UNCLASSIFIED

AD NUMBER

AD820759

NEW LIMITATION CHANGE

TO

Approved for public release, distribution unlimited

FROM

Distribution authorized to U.S. Gov't. agencies and their contractors; Critical Technology; MAY 1967. Other requests shall be referred to Naval Air Systems Command, Washington, DC 20360.

AUTHORITY

USNASC notice, 23 Dec 1970

THIS PAGE IS UNCLASSIFIED

HSER 4348
VOLUME 1 of 4

ENGINEERING REPORT

SHROUDED PROPELLER TEST PROGRAM DATA ANALYSIS

AD820759

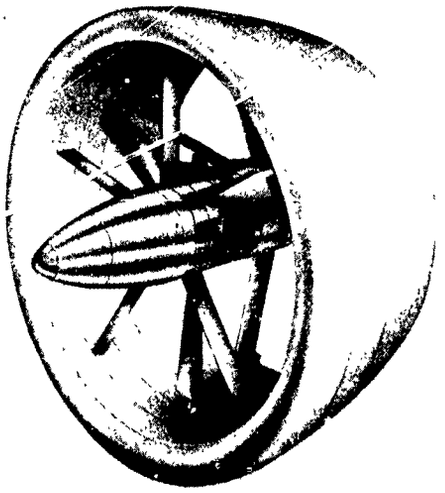

PHASE 1

CONTRACT NO. 64-0707-d
MAY, 1967

Hamilton Standard
DIVISION OF UNITED AIRCRAFT CORPORATION

HSER 4348
VOLUME 1 of 4

ENGINEERING REPORT

SHROUDED PROPELLER TEST PROGRAM DATA ANALYSIS

PREPARED BY: D. M. Black

D. M. BLACK - SENIOR ANALYTICAL ENGINEER

Hans S. Wainauski

H. S. WAINAUSKI - SENIOR ANALYTICAL ENGINEER

APPROVED BY: Carl Rohrbach

C. ROHRBACH - HEAD OF AERODYNAMICS & HYDRODYNAMICS

W. S. Fortmann

W. FORTMANN - CHIEF OF TECHNICAL STAFF

A. D. Croxall

A. D. CROXALL - CHIEF PROJECT ENGINEER

DDC
RECEIVED
OCT 5 1967
C

PHASE 1
CONTRACT NO. N64-0707-d
MAY 1967

STATEMENT #2 UNCLASSIFIED

This document is subject to special export controls and each transmittal to foreign governments or foreign nationals may be made only with prior approval of Naval Air Systems Command Code - AIR-604 Wash DC 20360

Hamilton Standard
DIVISION OF UNITED AIRCRAFT CORPORATION

CONTENTS

Section		Page
	VOLUME I	
I	SUMMARY	I-1
II	INTRODUCTION	II-1
III	OBJECT	III-1
IV	CONCLUSIONS	IV-1
V	RECOMMENDATIONS	V-1
VI	DESCRIPTION	VI-1
	6.1 General Description of Test Program	VI-1
	6.2 Model Notation	VI-2
VII	METHOD	VII-1
	7.1 Model Variables	VII-1
	7.1a Selection of Test Variables	VII-1
	7.1b Design of Test Models	VII-4
	7.2 Test Equipment	VII-8
	7.2a Wind Tunnel	VII-8
	7.2b Propeller Test Rig	VII-9
	7.2c Support Equipment	VII-10
	7.2d Shrouds	VII-11
	7.2e Propellers	VII-11
	7.3 Accuracy of Results	VII-11
VIII	RESULTS AND DISCUSSION	VIII-1
	8.1 Introduction	VIII-1
	8.2 Data Presentation	VIII-2
	8.2a Performance of the Basic Model (B1-3WT)	VIII-2
	8.3 Effect of Propeller and Shroud Shape Variables on Performance	VIII-6
	8.3a Area Ratio	VIII-6
	8.3b Shroud Lip Shape	VIII-10
	8.3c Shroud Length	VIII-11
	8.3d Propeller Position	VIII-13

CONTENTS (Cont.)

Section		Page
	8.3e Inlet Vanes	VIII-14
	8.3f Exit Vanes	VIII-16
	8.3g External Shape	VIII-17
	8.3h Propeller Planform	VIII-18
	8.3i Number of Blades	VIII-19
	8.3j Tip Clearance	VIII-21
	8.3k Basic Propeller without a Shroud	VIII-22
	8.4 Pressure and Velocity Data	VIII-23
	8.4a Shroud Surface Pressure Distributions	VIII-23
	8.4b Shroud Exit Plane Total Pressures	VIII-25
	8.4c Shroud Exit Plane Static Pressures	VIII-30
	8.4d Axial Velocity Distributions	VIII-31
IX	LIST OF SYMBOLS, SUBSCRIPTS & DEFINITIONS	IX-1
X	REFERENCES	X-1
XI	FIGURES AND CURVES	XI-1
XII	APPENDICES	XII-1
	12.1 Static Extrapolation	XII-1
	12.2 Conversion of Experimental Data from Coefficient Form	XII-5
	12.3 Shroud Surface Pressure Distribution and Friction Drag	XII-7
	12.4 Propeller Thrust and Power Distribution	XII-14
	12.5 Calculation of Slipstream Contraction and Net Thrust from Pressure Distribution	XII-28
	12.6 Application to X-22	XII-31
	BASIC TEST DATA	VOLUME II
	TABULATED TEST DATA (FORCE AND VELOCITY)	VOLUME III
	TABULATED TEST DATA (VELOCITY AND PRESSURE)	VOLUME IV

INDEX TO CONTENTS OF VOLUMES

	Volume	Contents	No. of Pages
I	Data Analysis	Analysis of the test data showing the effect of a variable change on performance.	400
II	Test Data (UAC Report E330590-1)	Contains a detailed description of the test equipment, methods and data reduction, run log and plots of shroud and propeller performance.	334
III	Data Tabulation (UAC Report E330590-1)	Contains tabulated force data and 18 foot test section inlet velocities.	392
IV	Data Tabulation (UAC Report E330590-1)	Contains tabulated 18 and 8 foot test section velocity and pressure data.	414

ILLUSTRATIONS

Figure

1	UARL Large Subsonic Wind Tunnel
2	Complete Shroud Model
3	Schematic Representation of Shrouds and Propeller Test Rig
4	Shroud Shapes
5	Shroud Thickness Ratio Distribution
6	Shroud Camber Line Slope Distribution
7	Propeller Test Blades
8	Model Blade Characteristics Common to All Blades
9	Model Blade Characteristics
10	Model Blade Calculated Circulation Distribution
11	Typical Pressure Transducer Trace
12	Sign Convention for Propeller and Vane Angles
13	Bare Propeller Test Rig with Shroud Support System
14	Test Rig with Three Way Rectangular Propeller
15	Shroud Support Ring
16	Shroud Diffuser and Exit Vane Installation
17	Shroud Center Section and Lip Installation
18	Rear View of Complete Model Showing Exit Vanes and Exit Rake Installation
19	Rear View of Shroud with Dummy "A" Frame Installed
20	Rear View of Shroud with Dummy Side Arm Installed
21	Bolt Damage to Fiberglass Tip of Rectangular Blades

ILLUSTRATIONS (Cont)

Figure

	Basic Force Data
22-27	Tnet/BHP Versus $\frac{BHP\ (\rho o/\rho)}{D^2}$
28-33	T/BHP Versus $\frac{BHP\ (\rho o/\rho)}{D^2}$
34-45	Tnet/T Versus $\frac{BHP\ (\rho o/\rho)}{D^2}$
46-75	Tnet/Tnet Basic Versus $\frac{BHP\ (\rho o/\rho)}{D^2}$
76-104	T/Tbasic Versus $\frac{BHP\ (\rho o/\rho)}{D^2}$
105-117	Lip Shape Effect Tnet/Tnet Basic and T/Tbasic Versus Non-Dimensional Lip Radius
118-128	Exit Area Ratio Effect Tnet/Tnet Basic and T/Tbasic Versus Area Ratio
129-140	Shroud Chord/Diameter Ratio Tnet/Tnet Basic and T/Tbasic Versus Shroud Length
141-152	Propeller Position Effect Tnet/Tnet Basic and T/Tbasic Versus Propeller Position
153-158	Inlet Vane Effect Tnet/Tnet Basic and T/Tbasic Versus Inlet Vane Angle
159-164	Exit Vane Effect Tnet/Tnet Basic and T/Tbasic Versus Exit Vane Angle
165-176	Blade Planform Effect Tnet/Tnet Basic and T/Tbasic Versus Blade Tip Chord/Propeller Diameter
177-188	Number of Blade Effect Tnet/Tnet Basic and T/Tbasic Versus Number of Blades
189-200	Tip Clearance Effect Tnet/Tnet Basic and T/Tbasic Versus Tip Clearance

ILLUSTRATIONS (Cont)

Figure

201-203	Unshrouded Propeller Tuns/Tnet Basic and Tuns/Tbasic Versus $\frac{BHP \times \rho o/\rho}{D^2}$
	Pressure Data
204-212	Inside Pressure Distribution
213-221	Outside Pressure Distribution
222-231	Shroud Pressure Distribution
232-249	Shroud Inlet Axial Velocities
250-272	Total Pressure Distributions at Shroud Exit
273-285	Static Pressure Distribution at Shroud Exit
286-302	Shroud Exit Velocity Distribution

I

SUMMARY

This report contains and summarizes the shrouded propeller test data obtained in a comprehensive wind tunnel test conducted by Hamilton Standard in the United Aircraft Subsonic Wind Tunnel test facility. These data include the effects of varying the shroud parameters of lip shape, exit area ratio, propeller position, shroud chord length, and exterior shape, and propeller parameters such as planform distribution, number of blades and tip clearance. Each of these parameters was tested over a wide range of propeller power loadings, tip speeds and free-stream Mach numbers. These data were then reduced in a manner in which the effect of variations of each parameter change on performance could be separately evaluated.

This work was undertaken as Phase I of Contract NOw-64-0707-d awarded by the Bureau of Naval Weapons in November of 1964.

II INTRODUCTION

The advent of V/STOL aircraft has accentuated the need for propulsive devices that produce high thrust at static and low speed flight conditions. One means of attaining high static thrust without resorting to large diameter propellers is through the use of shrouded propellers. As air is drawn through the shroud, a low pressure region is created on the lip of the shroud and, this, coupled with diffusion behind the propeller, creates a force in the thrust direction. The sum of the shroud force and the propeller thrust results in a greater net thrust on the shroud-propeller unit than could have been obtained with the same diameter unshrouded propeller.

A great deal of prior experimental work has been conducted on shrouded propellers to substantiate the concept and to define performance levels. Unfortunately, there had been no coordinated planning between the many individual test programs and, in fact, a large portion of the data apply only to specialized configurations or design problems. Consequently, these data have been unamenable to parametric analysis.

Mutual recognition of the need for a comprehensive experimental program on shrouded propeller aerodynamics led to a Bureau of Naval Weapons contract with Hamilton Standard for the conduct of the following three-phased program:

1) Phase I, a wind tunnel test covering a systematic variation in the important shroud-propeller variables.

2) Phase II, a wind tunnel test of a variable camber shrouded propeller.

3) Phase III, the development of a reliable shrouded propeller performance prediction method.

Work was initiated on this program under contract NOw-64-0707-d on November 1, 1964.

This report covers the first phase of this program which, as indicated above, involves a systematic wind tunnel test of the important shroud-propeller variables in the United Aircraft Research Laboratories test facility. In this Phase the following variables were investigated:

II (Continued)

PROPELLER VARIABLES

1. Propeller Blade Planform
2. Number of Blades
3. Tip Clearance

SHROUD VARIABLES

1. Lip Shape
2. Exit Area Ratio
3. Shroud Chord/Diameter Ratio
4. Propeller Position
5. Exterior Shape
6. Inlet Vanes
7. Exit Vanes

Each of the above variables was investigated with at least two configurations over a wide range of propeller power loadings and flight conditions. This report covers a presentation and analyses of the data gathered during the testing. Volume I covers the analysis of the data and includes a description of the effect of each variable change on performance.

The data are presented in a dimensional form which allows the rapid evaluation of the effect of a variable change, directly in terms of pounds of thrust for a given input horsepower, propeller diameter, tip speed, and flight Mach number. Both net (combined propeller and shroud thrust) and propeller alone performance are given.

Volume II contains a detailed description of the test facility and test techniques, and plots of the force test data in terms of propeller power coefficient, thrust coefficient, advance ratio and propeller and shroud efficiency. Volumes III and IV contains tabulated force and pressure test data.

III OBJECT

The object of Phase I of this program is two-fold:

1. To provide empirical data, with systematic variations in the important shroud-propeller shape variables, that may be used to design efficient shrouded propellers.

2. To supplement the development of a reliable analytical performance prediction method.

IV CONCLUSIONS

From the test results the following conclusions have been drawn:

SHROUD VARIABLES

1. Of the two shroud lip shapes which were tested, the net thrusts with the basic lip are 1% to 2% higher at M = 0, generally the same at M = 0.10 and 1% to 4% lower at M = 0.20. At higher Mach numbers the thrust comparisons are very dependent upon power loading and tip speed. At M = 0.50 the B2-3WT model produces from 10% more to 60% less net thrust than the basic or B1-3WT model.

2. At low speeds, below M = 0.20, the 1.3 area ratio shroud model produces the most net thrust for a given propeller input power. Above M = 0.20, however, the 1.1 area ratio shroud produces the best performance. The average changes in net thrust for the 1.3 compared to the basic or 1.1 area ratio shroud model are 9% at M = 0 and -69% at M = 0.50.

3. Of the two shroud chord lengths tested, the longer or basic length model produces considerably more net thrust at 0.40 and 0.50 Mach number. At lower Mach numbers the differences in performance are quite small ranging between plus and minus 2%. The net thrust for the basic shroud length is an average 3.5% and 18.5% higher at M = 0.40 and 0.50 respectively.

4. The net thrusts are quite dependent upon the position of the propeller within the shroud. With the propeller in the forward position, the net thrusts are consistently higher at and above M = 0.20 and are an average 13% higher at M = 0.50. At lower speeds the net thrusts are highest in the basic position and are an average 3% higher in that position at M = 0.

5. The external shape of the basic shroud model is considerably more favorable to net performance than the NACA series 16 external fairing. Up to M = 0.20 the performance for these two models is quite similar, but is an average 3%, 4% and 14% better for the basic model at M = 0.30, 0.40 and 0.50 respectively.

6. For inlet vanes which are designed as structural support members the best overall vane pitch setting is 0°. Large performances losses result from preswirling the flow in the direction of the propeller rotation. At low Mach numbers some minor net thrust increases occur with the inlet flow preswirled opposite to the propeller rotational direction. On the average there is very little difference in net thrust with no inlet vanes and with inlet vanes set at 0°.

IV

(Continued)

7. For exit vanes which are designed as structural support members the net thrusts are generally highest at M = 0.05 with the vanes set at 10° while they are highest at M = 0.20 with the vanes set at 0°. For these settings the net thrusts were very nearly the same as with no exit vanes at all. At higher Mach numbers the net thrusts were greater with the vanes set at 0° than with no vanes, and by an average 10% at M = 0.50.

PROPELLER VARIABLES

1. Of the three propeller planforms tested the superiority of any one for producing net thrust is dependent upon both Mach number and power loading. In general the narrow tip trapezoidal planform propeller is superior up to M = 0.20. At M = 0.3, 0.4 and 0.5 the superiority is shared by the rectangular and wide tip trapezoidal planform propeller models.

2. The net thrusts are generally higher with the three bladed propeller than with the four bladed propeller at Mach numbers of 0, 0.10 and 0.20, and are accentuated as the propeller power loading increases. Above M = 0.20 the four bladed propeller produces the most net thrust. The average ratios of net thrust for the four bladed model to the three bladed model are .978 and 1.062 at M = 0 and 0.50 respectively. At low speeds the net thrust trends are mostly the result of the propeller thrust comparisons while at M = 0.30, 0.40 and 0.50 both the shroud and propeller are favorably affected by the four bladed propeller.

3. Increasing the propeller tip clearance to diameter ratio is detrimental to both the propeller and shroud thrusts at 0, 0.10 and 0.20 Mach number. At higher speeds, however, the net thrusts increase at the maximum tip clearance and at M = 0.30 and 0.50 are an average 2% and 4% higher than the minimum tip clearance.

GENERAL

1. The basic shrouded propeller model produces considerably more thrust than the same propeller without a shroud at 0.05, 0.10 and 0.20 Mach number. The average increases in thrust are 65%, 35% and 3% at these three Mach numbers. The thrust of the propeller alone for the basic shroud model is very nearly the same at 0.05 and 0.10 Mach number as the unshrouded propeller thrust and about 5% lower at M = 0.20.

2. The shroud thrusts are very much affected by the propeller power loading. The axial force on the shrouds can be kept positive to increasingly higher Mach numbers as the propeller loading is increased.

IV (Continued)

3. The ratios of net to propeller thrust at M = 0 are generally within 2 or 3% of the value predicte by simple one dimensional monentum theory, which states that $T_{NET}/T = 2A4/A2$.

4. It is difficult to evaluate the shroud friction drag from the shroud surface pressure distributions. Some positive results have evolved from efforts to do this and have yielded reasonable generalizations of the shroud friction drags.

5. The static pressures at the shroud exit plane are generally greater than the atmospheric static pressure. From this it is concluded that the slipstream contracts downstream of the shroud exit.

6. The pressure measurements are sufficiently accurate to determine the propeller thrust gradients but not the propeller power gradients.

7. The experimental data obtained in this program is sufficient to allow the selection of the shroud and propeller variables for efficient performance.

8. Sufficient data was obtained to aid in the development of a performance prediction method in Phase III of this contract.

9. Aerodynamically the performance of the X-22A can be improved for some flight conditions by changes in the shroud shape and propeller characteristics. (See Appendix 12.6)

RECOMMENDATIONS

Based on the test results the following recommendations may be made:

1. Shrouds with lip thickness to diameter ratios less than 0.10 should be tested in attempt to improve high speed performance. These shrouds should be tested in small increment thickness changes so that the thickness at which the low speed performance begins to decrease can be determined.

2. Shrouds with chord to diameter ratios less than 0.50 should be tested. This test should be made compatible with the lip thickness shroud test employing both 0.10 and thinner lip to diameter ratios.

3. Further tip clearance tests should be conducted to evaluate the increased high Mach number performance that was observed for the maximum clearance in this test program. This test program should be planned so that both the clearance to diameter and clearance to propeller tip chord can be evaluated.

4. Additional testing should be conducted to further evaluate the effect of the number of propeller blades and to evaluate the effect of propeller solidity. The number of blades should be varied from three to thirteen with total activity factors ranging from 500 to 2000.

5. An experimental program should be conducted wherein the effect of centerbody shape and size on performance is evaluated. This should include rotating and non-rotating spinners. The aerodynamic loads on the centerbodies should be measured separately from the shroud and propeller forces.

6. The effect of the propeller test rig blockage on performance should be determined. This could be conducted as a part of the centerbody evaluating experimental program in recommendation number 5.

7. A test program should be conducted to evaluate the effect of inlet guidevanes and swirl recovery vanes on performance. These vanes should be designed to straighten the flow leaving the shroud. Several sets of vanes should be tested which are designed for different test conditions and for different propeller solidities.

8. A test program should be conducted on shrouded propellers at inflow angles other than zero to extend the range of these data.

VI DESCRIPTION

6.1 General Description of Test Program

In order to attain the objectives of this program, a parametric series 2.5 foot diameter shrouded propeller models were tested from near static velocities to a Mach number of 0.5 over a range of propeller power loadings and tip speeds. These models incorporated interchangeable shroud lips, exit sections and propellers so that the effect of a variable shape change in either shroud, propeller, or shroud-propeller combination could be investigated. Only those shape variables deemed to have a major influence on shroud-propeller performance were chosen for testing.

The shroud shape variables investigated in this program consisted of lip shape, area ratio, chord length, exterior shape, vanes, and propeller position within the shroud. The propeller shape variables included planform, number of blades and tip clearance. Each of the shroud variables could have been investigated with each of the propeller variables. However, this would have resulted in a prohibitively large test program. It was therefore necessary to select one propeller to investigate all the shroud variables and then, similarly, select one shroud to investigate all the propeller variables.

Each shroud-propeller model was tested in the United Aircraft Research Laboratories 18 foot low speed and 8 foot high speed wind tunnel test facility on the United Aircraft propeller test rig. All the low speed testing was accomplished in the 18 foot throat which allows testing from an Mach number of 0.02 to a Mach number of 0.2. The high speed testing was accomplished in the 8 foot throat which allows testing from a Mach number of 0.2 to a Mach number of 0.5. This facility, shown in figure 1, is capable of higher Mach numbers, but the mechanical flexibility of the shroud support system limited testing to a Mach number of 0.5.

Each shroud-propeller model was tested on the propeller test rig over a sufficient range of blade angles and tip speeds to define the effect of each variable change over a range of power loadings appropriate for both low and high speed flight conditions. At each test point, shroud and propeller forces were measured through the use of an integral strain-gaged thrust and torque system in the propeller test rig and a strain-gaged shroud force system consisting of Baldwin-Lima-Hamilton load cells. The rotational speed of the propeller was measured by a Berkely EPUT meter and signal generator. In addition, velocities and pressures were measured in and around the shrouds. A typical shroud installed on the test rig is shown in figure 2.

Two types of data were obtained in this test program. The first is the force data which consisted of measured reaction forces on the shroud and propeller. The second is the pressure and velocity data in which velocities and pressures in the shroud inlet and exit, as well as shroud surface static pressures, were measured. Particular care was taken to make sure that the force and pressure testing did not interfere with each other by conducting the pressure testing entirely separately from the force testing. This eliminated any drag on the shroud force measuring system due to the large bundle

6.1 (Continued)

of tubing required to measure the shroud surface pressures.

All of these force and pressure data were reduced to either coefficient or parametric forms which can be easily compared. One shroud-propeller model was chosen as the base or "yardstick" against which the effect of a parameter change could be compared. In addition some of the velocity and pressure data were plotted and analyzed to correlate changes in the force data with observed changes in the shroud velocities and pressures.

In the following section, the reasons for the selection of these variables, the aerodynamic design of the variables, and a brief discussion of the test equipment and methods will be presented. A detailed description of the test models, test equipment, location and size of the test equipment is contained in volume II of this report.

6.2 Model Notation

In order to describe the shroud-propeller models simply, it was necessary to devise an adequate shorthand notation. The notation used is contained in Table I below for the shrouds. Figures 3 and 4 present sketches of these shroud shapes.

TABLE I

SHROUD NOTATION	LIP TYPE	PROP/CHORD LOCATION	AREA RATIO	CHORD LENGTH INCHES	DIFFUSER TYPE
B1	LIP 1	0.4C	1.1	20	BASIC
B2	LIP 2	0.4C	1.1	20	BASIC
B3	LIP 1	0.4C	1.2	20	BASIC
B4	LIP 1	0.4C	1.3	20	BASIC
B5	LIP 1	0.25C	1.1	20	BASIC
B6	LIP 1	0.4C	1.1	20	SERIES 16
B7	LIP 1	0.4C	1.1	15	BASIC

In a similar manner, the propeller configurations can be described by referring to the tip shape and number of blades in each propeller. This designation is contained in Table II below. A photograph of the blades is shown in figure 7.

6.2 (Continued)

TABLE II

BLADE DESIGNATION	NUMBER OF BLADES	TIP SHAPE
3R	3	RECTANGULAR
3WT	3	WIDE TIP
3NT	3	NARROW TIP
4NT	4	NARROW TIP

With this notation therefore, a shroud-propeller configuration can be described as:

B1-3WT

(which is a shroud with Lip 1, 1.1 area ratio and a 20" chord and a three bladed, wide tip propeller).

This notation is used in presenting the data in Volume I of this report.

The UAC model notation, as contained in Volumes II, III and IV of this report, differs from the Hamilton Standard notation previously described. The correlation of the Hamilton Standard and UAC notation is contained in Table III below.

TABLE III

HS NOTATION	UAC NOTATION
B1	L1C1E1
B2	L2C1E1
B3	L1C1E2
B4	L1C1E3
B5	L1C2E1
B6	L1C1E4
B7	$L_{isc}C_{isc}E_{isc}$
3R	B3PR
3WT	B3PWT
3NT	B3PNT
4NT	B4PNT

THIS
PAGE
IS
MISSING
IN
ORIGINAL
DOCUMENT

7.1a (Continued)

slightly modified pitch distributions to vary the circulation distributions along the blade were tested. These blades are shown in figure 7a, b and c.

Tip Clearance

Because of manufacturing tolerances and mounting flexibility of the shroud and propeller, clearance must be left between the propeller blade tip and the shroud inner surface. Most references indicate that this clearance should be kept to a minimum in order to maximize shroud-propeller performance. Three tip clearances were investigated in this program corresponding to approximately 1/4, 1/2 and 1 percent of the propeller diameter with the maximum clearance representing an easily obtained design tolerance for this type of hardware.

Number of Blades

Present design methods for shrouded propellers define only the total propeller solidity required for a given operating condition and do not explicity indicate the number of blades required to obtain that solidity. However, theory indicates that the flow periodicity induced by the blades could significantly influence shroud pressure distribution and therefore shroud performance.

To investigate the effect of number of blades, both a 3 bladed and a 4 bladed propeller of the same total solidity were included in this test program. Both propellers incorporated trapezoidal planform blades as indicated in figure 7d with the 3 way blade 25% wider than the 4 way blade. All of the other shape parameters for both propeller blades were the same.

Shroud Variables

Shroud Exit Area

The ratio of the open area at the exit of the shroud to the open area at the propeller plane, theoretically affects shroud thrust at static and near static conditions as can be seen from the theoretical relationship, thrust total = 2x area ratio x propeller thrust as contained in Reference 1. However, the increased induced mass flow and diffuser drag adversely affect cruise performance, which implies an optimum magnitude of area ratio, dependent on the design operating condition. Prior testing has indicated that an area ratio of 1.0 and possibly less would provide optimum high speed cruise performance but relatively poor static thrust performance. On the other hand, data also indicate that an area ratio of 1.4 could give high static thrust performance with correspondingly poor high speed performance. Accordingly, area ratios of 1.1, 1.2 and 1.3 were investigated in this program. It was anticipated that somewhere within this range of area ratios, a good compromise between high static thrust and good high speed performance could be effected. Sketches of these shrouds are shown in figures 3 and 4.

7.1a (Continued)

Shroud Lip Shape

Shroud thrust is developed primarily by accelerated flow induced by the propeller which generates a reduced static pressure on the inlet lip. This reduced lip pressure tends to produce an adverse pressure gradient with respect to the boundary layer along the inside shroud surface between the shroud inlet and the propeller plane. Thus, improper design of the inlet lip can result in separation of the boundary layer from the inside surface of the shroud with resultant loss in both shroud and propeller thrust. Therefore, it is apparent that the shroud lip shape is the single most critical element in the design of a shroud in that it must support high loadings without separation at static conditions and yet must be thin enough to minimize drag in high speed flight conditions.

In this Phase, two lips were tested. These lips were designed to be suitable for both high and low speed flight. The configurations of these lips, which are very similar, are shown as shrouds B1 and B2 in Figure 4 and in Figure 3 with the area ratio 1.1 shroud.

Diffuser Exterior Shape

During the course of the design analysis of the shroud exterior contours, it became apparent that the exterior shape of the diffuser could significantly effect the performance of a shroud-propeller combination. Accordingly this variable was added to the test program.

This addition included building and testing a fourth diffuser section which had the exterior shape of the rear half of a Series 16 airfoil. This is indicated as shroud B6 in Figure 4. The effect of using this section can be seen by comparing shroud B6 with B1 which has the same area ratio and lip shape as shroud B6 or by comparing the sketches of Figure 3.

Shroud-Chord to Diameter Ratio

The shroud chord must be large enough to permit fully developed shroud thrust at static conditions and provide adequate lift for those applications where the shroud is used as a ring wing. Yet the shroud must be as short as possible to avoid excessive drag in cruise operation. However, as the shroud becomes shorter, the diffuser angle for a given area ratio becomes larger, but this angle must be kept as small as possible to avoid diffuser separation. Therefore, two shroud chord to diameter ratios were tested. The larger of these, .667, permits low diffuser angles up to and including an area ratio of 1.3. The smaller one, .5 incorporates the shortest shroud which can be utilized without going to large diffuser angles at relatively low area ratios.

7. (Continued)

Propeller Location

The location of the propeller within the shroud may have an important effect on performance and on propeller blade structure when the shroud is inclined to the flight direction. In general, it is expected that the largest circumferential and radial variations in velocity at the propeller disk under yawed conditions will occur with the shortest shroud length ahead of the propeller as the shroud tends to straighten the inflow into the propeller. Accordingly, two propeller locations were investigated in this phase. One location was at 25% of the chord from the leading edge and the other location was at 40% of the chord distance from the shroud leading edge.

Exit and Inlet Guide Vanes

In this test program all the models could be tested without inlet or exit vanes because of the unique shroud support system used. However, it is realized that in the practical sense, some provision must be made to keep the centerbody-propeller unit at a fixed distance from the shroud internal surface. The conventional means of doing this is through a vane support system. To determine the effect of a vane support system on performance, one set of inlet and one set of exit vanes were tested on the B1 shroud.

7. Design Considerations

Shrouds

Two analytical methods were used to establish the shroud shapes that were investigated in this Phase. The Therm performance prediction method (Reference 2) was used to determine the shroud velocity distributions and shroud performance at forward flight conditions and the Von Neumann potential flow calculation method (Reference 3) was used to determine shroud lip pressure and velocity distributions at static operation. Since a design requirement for good propeller and shroud efficiency is that no flow separation occur on the shroud lip, velocity distribution from both of these methods were then used in a boundary layer calculation procedure, to assure that flow separation would not occur on any shroud configuration included in this test program. These calculation methods were programmed on the IBM 7090 high speed computer permitting the rapid evaluation of a large number of shroud configurations. Thus numerous shroud shapes were analytically investigated to establish the optimum configuration. Among the shroud shapes studied, several incorporated airfoil shapes commonly used for aircraft wings and propeller blades. In particular, the NACA four digit, Series 6 and Series 16 airfoil families were investigated. Each of these families has at least one characteristic which would make it suitable for a shroud profile. For example, the four digit airfoil family with its large leading edge radius has a favorable pressure distribution necessary to avoid lip separation; the Series 6 airfoil family exhibits low minimum drag coefficients and high critical Mach numbers; and the Series 16 airfoil family has the highest critical Mach numbers of any currently available airfoil family. In order to take full advantage

7.1b (Continued)

of these favorable characteristics, some of the shroud profiles investigated were combinations of these airfoil families, i.e., the tail of a Series 6 airfoil might be joined to the nose of a four digit airfoil, etc.

These investigations led to the conclusion that no one airfoil family was ideally suited for use as a shroud shape. For instance, the Series 16 airfoil family has high critical Mach numbers, but an adverse shroud lip pressure distribution because of this family's small leading edge radius. Likewise, each of the other airfoil families has at least one desirable characteristic when utilized as a shroud profile. In addition, it was found necessary to modify the portion of the airfoil surface in the propeller plane in order to maintain a uniform blade tip clearance across the blade width. Following these preliminary investigations the final study was concentrated on shroud lips that consisted of analytically determined section shapes. The lip shape chosen for this test program follows the following mathematical equation:

$$y = \left\{ \pm .2065 \sqrt{52.75-(3.75-X)^3} + \frac{h}{b} (3.75-X)^3 (.028457) \right\} + 1.5$$

where

$$\frac{h}{b} = \frac{1}{3} \text{ for lip 1}$$

$$\frac{h}{b} = \frac{1}{6} \text{ for lip 2}$$

These lip shapes were previously analytically studied in Reference 4.

One important result of the study conducted to define the lip shapes for this test program was that the shroud lip section thickness as measured at the propeller plane should be at least ten percent of the propeller diameter in order to avoid separation at static conditions. With the shroud thickness fixed, two lip shapes were finally chosen for the wind tunnel test. The first, or lip 1, was conservatively chosen to avoid separation in either static or cruise operation. A very cursory, visual tuft study conducted in the 18-foot tunnel did, indeed, indicate no evidence of separation. The second lip was aimed at increasing the critical Mach number of the shroud. In order to accomplish this, it was necessary to make the leading edge radius of the shroud smaller and therefore more susceptible to lip separation.

With lip number 1 as the basic inlet, several different diffuser shapes were considered in order to determine the most desirable shroud cross-section shape for a given area ratio. The internal surface distribution of the diffuser was determined by the area ratio desired between the plane of the propeller and the shroud exit. A straight line was then drawn from the straight, cylindrical portion of the internal surface at the propeller plane to the shroud exit.

(Continued)

These diffuser studies indicate that diffuser sections modified from the rear portion of Series 6 airfoils and representative of current state-of-the-art, as investigated in previous wind tunnel tests, yield good static and high speed performance. However, these studies also indicated that shrouds with diffuser sections consisting of the rear halves of Series 16 airfoils were capable of improved performance at some flight conditions. Because of the uncertainty of the absolute levels of performance indicated by present analytical methods, it was decided that the basic diffusers should incorporate exterior shapes representative of the current state-of-the-art flight hardware. However, an additional diffuser consisting of the rear half of a Series 16 airfoil was included in the test program to investigate its potential.

The characteristics of these various shrouds are shown in Figures 5 and 6. As can be seen from these figures, the shape of the shroud mean camber line is primarily a function of the desired lip shape and shroud exit area ratio with the larger exit area ratio causing the most deviation from what may be considered a normal airfoil type of camber line slope.

The vane configurations for this test program were selected after careful consideration of such factors as drag, position, angle of attack and function. These vanes were included as support members only and were not intended to add or remove any swirl from the flow through the shroud. These considerations led to the selection of a ten percent thick, symmetrical, Series 16 airfoil section for the vane cross-section shape and a constant vane width. The number of vanes (5) was chosen so as to not to aerodynamically excite either the three or four bladed propeller. The position of the vanes within the shroud was chosen to avoid any possibility that the vanes would trigger separation on either the shroud lip or diffuser section.

Propellers

Planform Distribution

With the shroud internal flow fields defined by either the Hamilton Standard three-dimensional shrouded propeller performance prediction method or the Von-Neumann potential flow calculation method, the aerodynamic characteristics of the propeller blade configurations were determined. The objective was to define a series of three propeller designs which differed in blade radial circulation distribution and yet gave essentially the same calculated performance at the design conditions. In this manner, the effect of blade circulation distribution on shroud performance could be evaluated from the wind tunnel test data.

As prime design points, velocities, power coefficients and advance ratios were chosen which are representative of a design static and cruise operating condition of the current Bell X-22 flight test vehicle incorporating shrouded propellers. This results in an

7.1b (Continued)

$SHP/D^2 \times \rho_0/\rho$ of 16 for the zero velocity condition and 12 for a M = 0.338 case. On the basis of the aerodynamic design study, a three way propeller incorporating blades of 168 activity factor and an integrated design camber of 0.400 was selected to meet these design points.

As stated previously, the performance of a propeller within a shroud is very intimately associated with the performance of the shroud itself. The flow field induced by an operating propeller determines the pressure distribution on the shroud surface and, correspondingly, the flow field generated by the internal surface distribution of the shroud influences the propeller performance. Accordingly, each specific shroud shape should have a propeller designed for the flow field induced by that shroud shape. It is readily apparent, considering the large number of shroud shapes investigated in this Phase, each with its own flow field for a given operating condition, that this would have required the design and testing of a prohibitively large number of propeller blade designs. For example, the mass flow and flow distribution of the 1.3 area ratio shroud is different than that of the 1.1 area ratio shroud for a given velocity and horsepower input into the propeller. Obviously, a propeller designed specifically for an area ratio of 1.3 would have slightly different characteristics than a propeller designed for an area ratio of 1.1. Therefore, one shroud shape was chosen as the basic design and its flow field was used to design the propeller blades used in this phase. This shroud shape has an area ratio of 1.1, a chord to propeller diameter ratio of 0.667, a propeller location at 40% of the shroud chord, and a shroud lip section thickness to propeller diameter ratio of 0.10 as shown in Figure 4 as B1.

With this basic shroud configuration, a series of three propellers with the same activity factor, camber, and number of blades were designed. The first of these was a rectangular planform blade, designed to give the best performance at the previously mentioned design points. This blade design resulted in a specific distribution of circulation along the blade radius as defined by the performance prediction method. The characteristics of this blade (3R) are shown in Figures 8 and 9 and the circulation distribution is shown in Figure 10.

With the rectangular blade planform as a base, the circulation distribution was first varied by increasing the blade tip width and twist to get a desired nominal variation in blade circulation. These changes in the base blade are reflected as 3WT in Figures 8 and 9.

The objective of the third blade design was to reduce the circulation at the blade tip. This was done by reducing the blade tip width and adjusting the blade twist distribution until the desired nominal level of circulation was reached. These changes are also reflected as 3NT in Figures 8 and 9. Thus, with these three propellers, differing in circulation distribution, the effect on shroud-propeller performance could be analyzed from the wind tunnel data.

7.1b (Continued)

This change in circulation distribution as previously mentioned, is accompanied with a change in the induced velocity near the tip of the blade. This velocity when added to the flow field of the shroud must be such that the shroud does not separate. Conversely, a thin shroud with a marginal pressure gradient with regard to boundary layer separation near the propeller plane could, theoretically, be helped by increasing the circulation and induced velocity. However, present shroud-propeller analytical design methods do not explicitedly define how the shroud boundary layer and propeller tip circulation inter-act nor do they define the resultant pressure distribution on the shroud surface, which is an important consideration in determining boundary layer separation. Therefore, this information must be obtained in a test program.

Number of Blades

Present shrouded propeller design methods primarily specify only the total propeller solidity required for a given operating condition. These methods do not specify how this solidity should be obtained. For example, if a total solidity of 600 is specified, this may be arrived at with a three-bladed propeller with each blade having a solidity of 200 or a four-bladed propeller with each blade having a solidity of 150 or with a six-bladed propeller with each blade having a solidity of 100. Theoretically, each of these propellers should perform in the same manner.

In addition, it is known that the passage of each blade tip past a fixed point within the shroud produces a momentary rise and fall in the static pressure at that point. This is illustrated in Figure 11 which is a trace of the pressure variation on the shroud surface as recorded by electrical pressure transducers located immediately upstream of the propeller plane of rotation. It was observed as expected that for one revolution of the propeller, three distinct pressure peaks and valleys were recorded by the transducer for a three bladed propeller. The frequency and amplitude of these pressure fluctuations become important considerations in the design of a shroud in that they must not create adverse pressure gradients on the shroud. In a separate phase of this program the harmonic content of these instantaneous pressure fluctuations will be analyzed to determine its effect on shroud performance.

In order to provide a variation in the frequency and amplitude of the pressure fluctuation and in order to provide an indication of the effect of number of blades on shroud-propeller performance, a four-bladed propeller was included in the test program. This was accomplished by scaling down the three-way, narrow tip propeller to a four-bladed propeller of the same total solidity.

7.2 Test Equipment

7.2a The experimental test program reported herein was conducted in the UAC subsonic wind tunnel test facility. The UAC subsonic wind tunnel shown in figure 1 is a single return, closed throat facility having either an 8 foot or an 18 foot octagonal test section. The 18 foot test section is part of the fixed tunnel structure while the 8 ft. test section is a

7.2a (Continued)

movable cart which inserts into the 18 foot section. The 18 foot section is a low speed facility that may be operated at velocities as high as 200 MPH. The 8 foot test section free from supports and models and with special wall inserts may be operated at Mach numbers as high as 0.95. However, for the present series of tests, shroud support system flexibility restricted the bulk of the testing to Mach numbers of 0.5 and less. Total pressure in the tunnel is atmospheric since the circuit is vented to the atmosphere in the return circuit through air exchangers which also allow a means of controlling stagnation temperature.

7.2b The propeller dynamometer consists of two variable-speed motors mounted in a tandem configuration within a slender streamlined body. The variable-speed motors are coupled together and provide a maximum torque of 330 ft-lbs through a speed range up to 12,000 rpm. The motors are mounted on hydrostatic bearings to provide restraint to all motion except axial motion along, and rotational motion about, the longitudinal axis of the dynamometer. These motions are restrained by load cells which measure thrust and torque of the model propeller. The rotational speed of the propeller is measured by a Berkley EPUT meter and signal generator. In this test a special nose was fabricated for the propeller test rig. This nose allowed the transfer of the propeller plane upstream and further away from the body of the test rig. In addition a non-rotating, sting-supported, Series 1 spinner was designed and fabricated for use directly in front of the rotating hub. The sting not only supports the spinner but also allowed a convenient means of routing the pressure leads from the inlet rake, upstream and out of the tunnel.

A strain-gaged shroud force measuring system consisting of Baldwin-Lima-Hamilton load cells was attached to the outside cowl of the propeller test rig as shown in figure 13. The exact details of the shroud force measuring system i.e., location of balances, direction of forces, etc. is contained in Volume II of this report. It should be pointed out that this shroud system is independent of the propeller force measuring system. Prior to the test program, extensive calibrations of the propeller and shroud force measuring systems were performed. The wind tunnel itself was calibrated with and without a shroud model to determine the effects of the shroud on tunnel velocity setting. These calibrations are discussed and explained in Volume II of this report.

The testing technique in both throats consisted of setting up a particular shroud-propeller model in the wind tunnel and setting the blade angle of the propeller. The velocity of the tunnel was then set to the desired level and the propeller rpm varied from 4500 rpm to the maximum desired for that configuration. At discrete rpm values during the run, the shroud and propeller force data were recorded. Running plots of these data were kept and any obviously out-of-line points were repeated. After the maximum rpm point had been reached, a new wind tunnel velocity was set and the rpm excursion repeated or the wind tunnel was shutdown and a new blade angle set and the process repeated. This procedure was repeated until all the blade angle-mach number combinations for a particular configuration were completed and then a new shroud-propeller configuration was installed and tested in a similar manner. A complete run schedule is contained in Table III of Volume II.

7.2b (Continued)

After all the force testing had been completed, the tubing required to measure the shroud pressures was installed, and shroud surface pressures and exit velocities were measured for a selected range of propeller blade angles, rotational speeds, and tunnel velocities. This method of testing was undertaken to insure that there would be no interference effects on the shroud force measurements from the considerable bundle of tubing required to measure the shroud surface pressures. This tubing was exposed to the propeller slipstream and could have caused an interference with the shroud chord force readings if the force and pressure data were taken simultaneously.

7.2c In addition to the tunnel and shroud and propeller test instrumentation, inlet velocity and exit total pressure rakes were fabricated and installed for certain pressure measurements. The inlet rakes sensed the distribution of velocity from the shroud centerbody to the inner surface of the shroud near the shroud lip and directly in front of the propeller plane of rotation. The exit rake consisted of 25 Kiel probes located at the shroud trailing edge and extending radially from the centerbody to the shroud exit. This rake sensed the increase or decrease in total pressure at the shroud exit.

Also utilized was a remotely operated United Sensor and Control Corp DAT-250 traversing probe which traversed radially outward from the shroud centerbody at the shroud exit. This probe sensed yaw and pitch angles, total and static pressures and temperature. All of these quantities were measured at sufficient radial locations across the shroud exit to completely define the flow at this location. Although the bulk of the data obtained using the traversing probe is for conditions at the shroud exit, a limited amount of data was obtained with the probe in a position immediately downstream of the propeller plane. The location of this instrumentation is shown in figure 3.

Instrumentation also included transient pressure transducers located immediately upstream of the propeller on the inner and outer surfaces of the shroud. The purpose of these transducers was to determine the characteristics and magnitude of the harmonic content of the shroud surface pressure distribution due to the operation of the propeller. This information is to be used in the development of a calculation method under Phase III of this overall program.

7.2d Model Construction

The shrouds used in this program were of a composite wood and metal construction with the lip and diffuser sections constructed of laminated mahogany rings. These sections were attached to a heavy metal support ring through the use of bolts. Provisions were made in the lip and diffuser sections for surface pressure measurements at two azimuthal locations on the shroud. The complexity of a typical shroud is shown in figures 13 through 20. The complexity of these shrouds caused some problems during the course of testing. First, the models required more care and time to install and change configurations than had been anticipated and secondly, on three occasions one of the shroud assembly bolts worked its way loose and caused considerable

7.2d (Continued)

damage to the model blades as can be seen in figure 21. This required the institution of an inspection procedure after every performance run to insure that all the components were properly fastened.

7.2e The model propeller blades used in this program were constructed of solid aluminum with the exception of the rectangular planform blades which incorporated a fiberglass tip. These tips were cut down in planned increments to investigate the effect of blade tip clearance on shroud-propeller performance. This method was chosen after careful consideration of other mechanical means which were judged to be too costly and complex.

7.3 Accuracy of Data

Two general categories of data were obtained in this test. The first of these is the source data in which the loads and forces generated by the shroud and propeller were measured with strain-gaged load cells. The second category is the pressure data. These pressure data can be broken down still further into pressure data obtained with rakes and the traversing probe and static pressure distributions on the shroud surface. The force data was recorded by visually reading the output of the force system and then reducing the data to coefficient form on an LGP 30 desk-type computer. The pressure data was photographically recorded on a manometer board and also electrically recorded through pressure transducers and stored on magnetic tape. The taped pressure data was then reduced on an IBM 7090 computer at a later date.

The accuracy of the force measurements based on a statistical analysis of the data is as follows:

TABLE IV
DATA ACCURACY

MEASUREMENT	MEASURED VALUE	COEFFICIENT@ 5000 RPM
PROPELLER THRUST, LBS	± 0.93	± 0.002 (C_T)
PROPELLER TORQUE, FT-LBS	± 0.54	± 0.002 (C_P)
PROPELLER RPM	± 1	± 0.0002 (J)
SHROUD CHORD FORCE, LBS	± 1.26	± 0.004 (C_C)
PROPELLER BLADE ANGLE, DEG.	± 0.1	
TUNNEL MACH NUMBER	± 0.005	± 0.005 (J)

7.3 (Continued)

These values apply to all the data taken at a tunnel test Mach number of 0.05 or greater. However at tunnel test Mach numbers less than 0.05, it was extremely difficult to hold and maintain a fixed tunnel velocity during a performance run because of the pumping action produced by the propeller model as the rpm was varied. Therefore, at Mach number of 0.02 the velocity varied by as much as ten per cent during a performance run from low to high rpm. This could not be eliminated.

The first category of pressure data is the static pressure distributions on the shroud itself. In general these data are quite accurate. The location of the static pressure taps on the shrouds was controlled to within ± 0.010 of an inch.

The total pressure data has obtained with an exit rake. This rake was rigidly attached to the propeller test rig itself so that it could not interfere with the force measurements.

The inlet rake was attached to the spinner which in turn was free to float independently of the shroud and propeller force systems. However, in order to keep the diameter of the instrumentation sting supporting the spinner down to a reasonable value, it was necessary to use small diameter tubing leading from the rake to the pressure read out systems. The use of this small diameter tubing introduces a time lag between a velocity change and the resulting manometer reaction. It was noted during the course of the testing that the inlet velocities tended to increase if a data point were held for a period of two or three minutes and would reach a final stabilized value. This final value was at times as much as 10% higher than the initial value. To have waited until the values stabilized, would have required an additional 300 hours of testing. Not enough data was taken to permit all of the inlet velocity data to be corrected for each test data point presented in Volumes III and IV. The inlet velocities measured during the traversing probe testing, however, do not have to be corrected as considerable time was spent on each probe point. This time allowed the measured inlet velocities to reach stabilized values. These are the values presented in the comparison made in this volume.

It is difficult to tie values of accuracy to the traversing probe data as the accuracy is not only a function of how well the pressures can be sensed but also a function of how accurately the probe is calibrated and how well the mechanical system for extending the probe will repeat itself. Each of these items could cause an error in the final tabulated velocity. The calibration used to reduce the data from the probe was examined in detail and is the best calibration of this probe over the range of Mach numbers and angles investigated. This calibration is explained in detail in Volume II. The probe mechanical repeatability also appears to be accurate at least in the ability to extend the probe to a fixed radial location. It was found that each radial location could be repeated within ± 0.012 inches. The repeatability of the swirl angle setting, however, is not as accurate as would be desired. Analysis of the data indicates that this angle can only be mechanically repeated within ± 0.5°. Coupled with this is the

7.3 (Continued)

difficulty of the probe operator in determining when the probe is balanced in the air stream, for a mis-alignment of the fluid in the probe balancing tubes as little as 0.1 of an inch of water could cause an error of 1 degree in the swirl angle. It was possible to balance the probe to within ± 0.05 inches of water which results in a cumulative error in the swirl angle of approximately ± 1°.

This angle is extremely important in the integration of the rake measurements to obtain the power absorbed by the propeller which could serve as an indication of the accuracy of the force measurements. However, because the swirl angle measurement is not as accurate as would be desired, the correlation between measured torque and the torque integrated from pressure measurements is poor. The integration of the probe data for thrust, however, is rather good. These integrations are discussed in more detail in the results and discussion section of this report.

Although all the standard wind tunnel blockage corrections have been applied to the data to account for the effect of the shroud and propeller in tunnel velocity, the possible effect of the shape of the propeller test rig on the shroud and propeller forces has not been accounted for. It is realized that the shape of the test rig causes a slightly different distribution of velocity to be imposed at the shroud exit plane than if the test rig were not there. The effect of this different velocity gradient at the shroud exit was analytically examined using the calculation method being developed in Phase III of this program. This investigation indicates that the effects, if any, are small. Furthermore, ratioing the performance of one model variable to another, where the centerbody and test rig was kept fixed, tends to eliminate the effect of the test rig for most of the configurations investigated. This is not true for the case of the short chord shroud nor for the case where propeller position was investigated. In the case of the short chord shroud, the shroud is further away from the test rig than any other shroud and therefore any effect of the rig is reduced. On the other hand, to investigate propeller position, the shroud was pulled back closer to the test rig but even here the effect is throught to be small. Further work should be done in this area if absolute levels of performance are desired. However, for this series of tests, it is felt that the effect of any one shape variable has been established.

VIII RESULTS AND DISCUSSION

8.1 Introduction

This wind tunnel test program has made possible a systematic evaluation of many of the important shroud and propeller shape variables. The extensive scope of the program has allowed the acquisition of what are probably the most complete force and pressure measurements on this subject. The data presented in this report clearly shows the effect of each shape variable investigated upon propeller performance (thrust and power relationships for each propeller in a shroud) and net performance (thrust and power relationships for the shroud and propeller combination). The data showing these effects are shown in four basic series of curves which are described below. The experimental data is completely tabulated in coefficient form in Volumes III and IV.

1. One shroud and propeller combination was designated the basic model and is referred to as B1-3WT(1). This model is the performance "yardstick"; and the thrust and power of the other models are compared to it. The performance for this model is shown in figures 22 through 33. These figures depict the propeller thrust per horsepower and the net thrust per horsepower as a function of power loading at three tip speeds and seven Mach numbers (0 to .6).

2. The propeller thrusts and the net thrusts of each model are then compared to those for B1-3WT. These data are shown in figures 46 through 104 and depict the thrust comparisons as a function of power loading at three tip speeds and six Mach numbers. These curves were generated as a means of obtaining the next set of curves to be described, but have been included in this report because they provide additional information which is not directly shown in the model parameter comparison curves.

3. The effect on performance of each of the shape variables is shown in figures 105 through 200. These curves depict the ratios of propeller and net thrust of each model to those of the "yardstick" model(2) plotted against a measure of each geometric shape parameter. For example, figure 118 shows the effect of shroud exit area ratio upon net thrust.

   In the ensuing discussion sections for each of the shape parameters, average values of the thrust ratios are tabulated. These represent arithmetic averages of the data shown in the figures and provide the information which permits a quick assessment of each shape parameter upon performance.

4. The ratio of net to propeller thrust for each model is shown in figures 34 through 45. These curves define the effectiveness of the shroud at one selected tip speed and six Mach numbers for a range of power loadings.

---

(1) a complete model definition appears in the Model Notation section.

(2) in these comparisons B1-3WT is not always the "yardstick". For example, when the tip clearance parameter is described, B1-3R is the "yardstick" and B1-3R1/2 M and B1-3RM are compared to it.

8.1 (Continued)

Experimental data were obtained at .02, .05, .10, .20, .30, .40 and .50 Mach numbers (0.60 for B1-3WT) and were recorded inpropeller coefficient form. Static (M = O) data was obtained through a systematic extrapolation of the low speed measurements. The extrapolation technique is described in Appendix 12.1, and the conversion of the coefficients to thrusts and powers is described in Appendix 12.2.

A great number of pressure measurements were taken in this experimental program to enhance the understanding of the performance data and to aid in the formulation of an accurate theoretical method to be accomplished in Phase III of this contract. These measurements are described in the Test Methods section, are summarized in figures 204 through 302, and depict the following: (1) shroud surface pressure distribution, (2) propeller inlet axial velocity distributions, (3) shroud exit plane total pressure distributions, (4) shroud exit plane axial velocity distributions and (5) shroud exit plane static pressure distributions. The pressure and velocity data were used to compute propeller thrust and power loading distributions, shroud drag and shroud slipstream contraction. The pressure data are presented in a manner which shows the effect of blade angle, Mach number and tip speed on these five distributions for B1-3WT. The effects of many of the shroud and propeller shape variables upon these distributions are also shown at selected Mach numbers and tip speeds. Unlike the performance data presentation, it was not feasible to present pressure and velocity curves for fixed values of power loadings. However, complete tabulations of these data are presented in Volumes III and IV of this report and can be employed to suit various needs. The pressure and velocity distributions are referred to in the performance comparison discussions where they clarify the trends shown there and are described in further detail in the Pressures and Velocities section.

8.2 Data Presentation

8.2a Performance of the Basic Model (B1-3WT)

The B1-3WT model consisted of the basic three blade,wide-tip (3WT) propeller and the basic shroud (B1). The basic shroud had a chord-diameter (C/D)(3) ratio of .667, a maximum thickness/chord (x/c) ratio of .15 and a 1.1 exit-propeller plane flow area ratio. The propeller was located at the 40% shroud chord point and had a .0012 nominal gap-shroud diameter tip clearance. In its basic configuration, B1-3WT had no inlet or exit vanes, and like all other models tested it had a .25 hub-shroud diameter ratio. The basic and, in fact, all the propellers were designed to be compatible with

(3) When a shroud diameter is referred to it is the shroud ID at the propeller plane and is 2.5 feet for all models.

(Continued)

the basic shroud at two selected design conditions. (4) However, due to the broad scope and diversified intent of this program, these design conditions were of no greater significance than the multitude of other conditions tested. It should be borne in mind, however, that these conditions did directly influence the selected propeller solidities and hence the range of power loadings for which these propellers would operate efficiently without excessive blade stalling.

The performance of the basic model is shown in figures 22 through 33. These curves depict the propeller (5) and the net thrust per horsepower vs power loading characteristics. From these data power, diameter, tip speed and Mach number can be assessed against any given performance requirements. For example, the figures justify the tip speed selections for the two X-22A design conditions. In fact, the tip speed for best net thrust is highest at low Mach numbers and high loadings but decreases as Mach number increases and/or as the loading ($BHP/D_x^2 \rho_o/\rho$) decreases.

The propeller thrusts per horsepower generally increase at a given Mach number and tip speed as the loading diminishes. The net thrusts per horsepower, on the other hand, do not continue to increase as the loading diminishes. That is, the maximum net thrusts per horsepower generally occur at higher power loadings than the propeller thrusts per horsepower and diminish quite sharply thereafter. This trend in the values of net thrust per horsepower implies that the shroud thrust per horsepower diminishes as the loading decreases, and is clearly shown in Table V.

TABLE V

ROTATIONAL TIP SPEED= 785 FPS

	M= .30			M =.50		
$BHP/D^2 X \rho_o/\rho$	T/BHP	TNET/BHP	TSHROUD/BHP	T/BHP	TNET/BHP	TSHROUD/BHP
10	1.337	1.143	−0.194			
15	1.327	1.218	−0.109	0.832	0.426	−0.406
20	1.295	1.227	−0.068	0.841	0.559	−0.282
25	1.242	1.207	−0.035	0.839	0.630	−0.209
30	1.188	1.183	−0.005	0.834	0.666	−0.168
35	1.150	1.170	0.020	0.828	0.677	−0.151
40				0.817	0.677	−0.140
45				0.802	0.673	−0.129
50				0.781	0.670	−0.111

(4) The test propellers were designed to the one engine out hover and the 225 knot Bell X-22A conditions. M = O and .338; $BHP/D^2 X \rho_o/\rho$ = 16 and 12; tip speed 950 and 675 fps respectively.

(5) Unless otherwise stated, propeller thrusts will mean the thrust of the propeller in a shroud.

8.2a (Continued)

For a given Mach number, the propeller induces more flow through the shroud as the power loading increases. The increased flow raises both the shroud lip suction thrust and viscous drag, but in a manner whereby the resultant shroud force becomes more positive. The higher flows and suction pressures are clearly shown in the velocity and shroud surface pressure distributions at the end of this report. Many of the shroud surface pressure distributions were integrated in an attempt to evaluate the effect of propeller loading upon the pressure and viscous forces on the shroud. The method which was employed to determine these forces is described in Appendix 12.3. Although this attempt to evaluate shroud friction drag was not altogether successful, it did lead to a better understanding of the shroud force and its distribution over the shroud surface. The friction drags from these pressure integrations were correlated with values predicted from empirical methods as described in references 1 and 5. These findings are summarized in table VI. Whereas it appears that it is only necessary to keep the power loading high to assure good shroud performance, it can be seen when more closely examined, that this is a difficult task. Of the two ways in which the loading can readily be increased (by increasing horsepower and by reducing diameter) only reducing the diameter offers an attractive possibility. However, should the vehicle being investigated have a high static thrust requirement (6), then reducing the diameter to improve shroud performance and higher speeds loses its appeal. This effect is exemplified in Table VII where a propeller diameter reduction of three feet was considered for two operating conditions close to those for the Bell X22A aircraft. Obviously the thrust trade-offs (ΔT_{net}) shown in Table VII are far too unbalanced to be of practical value. However, it is interesting to note that a three foot reduction in propeller diameter increases the net thrust 15% at M = 0.4. Furthermore, had the propeller been designed for this higher power loading the thrust increase would have been yet larger.

TABLE VI

M = .3

$\frac{BHP}{D^2} \times \rho_o/\rho$	MEASURED SHROUD THRUST, #	PRESSURE THRUST, #	FRICTION DRAG, #
0	−17	−3	14
10	−14	1	15
20	−8	8	16
30	1	17.5	16.5
40	11	28	17

(6) All the experimental models are representative of fixed geometry shrouds designed to assure maximum static and low speed performance and it is therefore presumed that static thrust is of prime importance.

8.2a (Continued)

TABLE VII

BHP	M	D	ρ_o/ρ	BHP/D2 X ρ_o/ρ	TNET/SHP	TNET	ΔTNET	% CHANGE
735	0	7'	1.0	15.0	4.78	3513		
735	0	4'	1.0	46.0	2.98	2190	−1323	−37.7
586	.4	7'	1.0	12.0	.797	467		
586	.4	4'	1.0	36.8	.913	535	68	14.5

Figures 28 through 33 (T/BHP vs BHP/D^2xρ_o/ρ) shows rather sharp declines in propeller thrust per horsepower at some of the higher power loadings. At high powers, the propeller tends to become stalled (high angles of attack) and a loss in efficiency ensues. A propeller of higher solidity (more activity factor per blade or more blades) would avoid blade stall at high power loadings and would result in higher thrusts. However, higher solidity propellers would be less efficient at the lower loadings for which these models were designed.

The ratio of net thrust to propeller thrust for the basic configuration is shown in figure 34 at 915 feet per second tip speed for Mach numbers from 0 - .5. The value of this ratio where the shroud thrust is zero is 1.0. For the static case simple momentum theory predicts that this ratio is two times the shroud area ratio, or 2.2 for this model. Figure 34 shows that this value was very nearly achieved. It can also be seen that the Mach number at which $T_{net}/T = 1.0$ increases as the power loading increases. Which again exemplifies the effect of power loading on the shroud effectiveness. However, at the very highest loadings the propeller becomes less efficient whereby T decreases and T_{net}/T increases. The shroud thrust, however, does not continue to increase at a consistent rate as the propeller efficiency decreases and the ratio T_{net}/T is, in a very complex way, mutually affected by both the shroud and propeller. The shroud thrust is dependent upon the lip suction pressure which is dependent upon the propeller induced flow, and the flow is dependent upon the propeller efficiency.

Effect of Propeller and Shroud Shape Variables on Performance

8.3a Area Ratio

The effect of shroud exit to propeller plane flow area ratio was experimentally evaluated with shroud models B1, B3 and B4, each with the 3WT propeller. These formed the B1-3WT B3-3WT and B4-3WT models. These three shrouds employed the same shroud leading edge, but different aft sections which were designed to accomodate the three area ratios (1.1, 1.2 and 1.3). These shrouds are completely defined in the Model Notation section and are shown in figures 3 and 4. Geometrically these models differ in area ratio, diffuser angle and external fairing. Moreover, these models differ aerodynamically in airfoil profile. These differences are shown in figures 5 and 6 which show the camber line slopes and thickness distributions for each shroud model.

The effect of area ratio on propeller thrust and net thrust is presented in figures 117 through 128. These figures show the performance at constant power, tip speed and Mach number of the 1.2 and 1.3 shroud area ratio models in relation to the performance of the "yardstick" or 1.1 shroud area ratio model. The average (1) effect of shroud exit area ratio upon both propeller and net thrust is shown in Table VIII. This tabulation quite clearly indicates the performance compromise decisions that must be made in high speed vehicle designs. For example, an average 9% increase in take-off or hover net thrust associated with a 1.3 area ratio is accompanied by an average 69% decrease in net thrust at M = .5. These changes in average net thrust include average decreases in propeller thrusts of 10% and 30% for M = O and .5 respectively.

(1) The average effect of a shape variable upon performance represents the arithmetic average of the thrust ratios for the tip speeds and powers which are shown in the figures depicting the shape variable effect.

8.3a (Continued)

TABLE VIII
AVERAGE EFFECT OF AREA RATIO ON PERFORMANCE

M	$\frac{T_{NET}}{T_{NET\ B1-3WT}}$ A4/A2 = 1.1	1.2	1.3	$\frac{T}{T_{B1-3WT}}$ A4/A2 = 1.1	1.2	1.3
0	1.0	1.050	1.090	1.0	.950	.900
.1	1.0	1.030	1.040	1.0	.940	.890
.2	1.0	1.000	.970	1.0	.930	.860
.3	1.0	.950	.860	1.0	.915	.830
.4	1.0	.860	.640	1.0	.890	.780
.5	1.0	.670	.310	1.0	.800	.600

At each tip speed, Mach number and power loading the propeller thrust diminishes almost linearly as the area ratio increases from 1.1 to 1.3. The reduction in propeller thrust for the B3-3WT and B4-3WT models is associated with the higher propeller plane axial velocities attendant with the higher area shrouds as shown in figures 237, 238, 289 and 290. Defining a propeller efficiency as $\eta = TVa/550$ HP and recognizing that η remains nearly constant for a fairly wide range of axial velocities (Va), it can readily be seen that the propeller thrust rewritten as $T = 550\ HP\ \eta/Va$, will decrease as the area ratio increases for any specified power loading. The average axial velocities at the propeller plane for the B1-3WT and B3-3WT models at M = .4 as depicted in figure 238 are 1.1 x 430= 472 and 1.3 x 465 = 605. The ratio of propeller thrusts would then be .78 if the efficiencies are assumed to be equal, and this ratio agrees exactly with the average value in Table VIII. The change in propeller thrust with area ratio can also be seen in the exit rake total pressure distributions as shown in figures 256 and 257. These figures show that the exit total pressure is highest for the 1.1 shroud area ratio model and then decreases as the area ratio increases. The relationships between propeller thrust and exit total pressure and several numerical examples are shown in Appendix 12.4. Several thrust distributions were computed from

8.3a (Continued)

exit measurements and their integrations showed good correlation with the measured propeller thrusts. The velocity and pressure measurements will be employed more extensively in Phase III of this contract where they will provide detailed checkouts of the theoretical method. The detailed effect of shroud exit area ratio upon net thrust is shown in figures 117 through 122. These curves, like Table VIII, depict performance gains for the higher area ratio shrouds at and below .20 Mach number. The low speed gains, however, are accompanied by very severe performance losses at higher speeds. At M = O the net thrust, according to simple momentum theory, increases as the one third power of the area ratio. This would indicate net thrust increases of 1.0295 and 1.0572 above the 1.1 area ratio shroud model for the B3-3WT and B4-3WT configurations respectively. The actual values of these ratios were as high as 1.10 and 1.15 with averages of 1.05 and 1.09. Whereas the one third power is exceeded for both models, it is greater for B3-3WT. This and the shape of the net thrust ratio curves in figures 117 and 119 indicate that to increase static thrust by further increasing the area ratio requires longer diffusers with diffuser half angles no greater than the 12° on the B4 shroud (1). This conclusion has not been substantiated through observed diffuser separation, but the indicated tendency for the net thrust to begin to level off is enough warning to limit the rate of diffusion.

At M = .30 the general indication is that an area ratio of 1 1 is optimum. At higher speeds the curves of net thrust vs area ratio in figures 120 through 122 show that an area ratio less than 1.1 and perhaps less than 1.0 would be optimum. For Mach numbers equal to and below .20 the curves in figures 117 through 119 indicate that area ratios of at least 1.3 should be considered to achieve maximum net thrust. Depending, then, upon the application and upon the performance compromise situation area ratios both less than and greater than those tested in this program warrant further investigation (2). In order to achieve area ratios greater than 1.3 the added diffusion necessitates either lengthening the shroud or locating the propeller further forward in the shroud to allow more length for efficient diffusion.

---

(1) For shroud diffusers with boundary layer suction, vortex generators, grooves or possibly other than conical walls the required lengths to achieve efficient diffusion for area ratios greater than 1.3 might be shorter than for B4.

---

(2) Area ratios of .9 and 1.0 and 1.4 will be evaluated in a variable geometry shroud test by Hamilton Standard under Contract No. N00019-67-0087. This test will employ a new shroud design with 6% thick modified NACA Series 65 airfoils.

8.3a (Continued)

Looking ahead to the results for the shroud length and the propeller position experiments (figures 129 through 140 and 141 through 152 respectively) a probable solution for effectively achieving higher area ratios is indicated. At low speeds, where more diffusion is needed, moving the propeller nearer the inlet is detrimental to net thrust, while, increasing the shroud length improves both low and high speed performance. These results quite clearly indicate that lengthening the shroud is the best way to increase the area ratio and thereby produce more thrust.

The division of thrust between the shroud and the propeller is shown in figures 34, 41 and 42. Resorting again to simple momentum theory, the division of thrust at the static condition is two times the area ratio, or 2.2, 2.4 and 2.6 for these three models. About 98% of these values were achieved for the 915 foot per second tip speed shown. In each case the maximum value of the division of thrust occurs at the higher loadings, indicating again the benefits of heavily loading the propeller.

Table IX shows the effect of power loading upon the Mach number at which the shroud thrust is zero. This effect is shown for the three ratios and represents those Mach numbers in figures 34, 41 and 42 where $T_{net}/T = 1.0$. The pressure and viscous forces on the shroud are just balanced, and from this tabulation it can be seen that this occurs at a higher Mach number as the power loading increases. Furthermore, Table IX indicates that an area ratio between 1.2 and 1.3 allows operation at the highest Mach number before the shroud viscous drag becomes greater than the shroud pressure thrust. The reasons for this are not fully known, but as with the static condition, some mild and undetected separation may have been present with the B4 shroud diffuser causing a loss in shroud pressure thrust. That the Mach number is higher where $T_{net}/T = 1.0$ for B3-3WT than for B1-3WT does not, however, mean that the net thrust is greater for B3-3WT. When $T_{net}/T = 1.0$ all the thrust is propeller thrust and figures 123 through 128 show that the propeller thrust is considerably higher for the B1-3WT model and would be higher yet at area ratios less than 1.1.

TABLE IX
MACH NUMBERS WHERE SHROUD VISCOUS AND PRESSURE FORCES ARE EQUAL

AREA RATIO	1.1	1.2	1.3
$BHP/D2 \times \rho_0/\rho$	M	M	M
20	.266	.297	.297
30	.298	.356	.332
40	.326	.388	.364
50	.355	.407	.387

8.3a (Continued)

However, in investigating the shroud pressure distributions it was found (Appendix 12.3) that the pressure thrust and viscous drag both increase with area ratio. These increases apparently occur in such a manner that an optimum area ratio evolves.

8.3b Shroud Lip Shape

The shrouds for this experimental program were designed so that the maximum static thrust on the shroud lips would be realized. This means that the shrouds lips must be unseparated for the low suction pressure over them to be manifested as a shroud thrust. Provided that the flow is unseparated there are no limitations upon the lip thickness required to realize this static thrust. The prediction of the shroud surface pressure distributions and the boundary layer separation criteria indicated that the lip thickness needed to be 10% of the propeller diameter. In addition, the lip contour was also found to be quite critical in assuring attached flow. Two lips were designed with lip thickness to propeller diameter ratios of .10 with different contours. These two shroud modles were designated B1 and B2 and differed in the shroud leading edge thickness. The leading edge thickness is defined as one half of the difference between the shroud leading edge diameter and the shroud inside diameter. The leading edge diameter for B1 is 34.02 inches and for B2 is 33.50 inches. The leading edge thickness to diameter ratios for these two shrouds are 67% and 58.3% of the .10 overall lip thickness to diameter ratio. The larger leading edge thickness for B1 provided that model a better assurance of unseparated flow for the static condition whereas the more symmetrical shape for B2 provided it with a higher critical Mach number. The predicted critical Mach numbers were .52 and .57 for B1 and B2 respectively. The performance ratios for these two models are plotted against the leading edge to inside diameter ratio minus one. This parameter represents twice the non-dimensional leading edge thickness. The largest net and propeller thrust deviations between these two models occurs at the lowest of the three tip speeds (654 feet per second) at .3, .4 and .5 Mach numbers.

The average effect of the shroud lip shape is shown in Table X. The average net thrust ratios exhibit a very uniform trend with Mach number, with a maximum ratio of 1.017 at M = .2 and a minimum ratio of .903 at M = .5. The propeller thrust ratios do not exhibit as uniform a trend, but the spread in magnitude is somewhat smaller.

8.3b (Continued)

TABLE X
AVERAGE EFFECT OF SHROUD LIP SHAPE ON PERFORMANCE

M	TNET B2–3WT / TNET B1–3WT	TB2–3WT / TB1–3WT
0	.994	1.008
.1	.998	.992
.2	1.017	1.001
.3	1.015	.979
.4	.978	.980
.5	.903	.958

The higher critical Mach number which was designed with the B2 shroud was not actually evaluated experimentally since the test rig vibrations limited testing above .5 Mach number. Through the data which is tabulated in Volumes III and IV however, the shroud thrusts are generally found to be better at .4 and .5 Mach number for B2-3WT. From these data it would seem that the B2 shroud with its more symmetrical lip shape, is a better high speed airfoil. However, the net thrusts are generally poorer for B2-3WT model, indicating a less compatible union of propeller and shroud for this configuration. The average thrust ratios at M = .5 are highly influenced by the large thrust losses for both the propeller and shroud which occurred at the lowest of the three tip speeds. There is a strong indication in these results that the B2 lip was better at high Mach numbers and high power loadings, but considerably worse at low loadings.

8.3c Shroud Length

Two shrouds, with chord to inside diameter ratios of .667 and .50, were tested in this program. The effect of this parameter upon performance was evaluated with the 3NT propeller and the models were designated B1-3NT (C/D = .667) and B7-3NT (C/D = .50). The narrow tip propeller was employed in this investigation because the basic propeller was in the Hamilton Standard shop for repairs. A bolt had broken loose from the shroud and caused enough blade damage to require that it be repaired. In order not to lose valuable tunnel occupancy time the 3NT propeller was substituted for this series of tests.

3c (Continued)

These two shrouds, B1 and B7, had the same lip and the same exit area ratio. As airfoils, however, they had different thickness ratios and different mean camber lines. These two models were possible subjected to different interference effects from the propeller test rig. (1) The trailing edge of the B7 shroud was three inches further away from the test rig fairing than the B1 shroud. If there was significant blocking due to the propeller test rig it would have the effect of reducing performance as the distance from it was increased. Whether or not the test rig did create an effect upon performance which would influence the trends that are being attributed to the shape parameters is still being examined and will be discussed further in Phase III.

The net thrust and propeller thrust ratios for these two models are shown in figures 129 through 140. At 0., .1, and .2 Mach numbers there is only a relatively minor effect of shroud length upon net thrust at any tip speed or power loading. The propeller thrust ratios for these Mach numbers are also only slightly affected by power loading and tip speed but are generally 1-2% lower for B7-3NT. At .4 and .5 Mach numbers a large effect of shroud length is seen on both net and propeller thrust ratios. At M = .3 the net thrust is still only slightly affected by shroud length, but the propeller thrusts are 2-6% lower for the shorter shroud model. At M = .4 the net thrusts for B7-3NT fall 1-9% below those for B1-3NT while the propeller thrust ratios recover slightly from their apparent loss at M = .3. At .5 Mach number the net thrusts diminish quite sharply for the shorter chord shroud while the propeller thrust ratios again fall to their .3 Mach number level. The critical Mach number of the shorter chord shroud was estimated to be .46 and the large loss in net thrust at M = .5 is very likely attributable to exceeding this critical value.

The average effect of shroud length upon performance is shown in Table XI. Here the

TABLE XI
EFFECT OF SHROUD LENGTH ON PERFORMANCE

M	$\frac{T_{NET\ B7-3NT}}{T_{NET\ B1-3NT}}$	$\frac{T_{B7-3NT}}{T_{B1-3NT}}$
0	1.006	.991
.1	1.007	.985
.2	.996	.982
.3	1.000	.950
.4	.965	.977
.5	.815	.952

(1) The test rig blockage is described in some detail in the Accuracy of Data Section of this report.

8.3c (Continued)

near equality of these two models can be seen below M = .4 and the superiority of B1 3WT seen at M = .4 and .5.

Figures 280 and 281 indicate that of the two models the shorter chord shroud exit static pressures are closer to the atmospheric static pressure at both high and low Mach numbers. At the high Mach numbers (.3, .4 and .5) the static pressures are quite the same for the inner half of the annulus but fall closer to the atmospheric pressure for the outer half of the annulus. This pressure pattern is contrary to that which could be expected if the propeller test rig were acting as a flow or pressure block. The pressures and velocities will be employed in the Phase III study to help in the evaluation of this problem area.

8.3d Propeller Position

The effect of the propeller position within the shroud upon performance was determined experimentally with the basic shroud (B1) and the basic propeller (3WT). The propeller position on the propeller test rig was fixed and the shroud was moved in relation to this position. Two positions were tested and the model designations were B1-3WT and B5-3WT. For these two models the propellers centerlines were located 40% and 25% of the shroud chord length back from the shroud leading edge respectively. For the B5-3WT model the shroud trailing edge was located three inches closer to the enlarged diameter on the test rig. Therefore, if there was an effect upon performance due to the blockage effect of the propeller test rig, its effect might be different for these two models. The detailed effects, if any, of the propeller test rig upon performance will be evaluated in Phase III of this program.

It is important to evaluate the effect of propeller position on performance for two principal reasons. First, if the propeller can be positioned forward in the shroud without a performance loss more of the shroud length can be employed for either gentler diffusion or for more diffusion. Secondly, if the propeller can be located further back in the shroud without a performance loss, then the blade stressing could be less severe for inclined shroud operation usch as tilt shroud transition conditions. This latter effect was analyzed in an addition to this program at duct angles of attack to 28°. Very low blades stressing was observed with the propeller in either position, but this presumably would not have been true for higher duct angles of attack representative of transition maneuvers.

The effect of propeller position upon performance is shown in figures 141 through 152. It was impractical to test propeller positions forward of the 25% position or aft of the 40% position due to the lip and diffuser shroud contours. Therefore, these were the only positions tested and the data for these two configurations were connected with straight lines.

8.3d (Continued)

At zero Mach number the net thrust is consistently better in the basic or 40% position and is accentuated as the power loading increases. The propeller thrusts are affected quite similarly at M = O. However, the propeller thrust for B5-3WT does not continue to decrease as the loading increases but reaches a minimum value and recovers mildly. As the Mach number increases, however, the net thrust with the propeller in the forward position increases and above M = .2 it is greater than the net thrust in the basic position. The propeller thrusts on the other hand, recover only slightly in the forward position and only at selected power loadings and tip speeds exceed the propeller thrusts in the basic position. The average effect of this variable is shown in Table XII. There is an unexplainable loss in both net and propeller thrust at .4 Mach number which is not consistent with the average thrust trends established for the other Mach numbers. Excluding the unusual trend, the average net thrust in the forward position increases quite uniformly with Mach number to a 13% increase at M = .5. The propeller thrusts also exhibit a consistent trend, except at M = .4 and show very little position effect except at M = 0.

TABLE XII
AVERAGE EFFECT OF PROPELLER POSITION UPON PERFORMANCE

M	$\frac{T_{NET\ B5-3WT}}{T_{NET\ B1-3WT}}$	$\frac{T_{B5-3WT}}{T_{B1-3WT}}$
O	.970	.970
.1	.989	.999
.2	1.016	1.007
.3	1.053	.999
.4	1.025	.970
.5	1.130	.997

Figures 34 and 43 show the division of thrust (Tnet/T) for these two models at 7000 RPM (915 feet per second tip speed). At M = 0 both models exhibit a maximum division of thrust of about 2.14, which is about 3.5% below the momentum theory value of 2.20. As the Mach number increases, however, the division of thrust for the B5-3WT model increases slightly beyond the values for B1-3WT.

8.3e Inlet Vanes

The effect of inlet vanes on performance is shown in figures 153 through 158 at .05 and .2 Mach number and in figures 68 and 99 at higher Mach numbers. The inlet vanes were designed to represent shroud supports struts and were untwisted and un-

8.3e (Continued)

cambered constant chord airfoils. The angle setting for these inlet vanes could be changed to direct the propeller inflow either with (negative angle) or against (positive angle) the propeller rotational direction. The sense of the inlet and the exit guide vane angles is shown schematically in figure 12. At .05 and .20 Mach numbers -10°, 0° and +10° inlet vane angle settings were tested. These data were closely examined to evaluate the probable higher Mach number effect of the vanes and the vane setting upon performance. This evaluation was performed by considering the data at M = .2 and at 4500 and 5000 RPM as representative of .333 and .30 Mach numbers respectively at 7500 RPM. This investigation showed two important results; first, above M = .20 the net thrust is generally highest with no inlet vanes, and secondly, the least loss in net thrust at Mach numbers above .2 occurs with the inlet vanes set at 0°. Although some small increases in net thrust were exhibited (see Table XIII and figures 153 through 158) at M = .05 and .20, it was concluded that where support type inlet vanes are required they are best set in the neutral position. Therefore, the high speed testing was conducted at only the zero inlet vane angle setting.

With the inlet vanes pitched to direct the flow against the direction of rotation (positive angle) the propeller becomes more heavily loaded. Furthermore, the swirl leaving the propeller is reduced and a higher static pressure rise is produced. This higher static pressure rise is not necessarily manifested as a higher exit static pressure but more generally as a lower propeller inlet static pressure accompanied by more flow through the shroud. With the vanes set at a negative angle the opposite effect occurs. That is, the propeller is unloaded, the leaving swirl is greater and less flow and static pressure rise result for a given propeller blade angle. These observations are generally borne out in the pressure and velocity summary curves in this report.

Figures 153 through 158 depict the effect of inlet vane angle upon propeller and net thrust for a given power loading ($BHP/D^2 X \rho_0/\rho$). Therefore, the power loading effect of the vanes upon the propeller is not shown in these curves since the data have been selected at the appropriate propeller blade angles to equalize the propeller shaft input horsepower. However, for variable pitch propellers, these curves do depict the effect that the vanes would create for given vehicle operating conditions. The differences in performance as shown in these figures represents an interference and redistribution of loading effect upon the propeller and since the aerodynamic force on the vanes is measured with the shroud force, a direct change in shroud thrust. In these curves a very pronounced loss in net thrust occurs with the vanes set at -10° at both .05 and .20 Mach number. However, with the vanes set at 0° and +10° the net thrust is close to and sometimes greater than the net thrust with no vanes at all (B1-3WT). The average effect of the inlet vanes upon both propeller and net thrust is shown in Table XIII. It is noted that the effect of the vanes set at -10° is less detrimental to the propeller thrust than to the net thrust, and with the vanes set at +10°, the propeller thrust is increased more than the net thrust.

8.3e (Continued)

TABLE XIII
AVERAGE EFFECT OF INLET VANE ANGLE UPON PERFORMANCE

	NET THRUST/NET THRUST B1–3WT			THRUST/THRUST B1–3WT		
M	−10°	0°	10°	−10°	0°	10°
.05	.966	1.012	1.007	.978	.993	1.017
.20	.936	.995	1.011	.975	1.003	1.044
.40		.995			.997	
.50		.995			.985	

The average thrust ratios shown in Table XIII, at .4 and .5 Mach number, were derived from figure 68 and 99 generally represent high power coefficients (Cp). In the examination of the low speed test data (M = .2) at low RPM's, the net thrusts at each vane angle setting were seen to diminish quite rapidly above M = .3 at low propeller power loadings. As was found to be true for the shroud force, the drag on the inlet vanes is least detrimental to performance at the higher Mach numbers when the propeller is heavily loaded.

8.3f Exit Vanes

Like the inlet vanes, the exit vanes were designed as shroud support members. The exit vanes, then, are symmetrical, constant chord airfoils with no twist. The sense of the exit vane angle setting is shown schematically in figure 12. At .05 and .20 Mach numbers the exit vanes were set at -5°, 0° and +10°. It was concluded from these data, after conducting an investigation like the one described for the inlet vanes that the optimum exit vane angle is zero degrees for Mach numbers higher than .2.

The performance of the basic model with exit vanes is shown in figures 159 through 164 at .05 and .20 Mach number and in figures 73 and 102 at .4 and .5 Mach number. These figures depict the effect of exit vanes and their orientation upon performance for fixed levels of propeller input shaft horsepower. The net thrust is quite adversely effected by the exit vanes set at -5°. At 0° and 10° both the propeller and the net thrust are affected by the vanes in amounts that are dependent upon the propeller tip speed and power loading. The average effect is shown in Table XIV. The effect of the exit vanes upon the propeller thrust is generally quite small, but average losses in net thrust comparable with those seen with the inlet vanes set at 10° occurred with the exit vanes set at -5°. Although there might be more tendency to recover the propeller swirl energy with the exit vanes set at -5°, the vane angles of attack are quite high with attendent low lift to drag ratios and hence a detriment to the shroud and net

8.3f (Continued)

TABLE XIV
AVERAGE EFFECT OF EXIT VANES UPON PERFORMANCE

	NET THRUST/NET THRUST B1–3WT			THRUST/THRUST B1–3WT		
M	−5°	0°	10°	−5°	0°	10°
.05	.936	.969	1.0	1.0	.985	.991
.2	.969	1.012	.984	1.0	1.005	1.012
.4		1.035			1.003	
.5		1.10			1.008	

thrust results. At .4 and .5 Mach numbers the net thrust increases quite appreciably with the exit vanes set at 0°. This must have been the result of a very favorable orientation of the exit vane lift and drag vectors whereby a vane thrust was generated. The propeller thrusts for these two high Mach numbers still remained quite unaffected by the exit vanes.

8.3g External Shape

The analysis procedure which was employed in the design of the test models indicated that the exterior shape of the shroud surface could have a significant effect upon shroud and propeller performance. This design procedure is presently being evaluated for presentation in Phase III of this contract. Because of the analytical indication of differences in performance attributable to the exterior shroud shape, two external fairings for the 1.1 area ratio shrouds were built and tested. The basic shroud (B1) had a gradual fairing of the outside surface starting from the 25% chordal position. The exterior of the B6 shroud, on the other hand, was built with the camber side of a NACA Series 16 airfoil from the 50% chord position to the shroud trailing edge.

The performance for the B6 shroud with the 3WT propeller (B6-3WT) appears only in the curves depicting the net and propeller thrust ratios plotted against power loading in figures 64, 65, 94 and 95. Unlike the other models, B6 could not be represented by a non-dimensional shape parameter with thrust ratios plotted against that parameter.

These curves show some rather drastic losses in performance with the Series 16 exterior shroud shape above .2 Mach number. The loss in net thrust at the higher Mach numbers is quite sharply accentuated at low power loadings, and tends to recover to values close to the B1-3WT model as the power increases. The propeller thrusts are generally a little lower for B6-3WT but are not particularly dependent upon power load-

8.3g (Continued)

ing. The shape of the camber side of a Series 16 airfoil changes quite rapidly near the trailing edge making flow separation there very likely. As the propeller power loading increases the flow through the shroud increases and this high slipstream energy might be acting as a boundary layer control helping the external shroud flow to stay attached. There was no pressure testing for B6-3WT to substantiate this assumption.

The high performance losses with the B6 shroud at .3, .4 and .5 Mach numbers are not offset by appreciable performance gains at lower Mach numbers. Therefore, a Series 16 external shroud shape seems like a poor propulsive choice in view of these findings. The average effect of this shape variable is shown in Table XV. This tabulation quite clearly shows that the losses outweigh the gains with the B6 shroud.

TABLE XV
AVERAGE EFFECT OF SHROUD EXTERNAL SHAPE UPON PERFORMANCE

M	$\frac{T_{NET\ B6-3WT}}{T_{NET\ B1-3WT}}$	$\frac{T_{B6-3WT}}{T_{B1-3WT}}$
0	.992	.990
.1	1.000	1.00
.2	1.012	.992
.3	.970	.990
.4	.960	.985
.5	.860	.970

8.3h Propeller Planform

The effect of propeller planform on performance was evaluated in the basic shroud (B1) with the 3WT, 3NT and 3R propellers. These propellers and their design criteria are defined in previous sections of this Volume. The propellers were wide tip trapezoidal (3WT), narrow tip trapezoidal (3NT) and rectangular (3R) in planform. Each propeller had three blades and each had the same total activity factor or power absorbing capability. The 3WT propeller was designed to have a high tip thrust and power loading while the 3NT was designed for more loading near the blade roots.

The net thrust and propeller thrust ratios for these models are shown in figures 165 through 176 with the B1-3WT model as the "yardstick". In these figures the thrust ratios are plotted against the propeller tip width to diameter ratio. At 0, .1 and .2 Mach number the net thrust generally increases as the blade tip width decreases. That is, the B1-3NT model exhibits the highest net thrusts for these Mach numbers.

8.3h (Continued)

There is an exception to this observed trend at the lowest power loading for each of the three tip speeds. At higher Mach numbers B1-3R at M = .30 and B1-3WT at M = .40 and .50 generally produce the most net thrust of these three models. The propeller thrust ratios follow a similar pattern except that the performance of B1-3R and B1-3NT is generally equal at the lower Mach numbers. The average effect of propeller planform on net thrust and propeller thrust is shown in Table XVI.

TABLE XVI
AVERAGE EFFECT OF PROPELLER PLANFORM UPON PERFORMANCE

M	$\frac{T_{NET\ B1-3NT}}{T_{NET\ B1-3WT}}$	$\frac{T_{NET\ B1-3R}}{T_{NET\ B1-3WT}}$	$\frac{T_{B1-3NT}}{T_{B1-3WT}}$	$\frac{T_{B1-3R}}{T_{B1-3WT}}$
0	1.007	1.020	1.017	1.022
.1	1.007	1.005	1.020	.993
.2	1.013	1.008	1.010	.998
.3	.987	1.017	.99	1.000

The loading distributions for these three propellers can be seen in the total pressure distributions at .05 and .30 Mach numbers in figures 269 and 270. The loading ($H-H_\infty$) is shifted from the tip for B1-3WT towards the root for B1-3NT. Many shrouded propeller design methods employ free vortex axial and tangential velocity distributions. For these designs the axial velocities and total pressures are radially uniform, and the propeller planform, to accomplish the free vortex requirements, is usually similar to 3NT. None of these propellers represent a free vortex design, but the velocity distributions (figures 301 and 302) and total pressure distributions (figures 269 and 270) for 3NT do come the closest to the free vortex requirements. The 3NT planform, however showed only mild superiority at low Mach numbers and was generally inferior above .2 Mach number with an average net thrust loss of over 5% at M = .50.

8.3i Number of Blades

The effect of number of propeller blades upon performance was experimentally evaluated with the basic B1 shroud and the three and four way narrow tip propellers. These propellers were designated 3NT and 4NT and the complete models as B1-3NT and B1-4NT respectively. Both of these propellers had the same total activity factor, and the same product of number of blades and blade width at every radius. Furthermore, the thickness to chord ratios and camber and twist distributions for these propellers were identical. Therefore, any performance differences for these two models is attributed to the number of blades.

8.3i (Continued)

The performance comparison for these two models is shown in figures 177 through 188. Like some of the other shape parameter comparisons, these figures are two point plots where extrapolations in either direction could be erroneous. The "yardstick" in these figures is the B1-3NT model and the thrust ratios are thrusts for B1-4NT divided by the thrusts for B1-3NT.

The average effect of the number of blades upon net thrust and propeller thrust is shown in Table XVII. Both the figures and the tabulation of average performance

TABLE XVII
AVERAGE EFFECT OF NUMBER OF PROPELLER BLADES UPON PERFORMANCE

M	$\frac{T_{NET\ B1-4NT}}{T_{NET\ B1-3NT}}$	$\frac{T_{B1-4NT}}{T_{B1-3NT}}$
0	.978	.980
.1	.990	.982
.2	.998	.996
.3	1.046	1.020
.4	1.037	1.012
.5	1.062	1.033

disprove that the performance of a shrouded propeller is unaffected by number of blades for the same propeller solidity (same total activity factor). At Mach numbers up to 0.2 the effect of the number of blades is much the same on the net thrust and on the propeller thrust. This implies that the shroud thrust is nearly unaffected by the number of propeller blades at these Mach numbers. Above M = .2, however the net thrust superiority exceeds the propeller thrust superiority with the 4NT propeller and the associated shroud thrusts are higher for B1-4NT. This conclusion is impossible to substantiate with momentum concepts but will be thoroughly evaluated in Phase III. Possibly, the propeller induction is steadier with four bladed propeller, thereby producing more favorable shroud loadings at the higher Mach numbers.

Figures 177 through 188 generally show that up to M = .2, B1-3NT produces the most net thrust and its superiority is accentuated at the higher power loadings for each tip speed. The propeller thrust ratios follow a similar but less obvious power loading dependency. Above M = .2 however, neither the net nor the propeller thrusts follow a particular power loading dependency pattern.

The figures depicting the velocities and pressures for these models are rather inconclusive in their support of the performance trends. However, the tabulated velocity and pressure data in Volumes II and III generally substantiates the performance trends for equal power loadings.

8.3j Tip Clearance

The effect of propeller tip clearance on performance was investigated with the basic shroud (B1) and the three way rectangular planform propeller (3R). This propeller was fitted with fiberglass tips which were machined off in two increments to form the 3R1/2M and 3RM propeller models. The nominal radial tip clearances were .038, .078 and .168 inch for the 3R, 3R 1/2M and 3RM propellers respectively.

Figures 189 through 200 depict the effect of this variable upon propeller and net thrust. The "yardstick" for these comparisons is the B1-3R model and is noted in these figures. To get a quick estimate of the effect of tip clearance, the average values as depicted in figures 189 through 200 are shown in Table XVIII.

TABLE XVIII
AVERAGE EFFECT OF TIP CLEARANCE UPON PERFORMANCE

	PROPELLER THRUST		NET THRUST	
M	B1—3R M	B1—3RM	B1—3R M	B1—3RM
0	.985	.955	.980	.975
.1	.985	.965	.990	.990
.2	.995	.980	.995	.990
.3	.970	1.020	.985	.995
.4	.960	.970	.965	.985
.5	.990	1.040	1.00	1.00

Tip speed and power loading both have significant effects upon the thrust ratios. These detailed effects are shown in the figures but are difficult to catagorize. Generally the figures show that the net thrust diminishes as the tip clearance increases for Mach numbers up to .2. At Mach numbers above .2, however, there is a tendency for the net thrust to be minimum at the middle tip clearance (B1-3R 1/2M). In fact, much of the data above .2 Mach number indicates that the net thrust is highest with the maximum tip clearance. The reason for the apparent superiority of the larger tip clearances at .3 and .5 Mach numbers is not really understood, although it is probably due to a favorable interaction by which the blade tips energize the shroud boundary layer. This observed phenomenon will require careful attention in the Phase III investigations before the design theory is finalized.

The propeller loading differences for these three tip clearances can be seen in the total pressure plots in figures 271 and 272. These figures show that the total pressure increases above the atmospheric total pressure are sustained to a larger radius as the clearance diminishes. The velocity, shroud surface pressure distributions and shroud exit static pressure distributions figures at the end of this report are enlightening but the selected data does not offer any particular support of the observed performance trends.

8.3j (Continued)

This tip clearance investigation has shown the effect of clearance to propeller diameter on performance by reducing the diameter of a given propeller in the B1 shroud. It is possible that the tip clearance to propeller tip chord would also exhibit an effect upon the propeller and shroud thrusts. This would be difficult to evaluate without introducing a second shape variable change. That is, the blade tip chord could be changed for a given clearance, but this would introduce the effect of planform, number of blades or propeller total activity factor. If the clearance to propeller tip chord does produce a tip clearance effect on performance, it would have been shown as part of the effect which was, in this report, attributed to propeller planform and number of blades.

8.3k Basic Propeller Without a Shroud

A very limited amount of testing was conducted with the basic propeller (3WT) without a shroud. Although this was not part of the program plan, it provided some very interesting results which are shown in figures 201 through 203. These curves show ratios of unshrouded propeller thrust to net thrust and to propeller thrust (propeller in a shroud) at .05, .10 and .20 Mach numbers. At each point on these curves the tip speeds and power loadings of both the shrouded and the unshrouded propellers were the same. The blade angles shown are for the unshrouded propeller, while those for the shrouded propeller varied slightly to obtain fixed tip speeds and power loadings.

Referring again to simple momentum theory, the ratio Tuns/Tnet at M = 0 should be .769 and should increase as the Mach number increases. Similarly, the ratio of Tuns/T at M = 0 should be 1.69 and should decrease as the Mach number increases. These ratios are rarely achieved since the shrouded propeller tends to operate nearer to its momentum representation than does the unshrouded propeller. In fact figure 203 shows that even at M = .1 the ratio Tuns/Tnet is less than the static momentum expectation of .769. Furthermore, figures 201 through 203 show that the thrust of the propeller alone in the shroud is as great as the thrust for the unshrouded propeller (3WT) at M = .05 and .10, and only diminishes to about 95% of the B1-3WT thrust at M = .20.

8.4 PRESSURES AND VELOCITIES

A considerable number of flow and shroud surface pressure measurements were made in this experimental program. These data are completely tabulated in Volumes III and IV of this report. Figures 204 through 302 are selections from these data where the effect of test conditions and model shape parameters upon the flow and pressure distributions are shown. These data have been useful in developing an understanding of the performance trends and will be used in developing the theoretical method in Phase III of this contract.

The instrumentation and the test methods have been described in the Test Methods Section of this report as well as in Volume II. As was stated there, the flow and pressure measurements required (1) additional testing so as not to interfere with the shroud force measurements. Because a great amount of time was required for this additional testing, the models and test conditions were carefully selected for this aspect of the program. These test runs are referred to as "pressure runs" and the data obtained as "pressure data." The model configurations which were pressure tested are defined in the Wind Tunnel Run Log in Volume II.

These figures show the effect of RPM, blade angle and Mach number upon the velocity and shroud surface pressure distributions for the basic model (B1-3WT). The effect of many of the shroud and propeller shape parameters upon these distributions is shown for selected test conditions. The data were used to define propeller thrust and power loadings, shroud friction drag, net thrust and slipstream contraction. Several examples of this special usage of the pressure data is described later in this section and in the Appendices.

8.4a Shroud Surface Pressure Distributions - C_{P_L}

The shroud surface pressure distributions C_{P_L} are shown in figures 204 through 231. These curves depict the C_{P_L} distributions at M = .05 and .3. At M = .05 only the internal shroud surface pressures are shown, but are extended to the stagnation point on the outside surface. At M = .05 the external surface pressure coefficients are vary small in absolute magnitude relative to the internal C_{P_L} values. The test points shown on these figures represent the average of the values measured at two azimuthal locations. These two readings were generally in good agreement but exhibited differences which did influence the shroud integrated axial pressure force. These differences are discussed to some further length in Appendix 12.3. In closely examing some of the curves in figures 204 through 231 several irregularities were spotted. For example, in figure 207 a C_{P_L} inflection is shown at X = .2 for the B4-3WT model, and in figures 226 and 227 there appears to be a pressure fluctuation between X = .2 and X = .25 for

(1) Shroud exit rake total pressure and propeller inlet rake velocities data were taken for all runs. The inlet rake velocities taken during the performance testing are subject to some inaccuracy. This inaccuracy is described in the Accuracy of Data Section.

(Continued)

for the basic model with inlet vanes. These fluctuations were found to be the result of averaging the two azimuthal C_{P_L} measurements. That is, for one static pressure tap row the C_{P_L}'s do not exhibit these fluctuations but do for the other. Although both values were generally examined before the average was taken, several irregularities did find their way into the curves. In the cases which are cited here, however, it is not known that either azimuthal distribution is incorrect. If both are correct, then surface irregularities or flow asymmetry must have caused these surface pressure differences. The overall comparisons for which these curves were intended, however, are still generally valid. For detailed information derived from these distributions, special attention should be placed upon each test point as it was in the determinationof the shroud friction drag in Appendix 12.3. If recourse is made to the tabulated date in Volumes III and IV, two details that affect the correlation between the plotted and tabulated values of C_{P_L} found there should be noted. First, the tabulated values for runs 654 through 704 are in error by a constant C_{P_L} value of .06. That is, .06 must be added to each tabulated C_{P_L}. Secondly, in the comparisons for all other pressure runs, the date were corrected to the nearest nominal Mach number before plotting. That is, if a pressure run Mach number was 0.055 for one model and 0.05 for another, the C_{P_L} values at .055 were corrected by a constant multiplier equal to the ratio of the squares of the test to nominal Mach numbers.

These figures depict the shroud surface pressure coefficient, $C_{P_L} = P_L - P \;/q$, plotted against nondimensional shroud axial location ($X = \frac{\text{axial length}}{\text{shroud chord length}}$). The values of X which are of special geometric or physical significance are (1) X = .1875 denotes the end of the shroud lip contour both internally and externally except for the short chord shroud (B7) for which this X = .25; (2) X = .40 denotes the propeller axial position for the pressure runs, and the propeller disc extends from about X = .35 - .45; and (3) X = .50 denotes the diffuser entry axial location. Almost without exception C_{P_L} exhibits noticeable changes at these locations. Tracing a distribution from the leading to trailing edge along the inside surface the following trends are observed; (1) the surface pressure declines steeply from the leading edge to a minimum value near X = .05; (2) the pressure then increases until the end of the lip is reached (X = .1875); (3) the slope of the pressure increase diminishes slightly from X = .1875 to about X = .35 for which length the inside shroud surface is parallel to the flow axis; (4) the pressure rises sharply from X = .35 to X = .45 at M = .05 depicting the pressure rise of the propeller; (5) the pressure rise slope then tapers off and is continuous and smooth to the shroud trailing edge.

The shroud surface pressure coefficient curves show increased suction pressures on the inside lip surface as the propeller loading is increased through higher blade angles and higher RPM's. At M = .3 the suction pressure on the outside lip surface diminishes as the loading is increased (figures 213 and 214). A very good measure of the relative propeller thrust loading can be seen by the magnitude of the pressure jump across the propeller. In fact, a check of the propeller thrust magnitude from this pressure jump

8.4a (Continued)

agreed well with the measured propeller thrust for run #138 (figure 222). The measured thrust for run #138 was 290 pounds and the thrust deduced from the pressure measurements was 300 pounds.

All the pressure coefficients at M = .05 quite clearly show the trailing edge static pressure to be very close to the atmospheric static pressure. That is, C_{P_L} is very close to 0 at the trailing edge of the shrouds. The assumption that $P_L = P_\infty$ is very common in many of the simpler performance theories and in fact was the foundation assumption for Hamilton Standard's generalized performance handbook PDB 6220 (reference). Whereas this assumption seems to be quite well borne out at low Mach numbers its validity is not as good as the Mach number increases. The C_{P_L} plots indicate an average trailing edge value of about .25 for Mach numbers between .3 and .6. Although reading a C_{P_L} = .25 is beyond the curve accuracy at M = .05, the traverse probe static pressures, to be discussed later in this section, bear out that P_L is close to P_∞ at low Mach numbers.

Of the shape parameters investigated, area ratio exhibited the greatest effect upon the distribution and upon the magnitude of C_{P_L}. At both .05 and .3 Mach number the lip suction pressure is greater for the B4-3WT (1.3 area ratio) model and as should be expected more diffusion is accomplished in the 1.3 area ratio diffuser.

The effect of propeller planform upon C_{P_L} indicates the most inside surface lip suction for the rectangular planform propeller (3R) at M = .05 and for the wide tip trapezoidal planform propeller (3WT) at M = .3. At M = .05 there is considerably more diffuser pressure recovery with the narrow tip propeller (3NT).

The shroud length effect is somewhat obscured in the plots because of the shift in the pertinent X locations. However, at M = .05 the shorter chord shroud produces more inside surface lip suction than the basic shroud and has a higher rate of diffuser pressure recovery.

The other model shape parameters generally exhibit rather minor effects upon C_{P_L}. The distributions on the external shroud surface are shown for the higher Mach numbers and generally exhibit less dependence upon model shape and test conditions.

8.4b Shroud Exit Plane Total Pressures

Figures 250 through 271 show comparisons of shroud exit plane total pressure distributions for each model at two Mach numbers. Further comparisons are presented for the basic model to show the effect of blade angle and RPM. These curves depict the difference between exit total and free stream total pressures ($H-H_\infty$) in pounds per square inch plotted against the fractional distance from the rotational center line to the shroud trailing edge. These total pressure differences are a good measure of the propeller loading, as is discussed in Appendix 12.4. The total pressures were measured

(Continued)

on a fixed shrouded Kiel probe rake with twenty five pressure taps. Each of these points was used in drawing the curves but only every other one was symbolized. Except near the centerbody surface these measurements usually agreed very well with those taken during the pressure runs with the traverse probe. Due to the skewed flow near the centerbody the traverse probe is probably the better of the two measurements. However, so that the effect of every model could be shown, the exit rake pressures were chosen for these curves. The test run number is shown for each curve so that force measurements can be correlated with the pressure distributions.

Basic Model

Figure 252 shows the effect of propeller blade angle (Θ) upon total pressure for M = .05 and N = 7500 for B1-3WT. For a fixed RPM and Mach number the power loading increases as the blade angle increases, and therefore this curve shows the effect of power loading (Θ) upon $H-H_\infty$. At $\Theta = 15^\circ$ the loading ($H-H_\infty$) falls off beyond Xe = .70 while at 25° it increases smoothly to about Xe = .9 and then falls off quite sharply thereafter. The tip fall-off is characteristic of both the propeller loading and the diffuser pressure loss. At $\Theta = 30^\circ$ there is a very prominent hump in the distribution starting at X = .70. The humped distribution was observed frequently at the low Mach numbers beginning at about 7000 RPM for the higher blade angles. For these conditions where the humped distributions were observed, the propeller thrust and power coefficients changed noticeably from the expected trends and from the trends established at lower RPM's and blade angles. The effect upn C_p and Ct can be seen in the plots of these coefficients in Volume II. An interaction of airfoil compressibility and stall are believed to be responsible for the peculiar $H-H_\infty$ loading distributions. A very similar effect is shown in figure 250 for a fixed blade angle (30°) and Mach number (.05) while the RPM was varied. The humped distribution at N = 7500 is the same as in figure 252. This curve shows that the hump is not present as 5500 RPM and is barely noticeable at 6500 RPM.

Figures 251 and 253 are analogous to the two figures just discussed for M = .30. Here the RPM's are lower as they would likely be in a loiter or modurate speed cruise condition. The effect of power loading (Θ and RPM) is again shown in the magnitude of $H-H_\infty$, but the humped distribution is no longer present. For these curves, and for most of the remaining total pressure distributions at M = .3 or greater, the root values of $H-H_\infty$ are less than zero. This was not generally true with the traverse probe total pressures which are believed to be more accurate for skewed flow.

The effect of the model shape of the total pressure distribution is the most pertinent characteristic to observe in these curves. Where small differences exist in the magnitudes of $H-H_\infty$ it must be realized that they could be due to slight differences in power absorbed or thrust produced. That is, for a fixed Θ, N and M, power and thrust are not necessarily and in fact are not usually the same for different models.

8.4b (Continued)

Area Ratio

In almost every respect area ratio has the greatest effect of any of the shape variables. Figures 256 and 257 show the effect of area ratio on H-H∞ at M = 0.05, θ = 30°, N = 7500 and at M = 0.3, θ = 38°, N = 5500 respectively. Both figures show that the greatest magnitude of H-H∞ occurs for the lowest area ratio and decreases as the area ratio increases. Figure 256 shows that the humped distribution at Θ = 30° only existed for the 1.1 area ratio shroud model. For this model (B1-3WT) the axial velocities are considerably lower than for the 1.2 and 1.3 area ratio models. The lower velocity would tend to produce blade stall but would also tend to reduce blade relative velocities and ease the compressibility effect if stall were not present. Whereas both stall and compressibility are believed to be responsible for the H-H∞ humps, in this case the stall tendency seems to predominate.

The start of the total pressure decay begins at about the same value of Xe for each area ratio (.90 to .95 depending upon Mach number). This is a good indication that the flow was as well attached for the 1.3 area ratio as for the 1.2 and the 1.1 area ratio shrouds.

Shroud Lip Shape

The effect of the shroud lip shape on the total pressure distribution is shown in figure 254 at M = .05 and figure 255 at M = .30. At M = .05 the basic shroud total pressures are consistently 5 to 10% higher than for B2-3WT. The reason for this difference is not obvious since the propeller thrusts and powers were nearly identical. Figure 255 at M = .3 shows very similar pressure magnitudes with two H-H∞ cross overs at Xe = . .4 and .725. No particular significance, however, is attributed to these two crossovers.

Shroud Length

Figures 260 and 261 indicate that at both .05 and .3 Mach number the shorter chord shroud model (B7-3WT) produced lower magnitudes of total pressure than the basic model from Xe = .6 to Xe = 1.0. The propeller in the shorter chord shroud produced about 2.5% less thrust at M = .05 and 5% less at M = .3, and most of these differences can be seen in the higher tip values of H-H∞ . The comparisons between those two models is likely to be more affected by the propeller test rig blockage than the comparisons for most other models. The proximity of the shroud trailing edge to the test rig is different for these two models, with B1-3WT being three inches closer. It is not believed, however, that the effect of the test rig blockage would be manifested as a change in total pressure at the outer radii. If the blockage was of a significant magnitude it would change the propeller loading and the total pressures at the root sections.

8.4b (Continued)

Shroud External Profile Shape

There is no discernible difference in the total pressure distributions for the B1-3WT and B6-3WT models at either .02 (figure 258) or .3 (figure 259) Mach number. Since H-H∞ is primarily affected by the propeller loading and shroud internal shape, the similarity in these distributions was expected.

Propeller Position

The effect of propeller position within the shroud is shown in figures 262 and 263 to have only a small effect upon H-H∞ . At both .02 and .30 Mach number there is a crossover in the distributions. These are the only other two models (B1-3WT and B5-3WT) which were expected to be affected differently by the propeller test rig blockage. The B5-3WT shroud trailing edge is three inches closer to the test rig than B1-3WT. However, there is no evidence that the test rig affected the total pressure distribution.

Propeller Tip Clearance

The effect of propeller tip clearance on the H-H∞ is shown in figure 271 at M = .10 and figure 272 at M = .30. In both figures the highest total pressures occur for the minimum tip clearance and diminish as the tip clearance increases. It is worth noting again, however, that these figures represent total pressure distributions for a constant propeller blade angle for which thrust and power are generally different. Presumably if thrust or power were held constant these comparisons would be somewhat different. In both figures the drop off in total pressure near Xe = 1.0 is accentuated as the propeller tip clearance is increased.

Propeller Planform

The propeller planform shape directly affects the propeller loading distribution, and therefore this variable produced a very marked effect upon H-H∞ , as shown in figures 269 and 270. Although it is theoretically possible to design the three planforms to produce the same loading for a chosen condition, this was not done for these models. The wide tip planform propeller (3WT) was designed to have a high tip loading. The rectangular planform (3R) and the narrow tip planform (3NT) propellers were designed with sucessively lower tip loadings. The differences between the Xe = .9 and Xe = .5 values of H-H∞ presented in Table XIX show the effect of planform upon propeller loading.

8.4b (Continued)

TABLE XIX

MODEL	PLANFORM	(He--H∞) M = .05	(He - H∞) M = .30
B1-3WT	WIDE TIP	.44	.135
B1-3R	RECTANGULAR	.32	.060
B1-3NT	NARROW TIP	.04	--.020
B1-4NT	NARROW TIP	.06	--.020

The four way narrow tip propeller (4NT) is also shown on these curves. This propeller has the same planform shape as 3NT but the chord widths are reduced by twenty-five percent.

Number of Propeller Blades

Figures 264 and 265 both show that the total pressures for the 4NT propeller are higher than for the 3NT propeller, although the shapes are quite similar. The exit rake total pressures are time averaged values and as such the measured pressures would not be a reflection of the instantaneous or local pressure differences attributed to the number of blades. The large difference shown at M = .30 is attributed to a nearly 30% increase in propeller thrust and power. The large thrust difference is believed to be due to a blade angle setting error. For the same thrust or power the two distributions would be very nearly the same.

Exit and Inlet Vanes

The effect of exit vanes is shown in figure 268. The definition of the sense of the vane angles is shown in figure 12. The exit vanes were representative of shroud support members and as such were untwisted and uncambered with constant chord airfoils. The shape of the distributions are nearly the same for the basic model and for the basic model with the exit vanes set at 10°, 0° and -5°. There is an apparent increase in H-H∞ for 0° and -5° settings which is not seen in the performance comparisons.

The effect of inlet vanes at M = .05 is shown in figures 267. The total pressures are highest for a positive 10° vane angle setting and diminish as the angle reduces to 0° and -10°. This trend is in agreement with the performance trend which shows that both thrust and power increases as the inlet vane angle becomes more positive. This trend is to be expected since the propeller experiences higher angles of attach as the inlet vanes are set positively and hence produces more thrust, power and total pressure rise.

8.4b (Continued)

In figure 266 the effect of both inlet and exit vanes is shown at M = .30 with the vanes set in a neutral position. Although there are some differences in these $H-H_\infty$ distributions, there is no apparent correlation between these differences and the measured performance.

8.4c Shroud Exit Plane Static Pressures

The shroud exit plane static pressure distributions are shown for the "pressure runs" in figures 273 through 285. The static pressures were measured on the three dimensional traverse probe. The form of presentation is exactly like that used in the shroud exit plane total pressure distributions where the effects of test conditions and model parameters are shown.

A common assumption in many shrouded propeller theories is that the shroud exit static pressure is uniform and equal to the atmospheric pressure. This is a very convenient assumption in simple momentum theory since it defines the propeller wake as the shroud exit and allows a ready solution to the momentum equations. The theory currently being developed in Phase III generally predicts a static pressure in excess of P_∞ at the shroud T.E. This theory, then, implies that there is slipstream contraction. The curves in figures 273 through 285 directly show the relationship of the exit static pressure to the free stream value in plots of P_s-P_∞ vs Xe, and like the theory, generally indicate a static pressure in excess of P_∞.

Expressed nondimensionally as $(P_x-P_\infty)/q_\infty$ the static pressure differences (based upon the average exit static pressure) are quite similar at all Mach numbers. The values of this coefficient generally fall between .20 and 1.0 except for the 1.3 area ratio model (B4-3WT). For this model the exit pressure coefficient is negative at M = .05 and about one half the magnitude of the pressure coefficient for B1-3WT at M = .4 and .5. When P_s-P_∞ is positive the propeller slipstream has overexpanded and must subsequently contract in the ultimate wake where the static pressure again becomes atmospheric. For the 1.3 area ratio shroud model the negative values of P_s-P_∞ at M = .05 indicate that the slipstream will continue to expand beyond the shroud trailing edge; and the lower positive pressures at M = .4 and .5 indicate that the slipstream will contract less than for the 1.1 area ratio shroud model.

8.4d Axial Velocity Distributions

Radial distributions of axial velocity were measured at two shroud locations. (1) A fixed pitot static rake was placed 4.28 inches upstream of the propeller centerline to measure axial velocity distributions there. The ten static taps on this rake were oriented radially so that they were in the centers of equal annular areas. The arithmetic average of these ten velocities represents the volume flow average velocity (1). The dimensional details of this velocity rake are shown in figure II-2 of Volume II. (2) A traversing probe was placed at the shroud trailing edge plane to measure flow direction and magnitude. This probe is shown schematically in figure II-4 in Volume II. The traverse probe measurements of axial velocity were not taken at centers of equal annular areas. The inlet axial velocities are shown in figures 232 through 249 and the exit axial velocities in figures 236 through 302. The inlet velocities generally show a considerable amount of data scatter, especially at the lower Mach numbers. For these distributions (figures 232 through 249) only the "pressure run" data was used so that the inlet rake time lag could be avoided.

The effect of blade angle and rotational speed (RPM) has a large effect upon the magnitude of both velocities as is shown for the basic model. Figures 236 and 289 show the effect of flight Mach number upon the inlet and exit axial velocity distributions. These show that in general the exit velocities are less than the free stream velocities

---

(1) The velocities were evaluated using compressible fluid dynamics and represent the weight flow average velocity for density assumed to be constant with radius.

viz. $w = \sum_{n=1} \rho_n A_n V_n$

$$V \text{ average} = \frac{W}{\overline{n=1}\ \rho_n A_n} = \overline{V}_2$$

and $\overline{V}_2 = \sum_{n=1} \rho_n A_n V_n / \sum_{n=1} \rho_n A_n$

since $A_1 = A_2 = \ldots\ldots\ldots A_{10}$

and if $\rho_1 = \rho_2 \ldots\ldots\ldots 10$

then $\overline{V}_2 = \frac{1}{10} \sum_{n=1} V_n$

8.4d (Continued)

and that the two measured velocities are not in proportion to the shroud exit area ratio. The first of these observations implies that there must be a slipstream contraction for the net thrust to be greater than zero.(1) The second observation merely indicates that the flow cannot be treated as incompressible if good correlations are expected.(2) Treated compressibly, however, the mass flow checks are quite good.

"Pressure run" configuration velocity distribution comparisons are shown for selected Mach numbers and RPM's. The exit velocity distributions are quite similar in shape to the total pressure distributions due to the near uniformity of the static pressure distributions. The distributions of velocity at the inlet and exit are quite different in many cases indicating that there was a significant radial shift in flow streamlines.

---

(1) Since Tnet = ρ_e AeVe (Vjet-V∞), Vjet must be greater than V∞ for Tnet > 0 and therefore Vjet > Vexit and the slipstream contracts.

(2) Sample relationships between Vexit and Vinlet for compressible flow -

$\bar{V}e$ fps	Mexit $\bar{M}e$	Avg V2 for A4/A2=1.1 $\bar{V}_2$ for $A_4/_2$=1.1	Avg. V2 for A4/A2=1.3 $\bar{V}2$ for A4/A2=1.3	$\bar{V}2/\bar{V}e$ for A4/A2=1.1	$\bar{V}2/\bar{V}e$ for A4/A1 = 1.3
200	.179	220	262	1.10	1.31
400	.357	449	554	1.122	1.383
600	.536	700	choked	1.167	-
700	.625	962	choked	1.373	-

IX

LIST OF SYMBOLS, SUBSCRIPTS AND DEFINITIONS

List of Symbols

A_1	Shroud inlet open area, sq. ft.
A_2	Shroud open area directly ahead of propeller, sq. ft.
A_3	Shroud open area directly behind propeller, sq. ft.
A_4	Shroud open area at shroud exit, sq. ft.
b	Blade width, inches
BHP	Propeller Shaft Horsepower
C	Shroud Chord length, ft.
C_{L_D}	Propeller Blade Section Camber
C_p	Power coefficient, $P/\rho n^3 D^5$
C_t	Thrust Coefficient, $T/\rho n^2 D^4$
C_p	Shroud surface pressure coefficient, $\frac{P_\ell - P}{1/2\, \rho V_\infty^2}$
D	Internal diameter of shroud at propeller plane, ft.
D_p	Diameter of propeller, ft.
F_d	Shroud friction drag, lbs.
H	Total Pressure
h	Blade section thickness, inches
M	Mach number
N	Propeller rotational speed, rpm
n	Propeller rotational speed, rps
P	Static pressure, psi
R	Radius, ft.
r	Radius to propeller or shroud station, ft.

IX

(Continued)

T	Thrust, lbs.
V	Velocity, fps
X	Non-dimensional distance; for radial distance r/R; for shroud, percent chord from leading edge
Θ	Blade section twist, degrees
Γ	Circulation
μ	Viscosity
ρ_o	Air density, sea level standard day, slugs/ft^3
ρ	Air density, slugs/ft^3
$\frac{dC_p}{dx}$	Elemental Power Coefficient
$\frac{dC_t}{dx}$	Elemental thrust coefficient
$\frac{dy}{dx}$	Slope of shroud camber line

(Continued)

Subscripts

a	axial
e	shroud exit
exit	shroud exit
i	inside shroud surface
O	outside shroud surface
ℓ	local shroud surface
NET	Combined propeller and shroud thrust
s	shroud
UNS	Unshrouded propeller
ZETA	Flow pitch angle
1	Plane at shroud leading edge
2	Plane of shroud directly in front of propeller
3	Plane of shroud directly behind propeller
4	Plane at shroud exit
∞	Free stream conditions

(Continued)

Definitions

Area Ratio	-	The ratio of the open area at the shroud exit to the open area at the propeller plane.
Propeller Position	-	Defined as the distance of the propeller plane of rotation from the leading edge of the shroud divide by the shroud chord.
Shroud/Chord Diameter Ratio	-	The overall length of the shroud divided by the internal diameter at the propeller plane.
Tip Clearance	-	The ratio of the nominal clearance between the tip of the blade and the inner surface of the shroud divided by the shroud internal diameter at the propeller plane.

REFERENCES

1. Minassian, B. "Analytical Study of Shrouded Propellers"., Longren Report LR-501, May, 1956.

2. Ordway, D. E., Sluyter, M. M., and Sonnerup, B.O.U., "Three-Dimensional Theory of Ducted Propellers", Therm Research Report TAR-TR602, August, 1960.

3. Smith, A.M.O and Pierce, J. "Exact Solution of the Neumann Problem. Calculation of Non-Circulatory Plane and Axially Symmetric Flows About or Within Arbitrary Boundaries." Douglas Aircraft Report No. ES 26988, April, 1958.

4. Cahn, M. S. and Tee, J. T., "Preliminary Results of An Analytical Study of Shrouded Propeller Inlet Design Requirements." Douglas Aircraft Company Report ES 29735, July, 1960.

5. Horner, S.F., "Fluid-Dynamic Drag", 1958.

6. Anon, "Generalized Method of Shrouded Propeller Performance Estimation". Hamilton Standard Report PDB 6220.

7. Shapiro, A. H., "The Dynamics and Thermodynamics of Compressible Fluid Flow". The Ronald Press Co., 1953.

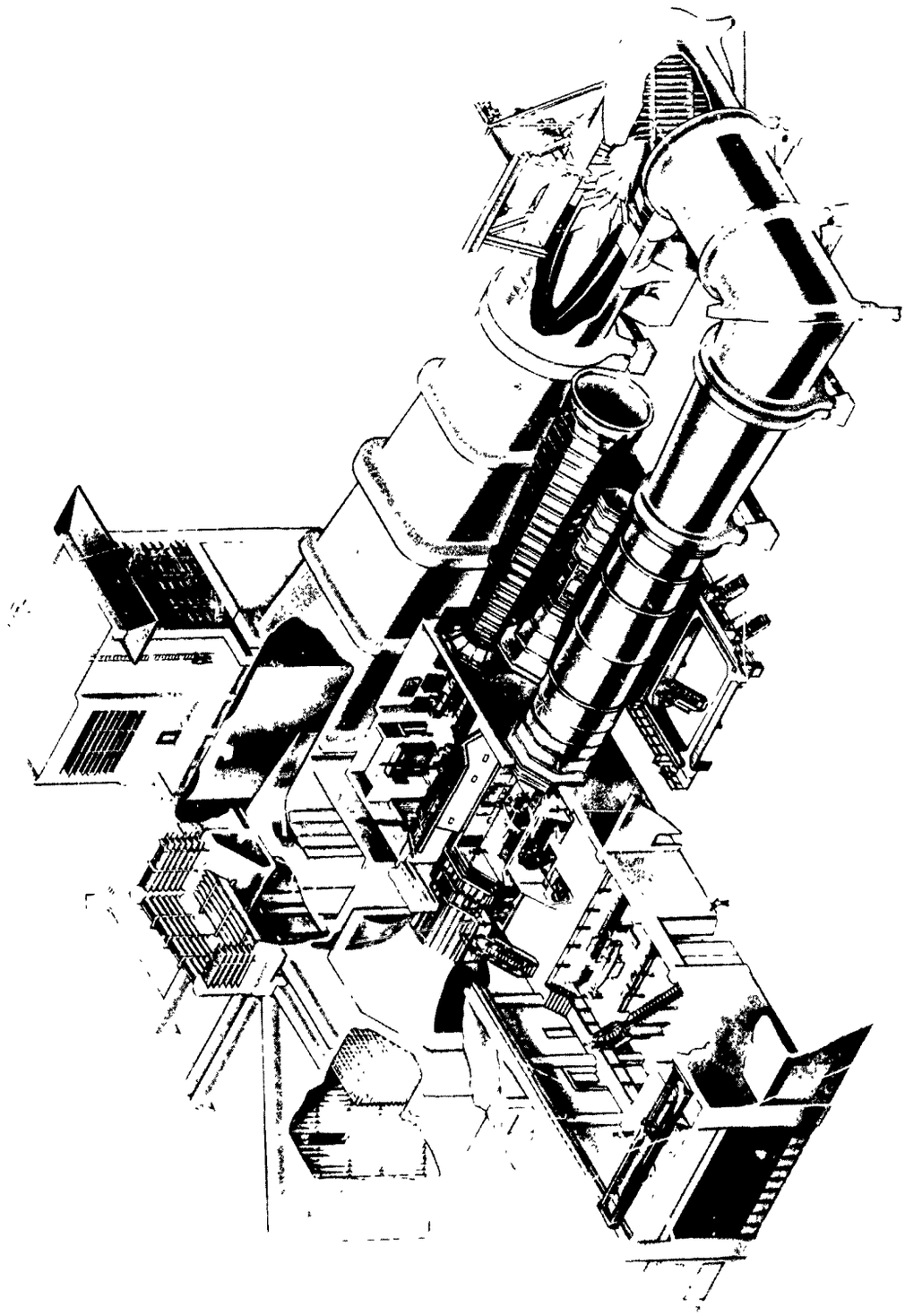

HS SHROUDED PROPELLER TEST
UAC LARGE SUBSONIC WIND TUNNEL

FIGURE 1

HS SHROUDED PROPELLER TEST

COMPLETE MODEL WITH SPINNER AND INLET VANES INSTALLED

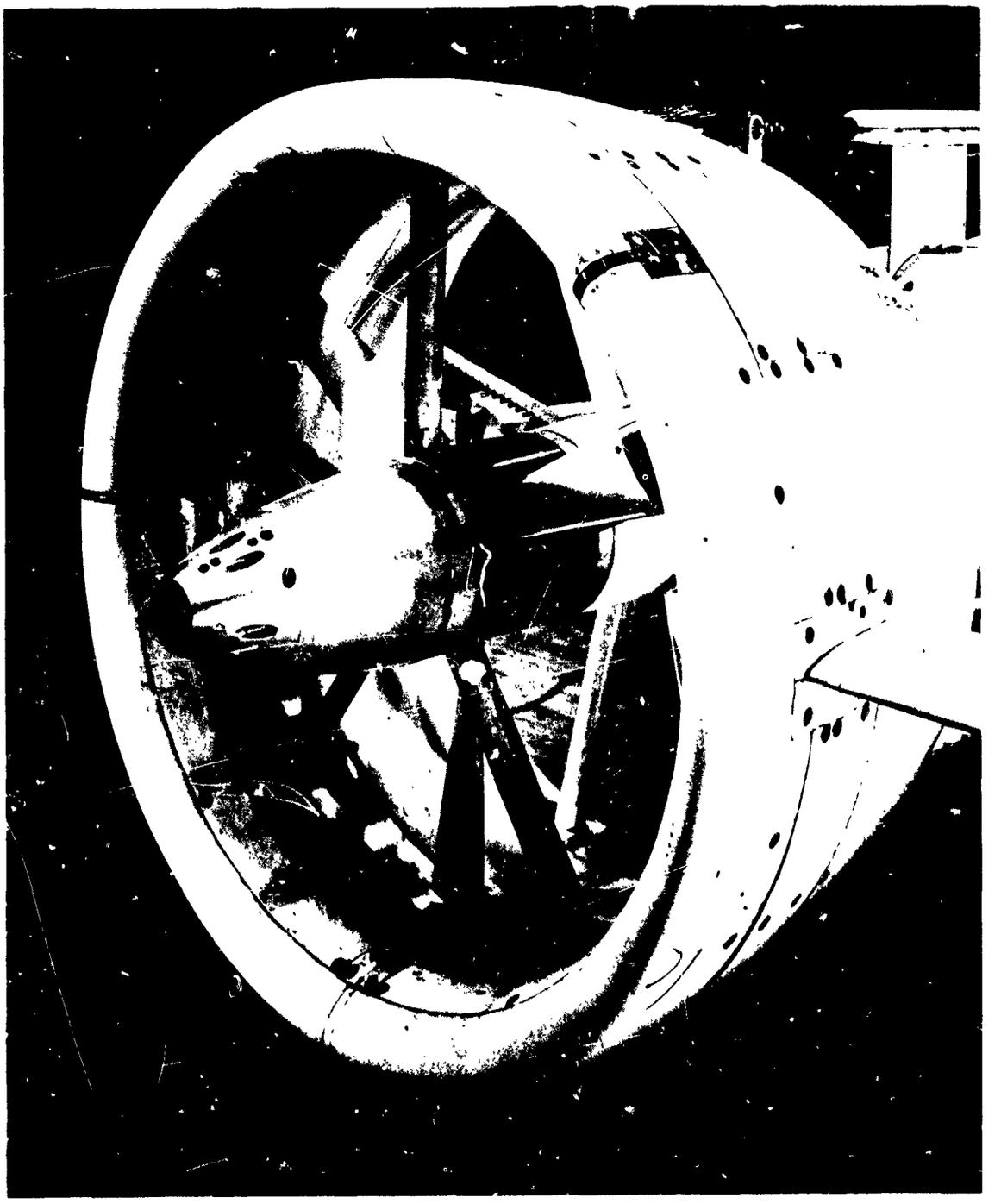

FIGURE 2

HS SHROUDED PROPELLER TEST

SCHEMATIC REPRESENTATION OF SHROUDS AND PROPELLER TEST RIG

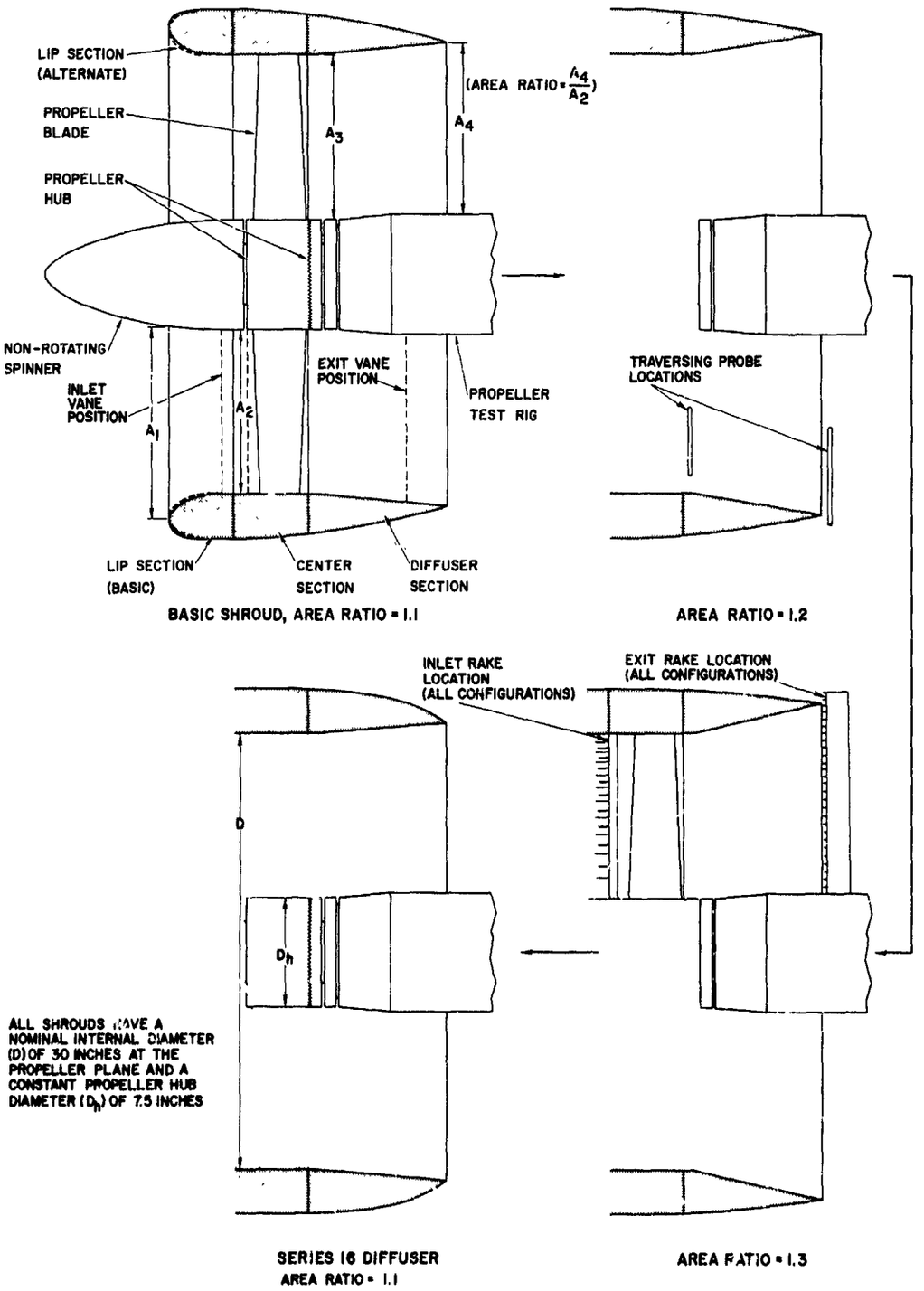

FIGURE 3

HS SHROUDED PROPELLER TEST

SHROUD SHAPES

EXTERIOR SHAPE	NOTATION
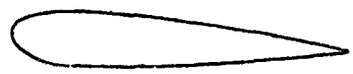	B1
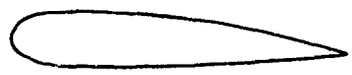	B2
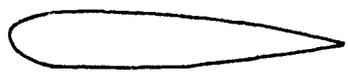	B3
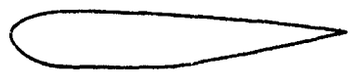	B4
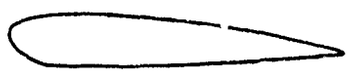	B5
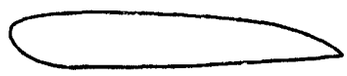	B6
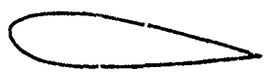	B7

FIGURE 4

HS SHROUDED PROPELLER TEST

SHROUD THICKNESS RATIO DISTRIBUTION

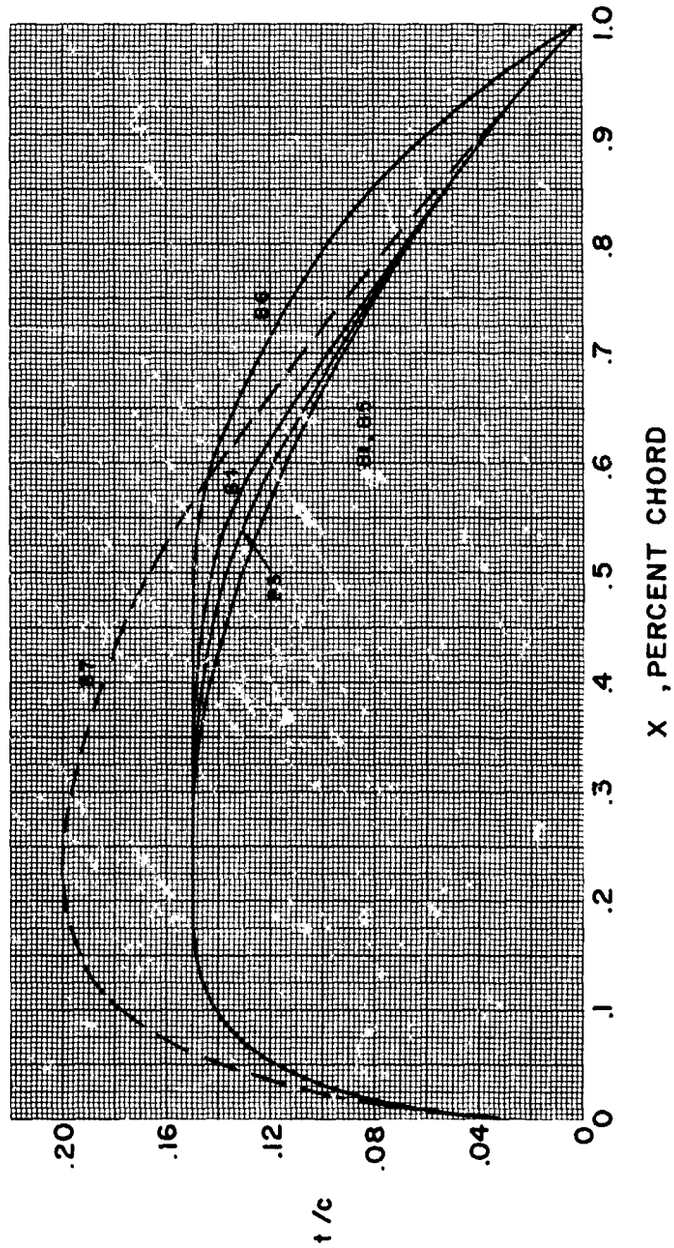

FIGURE 5

HS SHROUDED PROPELLER TEST

SHROUD CAMBER LINE SLOPE DISTRIBUTION

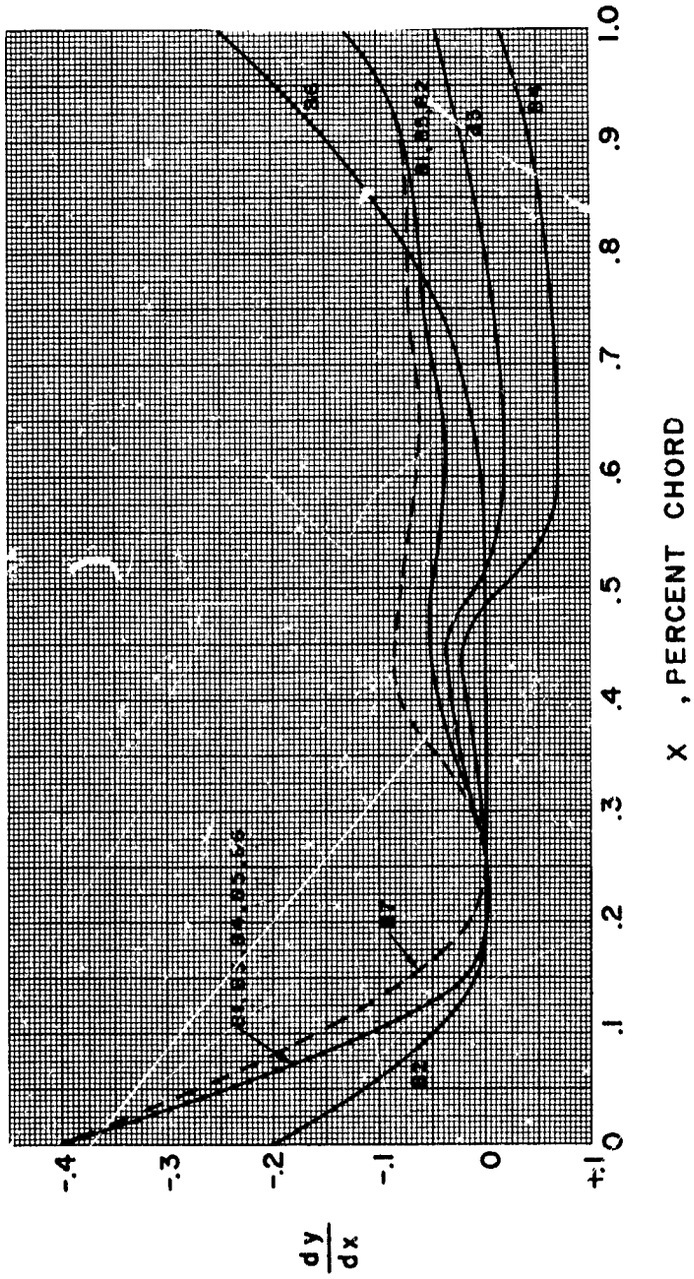

FIGURE 6

HS SHROUDED PROPELLER TEST

PROPELLER TEST BLADES

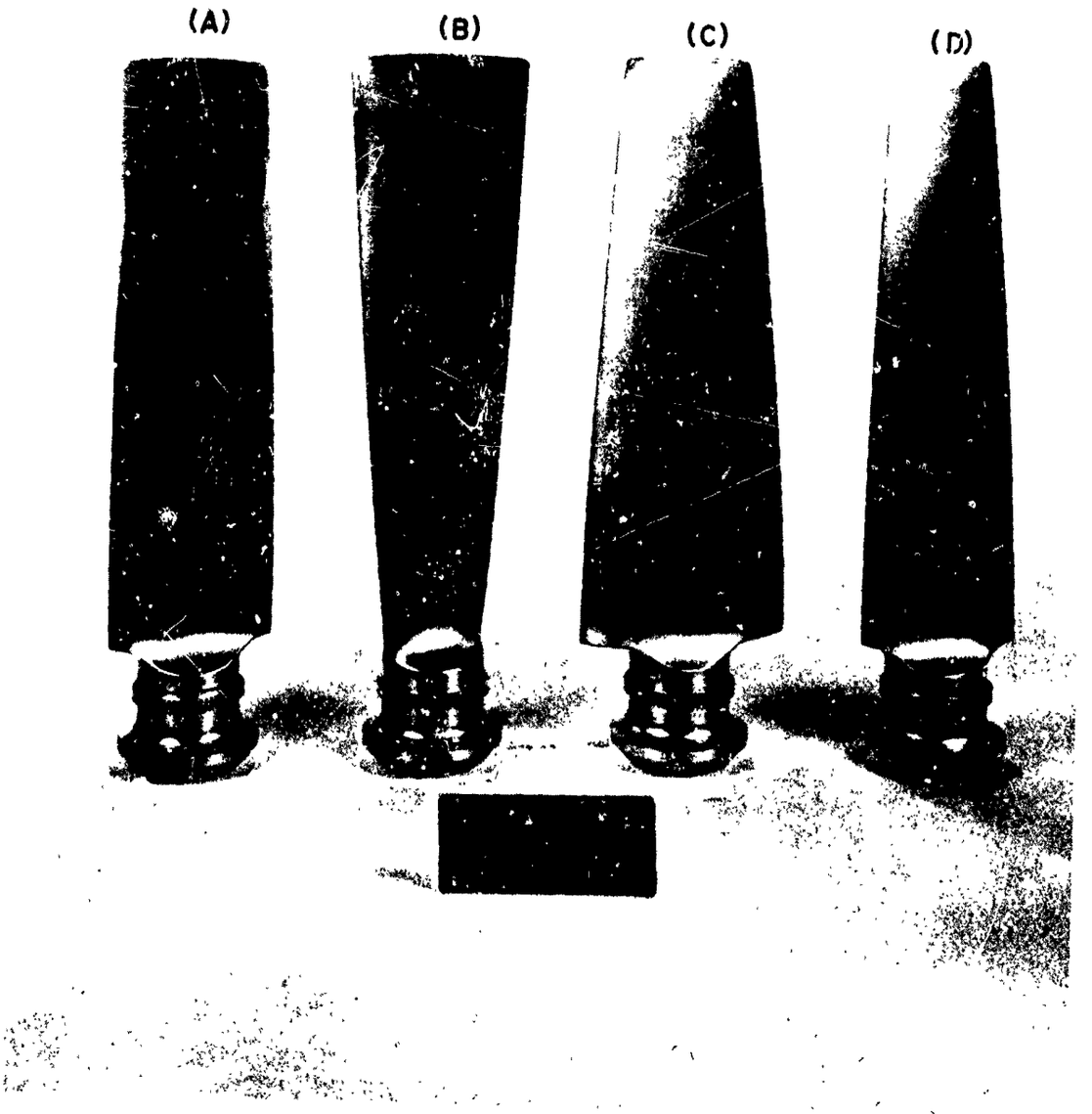

FIGURE 7

HS SHROUDED PROPELLER TEST

MODEL BLADE CHARACTERISTICS
COMMON TO ALL BLADES

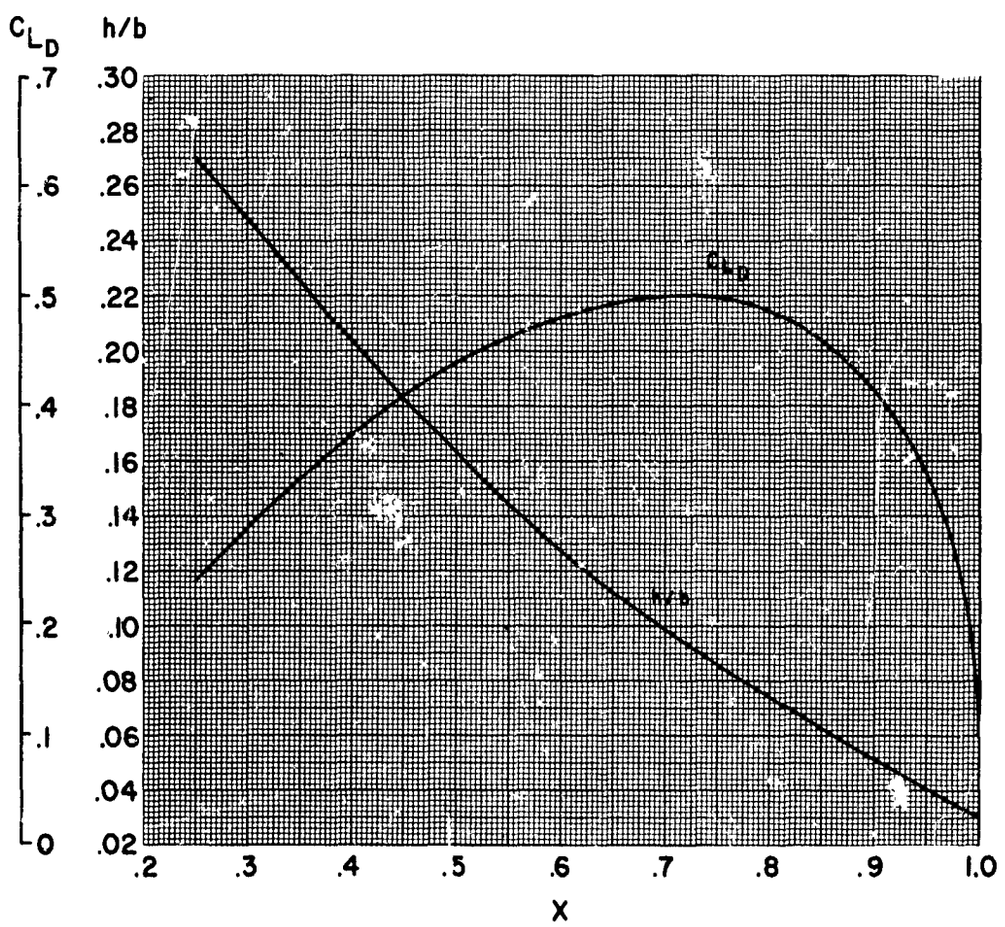

FIGURE 8

HS SHROUDED PROPELLER TEST

MODEL BLADE CHARACTERISTICS

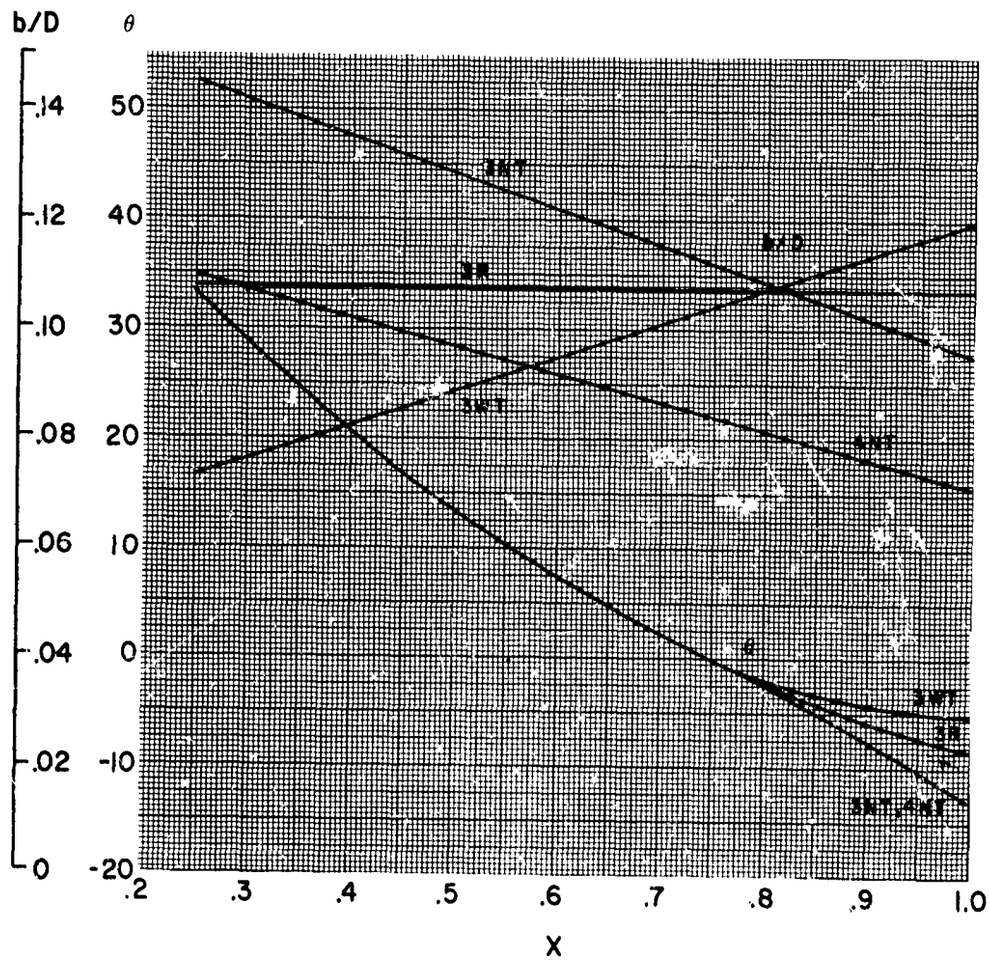

FIGURE 9

HS SHROUDED PROPELLER TEST

MODEL BLADE CALCULATED
CIRCULATION DISTRIBUTIONS

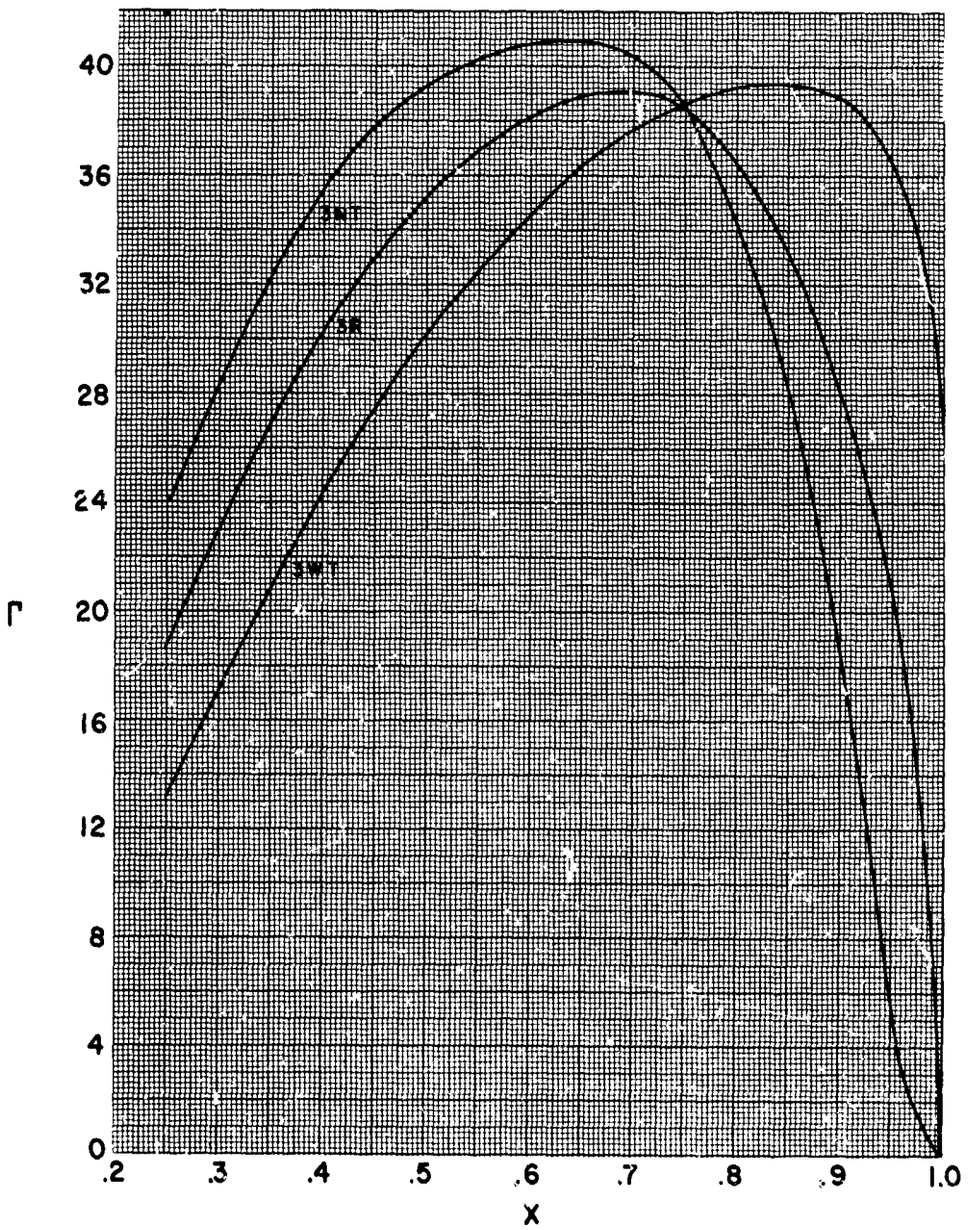

FIGURE 10

HS SHROUDED PROPELLER TEST

TYPICAL PRESSURE TRANSDUCER TRACE

RUN No. 671

POINT No. 3
M = 0.4
RPM = 6500

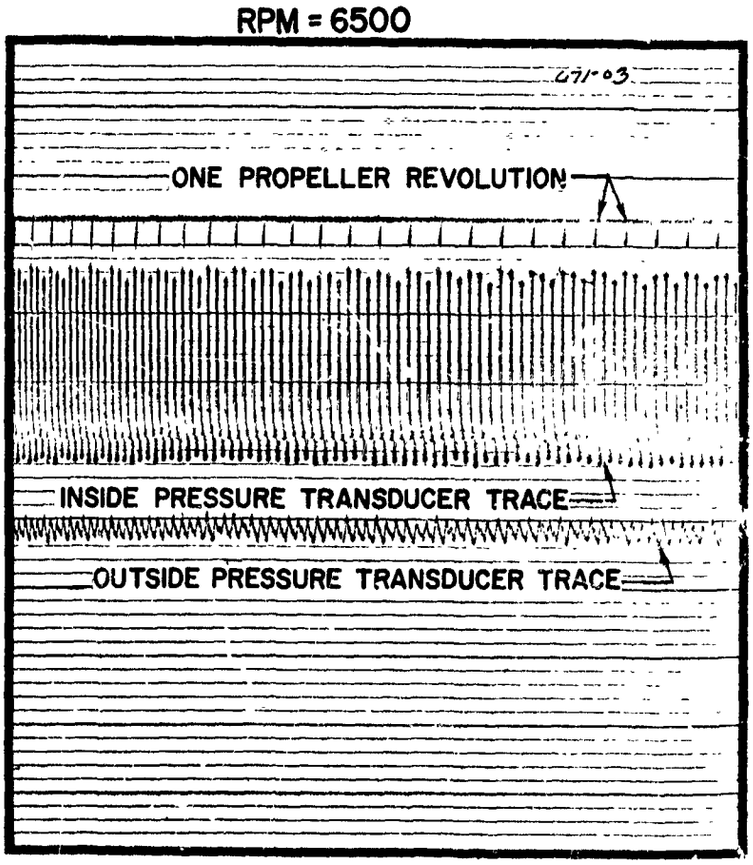

FIGURE 11

HS SHROUDED PROPELLER TEST

PROPELLER AND VANE ANGLE SIGN CONVENTION
WHEN VIEWED FROM VANE OR BLADE TIP

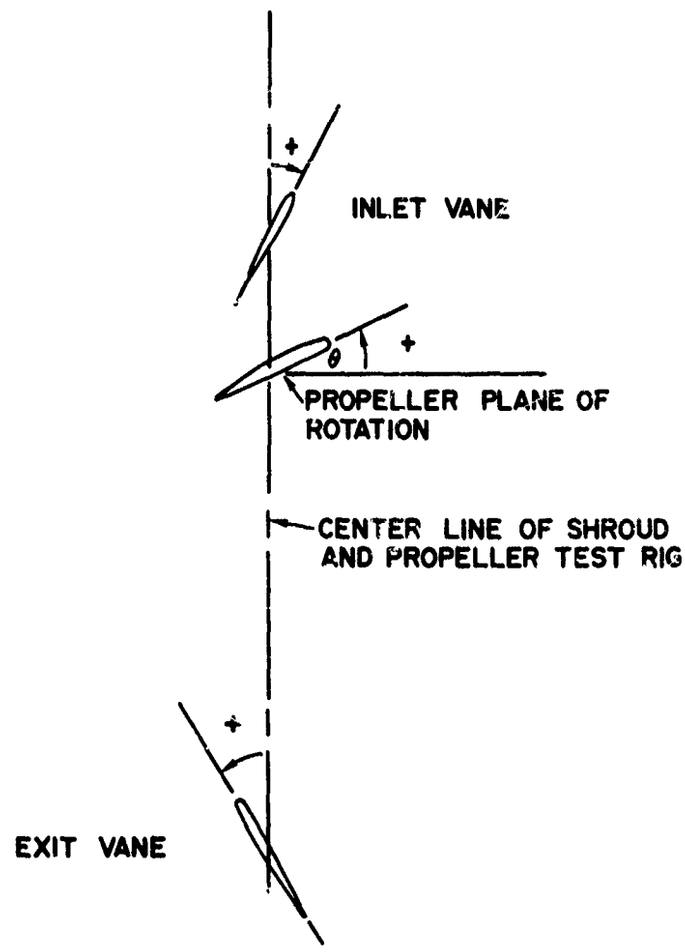

FIGURE 12

HS SHROUDED PROPELLER TEST

BARE PROPELLER TEST RIG WITH SHROUD SUPPORT SYSTEM

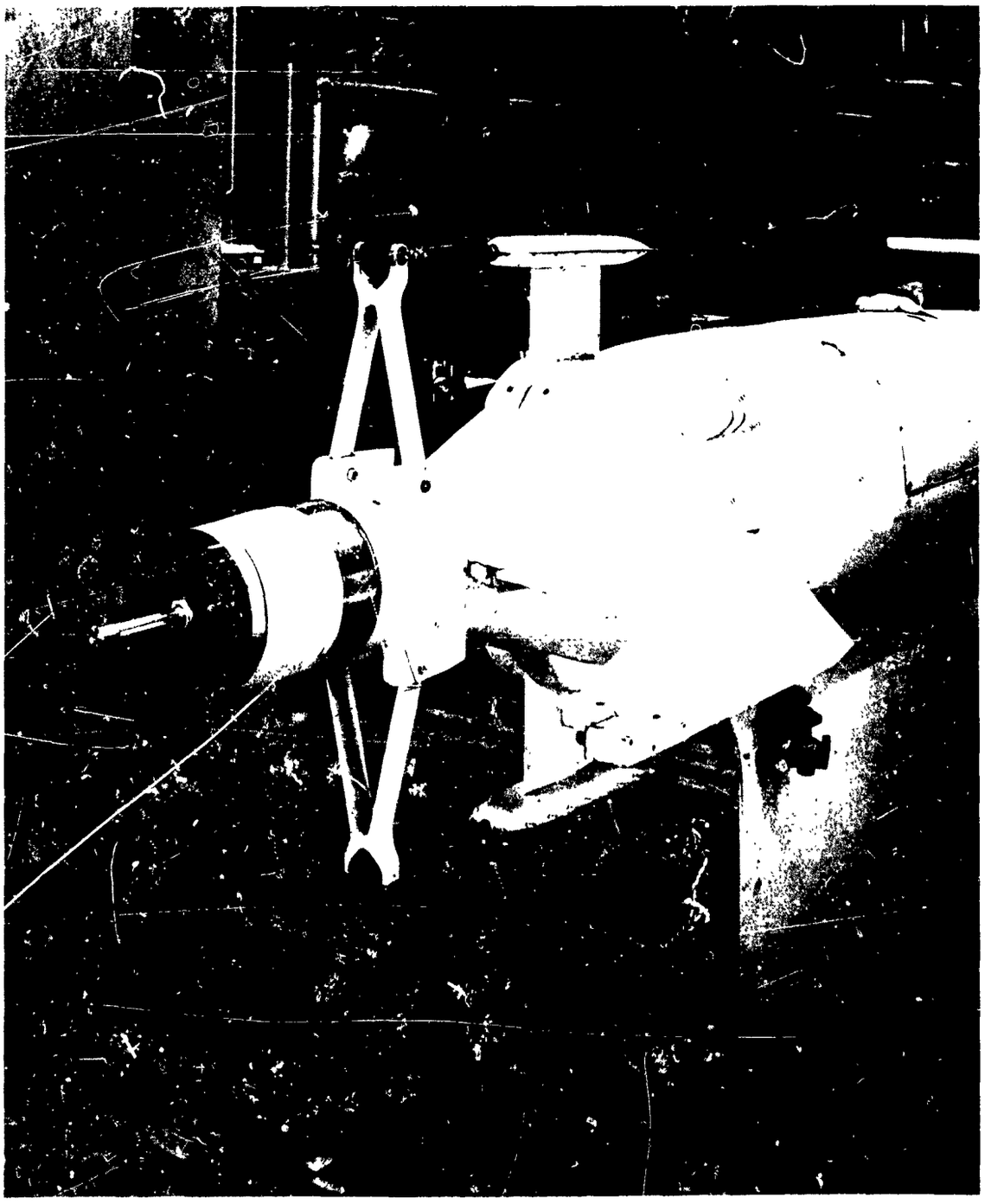

FIGURE 13

HS SHROUDED PROPELLER TEST

TEST RIG WITH THREE WAY RECTANGULAR PROPELLER

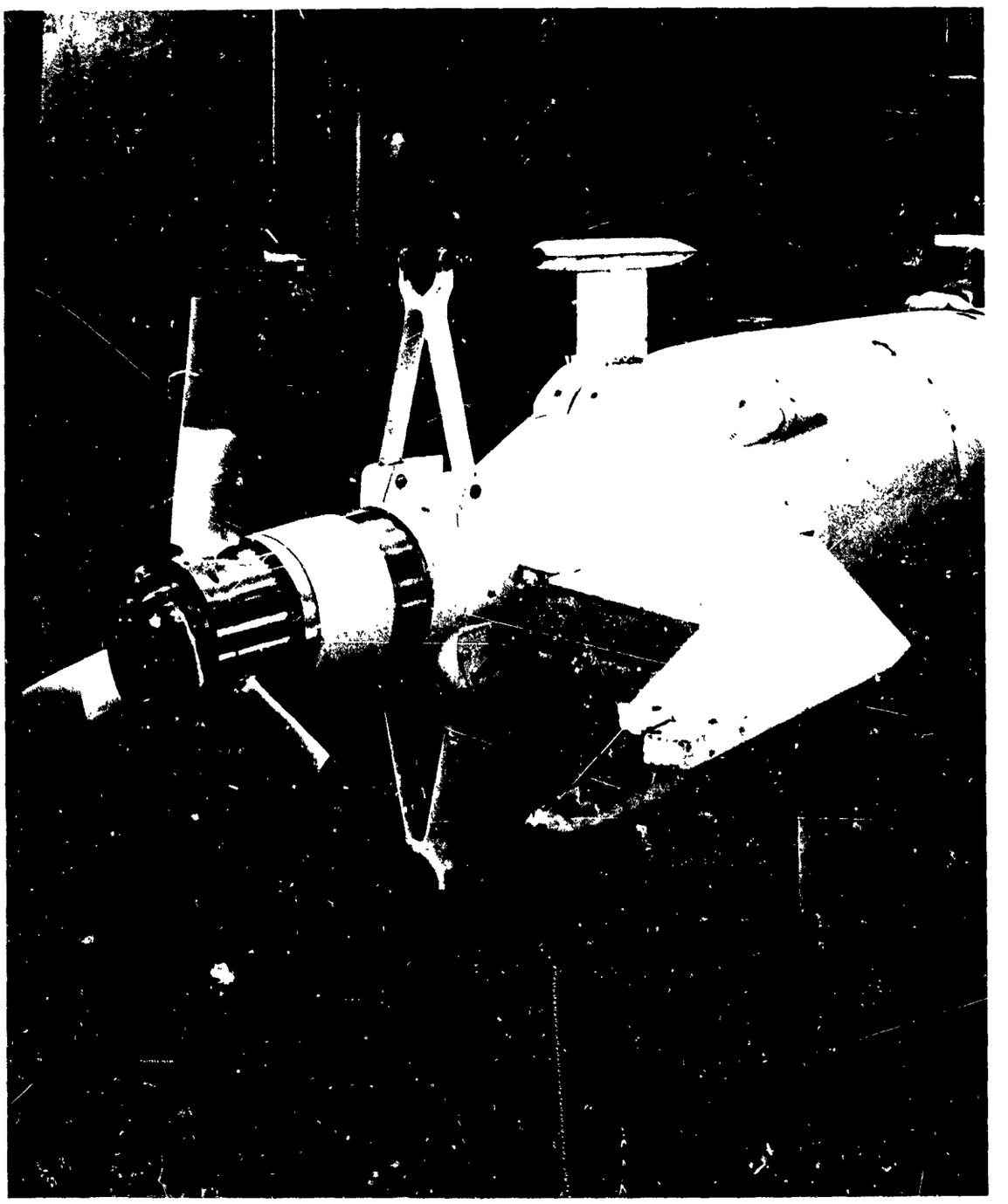

FIGURE 14

HS SHROUDED PROPELLER TEST

SHROUD SUPPORT RING

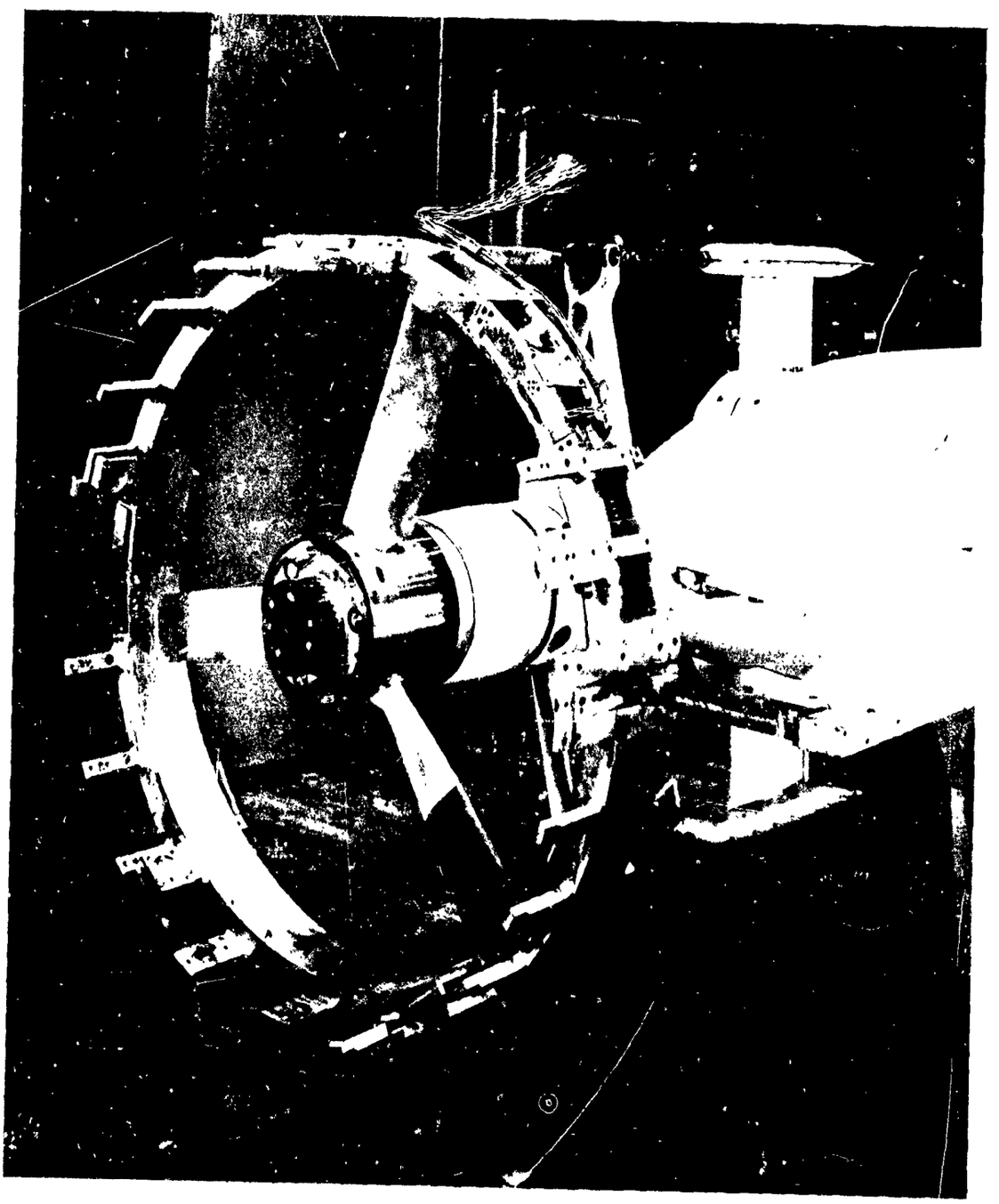

FIGURE 15

HS SHROUDED PROPELLER TEST

SHROUD DIFFUSER AND EXIT VANE INSTALLATION

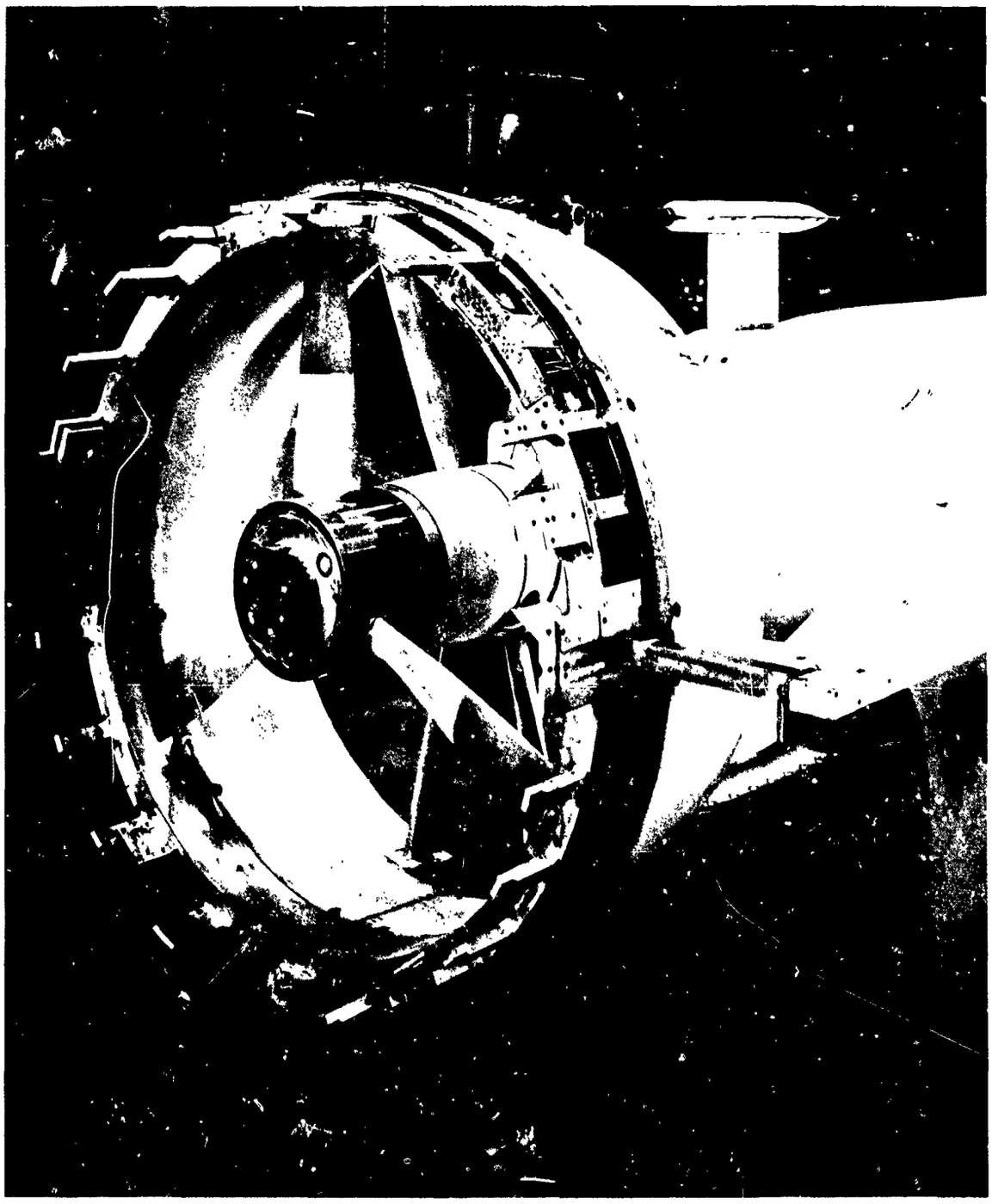

FIGURE 16

HS SHROUDED PROPELLER TEST

SHROUD CENTER SECTION AND LIP INSTALLATION

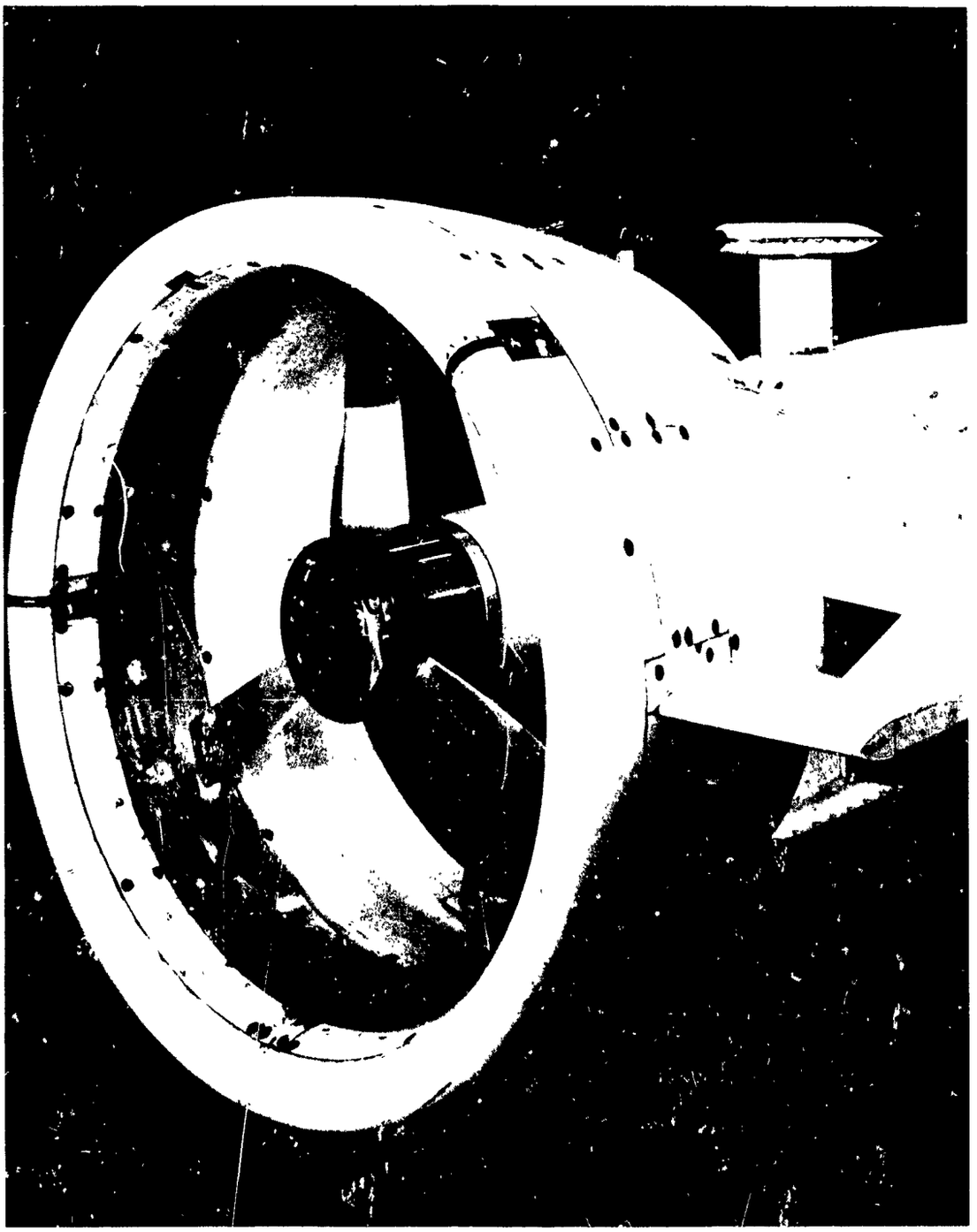

FIGURE 17

HS SHROUDED PROPELLER TEST

REAR VIEW OF COMPLETE MODEL SHOWING EXIT VANES AND EXIT RAKE INSTALLATION

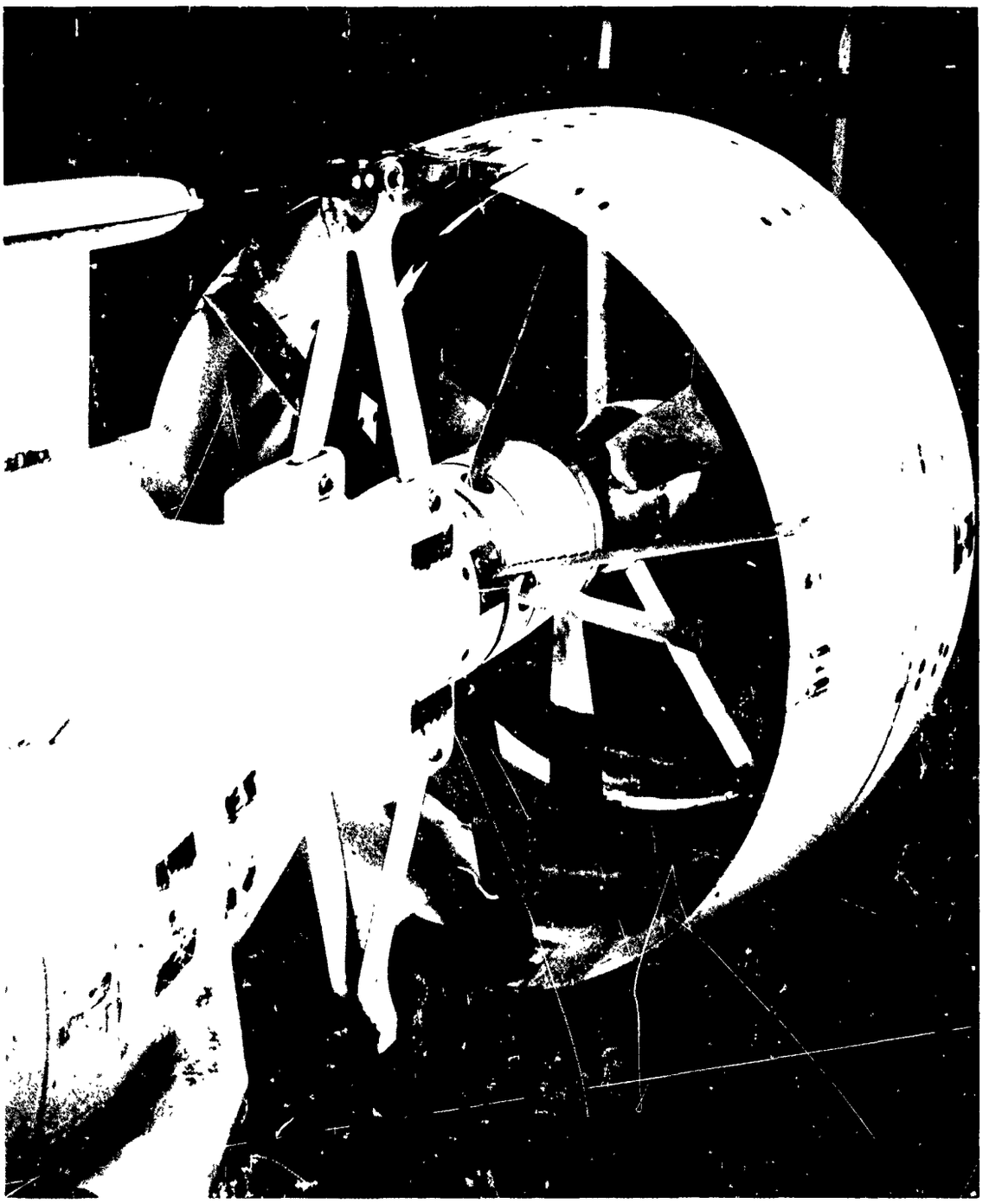

FIGURE 18

HS SHROUDED PROPELLER TEST

REAR VIEW OF SHROUD WITH DUMMY "A" FRAME INSTALLED

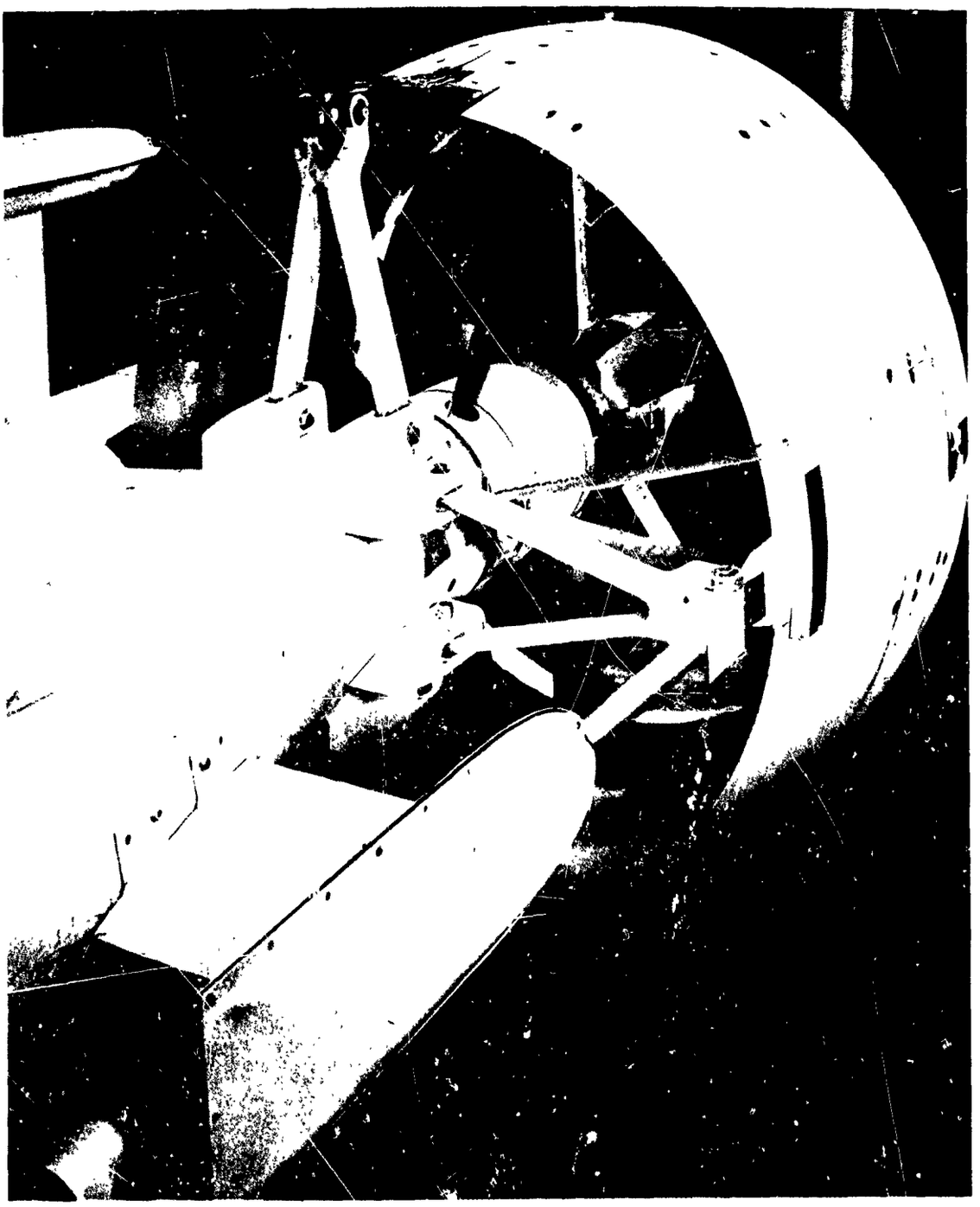

FIGURE 19

HS SHROUDED PROPELLER TEST

REAR VIEW OF SHROUD WITH DUMMY SIDE ARM INSTALLED

FIGURE 20

HS SHROUDED PROPELLER TEST

BOLT DAMAGE TO FIBERGLASS TIP OF RECTANGULAR BLADE

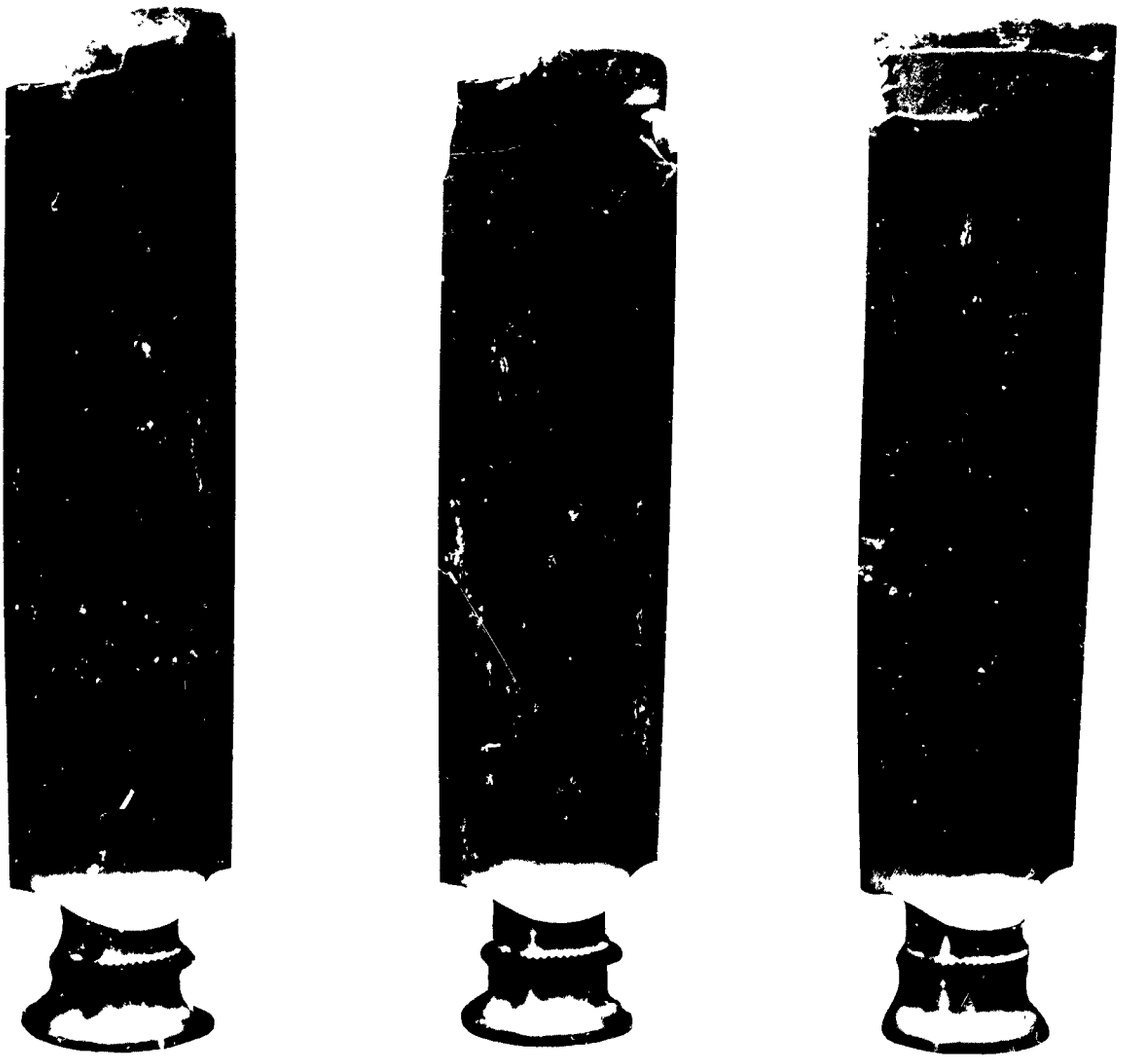

FIGURE 21

HS SHROUDED PROPELLER TEST

PHASE I - 18 FT TEST SECTION
VARIATION OF NET THRUST PER HORSEPOWER WITH
POWER LOADING FOR THE BASIC CONFIGURATION, B1-3WT.
TIP SPEED= 980 FPS

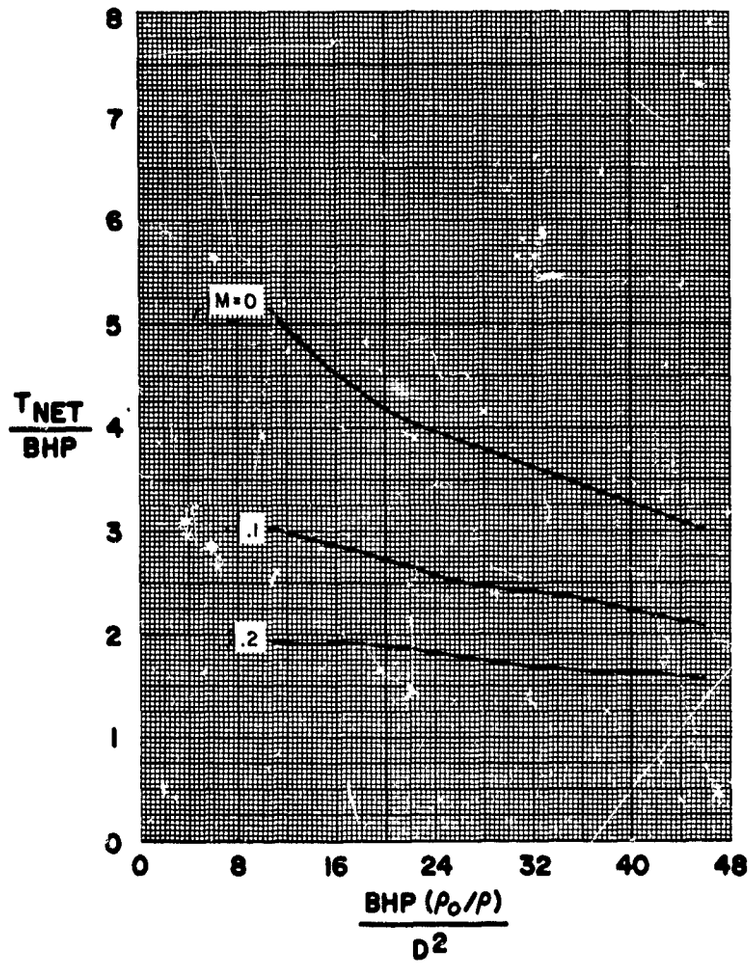

FIGURE 22

HS SHROUDED PROPELLER TEST

PHASE I - 18 FT TEST SECTION
VARIATION OF NET THRUST PER HORSEPOWER WITH
POWER LOADING FOR THE BASIC CONFIGURATION, B1-3WT.
TIP SPEED = 915 FPS

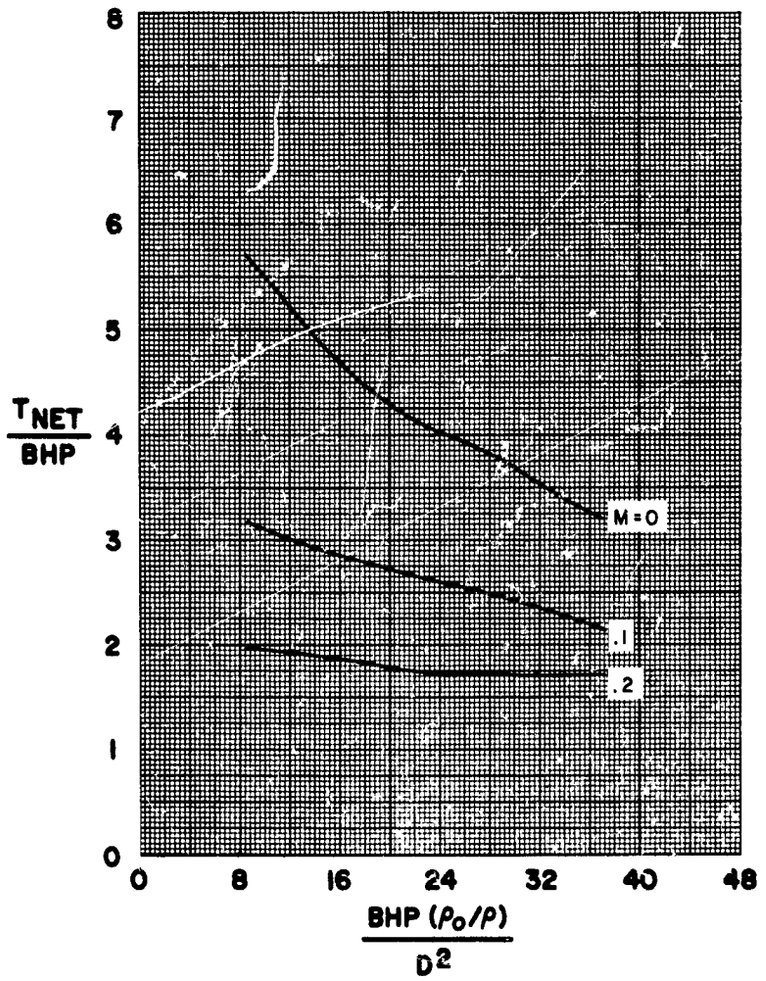

FIGURE 23

HS SHROUDED PROPELLER TEST

PHASE I - 18 FT TEST SECTION
VARIATION OF NET THRUST PER HORSEPOWER WITH
POWER LOADING FOR THE BASIC CONFIGURATION, BI-3WT.
TIP SPEED= 785 FPS

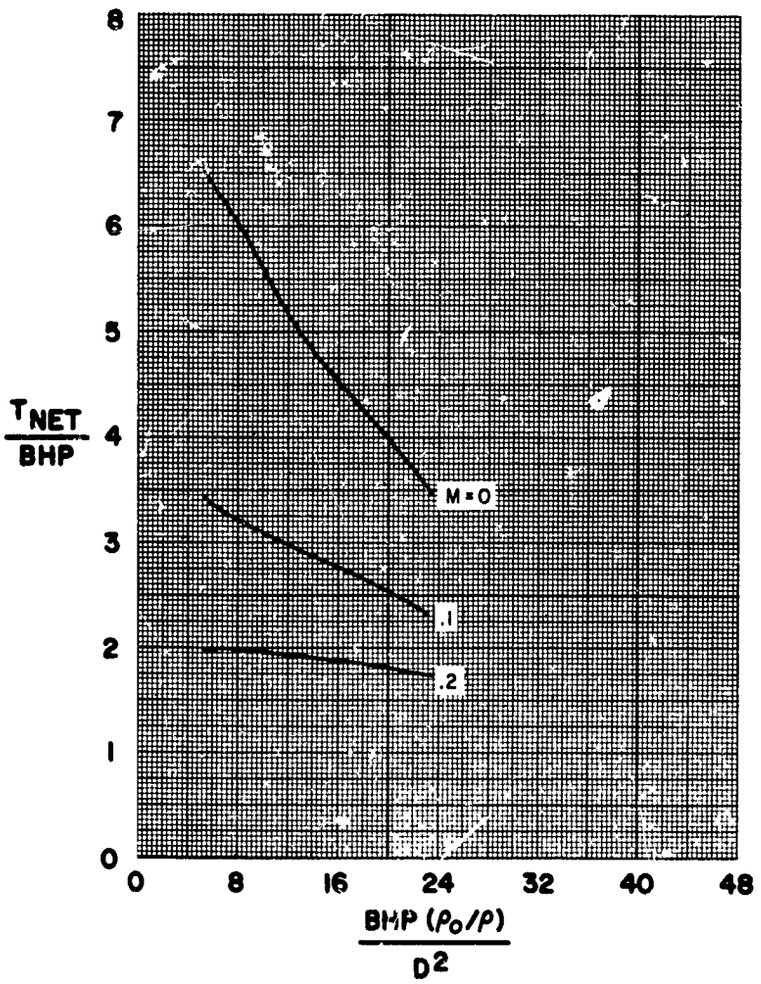

FIGURE 24

HS SHROUDED PROPELLER TEST

PHASE I-8 FT. TEST SECTION
VARIATION OF NET THRUST PER HORSEPOWER WITH POWER LOADING FOR THE BASIC CONFIGURATION BI-3WT

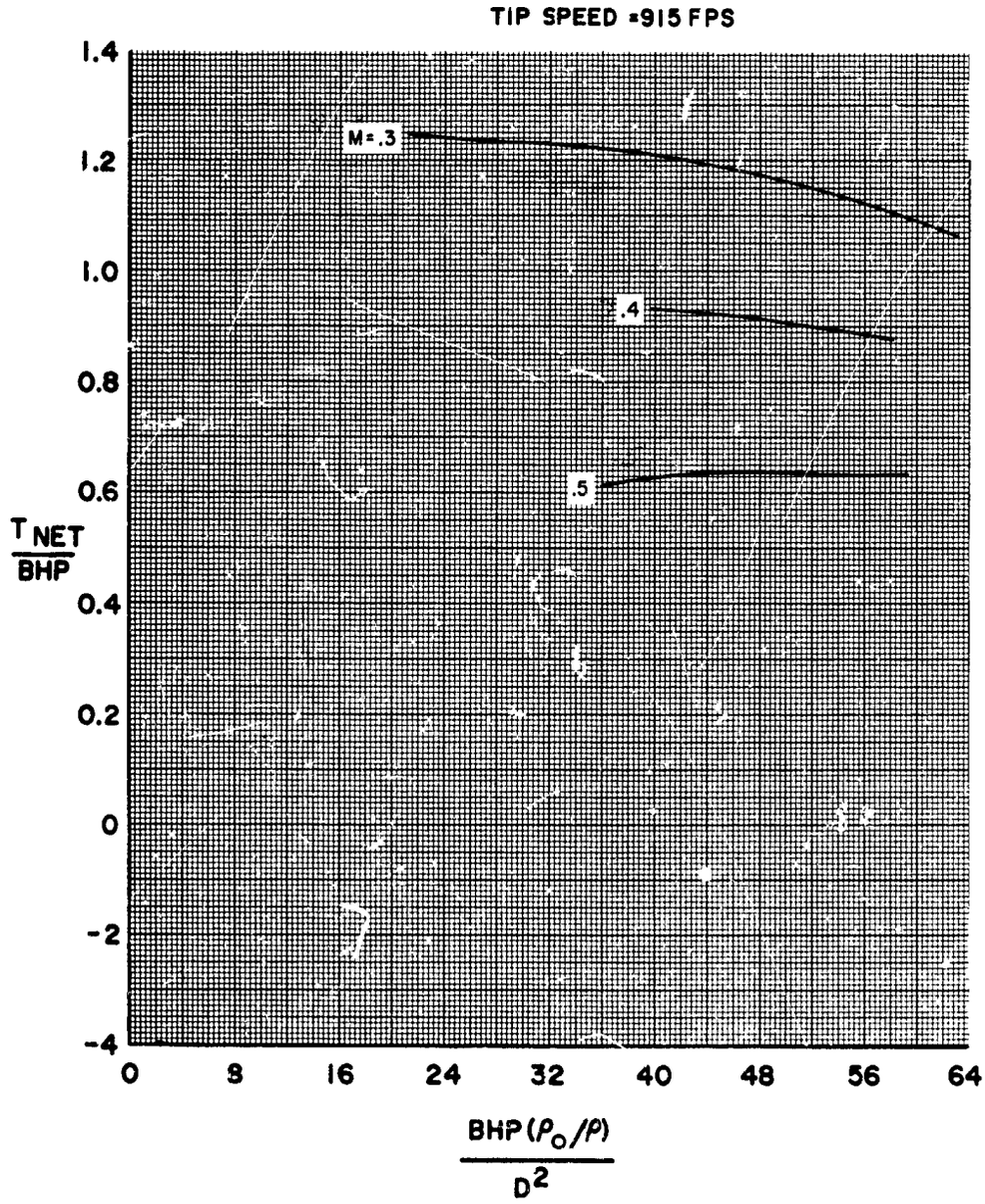

FIGURE 25

HS SHROUDED PROPELLER TEST

PHASE I-8 FT. TEST SECTION
VARIATION OF NET THRUST PER HORSEPOWER WITH POWER LOADING FOR THE BASIC CONFIGURATION BI-3WT

TIP SPEED =785 FPS

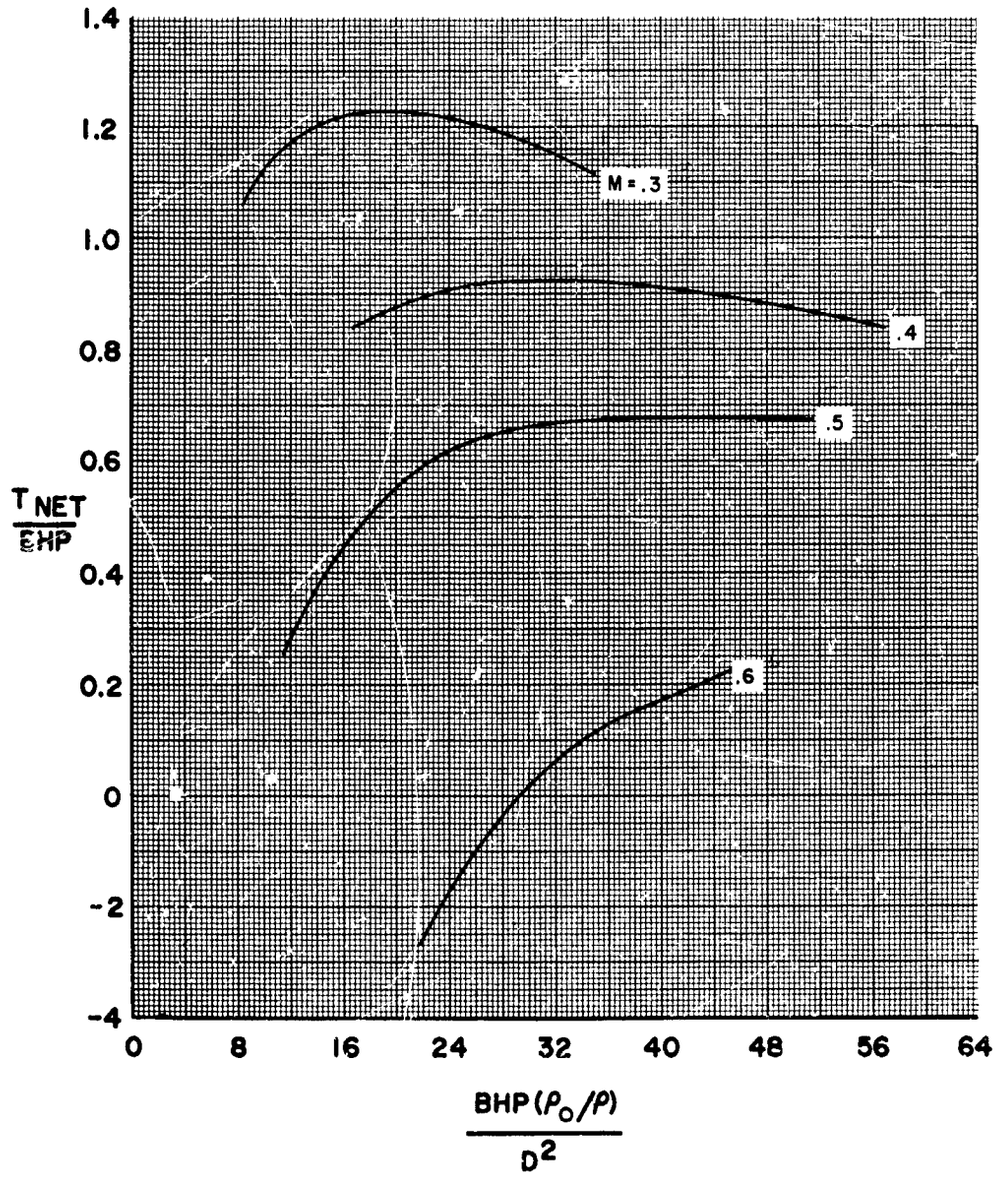

FIGURE 26

HS SHROUDED PROPELLER TEST

PHASE I-8 FT. TEST SECTION
VARIATION OF NET THRUST PER HORSEPOWER WITH POWER LOADING FOR THE BASIC CONFIGURATION BI-3WT

TIP SPEED = 654 FPS

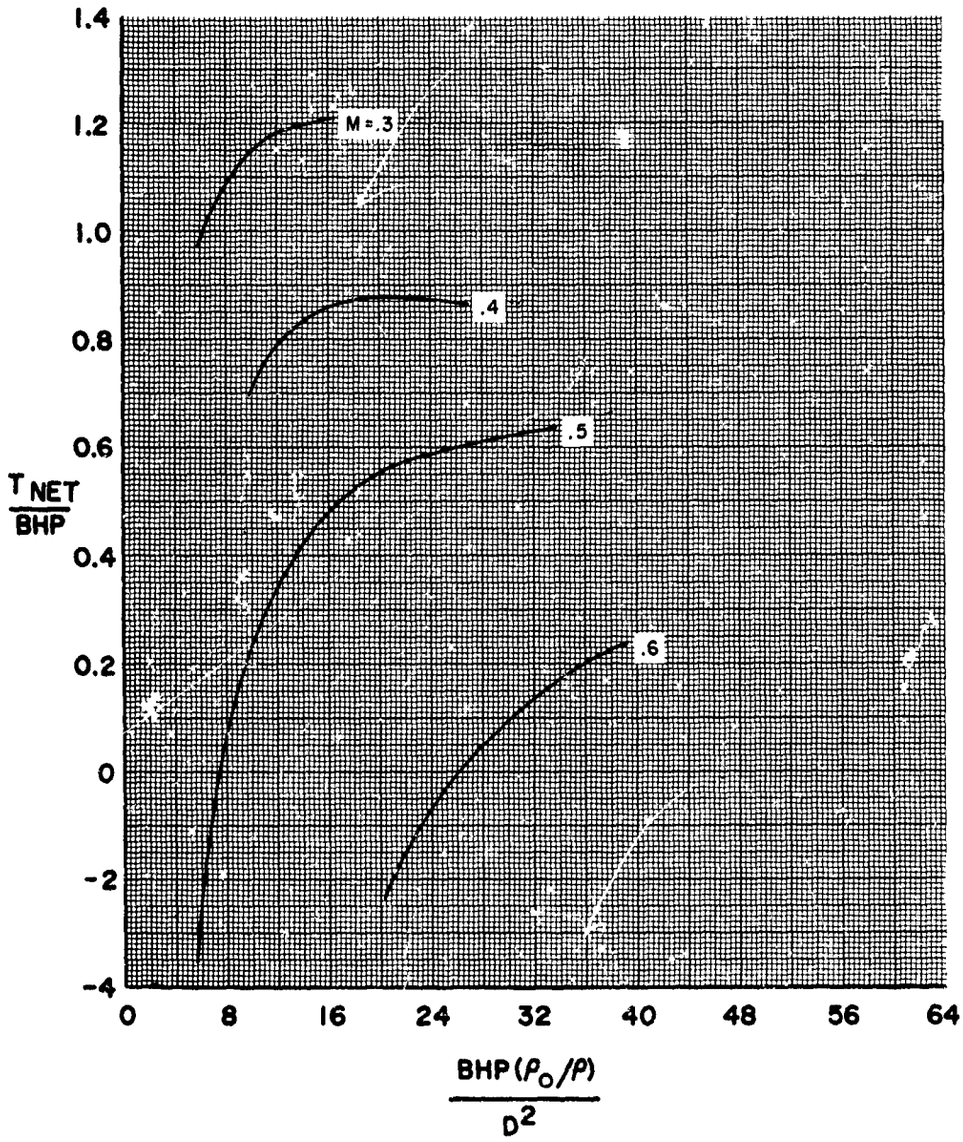

FIGURE 27

HS SHROUDED PROPELLER TEST

PHASE I-18 FT TEST SECTION
VARIATION OF PROPELLER THRUST PER HORSEPOWER WITH
POWER LOADING FOR THE BASIC CONFIGURATION, BI-3WT

TIP SPEED = 980 FPS

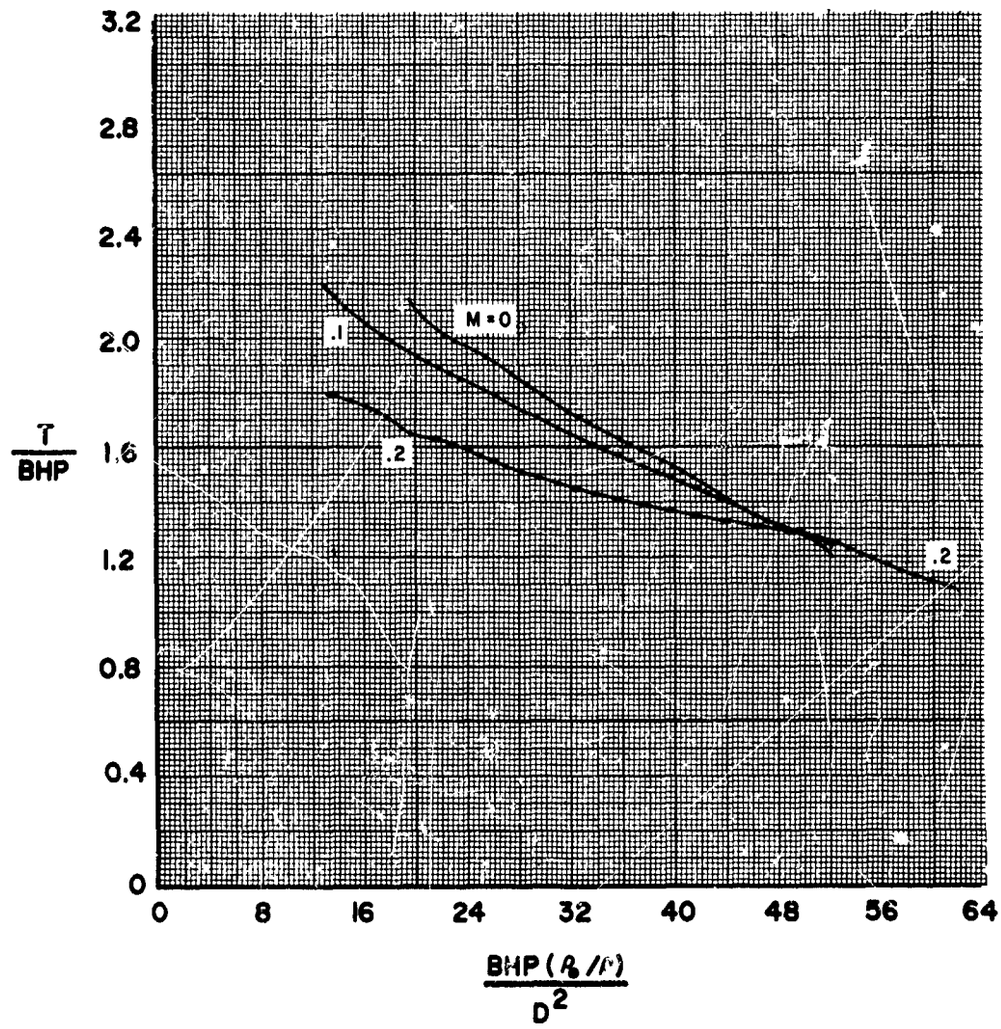

FIGURE 28

HS SHROUDED PROPELLER TEST

PHASE 1-18 FT TEST SECTION
VARIATION OF PROPELLER THRUST PER HORSEPOWER WITH
POWER LOADING FOR THE BASIC CONFIGURATION, BI-3WT

TIP SPEED = 915 FPS

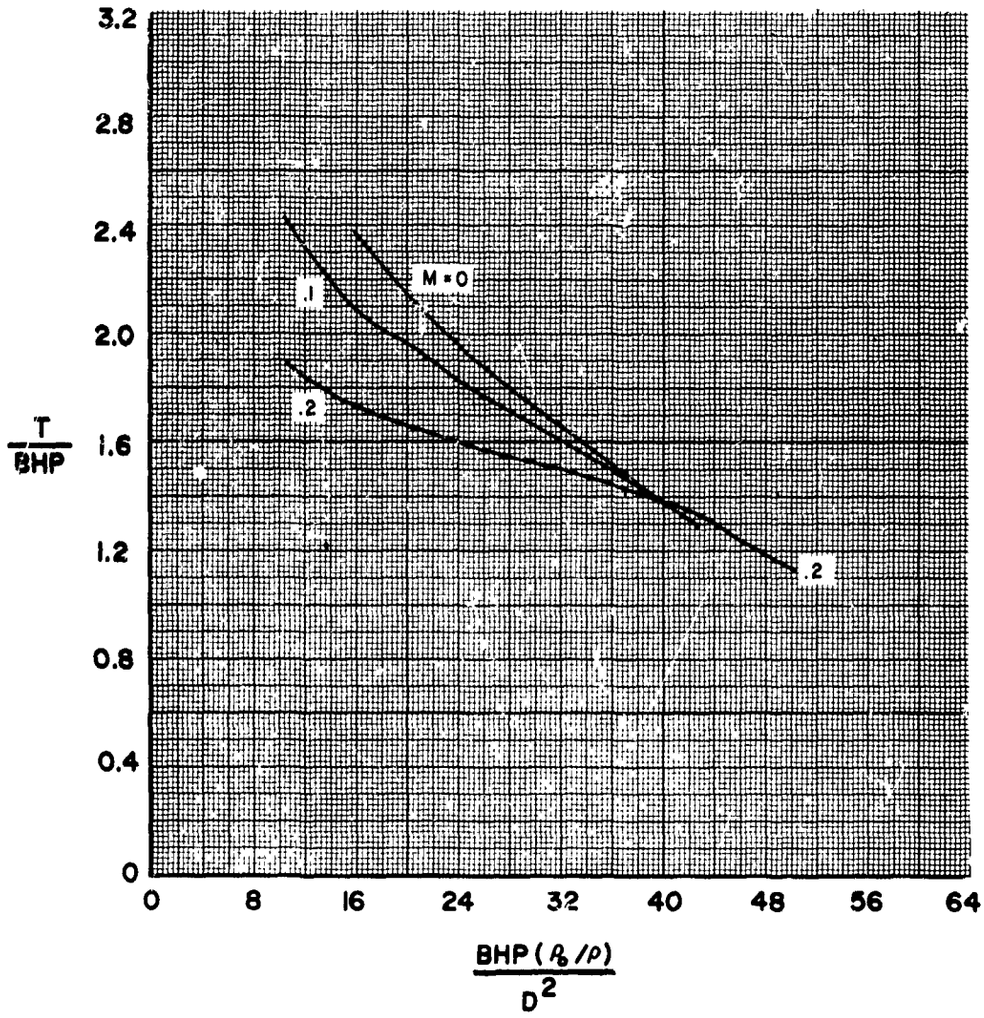

FIGURE 29

HS SHROUDED PROPELLER TEST

PHASE 1-18 FT TEST SECTION
VARIATION OF PROPELLER THRUST PER HORSEPOWER WITH
POWER LOADING FOR THE BASIC CONFIGURATION, B1-3WT

TIP SPEED = 785 FPS

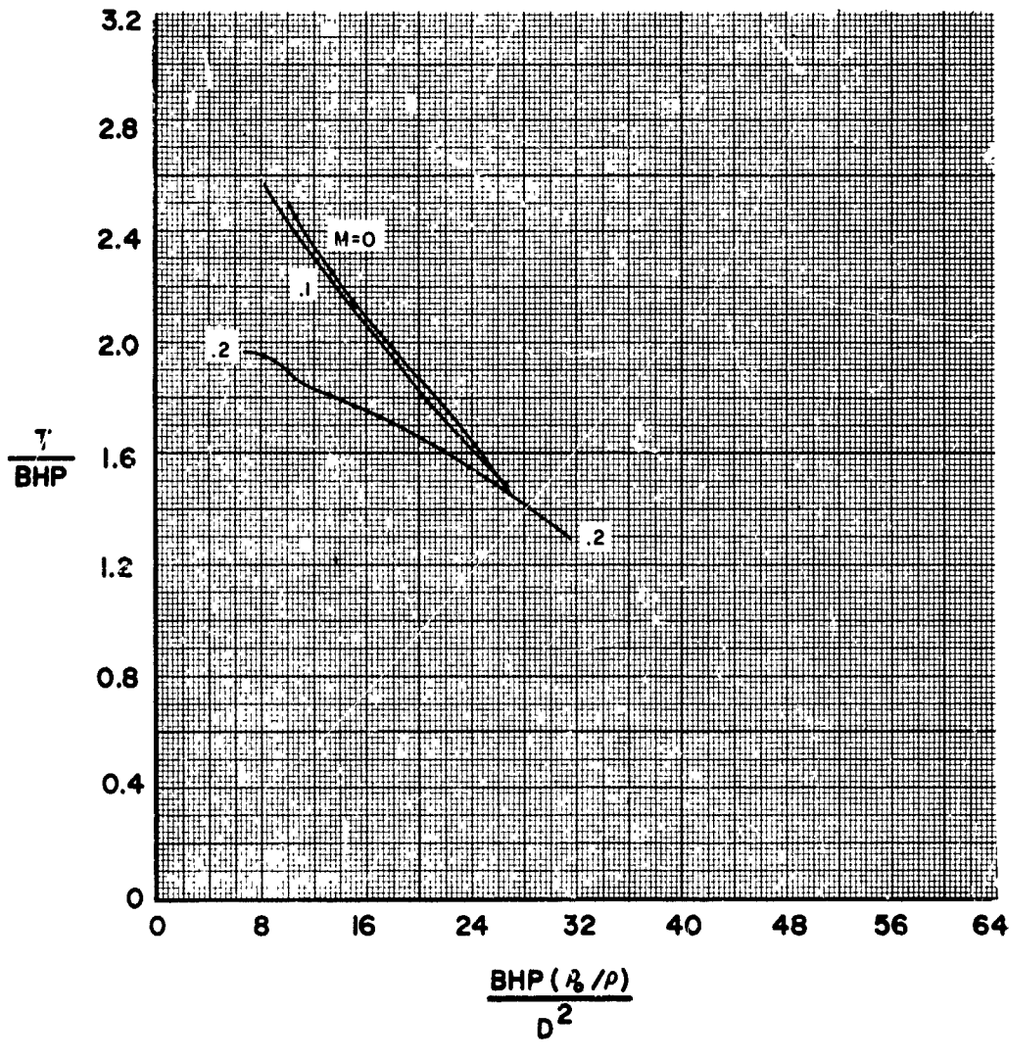

FIGURE 30

HS SHROUDED PROPELLER TEST

PHASE I - 8 FT. TEST SECTION
VARIATION OF PROPELLER THRUST PER HORSEPOWER WITH
POWER LOADING FOR THE BASIC CONFIGURATION BI - 3WT

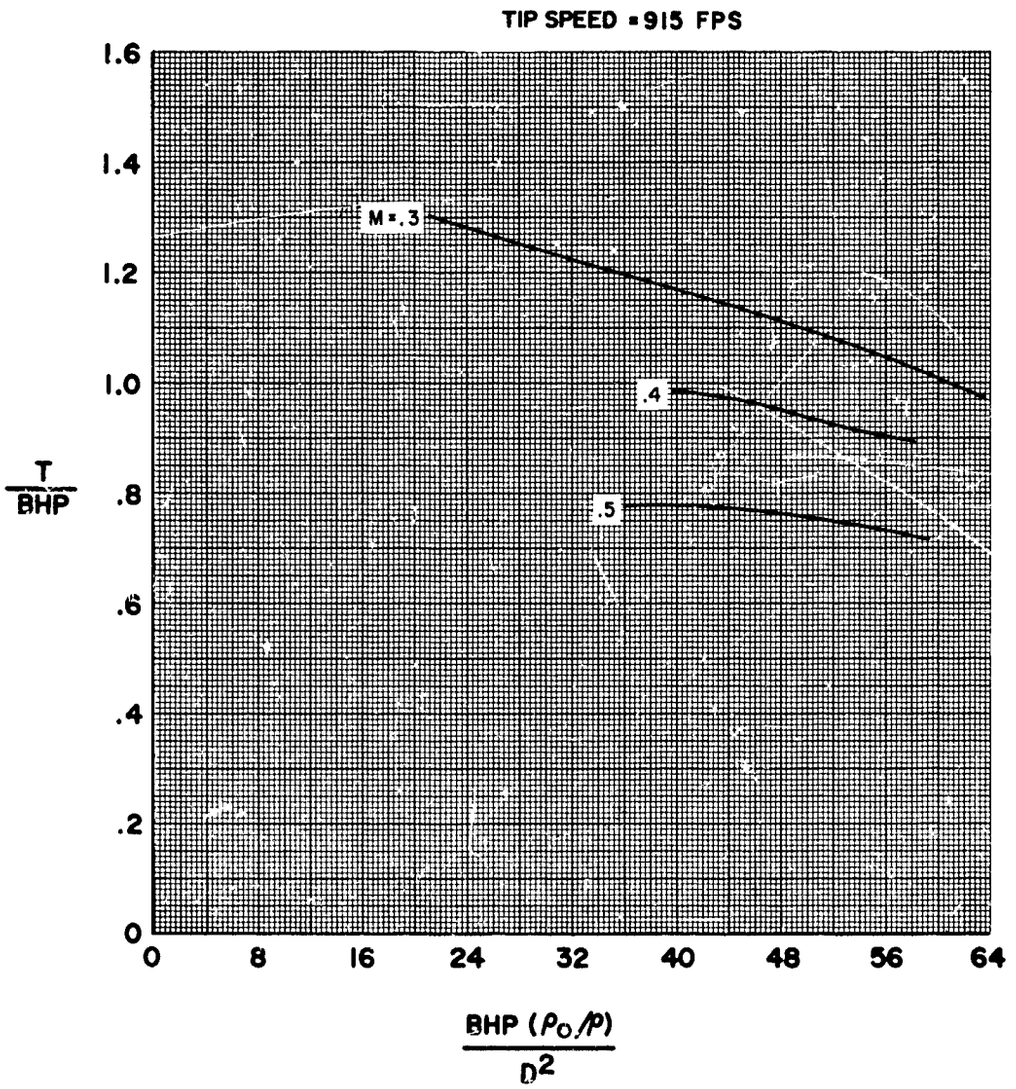

FIGURE 31

HS SHROUDED PROPELLER TEST

PHASE I - 8 FT. TEST SECTION
VARIATION OF PROPELLER THRUST PER HORSEPOWER WITH
POWER LOADING FOR THE BASIC CONFIGURATION BI - 3WT

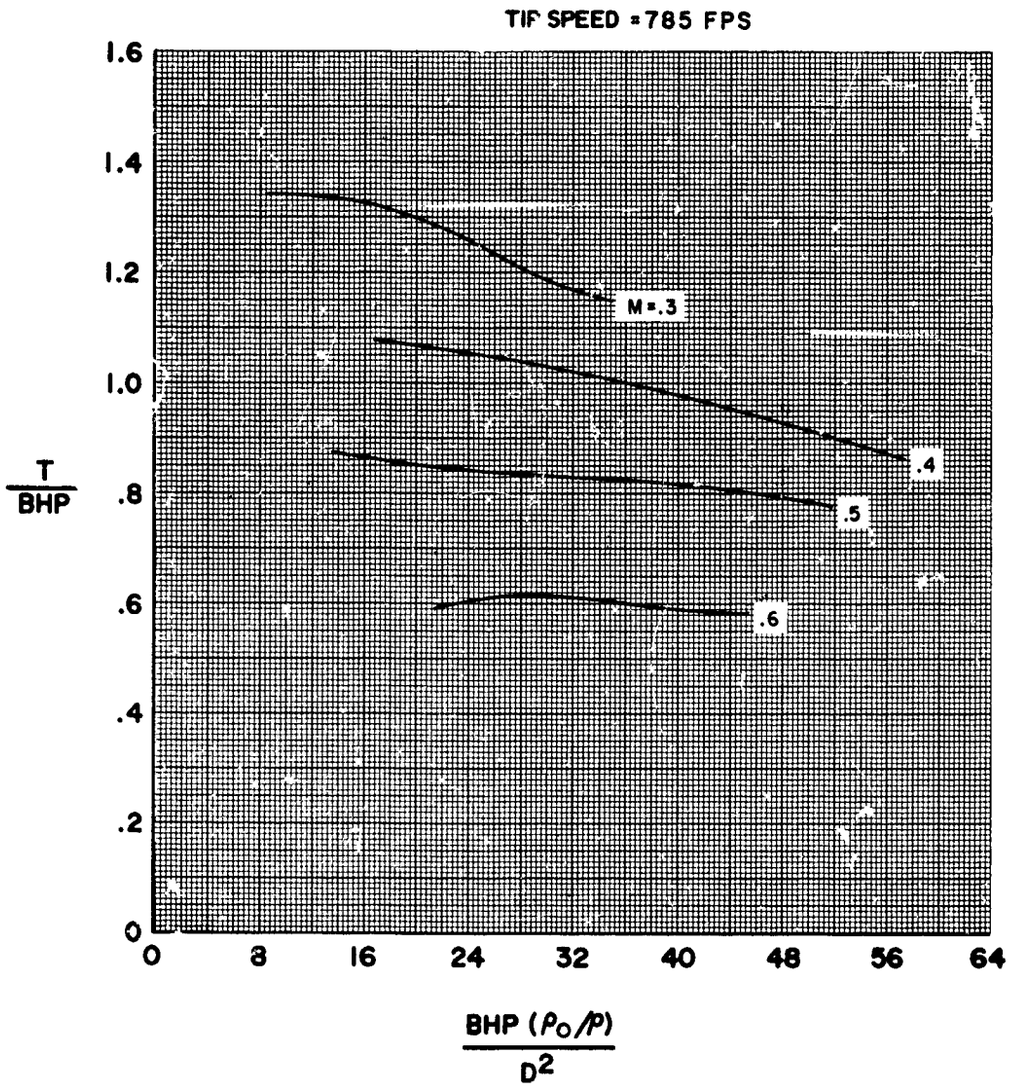

FIGURE 32

HS SHROUDED PROPELLER TEST

PHASE I - 8 FT. TEST SECTION
VARIATION OF PROPELLER THRUST PER HORSEPOWER WITH
POWER LOADING FOR THE BASIC CONFIGURATION BI - 3WT

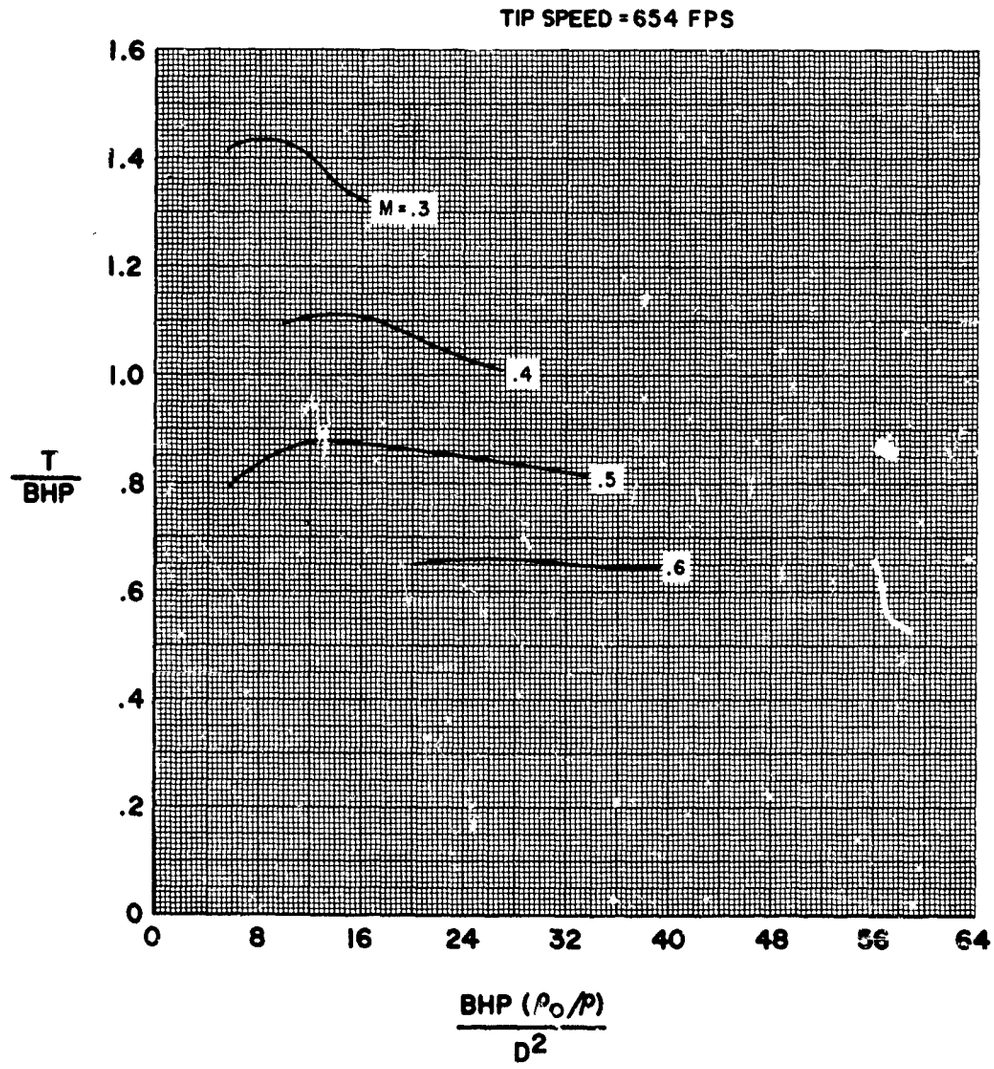

FIGURE 33

HS SHROUDED PROPELLER TEST

RATIO OF NET TO PROPELLER THRUST
CONFIGURATION 51-3WT
N=7000

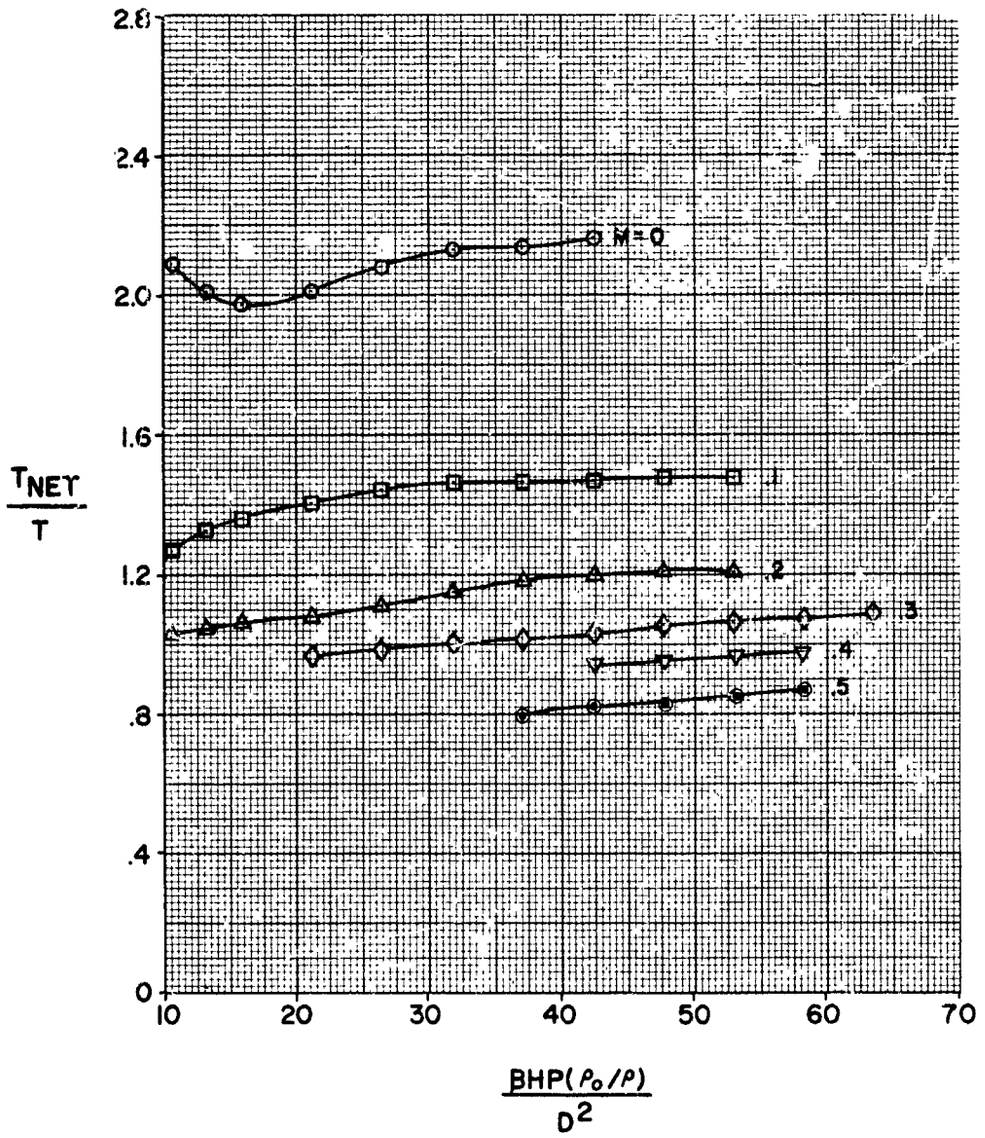

FIGURE 34

HS SHROUDED PROPELLER TEST

RATIO OF NET TO PROPELLER THRUST
CONFIGURATION BI-3R
N=7000

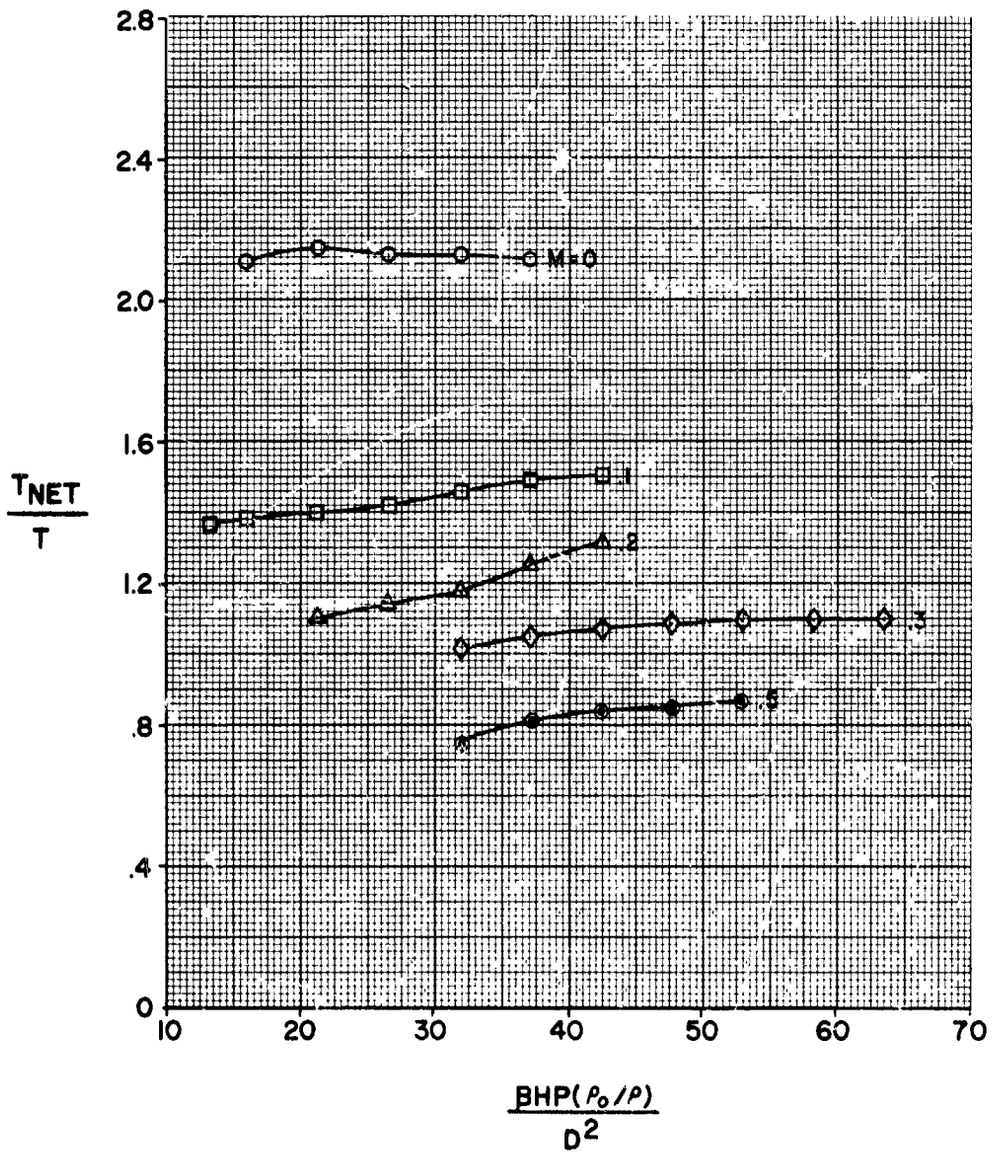

FIGURE 35

HS SHROUDED PROPELLER TEST

RATIO OF NET TO PROPELLER THRUST
CONFIGURATION BI-3R 1/2M
N=7000

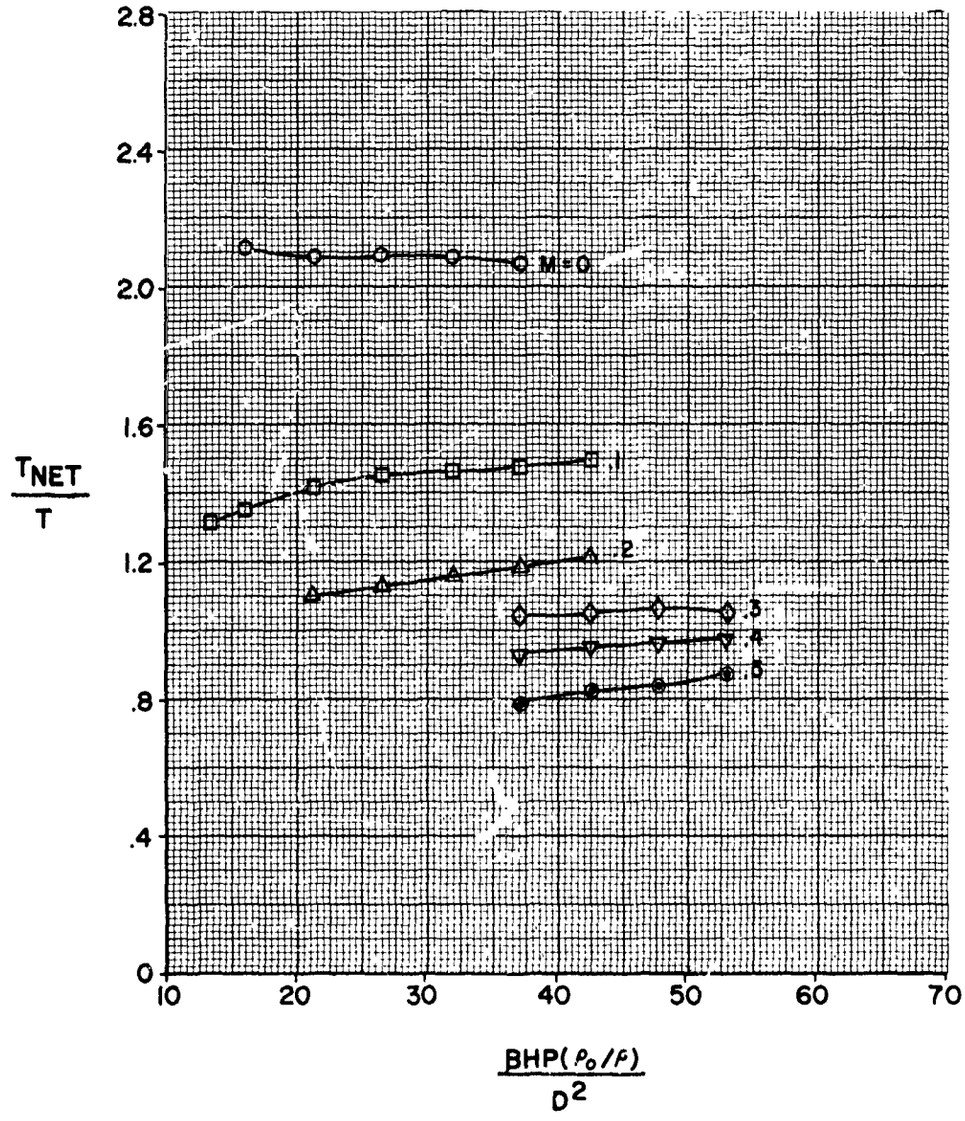

FIGURE 36

HS SHROUDED PROPELLER TEST

RATIO OF NET TO PROPELLER THRUST
CONFIGURATION BI-3RM
N=7000

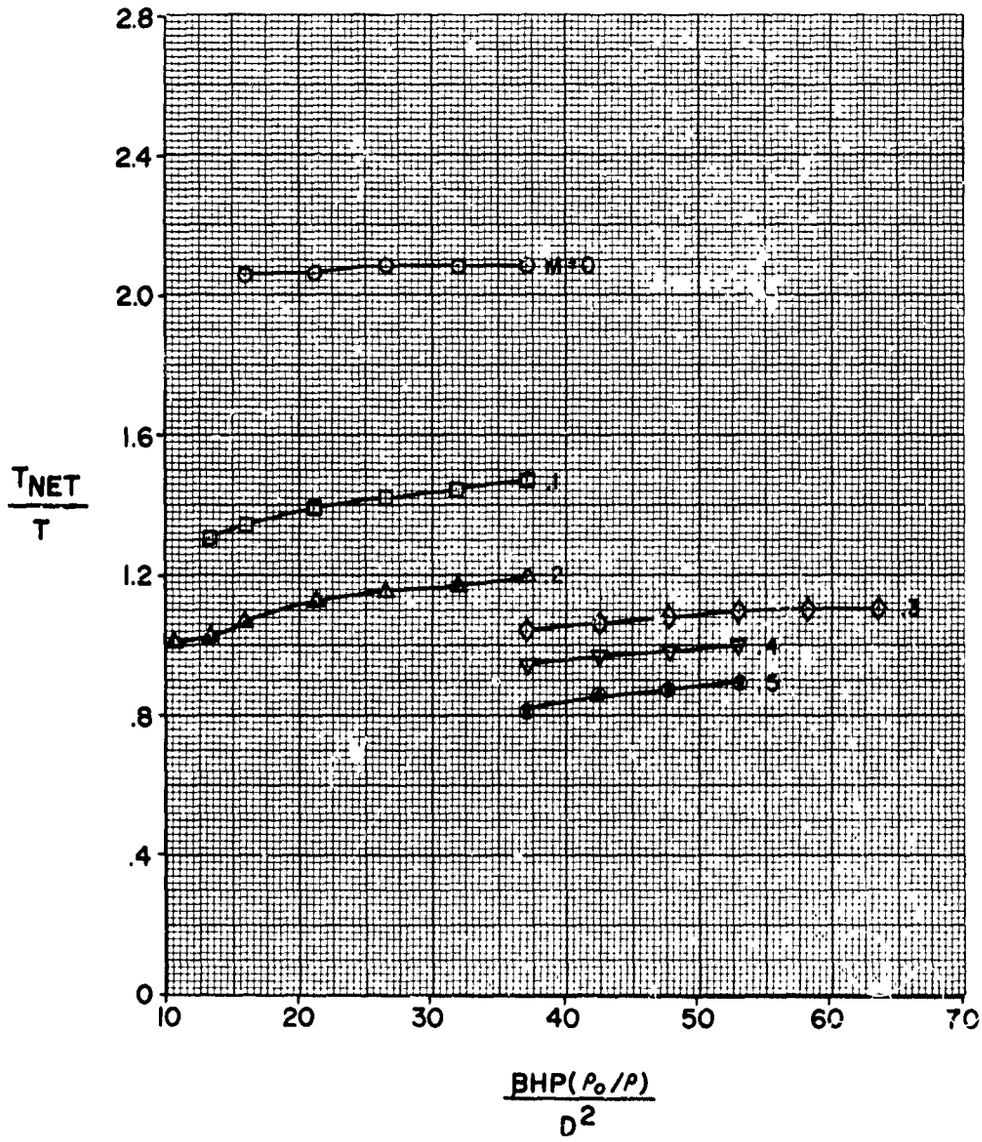

FIGURE 37

HS SHROUDED PROPELLER TEST

RATIO OF NET TO PROPELLER THRUST
CONFIGURATION BI-3NT
N=7000

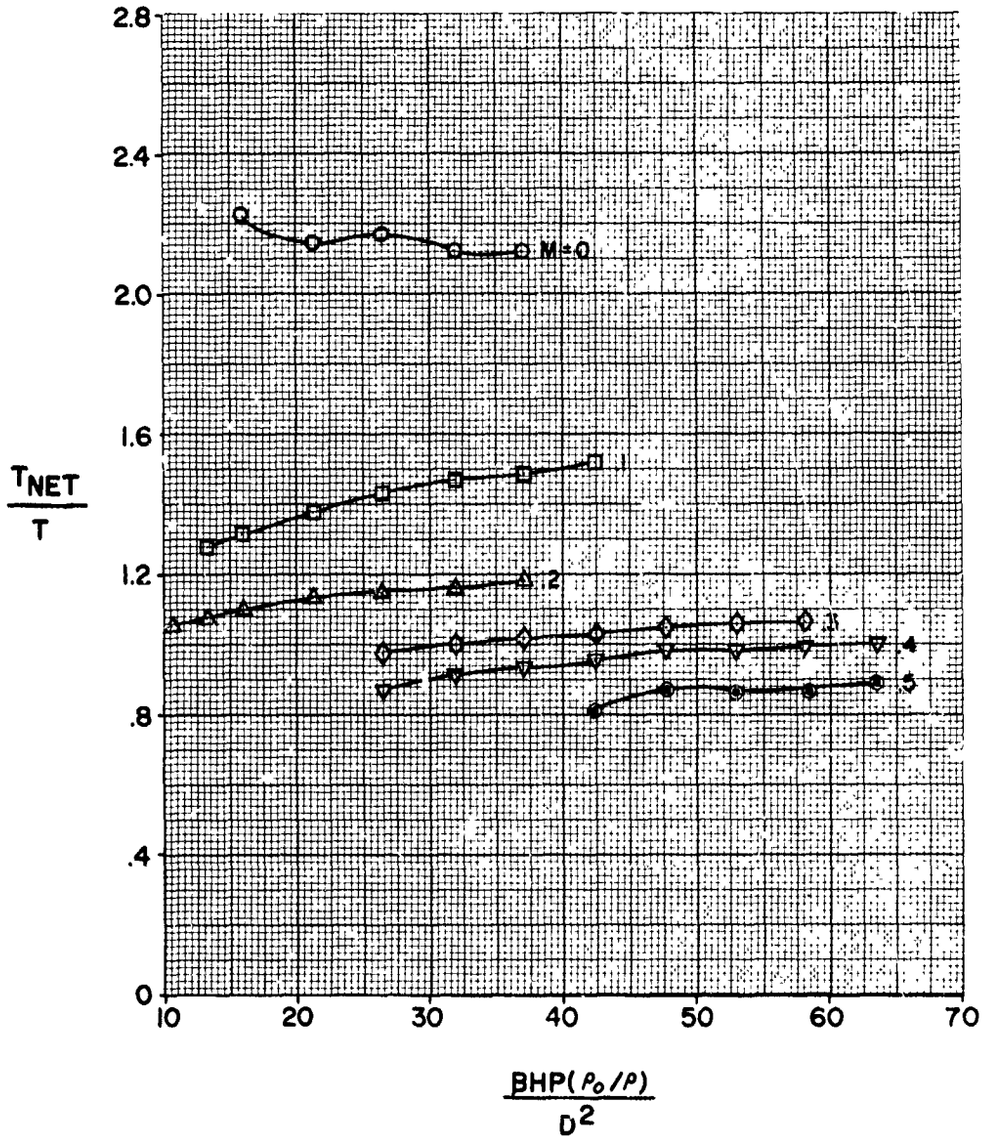

FIGURE 38

HS SHROUDED PROPELLER TEST

RATIO OF NET TO PROPELLER THRUST
CONFIGURATION BI-4NT
N=7000

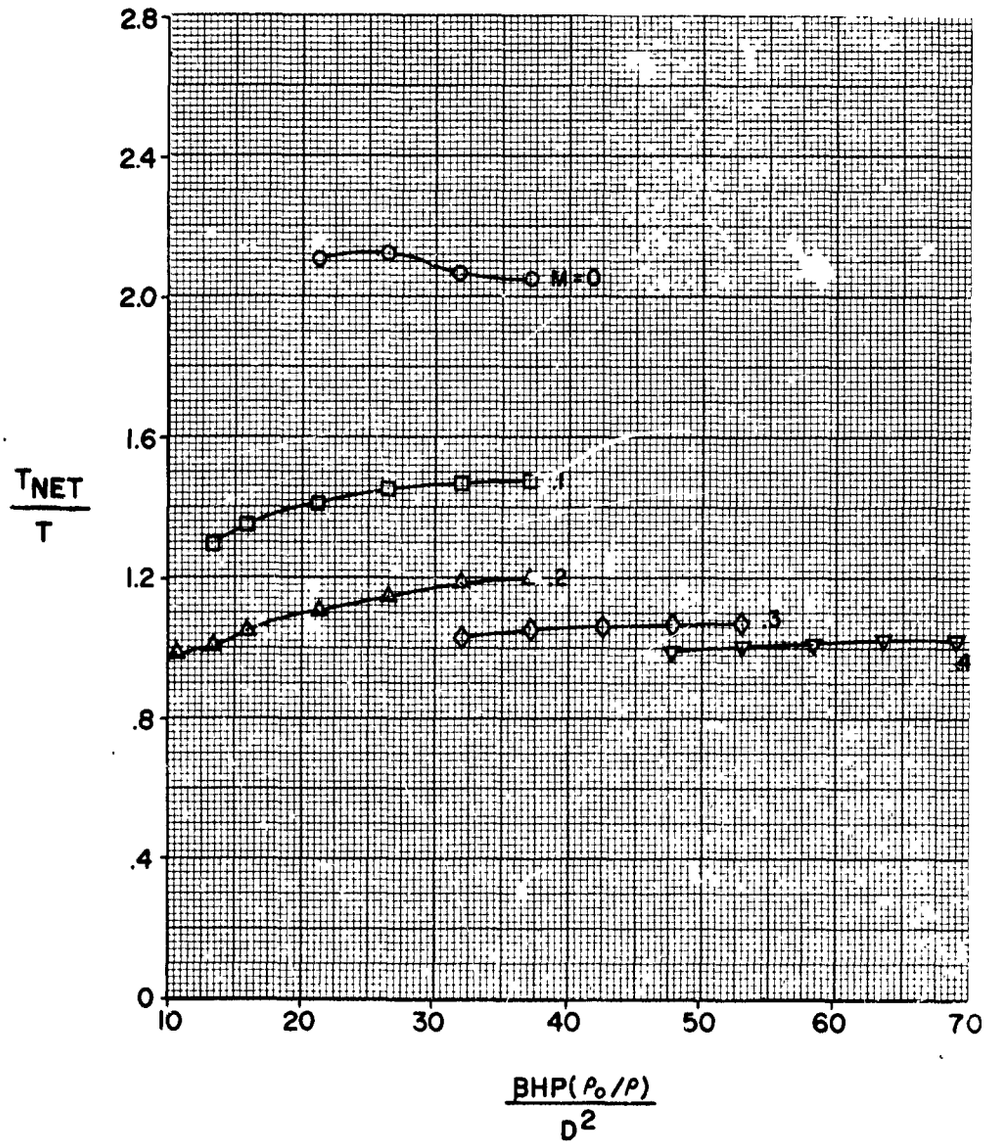

FIGURE 39

HS SHROUDED PROPELLER TEST

RATIO OF NET TO PROPELLER THRUST
CONFIGURATION B2-3WT
N=7000

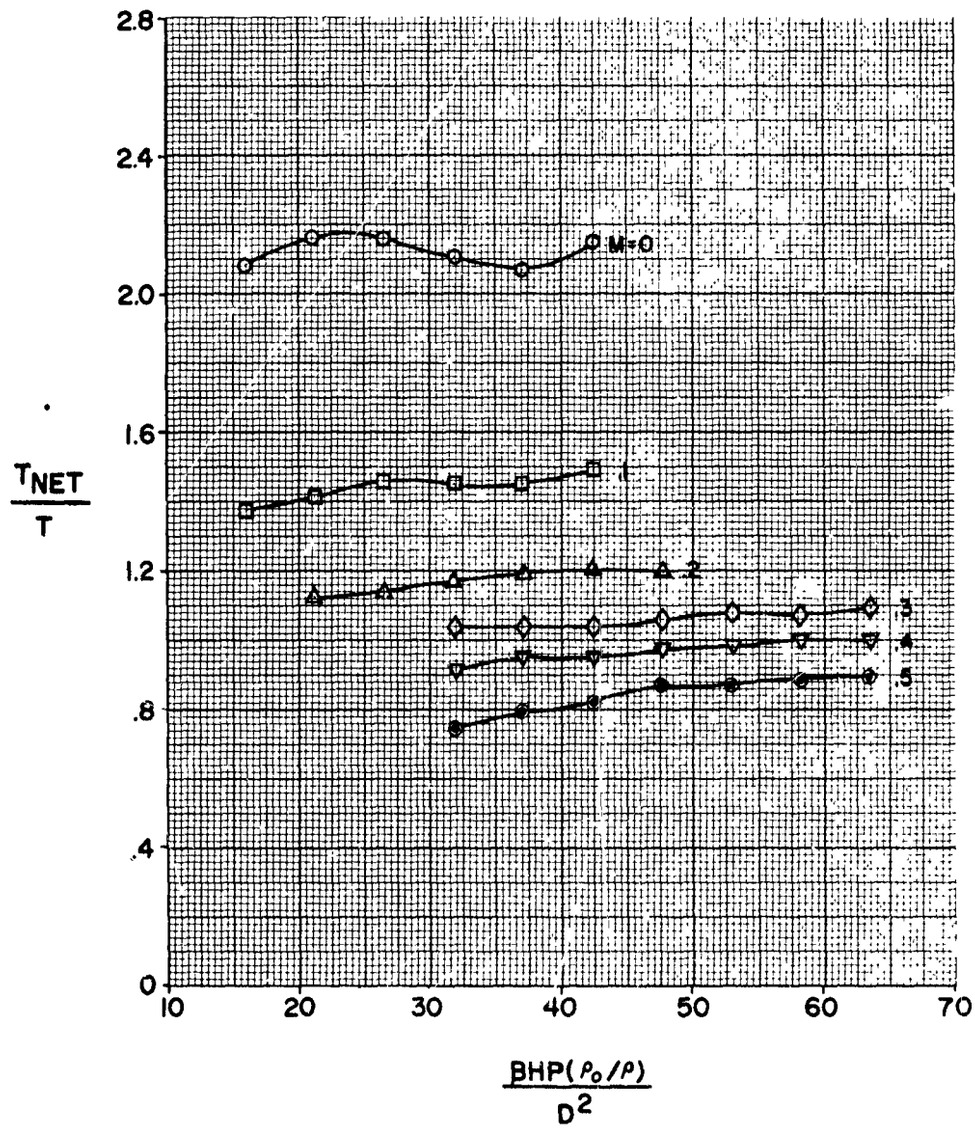

FIGURE 40

HS SHROUDED PROPELLER TEST

RATIO OF NET TO PROPELLER THRUST
CONFIGURATION B3-3WT
N=7000

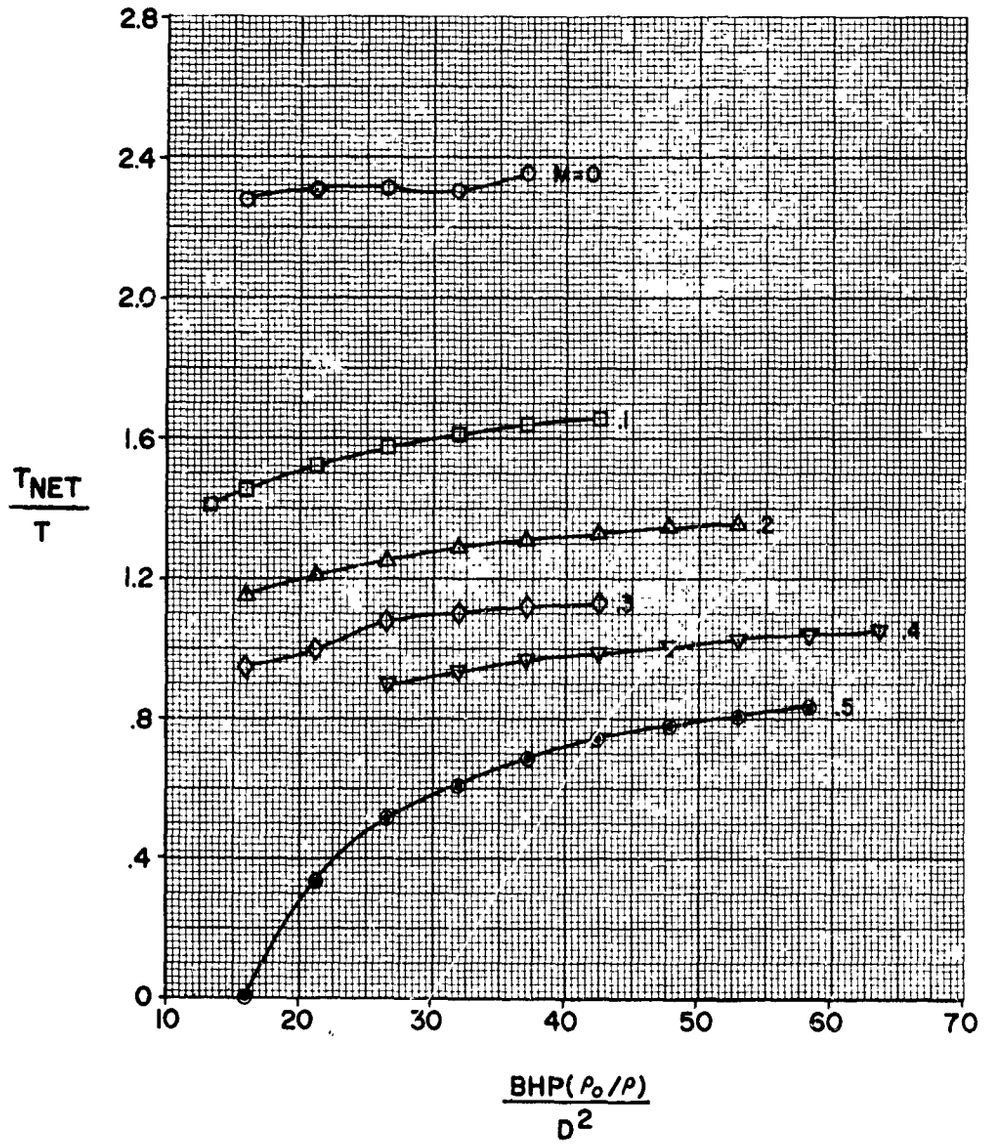

FIGURE 41

HS SHROUDED PROPELLER TEST

RATIO OF NET TO PROPELLER THRUST
CONFIGURATION B4-3WT
N=7000

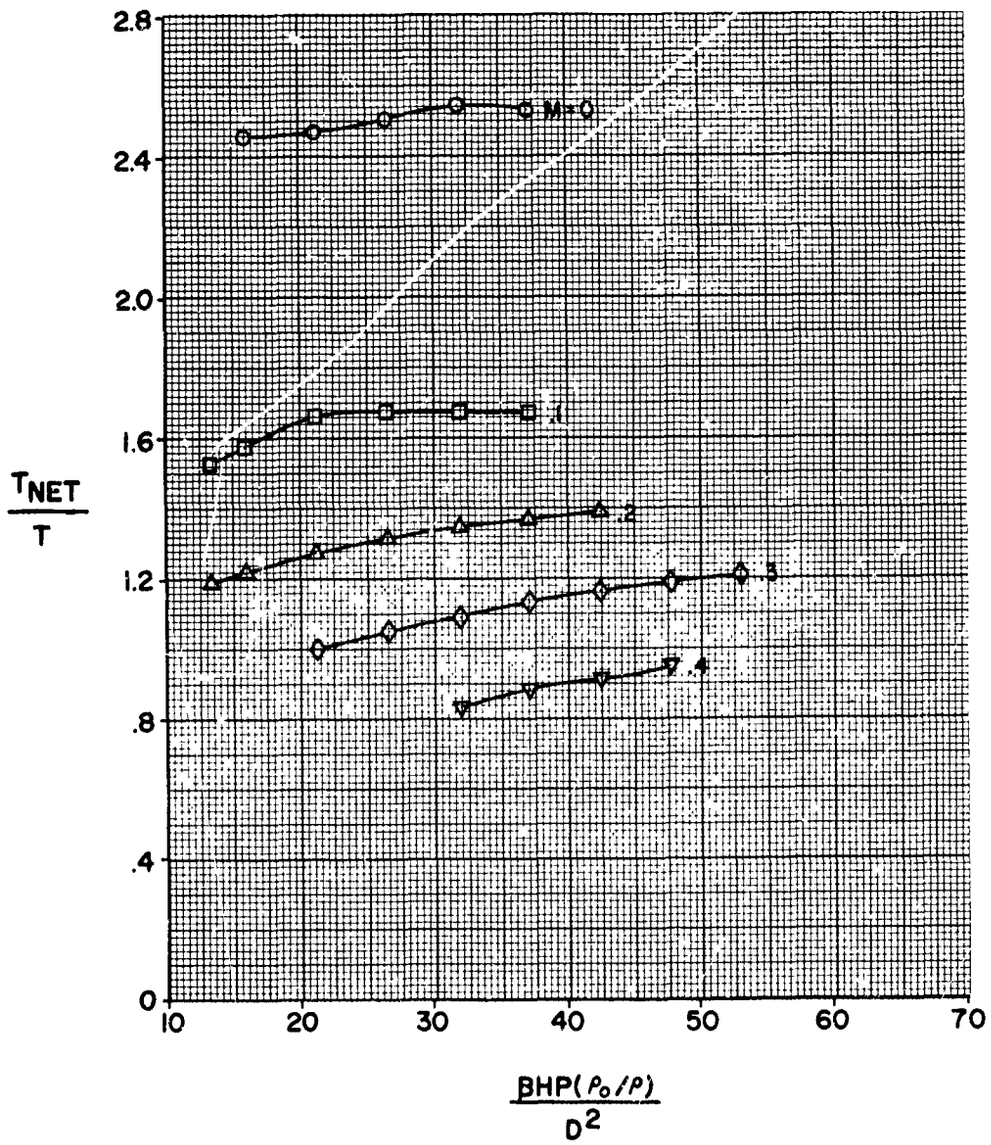

FIGURE 42

HS SHROUDED PROPELLER TEST

RATIO OF NET TO PROPELLER THRUST
CONFIGURATION B5-3WT
N=7000

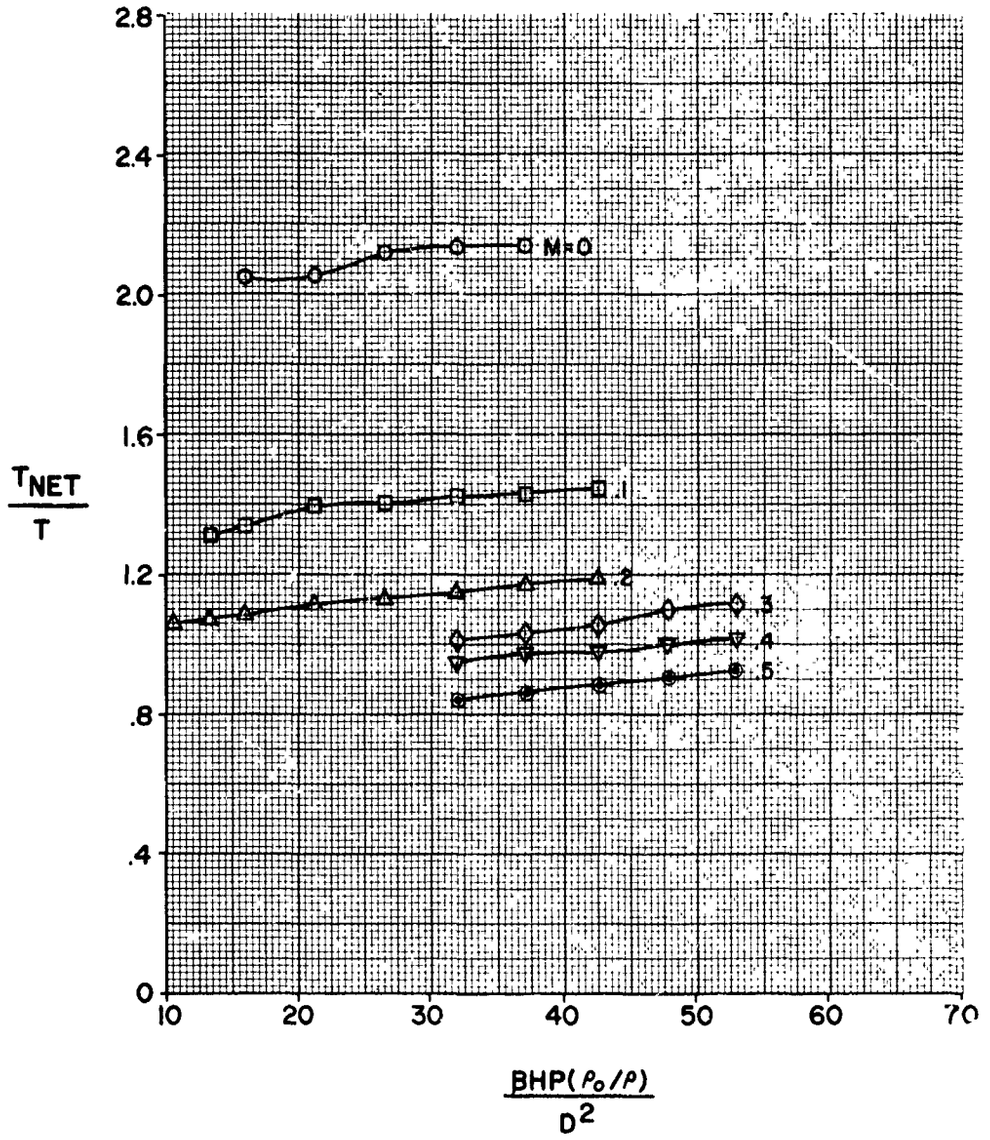

FIGURE 43

HS SHROUDED PROPELLER TEST

RATIO OF NET TO PROPELLER THRUST
CONFIGURATION B6-3WT
N=7000

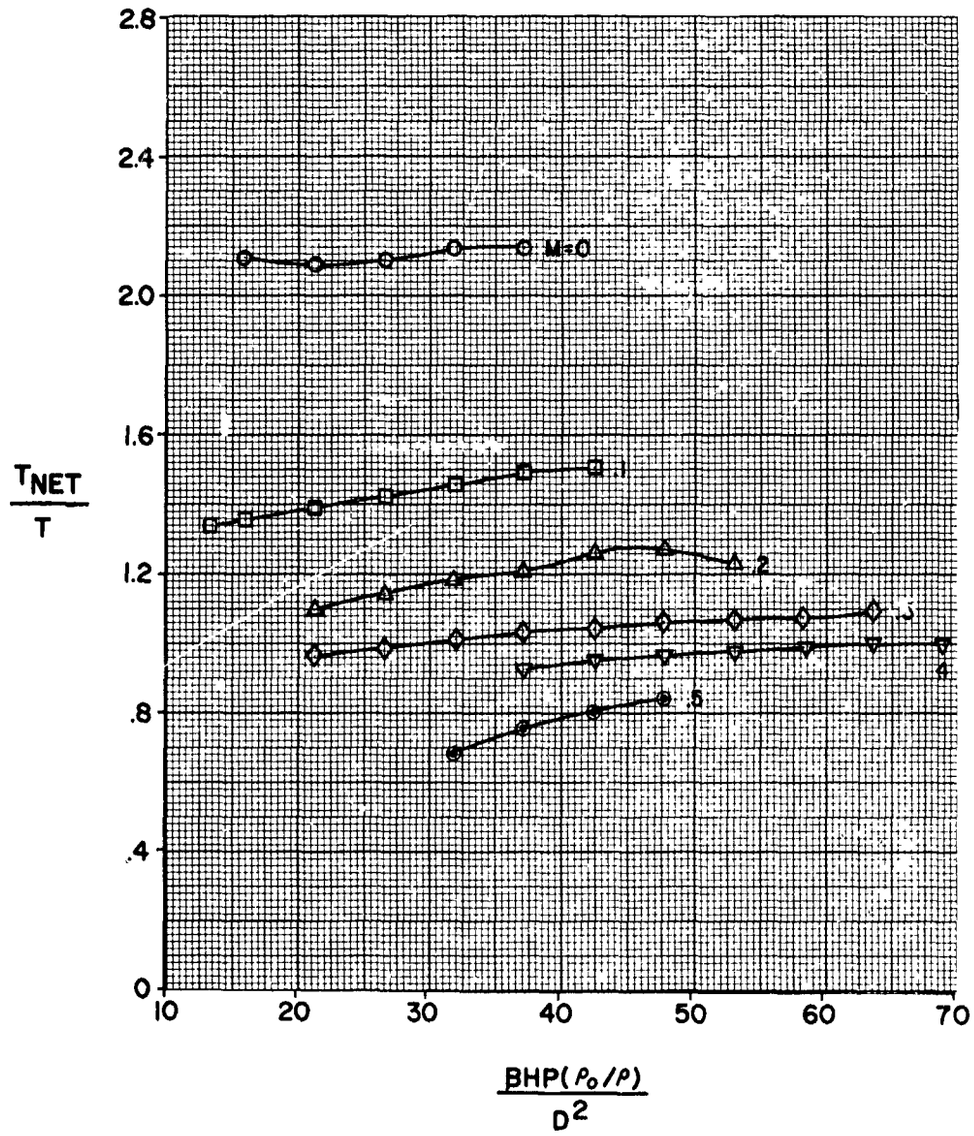

FIGURE 44

HS SHROUDED PROPELLER TEST

RATIO OF NET TO PROPELLER THRUST
CONFIGURATION B7-3NT
N=7000

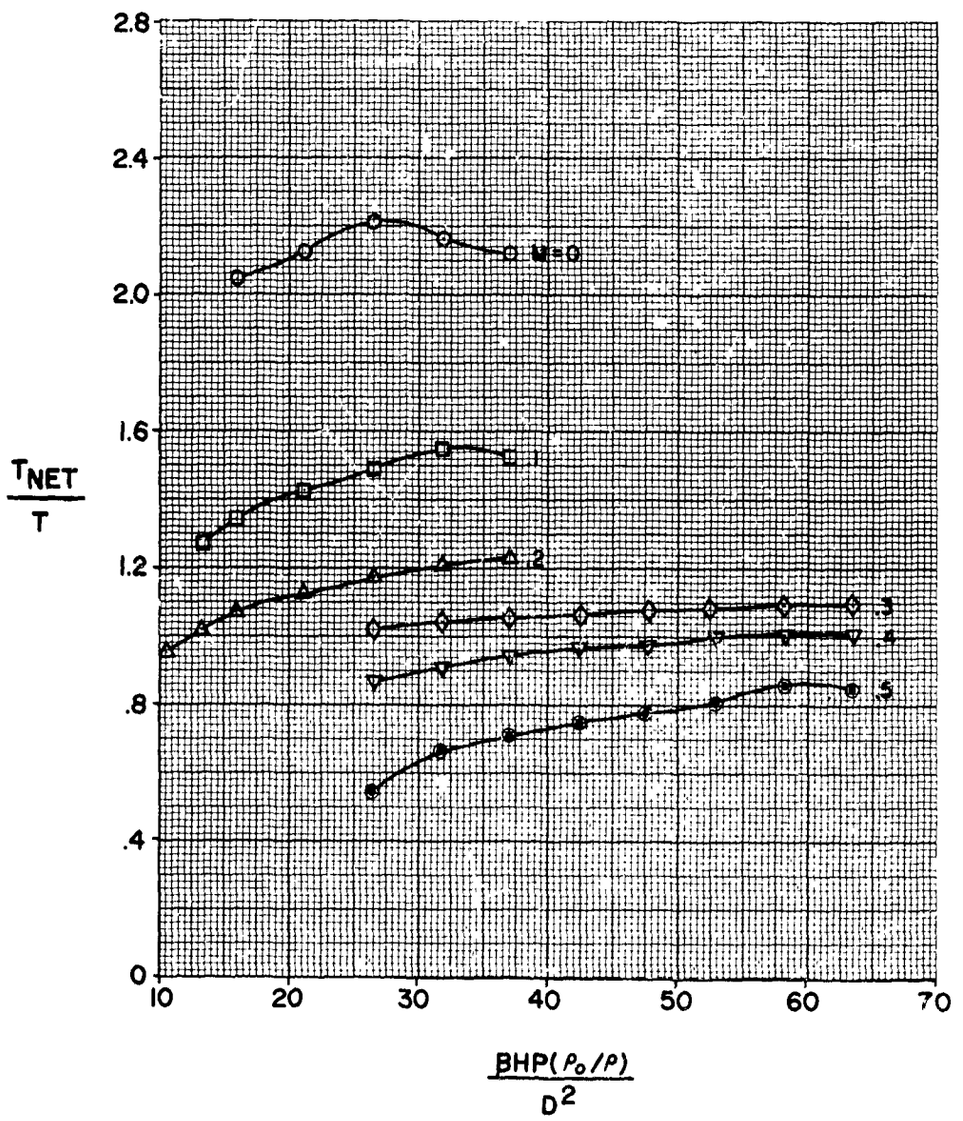

FIGURE 45

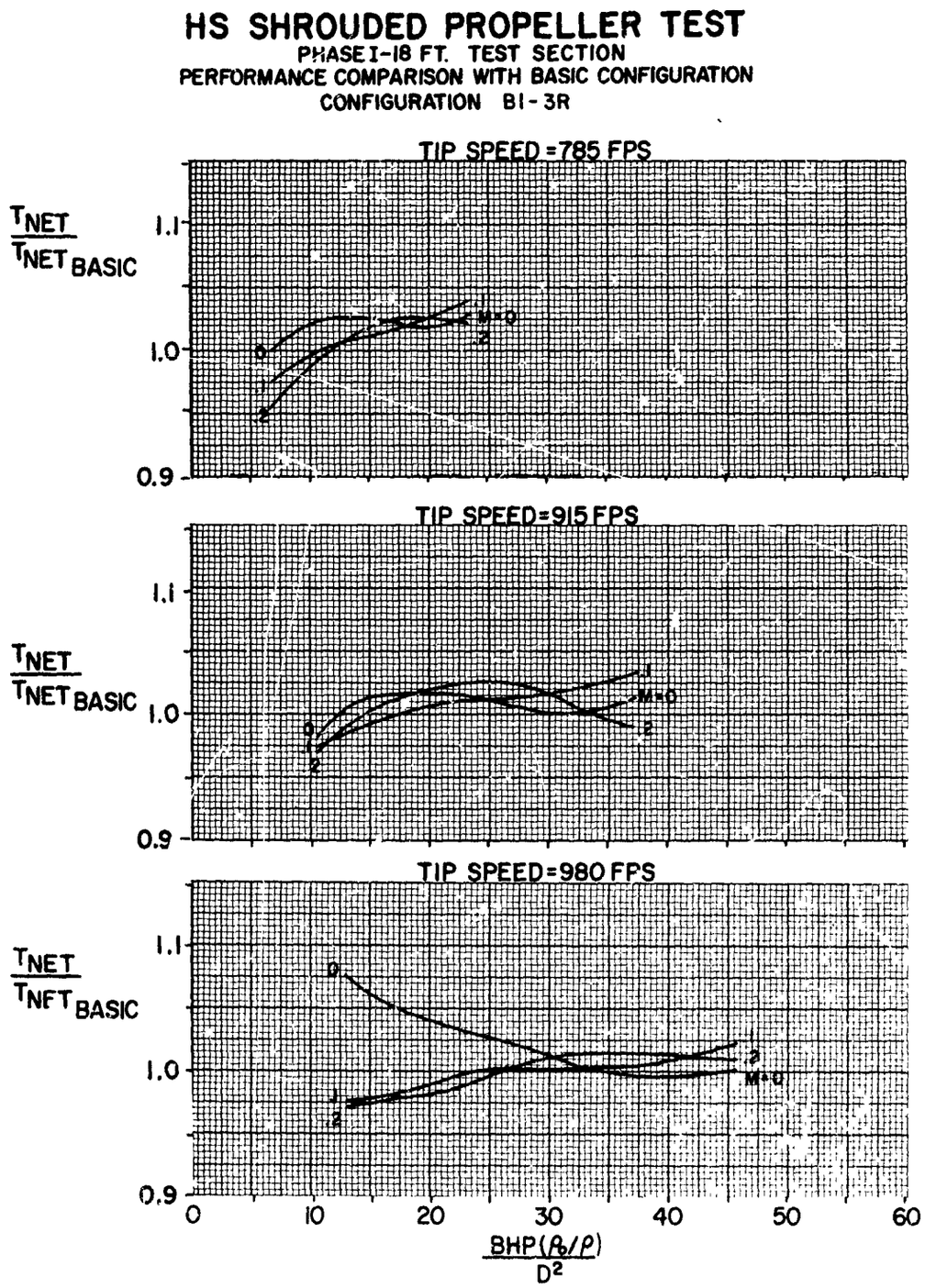
HS SHROUDED PROPELLER TEST
PHASE I-18 FT. TEST SECTION
PERFORMANCE COMPARISON WITH BASIC CONFIGURATION
CONFIGURATION B1-3R
TIP SPEED=785 FPS
TIP SPEED=915 FPS
TIP SPEED=980 FPS
TNET / TNET BASIC
TNET / TNFT BASIC
1.1
1.0
0.9
M=0
0
10
20
30
40
50
60
BHP(ρ0/ρ) / D2

FIGURE 46

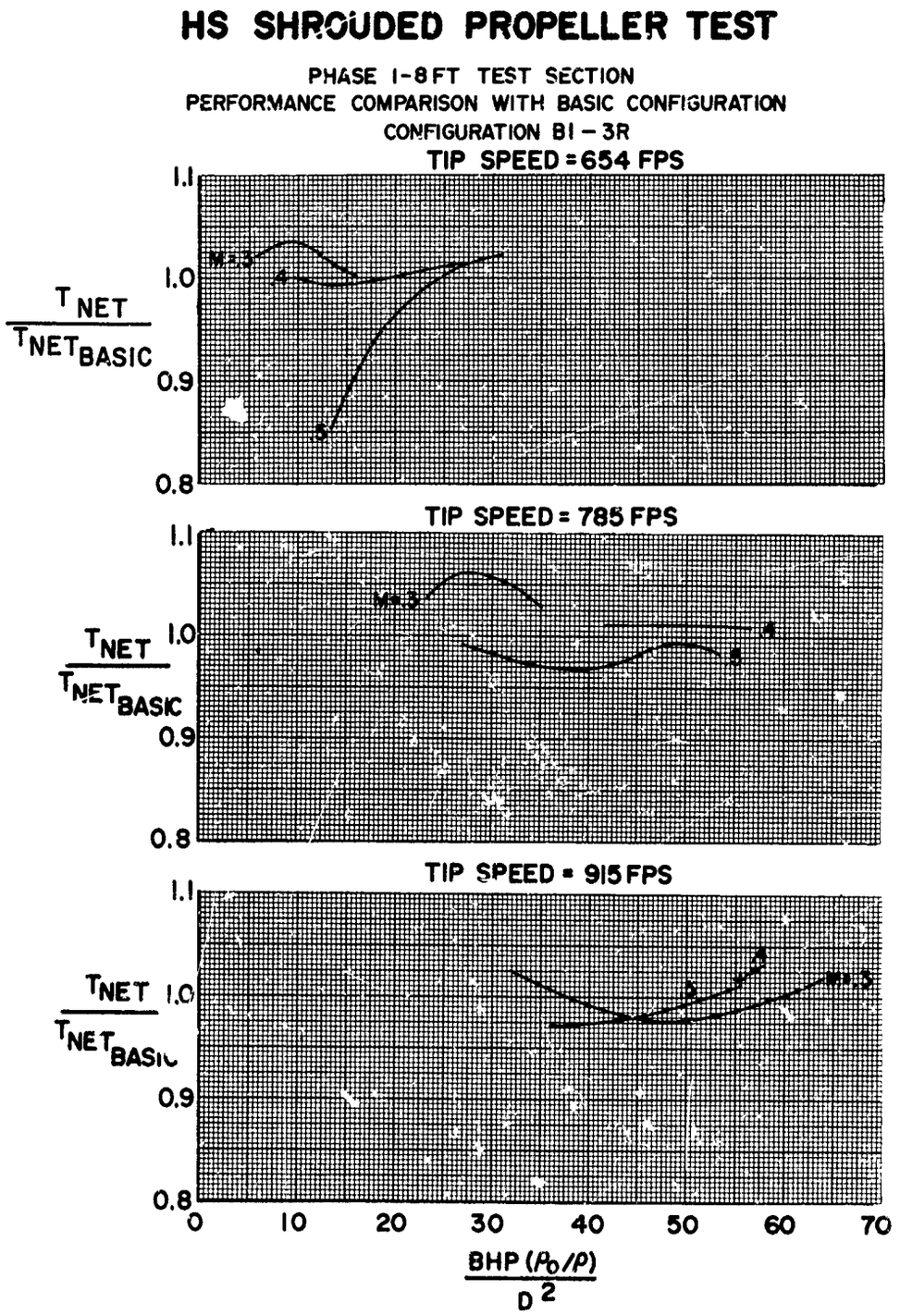
HS SHROUDED PROPELLER TEST
PHASE I-8 FT TEST SECTION
PERFORMANCE COMPARISON WITH BASIC CONFIGURATION
CONFIGURATION B1 – 3R
TIP SPEED = 654 FPS
TIP SPEED = 785 FPS
TIP SPEED = 915 FPS
T NET / T NET BASIC
1.1
1.0
0.9
0.8
M=.3
.4
.5
0
10
20
30
40
50
60
70
BHP (P0/P) / D 2

FIGURE 47

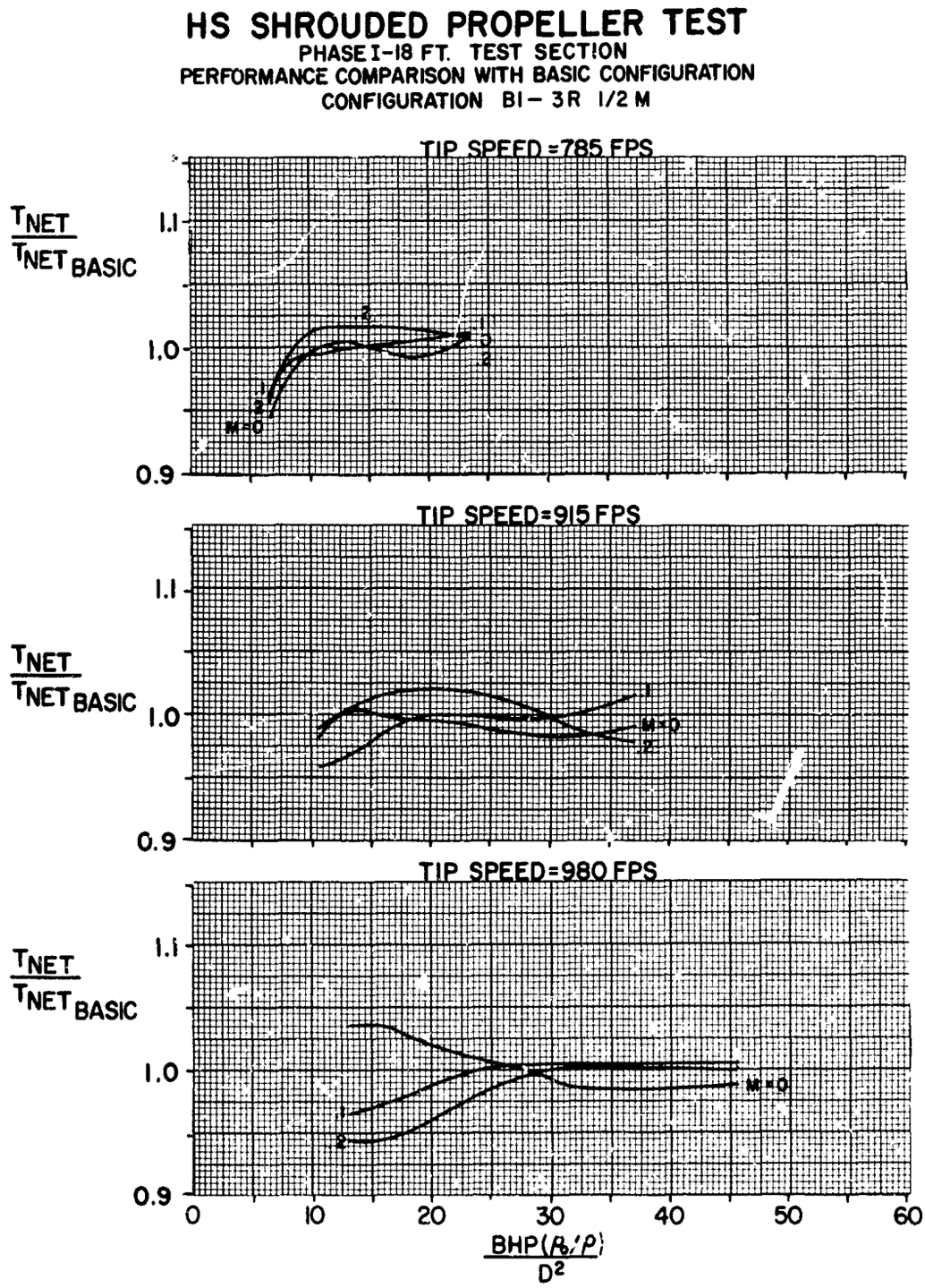
HS SHROUDED PROPELLER TEST
PHASE I-18 FT. TEST SECTION
PERFORMANCE COMPARISON WITH BASIC CONFIGURATION
CONFIGURATION BI-3R 1/2 M
TIP SPEED=785 FPS
TIP SPEED=915 FPS
TIP SPEED=980 FPS
TNET / TNET BASIC
1.1
1.0
0.9
M=0
0
10
20
30
40
50
60
BHP(Ab/P) / D2

FIGURE 48

HS SHROUDED PROPELLER TEST

PHASE 1-8 FT TEST SECTION
PERFORMANCE COMPARISON WITH BASIC CONFIGURATION
CONFIGURATION B1-3R 1/2 M

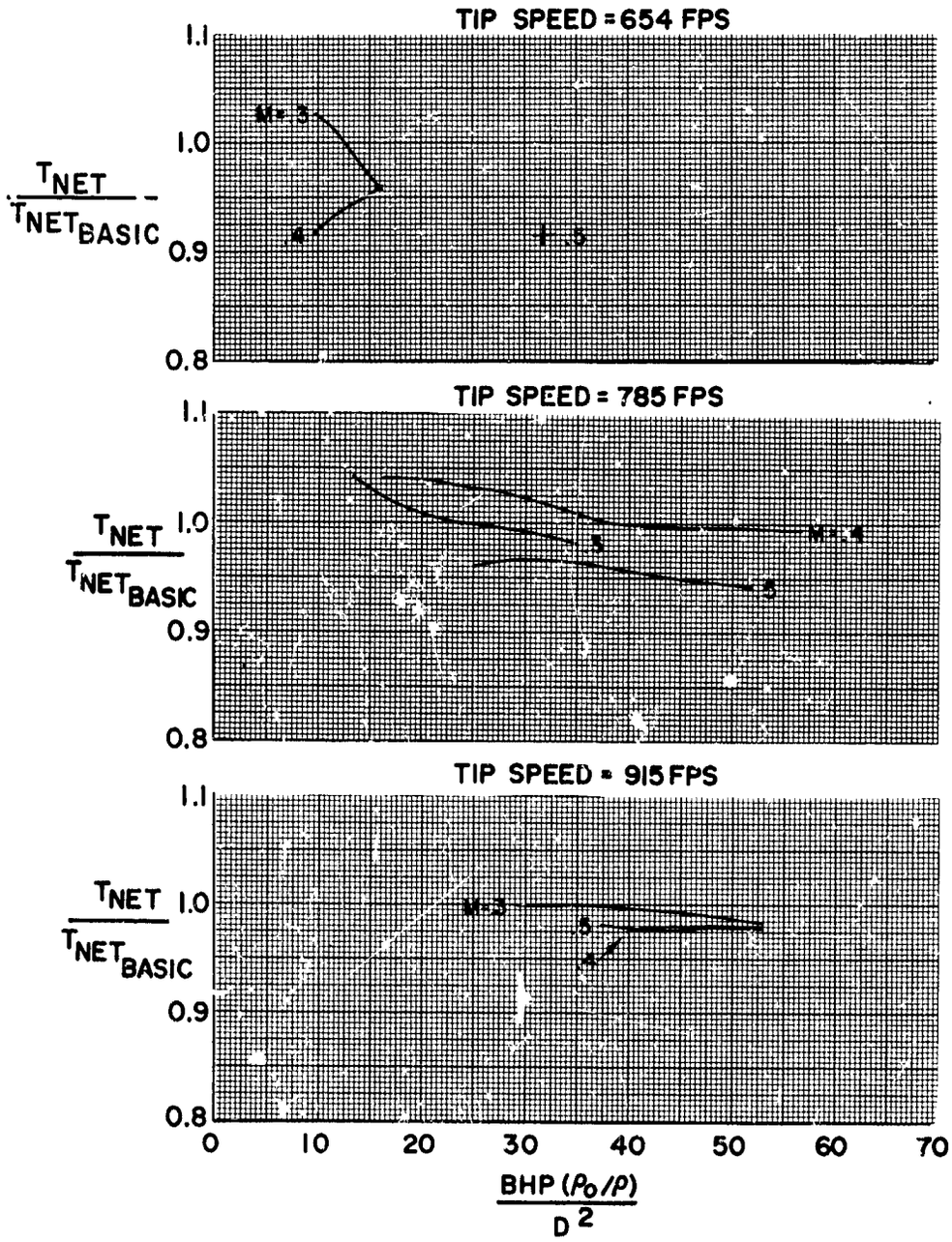

FIGURE 49

HS SHROUDED PROPELLER TEST

PHASE I-18 FT. TEST SECTION
PERFORMANCE COMPARISON WITH BASIC CONFIGURATION
CONFIGURATION B1-3RM

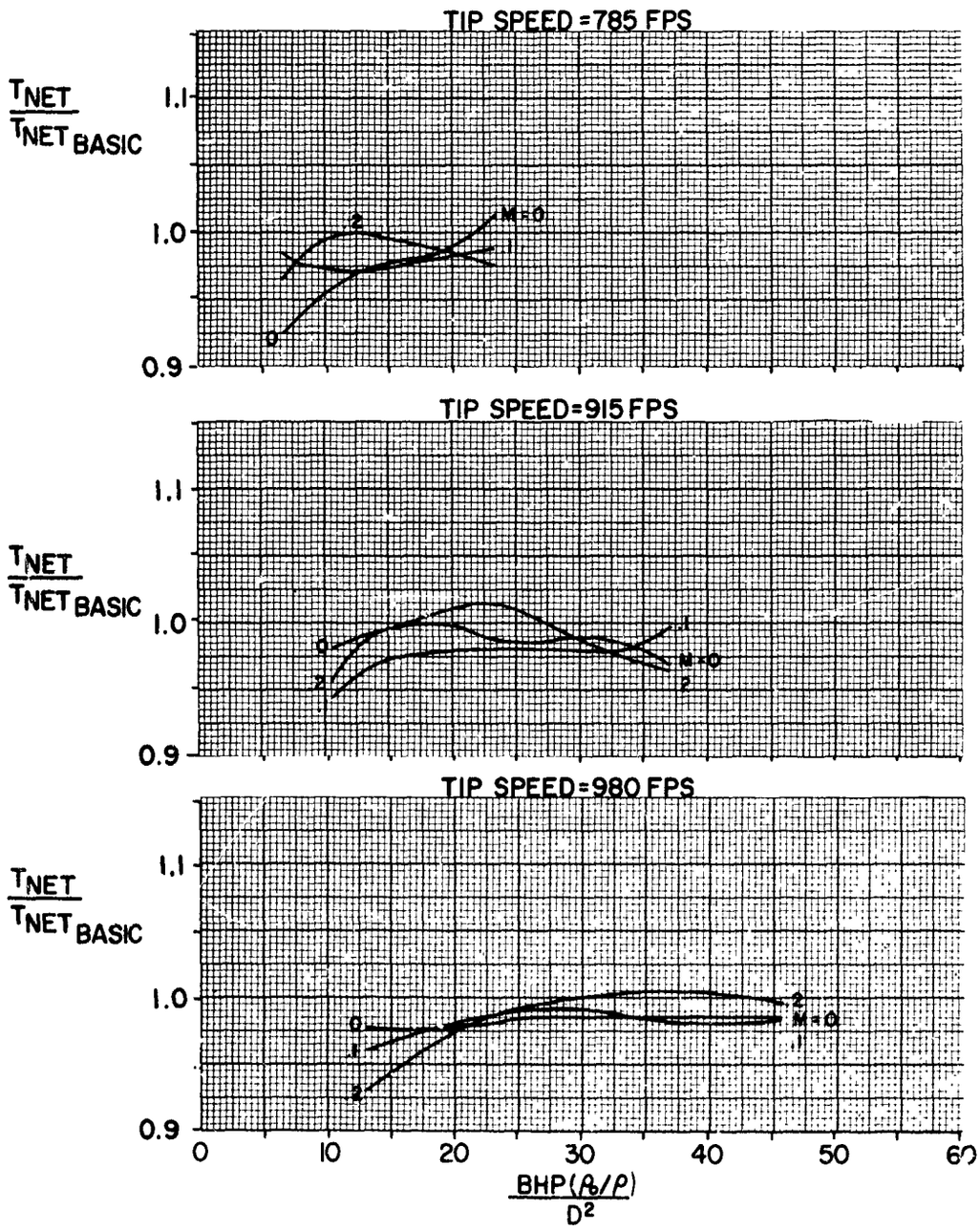

FIGURE 50

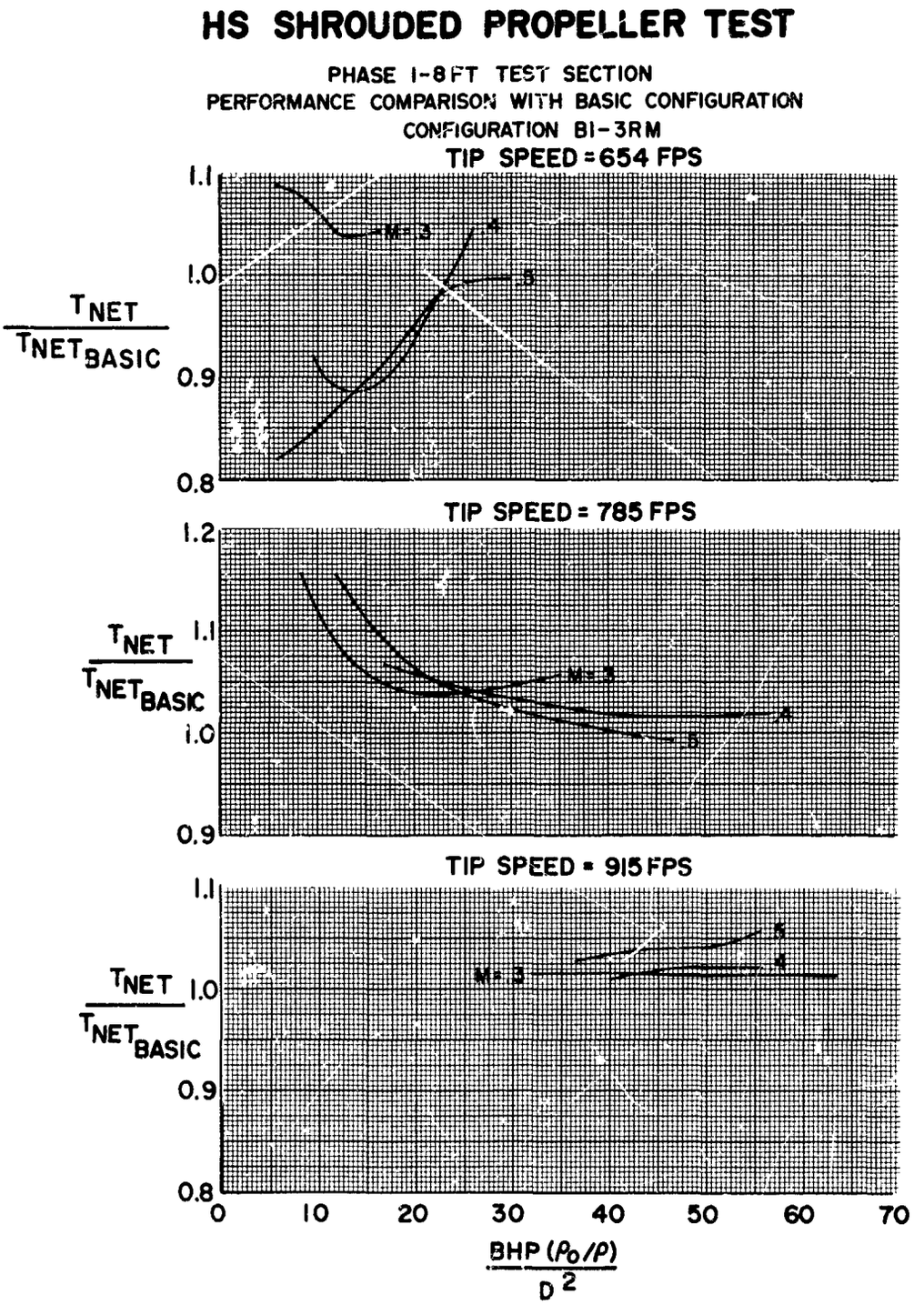
HS SHROUDED PROPELLER TEST
PHASE I-8 FT TEST SECTION
PERFORMANCE COMPARISON WITH BASIC CONFIGURATION
CONFIGURATION BI-3RM
TIP SPEED = 654 FPS
TIP SPEED = 785 FPS
TIP SPEED = 915 FPS
T_NET / T_NET BASIC
M = .3
.4
.5
1.1
1.0
0.9
0.8
1.2
0
10
20
30
40
50
60
70
BHP (ρ0/ρ) / D 2

FIGURE 51

HS SHROUDED PROPELLER TEST

PHASE I-18 FT. TEST SECTION
PERFORMANCE COMPARISON WITH BASIC CONFIGURATION
CONFIGURATION B1-3NT

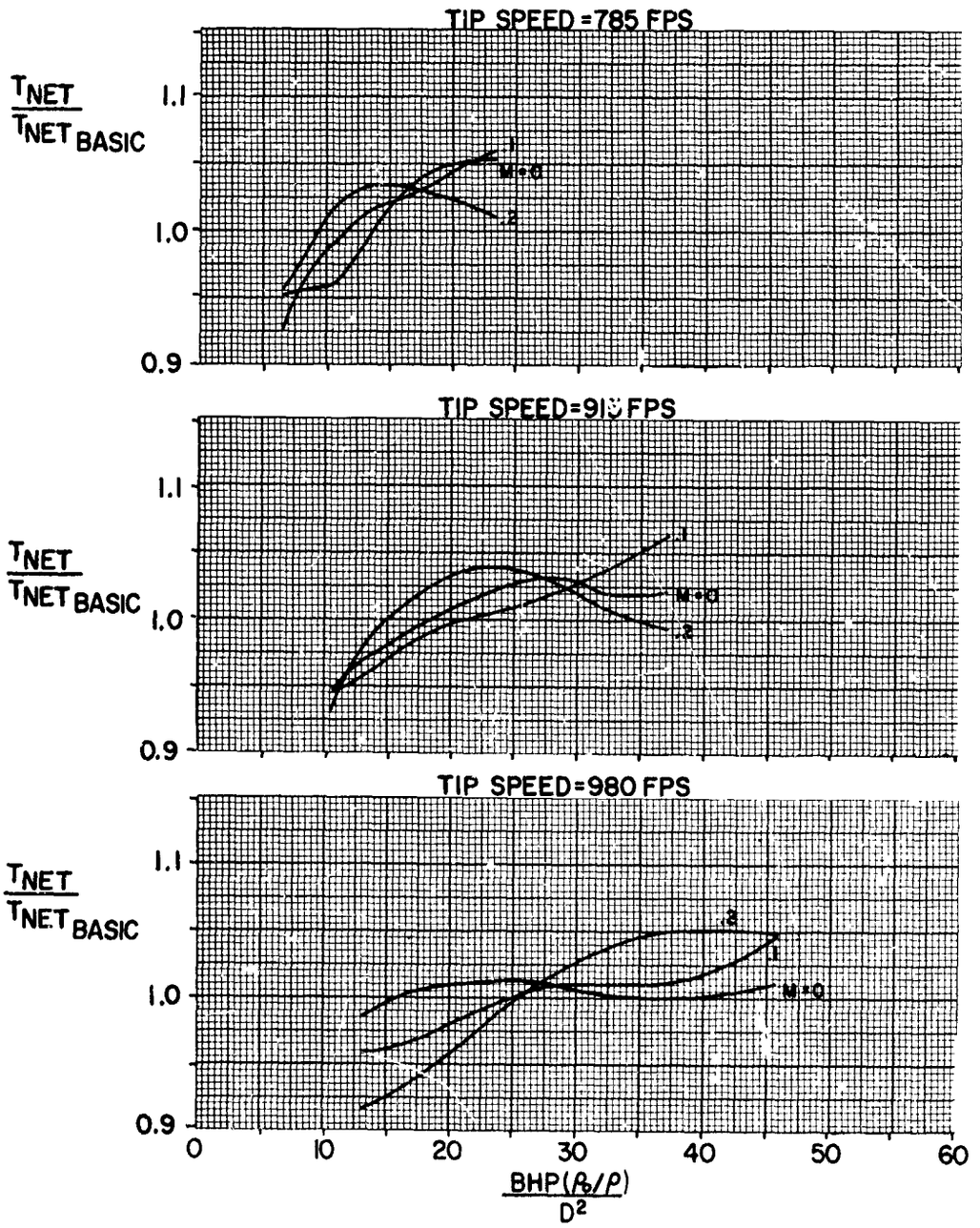

FIGURE 52

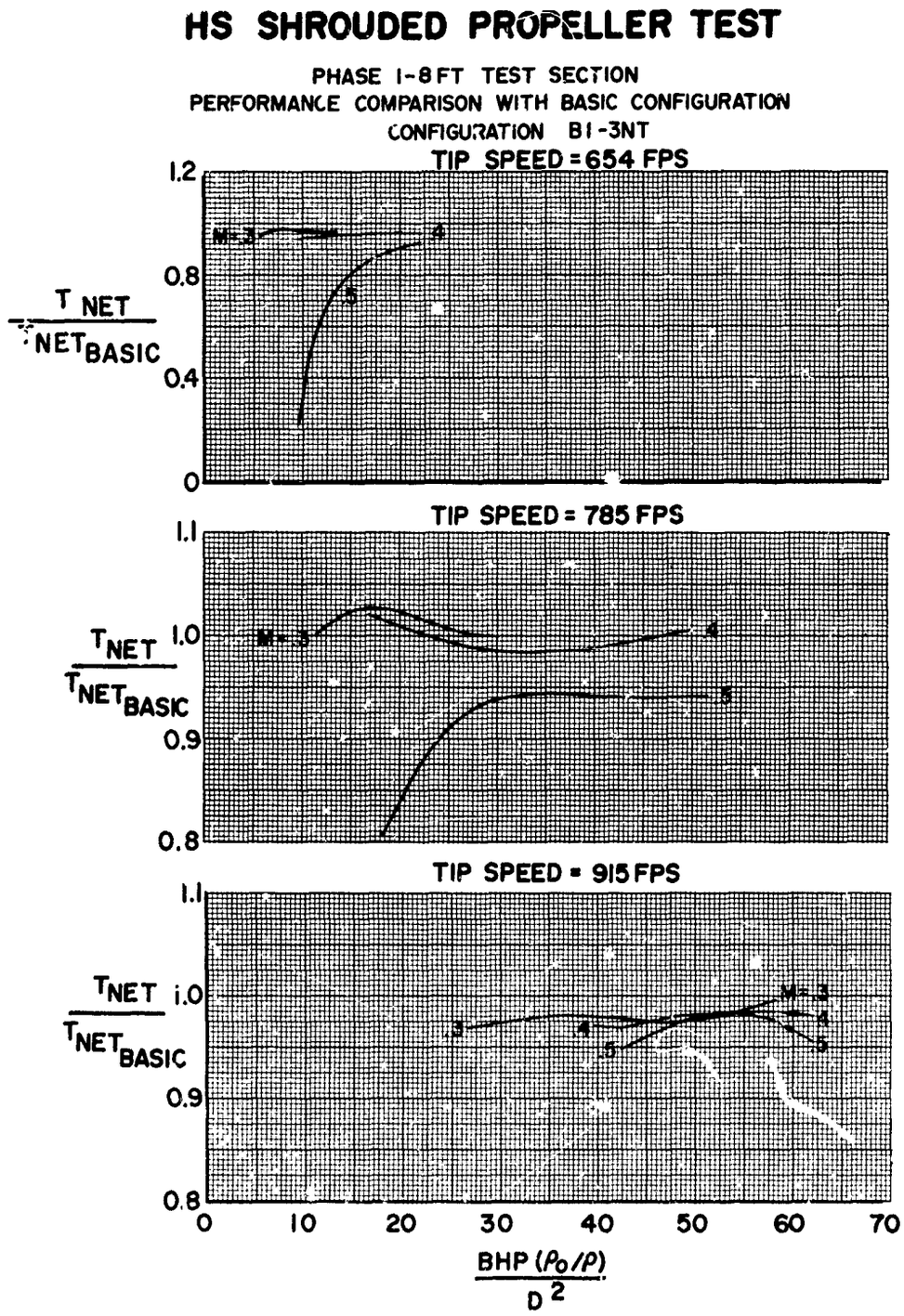
HS SHROUDED PROPELLER TEST
PHASE I-8 FT TEST SECTION
PERFORMANCE COMPARISON WITH BASIC CONFIGURATION
CONFIGURATION B1-3NT
TIP SPEED = 654 FPS
TIP SPEED = 785 FPS
TIP SPEED = 915 FPS
T NET / T NET BASIC
M=.3
.4
.5
1.2
1.1
1.0
0.9
0.8
0.4
0
10
20
30
40
50
60
70
BHP (ρ0/ρ) / D 2

FIGURE 53

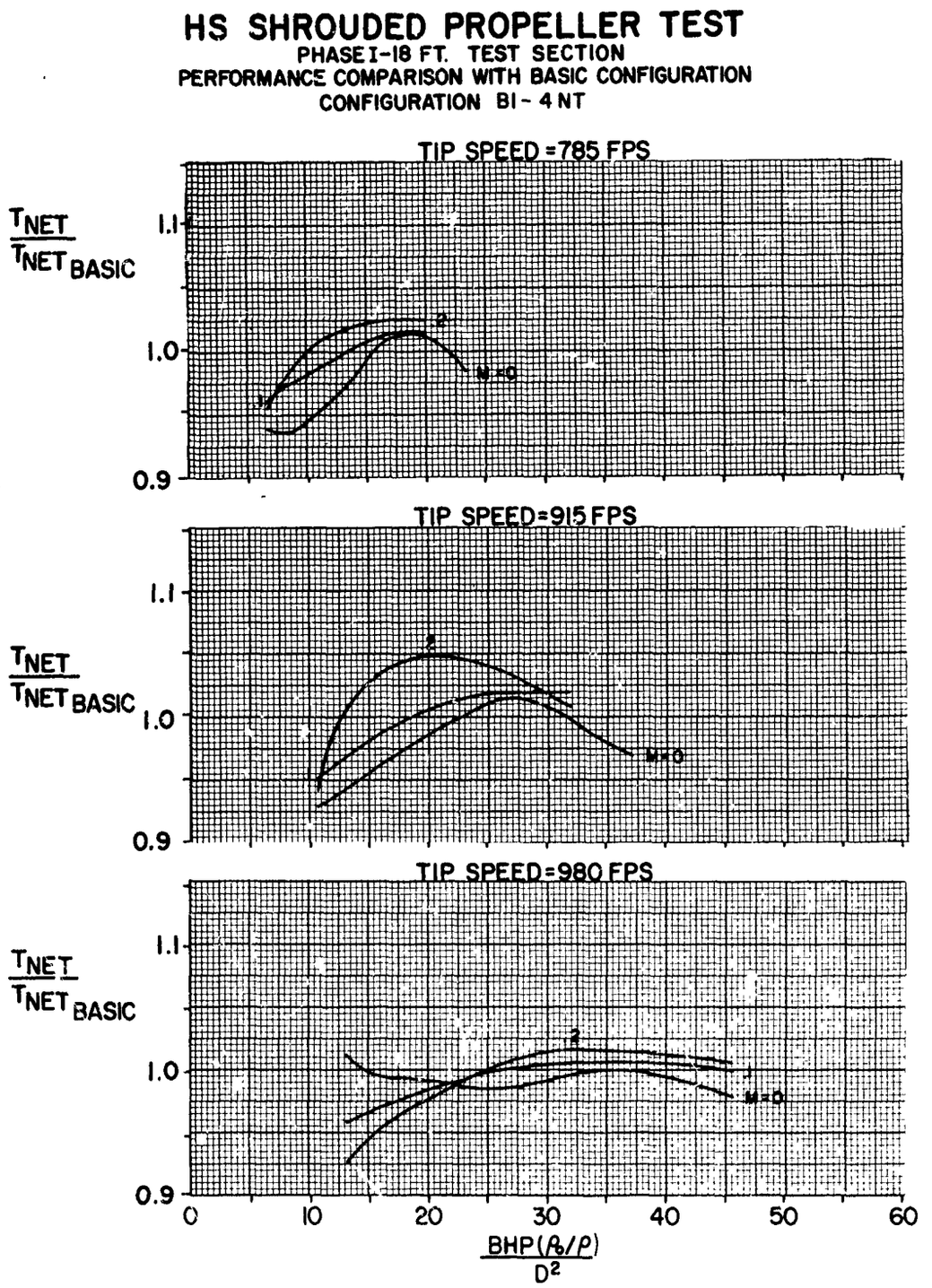
HS SHROUDED PROPELLER TEST
PHASE I-18 FT. TEST SECTION
PERFORMANCE COMPARISON WITH BASIC CONFIGURATION
CONFIGURATION BI-4NT
TIP SPEED=785 FPS
TIP SPEED=915 FPS
TIP SPEED=980 FPS
TNET / TNET BASIC
1.1
1.0
0.9
M=0
0
10
20
30
40
50
60
BHP(ρ0/ρ) / D2

FIGURE 54

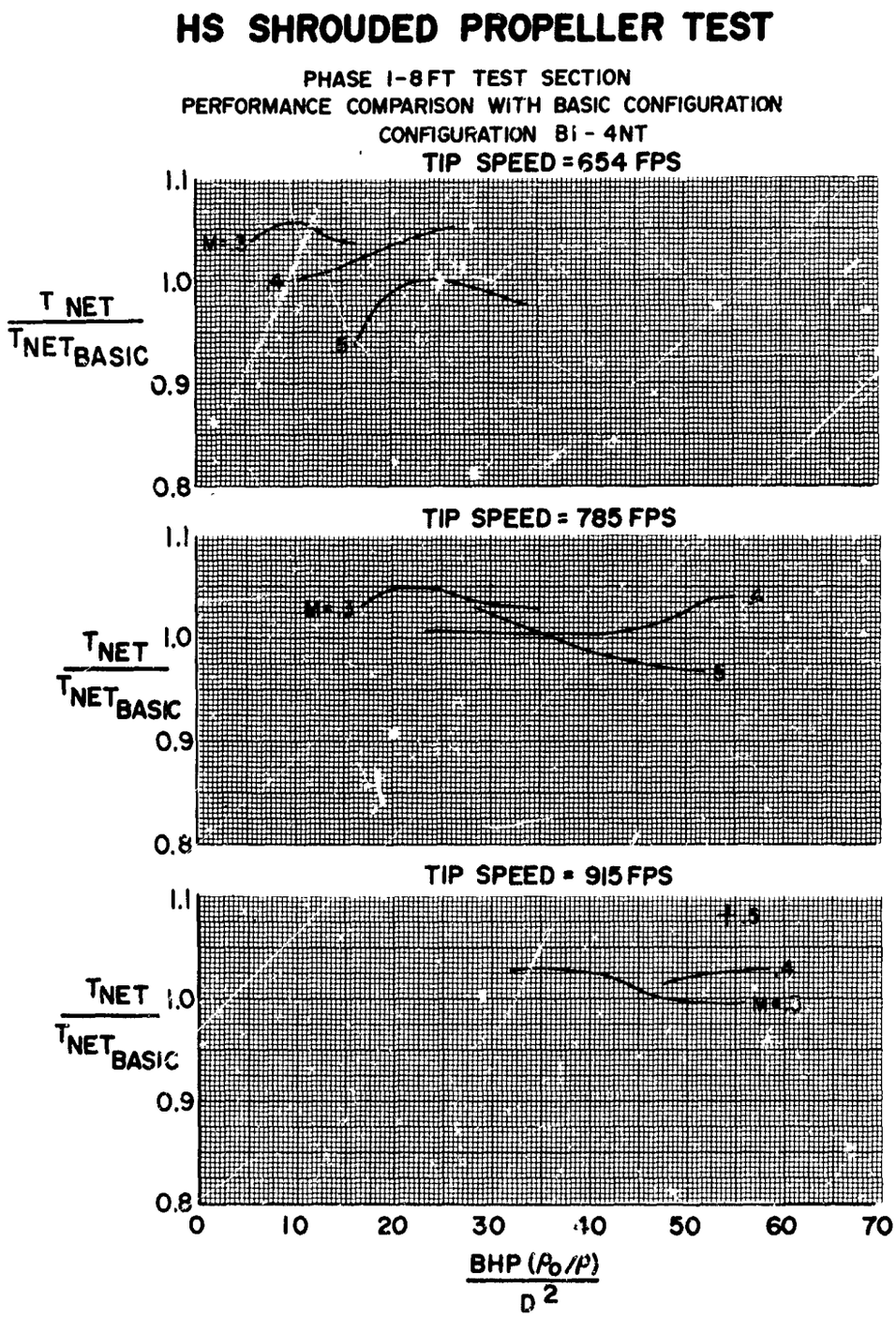
HS SHROUDED PROPELLER TEST
PHASE I-8 FT TEST SECTION
PERFORMANCE COMPARISON WITH BASIC CONFIGURATION
CONFIGURATION B1 - 4NT
TIP SPEED = 654 FPS
TIP SPEED = 785 FPS
TIP SPEED = 915 FPS
T NET / T NET BASIC
1.1
1.0
0.9
0.8
0
10
20
30
40
50
60
70
BHP (Po/P) / D 2

FIGURE 55

HS SHROUDED PROPELLER TEST

PHASE I-18 FT. TEST SECTION
PERFORMANCE COMPARISON WITH BASIC CONFIGURATION
CONFIGURATION B2-3WT

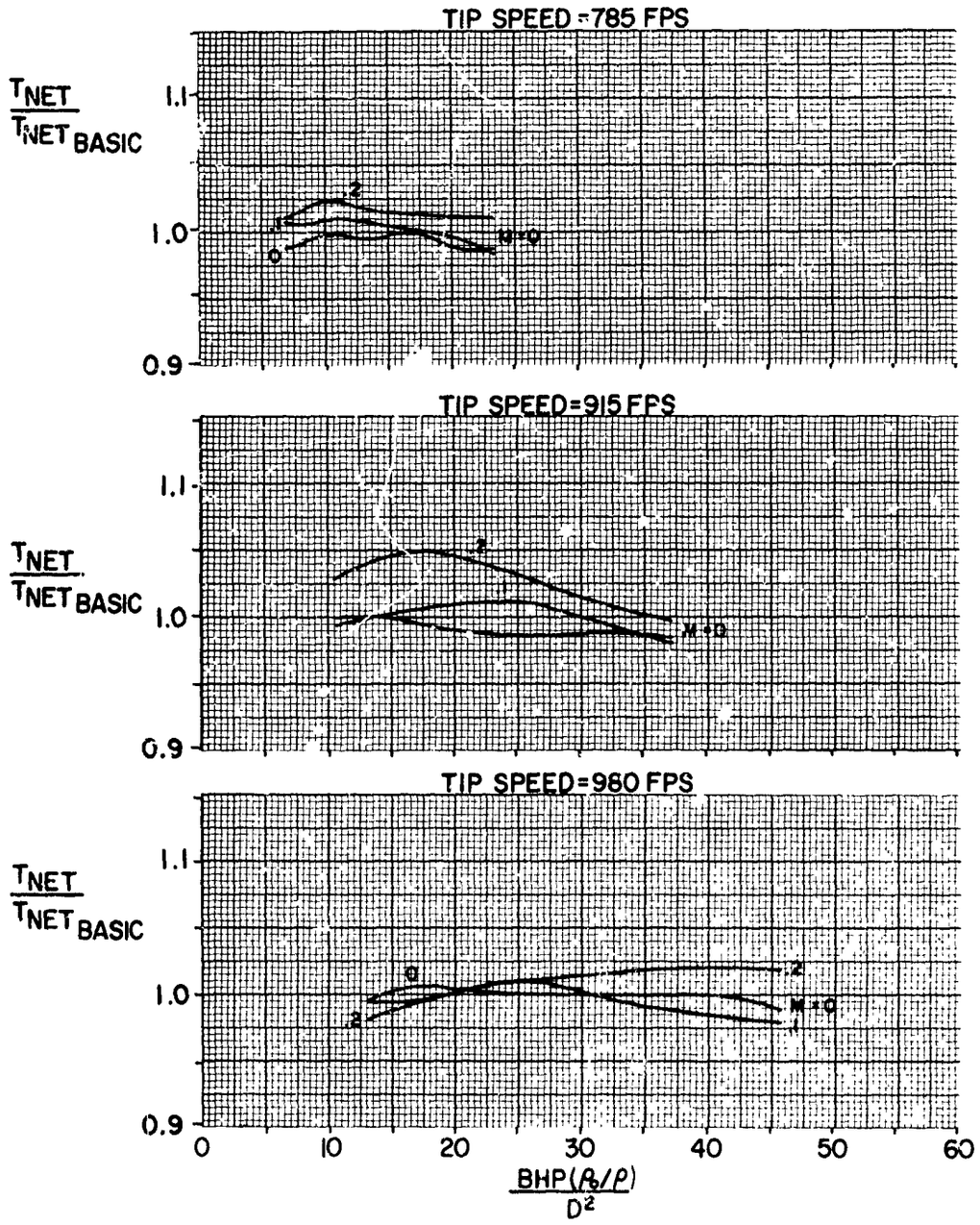

FIGURE 56

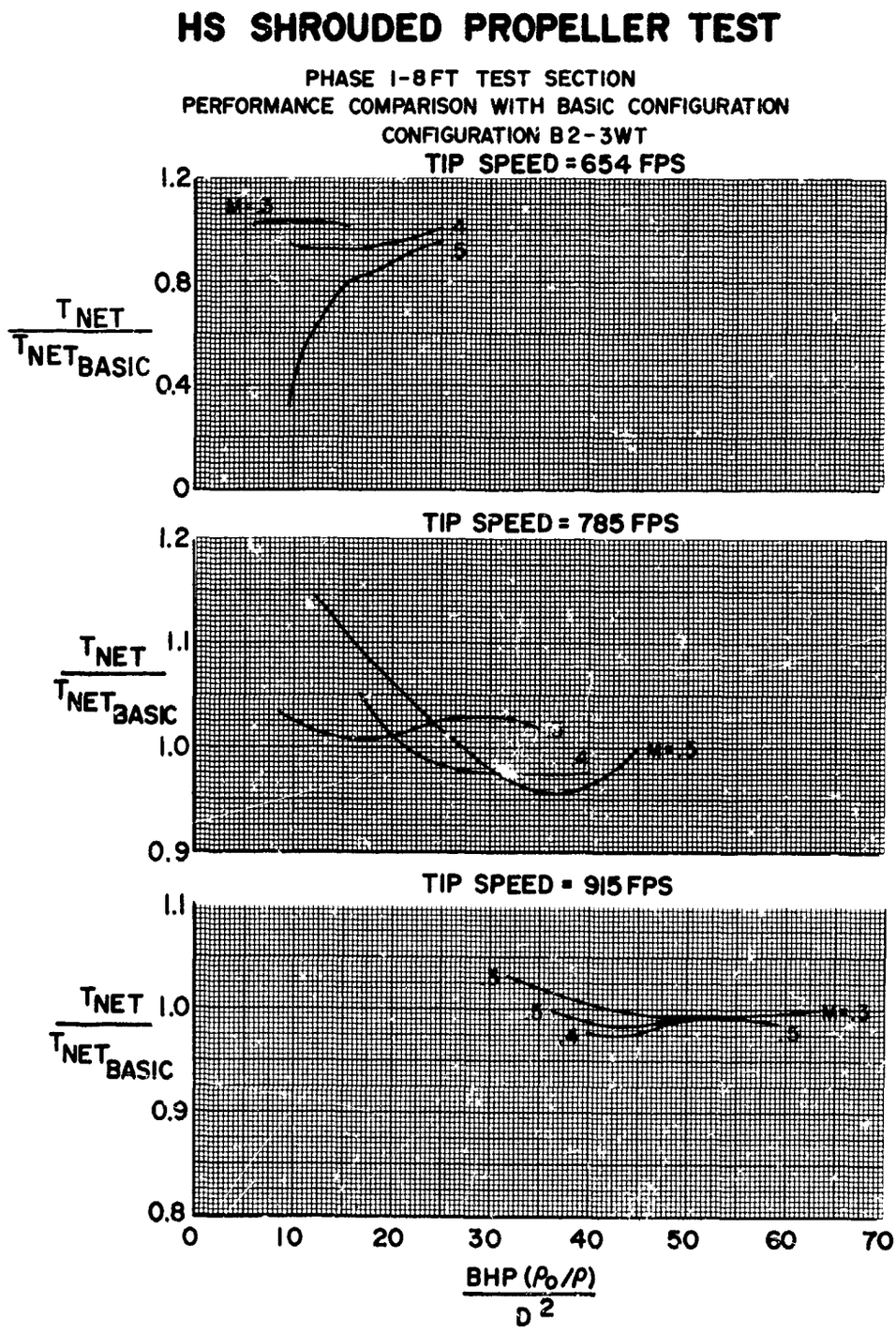
HS SHROUDED PROPELLER TEST
PHASE I-8 FT TEST SECTION
PERFORMANCE COMPARISON WITH BASIC CONFIGURATION
CONFIGURATION B2-3WT
TIP SPEED = 654 FPS
TIP SPEED = 785 FPS
TIP SPEED = 915 FPS
T NET / T NET BASIC
BHP (ρ0/ρ) / D 2
1.2
1.1
1.0
0.9
0.8
0.4
0
10
20
30
40
50
60
70
M=.3
M=.5
4
5

FIGURE 57

HS SHROUDED PROPELLER TEST

PHASE I-18 FT. TEST SECTION
PERFORMANCE COMPARISON WITH BASIC CONFIGURATION
CONFIGURATION B3-3WT

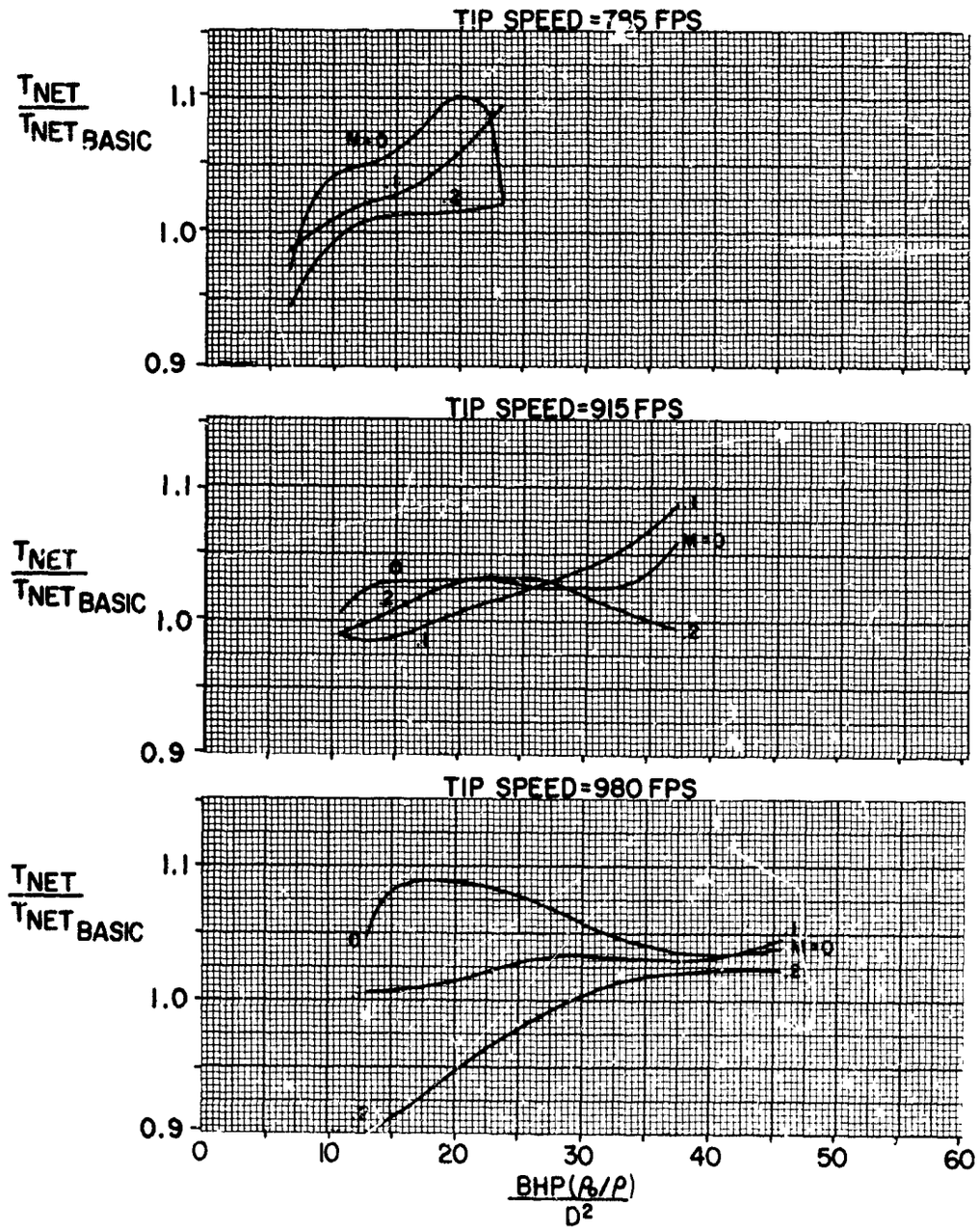

FIGURE 58

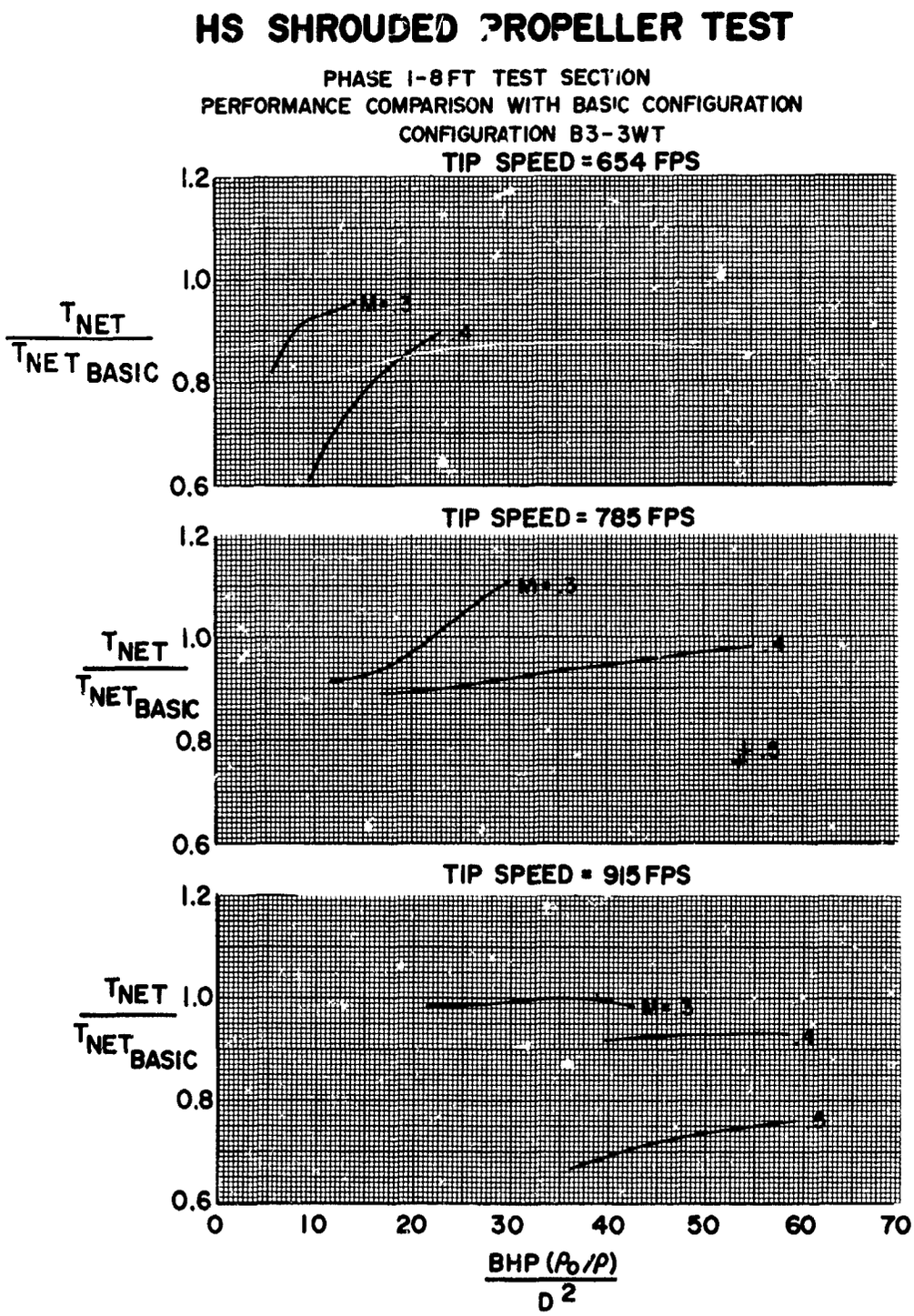
HS SHROUDED PROPELLER TEST
PHASE I-8 FT TEST SECTION
PERFORMANCE COMPARISON WITH BASIC CONFIGURATION
CONFIGURATION B3-3WT
TIP SPEED = 654 FPS
TIP SPEED = 785 FPS
TIP SPEED = 915 FPS
T_NET / T_NET BASIC
1.2
1.0
0.8
0.6
M = .3
.4
.5
0
10
20
30
40
50
60
70
BHP (ρ0/ρ) / D²

FIGURE 59

HS SHROUDED PROPELLER TEST

PHASE I-18 FT. TEST SECTION
PERFORMANCE COMPARISON WITH BASIC CONFIGURATION
CONFIGURATION E 4-3WT

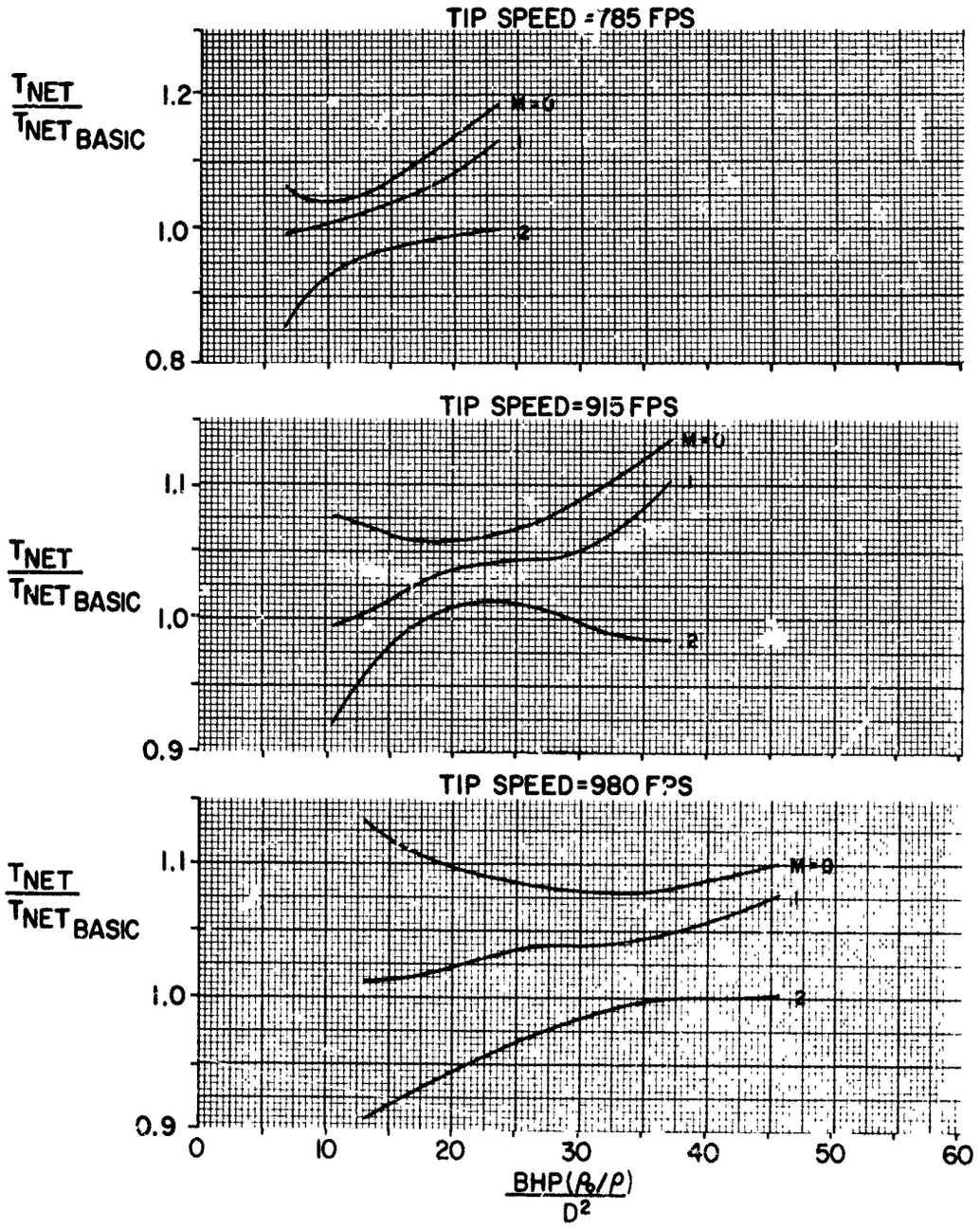

FIGURE 60

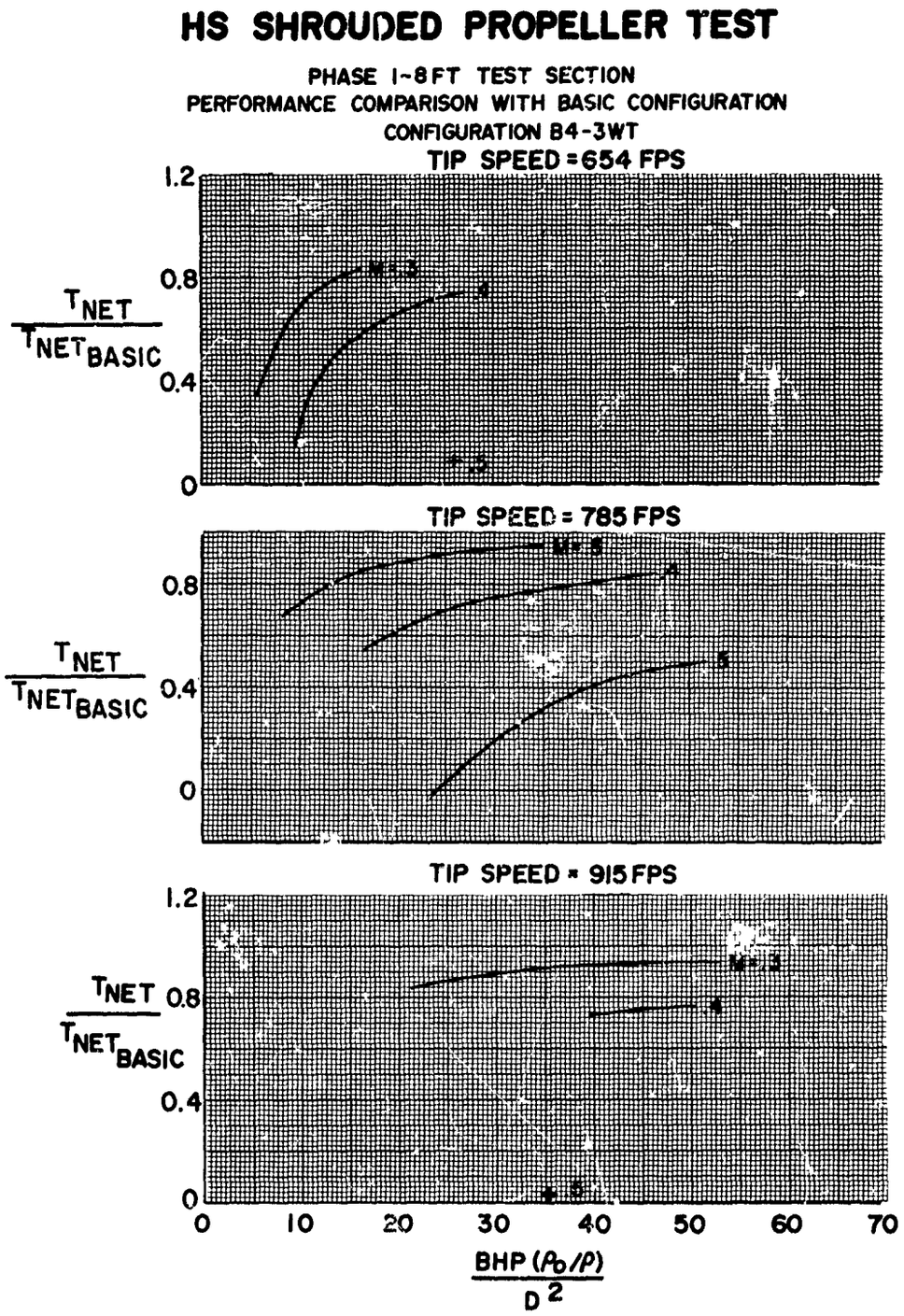
HS SHROUDED PROPELLER TEST
PHASE I-8 FT TEST SECTION
PERFORMANCE COMPARISON WITH BASIC CONFIGURATION
CONFIGURATION B4-3WT
TIP SPEED = 654 FPS
TIP SPEED = 785 FPS
TIP SPEED = 915 FPS
$T_{NET} / T_{NET_{BASIC}}$
1.2
0.8
0.4
0
0
10
20
30
40
50
60
70
$BHP (\rho_0/\rho) / D^2$

FIGURE 61

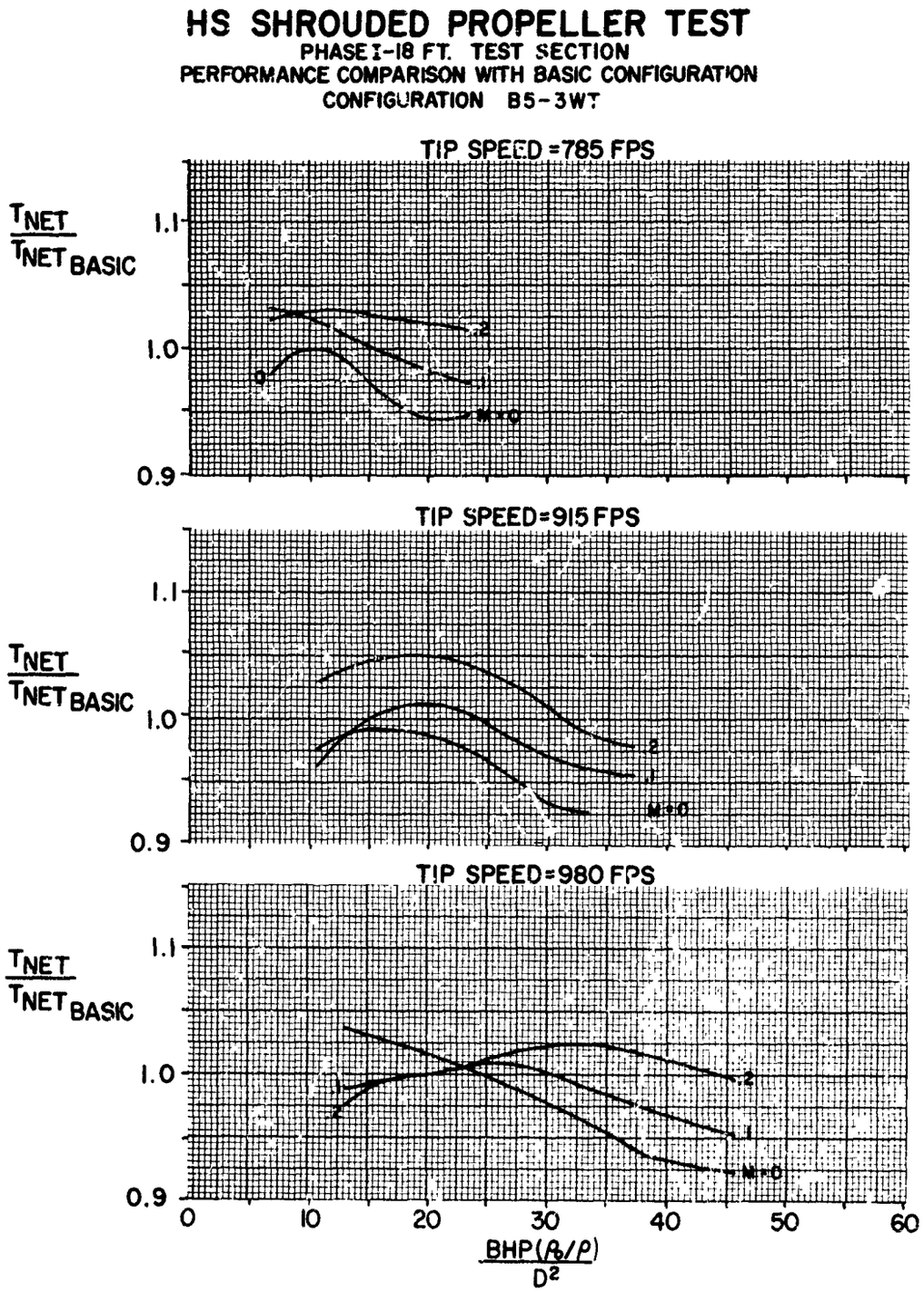
HS SHROUDED PROPELLER TEST
PHASE I-18 FT. TEST SECTION
PERFORMANCE COMPARISON WITH BASIC CONFIGURATION
CONFIGURATION B5-3WT
TIP SPEED=785 FPS
TIP SPEED=915 FPS
TIP SPEED=980 FPS
TNET / TNET BASIC
1.1
1.0
0.9
0
10
20
30
40
50
60
BHP(ρ0/ρ) / D2
2
1
M=0

FIGURE 62

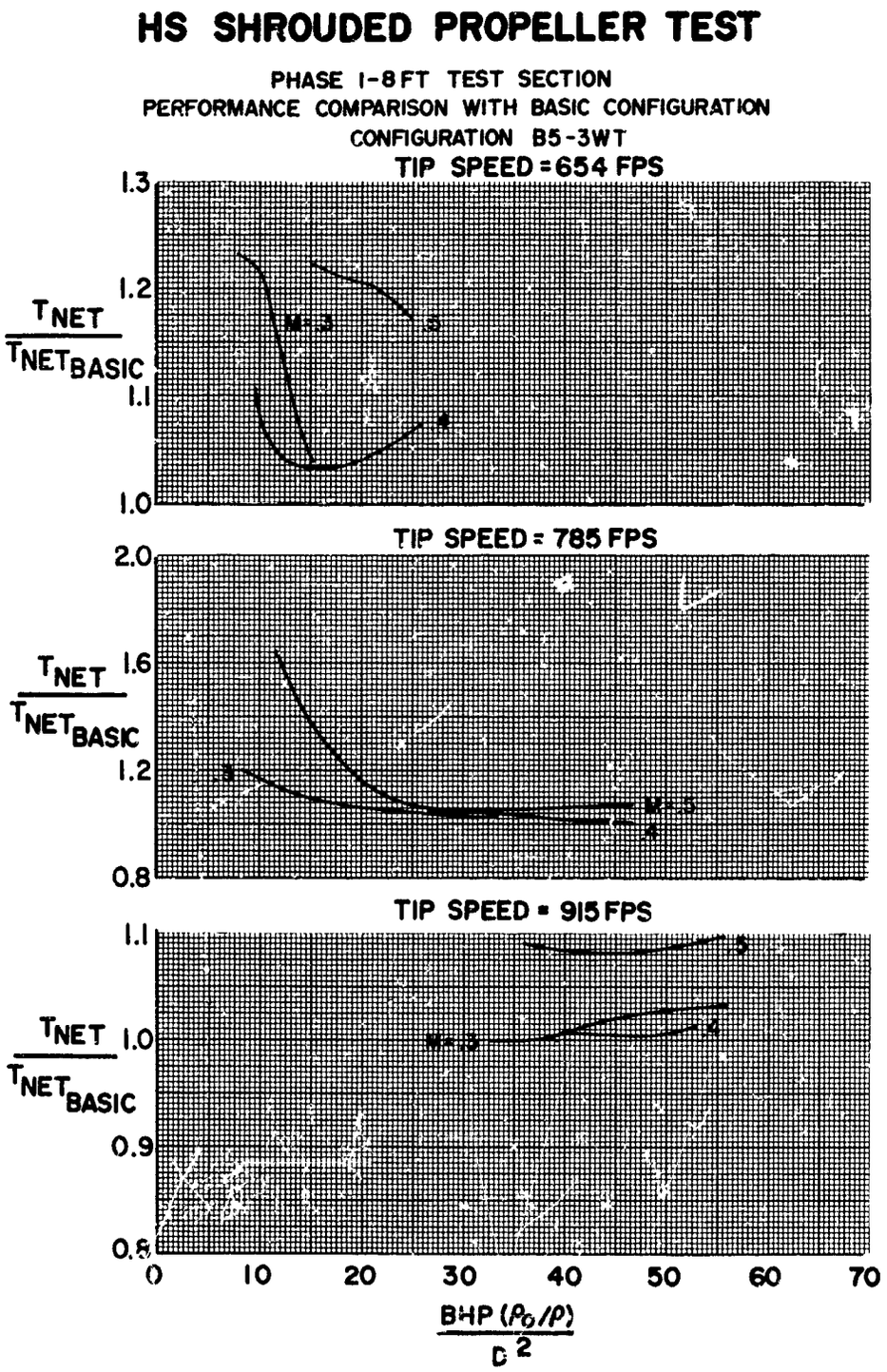
HS SHROUDED PROPELLER TEST
PHASE 1-8 FT TEST SECTION
PERFORMANCE COMPARISON WITH BASIC CONFIGURATION
CONFIGURATION B5-3WT
TIP SPEED = 654 FPS
TIP SPEED = 785 FPS
TIP SPEED = 915 FPS
T_NET / T_NET BASIC
1.3
1.2
1.1
1.0
2.0
1.6
1.2
0.8
0.9
0.8
M=.3
.5
.4
0
10
20
30
40
50
60
70
BHP (P0/P) / D 2

FIGURE 63

HS SHROUDED PROPELLER TEST

PHASE I-18 FT. TEST SECTION
PERFORMANCE COMPARISON WITH BASIC CONFIGURATION
CONFIGURATION B6-3WT

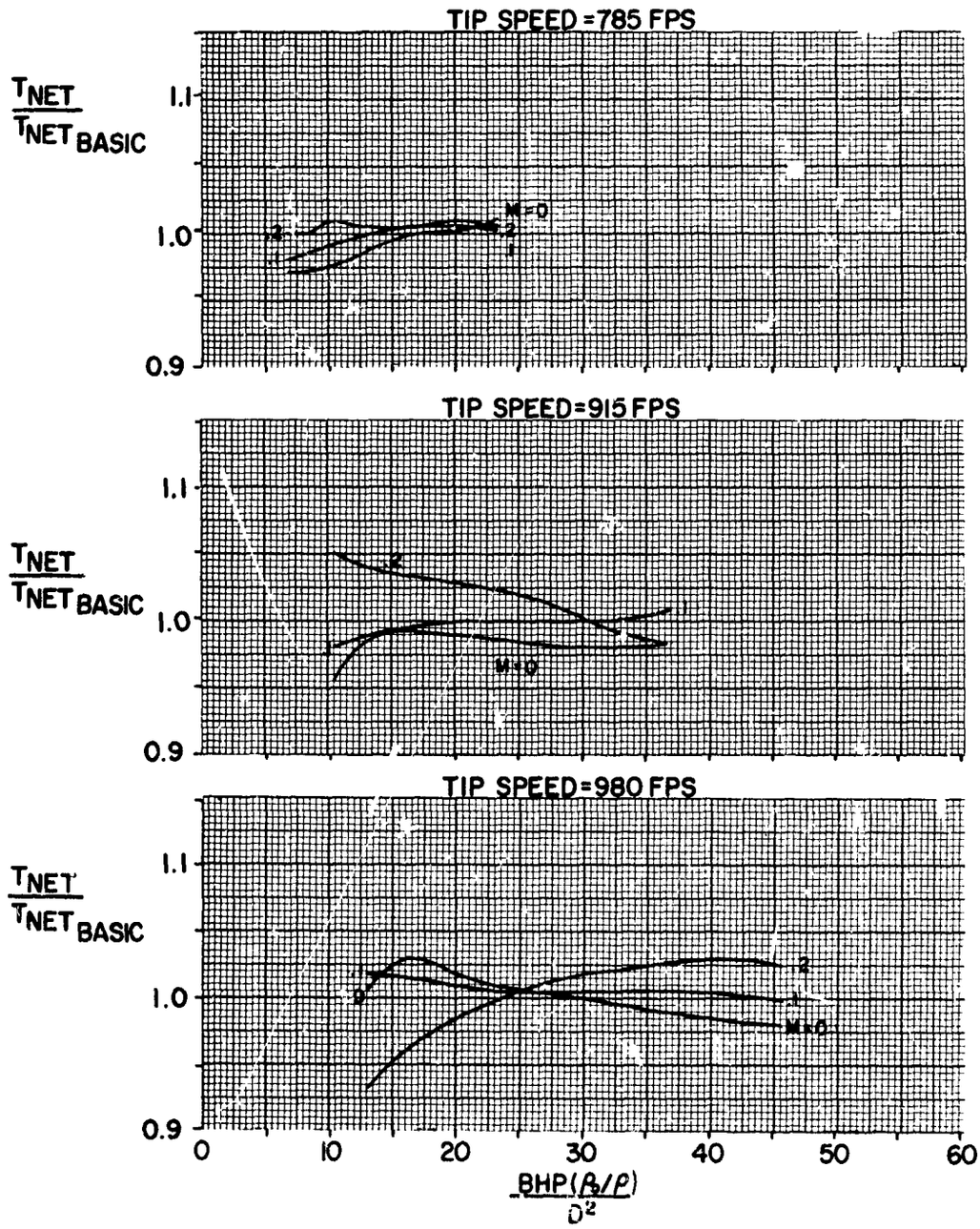

FIGURE 64

HS SHROUDED PROPELLER TEST

PHASE 1-8 FT TEST SECTION
PERFORMANCE COMPARISON WITH BASIC CONFIGURATION
CONFIGURATION B6-3WT

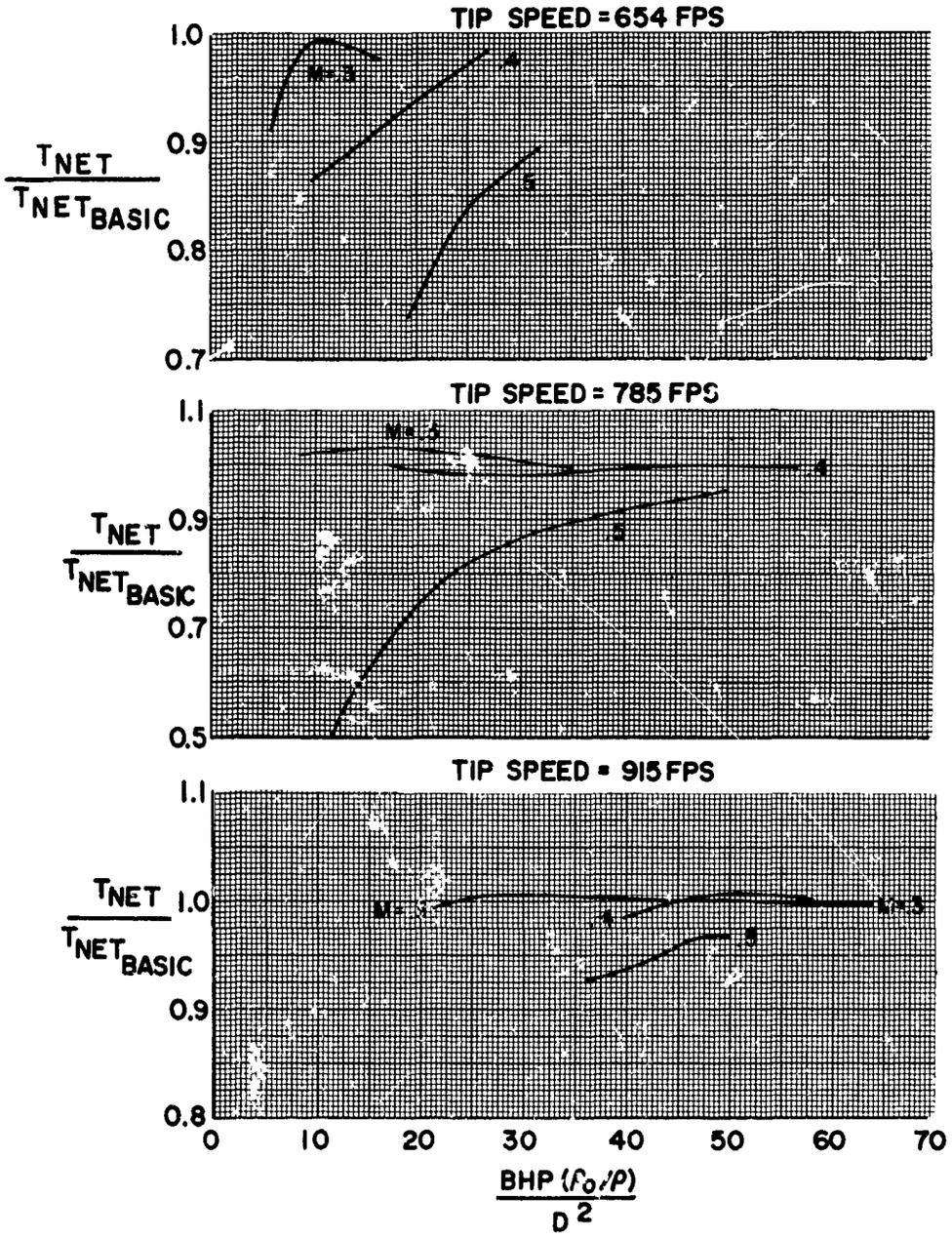

FIGURE 65

HS SHROUDED PROPELLER TEST

PHASE I-18 FT. TEST SECTION
PERFORMANCE COMPARISON WITH BASIC CONFIGURATION
CONFIGURATION B7-3NT

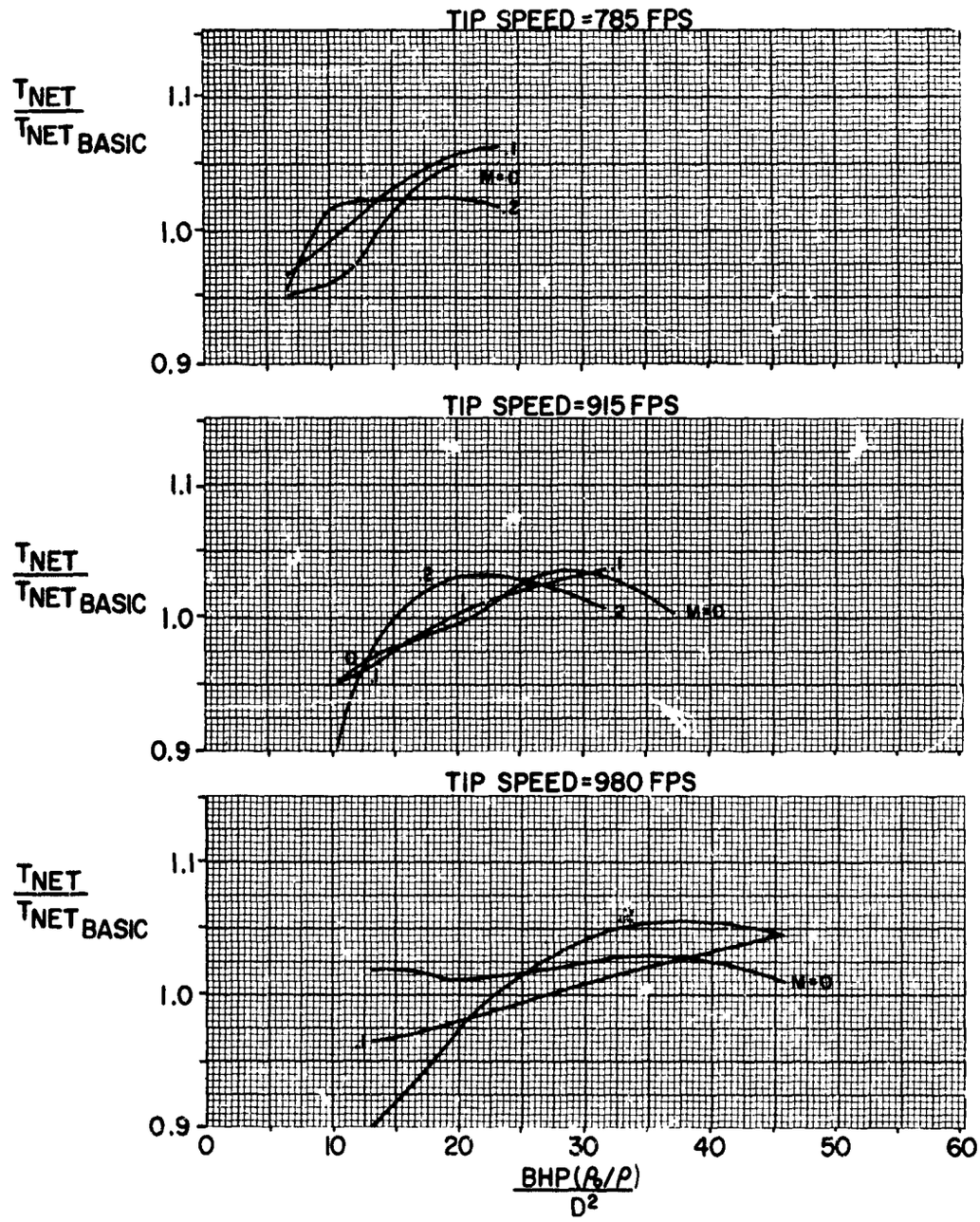

FIGURE 66

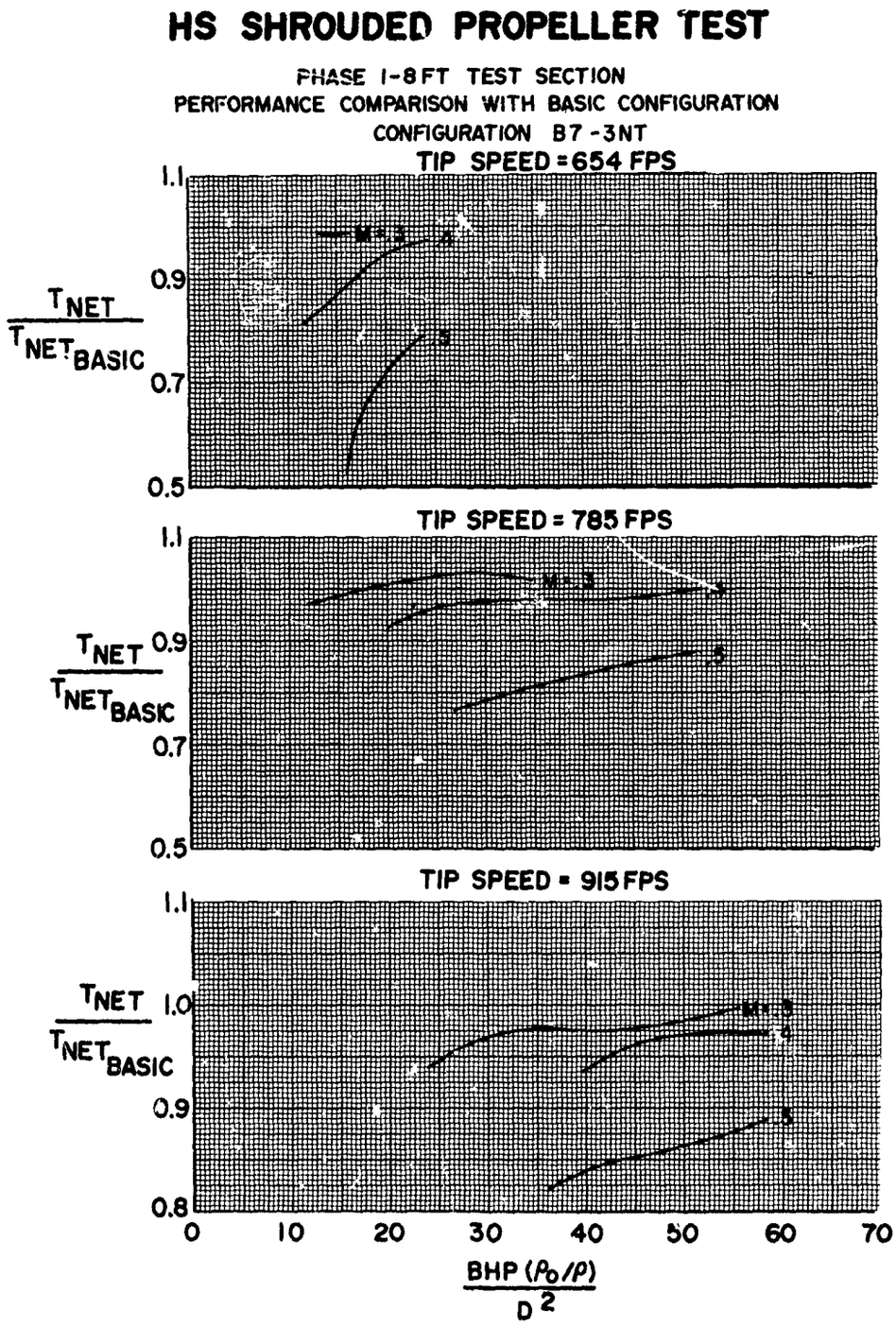
HS SHROUDED PROPELLER TEST
PHASE I-8 FT TEST SECTION
PERFORMANCE COMPARISON WITH BASIC CONFIGURATION
CONFIGURATION B7-3NT
TIP SPEED = 654 FPS
TIP SPEED = 785 FPS
TIP SPEED = 915 FPS
T_NET / T_NET BASIC
1.1
1.0
0.9
0.8
0.7
0.5
M=3
4
5
0
10
20
30
40
50
60
70
BHP (ρ0/ρ) / D²

FIGURE 67

HS SHROUDED PROPELLER TEST

PHASE I-18 FT. TEST SECTION
PERFORMANCE COMPARISON WITH BASIC CONFIGURATION
CONFIGURATION 31-3WT 1°

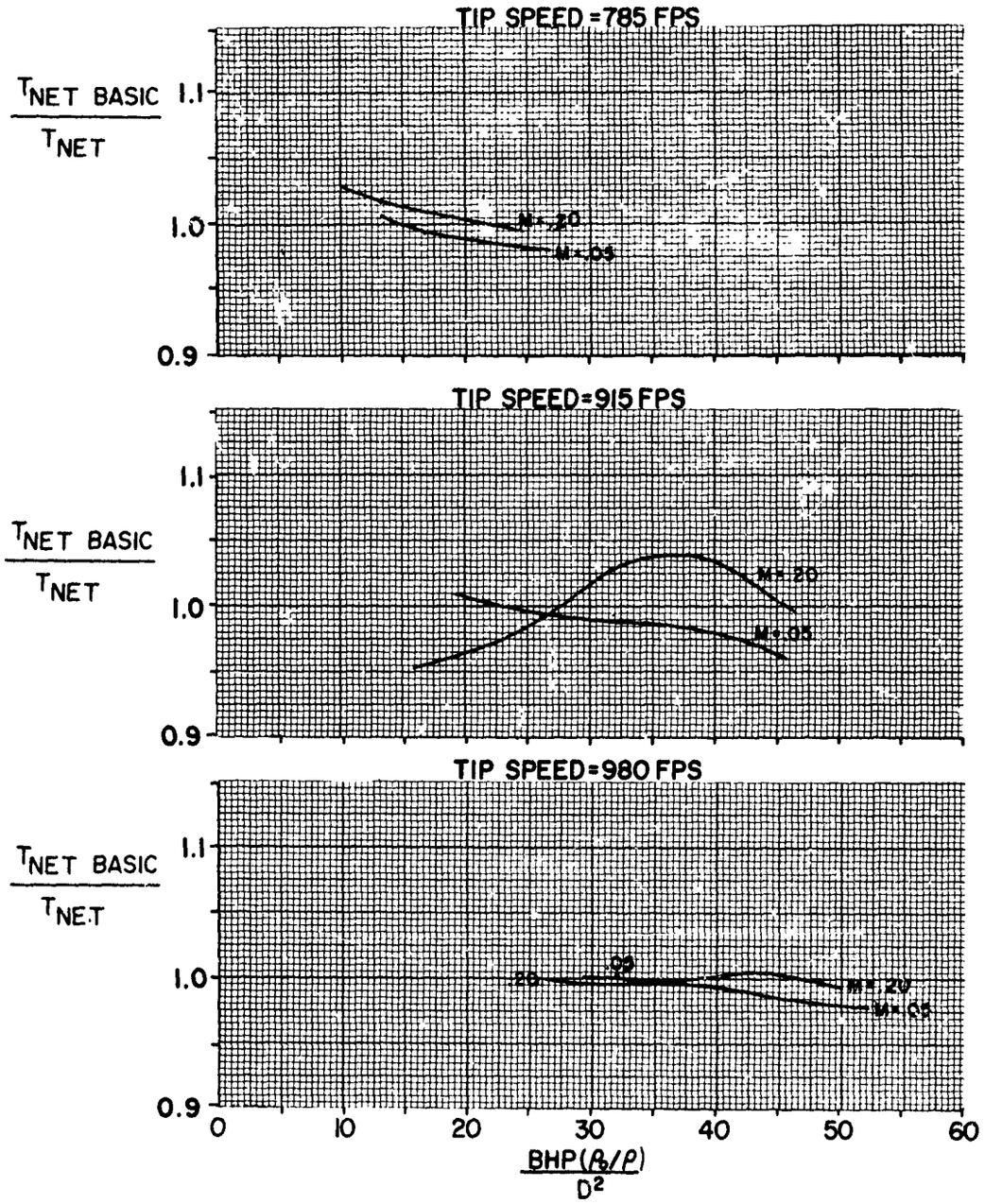

FIGURE 68

HS SHROUDED PROPELLER TEST

PHASE I-8 FT TEST SECTION
PERFORMANCE COMPARISON WITH BASIC CONFIGURATION
CONFIGURATION BI-3WT I°

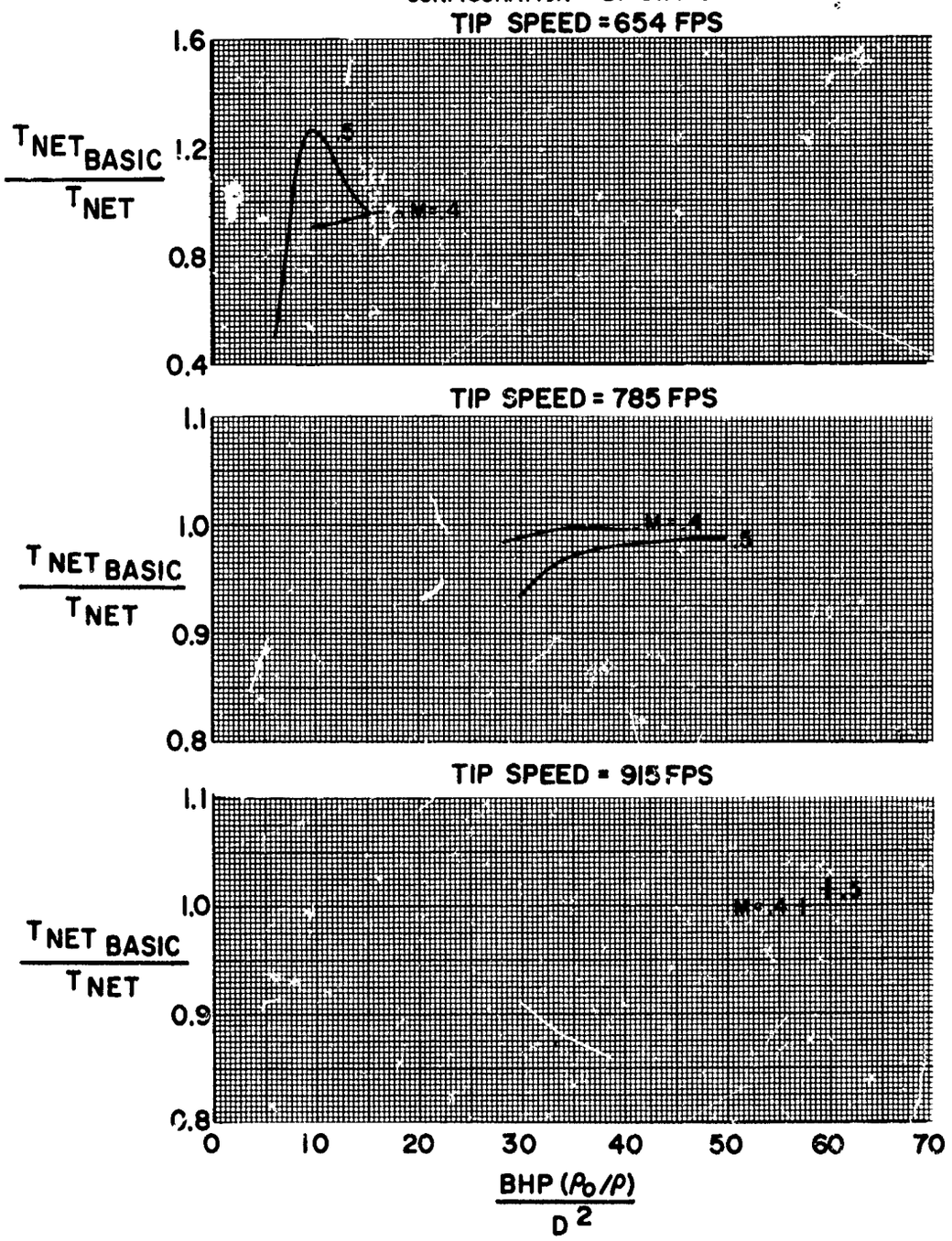

FIGURE 69

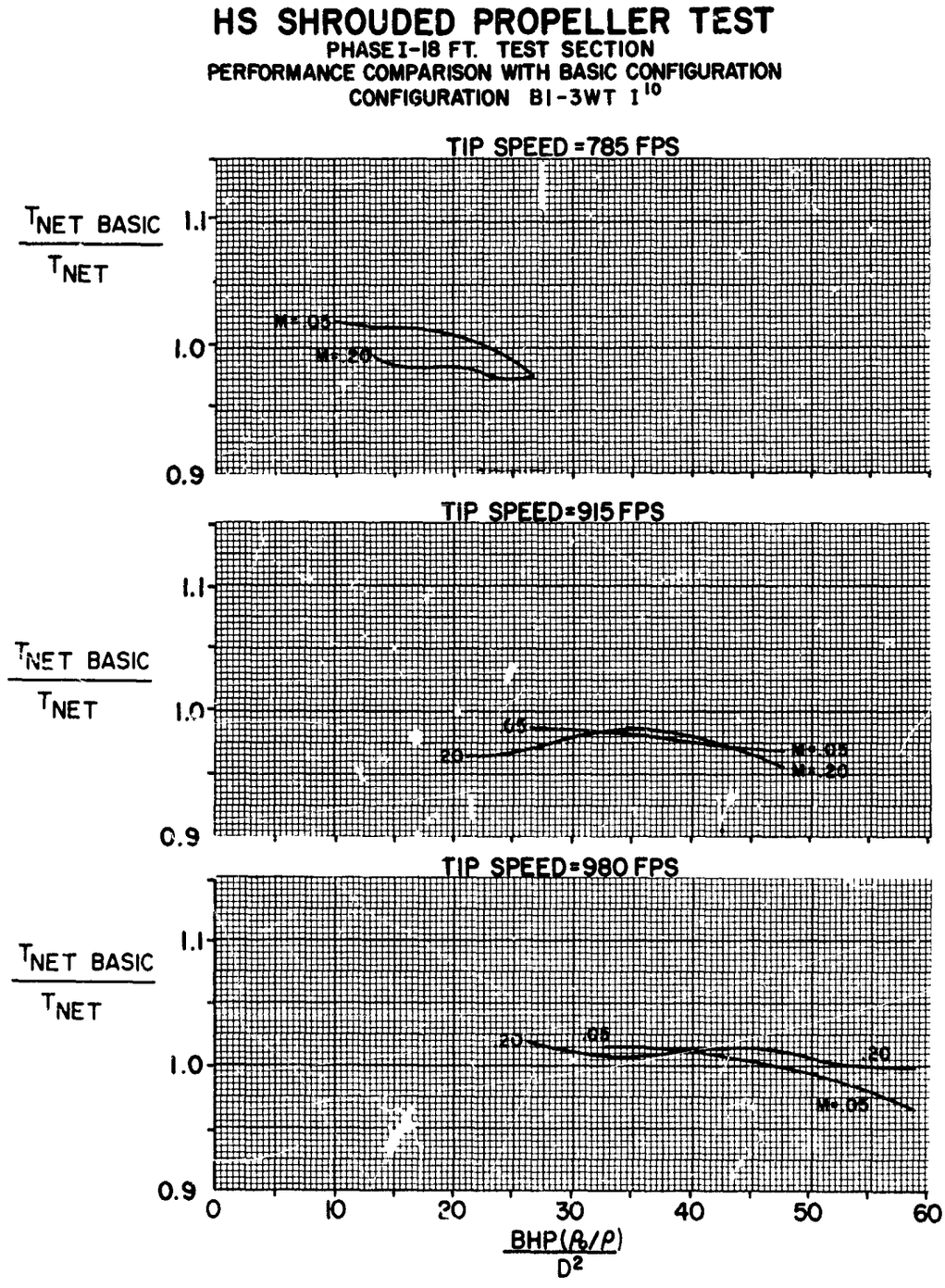
HS SHROUDED PROPELLER TEST
PHASE I-18 FT. TEST SECTION
PERFORMANCE COMPARISON WITH BASIC CONFIGURATION
CONFIGURATION BI-3WT I 10
TIP SPEED = 785 FPS
TIP SPEED = 915 FPS
TIP SPEED = 980 FPS
T NET BASIC / T NET
1.1
1.0
0.9
M = .05
M = .20
0
10
20
30
40
50
60
BHP(ρ₀/ρ) / D²

FIGURE 70

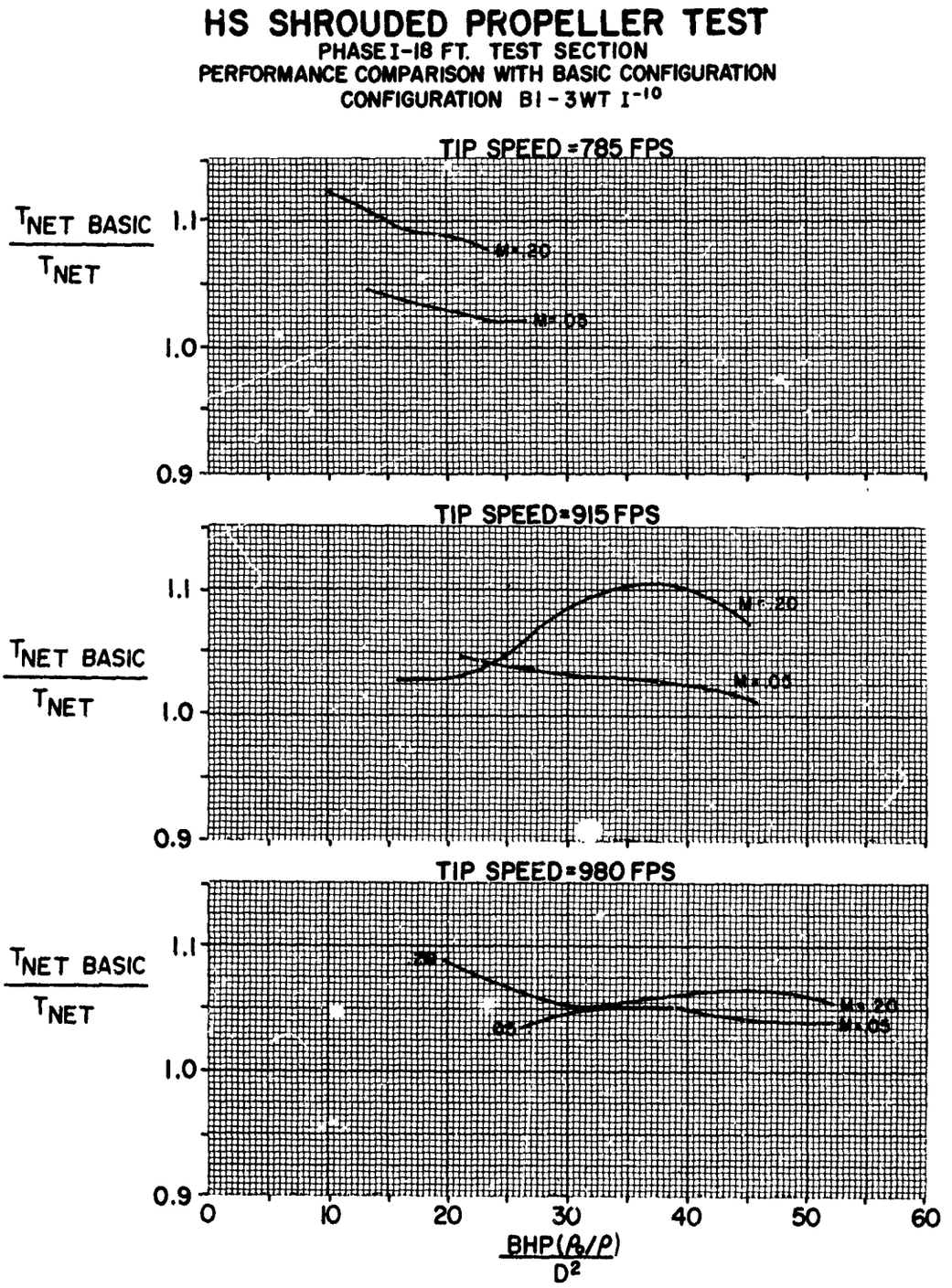
HS SHROUDED PROPELLER TEST
PHASE I-18 FT. TEST SECTION
PERFORMANCE COMPARISON WITH BASIC CONFIGURATION
CONFIGURATION B1-3WT I-10
TIP SPEED = 785 FPS
TIP SPEED = 915 FPS
TIP SPEED = 980 FPS
T NET BASIC / T NET
1.1
1.0
0.9
M = .20
M = .05
0
10
20
30
40
50
60
BHP(A/ρ) / D²

FIGURE 71

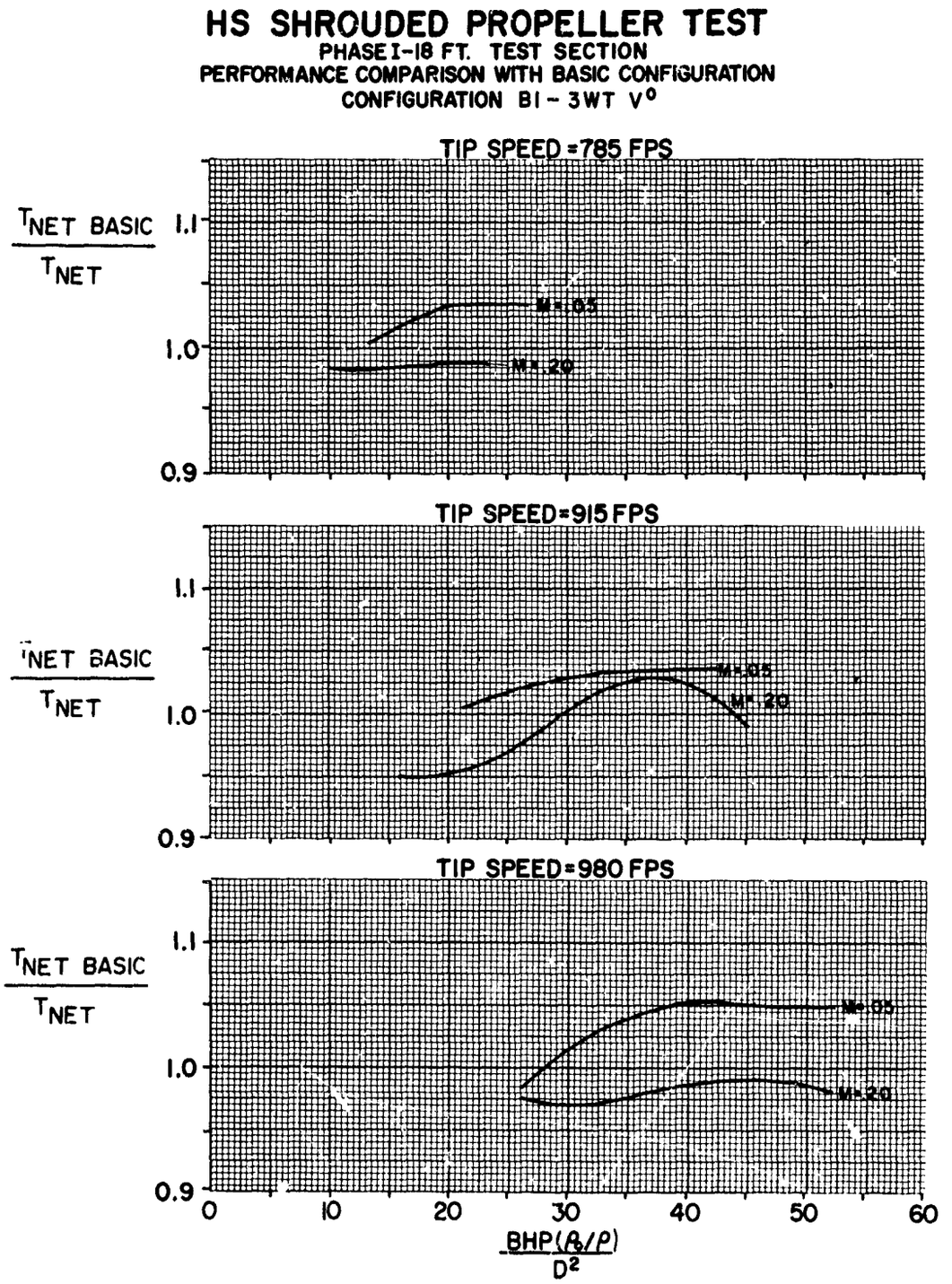
HS SHROUDED PROPELLER TEST
PHASE I-18 FT. TEST SECTION
PERFORMANCE COMPARISON WITH BASIC CONFIGURATION
CONFIGURATION B1 - 3WT V°
TIP SPEED = 785 FPS
TIP SPEED = 915 FPS
TIP SPEED = 980 FPS
T NET BASIC / T NET
1.1
1.0
0.9
M = .05
M = .20
0
10
20
30
40
50
60
BHP(ρ₀/ρ) / D²

FIGURE 72

HS SHROUDED PROPELLER TEST

PHASE 1-8 FT TEST SECTION
PERFORMANCE COMPARISON WITH BASIC CONFIGURATION
CONFIGURATION B1-3WT V°

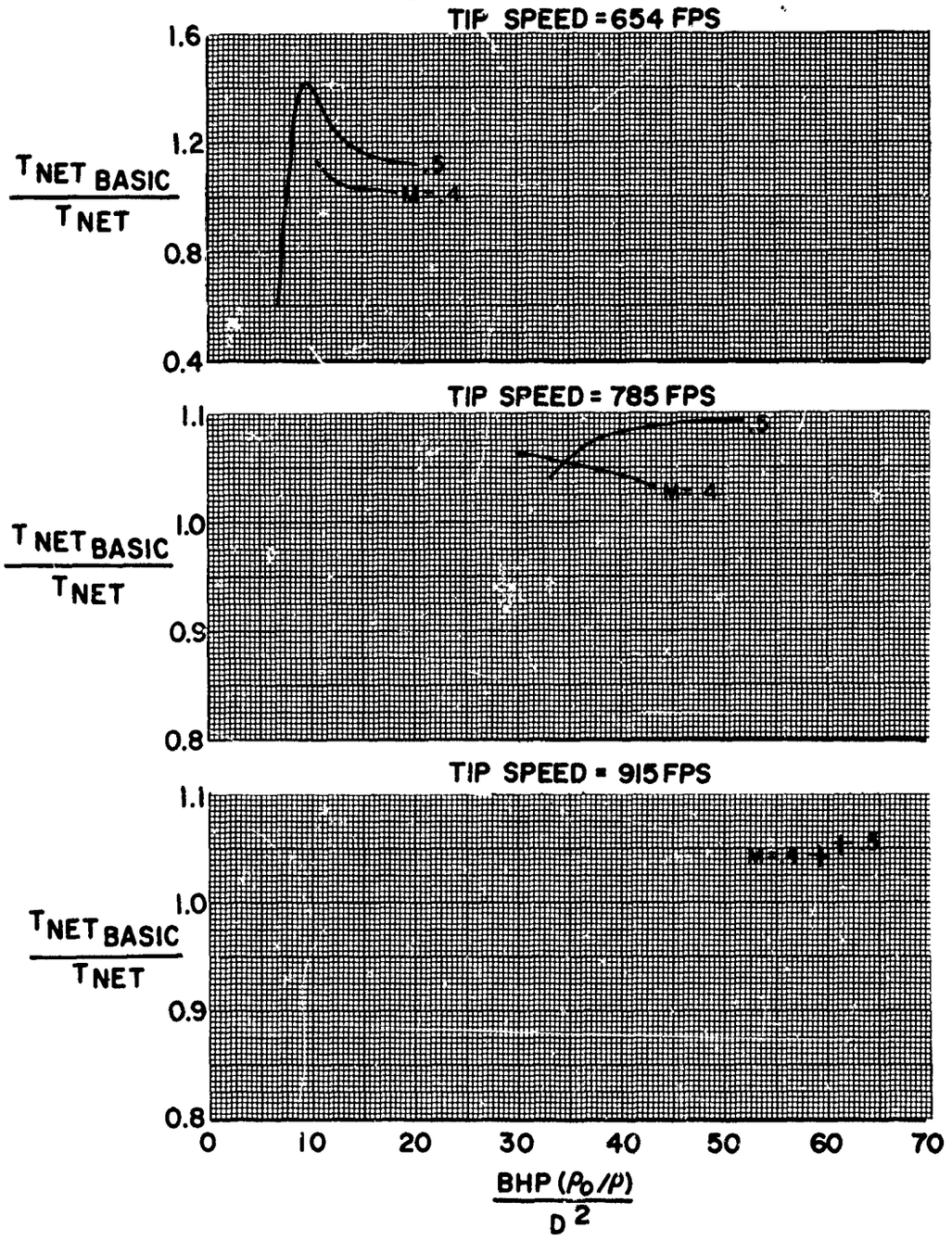

FIGURE 73

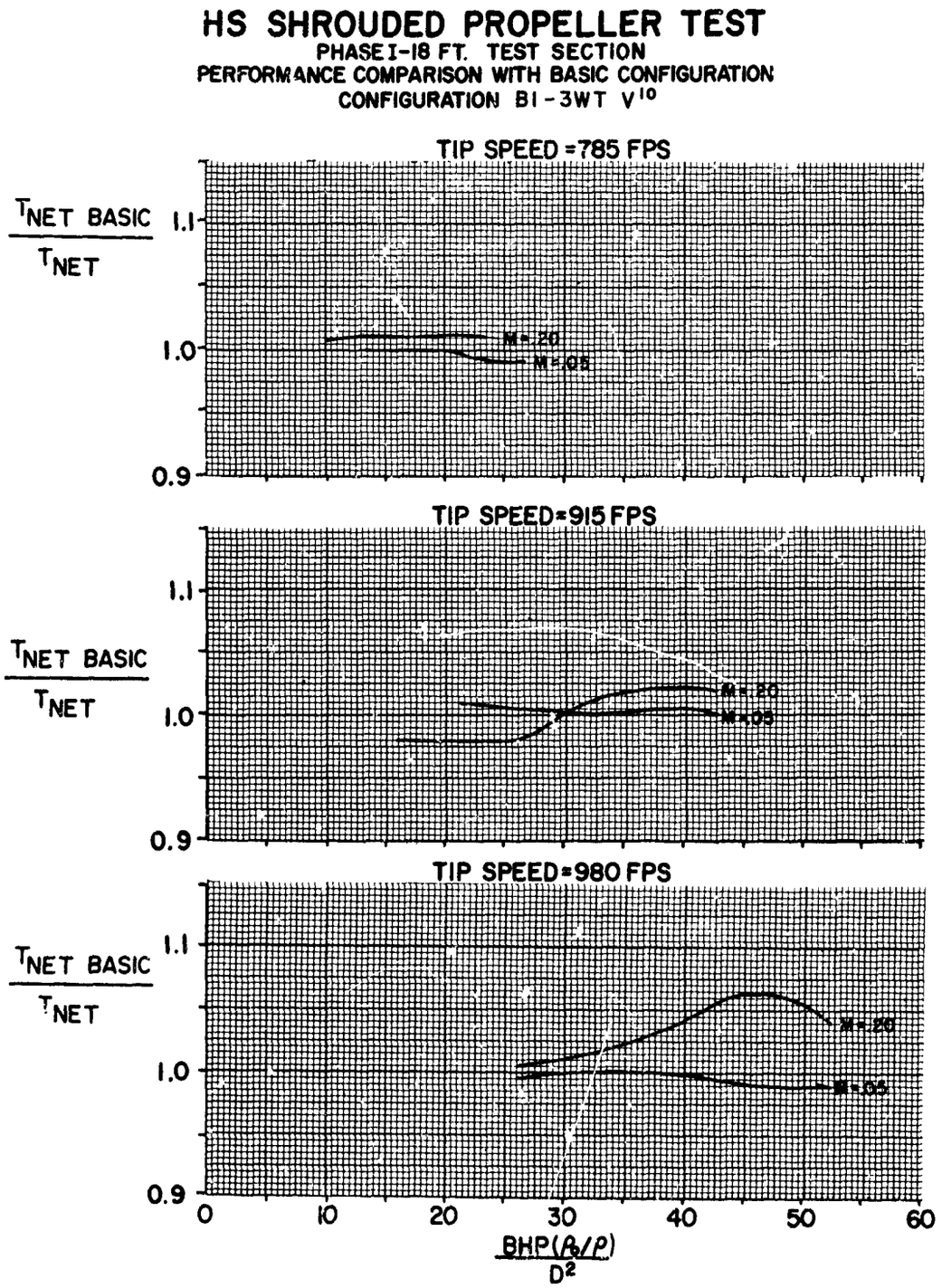
HS SHROUDED PROPELLER TEST
PHASE I-18 FT. TEST SECTION
PERFORMANCE COMPARISON WITH BASIC CONFIGURATION
CONFIGURATION B1-3WT V10
TIP SPEED = 785 FPS
TIP SPEED = 915 FPS
TIP SPEED = 980 FPS
TNET BASIC / TNET
1.1
1.0
0.9
M = .20
M = .05
0
10
20
30
40
50
60
BHP(ρ0/ρ) / D2

FIGURE 74

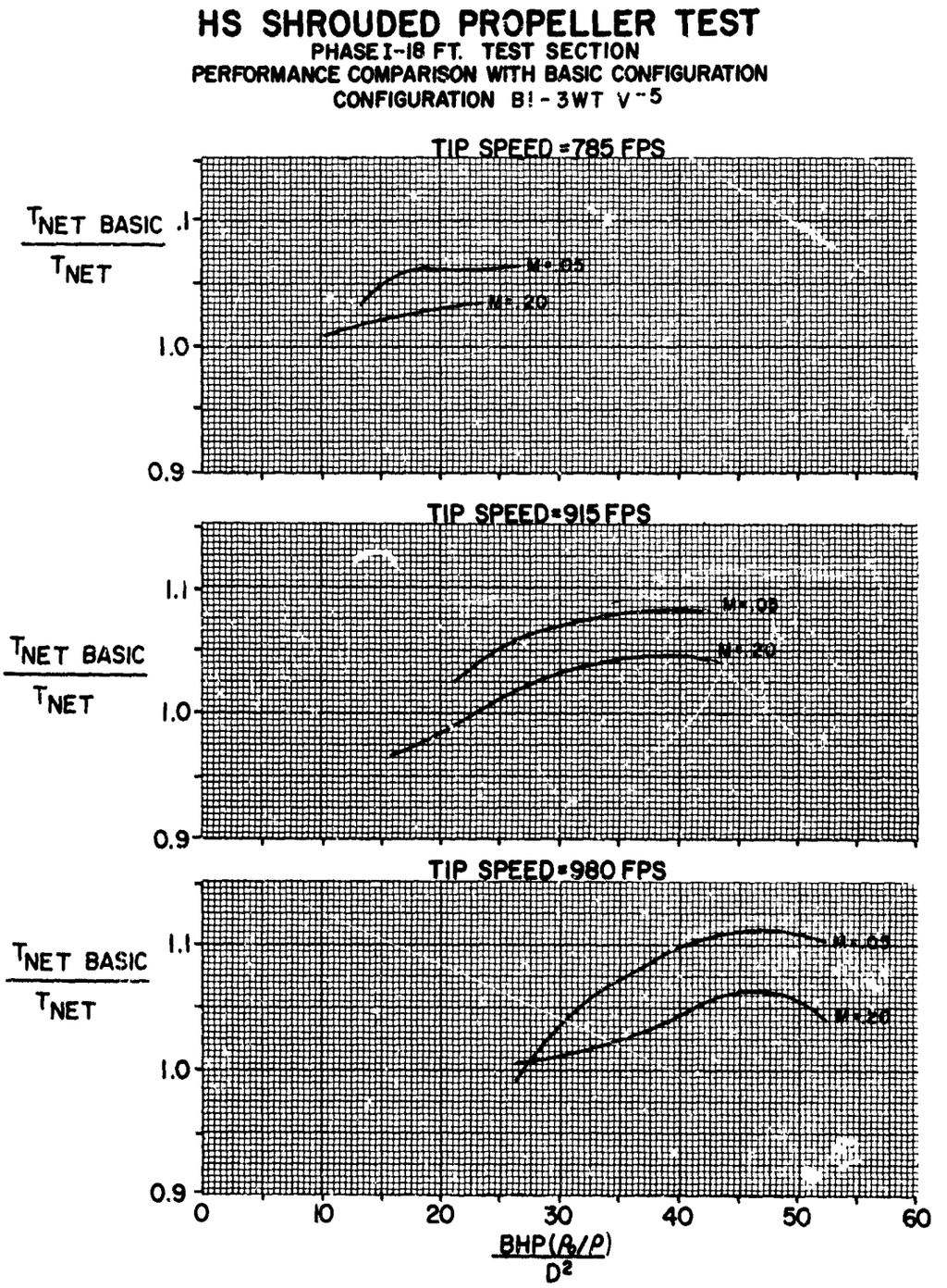
HS SHROUDED PROPELLER TEST
PHASE I-18 FT. TEST SECTION
PERFORMANCE COMPARISON WITH BASIC CONFIGURATION
CONFIGURATION B1-3WT V-5
TIP SPEED = 785 FPS
TIP SPEED = 915 FPS
TIP SPEED = 980 FPS
T NET BASIC / T NET
1.1
1.0
0.9
0
10
20
30
40
50
60
BHP(β/ρ) / D²

FIGURE 75

HS SHROUDED PROPELLER TEST

PHASE I - 18 FT. TEST SECTION
PERFORMANCE COMPARISON WITH BASIC CONFIGURATION
CONFIGURATION B1-3R

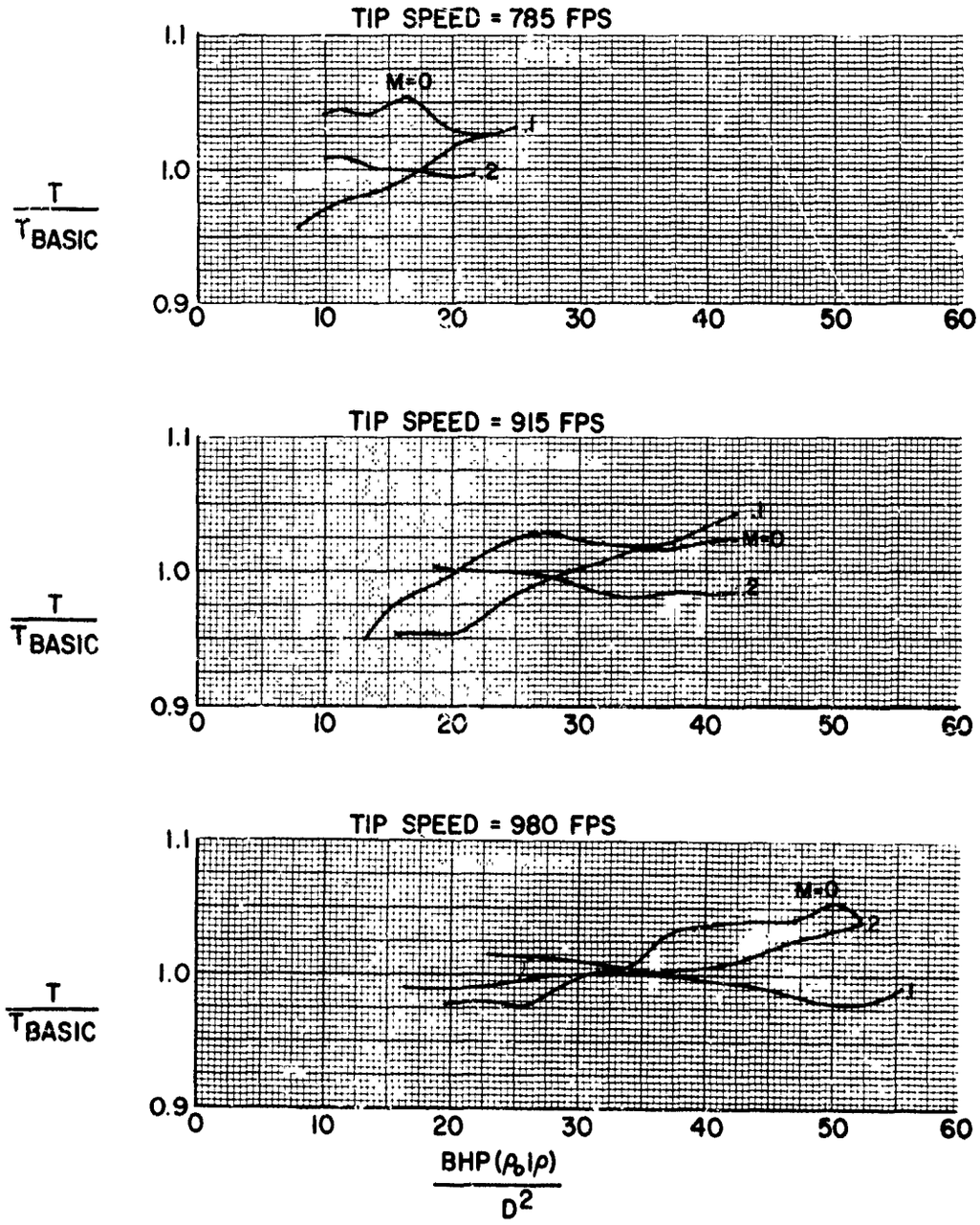

FIGURE 76

HS SHROUDED PROPELLER TEST

PHASE 1-8FT TEST SECTION
PERFORMANCE COMPARISON WITH BASIC CONFIGURATION
CONFIGURATION B1-3R

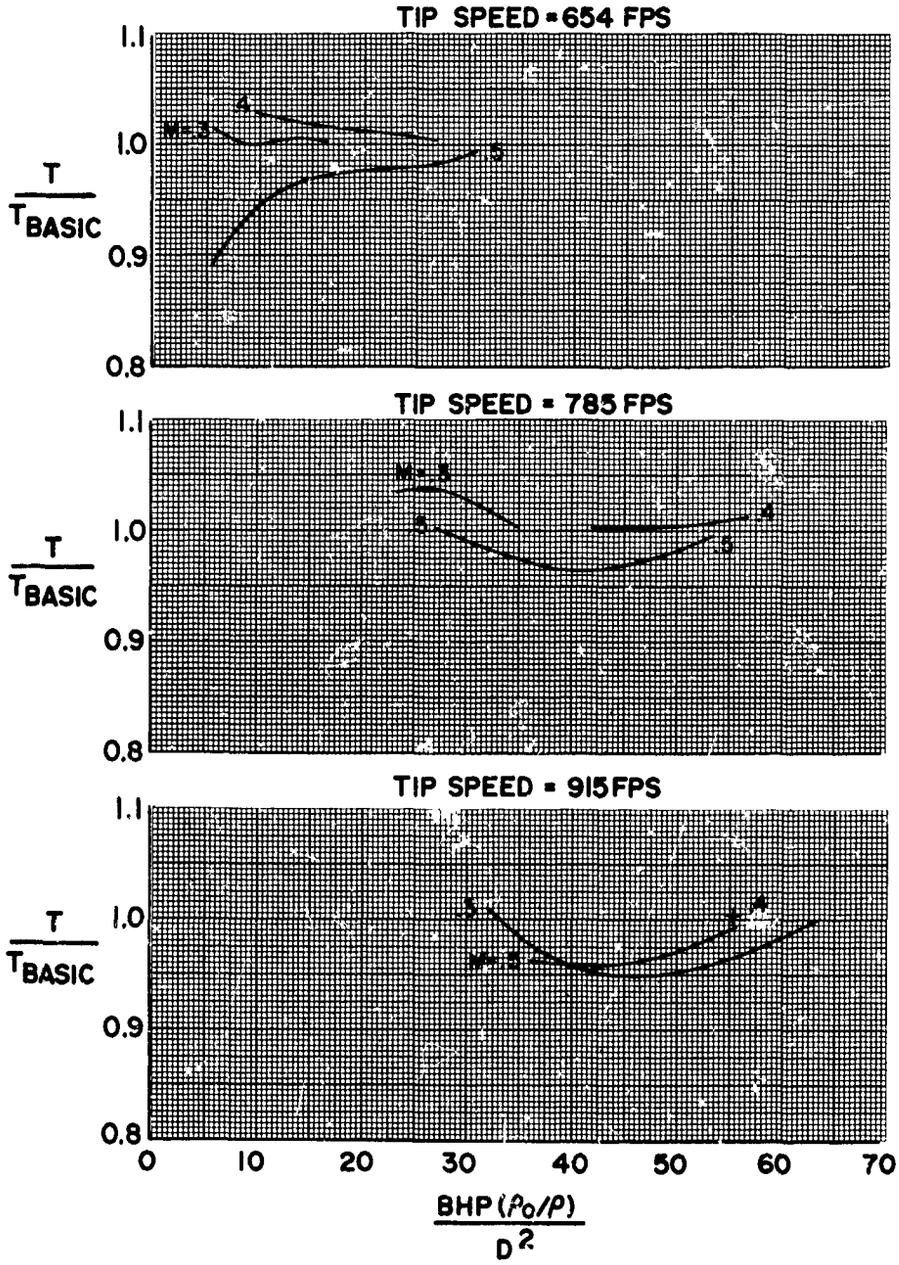

FIGURE 77

HS SHROUDED PROPELLER TEST

PHASE I - 18 FT. TEST SECTION
PERFORMANCE COMPARISON WITH BASIC CONFIGURATION
CONFIGURATION B1 - 3R 1/2M

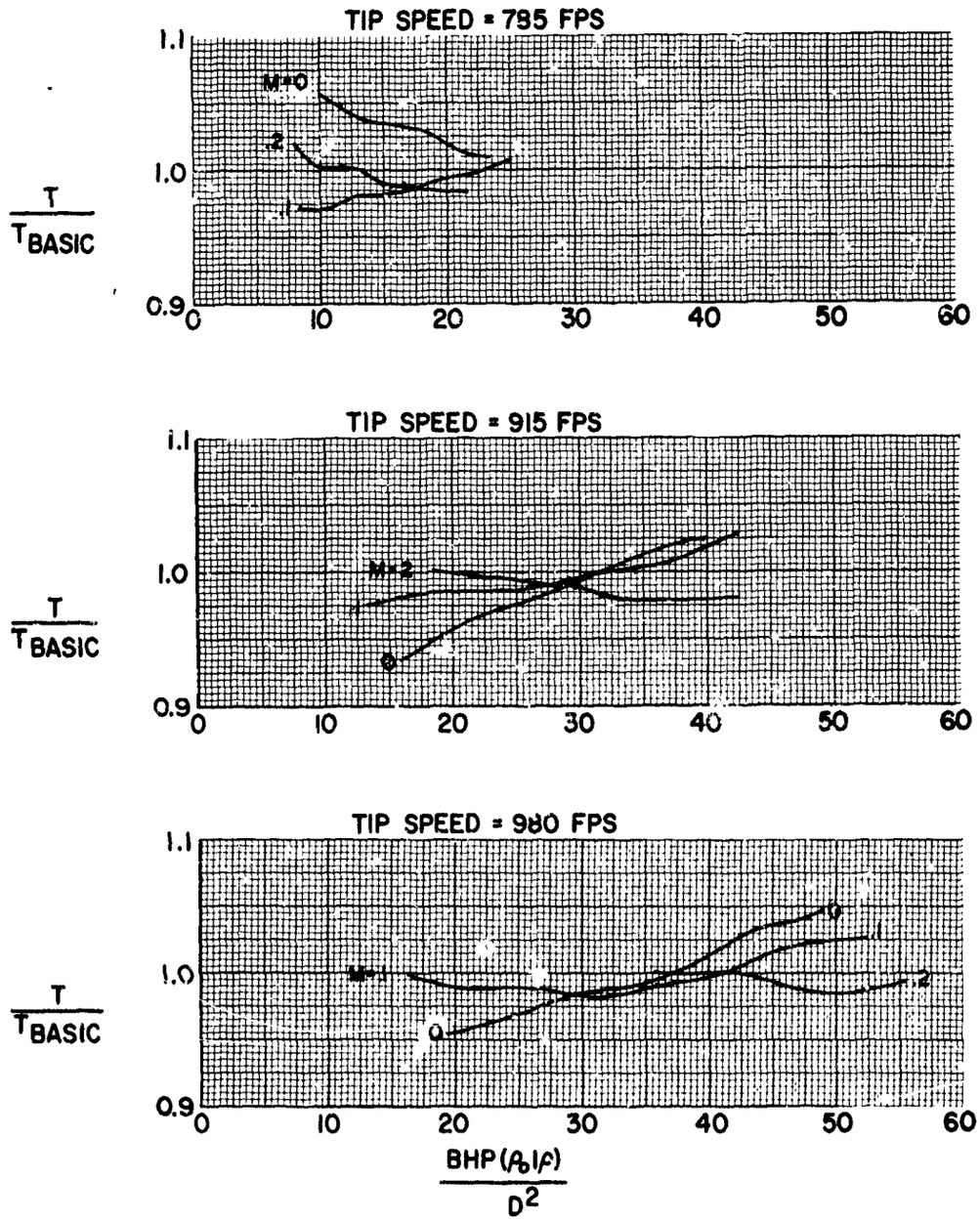

FIGURE 78

HS SHROUDED PROPELLER TEST

PHASE 1-8FT TEST SECTION
PERFORMANCE COMPARISON WITH BASIC CONFIGURATION
CONFIGURATION B1-3R 1/2M

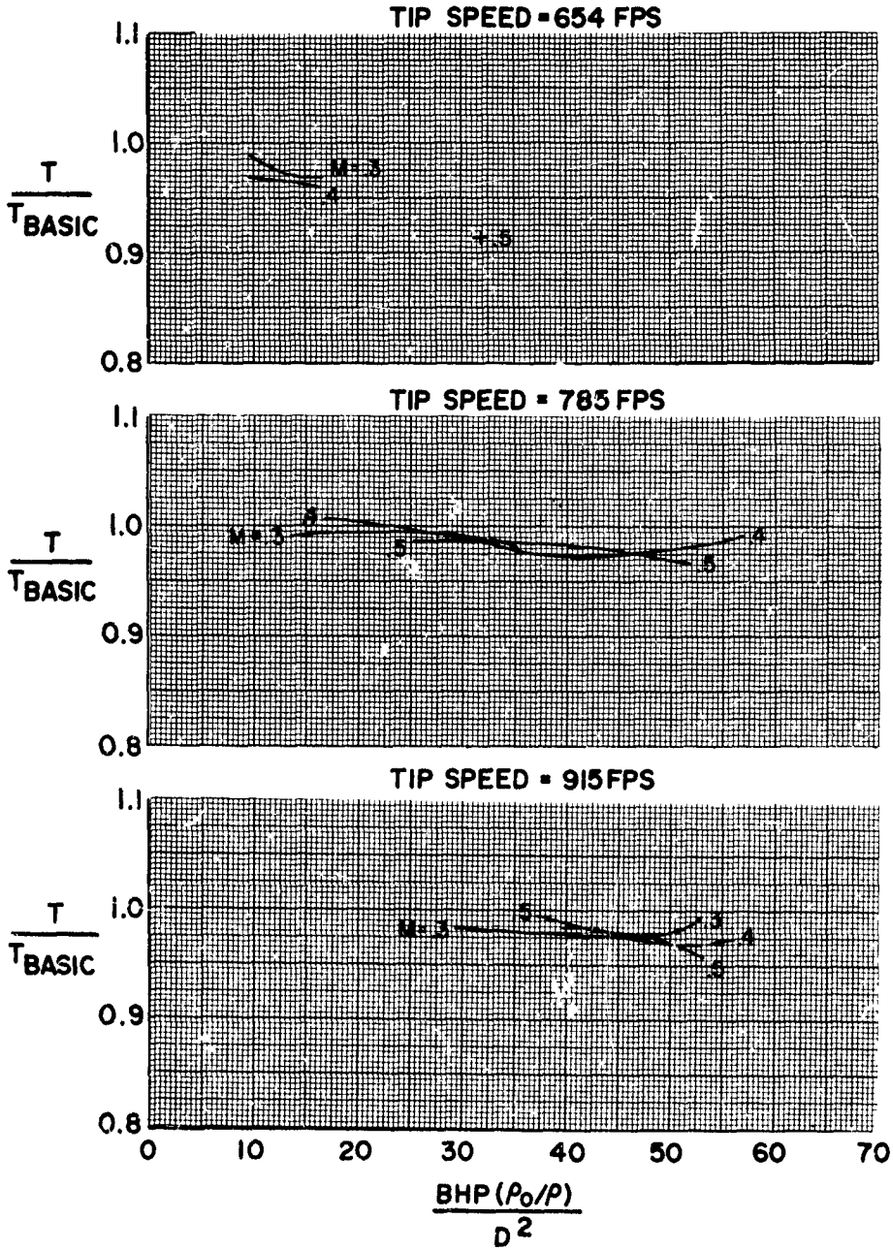

FIGURE 79

HS SHROUDED PROPELLER TEST

PHASE I - 18 FT. TEST SECTION
PERFORMANCE COMPARISON WITH BASIC CONFIGURATION
CONFIGURATION B1 - 3RM

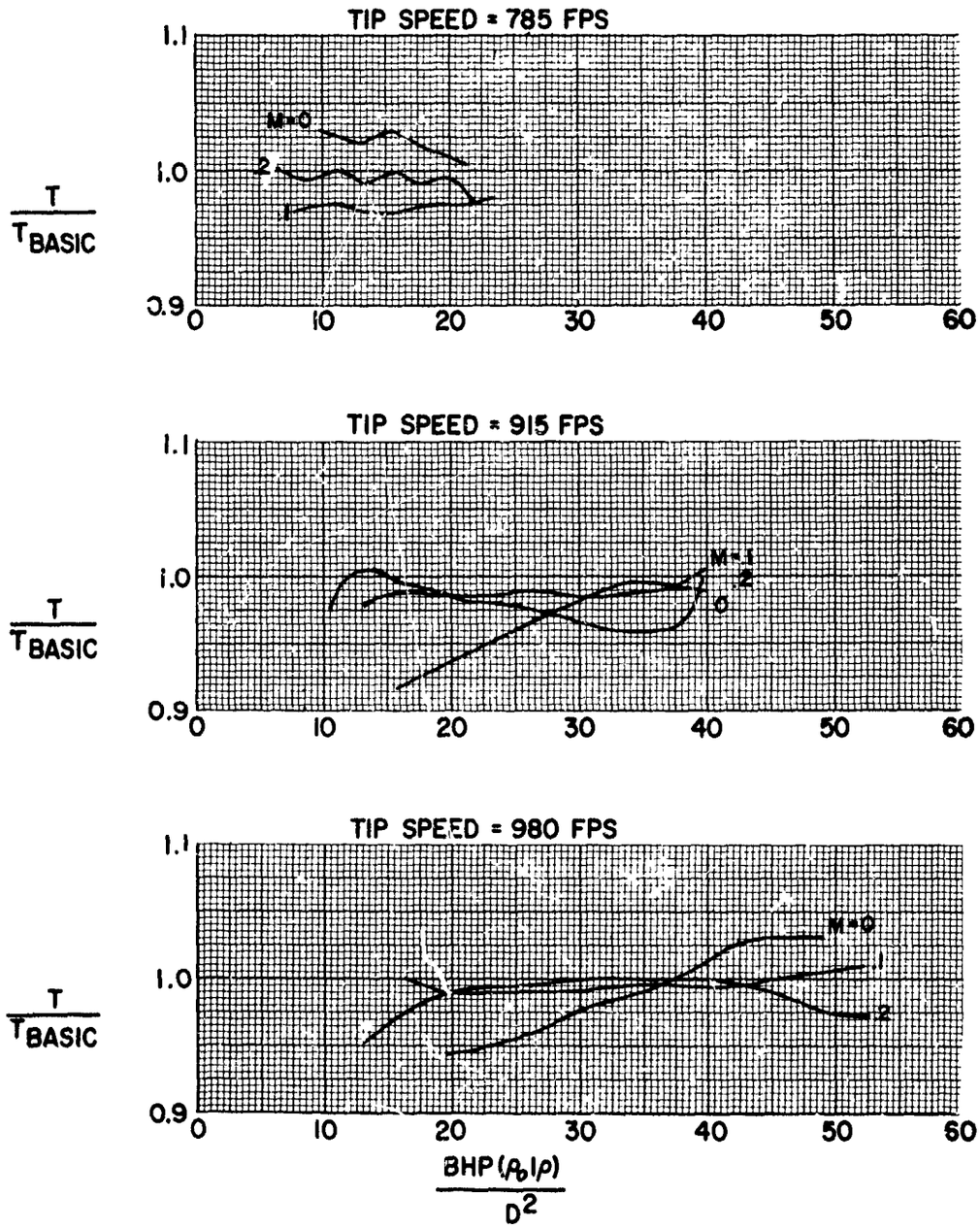

FIGURE 80

HS SHROUDED PROPELLER TEST

PHASE I-8FT TEST SECTION
PERFORMANCE COMPARISON WITH BASIC CONFIGURATION
CONFIGURATION BI-3RM

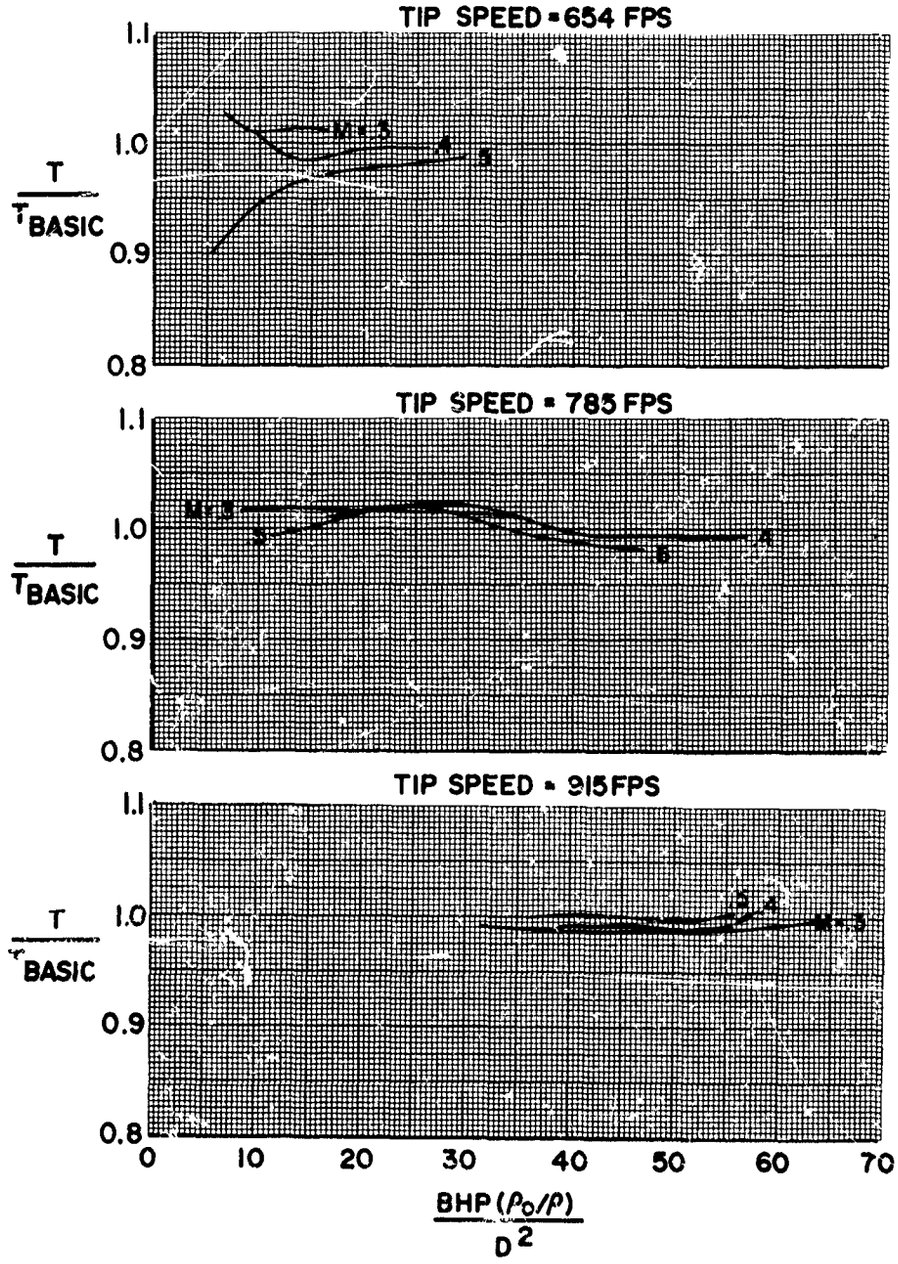

FIGURE 81

HS SHROUDED PROPELLER TEST

PHASE I - 18 FT. TEST SECTION
PERFORMANCE COMPARISON WITH BASIC CONFIGURATION
CONFIGURATION B1 - 3NT

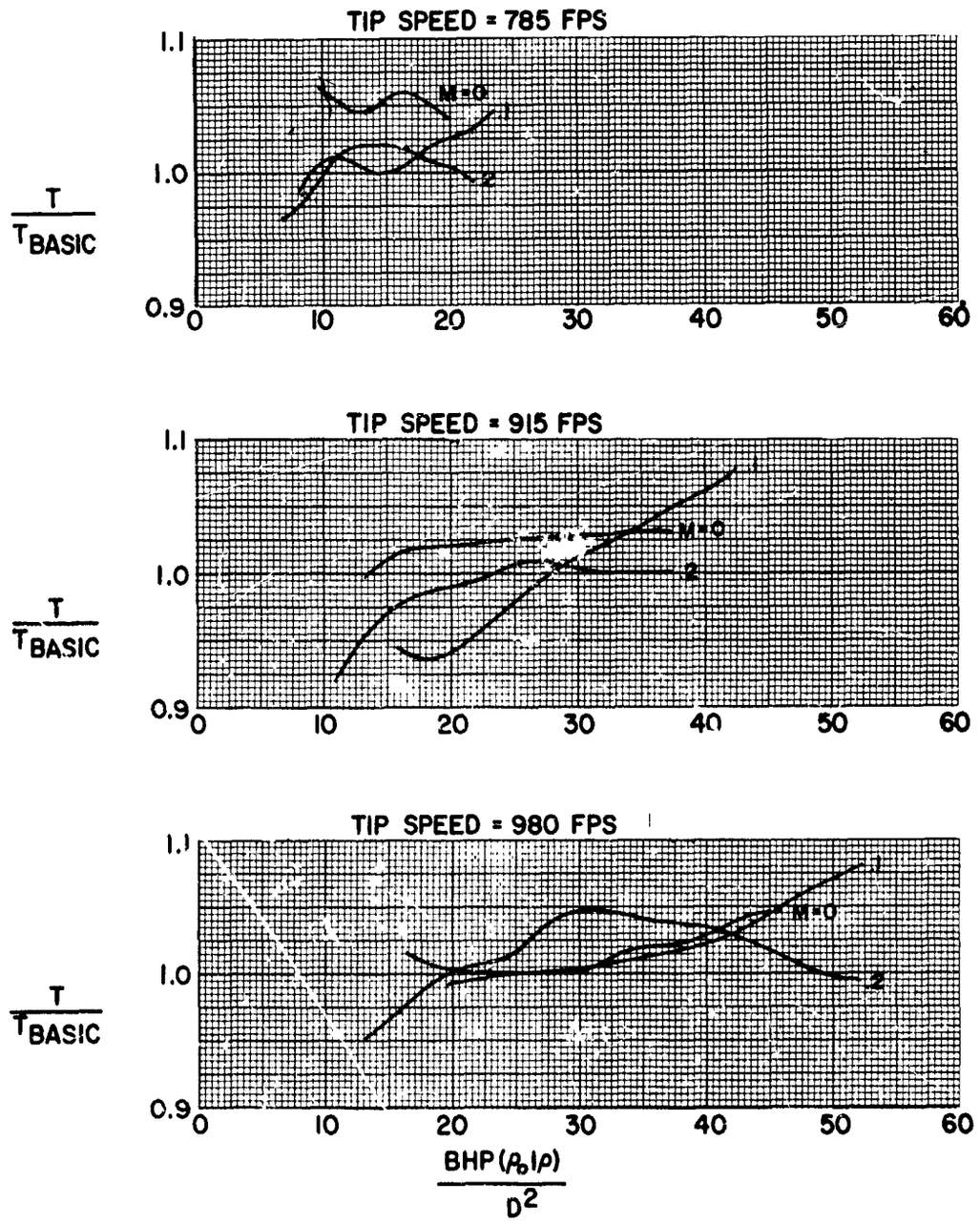

FIGURE 82

HS SHROUDED PROPELLER TEST

PHASE 1-8FT TEST SECTION
PERFORMANCE COMPARISON WITH BASIC CONFIGURATION
CONFIGURATION B1-3NT

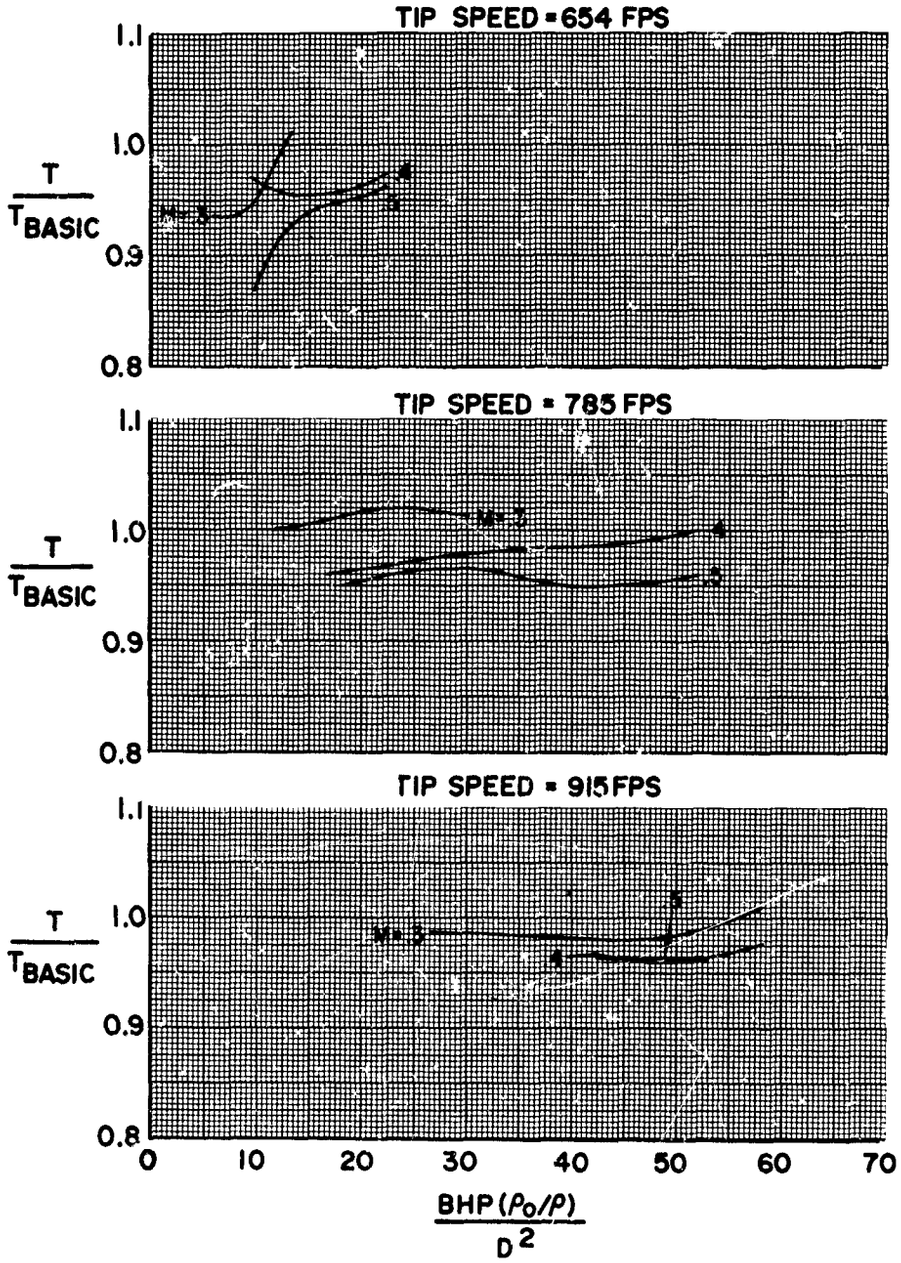

FIGURE 83

HS SHROUDED PROPELLER TEST

PHASE I - 18 FT. TEST SECTION
PERFORMANCE COMPARISON WITH BASIC CONFIGURATION
CONFIGURATION B1-4NT

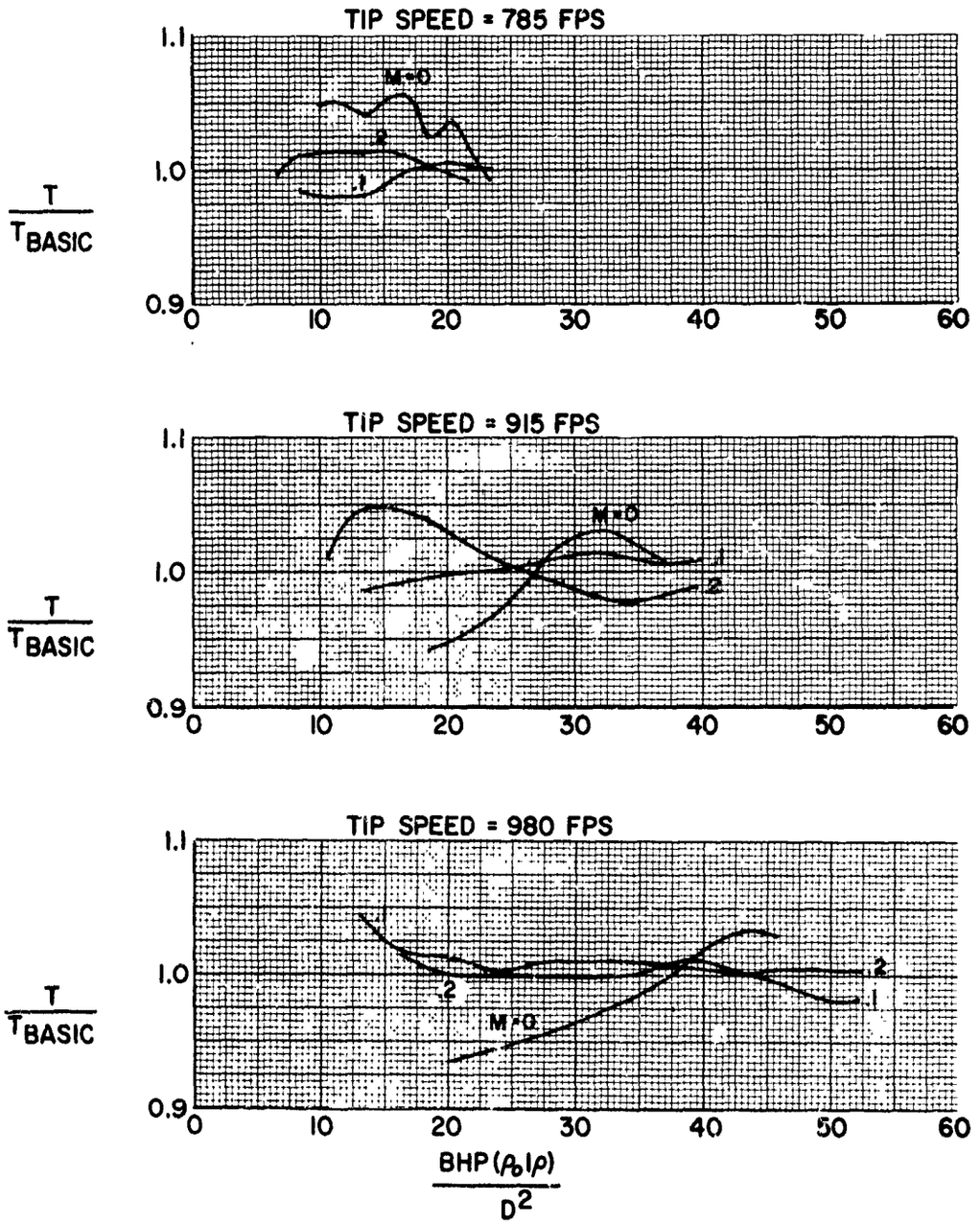

FIGURE 84

HS SHROUDED PROPELLER TEST

PHASE I-8FT TEST SECTION
PERFORMANCE COMPARISON WITH BASIC CONFIGURATION
CONFIGURATION B1-4NT

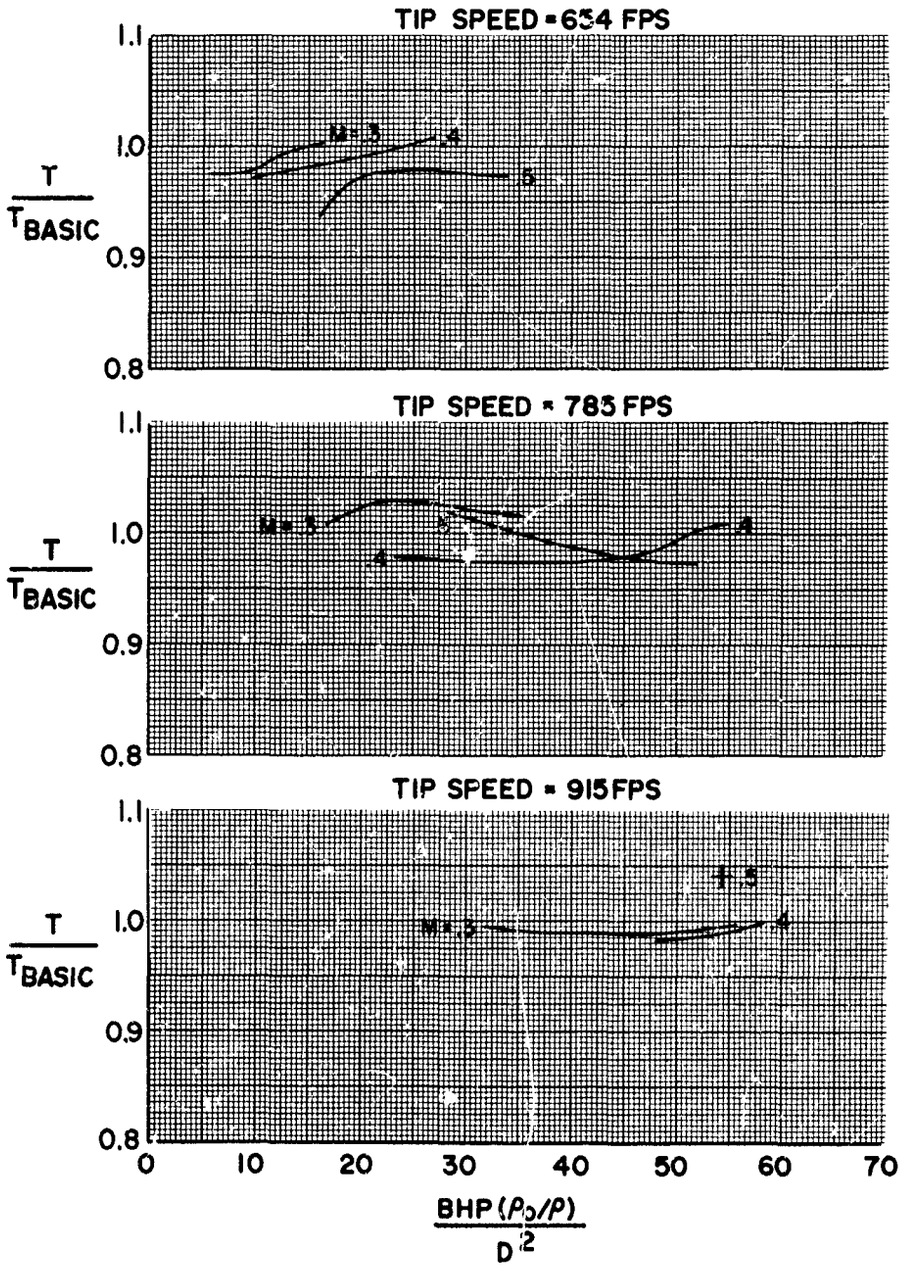

FIGURE 85

HS SHROUDED PROPELLER TEST

PHASE I - 18 FT. TEST SECTION
PERFORMANCE COMPARISON WITH BASIC CONFIGURATION
CONFIGURATION B2 - 3WT

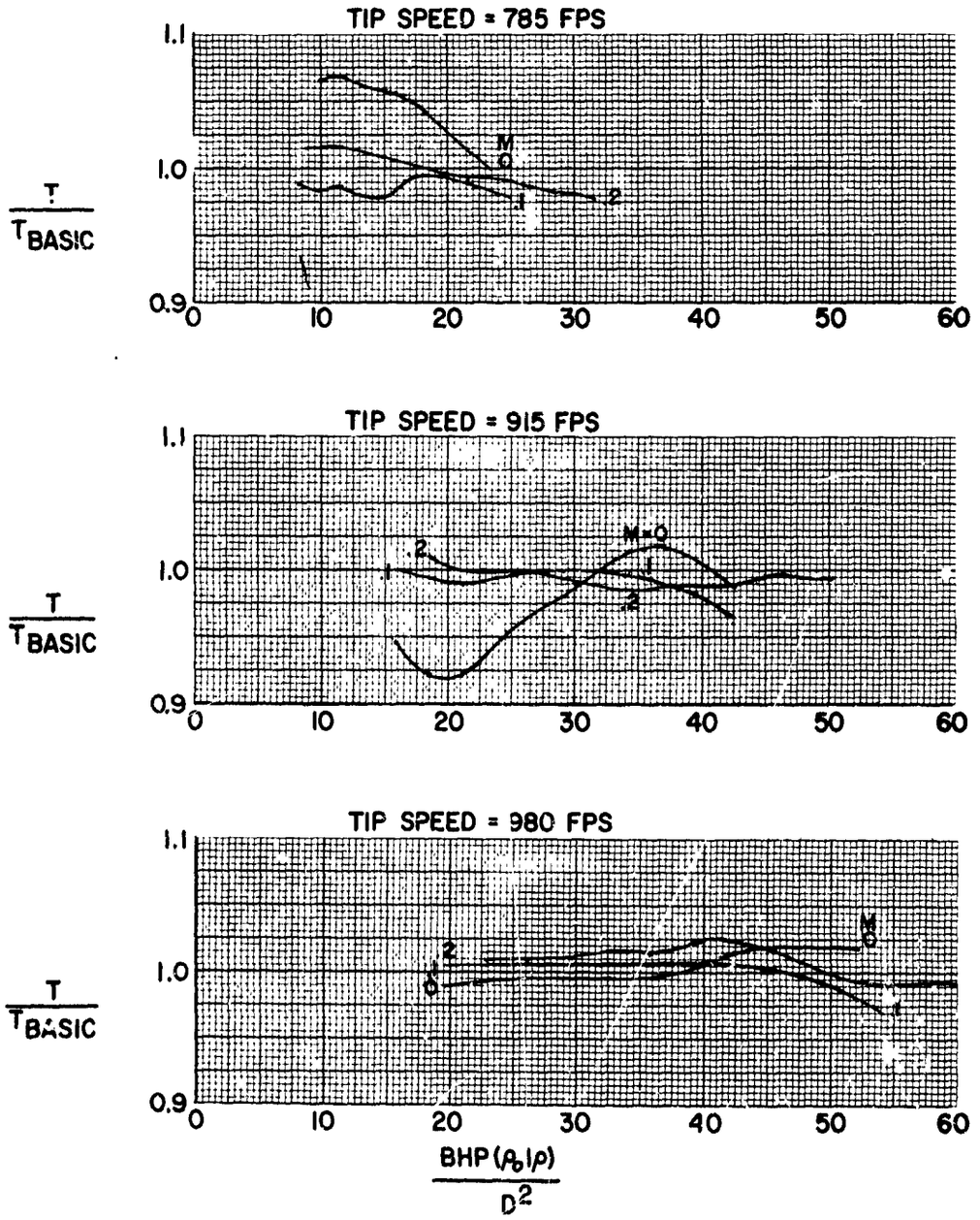

FIGURE 86

HS SHROUDED PROPELLER TEST

PHASE 1-8FT TEST SECTION
PERFORMANCE COMPARISON WITH BASIC CONFIGURATION
CONFIGURATION B2-3WT

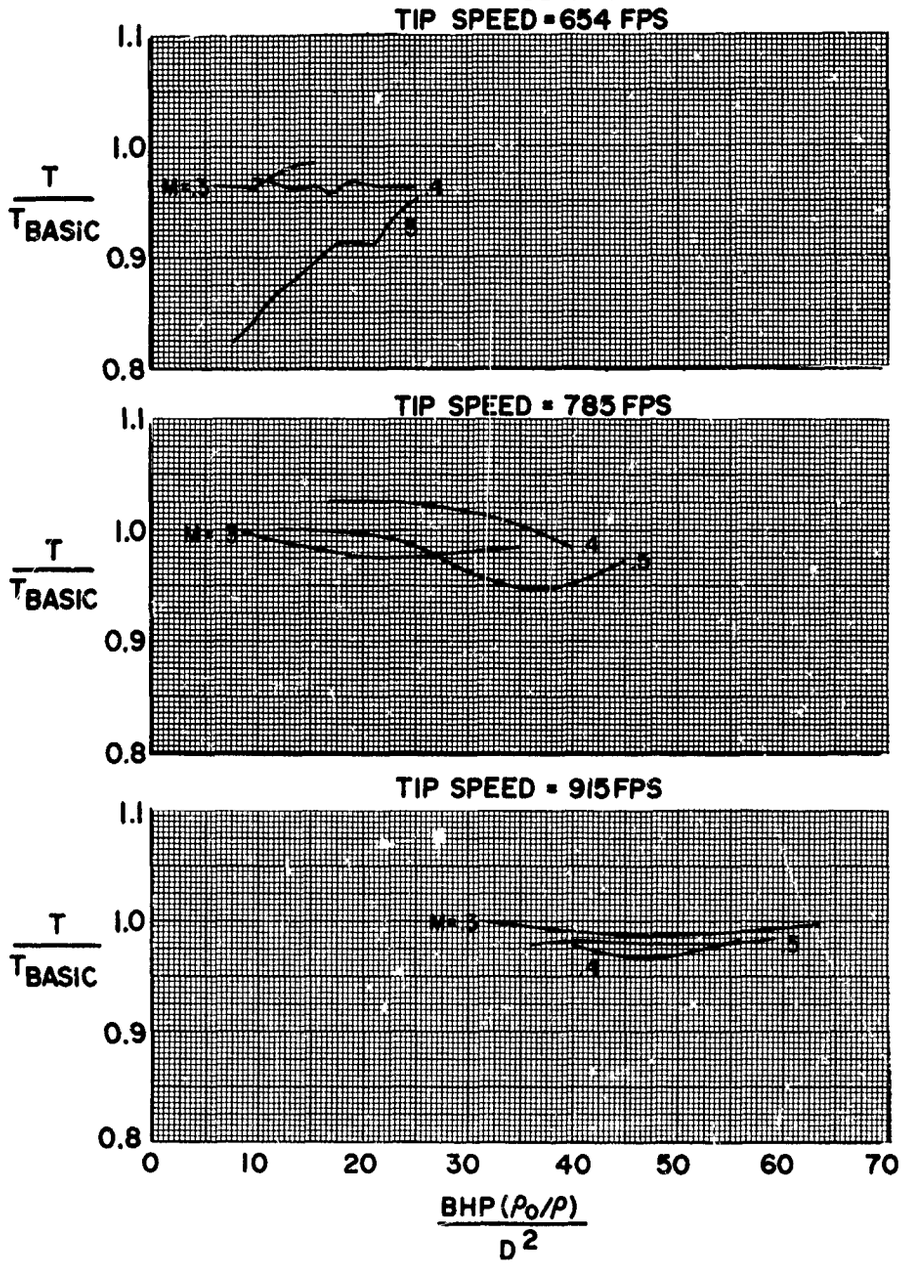

FIGURE 87

HS SHROUDED PROPELLER TEST

PHASE I - 18 FT. TEST SECTION
PERFORMANCE COMPARISON WITH BASIC CONFIGURATION
CONFIGURATION B3-3WT

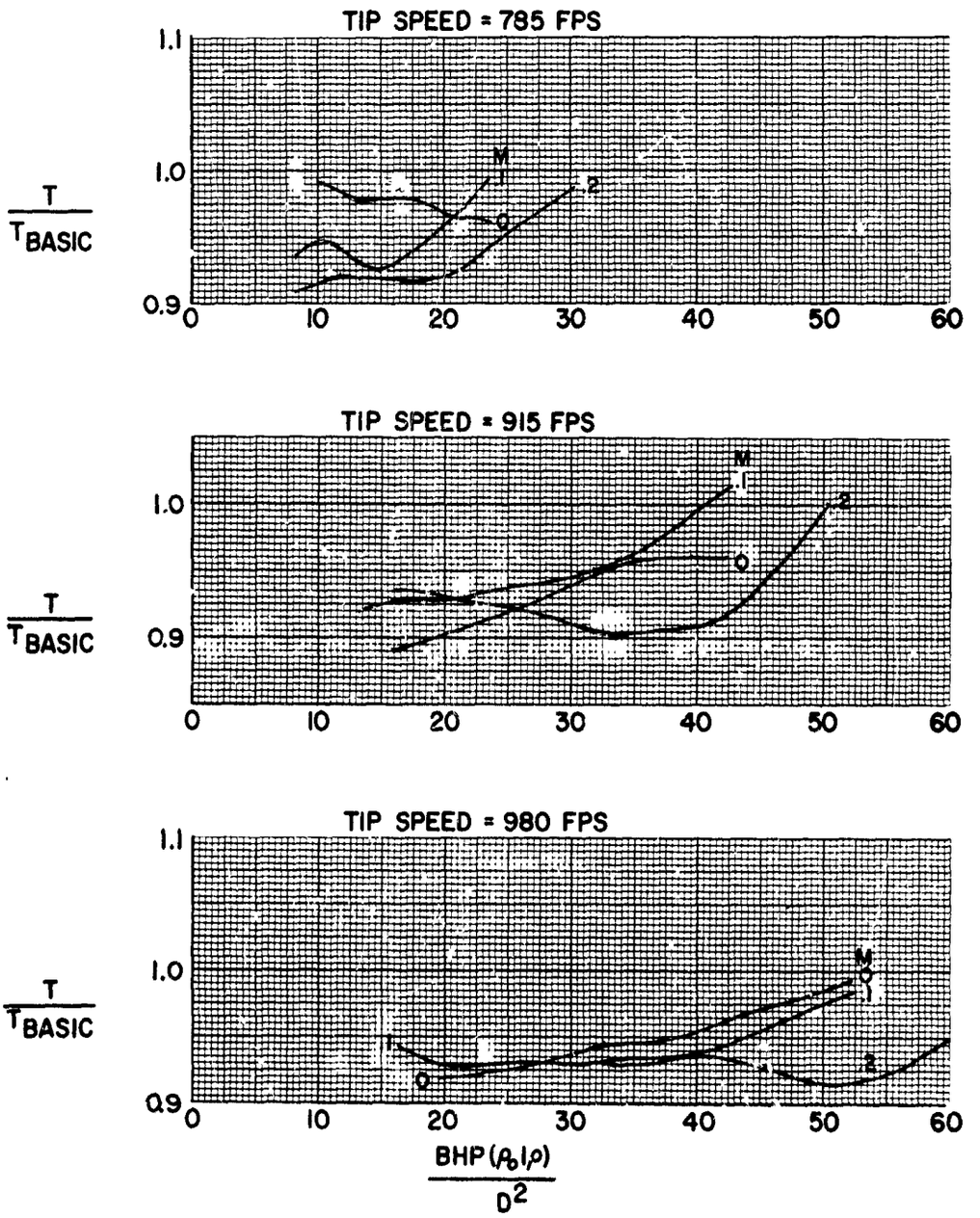

FIGURE 88

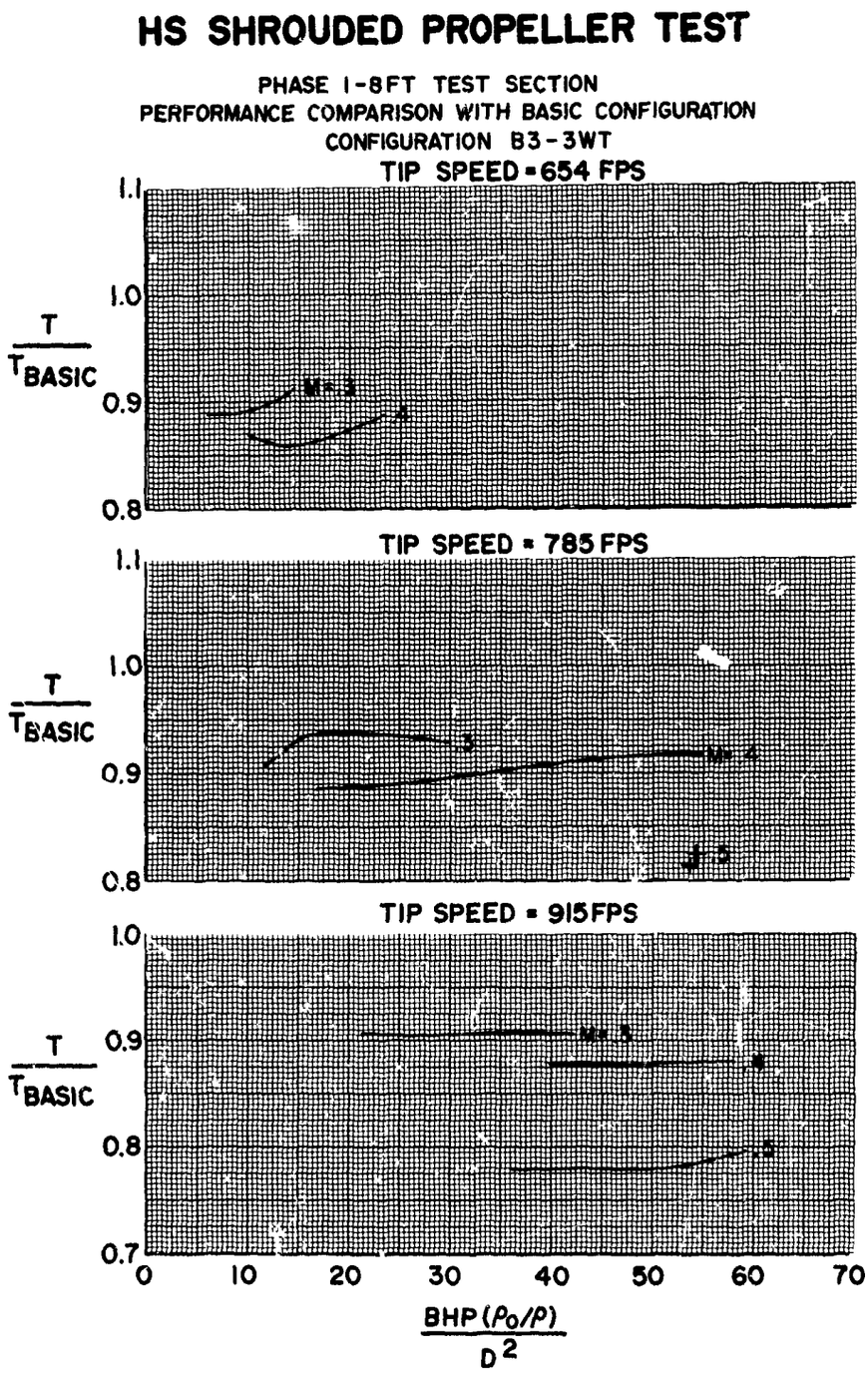
HS SHROUDED PROPELLER TEST
PHASE I-8FT TEST SECTION
PERFORMANCE COMPARISON WITH BASIC CONFIGURATION
CONFIGURATION B3-3WT
TIP SPEED = 654 FPS
TIP SPEED = 785 FPS
TIP SPEED = 915 FPS
T / T BASIC
1.1
1.0
0.9
0.8
0.7
0
10
20
30
40
50
60
70
BHP (ρ0/ρ) / D2

FIGURE 89

HS SHROUDED PROPELLER TEST

PHASE I - 18/FT. TEST SECTION
PERFORMANCE COMPARISON WITH BASIC CONFIGURATION
CONFIGURATION B4 - 3WT

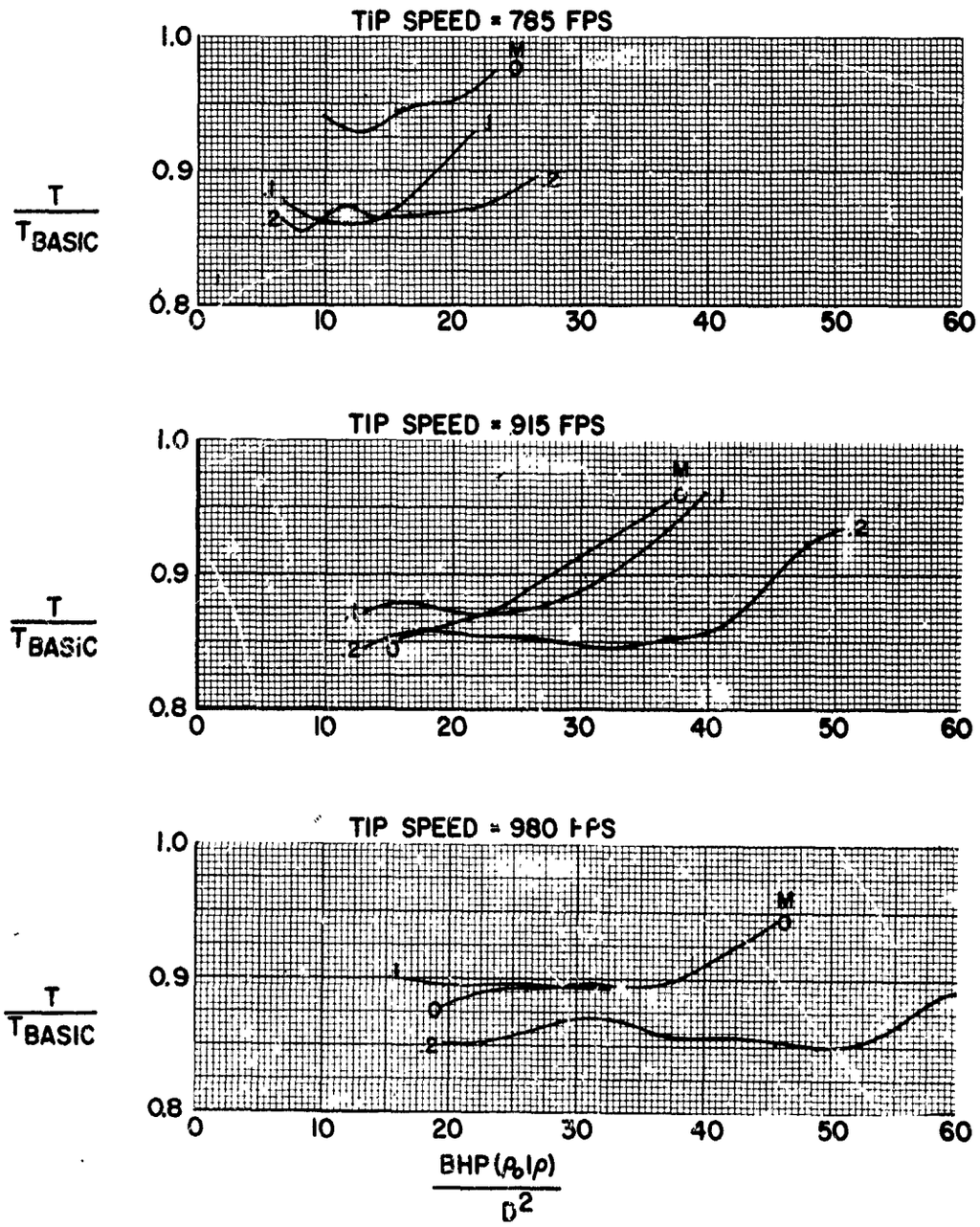

FIGURE 90

HS SHROUDED PROPELLER TEST

PHASE 1-8FT TEST SECTION
PERFORMANCE COMPARISON WITH BASIC CONFIGURATION
CONFIGURATION B4-3WT

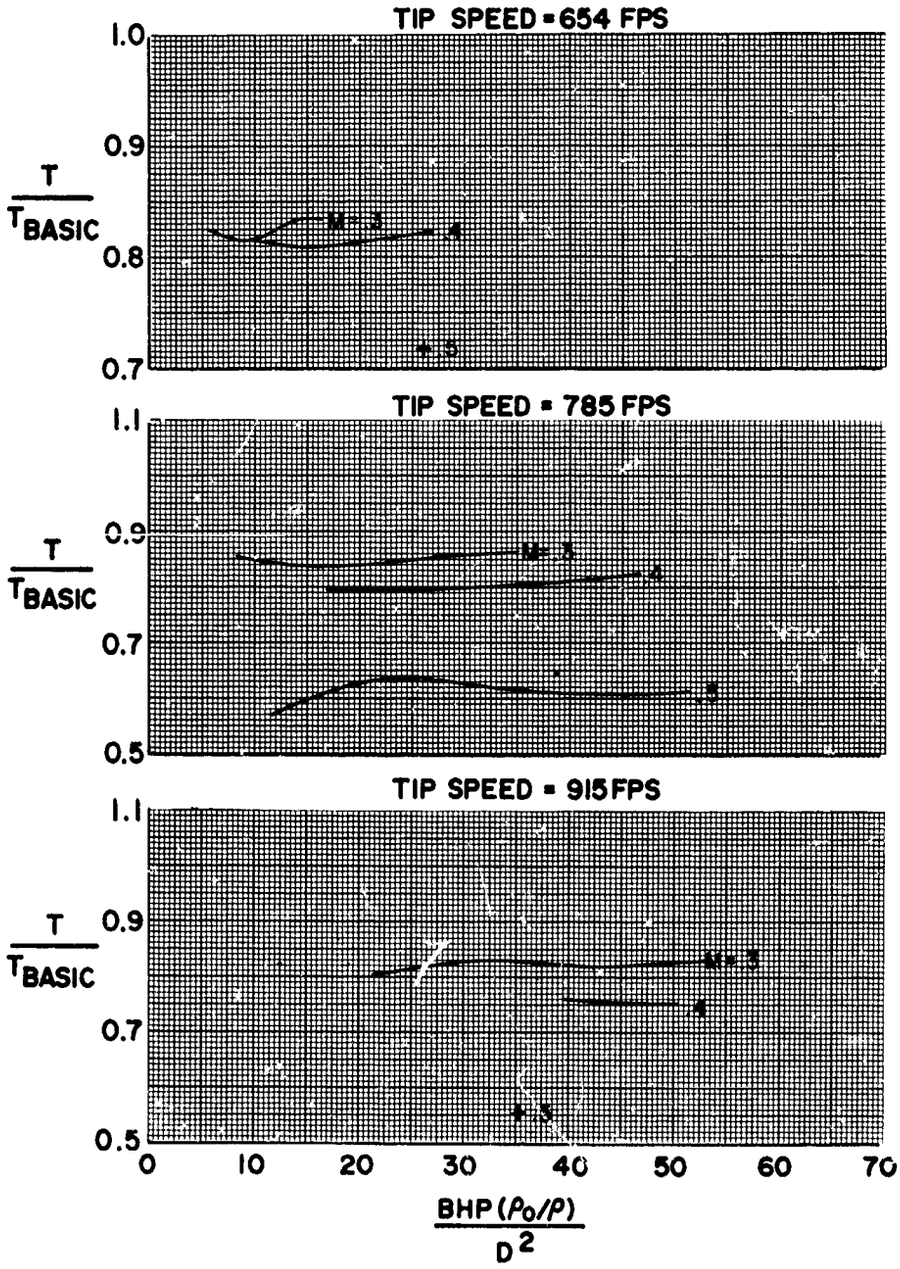

FIGURE 91

HS SHROUDED PROPELLER TEST

PHASE I - 18 FT. TEST SECTION
PERFORMANCE COMPARISON WITH BASIC CONFIGURATION
CONFIGURATION B5-3WT

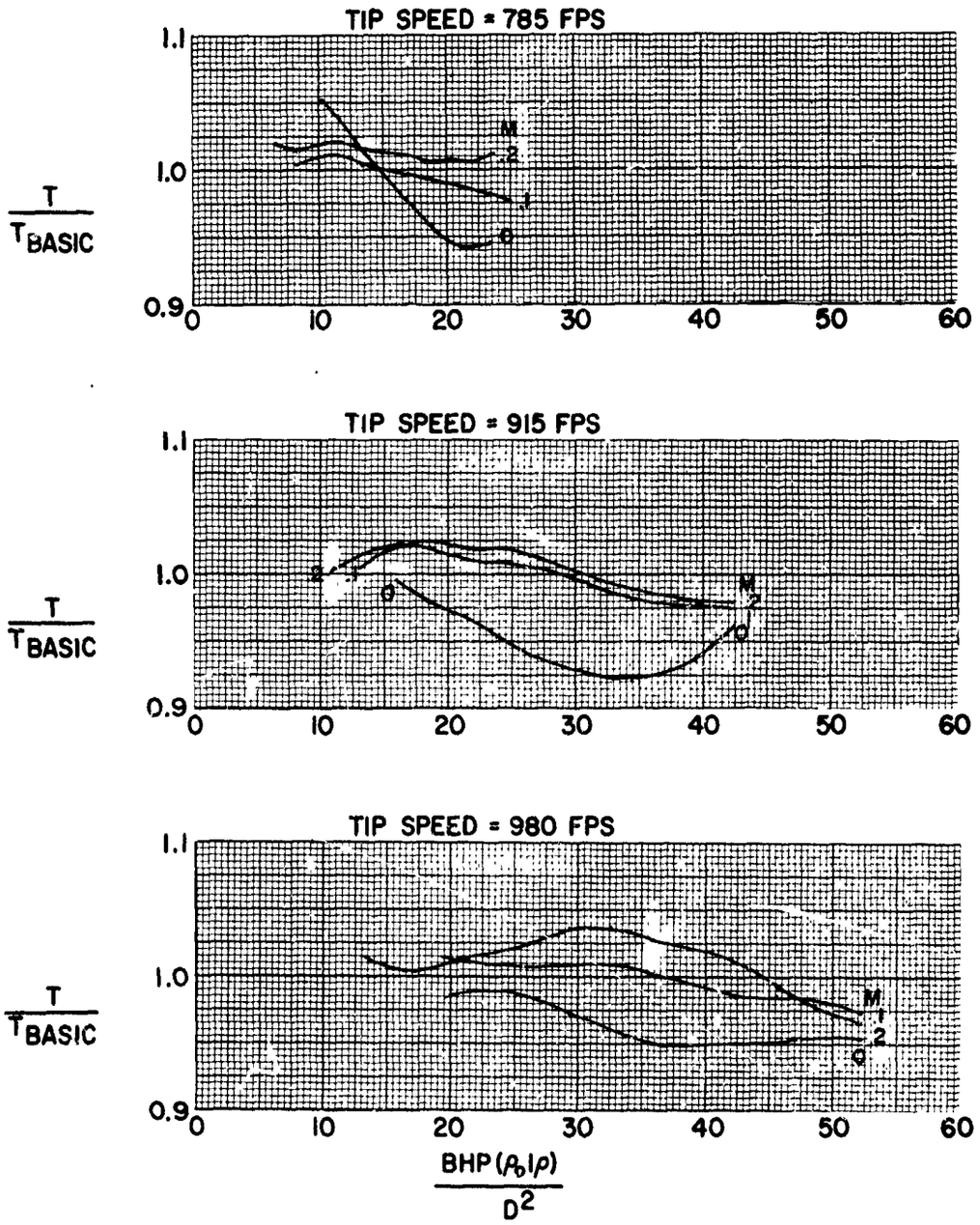

FIGURE 92

HS SHROUDED PROPELLER TEST

PHASE I-8FT TEST SECTION
PERFORMANCE COMPARISON WITH BASIC CONFIGURATION
CONFIGURATION B5-3WT

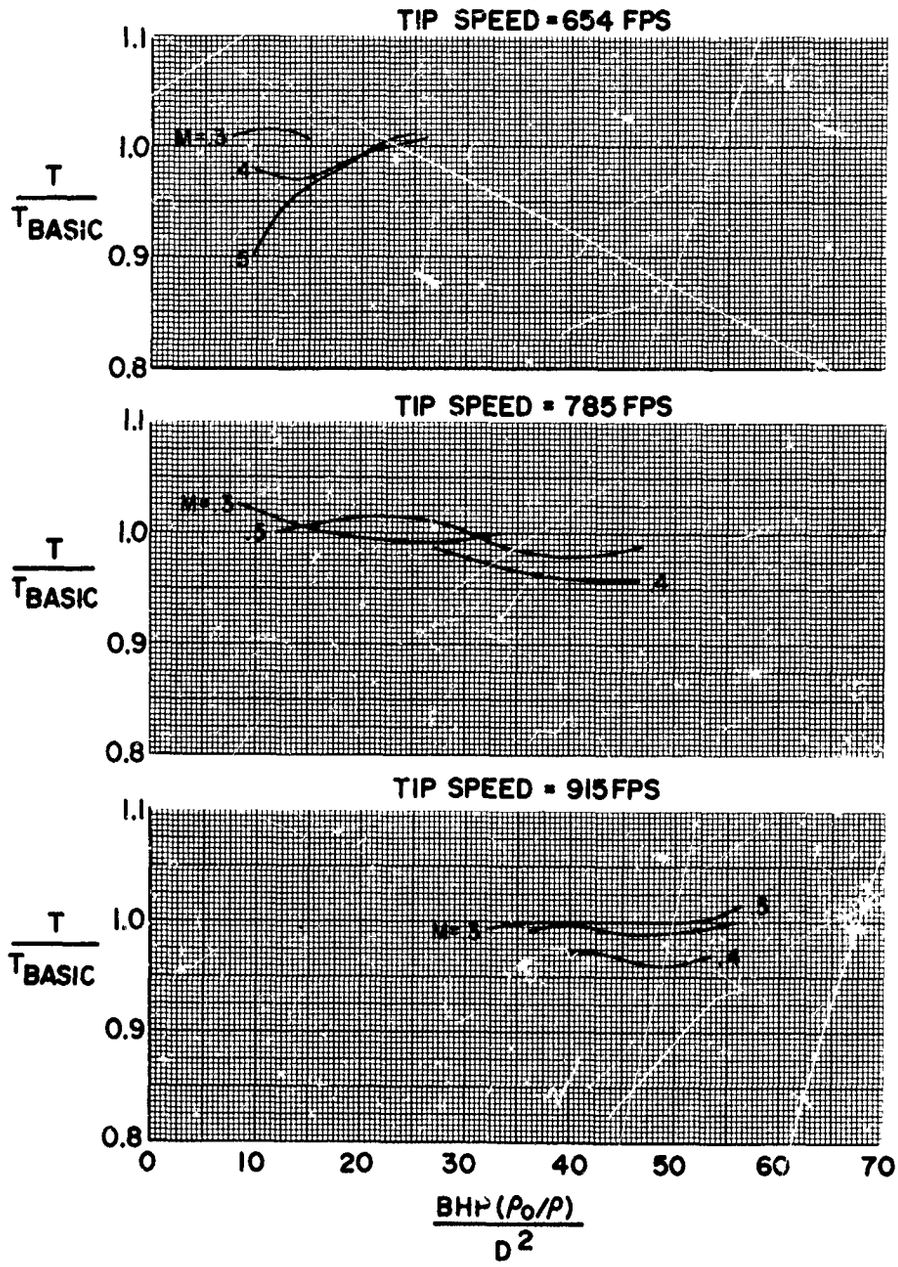

FIGURE 93

HS SHROUDED PROPELLER TEST

PHASE I - 18 FT. TEST SECTION
PERFORMANCE COMPARISON WITH BASIC CONFIGURATION
CONFIGURATION B6-3WT

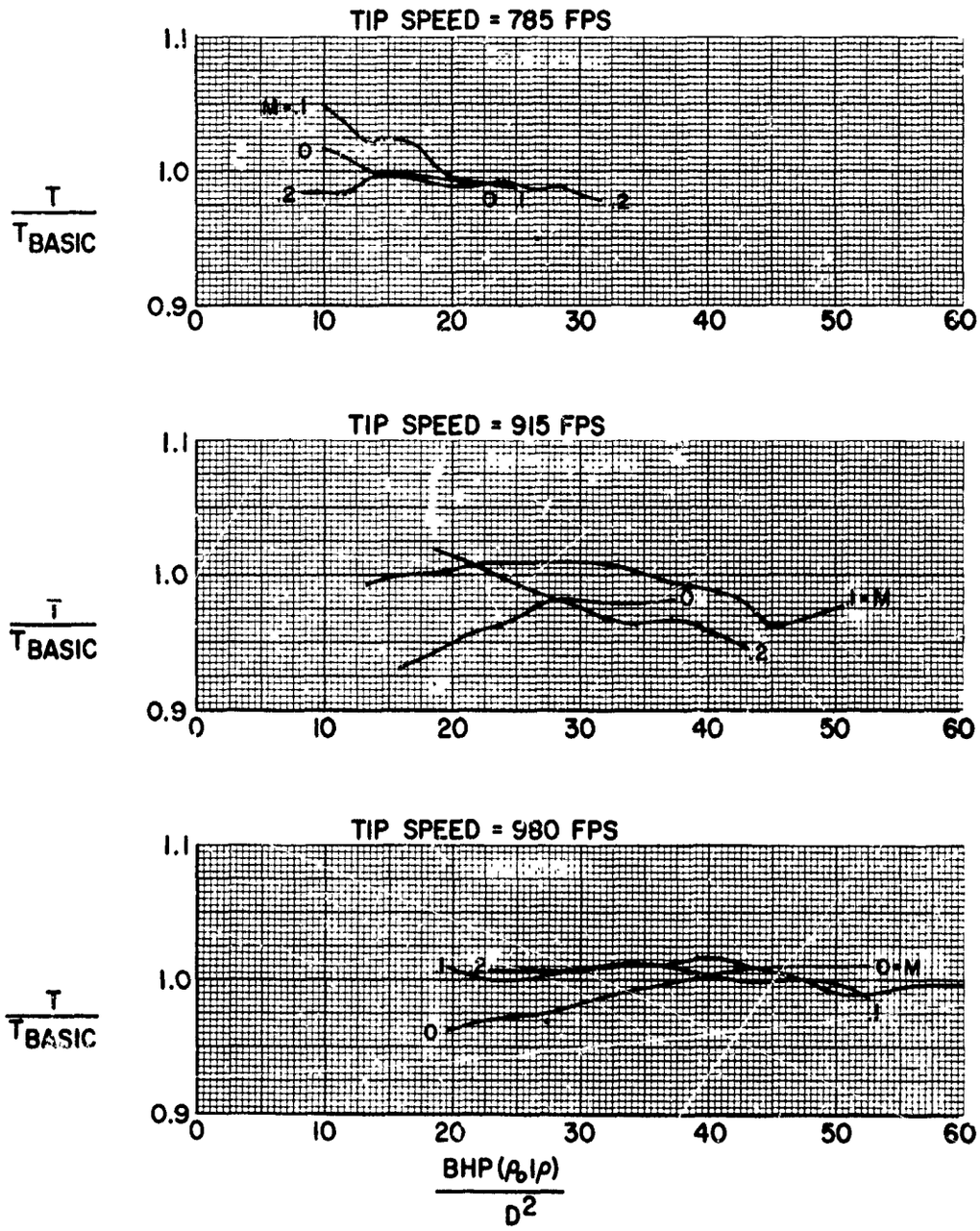

FIGURE 94

HS SHROUDED PROPELLER TEST

PHASE I-8FT TEST SECTION
PERFORMANCE COMPARISON WITH BASIC CONFIGURATION
CONFIGURATION B6 - 3WT

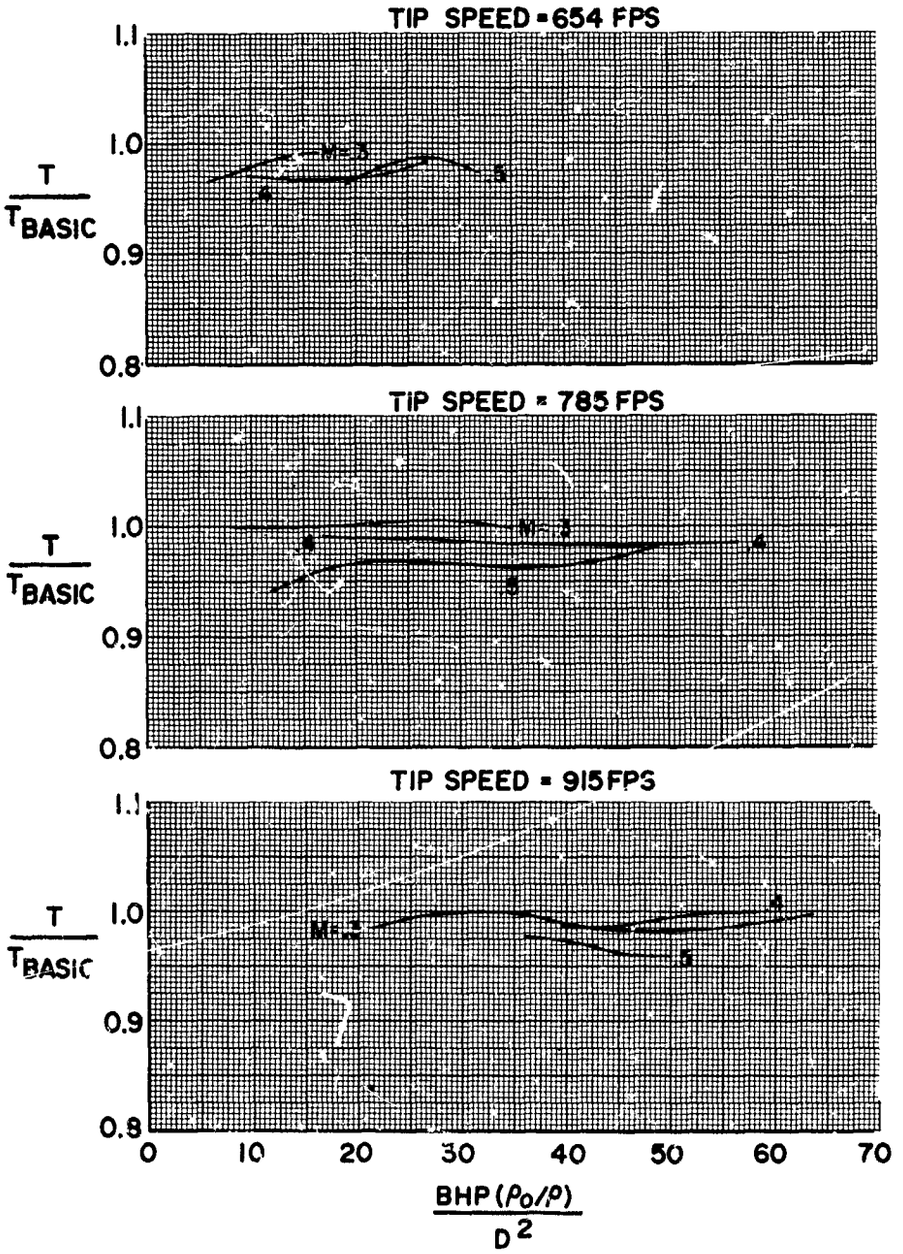

FIGURE 95

HS SHROUDED PROPELLER TEST

PHASE I - 18 FT. TEST SECTION
PERFORMANCE COMPARISON WITH BASIC CONFIGURATION
CONFIGURATION B7-3NT

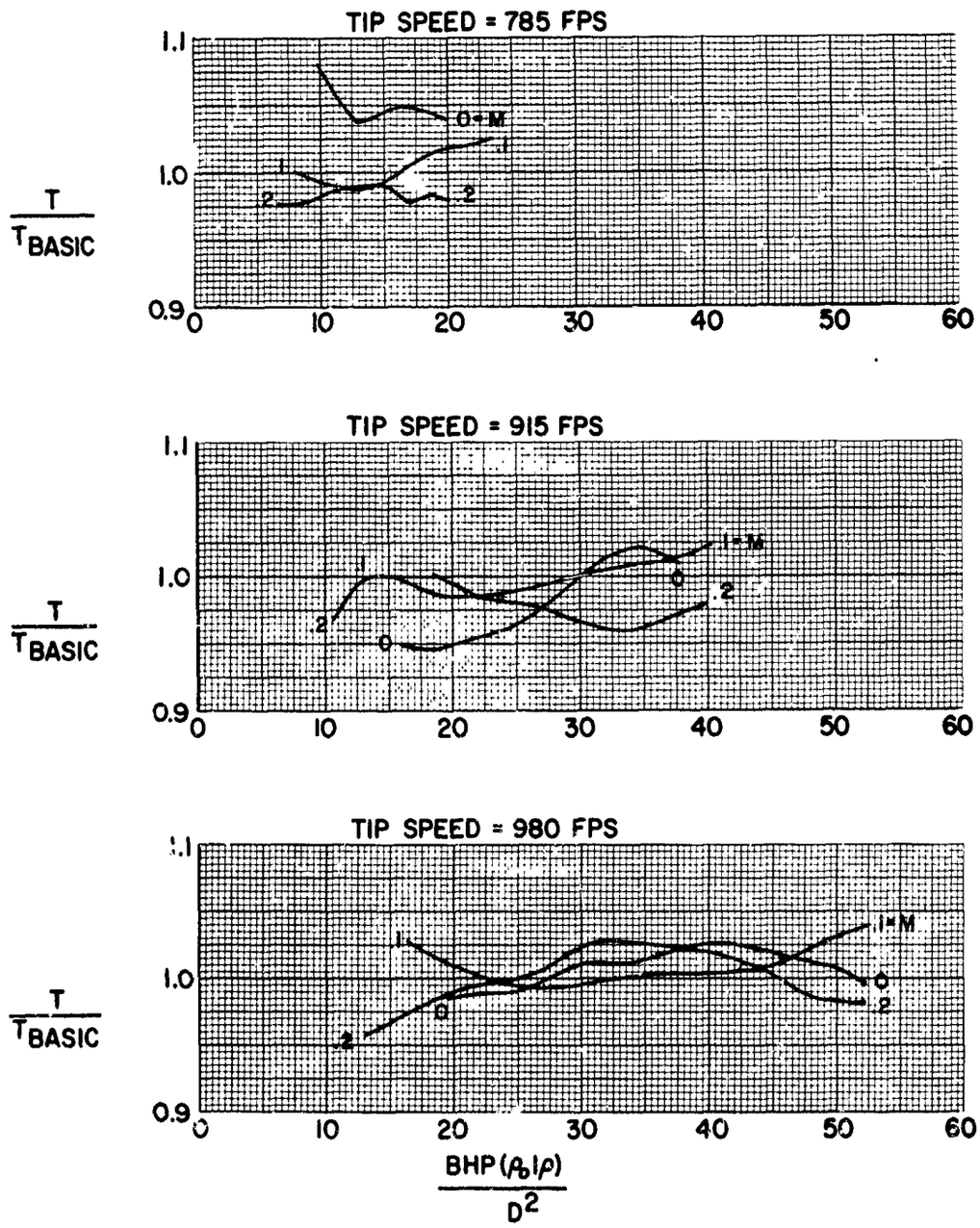

FIGURE 96

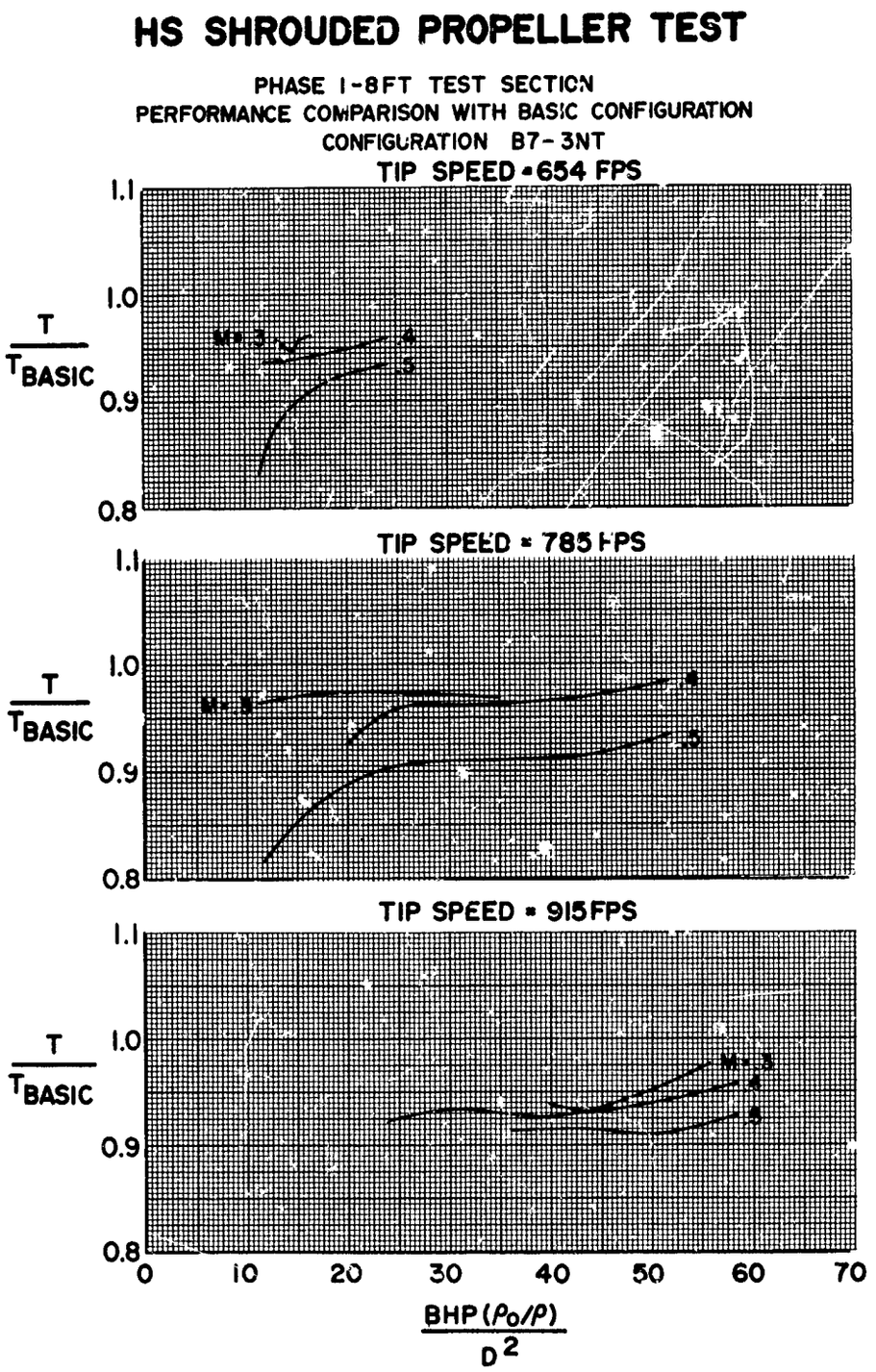
HS SHROUDED PROPELLER TEST
PHASE I-8FT TEST SECTION
PERFORMANCE COMPARISON WITH BASIC CONFIGURATION
CONFIGURATION B7-3NT
TIP SPEED = 654 FPS
TIP SPEED = 785 FPS
TIP SPEED = 915 FPS
T / T BASIC
1.1
1.0
0.9
0.8
M = .3
.4
.5
0
10
20
30
40
50
60
70
BHP (ρ0/ρ) / D2

FIGURE 97

HS SHROUDED PROPELLER TEST

PHASE I - 18 FT. TEST SECTION
PERFORMANCE COMPARISON WITH BASIC CONFIGURATION
CONFIGURATION BI - 3WT 1°

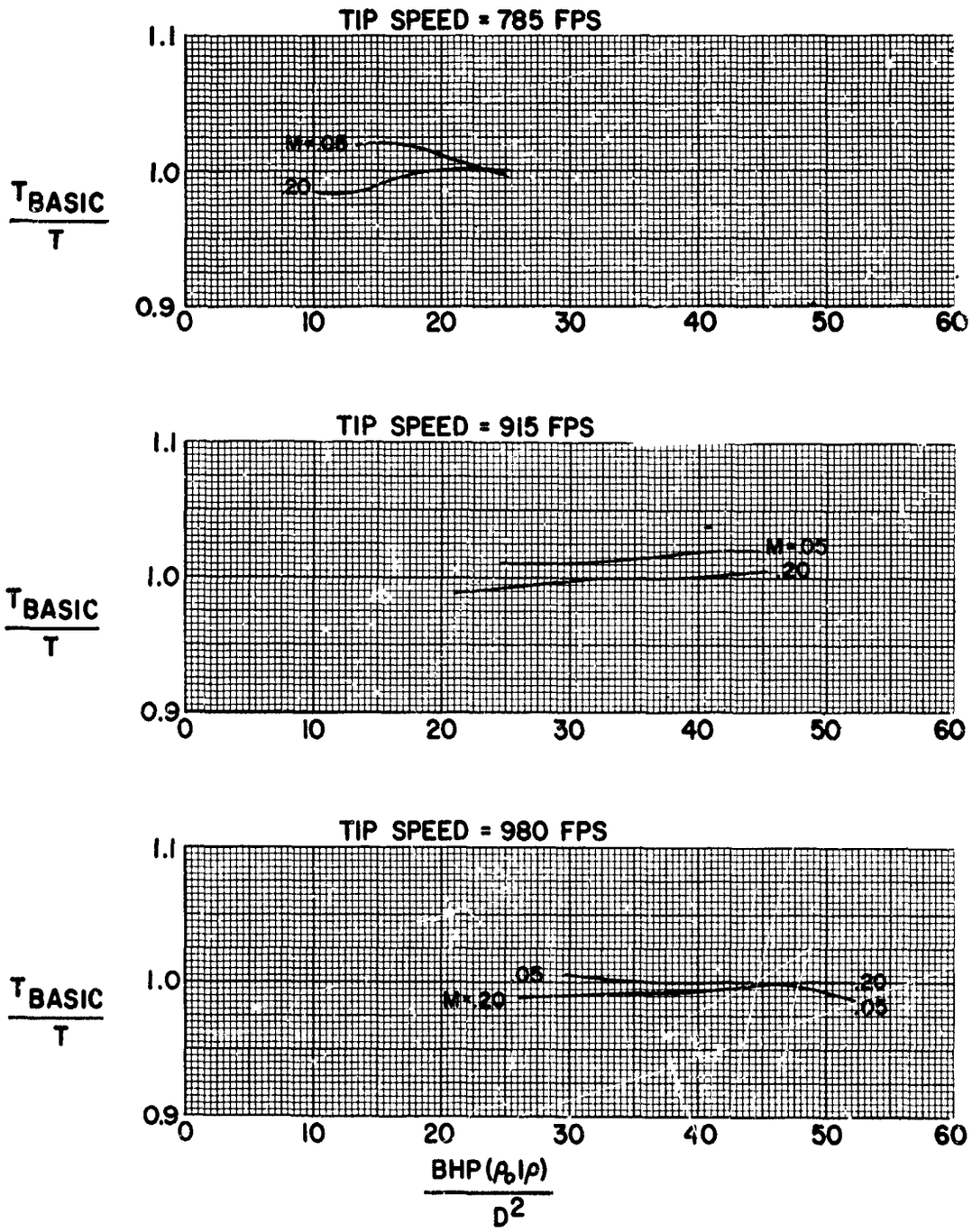

FIGURE 98

HS SHROUDED PROPELLER TEST

PHASE I-8FT TEST SECTION
PERFORMANCE COMPARISON WITH BASIC CONFIGURATION
CONFIGURATION B!-3WT I°

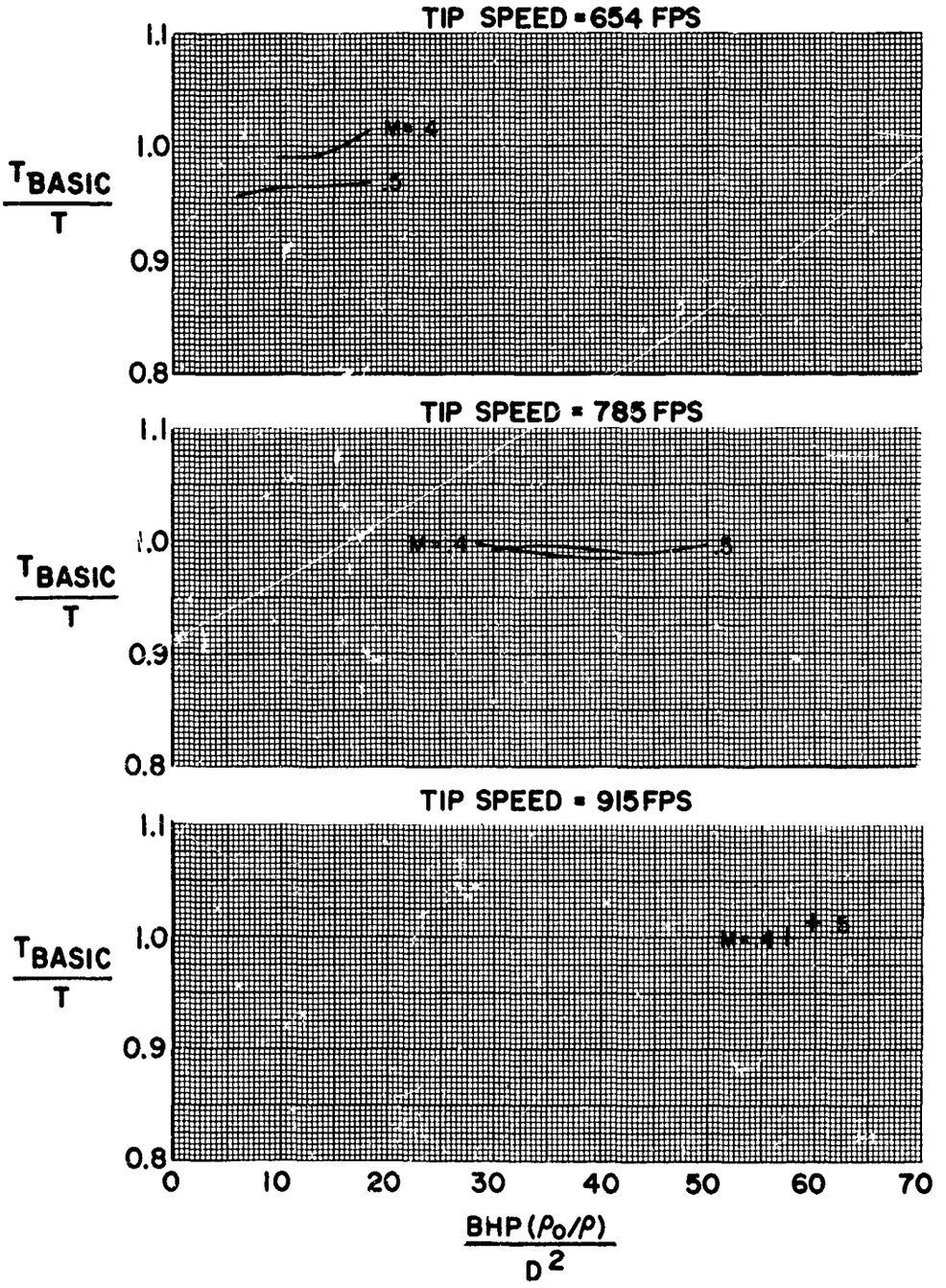

FIGURE 99

HS SHROUDED PROPELLER TEST

PHASE I - 18 FT. TEST SECTION
PERFORMANCE COMPARISON WITH BASIC CONFIGURATION
CONFIGURATION B1-3WT-110

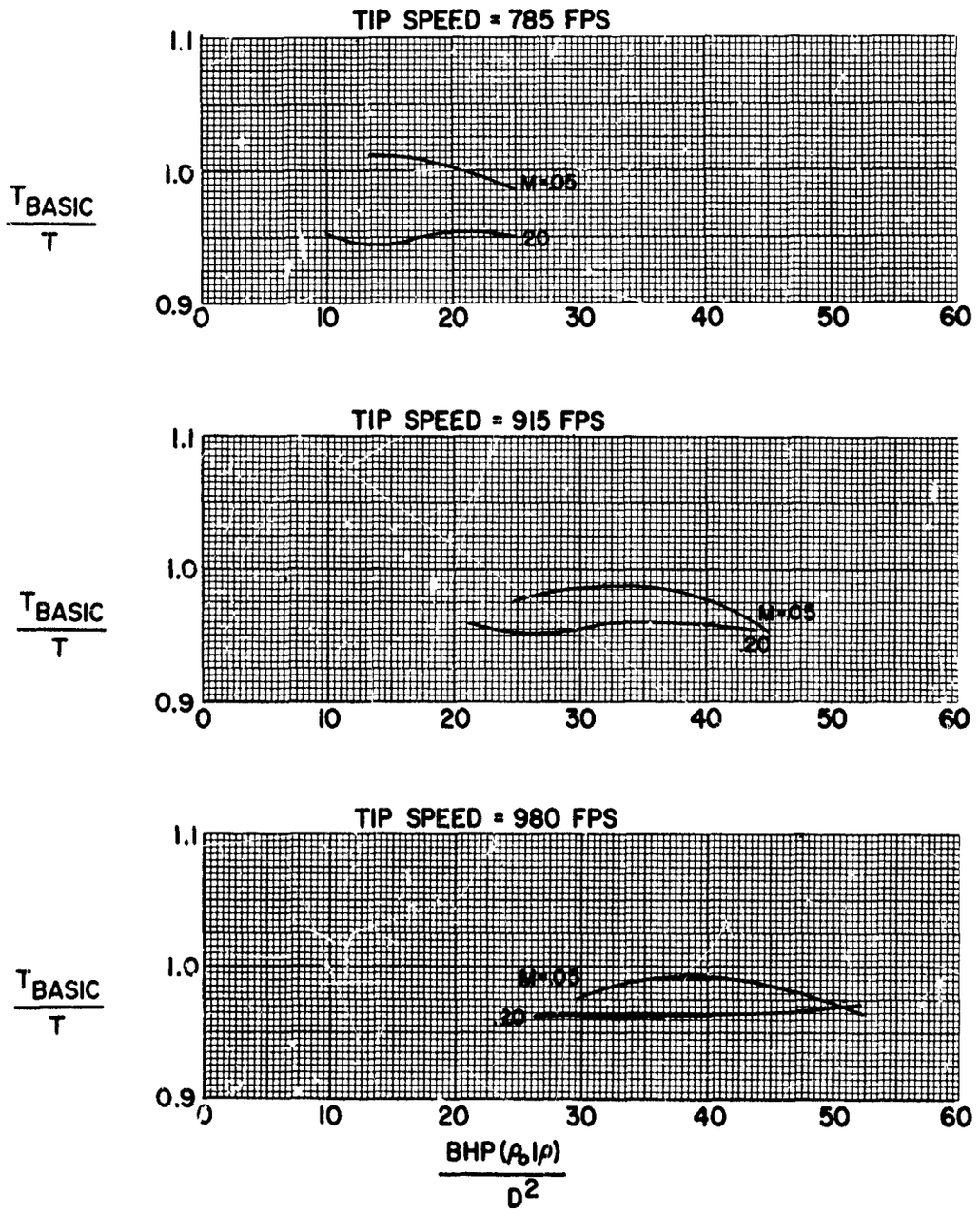

FIGURE 100

HS SHROUDED PROPELLER TEST

PHASE I – 18 FT. TEST SECTION
PERFORMANCE COMPARISON WITH BASIC CONFIGURATION
CONFIGURATION BI – 3WT V°

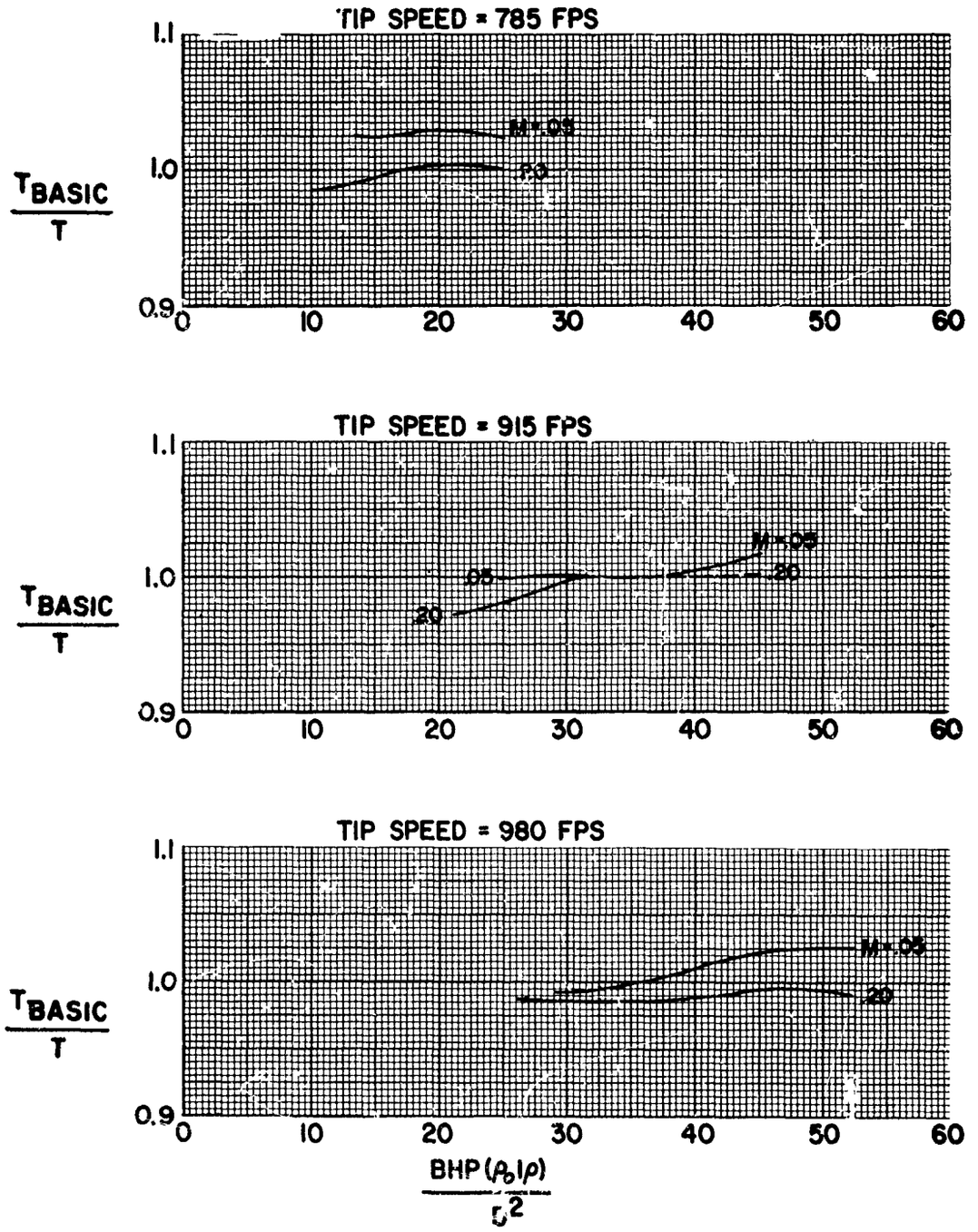

FIGURE 101

HS SHROUDED PROPELLER TEST

PHASE I-8FT TEST SECTION
PERFORMANCE COMPARISON WITH BASIC CONFIGURATION
CONFIGURATION BI-3WT V*

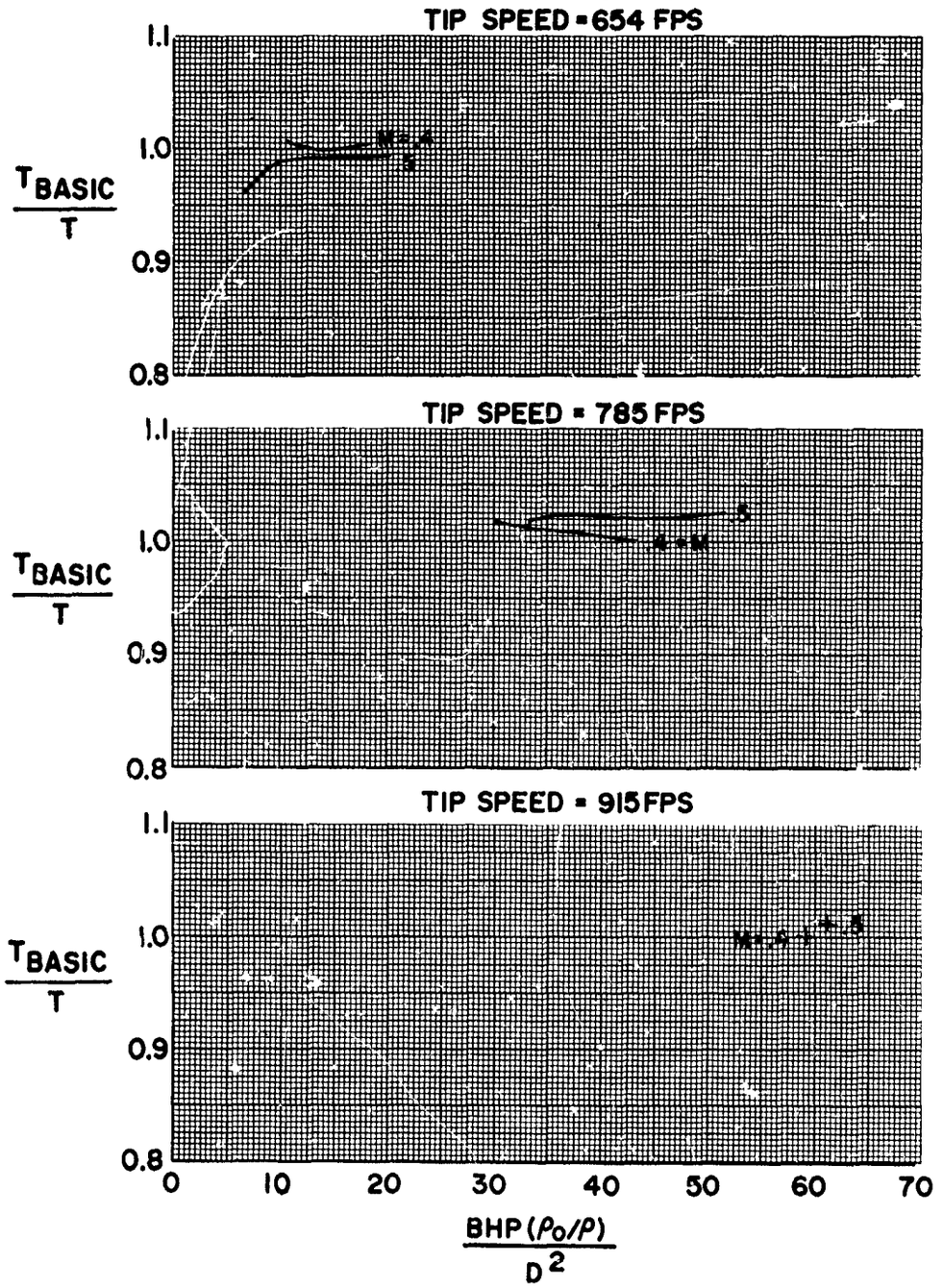

FIGURE 102

HS SHROUDED PROPELLER TEST

PHASE I – 18 FT. TEST SECTION
PERFORMANCE COMPARISON WITH BASIC CONFIGURATION
CONFIGURATION BI-3WT V10

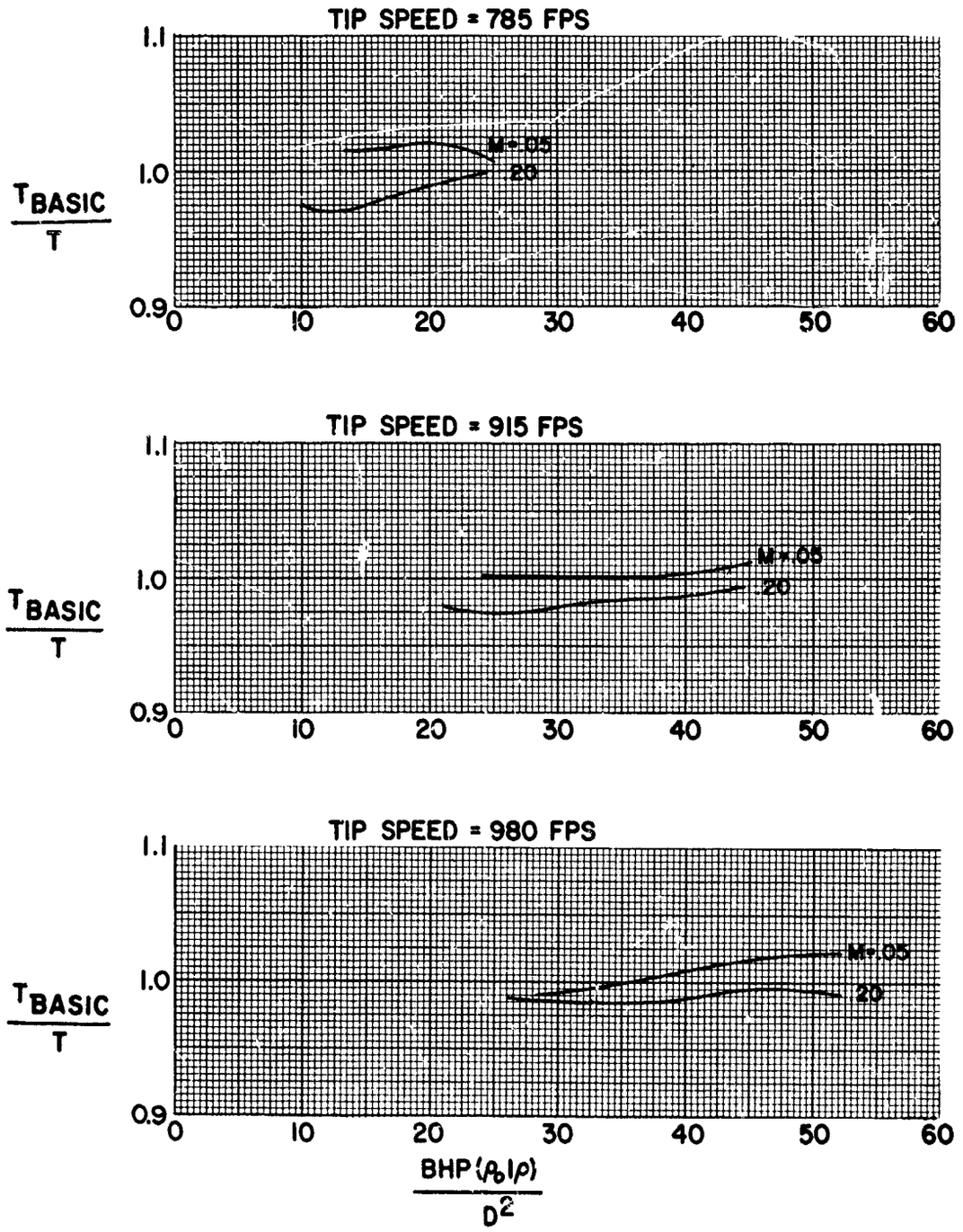

FIGURE 103

HS SHROUDED PROPELLER TEST

PHASE I - 18 FT. TEST SECTION
PERFORMANCE COMPARISON WITH BASIC CONFIGURATION
CONFIGURATION BI-3WT V-5

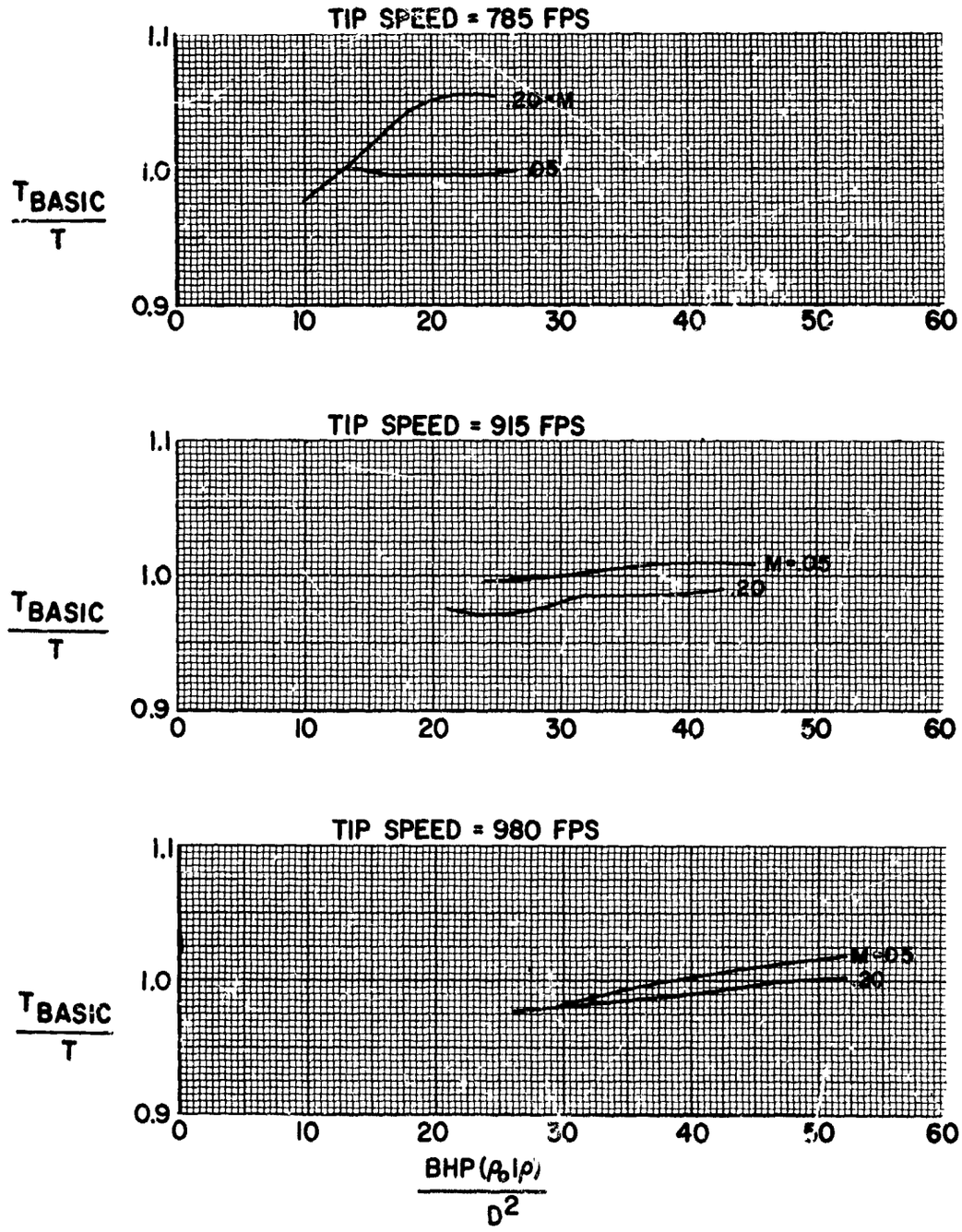

FIGURE 104

HS SHROUDED PROPELLER TEST

PERFORMANCE COMPARISON WITH BASIC CONFIGURATION, BI-3WT
EFFECT OF LIP
TIP SPEED = 980 FPS

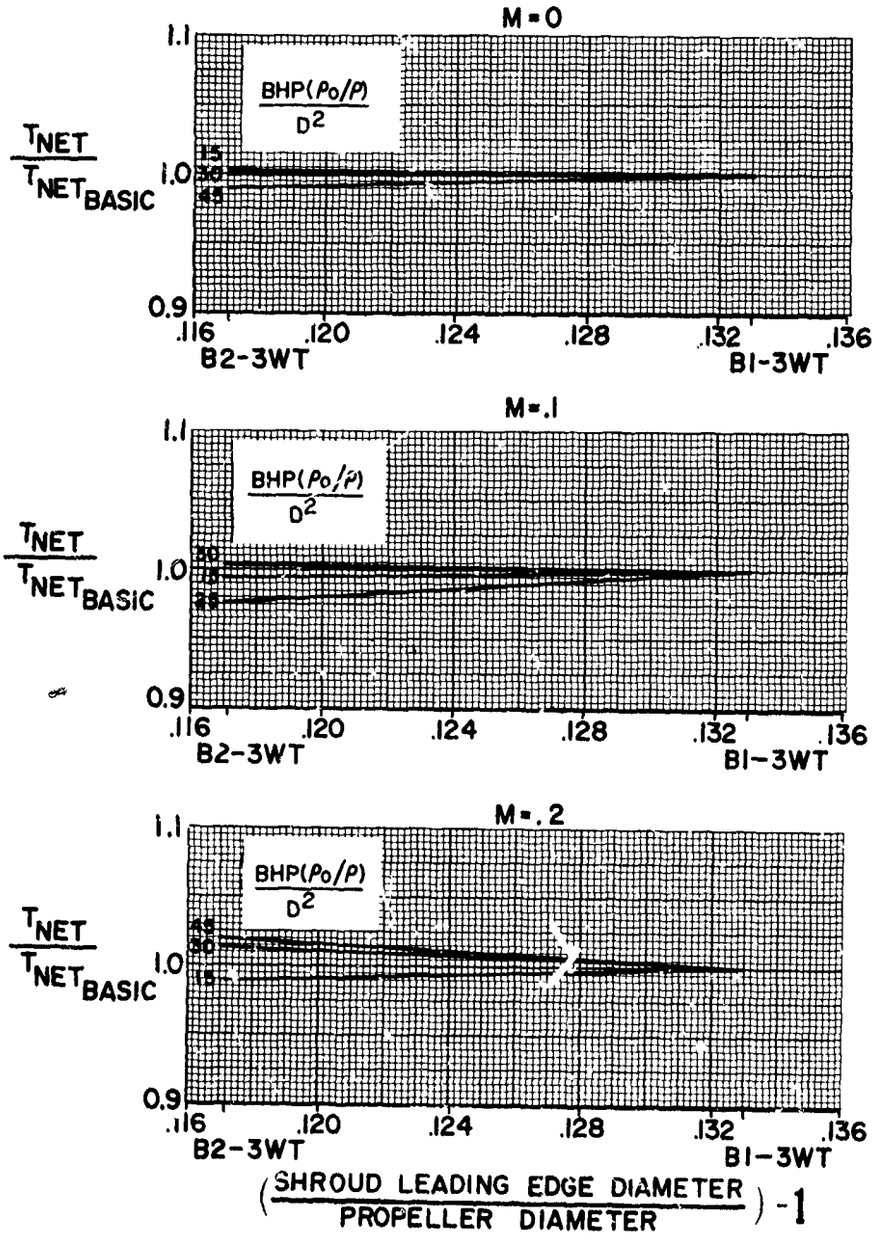

FIGURE 105

HS SHROUDED PROPELLER TEST

PERFORMANCE COMPARISON WITH BASIC CONFIGURATION, B1-3WT
EFFECT OF LIP
TIP SPEED = 915 FPS

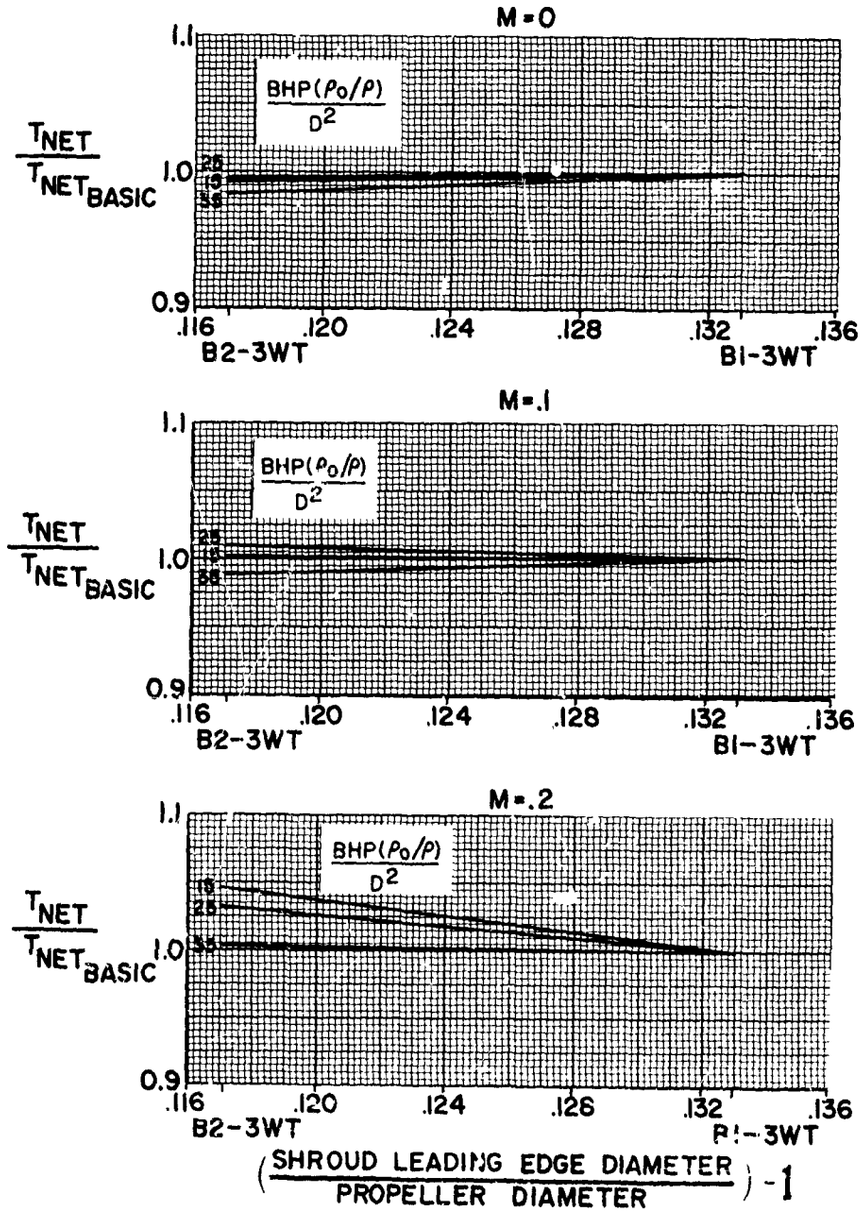

FIGURE 106

HS SHROUDED PROPELLER TEST

PERFORMANCE COMPARISON WITH BASIC CONFIGURATION, B1-3WT
EFFECT OF LIP
TIP SPEED = 785 FPS

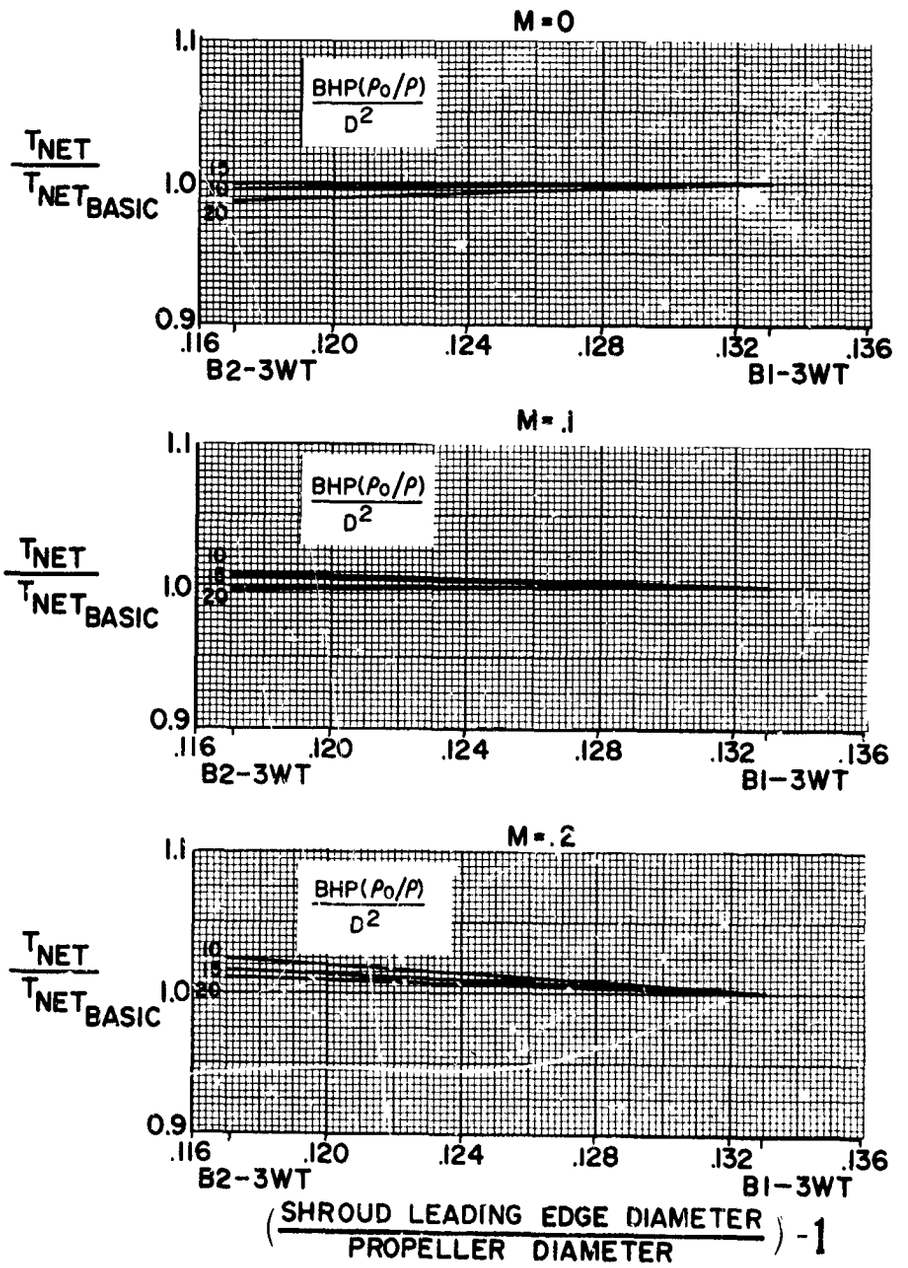

FIGURE 107

HS SHROUDED PROPELLER TEST

PERFORMANCE COMPARISON WITH BASIC CONFIGURATION, BI – 3WT
EFFECT OF LIP
TIP SPEED = 915 FPS

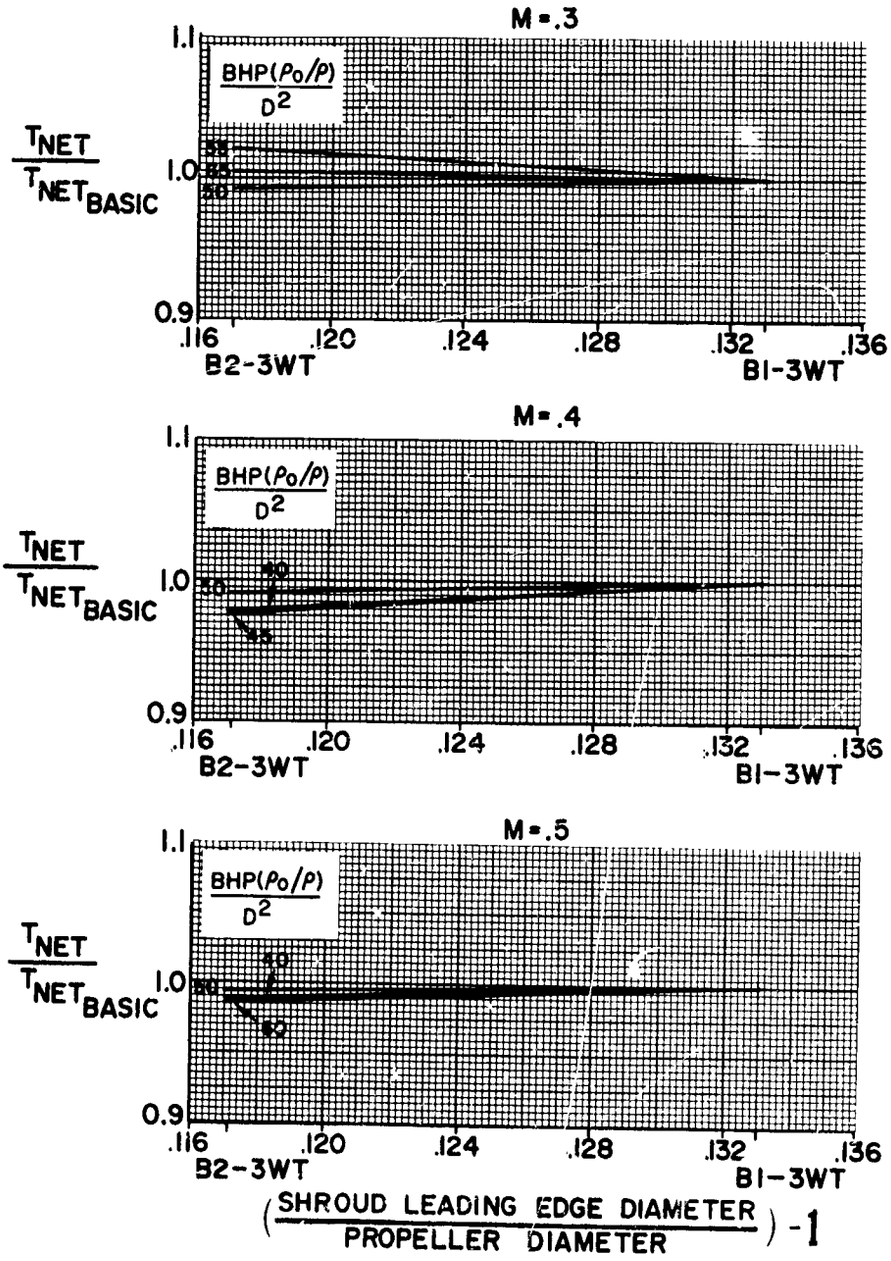

FIGURE 108

HS SHROUDED PROPELLER TEST

PERFORMANCE COMPARISON WITH BASIC CONFIGURATION, BI – 3WT
EFFECT OF LIP
TIP SPEED = 785 FPS

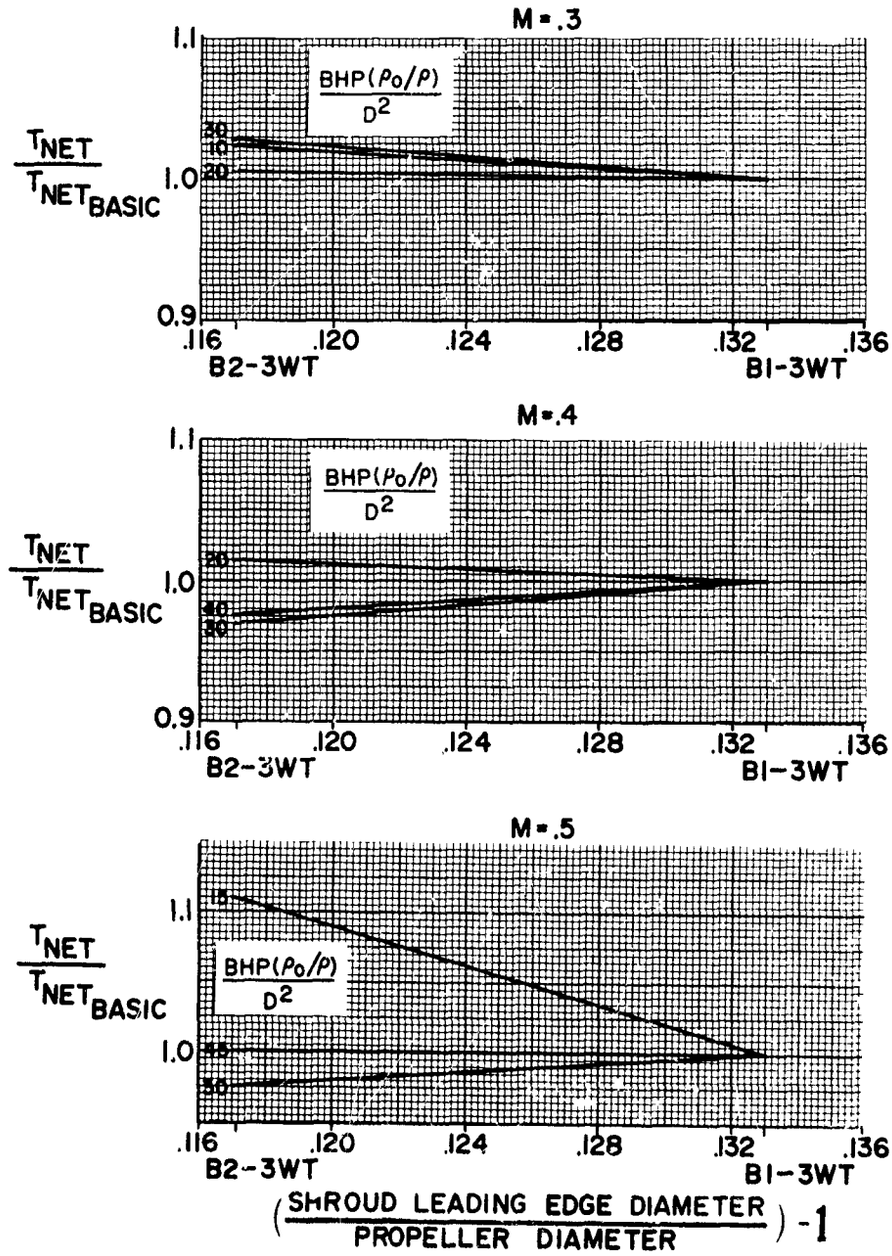

FIGURE 109

HS SHROUDED PROPELLER TEST

PERFORMANCE COMPARISON WITH BASIC CONFIGURATION, BI-3WT
EFFECT OF LIP
TIP SPEED = 654 FPS

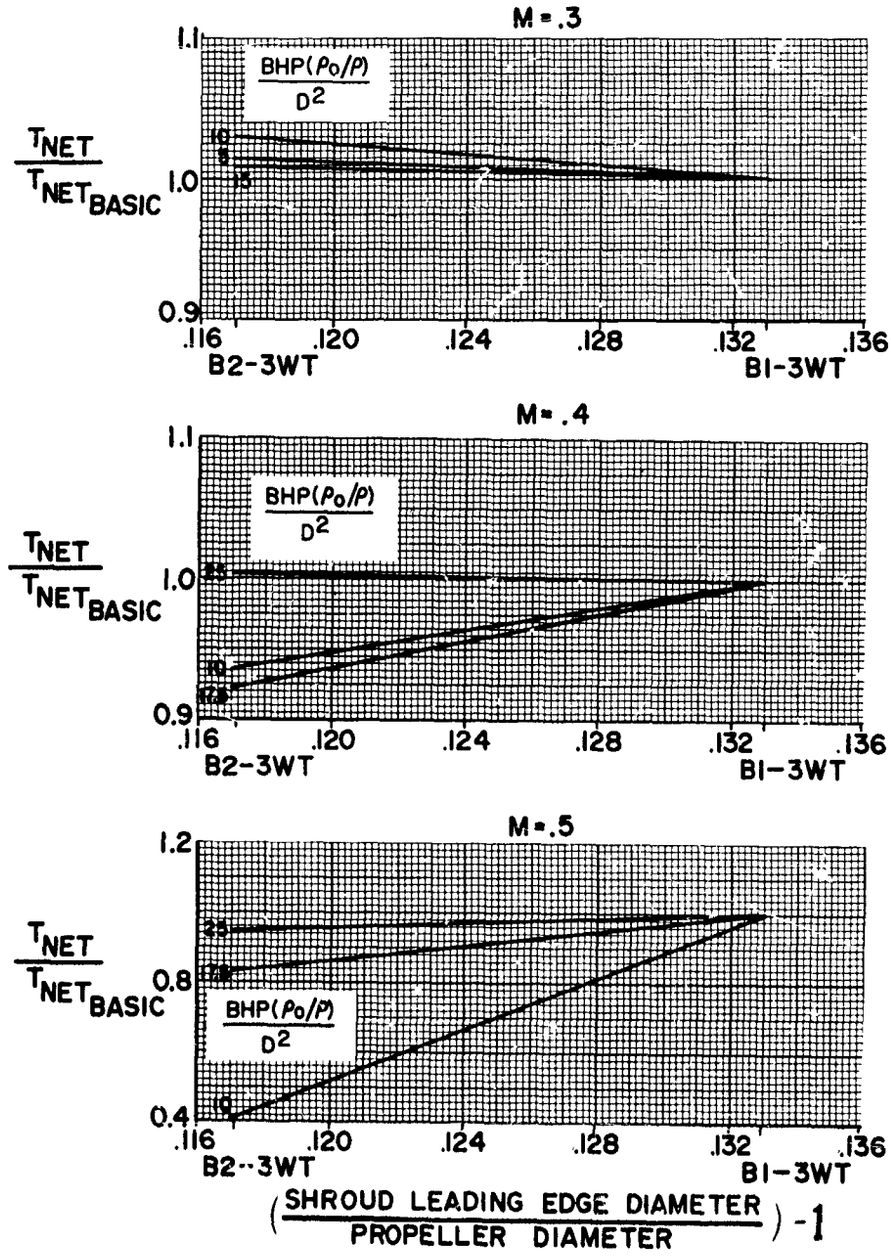

FIGURE 110

HS SHROUDED PROPELLER TEST

PERFORMANCE COMPARISON WITH BASIC CONFIGURATION, B1-3WT
EFFECT OF LIP
TIP SPEED=980FPS

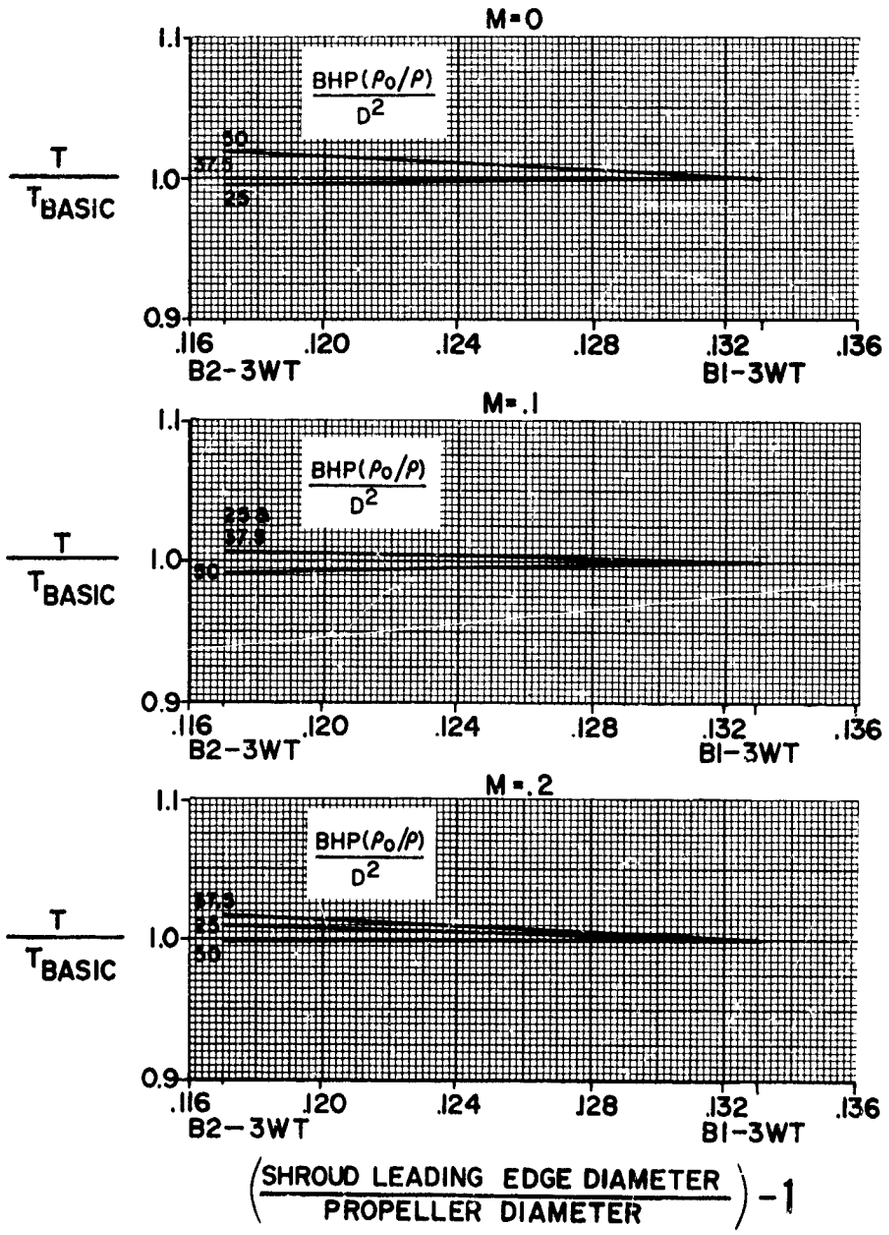

FIGURE 111

HS SHROUDED PROPELLER TEST

PERFORMANCE COMPARISON WITH BASIC CONFIGURATION, B1-3WT
EFFECT OF LIP
TIP SPEED=915 FPS

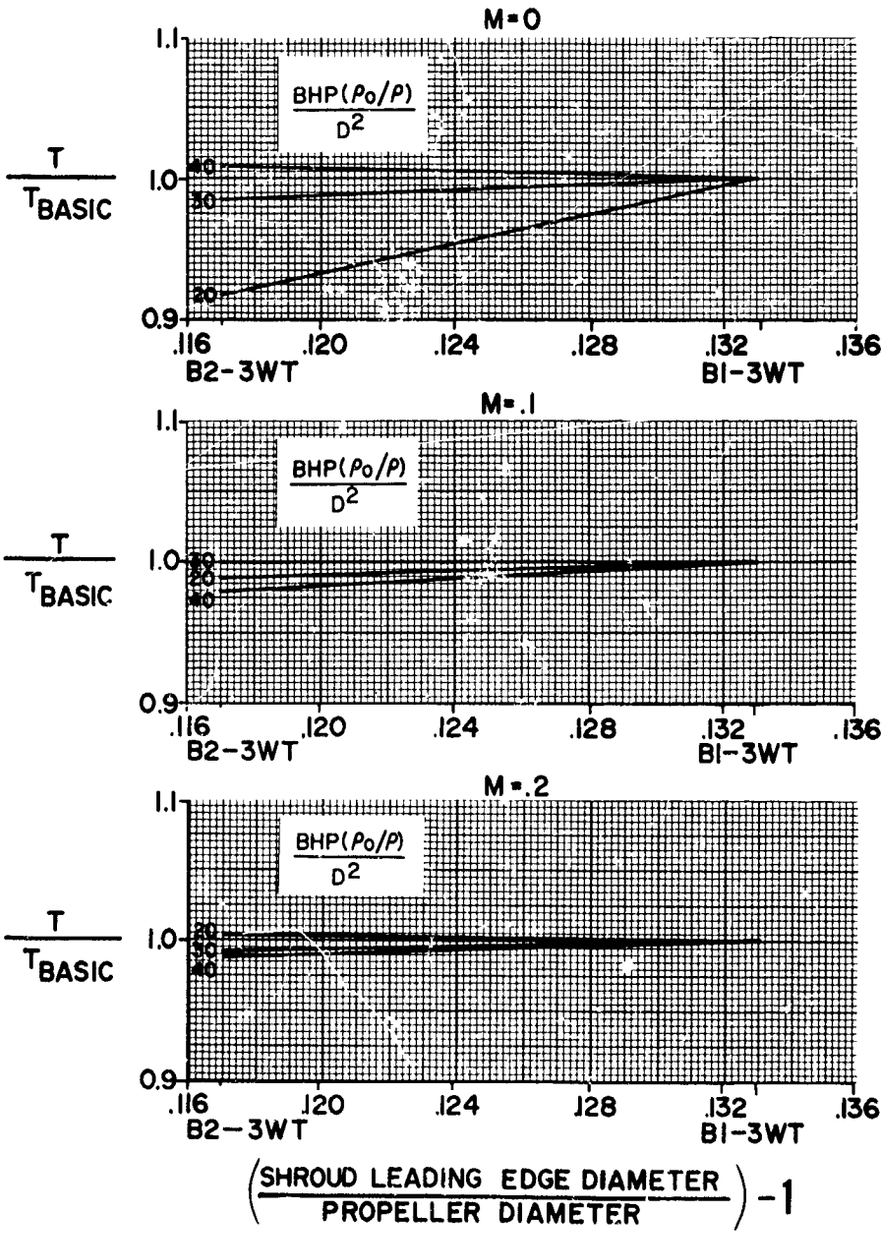

FIGURE 112

HS SHROUDED PROPELLER TEST

PERFORMANCE COMPARISON WITH BASIC CONFIGURATION, B1-3WT
EFFECT OF LIP
TIP SPEED = 785FPS

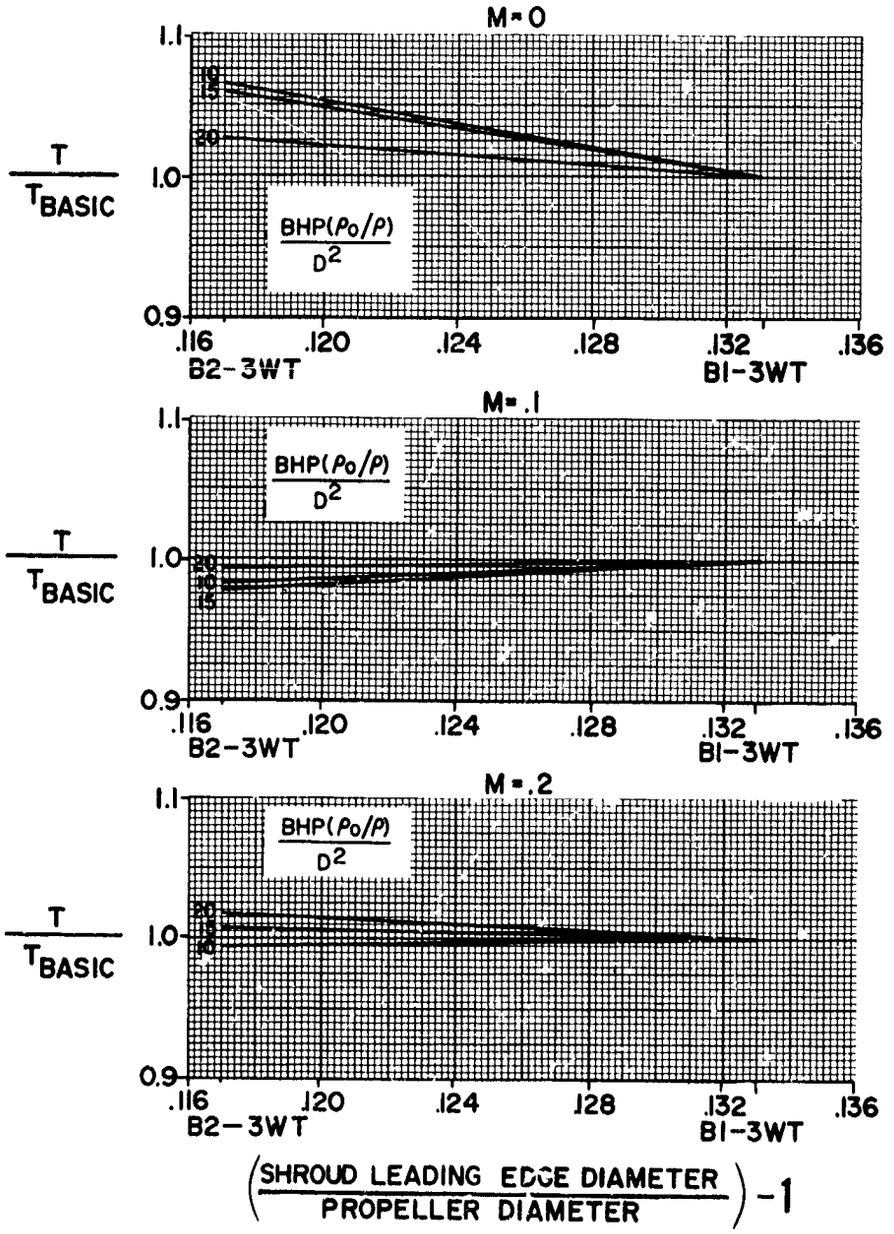

FIGURE 113

HS SHROUDED PROPELLER TEST

PERFORMANCE COMPARISON WITH BASIC CONFIGURATION, B1-3WT
EFFECT OF LIP
TIP SPEED=915 FPS

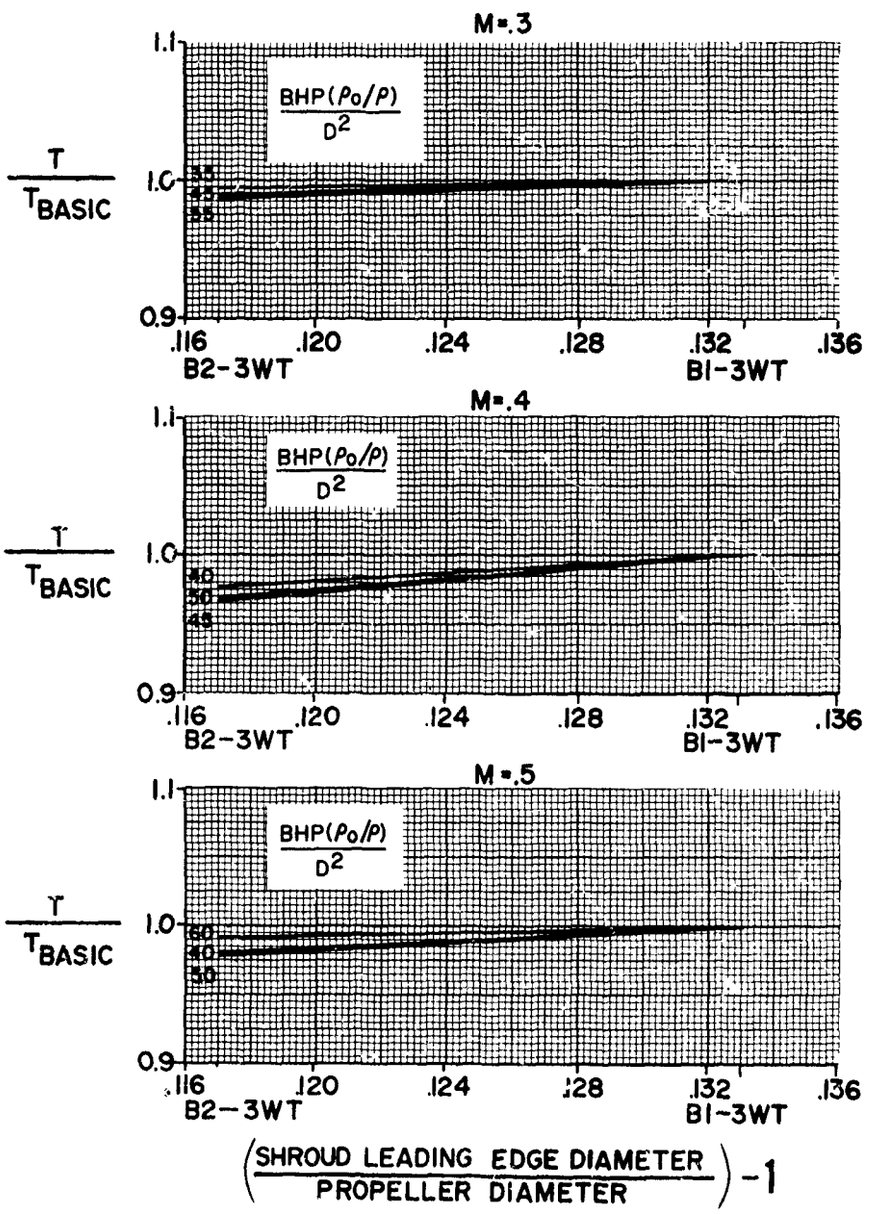

FIGURE 114

HS SHROUDED PROPELLER TEST

PERFORMANCE COMPARISON WITH BASIC CONFIGURATION, B1-3WT
EFFECT OF LIP
TIP SPEED=785 FPS

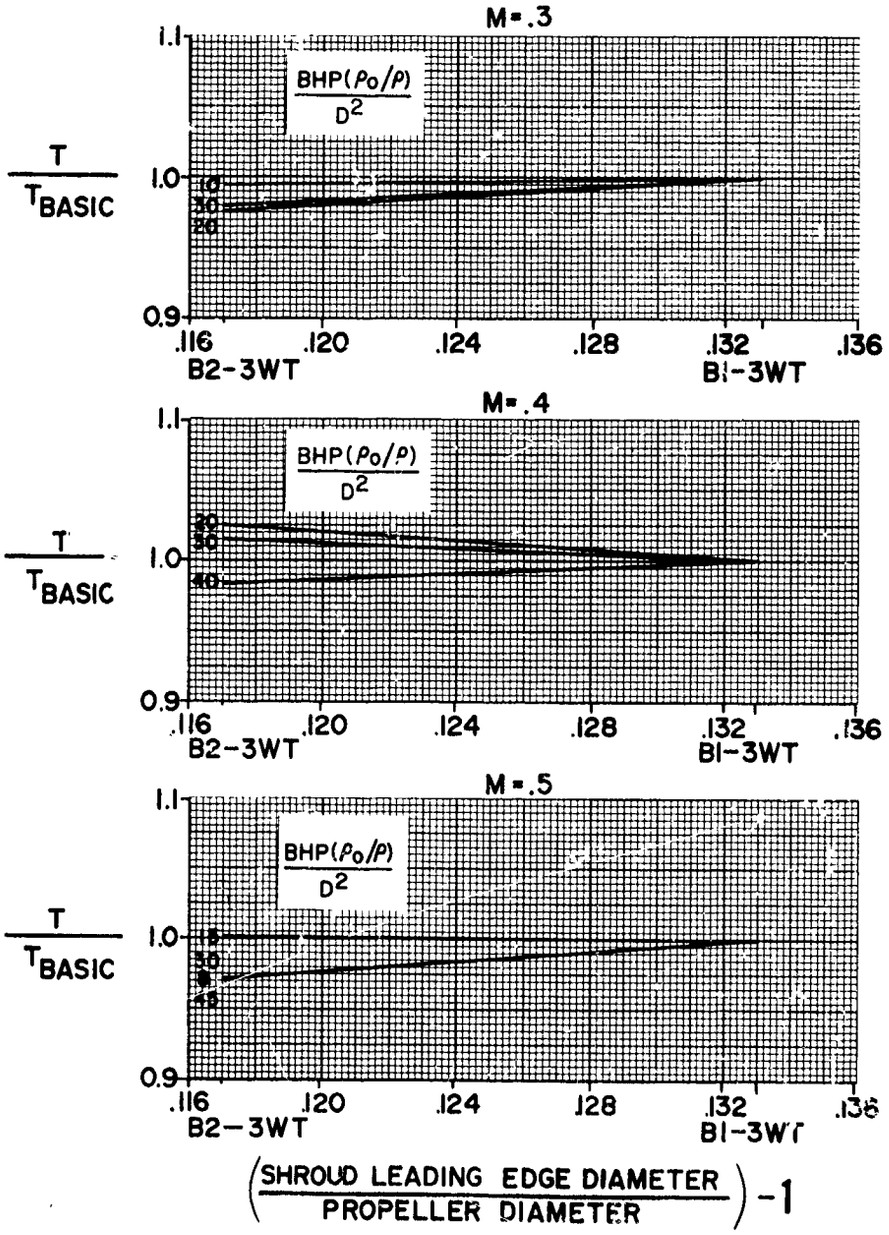

FIGURE 115

HS SHROUDED PROPELLER TEST

PERFORMANCE COMPARISON WITH BASIC CONFIGURATION, B1-3WT
EFFECT OF LIP
TIP SPEED=654 FPS

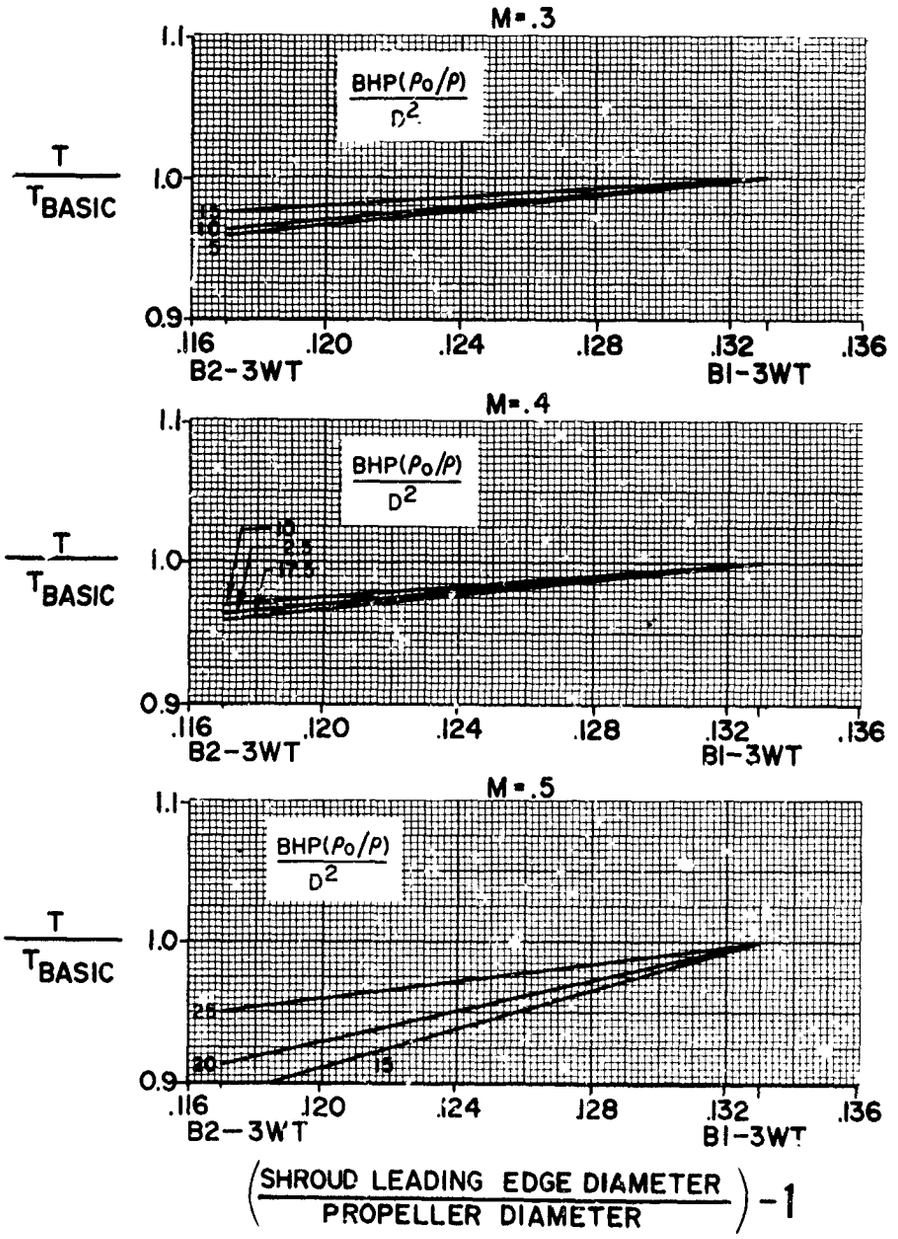

FIGURE 116

HS SHROUDED PROPELLER TEST

PERFORMANCE COMPARISON WITH BASIC CONFIGURATION, BI – 3WT
EFFECT OF AREA RATIO
TIP SPEED = 980 FPS

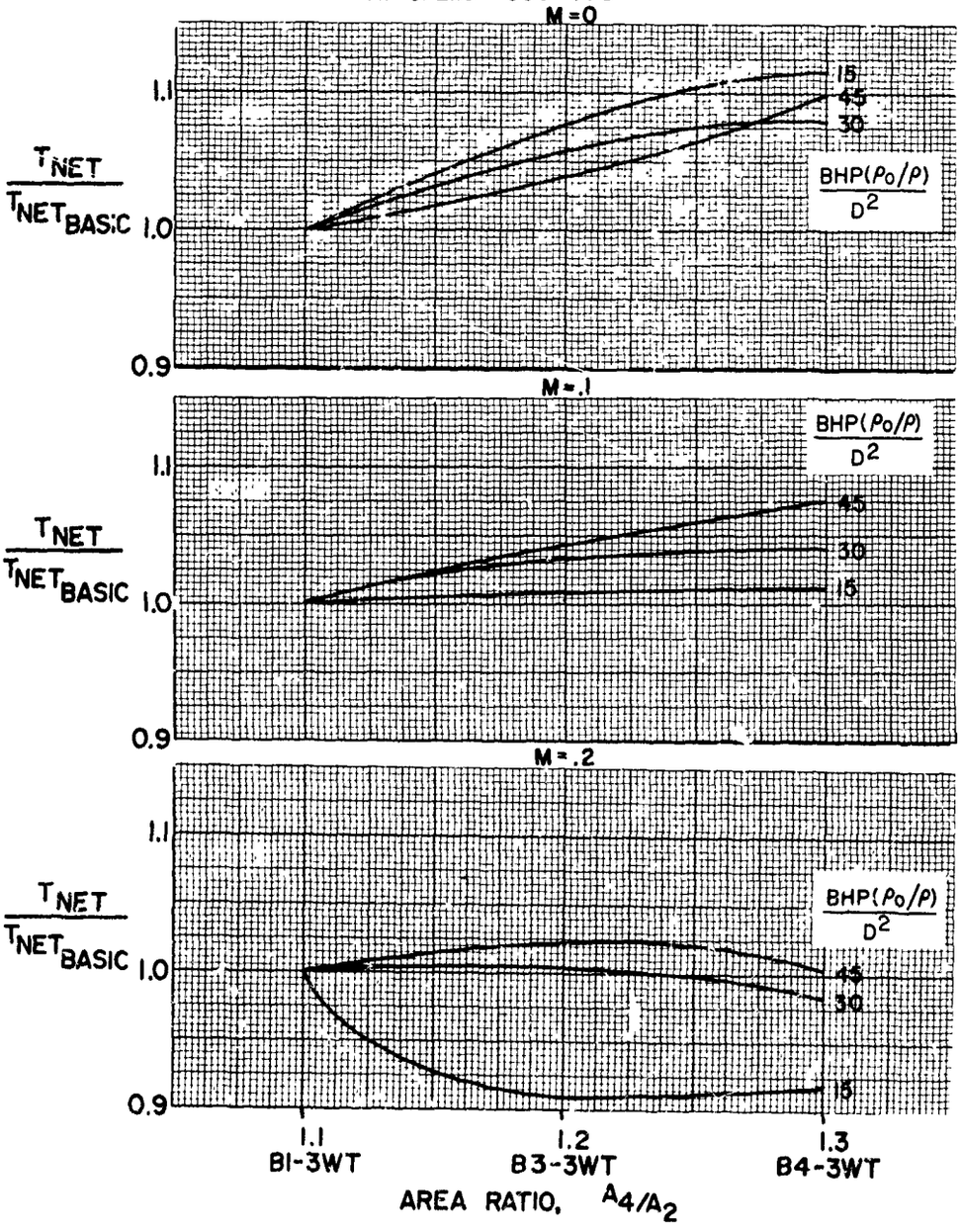

FIGURE 117

HS SHROUDED PROPELLER TEST

PERFORMANCE COMPARISON WITH BASIC CONFIGURATION, BI – 3WT
EFFECT OF AREA RATIO
TIP SPEED = 915 FPS

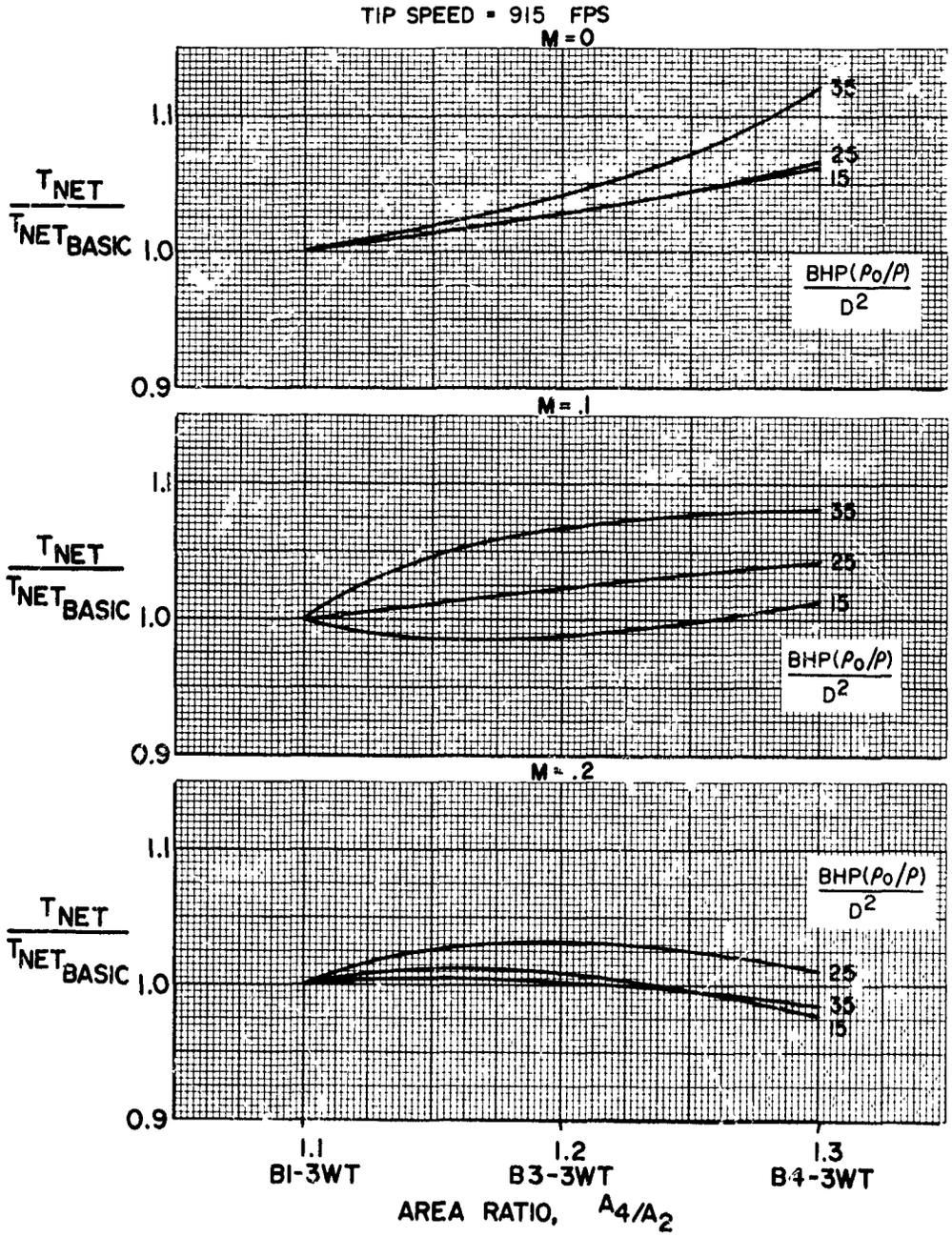

FIGURE 118

HS SHROUDED PROPELLER TEST

PERFORMANCE COMPARISON WITH BASIC CONFIGURATION, B1 – 3WT
EFFECT OF AREA RATIO
TIP SPEED = 785 FPS

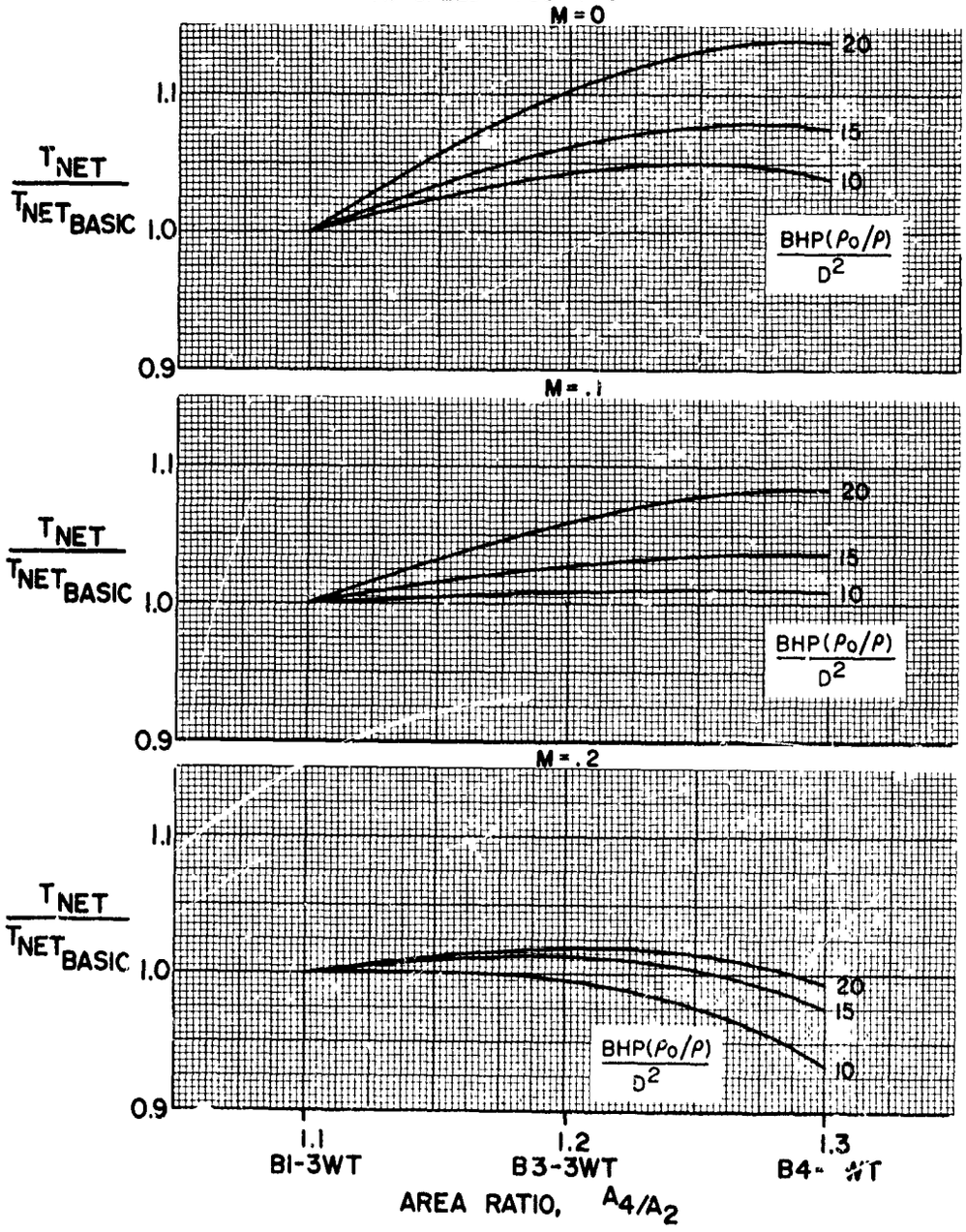

FIGURE 119

HS SHROUDED PROPELLER TEST

PERFORMANCE COMPARISON WITH BASIC CONFIGURATION, BI-3WT
EFFECT OF AREA RATIO
TIP SPEED = 915 FPS

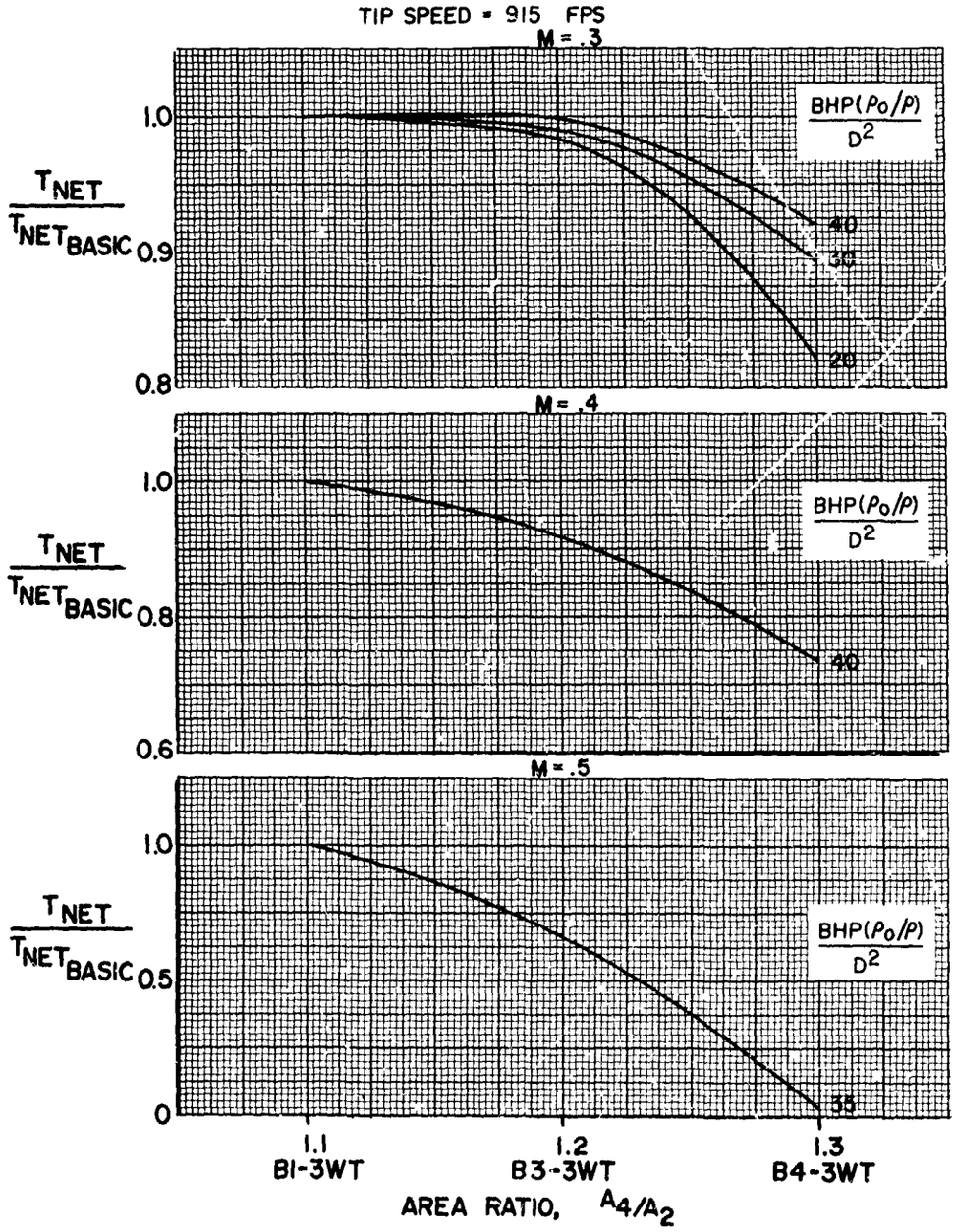

FIGURE 120

HS SHROUDED PROPELLER TEST

PERFORMANCE COMPARISON WITH BASIC CONFIGURATION, B1-3WT
EFFECT OF AREA RATIO
TIP SPEED = 785 FPS

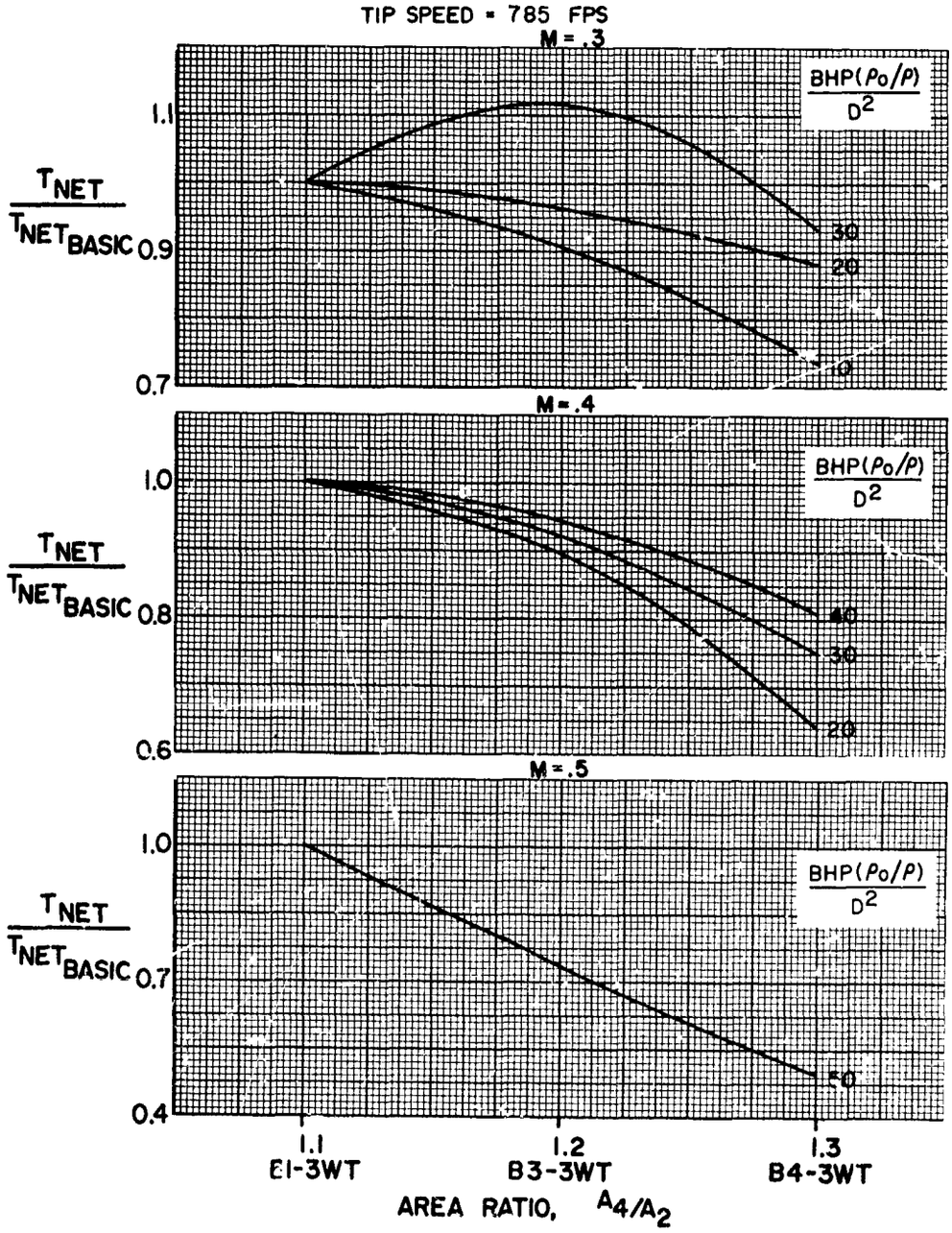

FIGURE 121

HS SHROUDED PROPELLER TEST

PERFORMANCE COMPARISON WITH BASIC CONFIGURATION, BI-3WT
EFFECT OF AREA RATIO
TIP SPEED = 654 FPS

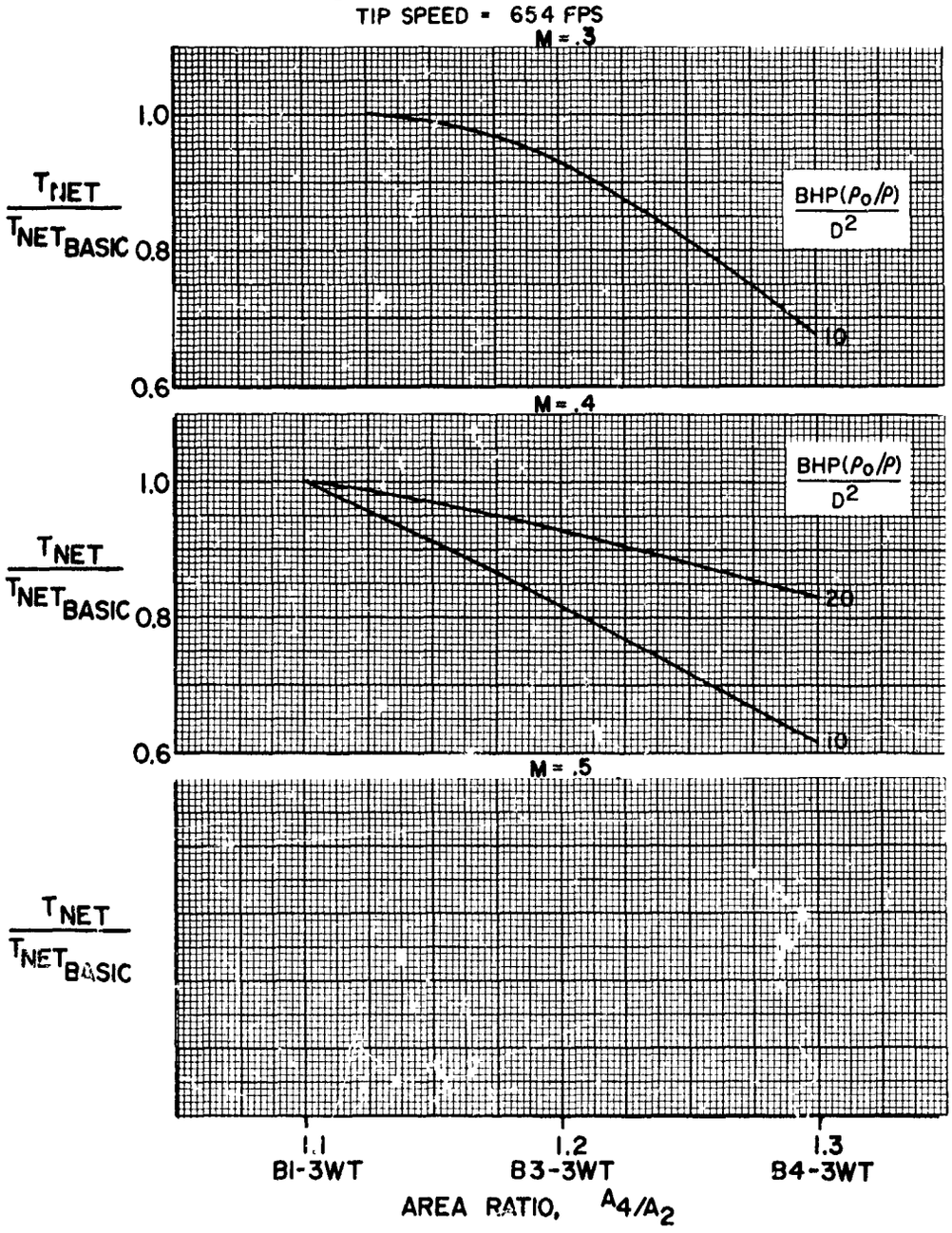

FIGURE 122

HS SHROUDED PROPELLER TEST

PERFORMANCE COMPARISON WITH BASIC CONFIGURATION, BI – 3WT
EFFECT OF AREA RATIO
TIP SPEED = 980 FPS

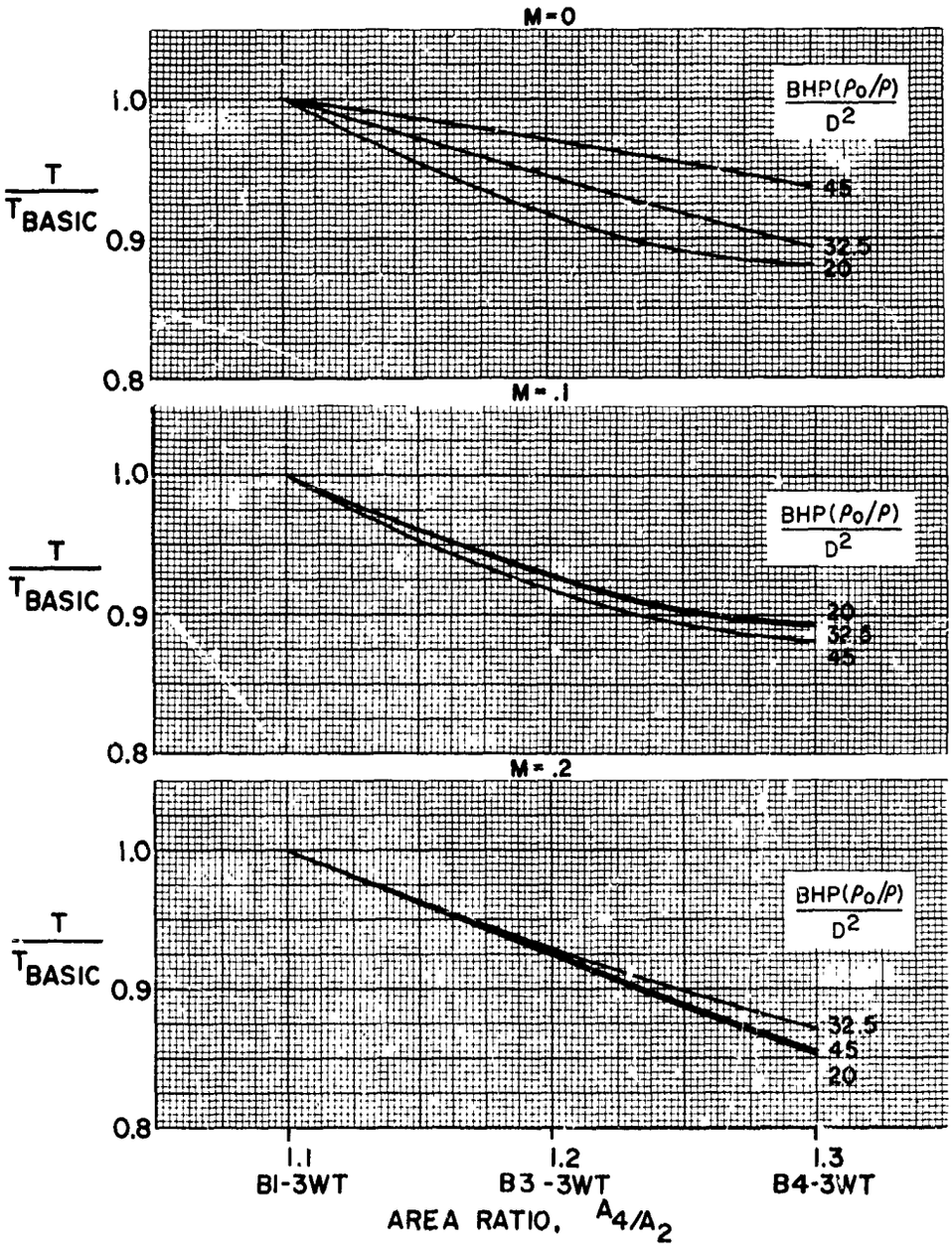

FIGURE 123

HS SHROUDED PROPELLER TEST

PERFORMANCE COMPARISON WITH BASIC CONFIGURATION, BI – 3WT
EFFECT OF AREA RATIO
TIP SPEED = 915 FPS

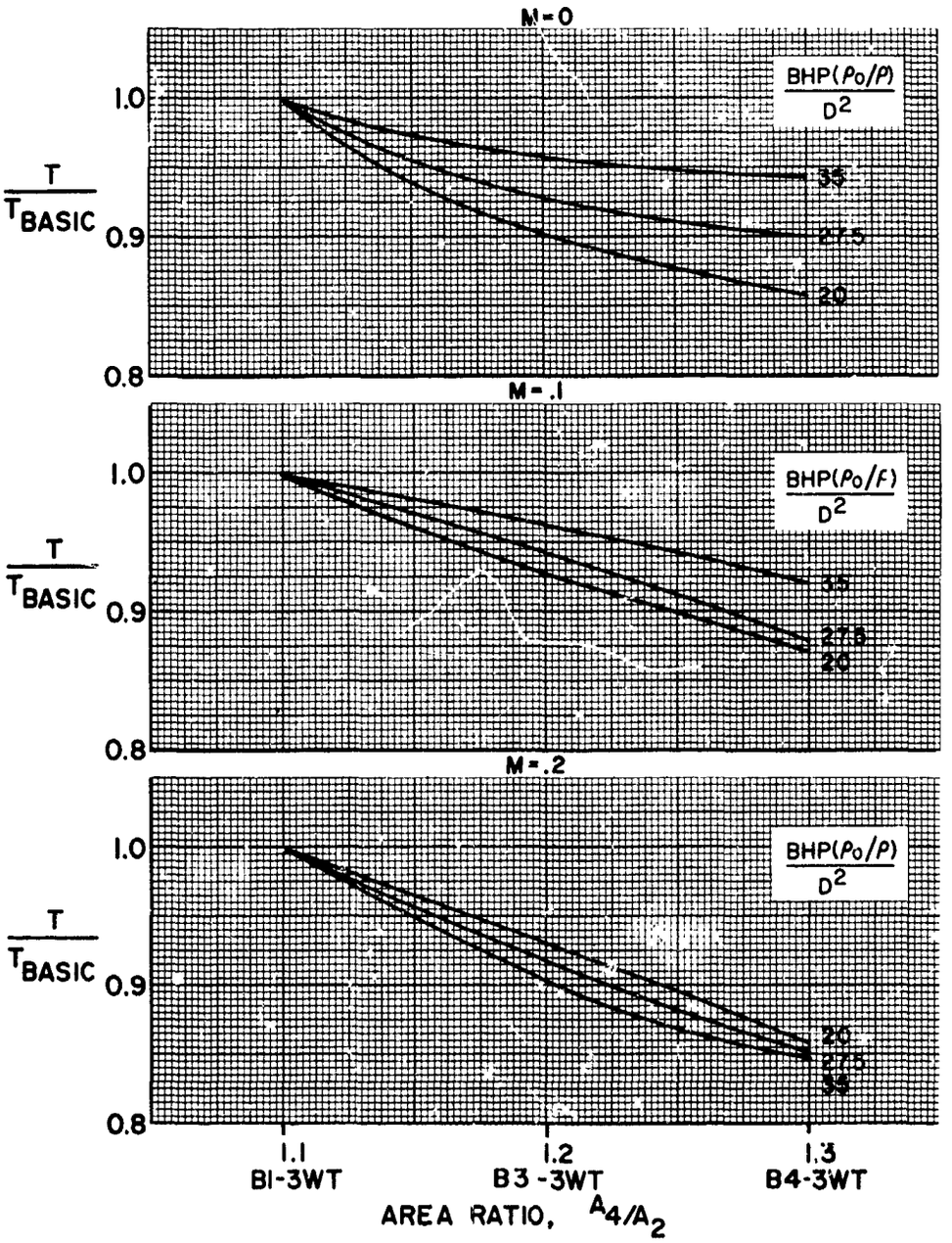

FIGURE 124

HS SHROUDED PROPELLER TEST

PERFORMANCE COMPARISON WITH BASIC CONFIGURATION, B1 – 3WT
EFFECT OF AREA RATIO
TIP SPEED = 785 FPS

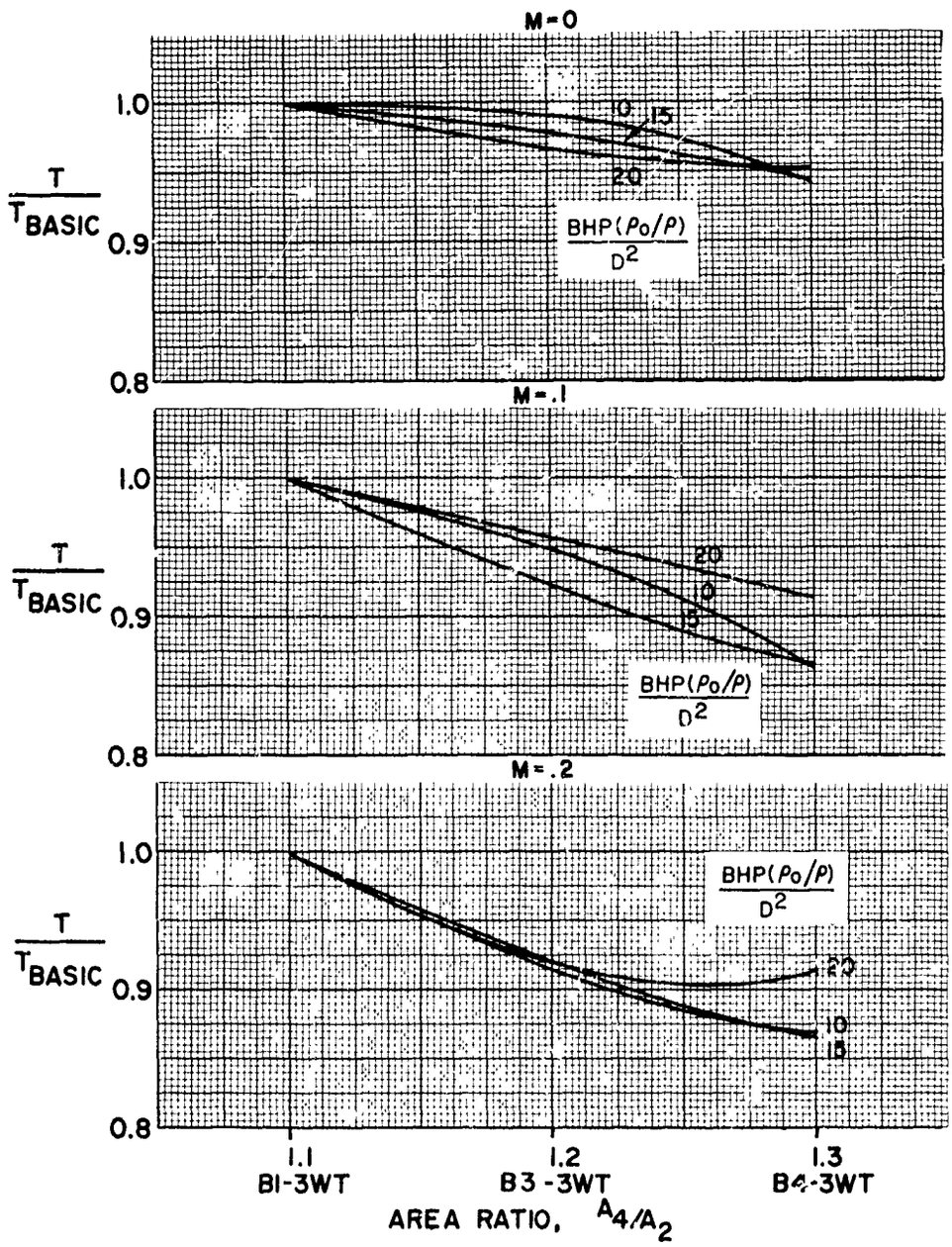

FIGURE 125

HS SHROUDED PROPELLER TEST

PERFORMANCE COMPARISON WITH BASIC CONFIGURATION, BI – 3WT
EFFECT OF AREA RATIO
TIP SPEED = 915 FPS

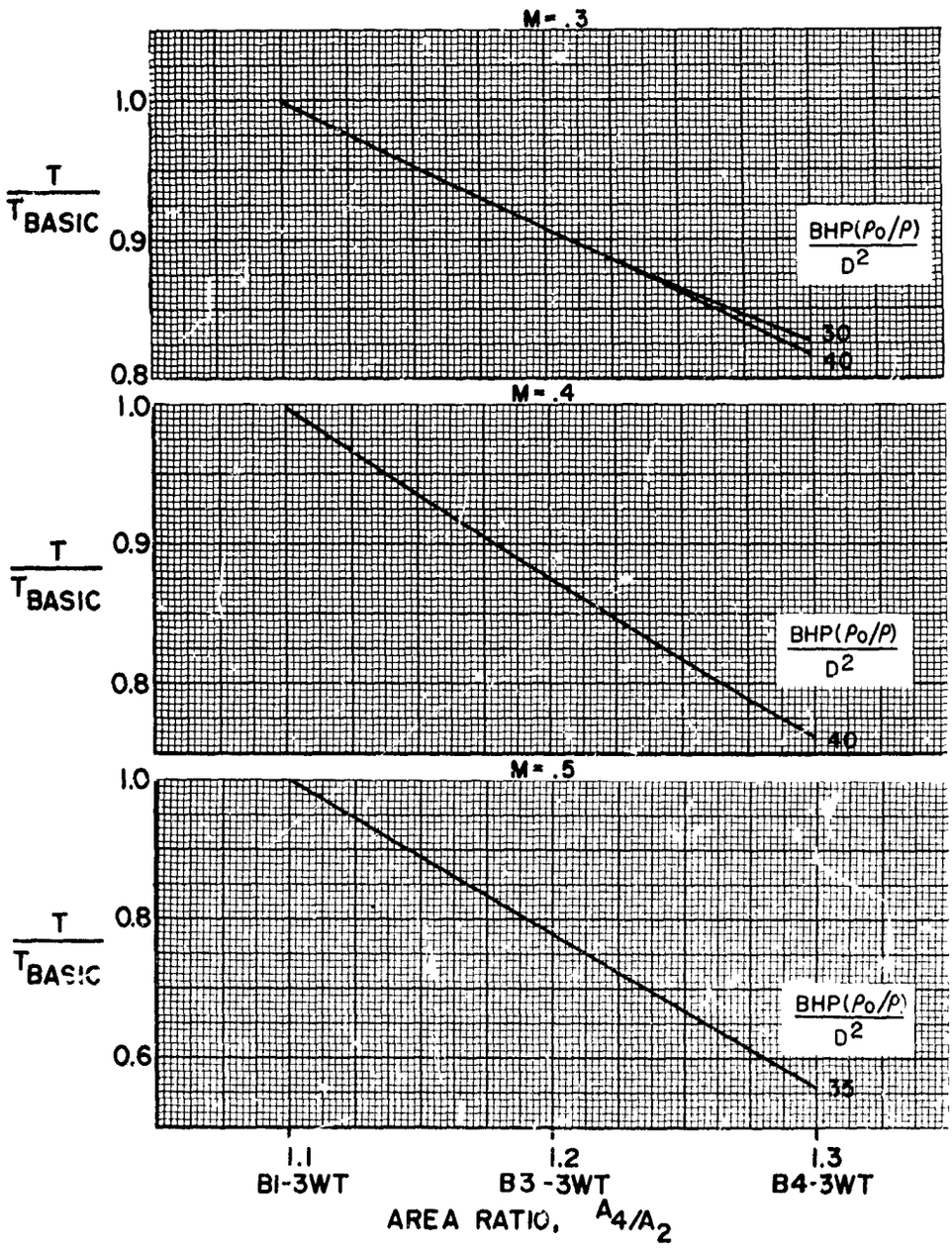

FIGURE 126

HS SHROUDED PROPELLER TEST

PERFORMANCE COMPARISON WITH BASIC CONFIGURATION, BI-3WT
EFFECT OF AREA RATIO
TIP SPEED = 785 FPS

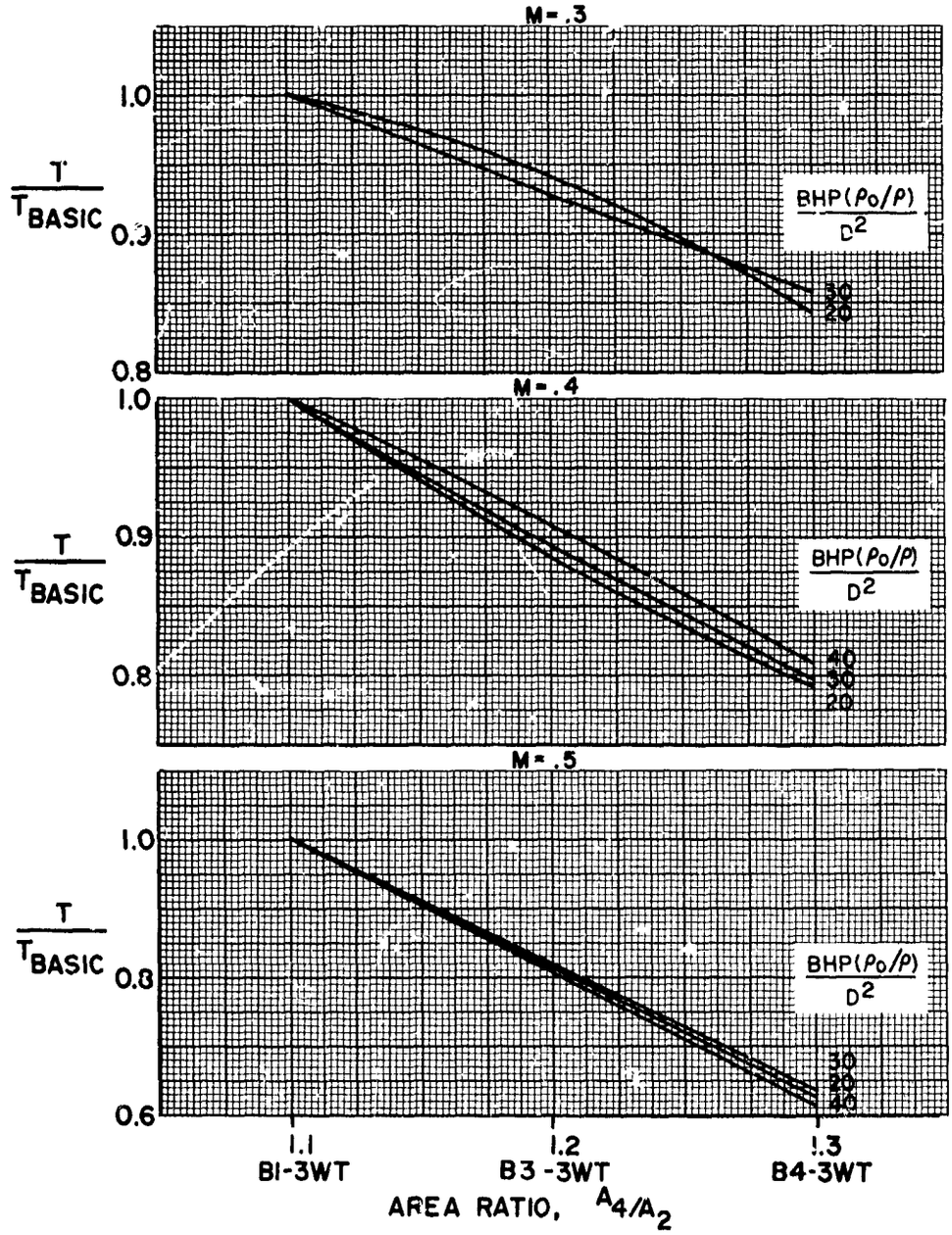

FIGURE 127

HS SHROUDED PROPELLER TEST

PERFORMANCE COMPARISON WITH BASIC CONFIGURATION, BI-3WT
EFFECT OF AREA RATIO
TIP SPEED = 654 FPS

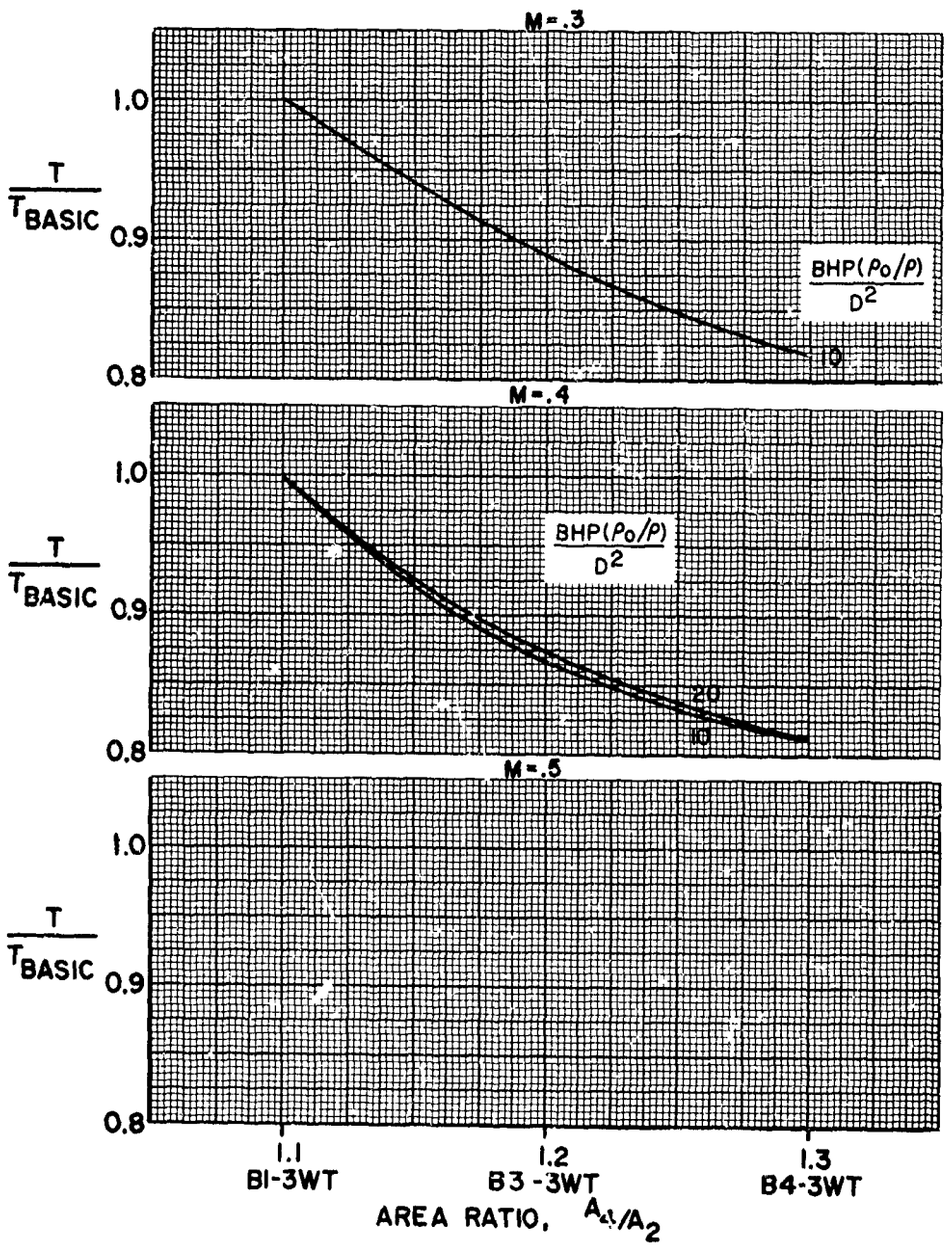

FIGURE 128

HS SHROUDED PROPELLER TEST

PERFORMANCE COMPARISON WITH CONFIGURATION B1 - 3NT
EFFECT OF SHROUD LENGTH
TIP SPEED = 980 FPS

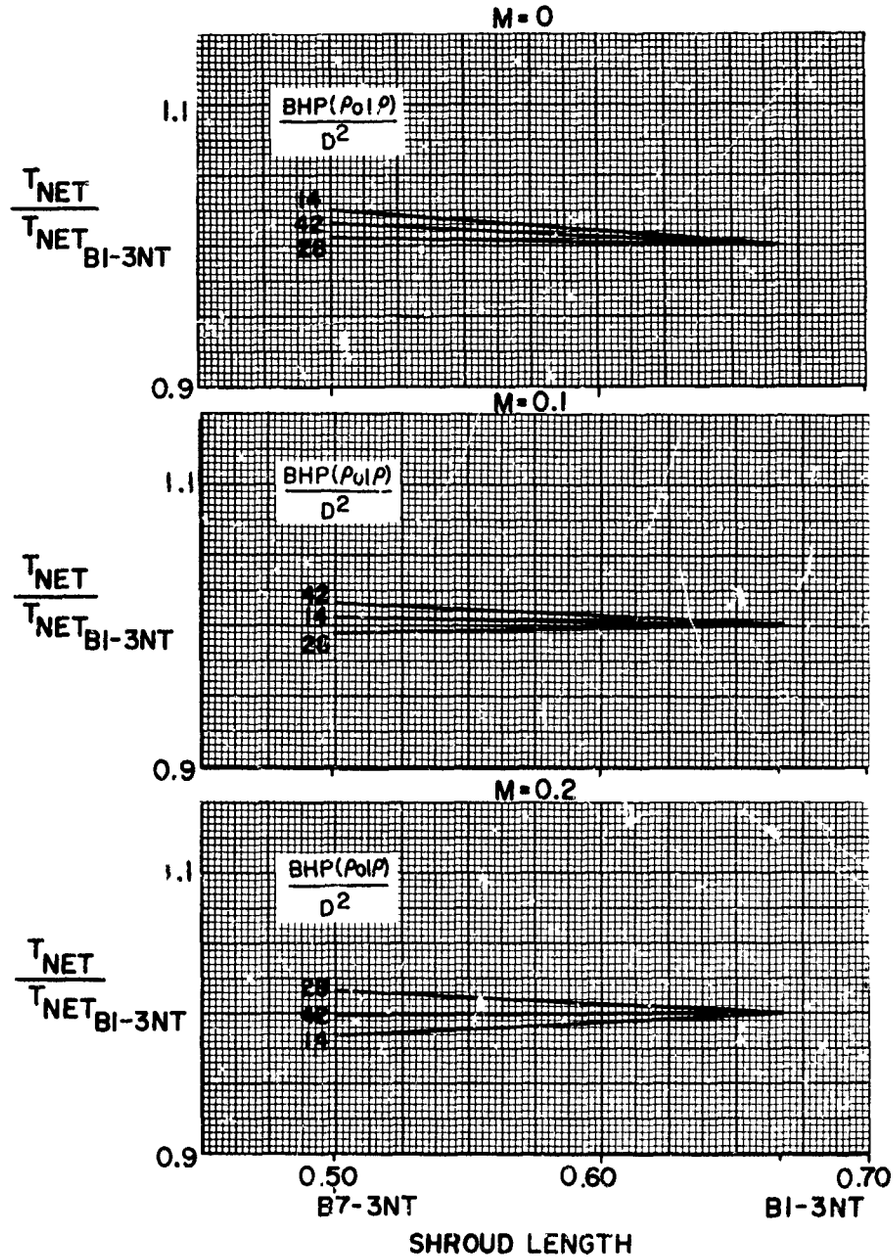

FIGURE 129

HS SHROUDED PROPELLER TEST

PERFORMANCE COMPARISON WITH CONFIGURATION BI - 3NT
EFFECT OF SHROUD LENGTH
TIP SPEED = 915 FPS

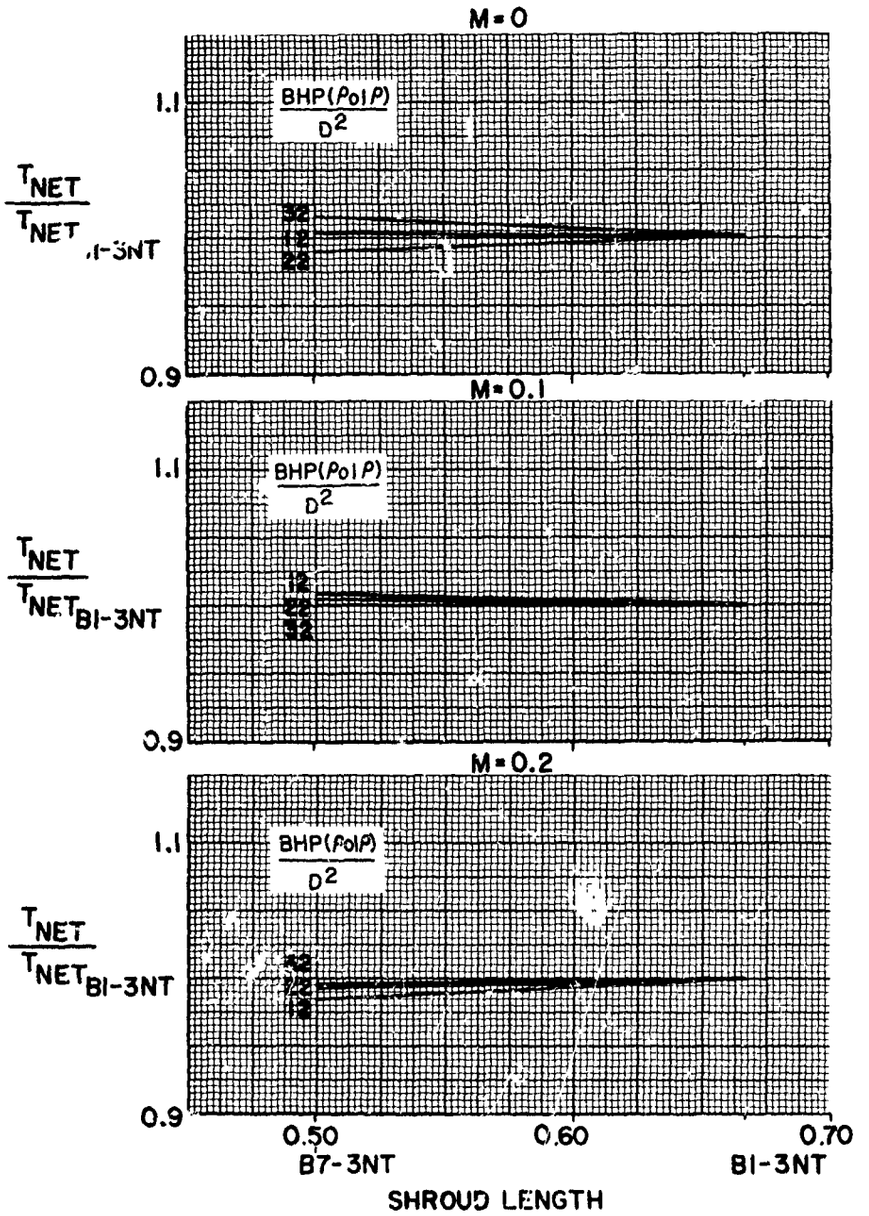

FIGURE 130

HS SHROUDED PROPELLER TEST

PERFORMANCE COMPARISON WITH CONFIGURATION BI - 3NT
EFFECT OF SHROUD LENGTH
TIP SPEED = 785 FPS

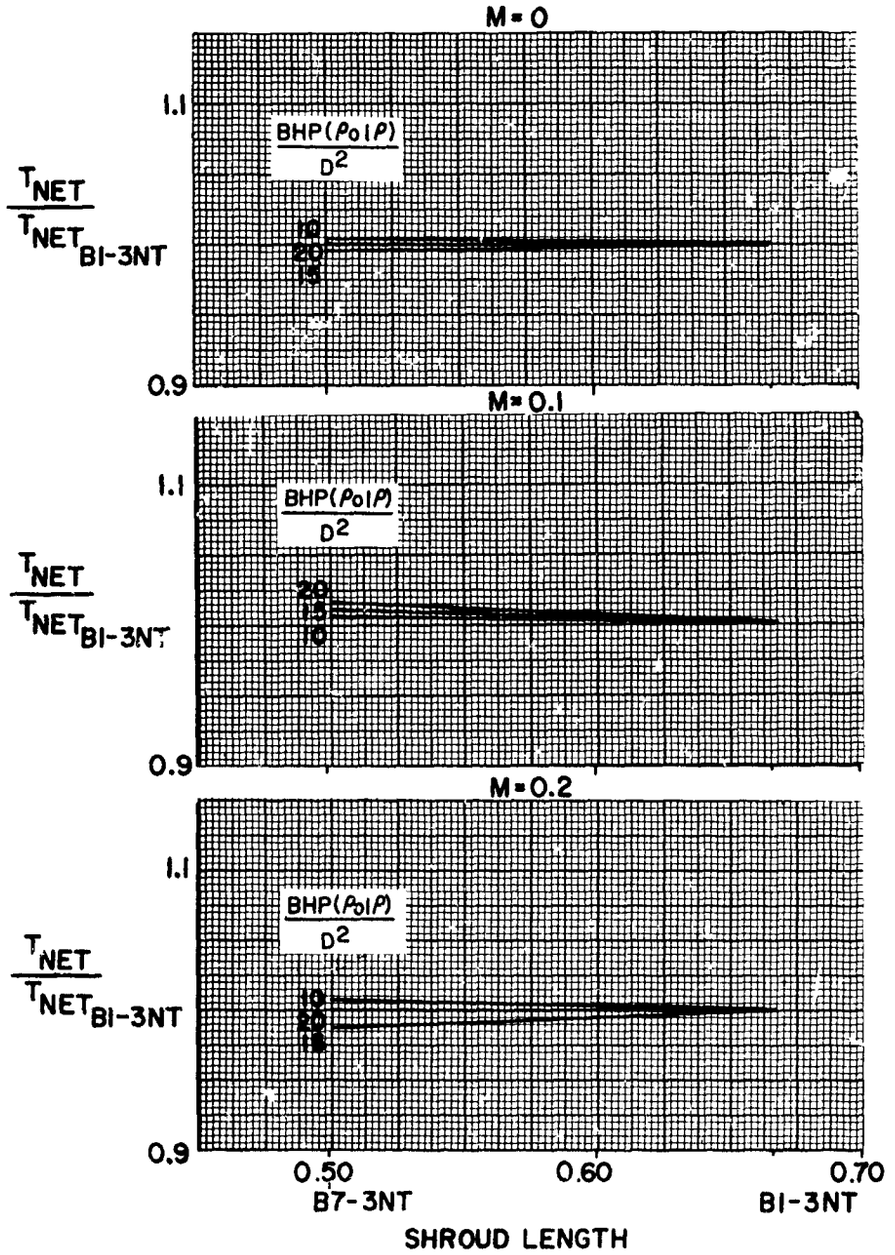

FIGURE 131

HS SHROUDED PROPELLER TEST

PERFORMANCE COMPARISON WITH CONFIGURATION B1 - 3NT
EFFECT OF SHROUD LENGTH
TIP SPEED = 915 FPS

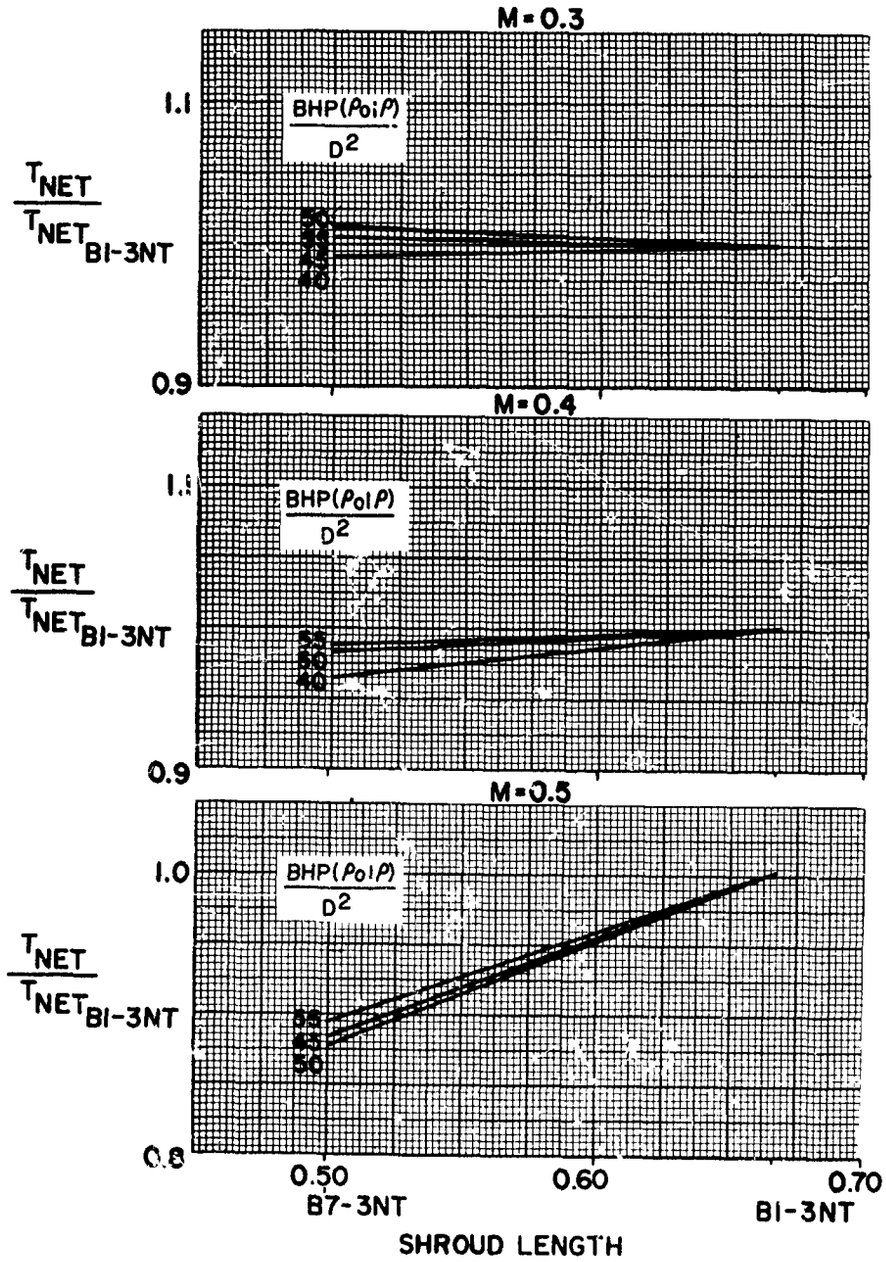

FIGURE 132

HS SHROUDED PROPELLER TEST

PERFORMANCE COMPARISON WITH CONFIGURATION BI - 3NT
EFFECT OF SHROUD LENGTH
TIP SPEED = 785 FPS

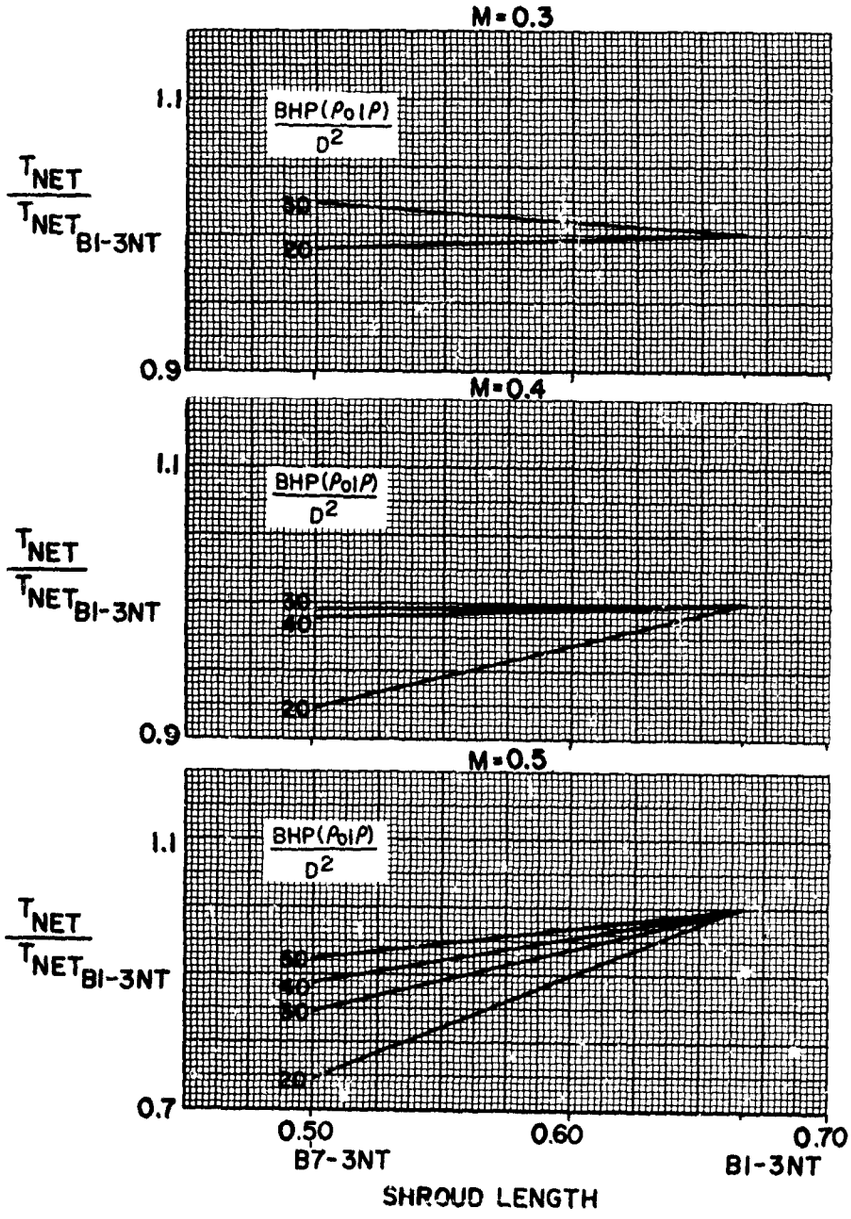

FIGURE 133

HS SHROUDED PROPELLER TEST

PERFORMANCE COMPARISON WITH CONFIGURATION B1 - 3NT
EFFECT OF SHROUD LENGTH
TIP SPEED = 654 FPS

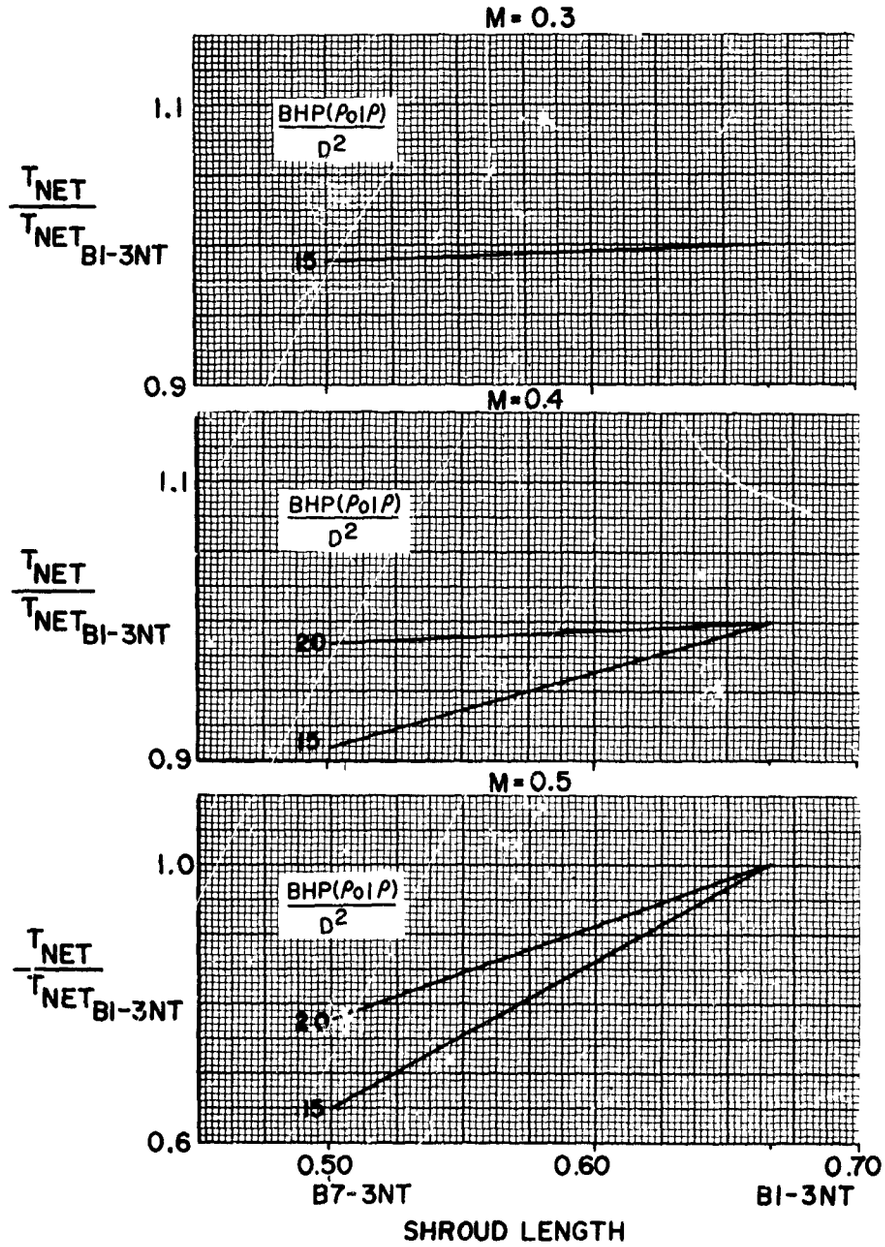

FIGURE 134

HS SHROUDED PROPELLER TEST

PERFORMANCE COMPARISON WITH CONFIGURATION, BI-3NT
EFFECT OF SHROUD LENGTH
TIP SPEED = 980 FPS

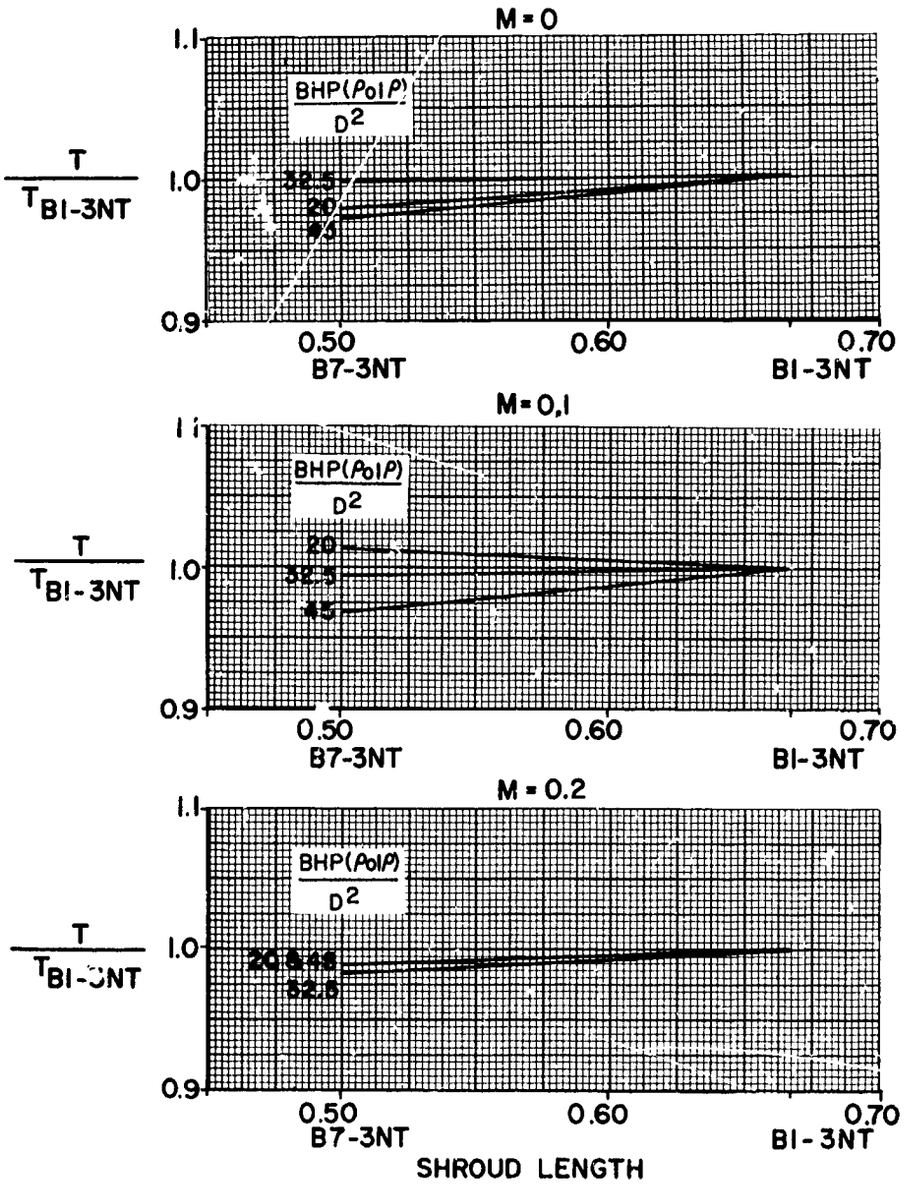

FIGURE 135

HS SHROUDED PROPELLER TEST

PERFORMANCE COMPARISON WITH CONFIGURATION, BI-3NT
EFFECT OF SHROUD LENGTH
TIP SPEED = 915 FPS

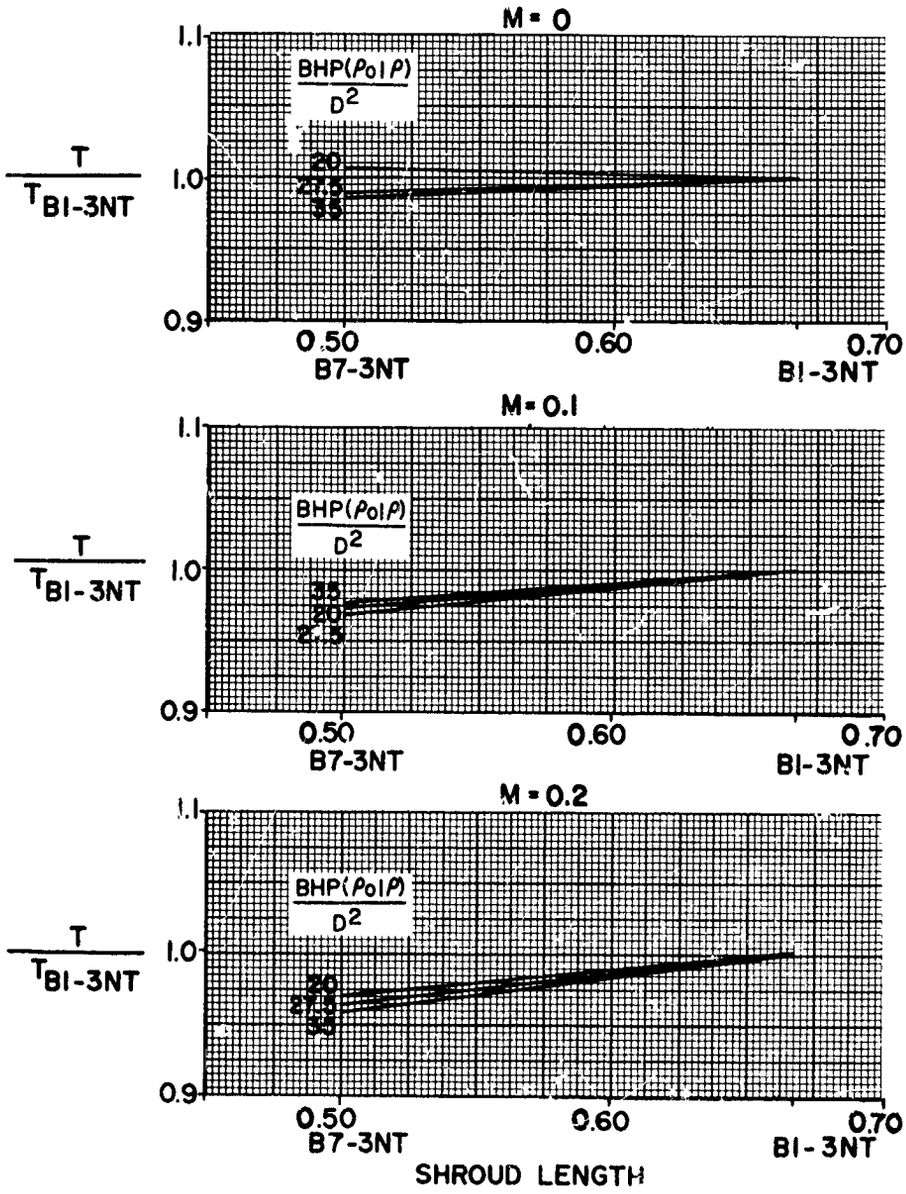

FIGURE 136

HS SHROUDED PROPELLER TEST

PERFORMANCE COMPARISON WITH CONFIGURATION, BI-3NT
EFFECT OF SHROUD LENGTH
TIP SPEED = 785 FPS

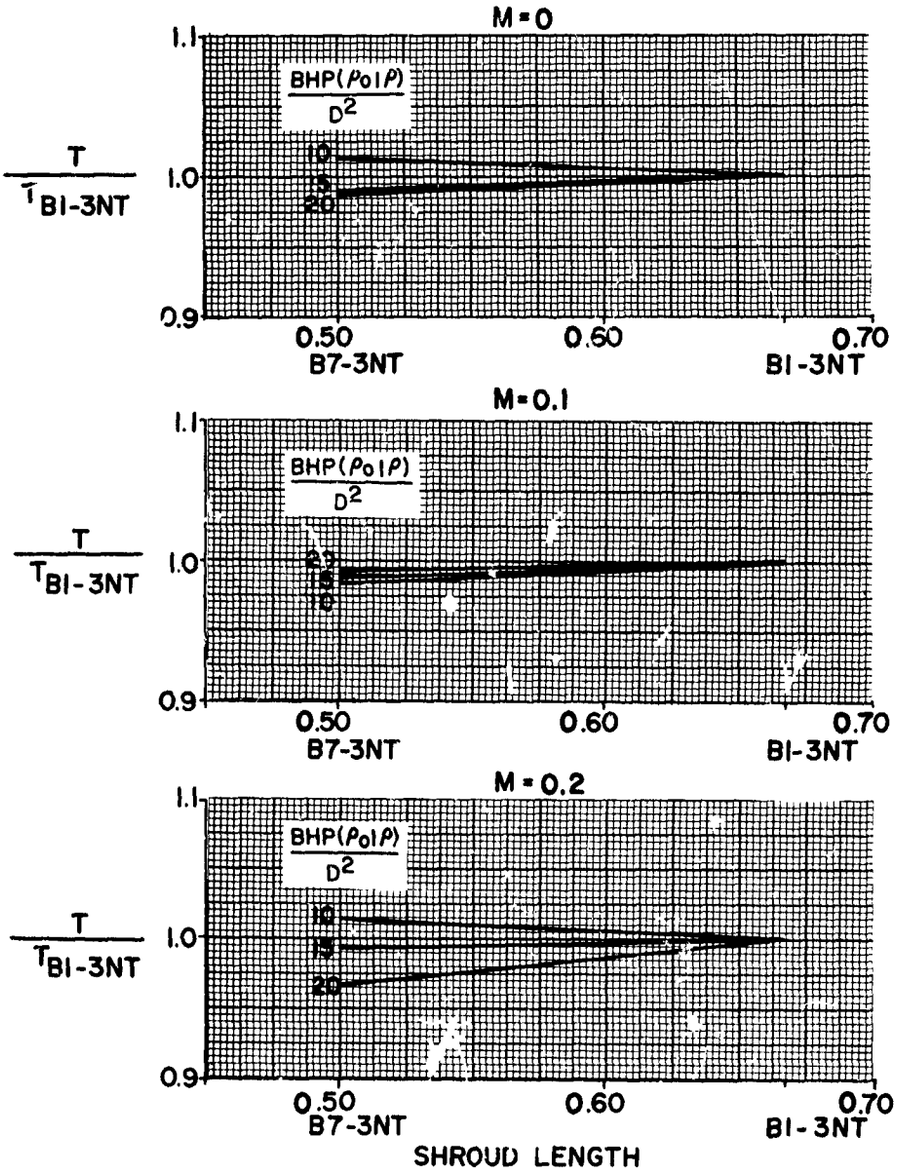

FIGURE 137

HS SHROUDED PROPELLER TEST

PERFORMANCE COMPARISON WITH CONFIGURATION, BI-3NT
EFFECT OF SHROUD LENGTH
TIP SPEED = 915 FPS

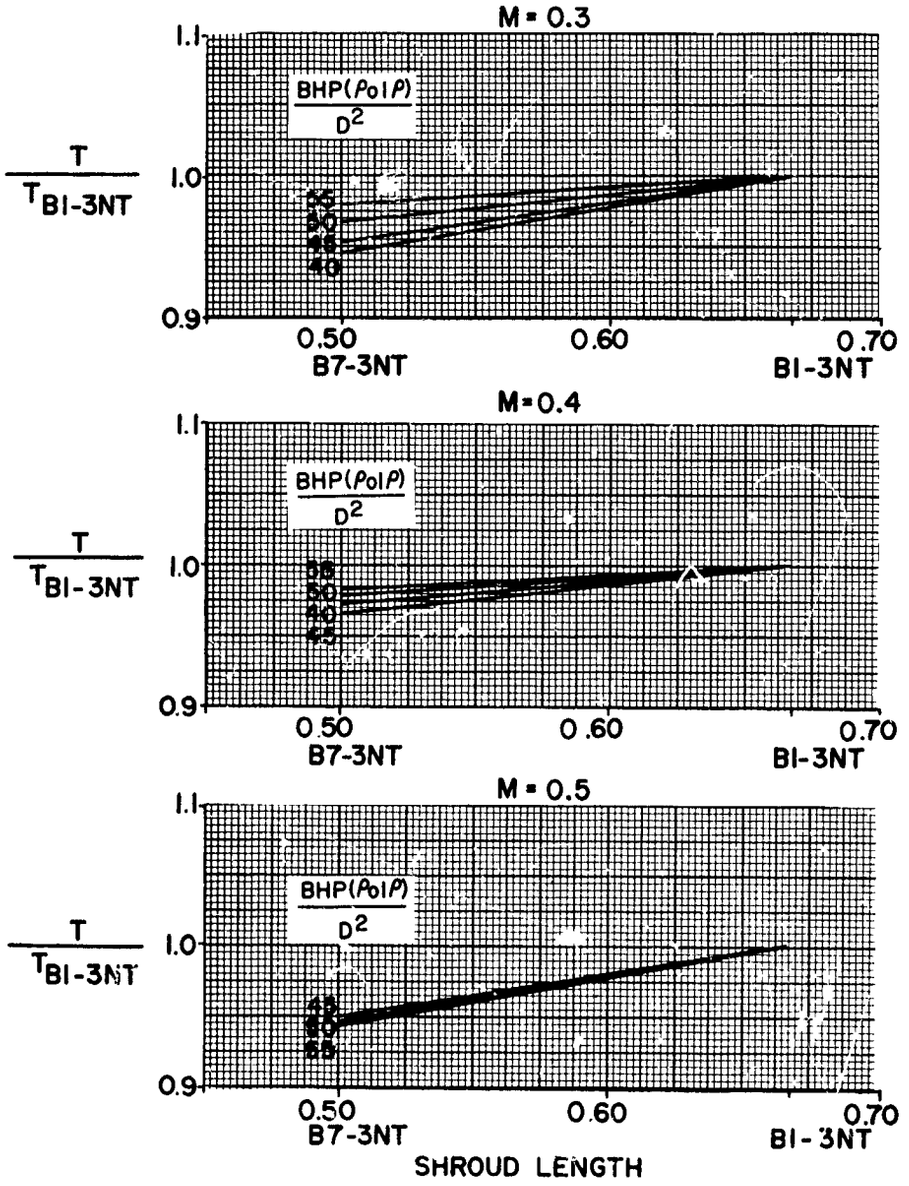

FIGURE 138

HS SHROUDED PROPELLER TEST

PERFORMANCE COMPARISON WITH CONFIGURATION, BI-3NT
EFFECT OF SHROUD LENGTH
TIP SPEED = 785 FPS

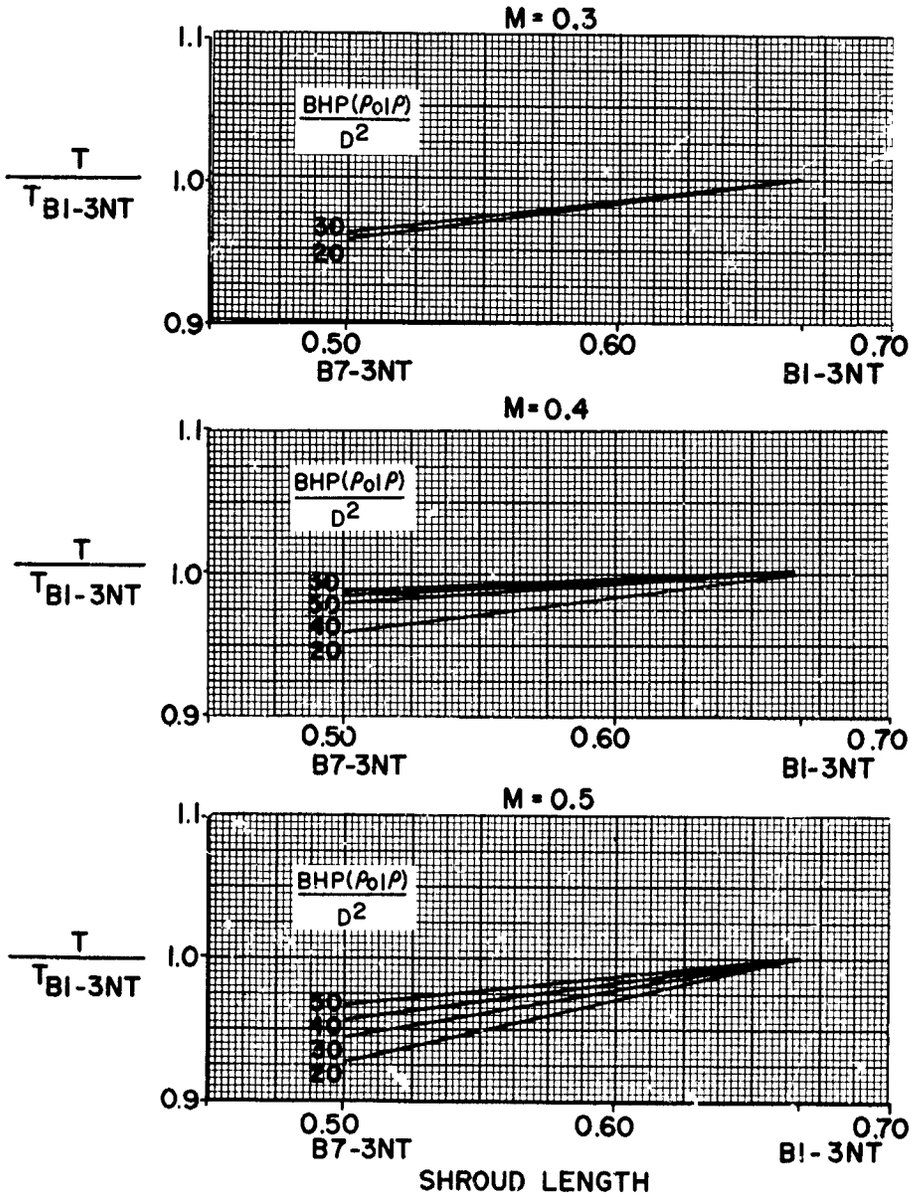

FIGURE 139

HS SHROUDED PROPELLER TEST

PERFORMANCE COMPARISON WITH CONFIGURATION, BI-3NT
EFFECT OF SHROUD LENGTH
TIP SPEED = 654 FPS

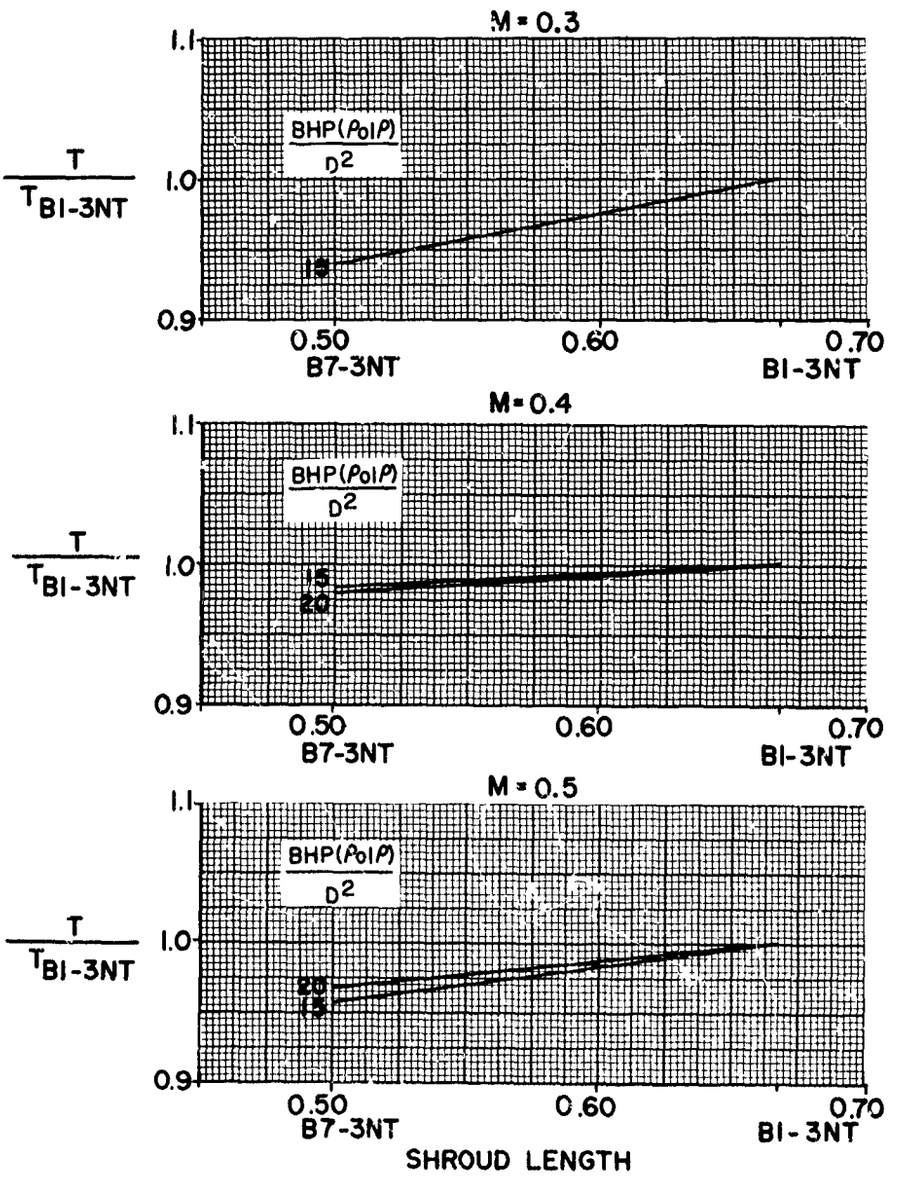

FIGURE 140

HS SHROUDED PROPELLER TEST

PERFORMANCE COMPARISON WITH BASIC CONFIGURATION, BI-3WT
EFFECT OF PROPELLER POSITION
TIP SPEED = 980 FPS

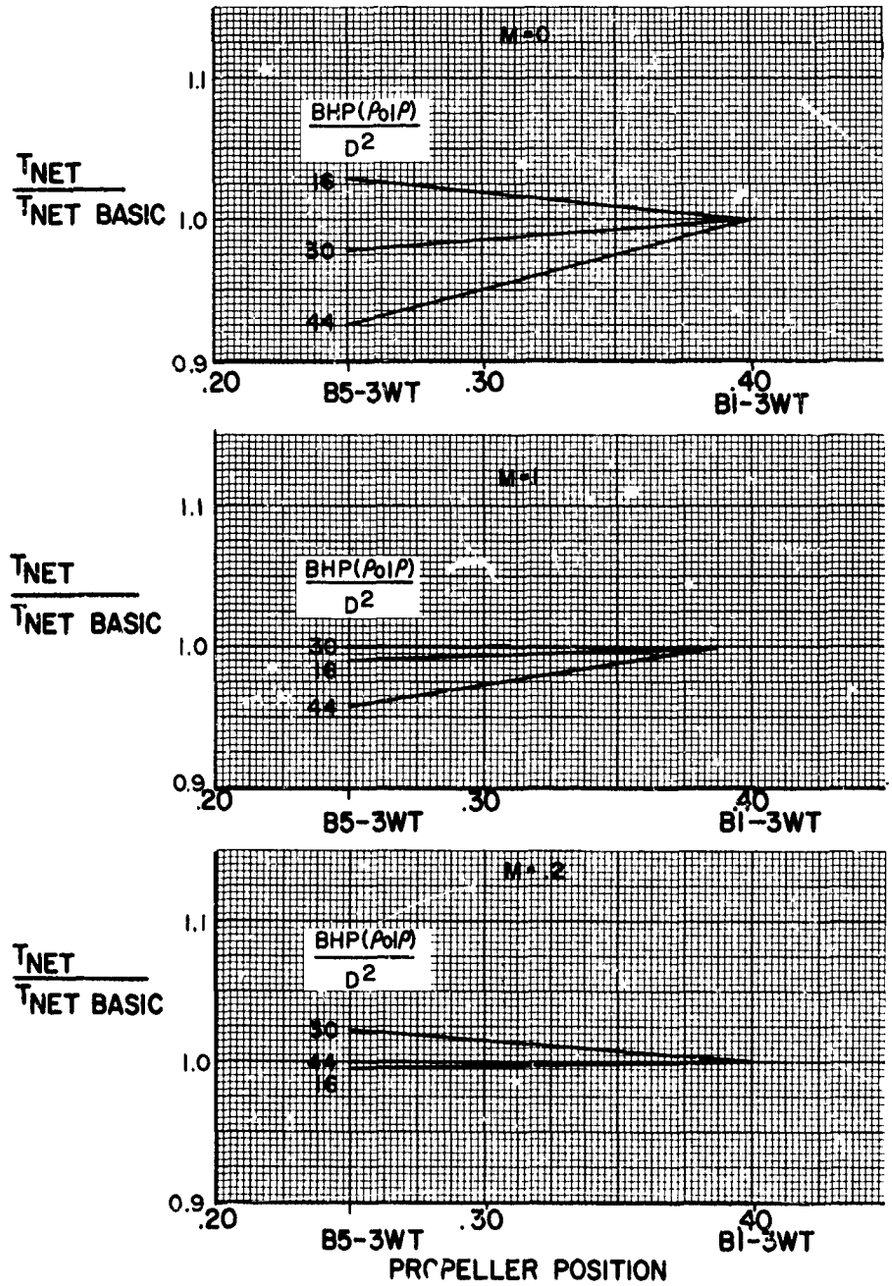

FIGURE 141

HS SHROUDED PROPELLER TEST

PERFORMANCE COMPARISON WITH BASIC CONFIGURATION, BI – 3WT
EFFECT OF PROPELLER POSITION
TIP SPEED = 915 FPS

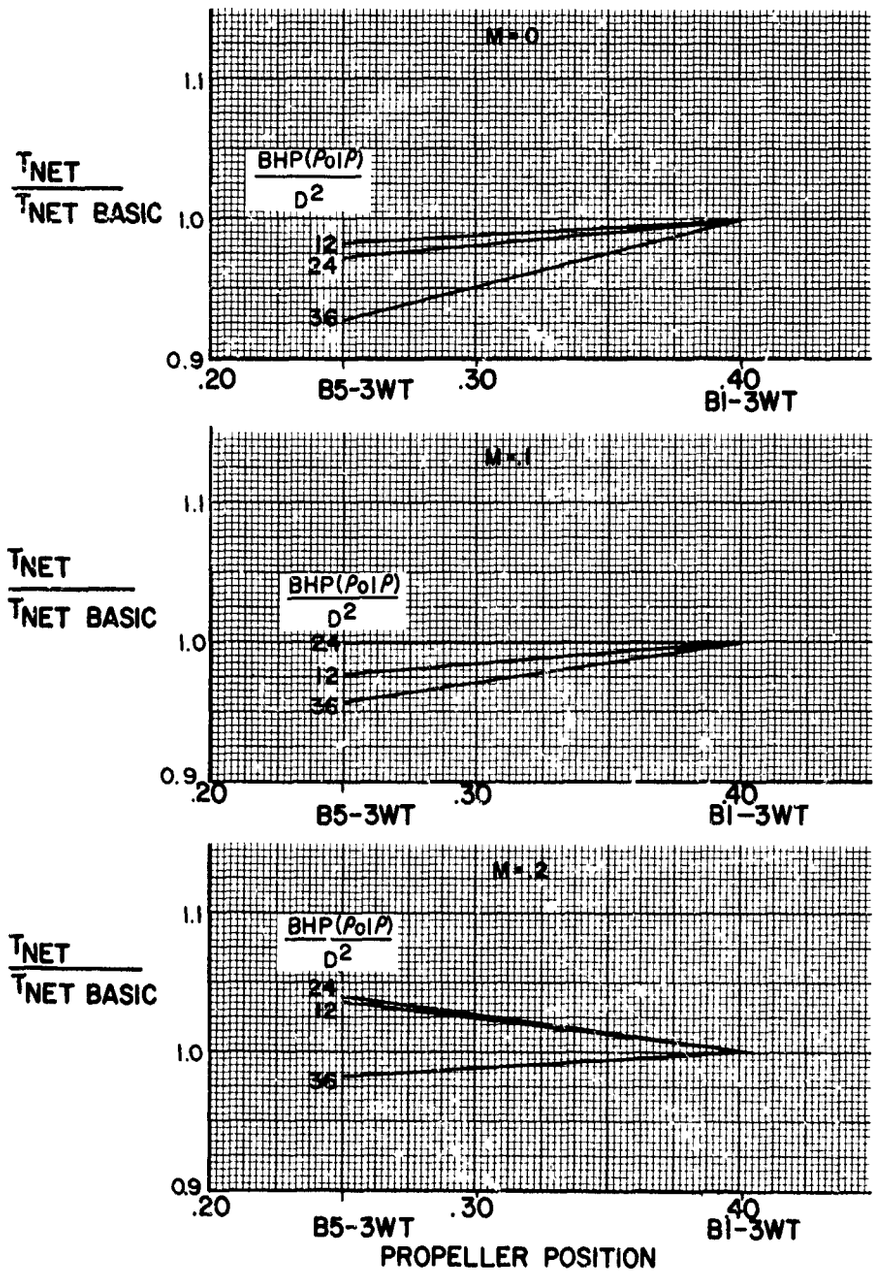

FIGURE 142

HS SHROUDED PROPELLER TEST

PERFORMANCE COMPARISON WITH BASIC CONFIGURATION, BI – 3WT
EFFECT OF PROPELLER POSITION
TIP SPEED = 785 FPS

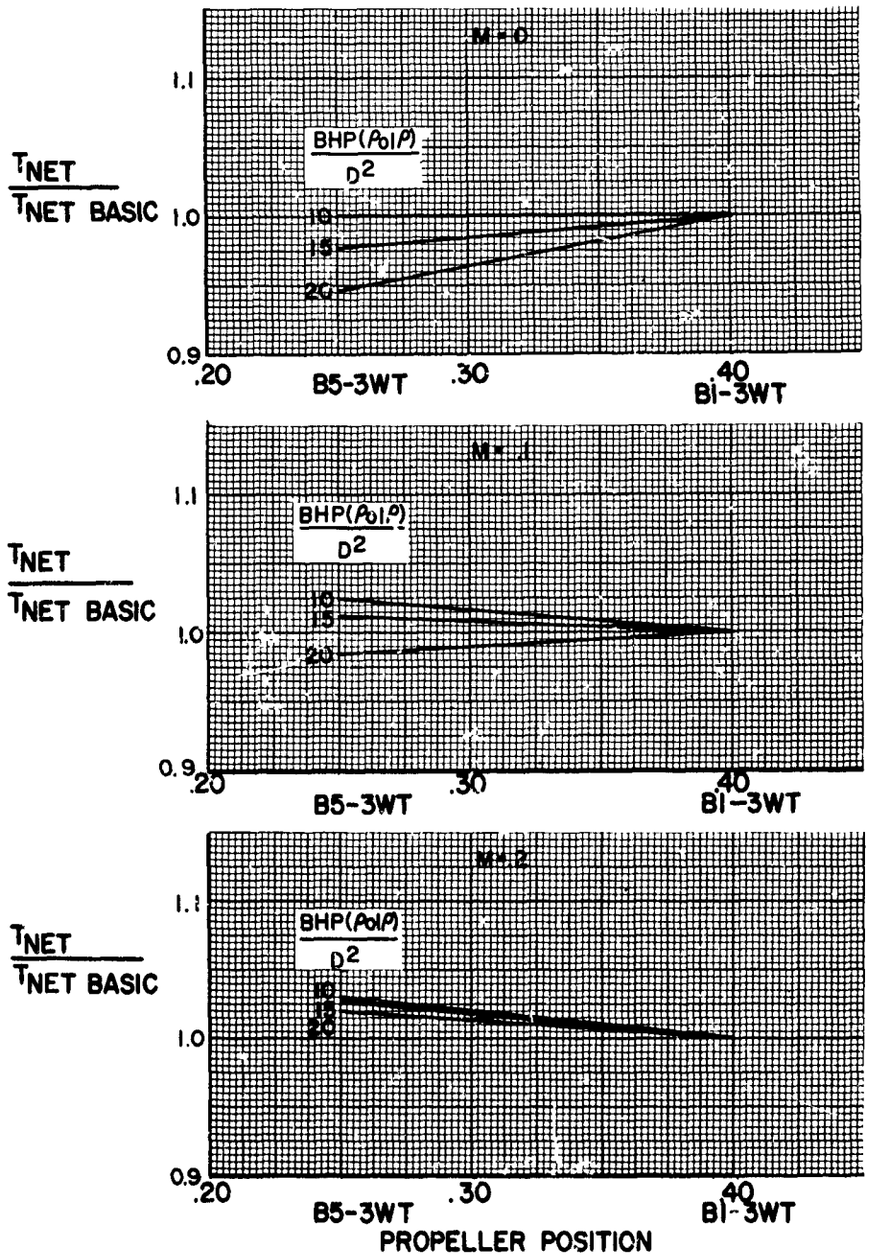

FIGURE 143

HS SHROUDED PROPELLER TEST

PERFORMANCE COMPARISON WITH BASIC CONFIGURATION, BI – 3WT
EFFECT OF PROPELLER POSITION
TIP SPEED = 915 FPS

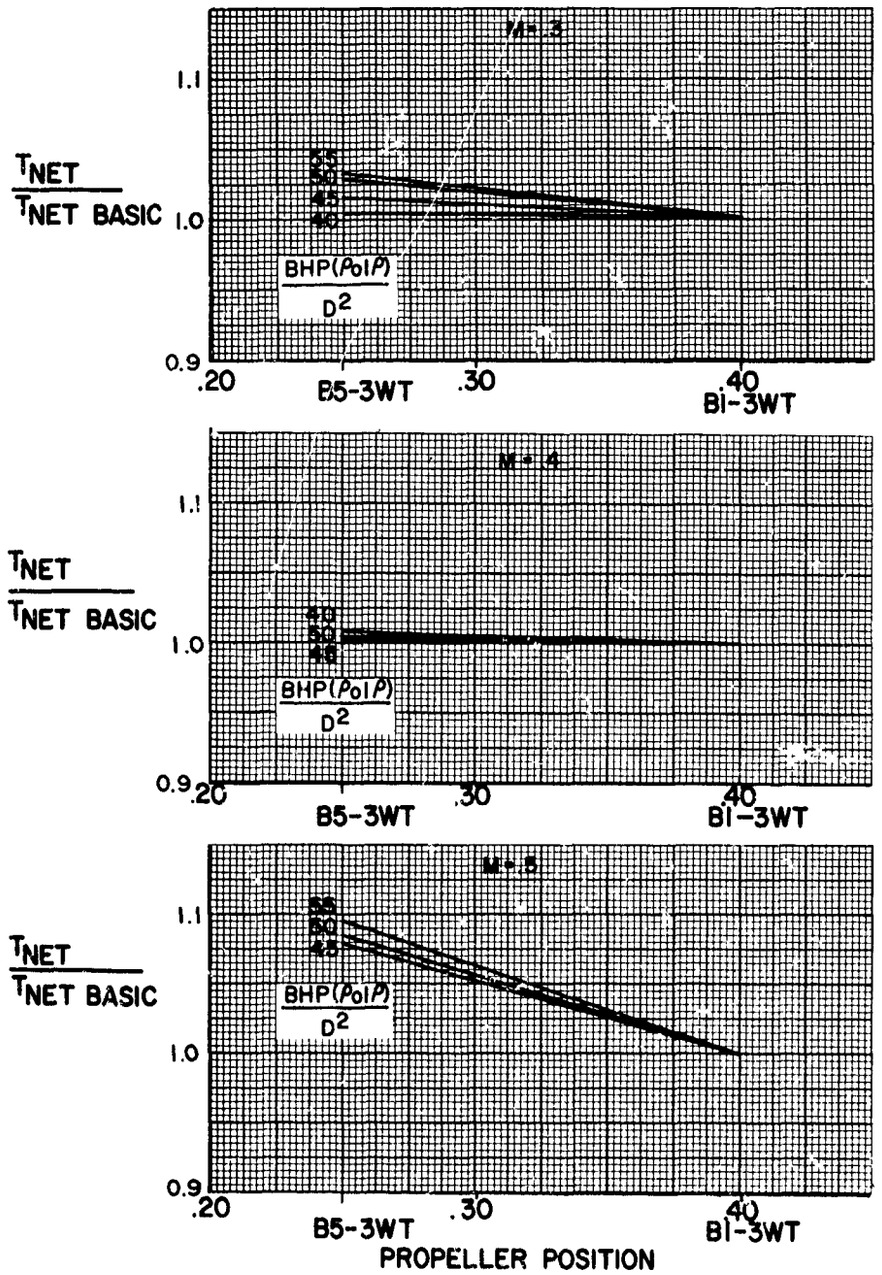

FIGURE 144

HS SHROUDED PROPELLER TEST

PERFORMANCE COMPARISON WITH BASIC CONFIGURATION, BI – 3WT
EFFECT OF PROPELLER POSITION
TIP SPEED = 785 FPS

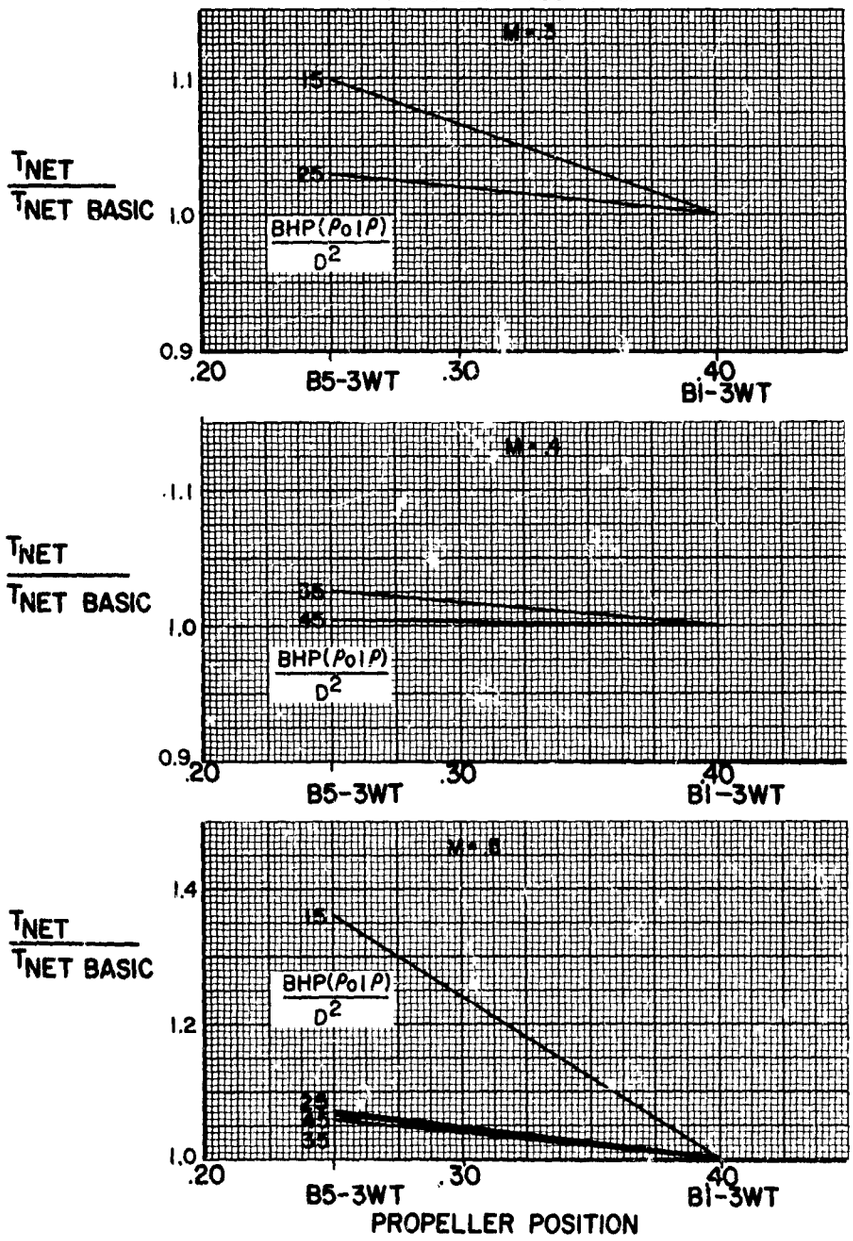

FIGURE 145

HS SHROUDED PROPELLER TEST

PERFORMANCE COMPARISON WITH BASIC CONFIGURATION, B1-3WT
EFFECT OF PROPELLER POSITION
TIP SPEED = 654 FPS

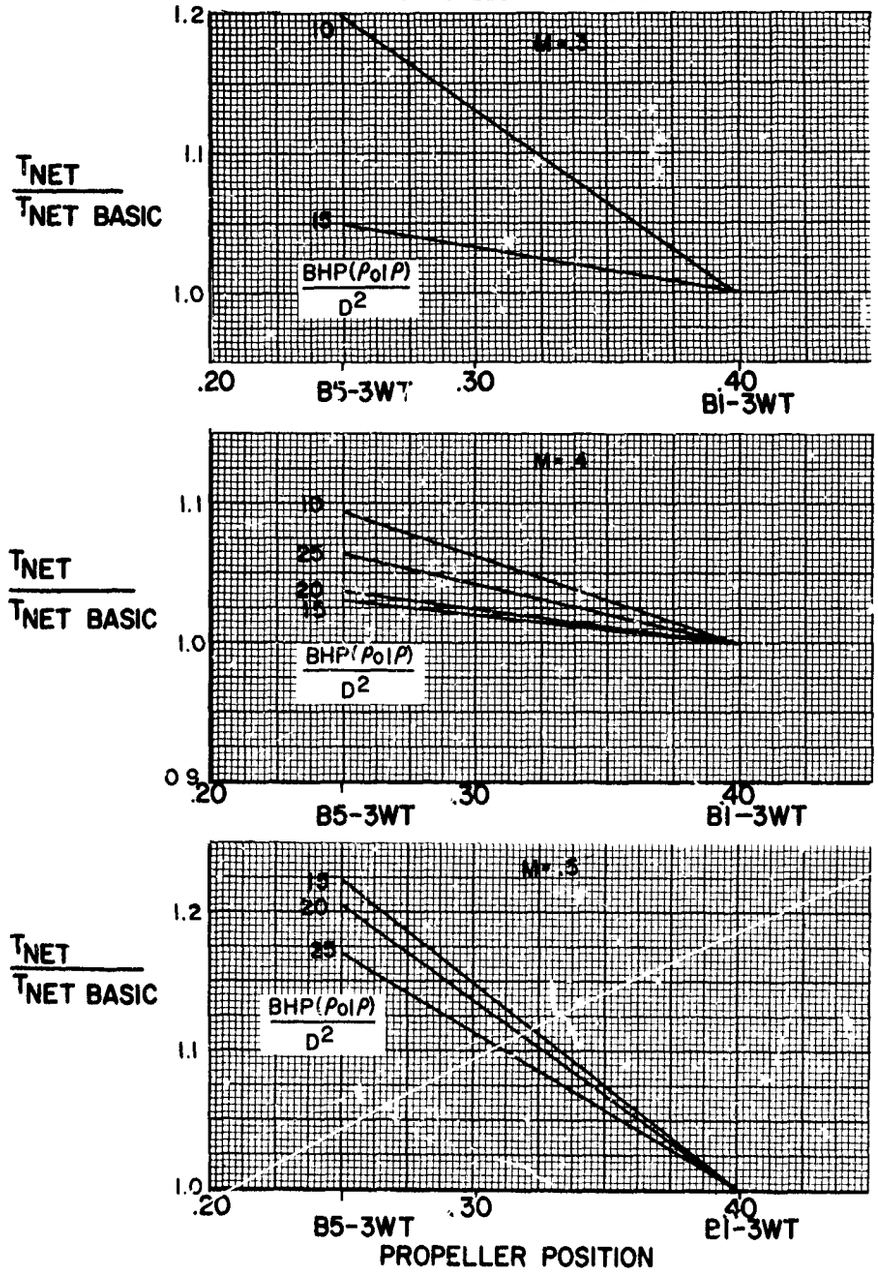

FIGURE 146

HS SHROUDED PROPELLER TEST

PERFORMANCE COMPARISON WITH BASIC CONFIGURATION, BI – 3WT
EFFECT OF PROPELLER POSITION
TIP SPEED = 980 FPS

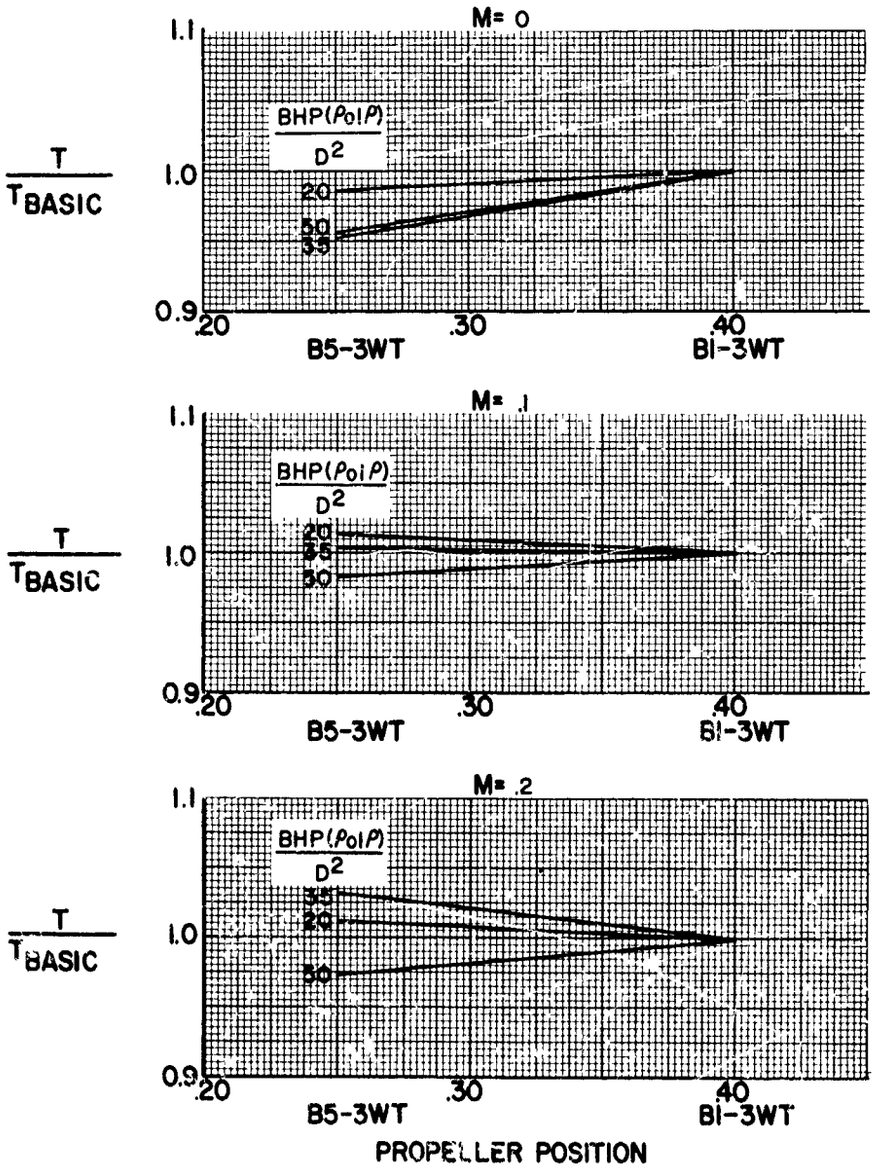

FIGURE 147

HS SHROUDED PROPELLER TEST

PERFORMANCE COMPARISON WITH BASIC CONFIGURATION, BI-3WT
EFFECT OF PROPELLER POSITION
TIP SPEED = 915 FPS

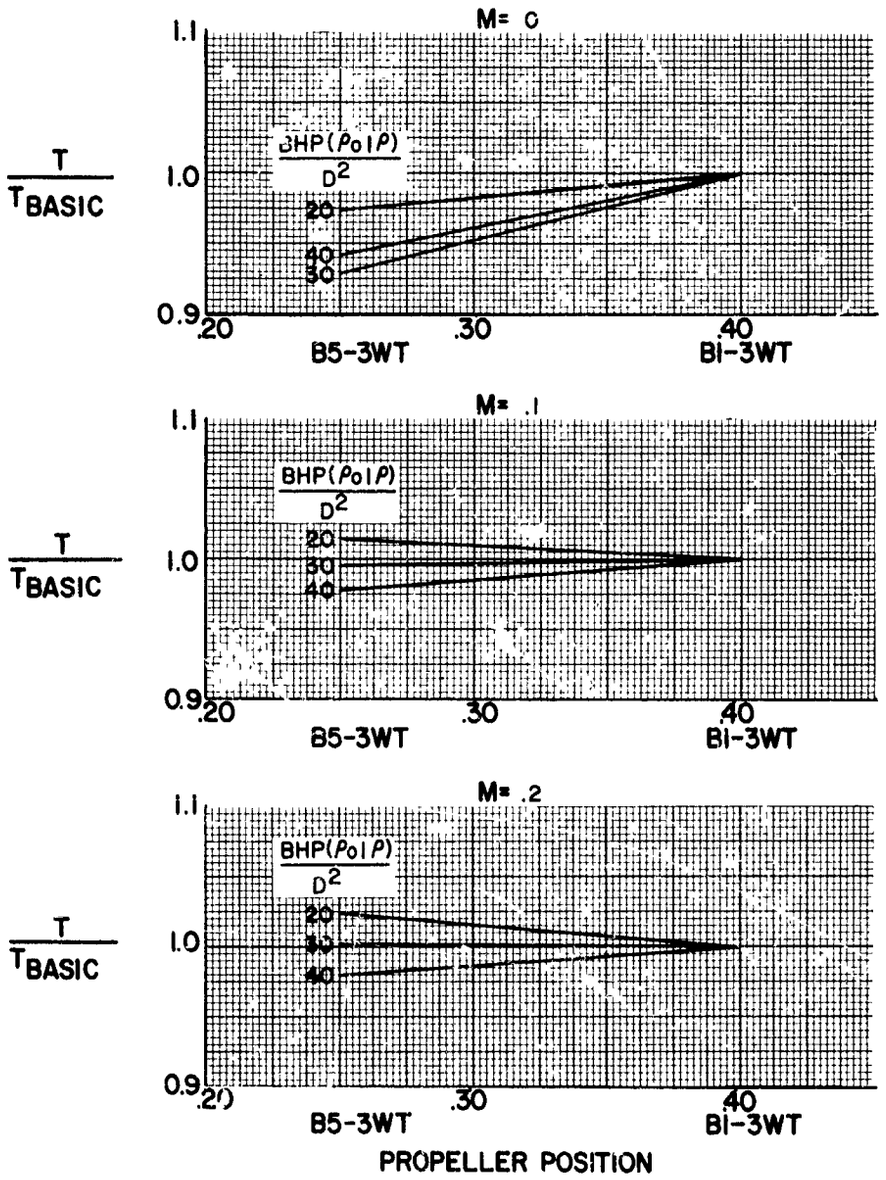

FIGURE 148

HS SHROUDED PROPELLER TEST

PERFORMANCE COMPARISON WITH BASIC CONFIGURATION, BI – 3WT
EFFECT OF PROPELLER POSITION
TIP SPEED = 785 FPS

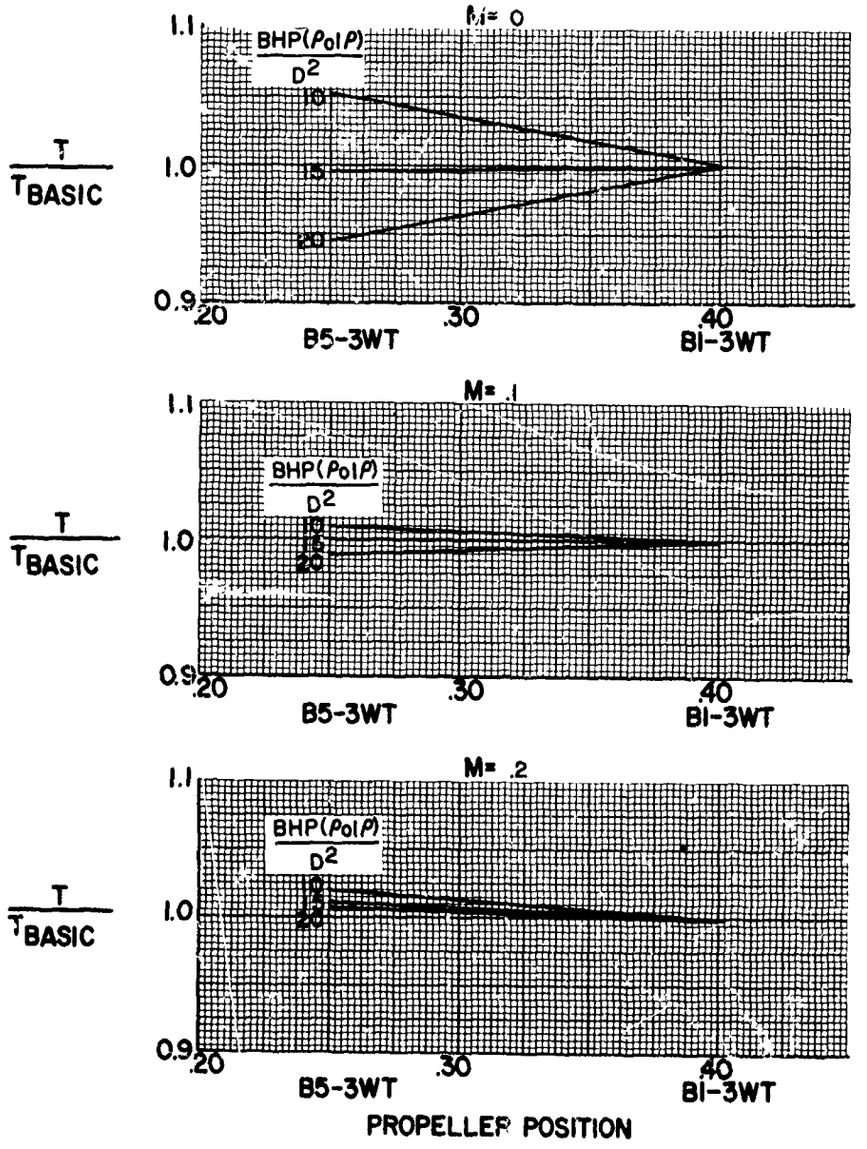

FIGURE 149

HS SHROUDED PROPELLER TEST

PERFORMANCE COMPARISON WITH BASIC CONFIGURATION, BI-3WT
EFFECT OF PROPELLER POSITION
TIP SPEED = 915 FPS

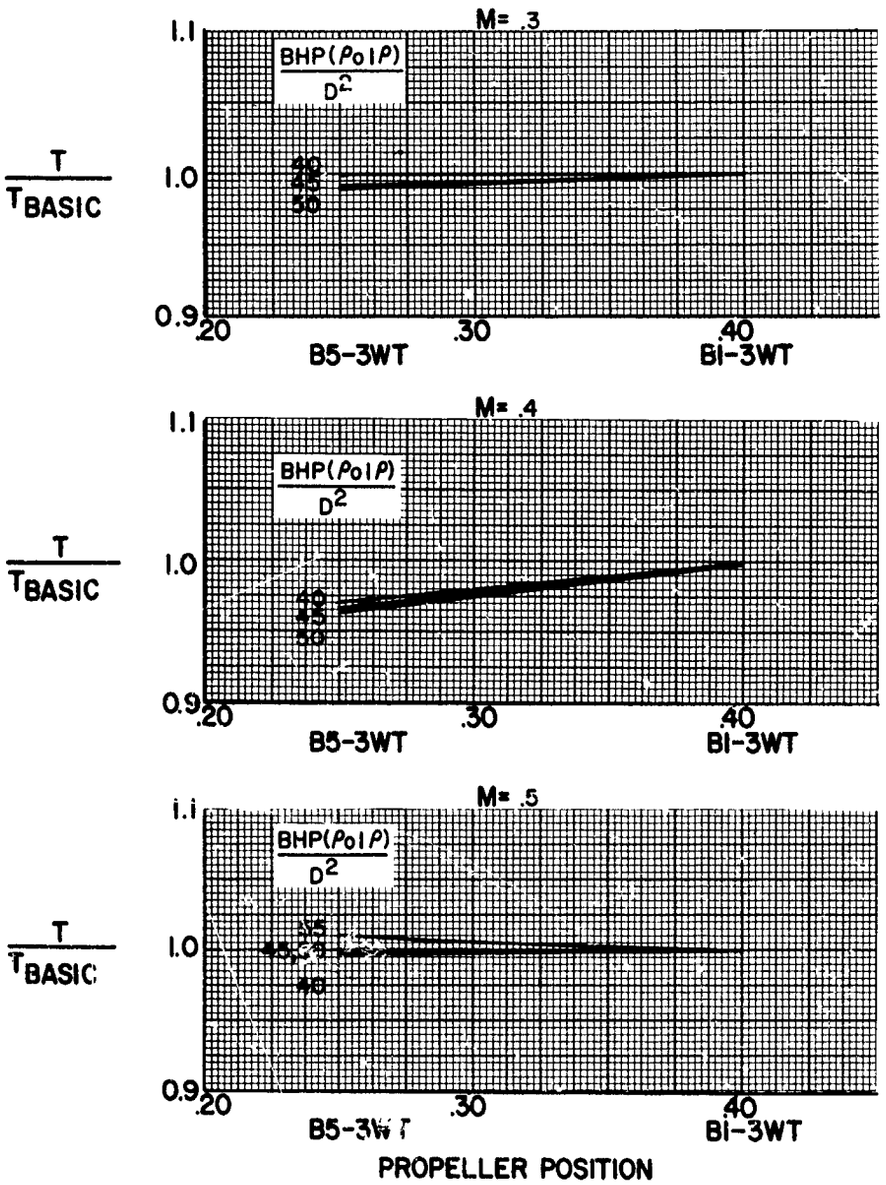

FIGURE 150

HS SHROUDED PROPELLER TEST

PERFORMANCE COMPARISON WITH BASIC CONFIGURATION, BI – 3WT
EFFECT OF PROPELLER POSITION
TIP SPEED = 785 FPS

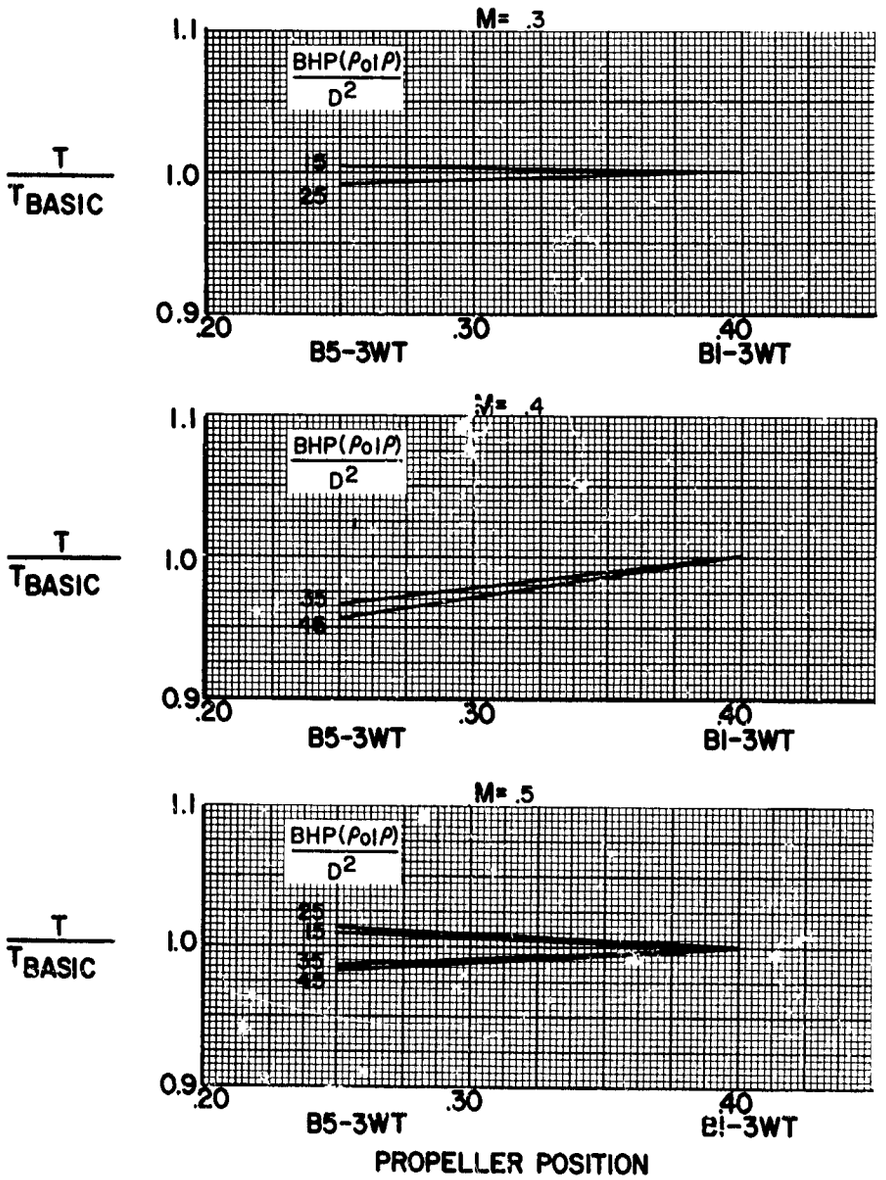

FIGURE 151

HS SHROUDED PROPELLER TEST

PERFORMANCE COMPARISON WITH BASIC CONFIGURATION, BI – 3WT
EFFECT OF PROPELLER POSITION
TIP SPEED = 654 FPS

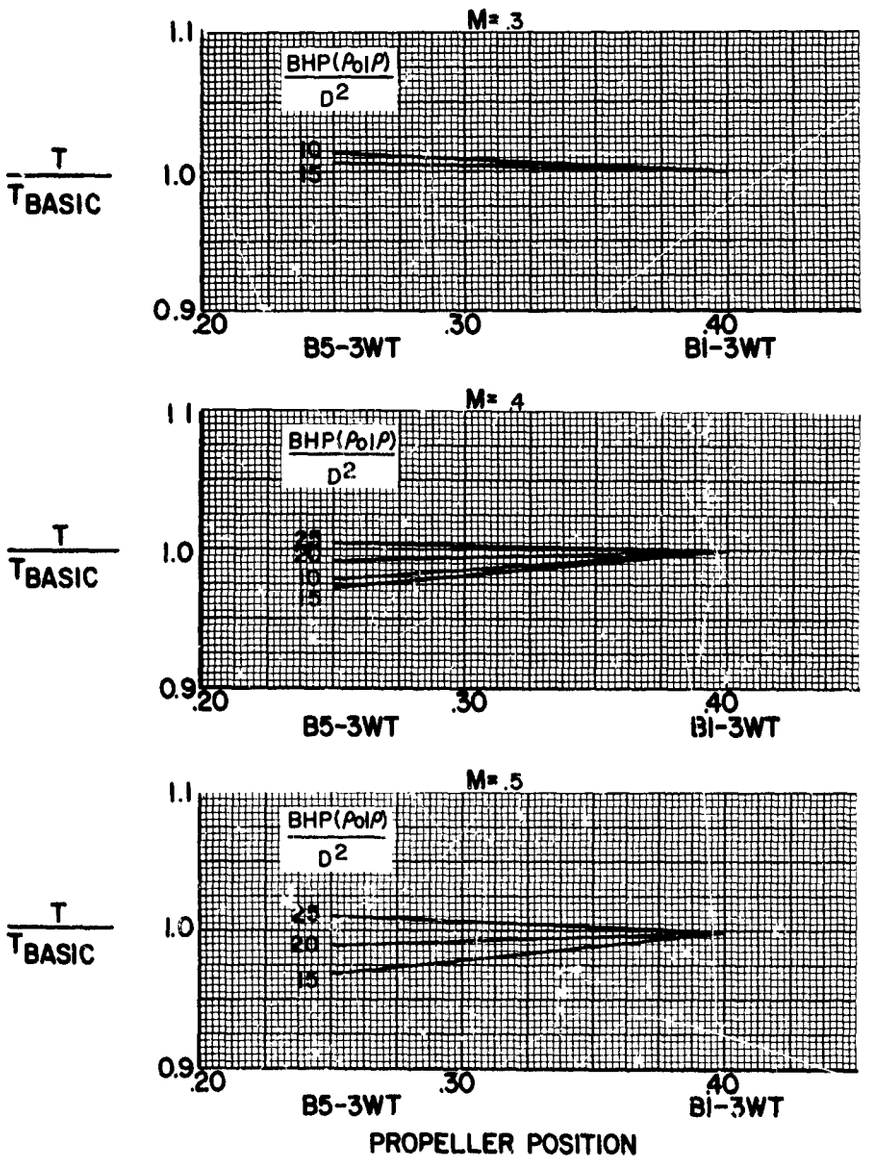

FIGURE 152

HS SHROUDED PROPELLER TEST

PERFORMANCE COMPARISON WITH BASIC CONFIGURATION, BI – 3WT

EFFECT OF INLET VANE
TIP SPEED = 980 FPS

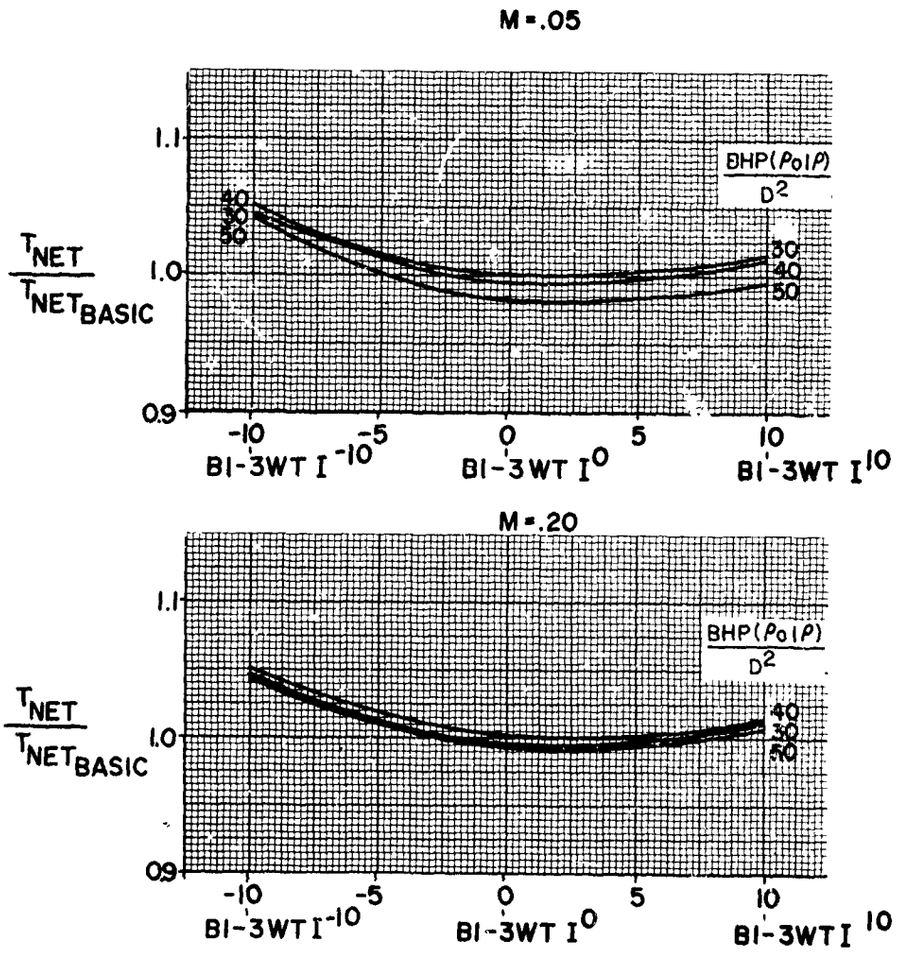

INLET VANE ANGLE

FIGURE 153

HS SHROUDED PROPELLER TEST

PERFORMANCE COMPARISON WITH BASIC CONFIGURATION, BI-3WT

EFFECT OF INLET VANE

TIP SPEED = 915 FPS

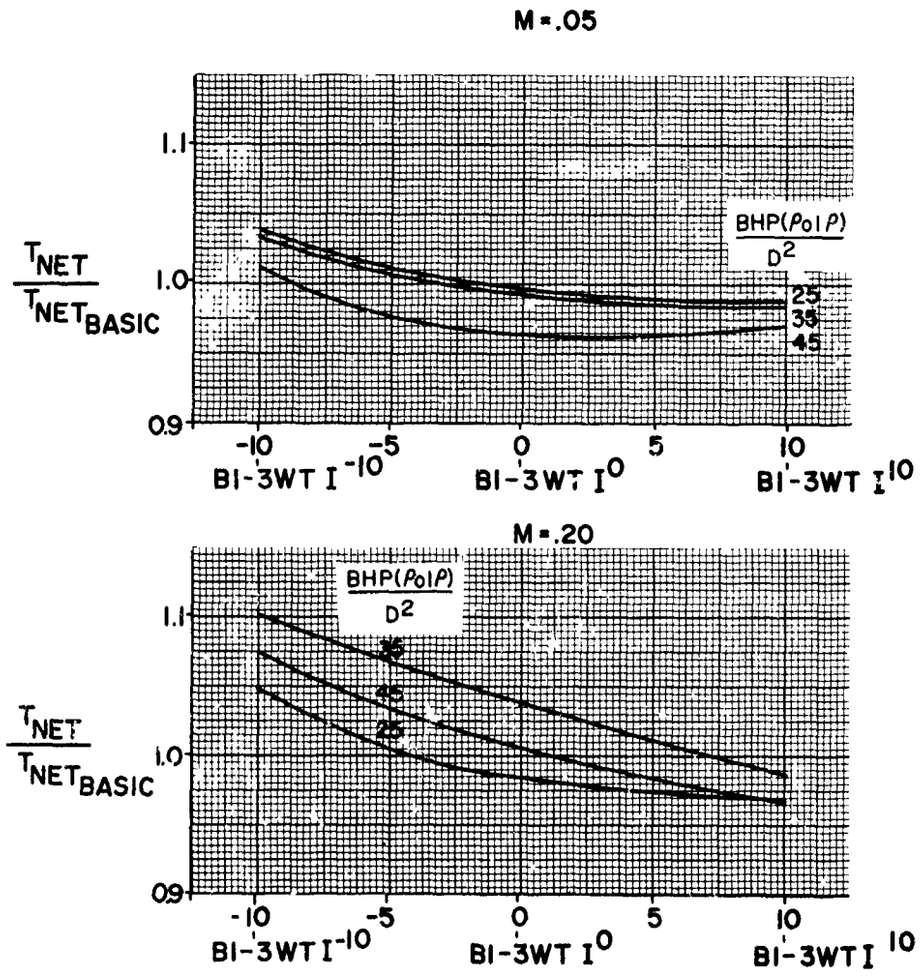

FIGURE 154

HS SHROUDED PROPELLER TEST

PERFORMANCE COMPARISON WITH BASIC CONFIGURATION, BI – 3WT

EFFECT OF INLET VANE
TIP SPEED = 785 FPS

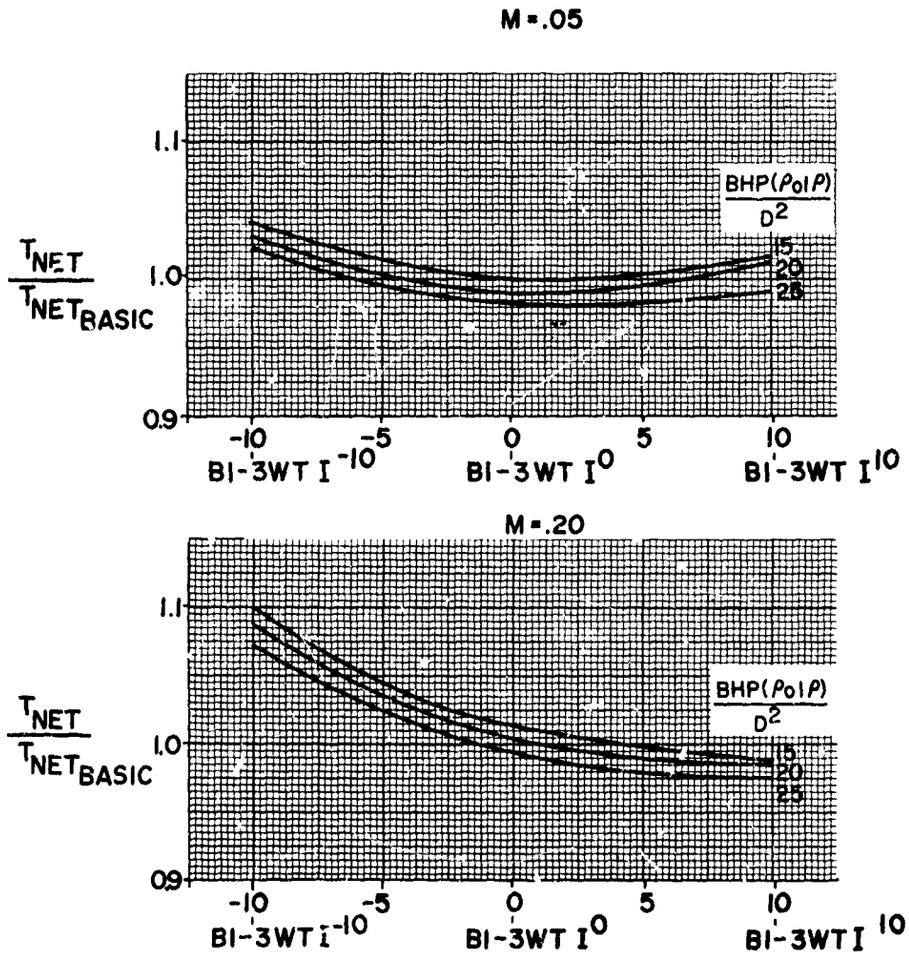

INLET VANE ANGLE

FIGURE 155

HS SHROUDED PROPELLER TEST

PERFORMANCE COMPARISON WITH BASIC CONFIGURATION, BI – 3WT
EFFECT OF INLET VANE
TIP SPEED = 980 FPS

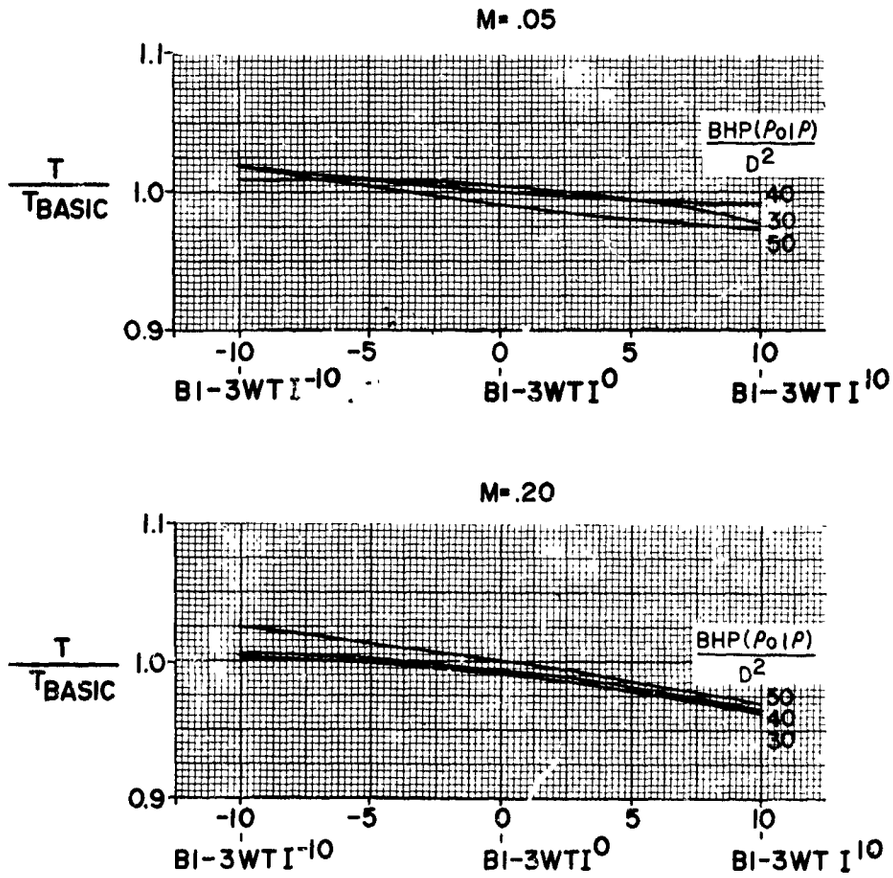

INLET VANE ANGLE

FIGURE 156

HS SHROUDED PROPELLER TEST

PERFORMANCE COMPARISON WITH BASIC CONFIGURATION, BI-3WT
EFFECT OF INLET VANE
TIP SPEED = 915 FPS

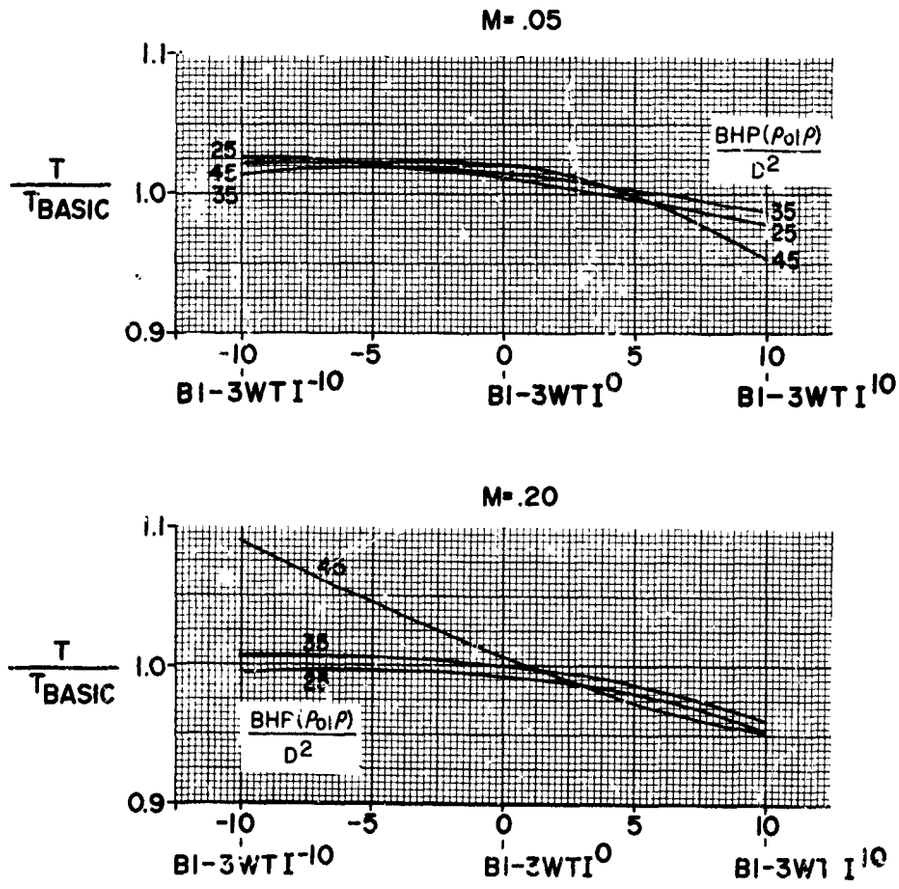

INLET VANE ANGLE

FIGURE 157

HS SHROUDED PROPELLER TEST

PERFORMANCE COMPARISON WITH BASIC CONFIGURATION, BI – 3WT
EFFECT OF INLET VANE
TIP SPEED = 785 FPS

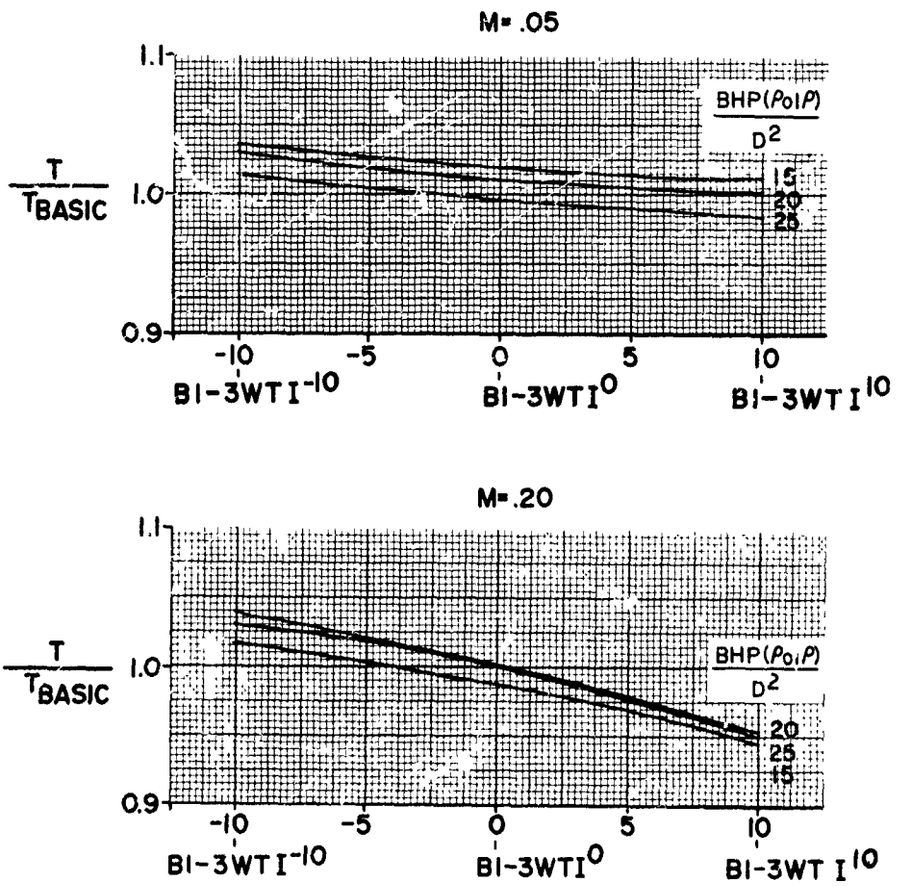

INLET VANE ANGLE

FIGURE 158

HS SHROUDED PROPELLER TEST

PERFORMANCE COMPARISON WITH BASIC CONFIGURATION, BI-3WT
EFFECT OF EXIT VANE
TIP SPEED = 980 FPS

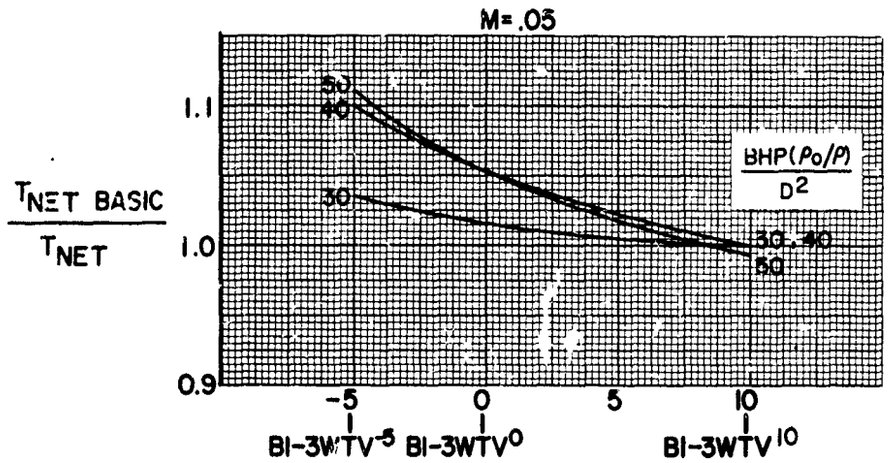

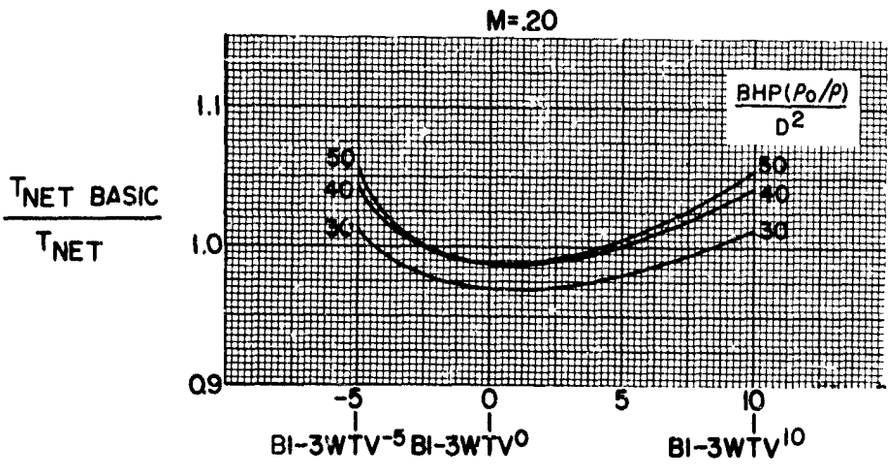

EXIT VANE ANGLE

FIGURE 159

HS SHROUDED PROPELLER TEST

PERFORMANCE COMPARISON WITH BASIC CONFIGURATION, BI – 3WT
EFFECT OF EXIT VANE
TIP SPEED = 915 FPS

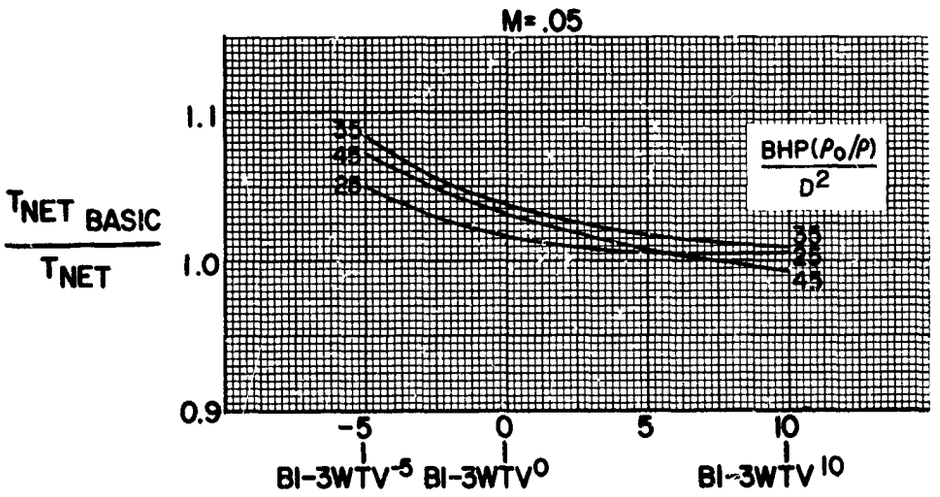

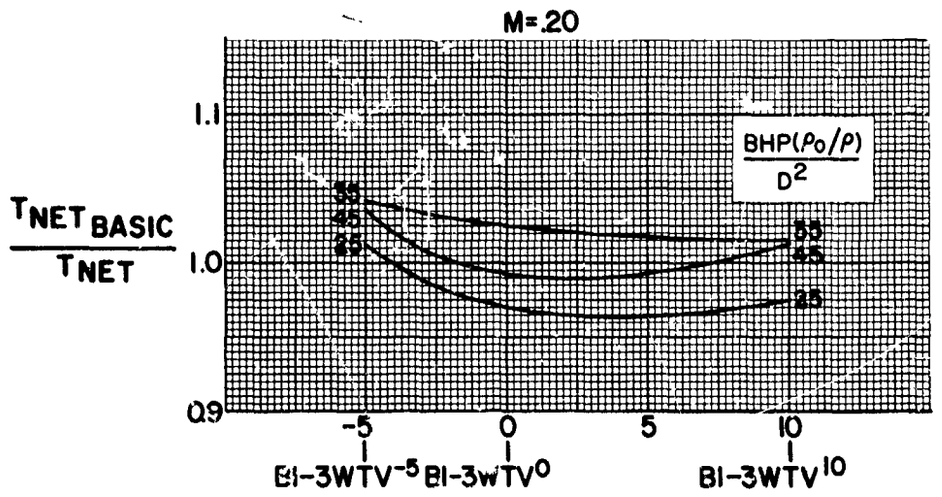

EXIT VANE ANGLE

FIGURE 160

HS SHROUDED PROPELLER TEST

PERFORMANCE COMPARISON WITH BASIC CONFIGURATION, BI-3WT
EFFECT OF EXIT VANE
TIP SPEED = 785 FPS

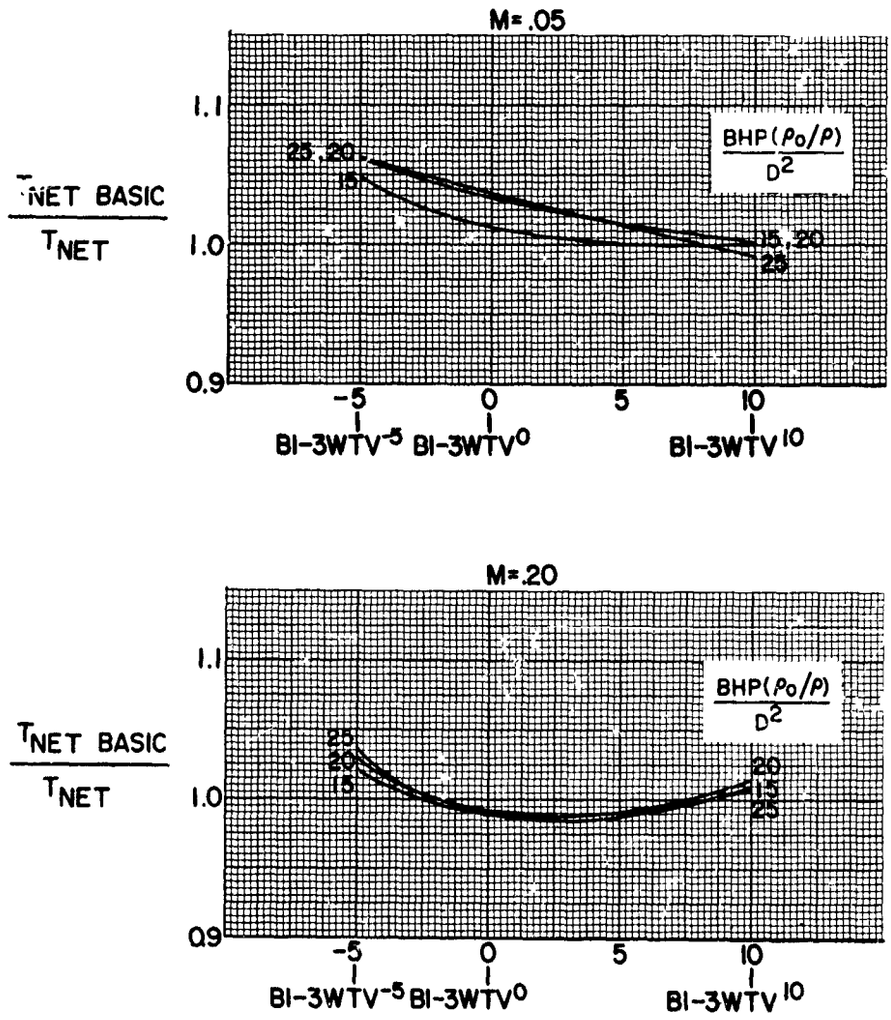

FIGURE 161

HS SHROUDED PROPELLER TEST

PERFORMANCE COMPARISON WITH BASIC CONFIGURATION, BI-3WT
EFFECT OF EXIT VANE
TIP SPEED = 980 FPS

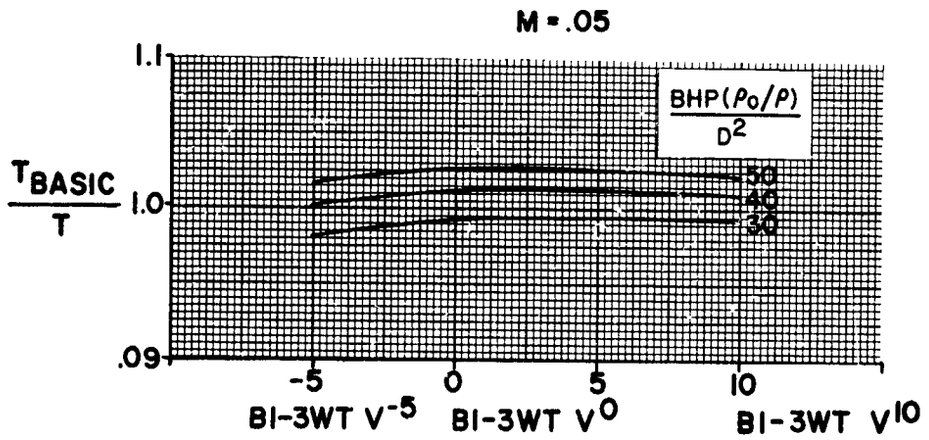

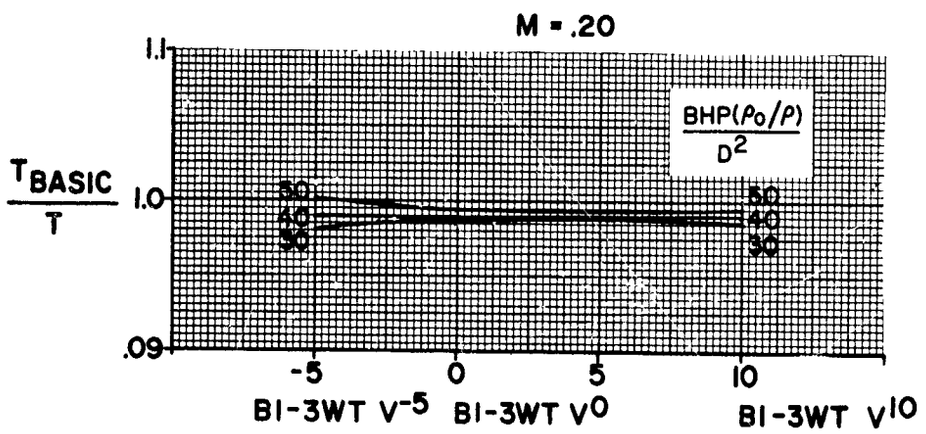

EXIT VANE ANGLE

FIGURE 162

HS SHROUDED PROPELLER TEST

PERFORMANCE COMPARISON WITH BASIC CONFIGURATION, BI-3WT
EFFECT OF EXIT VANE
TIP SPEED = 915 FPS

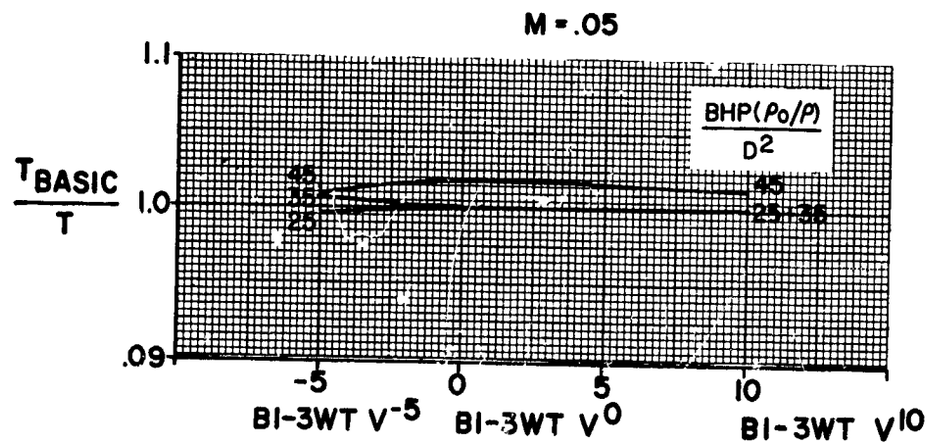

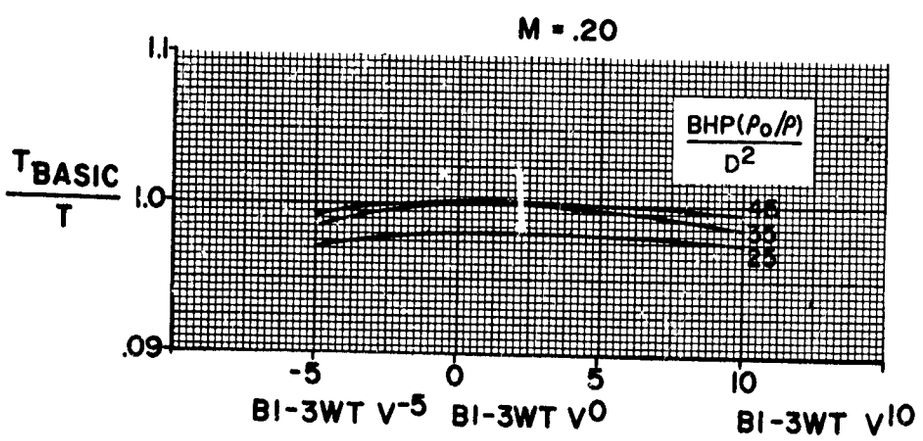

EXIT VANE ANGLE

FIGURE 163

HS SHROUDED PROPELLER TEST

PERFORMANCE COMPARISON WITH BASIC CONFIGURATION, BI – 3WT
EFFECT OF EXIT VANE
TIP SPEED = 785 FPS

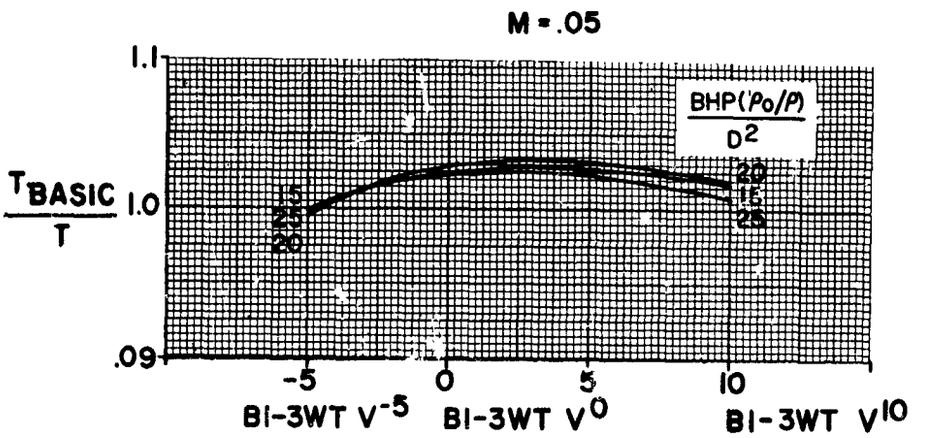

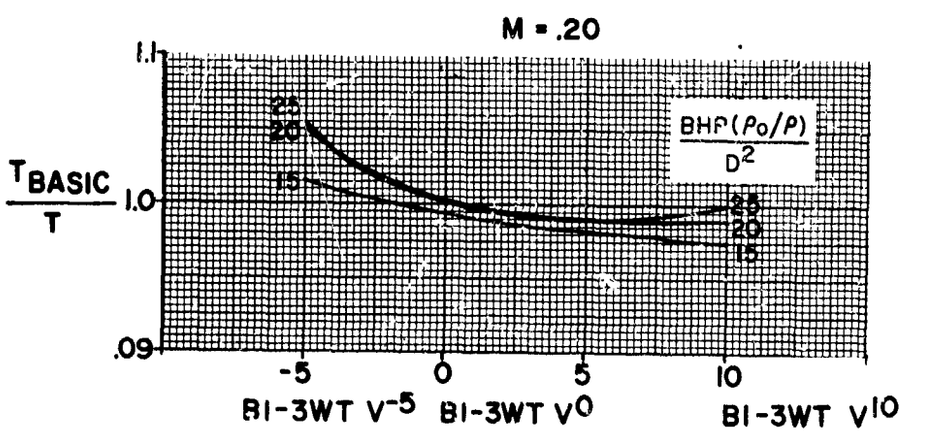

EXIT VANE ANGLE

FIGURE 164

HS SHROUDED PROPELLER TEST

PERFORMANCE COMPARISON WITH BASIC CONFIGURATION, BI-3WT
EFFECT OF PROPELLER PLANFORM
TIP SPEED = 980 FPS

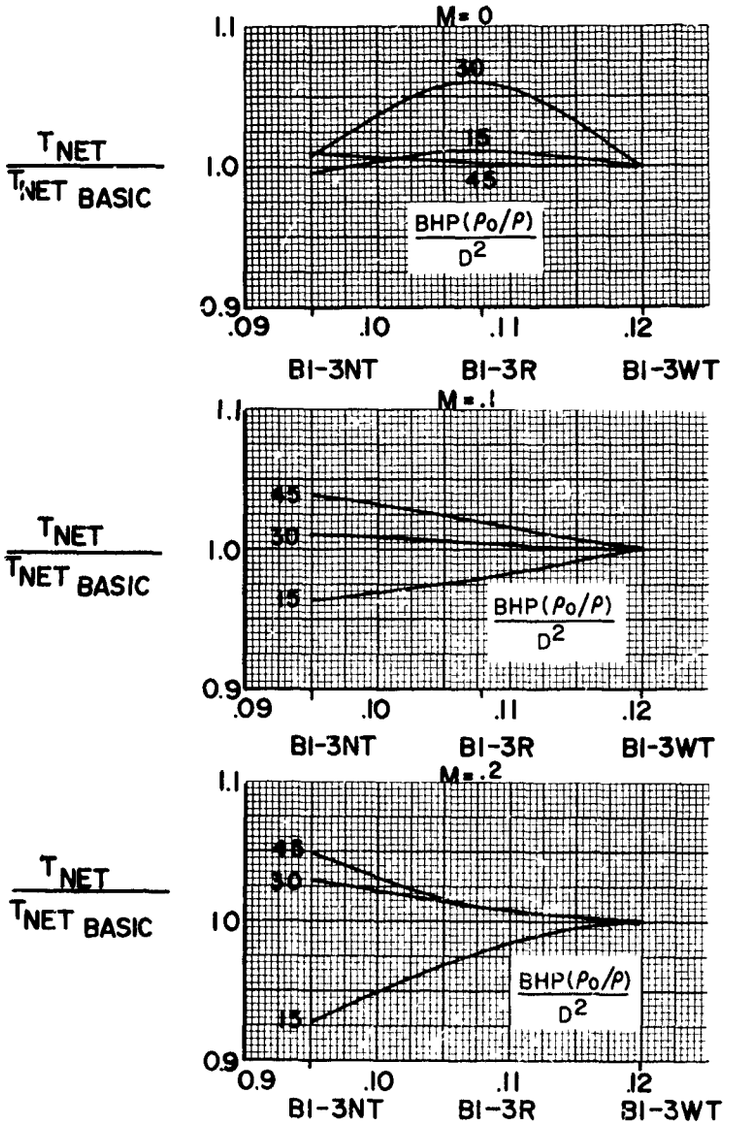

BLADE TIP CHORD / PROPELLER DIAMETER

FIGURE 165

HS SHROUDED PROPELLER TEST

PERFORMANCE COMPARISON WITH BASIC CONFIGURATION, BI-3WT
EFFECT OF PROPELLER PLANFORM
TIP SPEED = 915 FPS

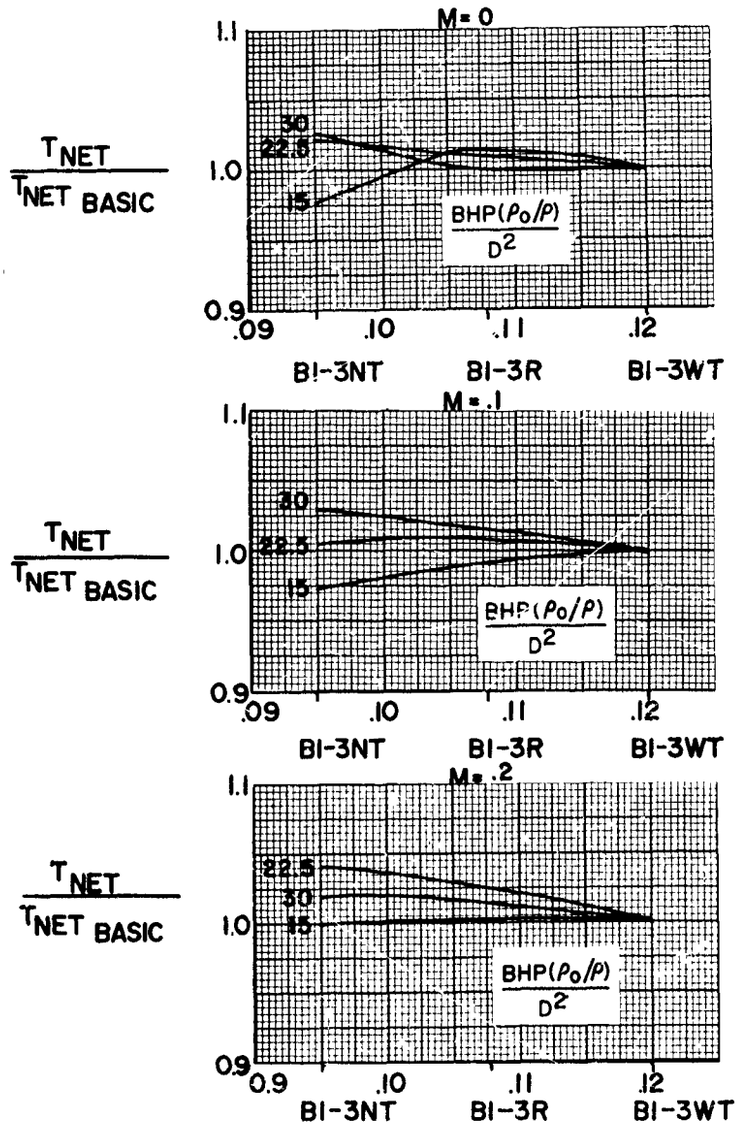

FIGURE 166

HS SHROUDED PROPELLER TEST

PERFORMANCE COMPARISON WITH BASIC CONFIGURATION, BI-3WT
EFFECT OF PROPELLER PLANFORM
TIP SPEED = 785 FPS

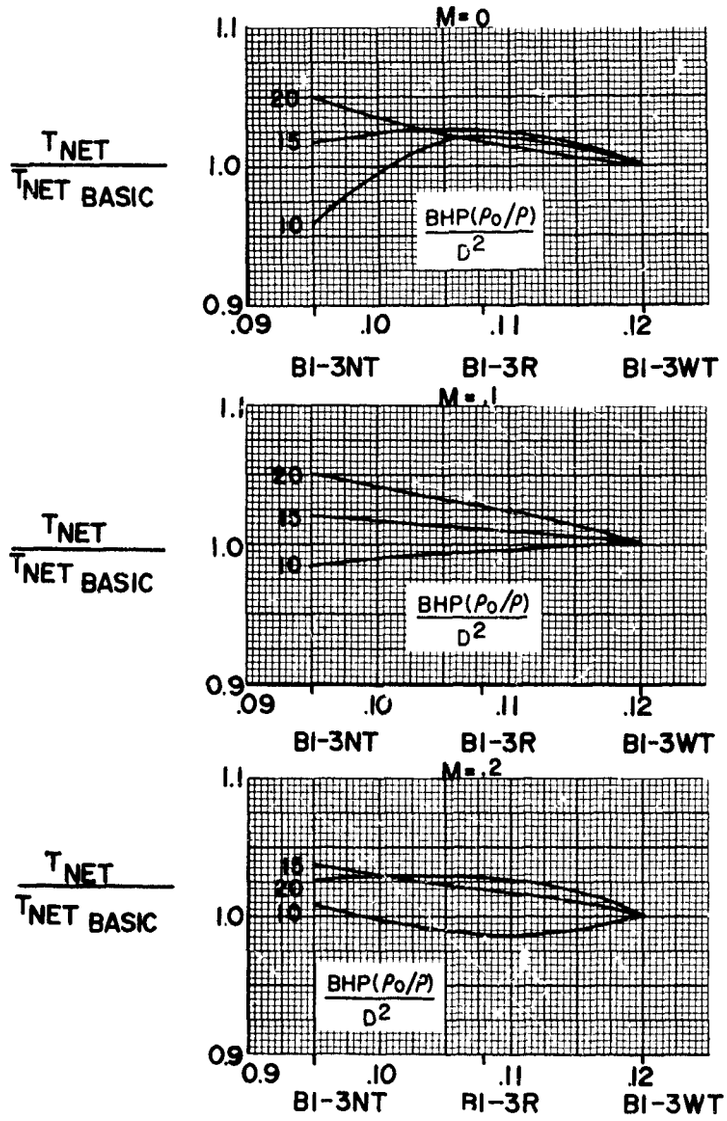

BLADE TIP CHORD/PROPELLER DIAMETER

FIGURE 167

HS SHROUDED PROPELLER TEST

PERFORMANCE COMPARISON WITH BASIC CONFIGURATION, BI-3WT
EFFECT OF PROPELLER PLANFORM
TIP SPEED = 915 FPS

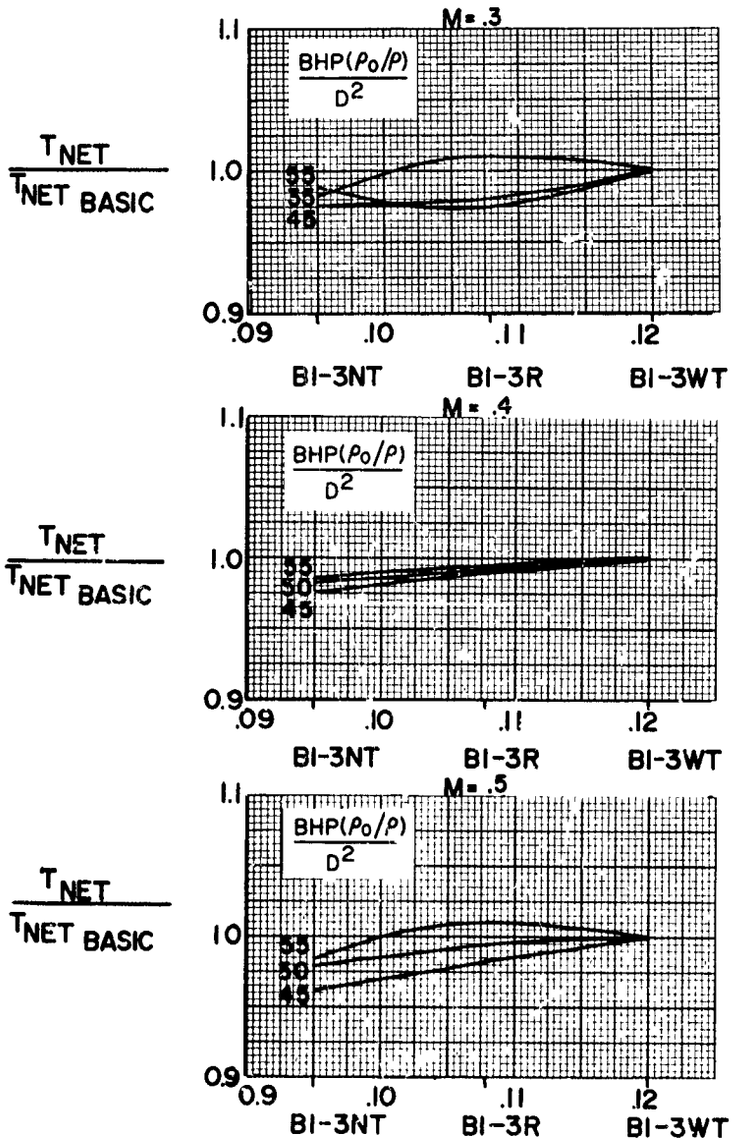

FIGURE 168

HS SHROUDED PROPELLER TEST

PERFORMANCE COMPARISON WITH BASIC CONFIGURATION, BI-3WT
EFFECT OF PROPELLER PLANFORM
TIP SPEED = 785 FPS

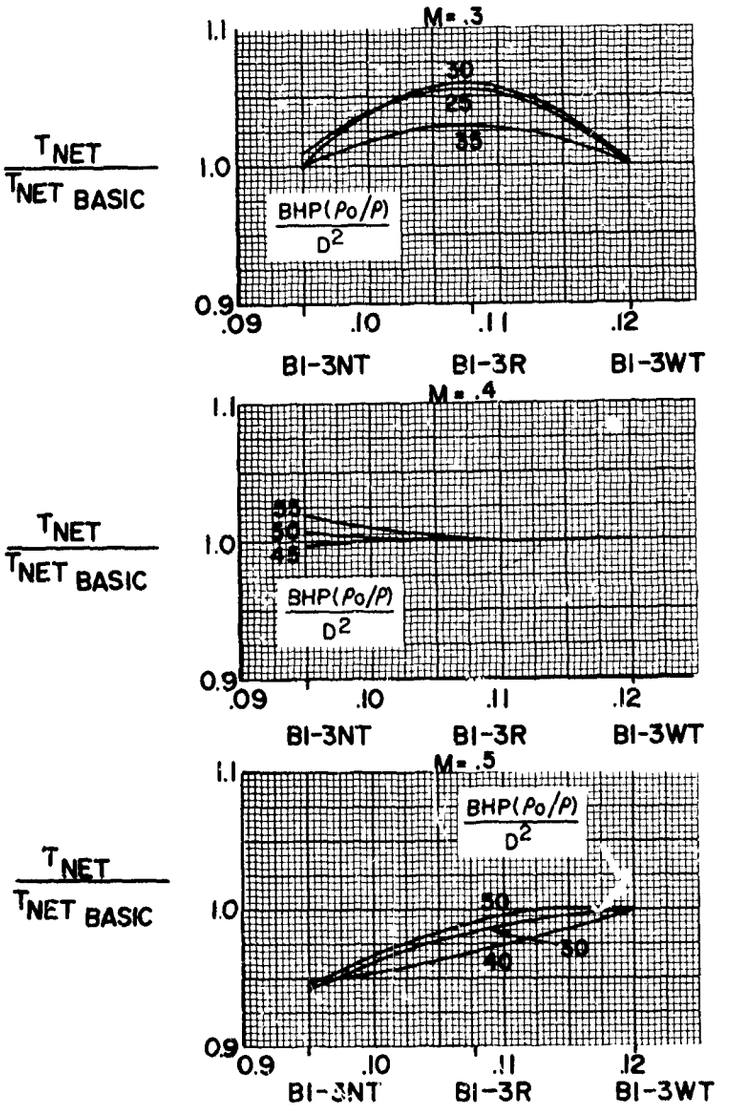

FIGURE 169

HS SHROUDED PROPELLER TEST

PERFORMANCE COMPARISON WITH BASIC CONFIGURATION, BI-3WT
EFFECT OF PROPELLER PLANFORM
TIP SPEED = 654 FPS

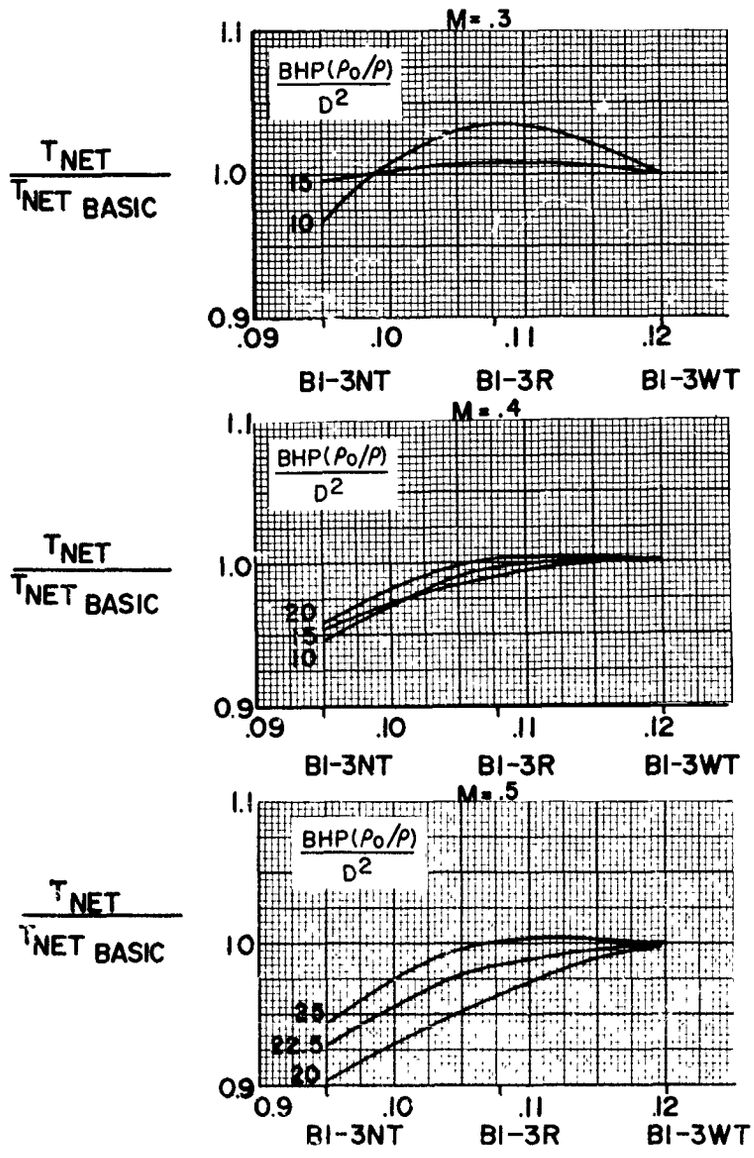

BLADE TIP CHORD / PROPELLER DIAMETER

FIGURE 170

HS SHROUDED PROPELLER TEST

PERFORMANCE COMPARISON WITH BASIC CONFIGURATION, BI-3WT
EFFECT OF PROPELLER PLANFORM
TIP SPEED = 980 FPS

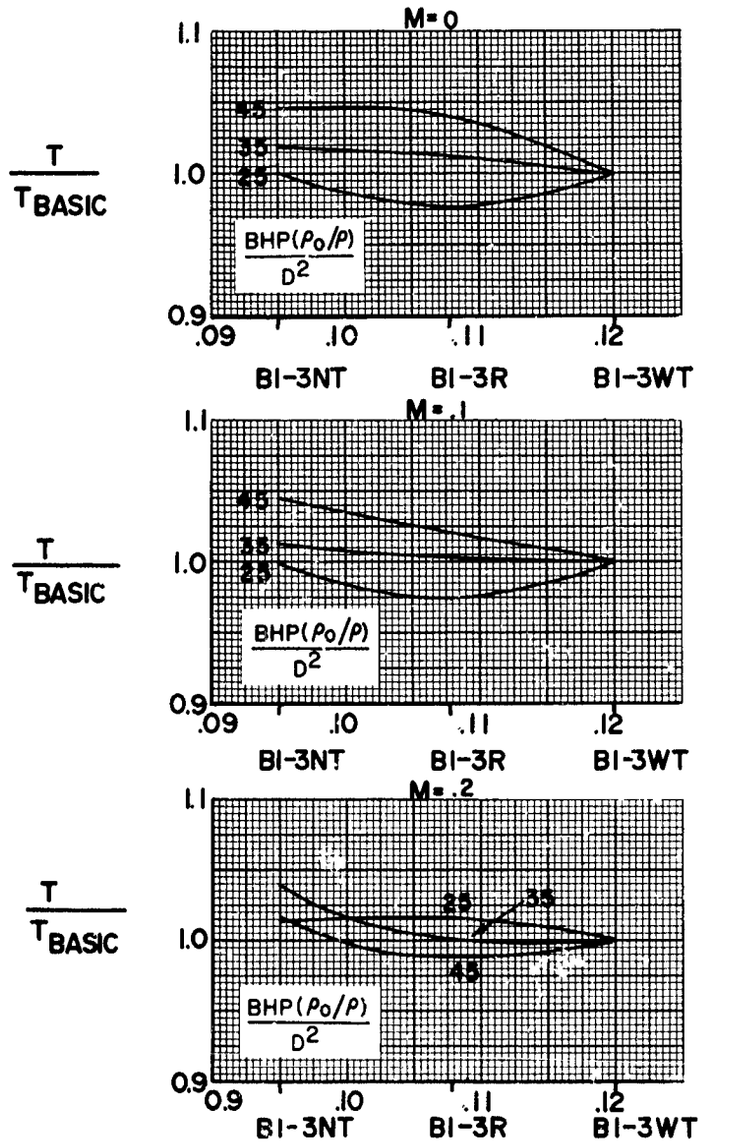

FIGURE 171

HS SHROUDED PROPELLER TEST

PERFORMANCE COMPARISON WITH BASIC CONFIGURATION, BI-3WT
EFFECT OF PROPELLER PLANFORM
TIP SPEED = 915 FPS

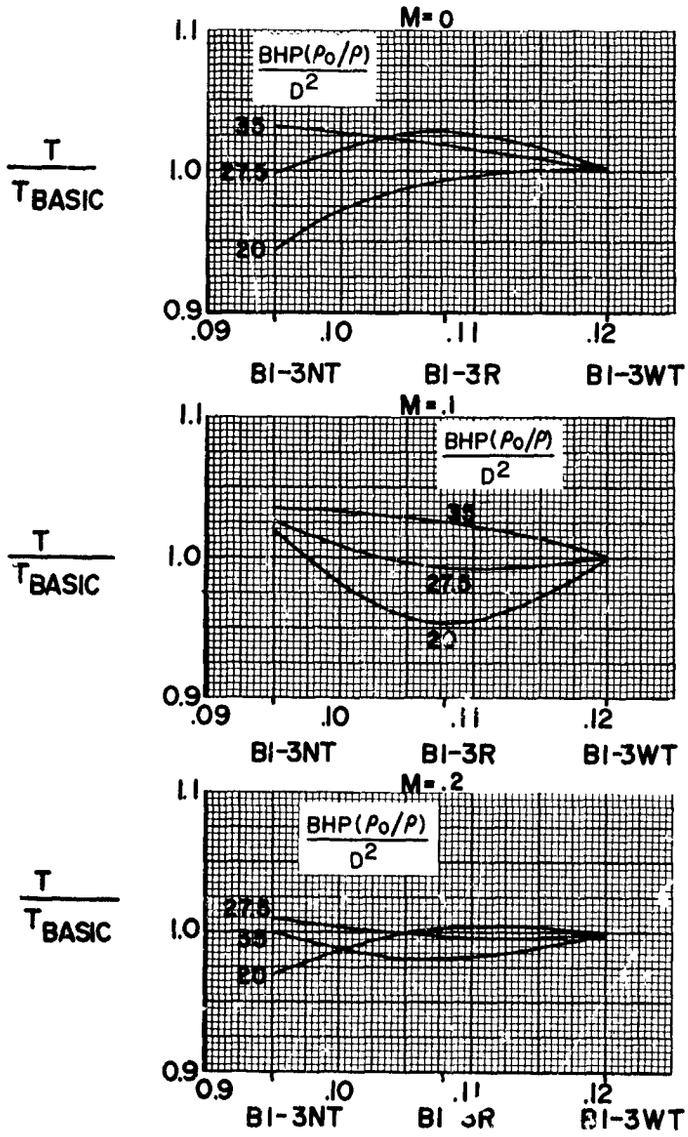

BLADE TIP CHORD/PROPELLER DIAMETER

FIGURE 172

HS SHROUDED PROPELLER TEST

PERFORMANCE COMPARISON WITH BASIC CONFIGURATION, BI-3WT
EFFECT OF PROPELLER PLANFORM
TIP SPEED = 785 FPS

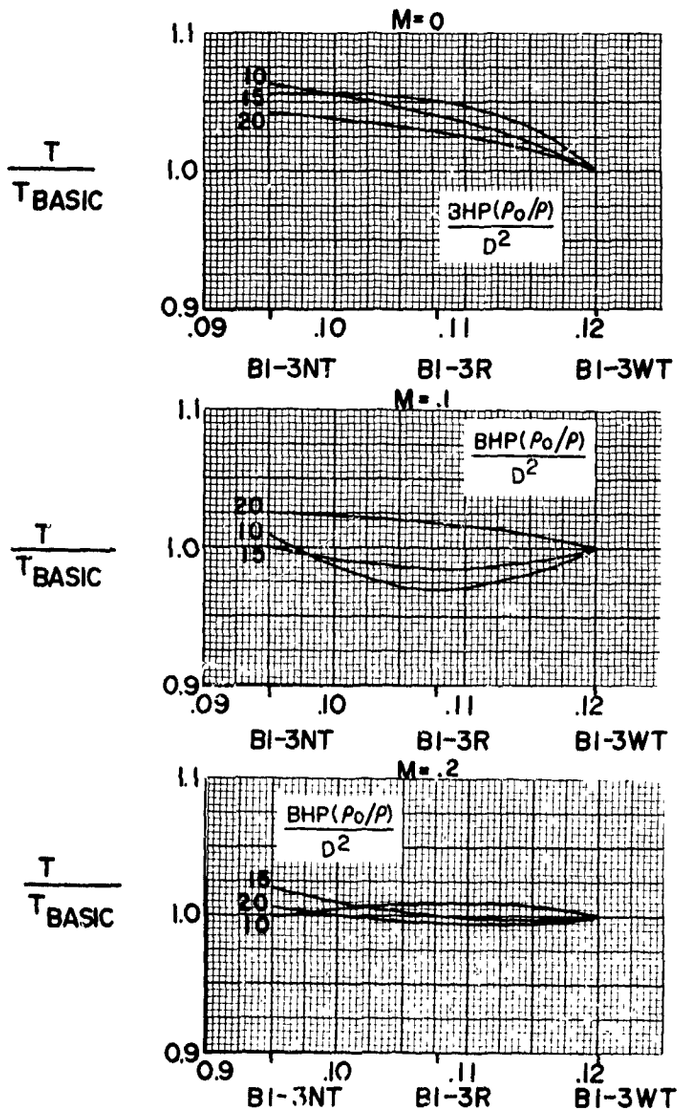

BLADE TIP CHORD/PROPELLER DIAMETER

FIGURE 173

HS SHROUDED PROPELLER TEST

PERFORMANCE COMPARISON WITH BASIC CONFIGURATION, BI-3WT
EFFECT OF PROPELLER PLANFORM
TIP SPEED = 915 FPS

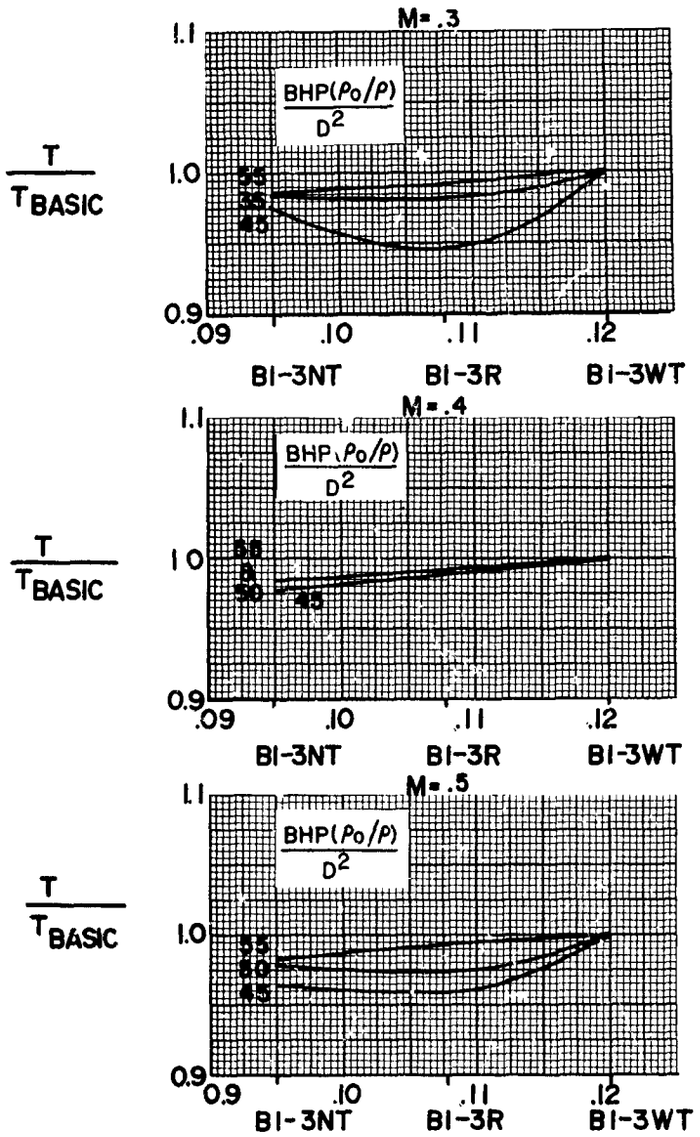

BLADE TIP CHORD/PROPELLER DIAMETER

FIGURE 174

HS SHROUDED PROPELLER TEST

PERFORMANCE COMPARISON WITH BASIC CONFIGURATION, BI-3WT
EFFECT OF PROPELLER PLANFORM
TIP SPEED = 785 FPS

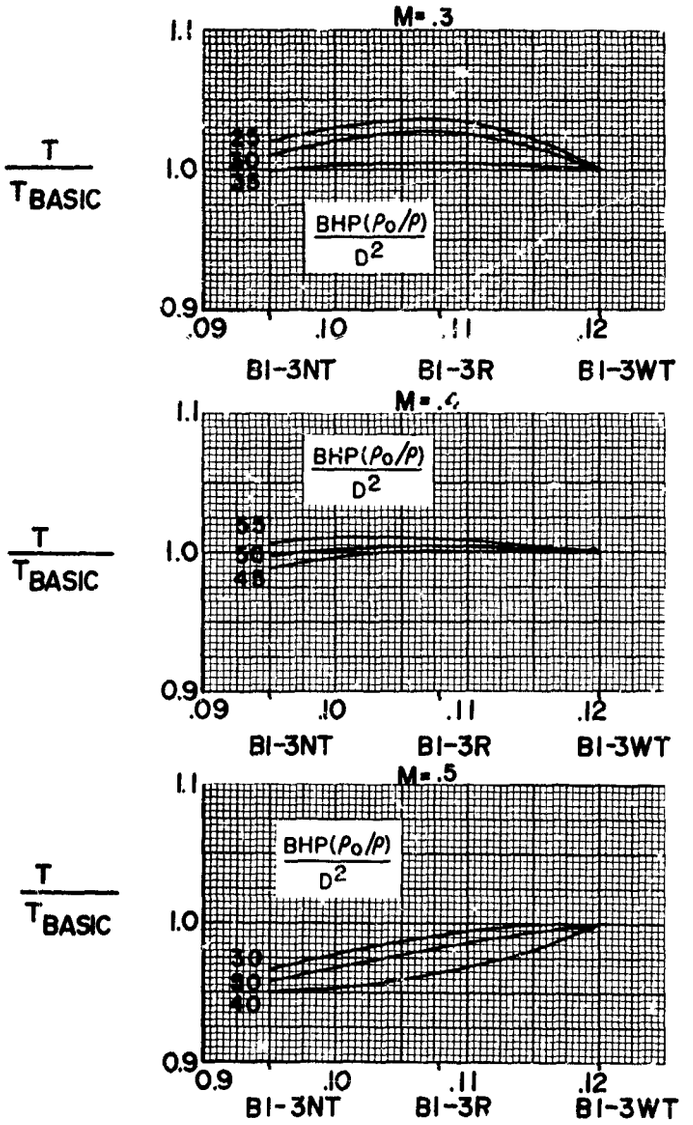

BLADE TIP CHORD / PROPELLER DIAMETER

FIGURE 175

HS SHROUDED PROPELLER TEST

PERFORMANCE COMPARISON WITH BASIC CONFIGURATION, BI-3WT
EFFECT OF PROPELLER PLANFORM
TIP SPEED = 654 FPS

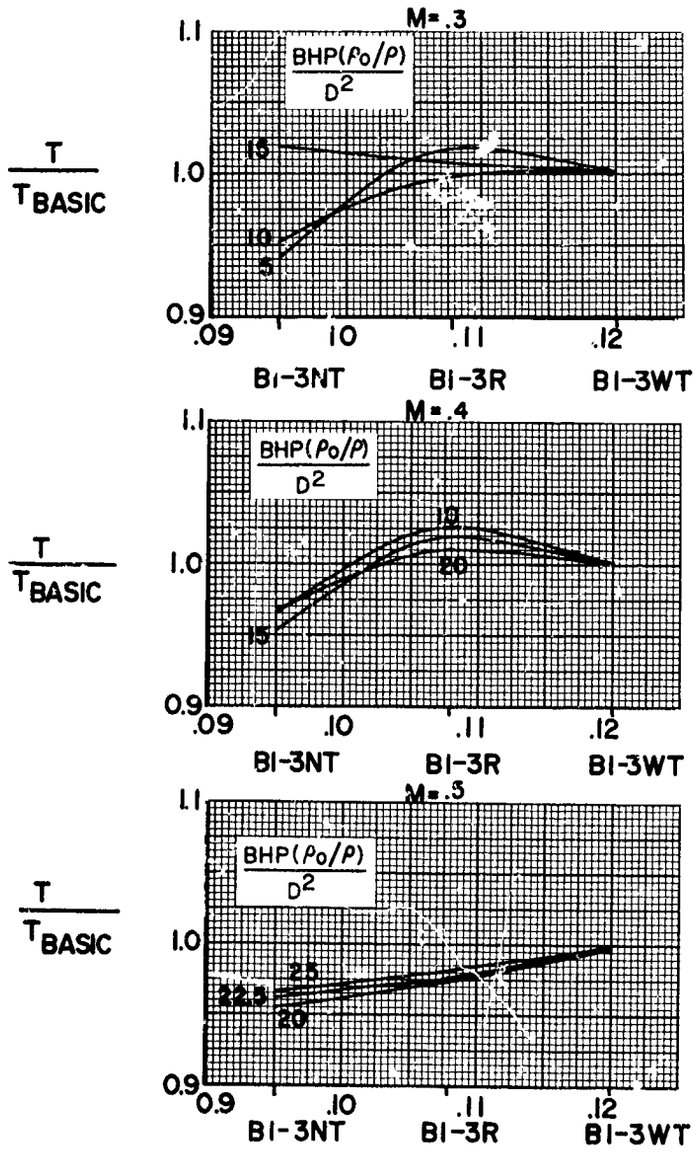

BLADE TIP CHORD / PROPELLER DIAMETER

FIGURE 176

HS SHROUDED PROPELLER TEST

PERFORMANCE COMPARISON WITH CONFIGURATION BI-3NT
EFFECT OF NUMBER OF BLADES
TIP SPEED = 980 FPS

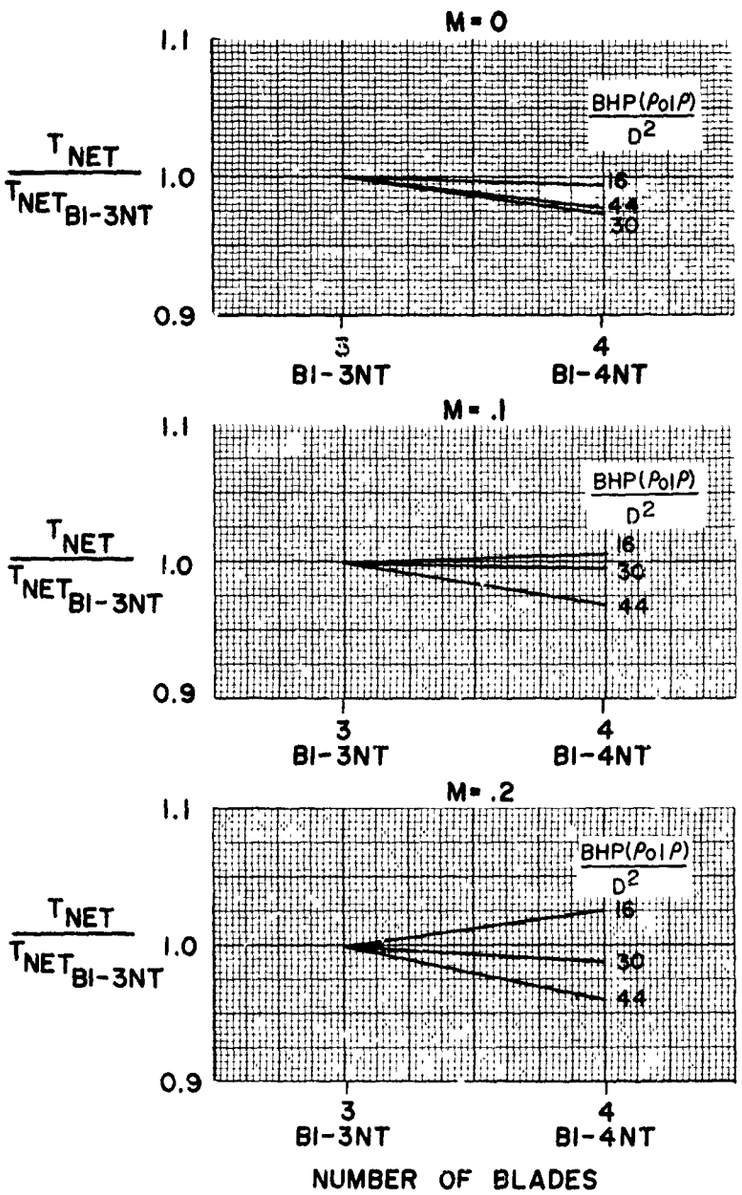

FIGURE 177

HS SHROUDED PROPELLER TEST

PERFORMANCE COMPARISON WITH CONFIGURATION BI-3NT
EFFECT OF NUMBER OF BLADES
TIP SPEED = 915 FPS

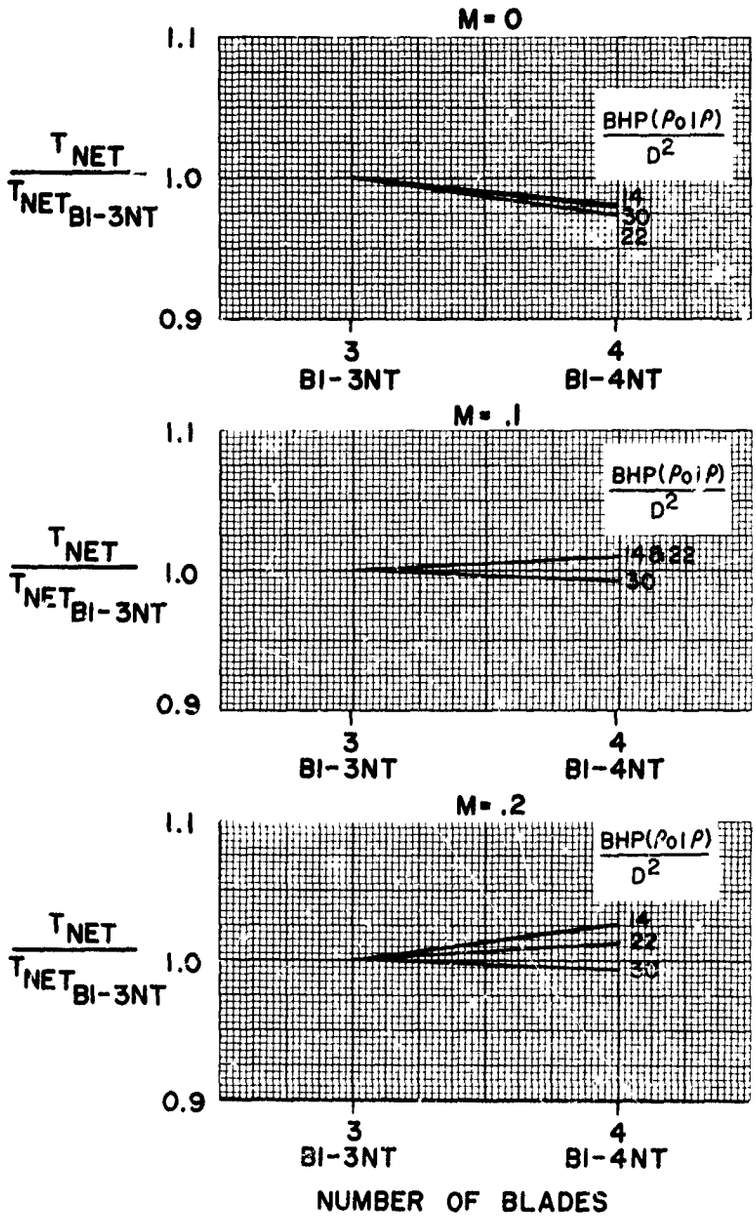

FIGURE 178

HS SHROUDED PROPELLER TEST

PERFORMANCE COMPARISON WITH CONFIGURATION BI-3NT
EFFECT OF NUMBER OF BLADES
TIP SPEED = 785 FPS

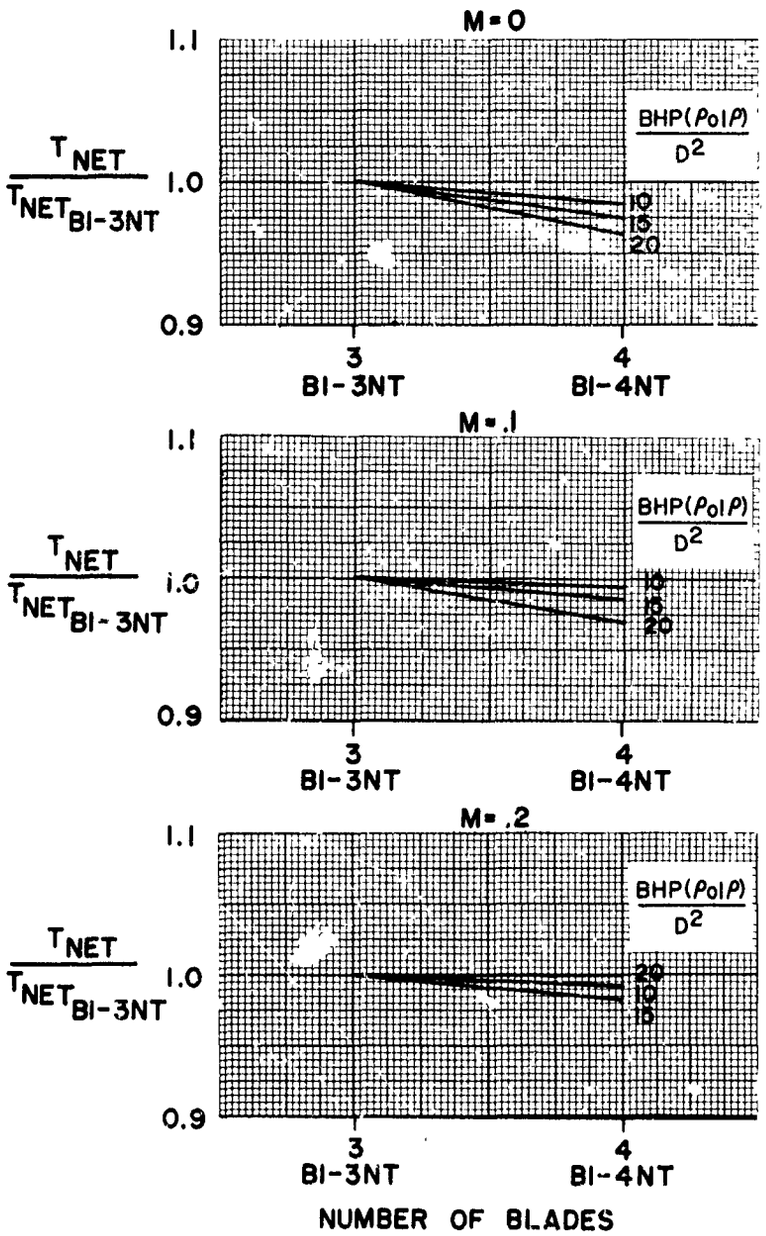

FIGURE 179

HS SHROUDED PROPELLER TEST

PERFORMANCE COMPARISON WITH CONFIGURATION BI-3NT
EFFECT OF NUMBER OF BLADES
TIP SPEED = 915 FPS

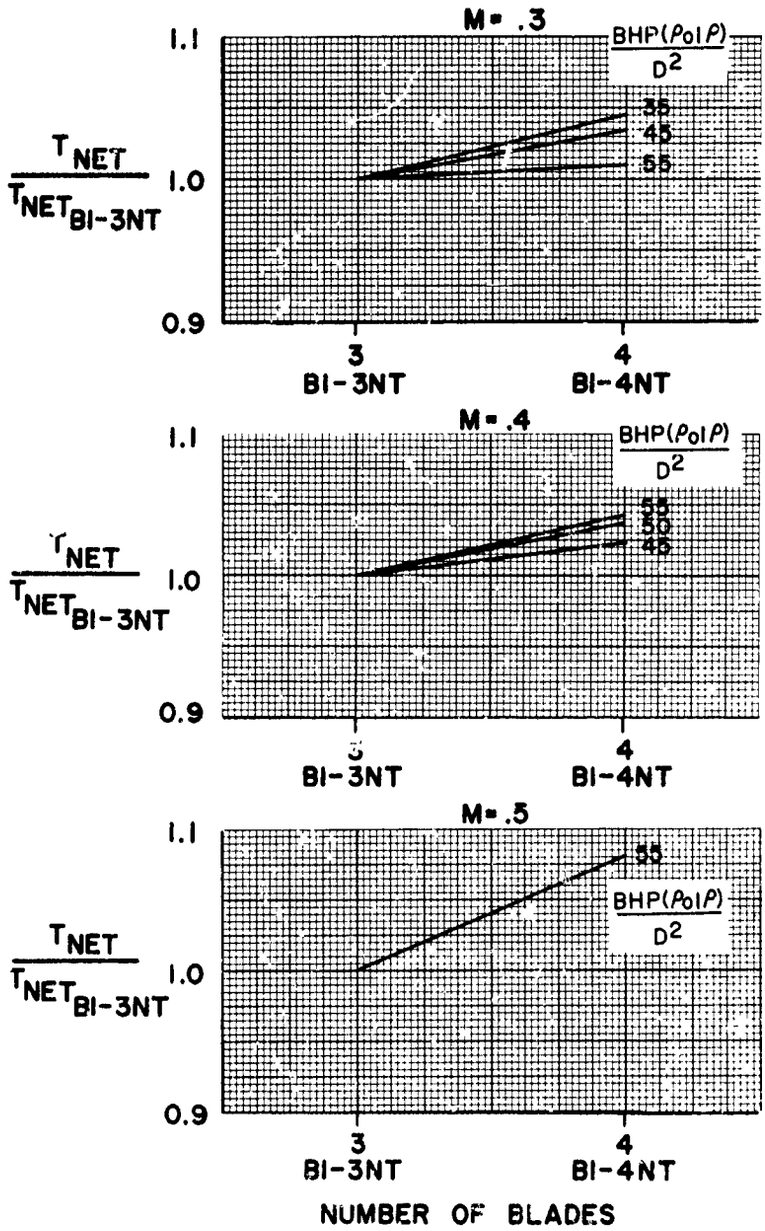

FIGURE 180

HS SHROUDED PROPELLER TEST

PERFORMANCE COMPARISON WITH CONFIGURATION BI-3NT
EFFECT OF NUMBER OF BLADES
TIP SPEED = 785 FPS

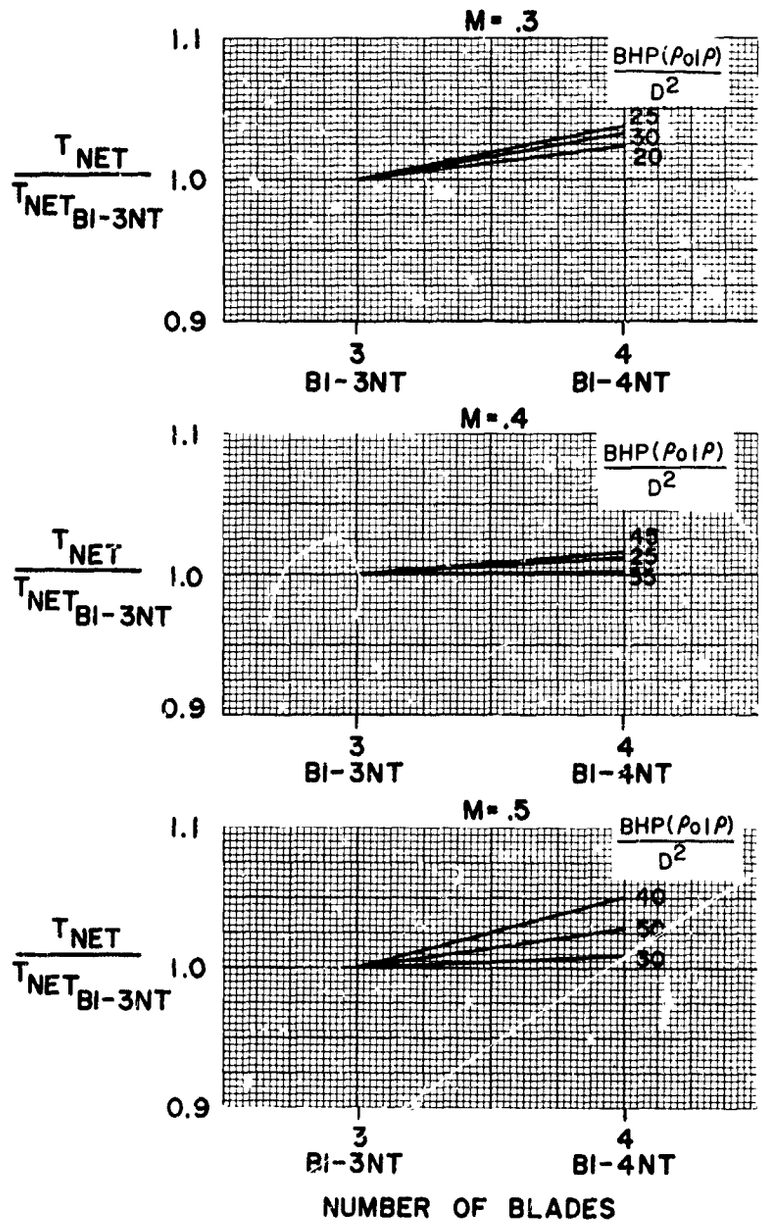

FIGURE 181

HS SHROUDED PROPELLER TEST

PERFORMANCE COMPARISON WITH CONFIGURATION BI-3NT
EFFECT OF NUMBER OF BLADES
TIP SPEED = 654 FPS

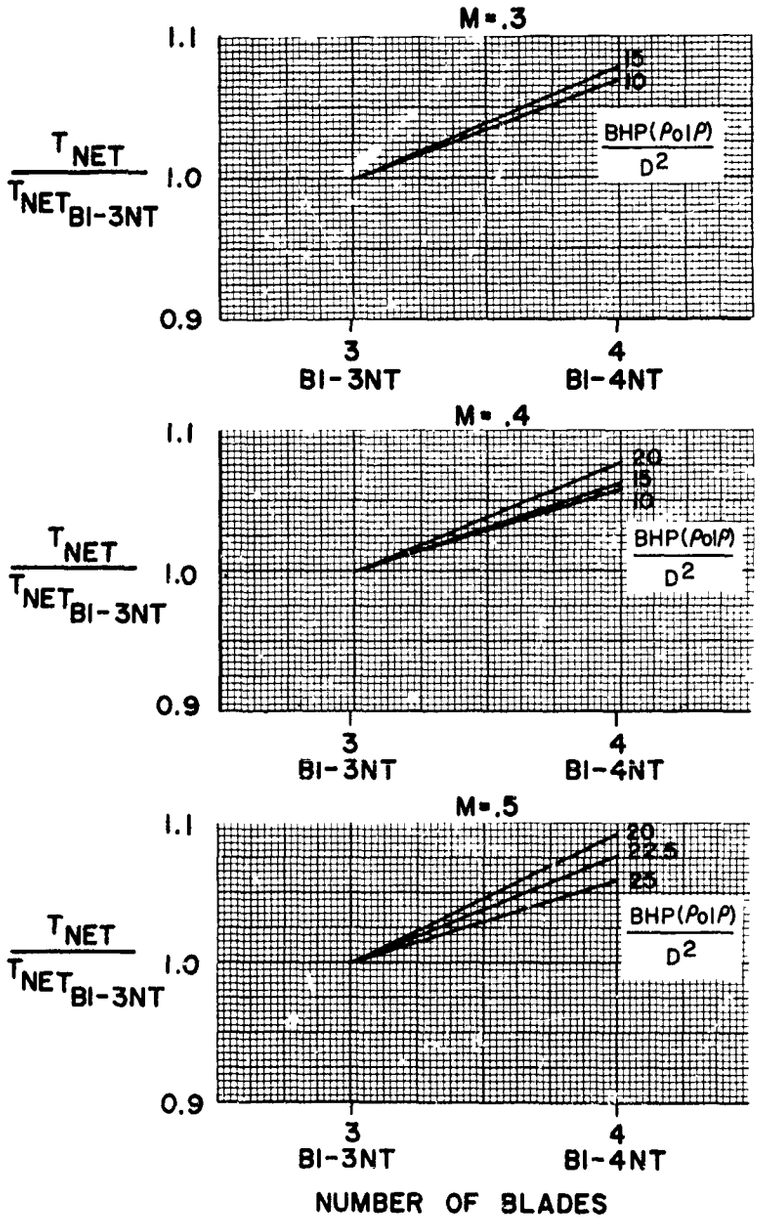

FIGURE 182

HS SHROUDED PROPELLER TEST

PERFORMANCE COMPARISON WITH CONFIGURATION BI-3NT
EFFECT OF NUMBER OF BLADES
TIP SPEED = 980 FPS

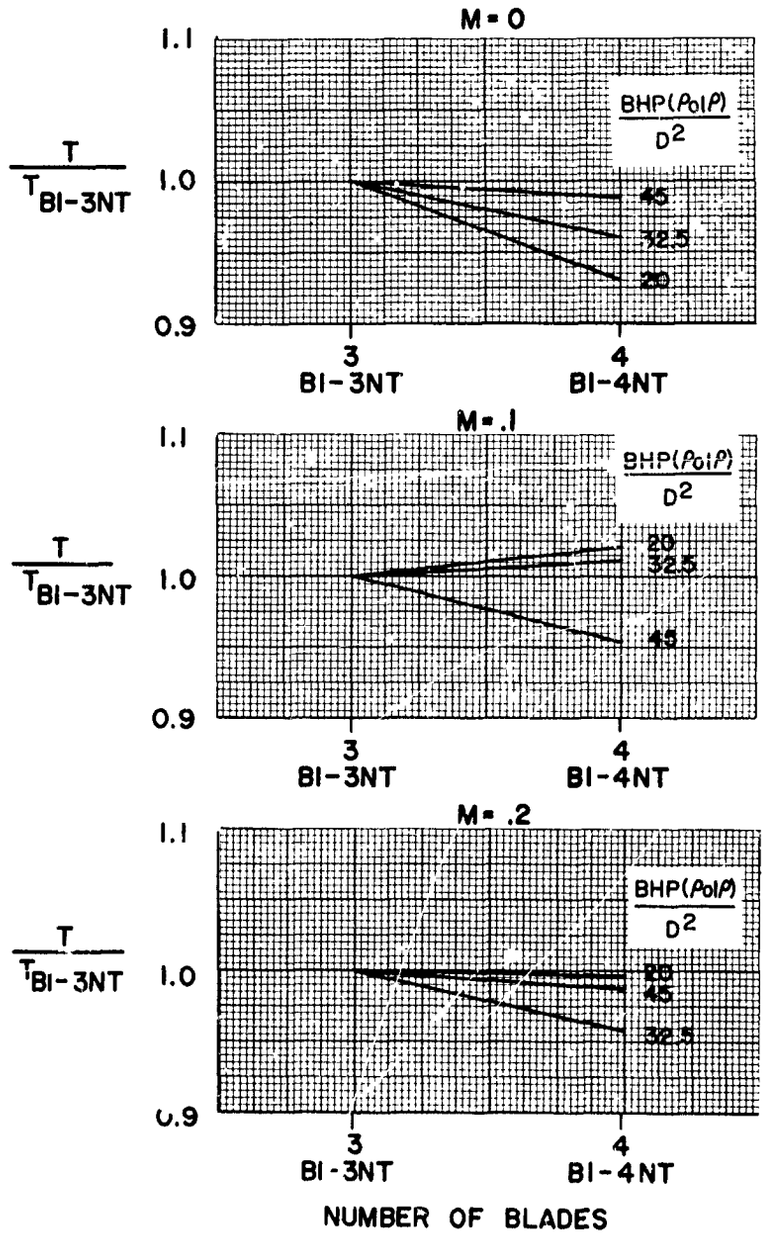

FIGURE 183

HS SHROUDED PROPELLER TEST

PERFORMANCE COMPARISON WITH CONFIGURATION BI-3NT
EFFECT OF NUMBER OF BLADES
TIP SPEED = 915 FPS

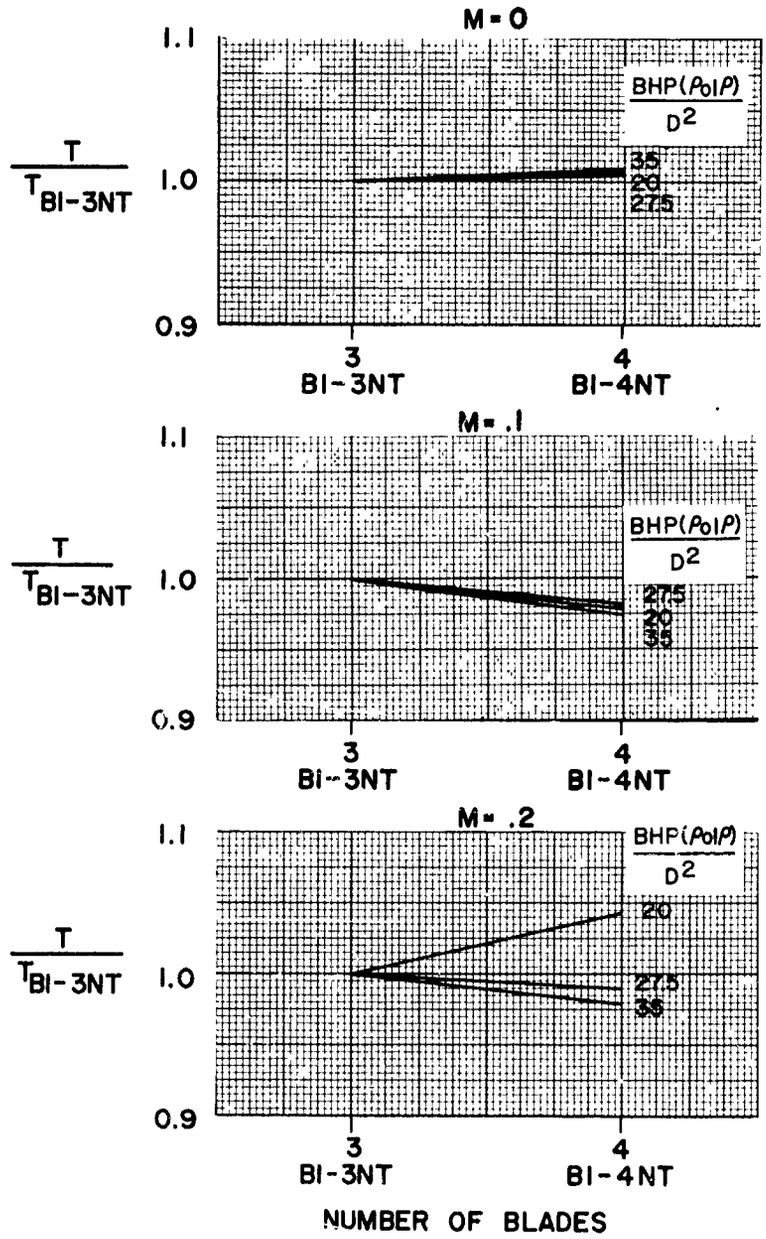

FIGURE 184

HS SHROUDED PROPELLER TEST

PERFORMANCE COMPARISON WITH CONFIGURATION BI-3NT
EFFECT OF NUMBER OF BLADES
TIP SPEED = 785 FPS

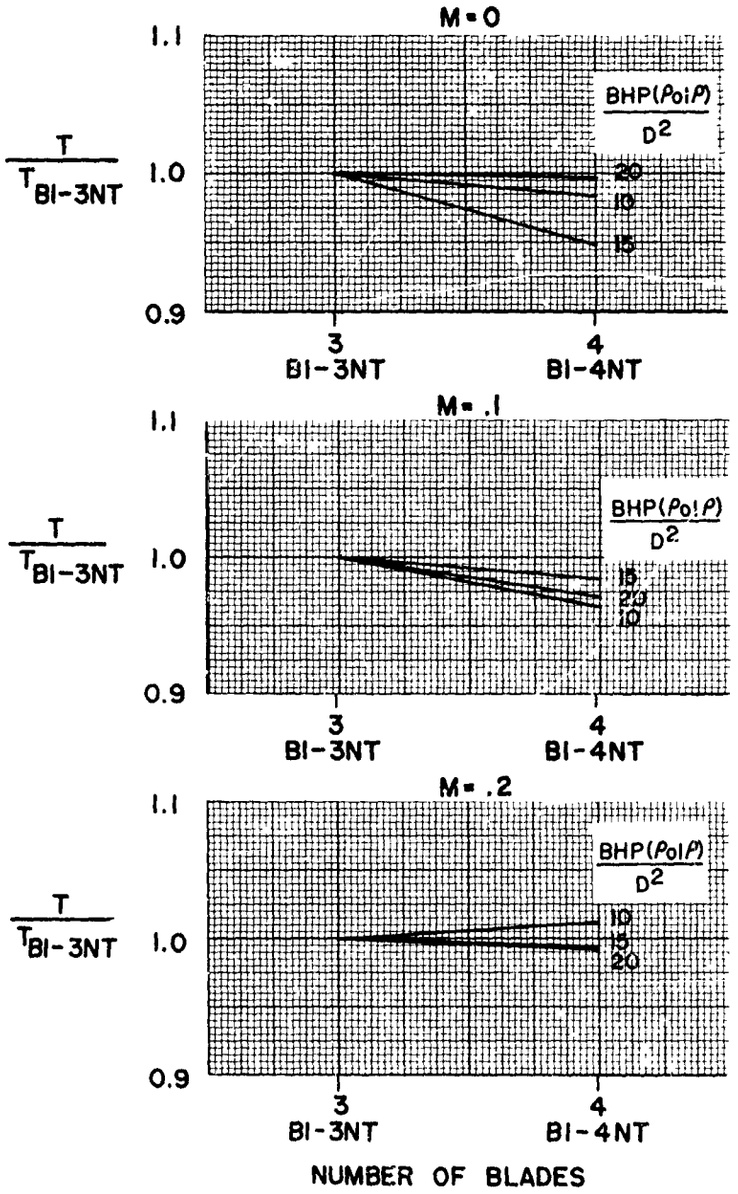

FIGURE 185

HS SHROUDED PROPELLER TEST

PERFORMANCE COMPARISON WITH CONFIGURATION BI-3NT
EFFECT OF NUMBER OF BLADES
TIP SPEED = 915 FPS

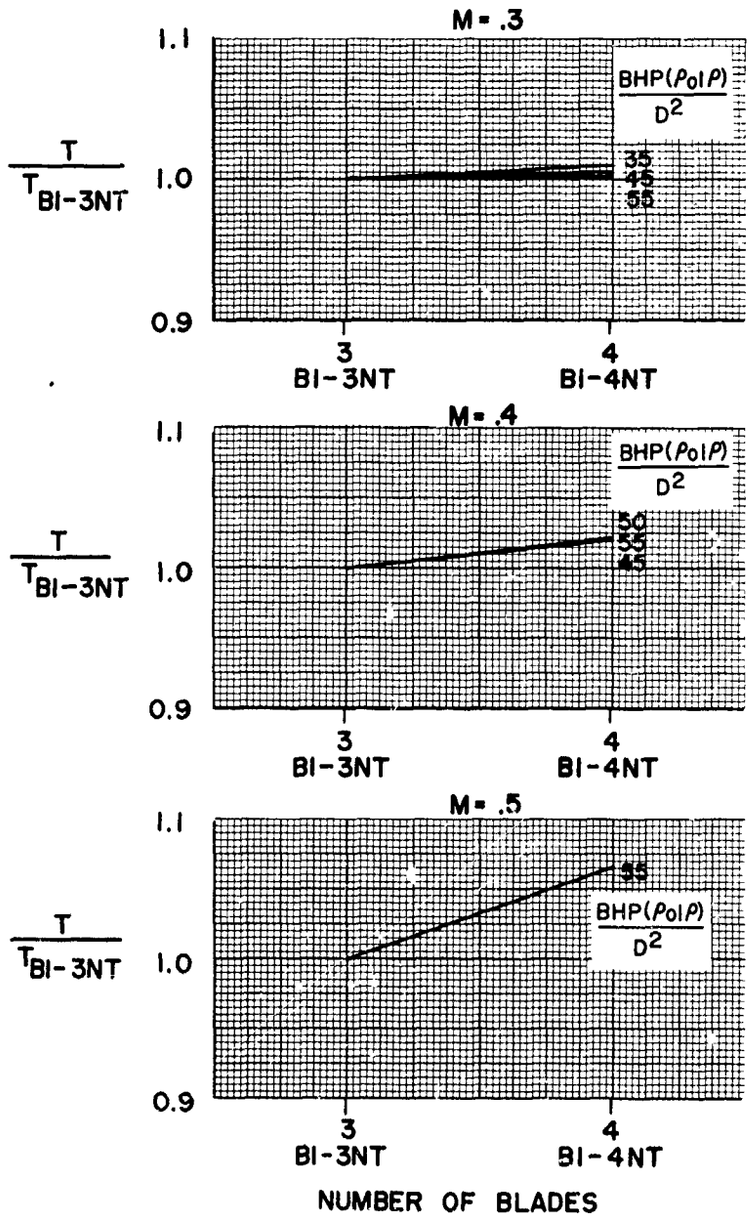

FIGURE 186

HS SHROUDED PROPELLER TEST

PERFORMANCE COMPARISON WITH CONFIGURATION BI-3NT
EFFECT OF NUMBER OF BLADES
TIP SPEED = 785 FPS

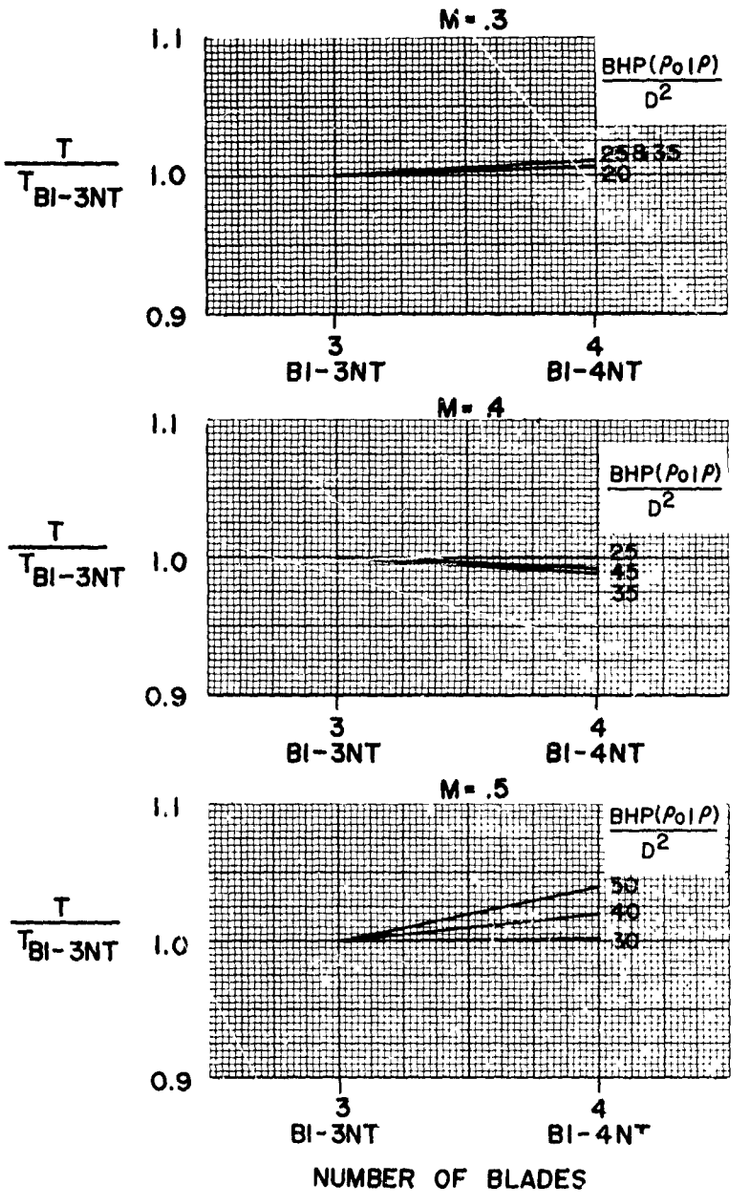

FIGURE 187

HS SHROUDED PROPELLER TEST

PERFORMANCE COMPARISON WITH CONFIGURATION BI-3NT
EFFECT OF NUMBER OF BLADES
TIP SPEED = 654 FPS

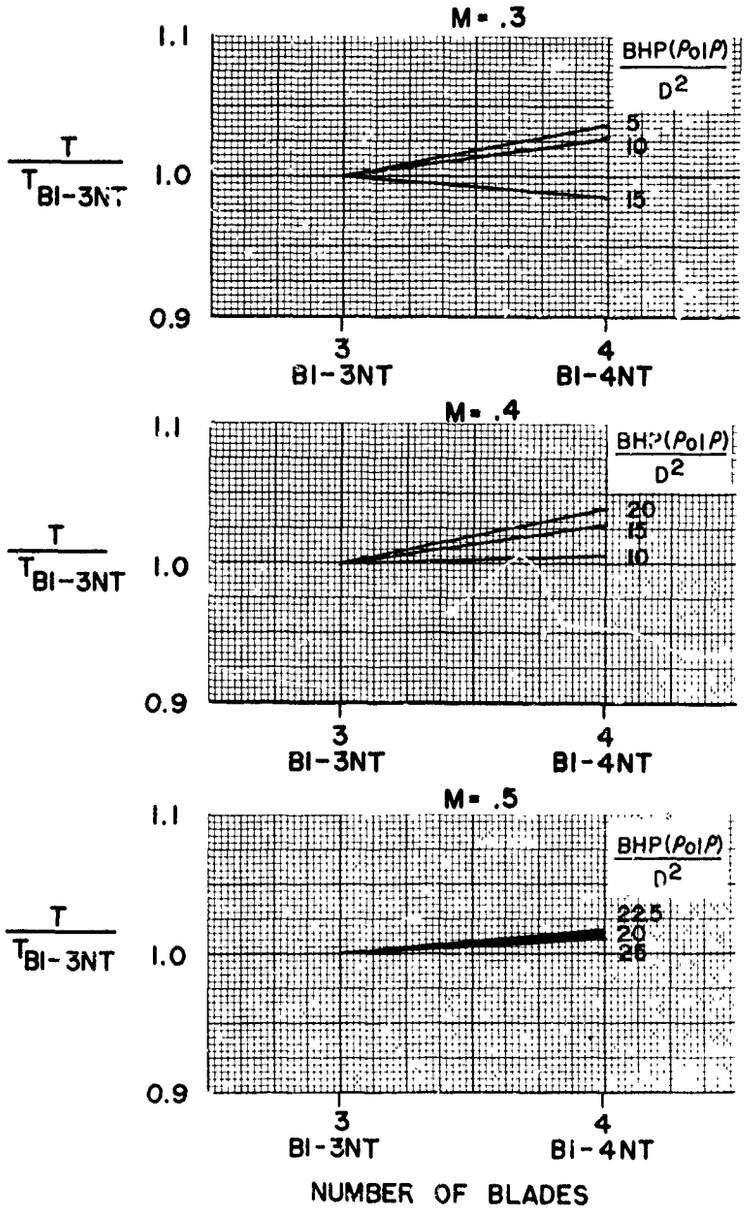

FIGURE 188

HS SHROUDED PROPELLER TEST

PERFORMANCE COMPARISON WITH CONFIGURATION, BI-3R
EFFECT OF TIP CLEARANCE
TIP SPEED = 980 FPS

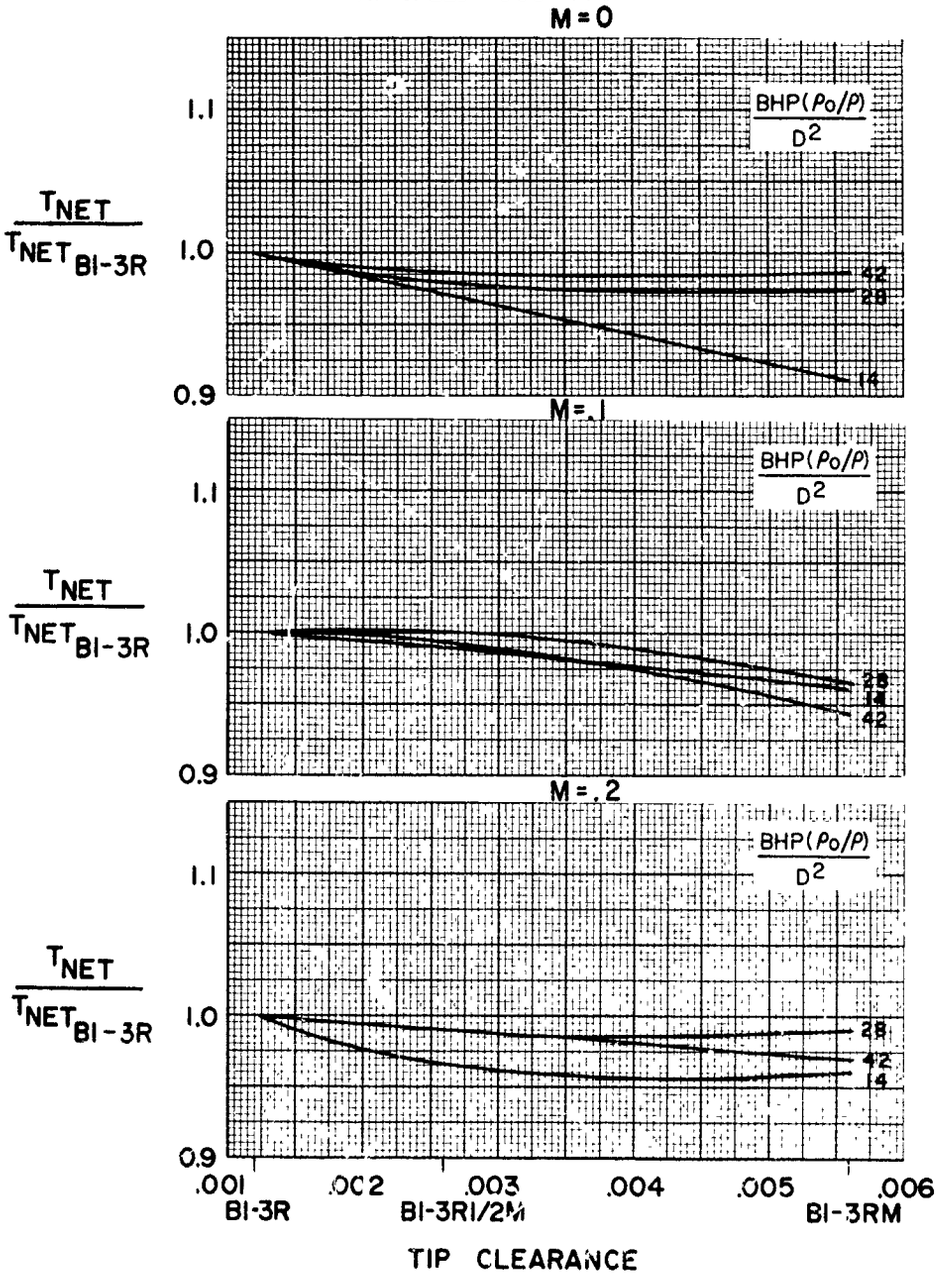

FIGURE 189

HS SHROUDED PROPELLER TEST

PERFORMANCE COMPARISON WITH CONFIGURATION, BI-3R
EFFECT OF TIP CLEARANCE
TIP SPEED = 915 FPS

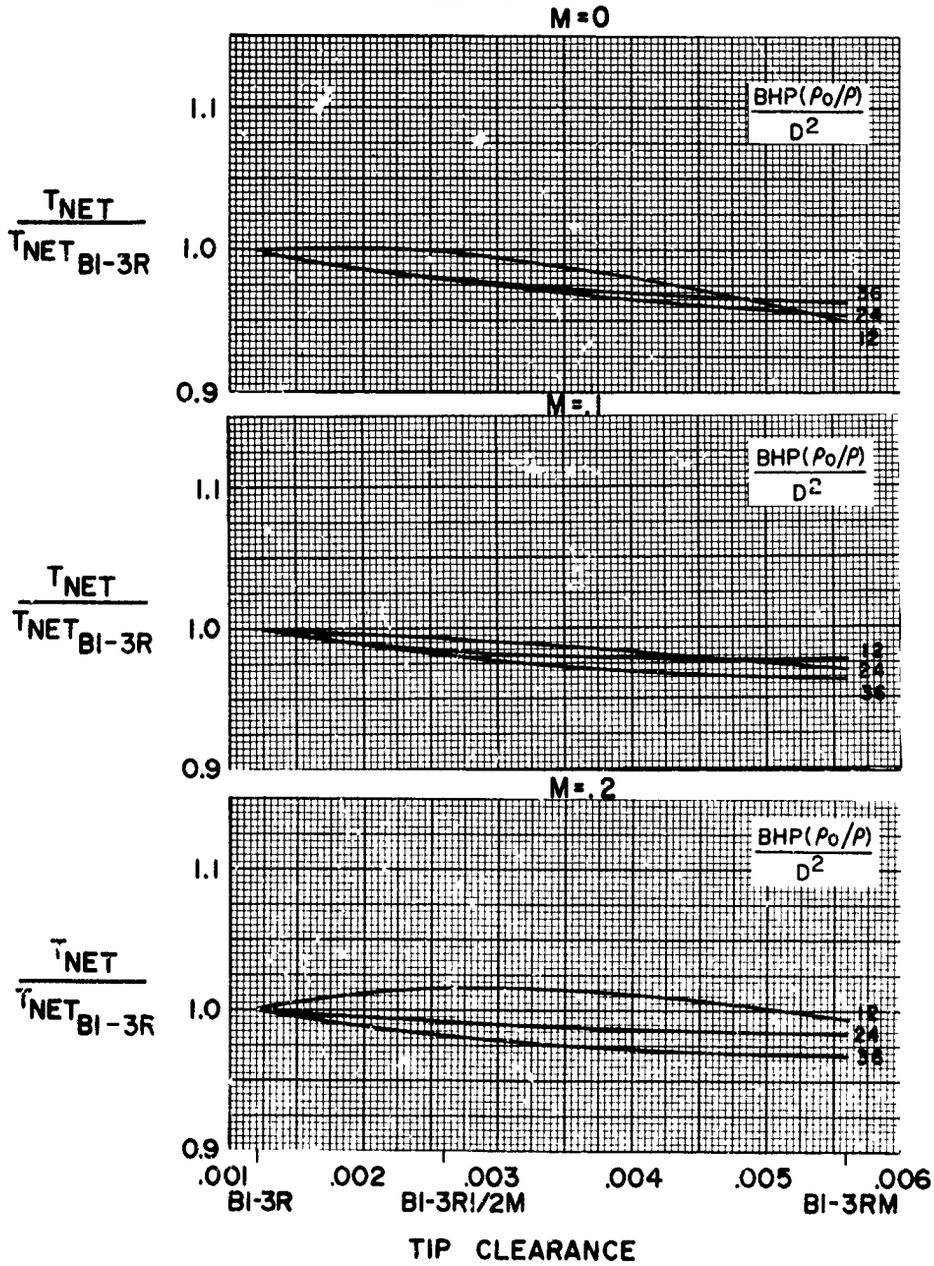

FIGURE 190

HS SHROUDED PROPELLER TEST

PERFORMANCE COMPARISON WITH CONFIGURATION, BI-3R
EFFECT OF TIP CLEARANCE
TIP SPEED = 785 FPS

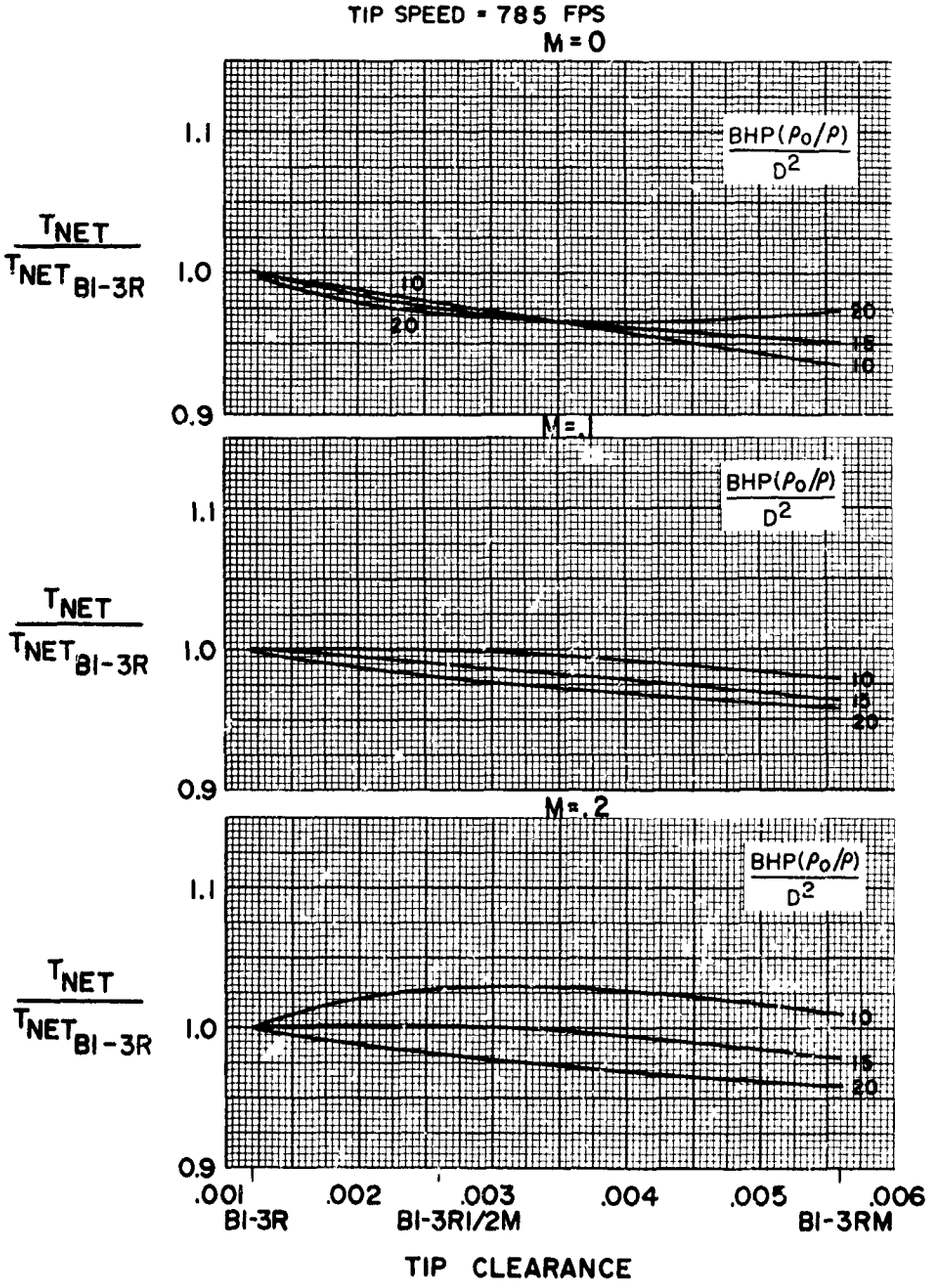

FIGURE 191

HS SHROUDED PROPELLER TEST

PERFORMANCE COMPARISON WITH CONFIGURATION, BI-3R
EFFECT OF TIP CLEARANCE
TIP SPEED = 915 FPS

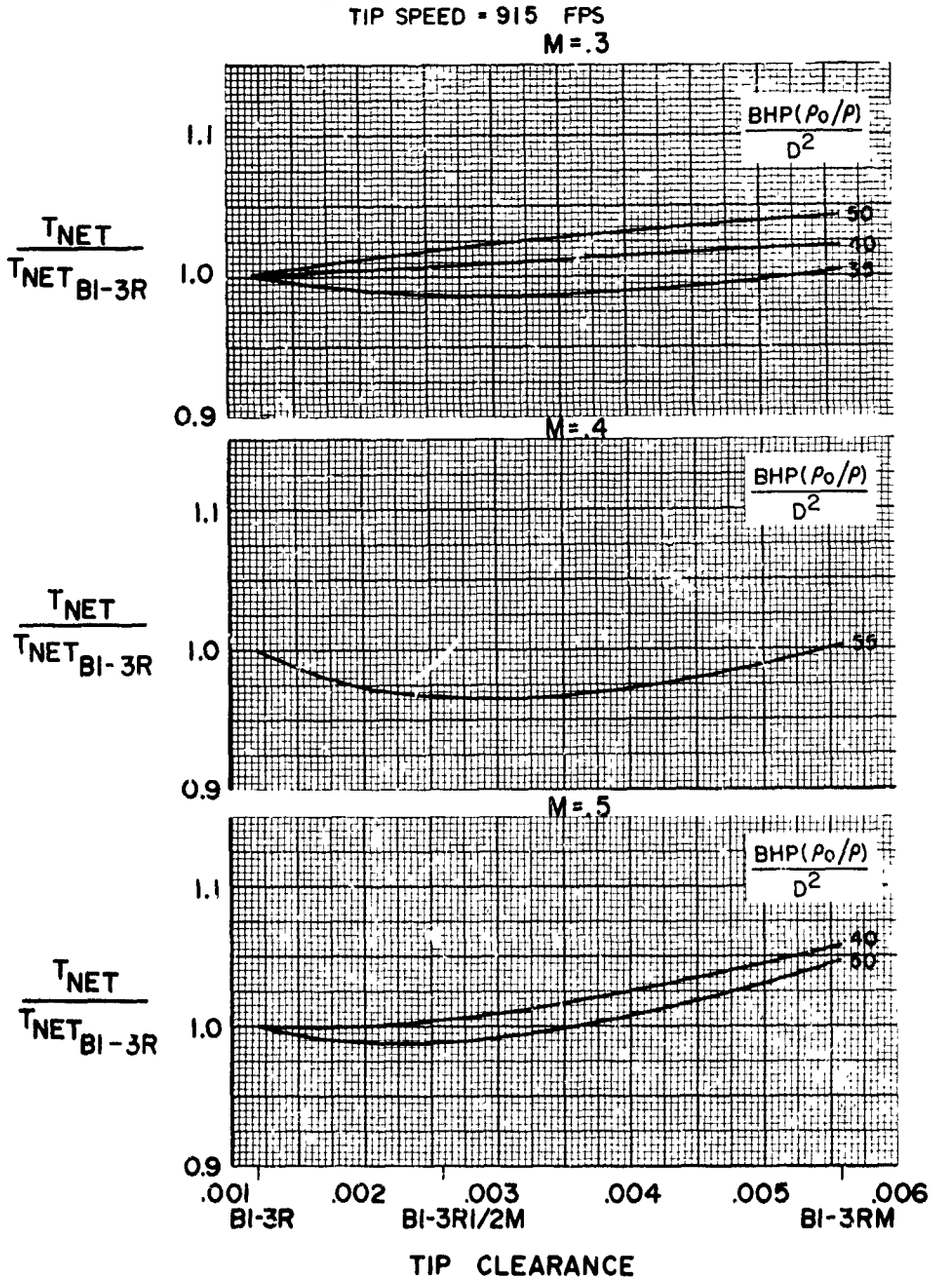

FIGURE 192

HS SHROUDED PROPELLER TEST

PERFORMANCE COMPARISON WITH CONFIGURATION, BI-3R
EFFECT OF TIP CLEARANCE
TIP SPEED = 785 FPS

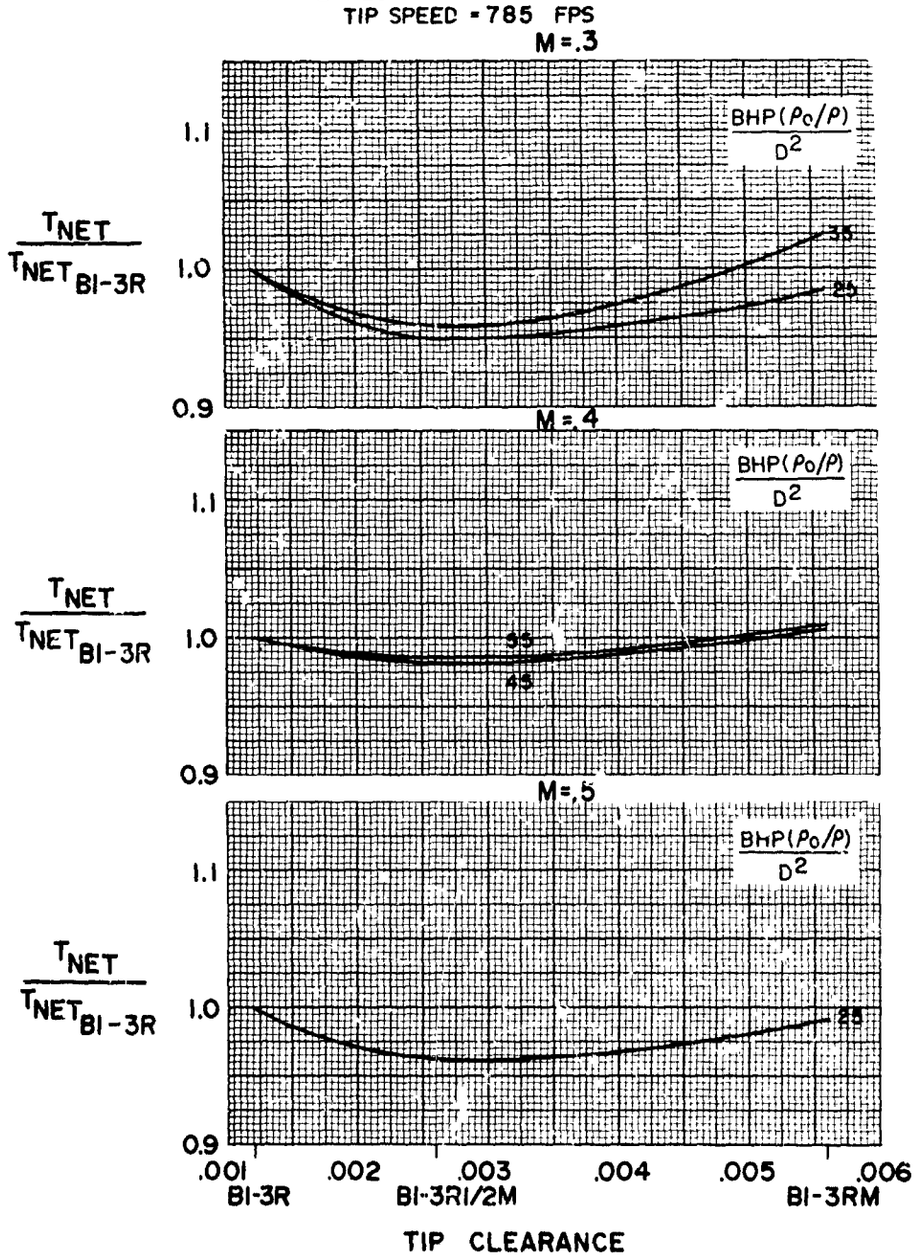

FIGURE 193

HS SHROUDED PROPELLER TEST

PERFORMANCE COMPARISON WITH CONFIGURATION, BI-3R
EFFECT OF TIP CLEARANCE
TIP SPEED = 654 FPS

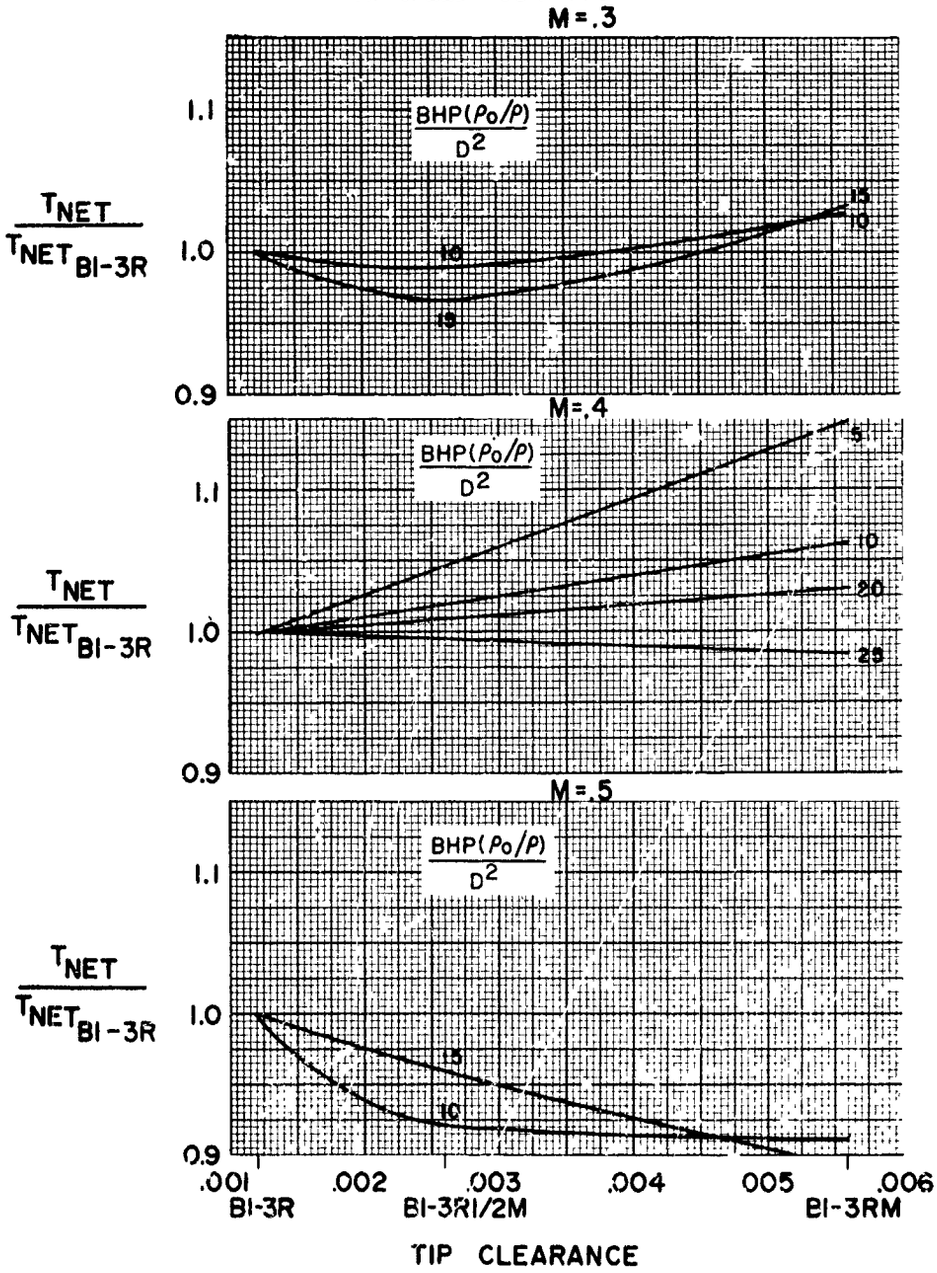

FIGURE 194

HS SHROUDED PROPELLER TEST

PERFORMANCE COMPARISON WITH CONFIGURATION, BI - 3R
EFFECT OF TIP CLEARANCE
TIP SPEED = 980 FPS

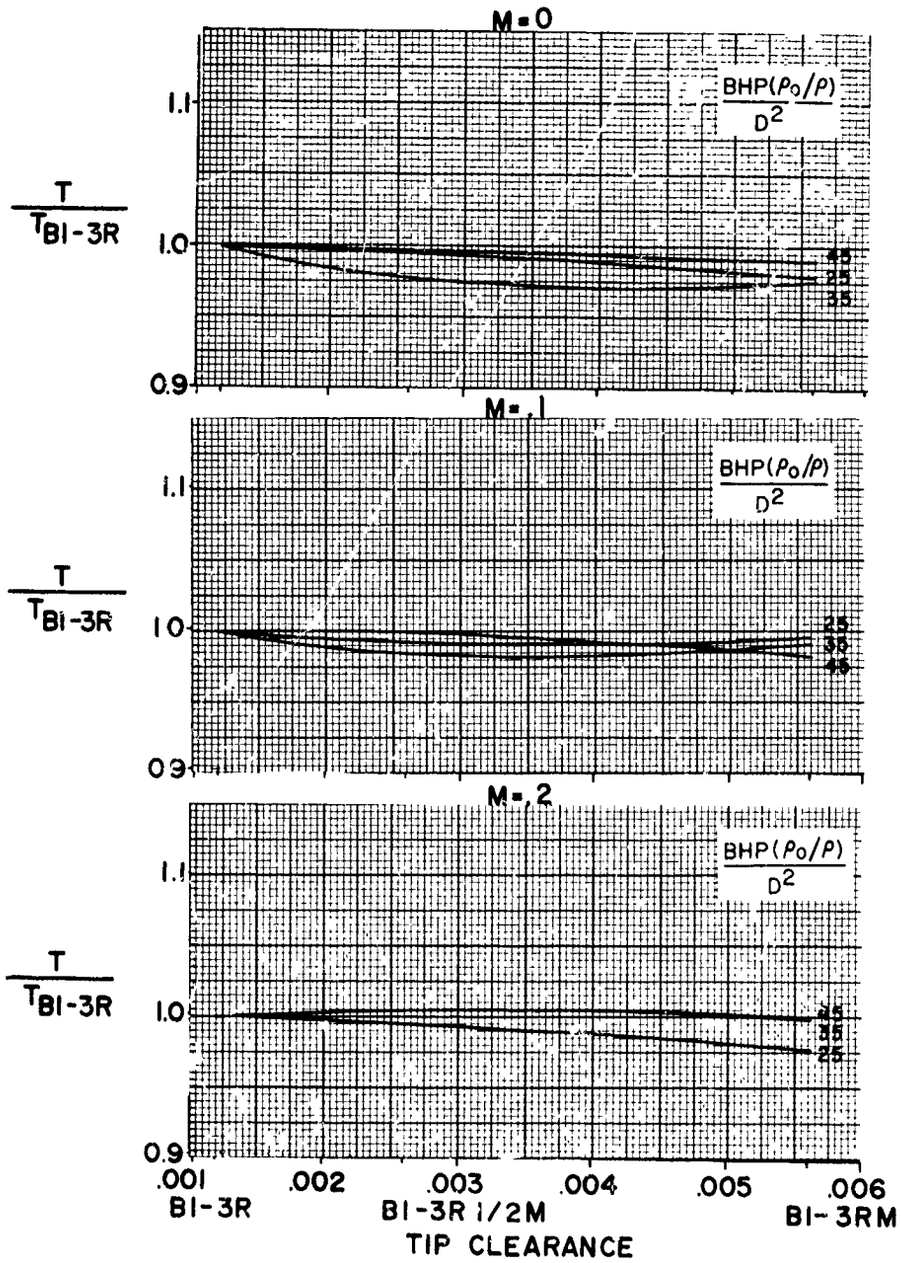

FIGURE 195

HS SHROUDED PROPELLER TEST

PERFORMANCE COMPARISON WITH CONFIGURATION, BI-3R
EFFECT OF TIP CLEARANCE
TIP SPEED = 915 FPS

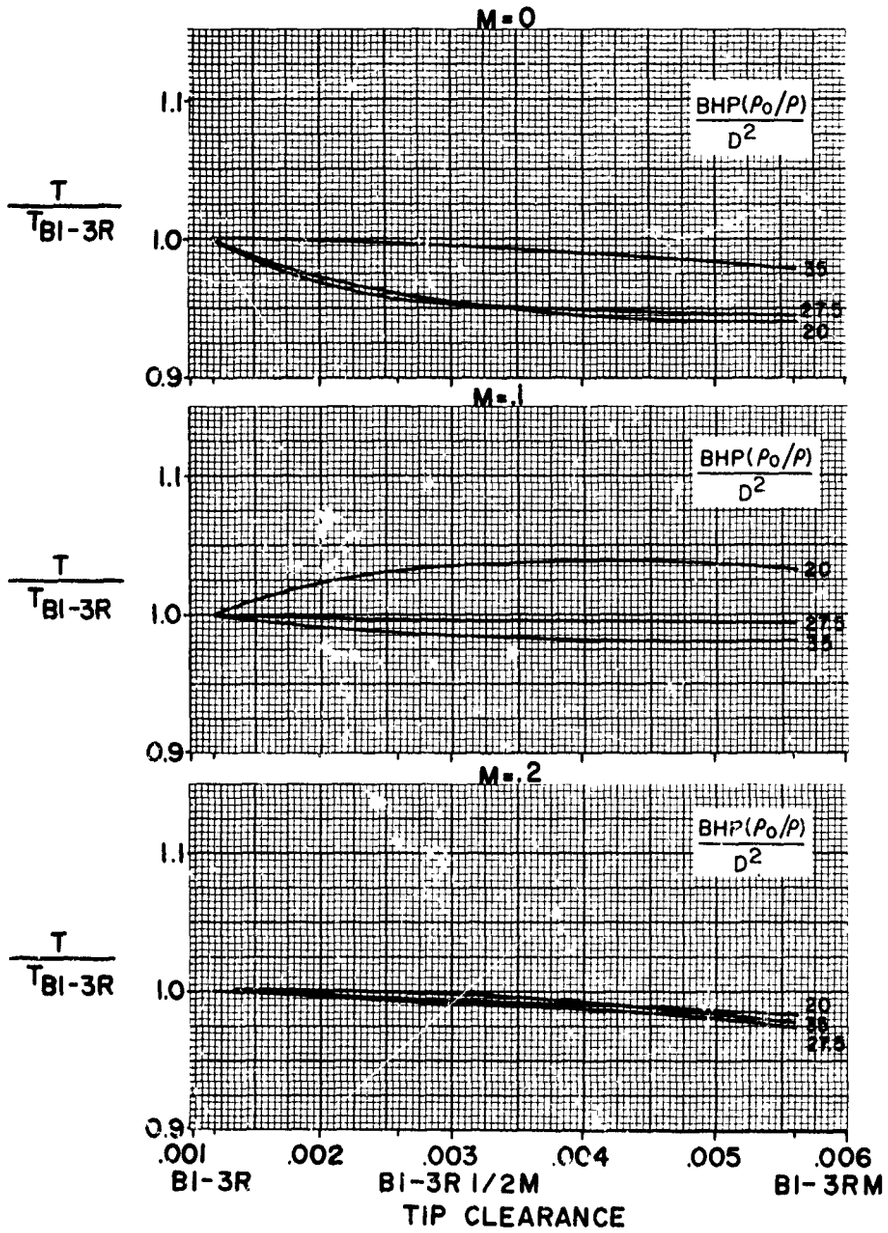

FIGURE 196

HS SHROUDED PROPELLER TEST

PERFORMANCE COMPARISON WITH CONFIGURATION, BI-3R
EFFECT OF TIP CLEARANCE
TIP SPEED = 785 FPS

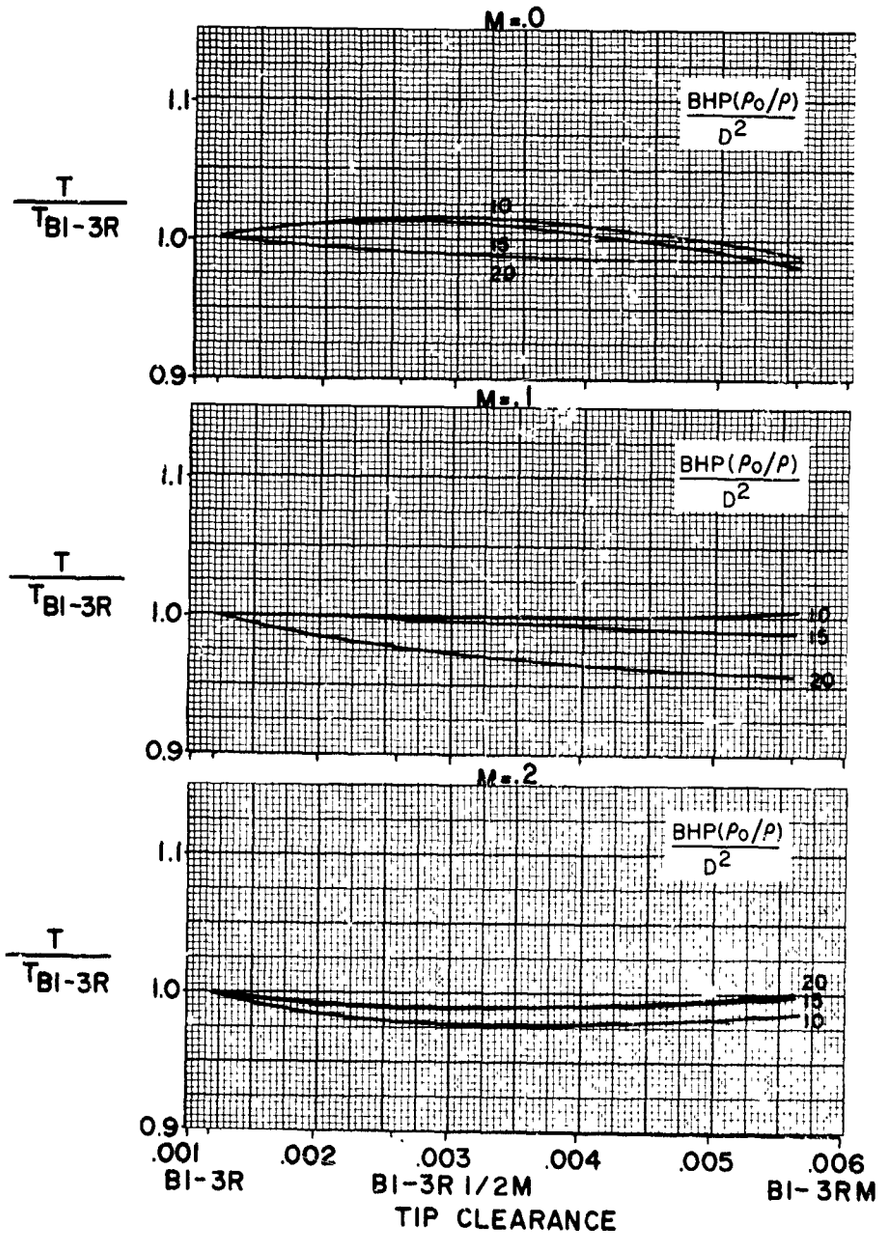

FIGURE 197

HS SHROUDED PROPELLER TEST

PERFORMANCE COMPARISON WITH CONFIGURATION, BI-3R
EFFECT OF TIP CLEARANCE
TIP SPEED = 915 FPS

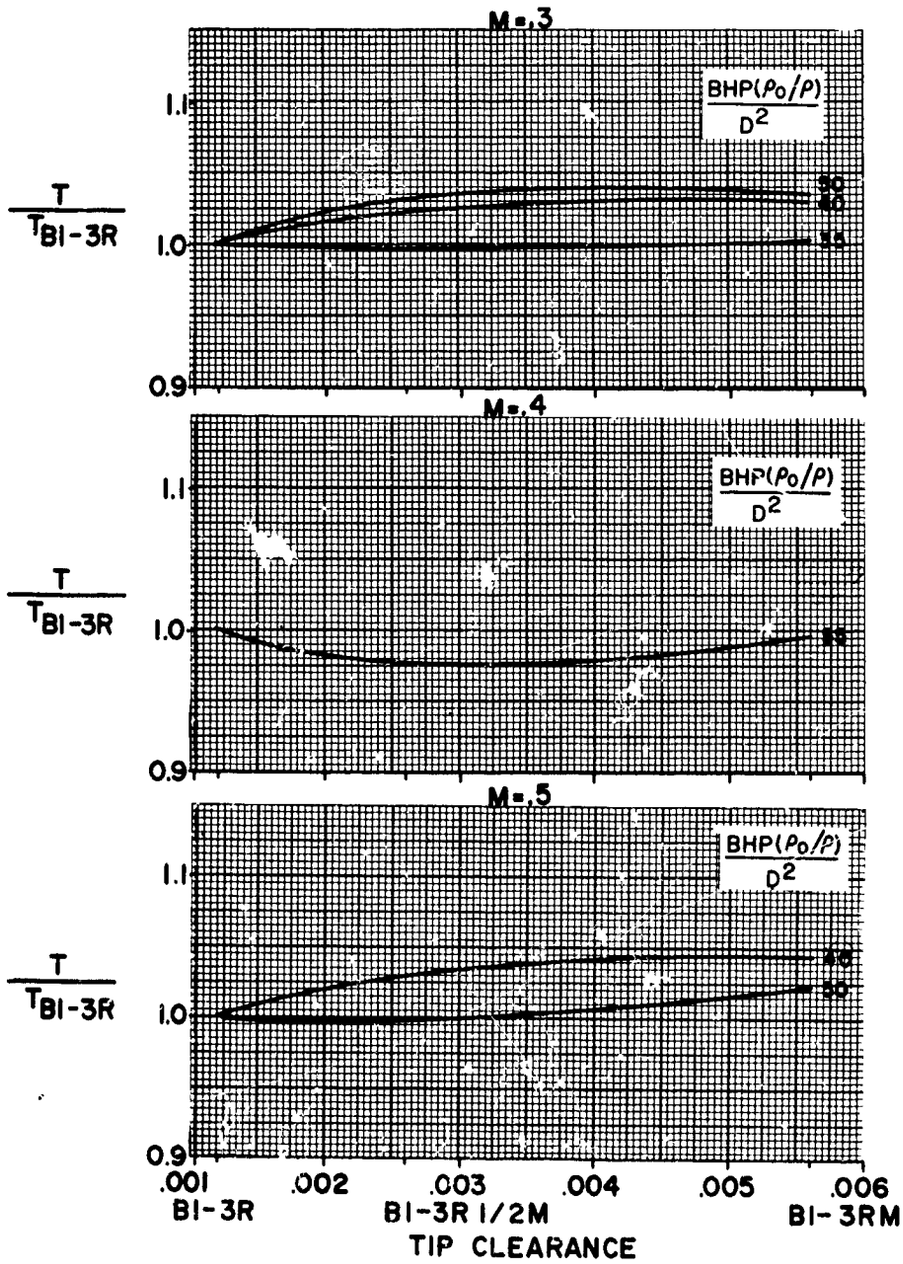

FIGURE 198

HS SHROUDED PROPELLER TEST

PERFORMANCE COMPARISON WITH CONFIGURATION, BI-3R
EFFECT OF TIP CLEARANCE
TIP SPEED = 735 FPS

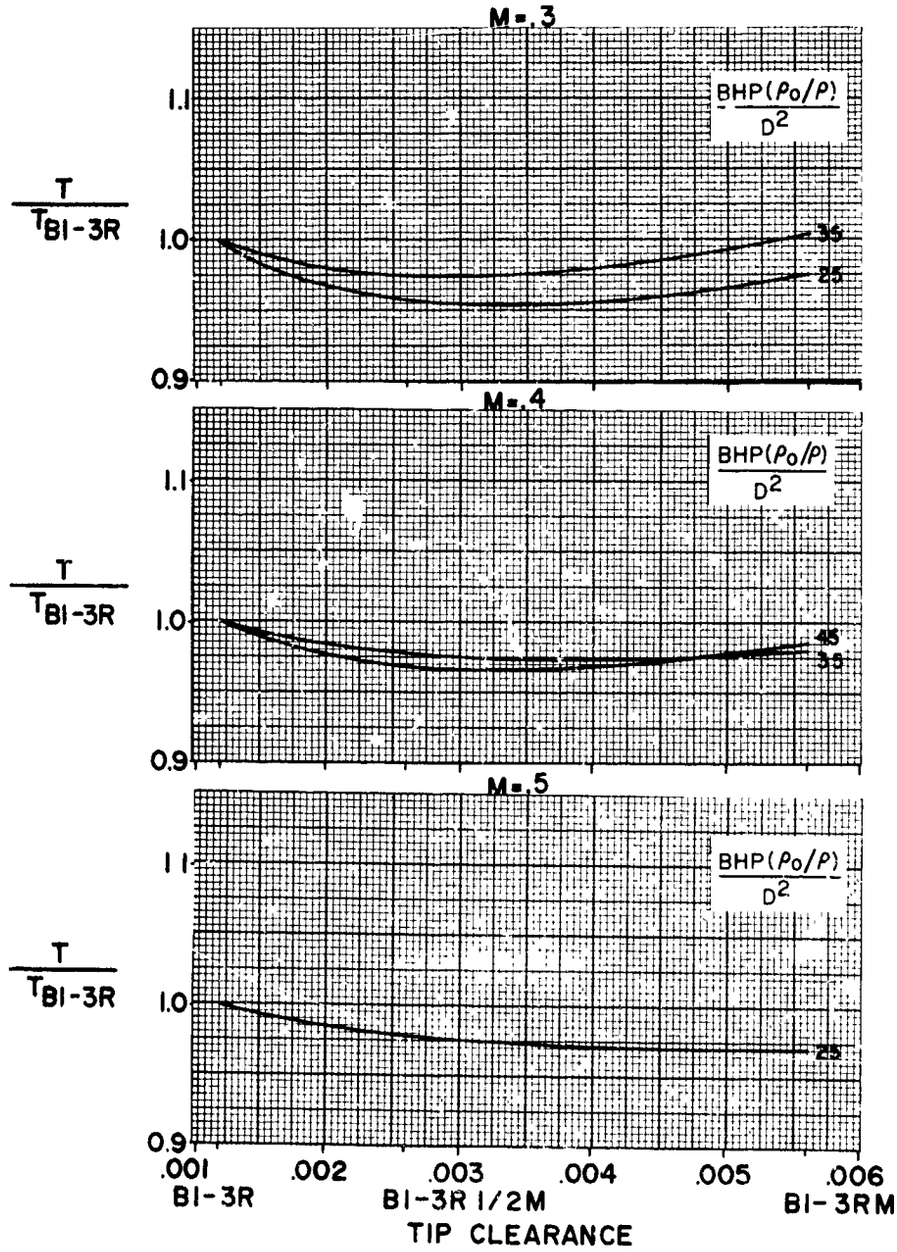

FIGURE 199

HS SHROUDED PROPELLER TEST

PERFORMANCE COMPARISON WITH CONFIGURATION, BI – 3R
EFFECT OF TIP CLEARANCE
TIP SPEED = 654 FPS

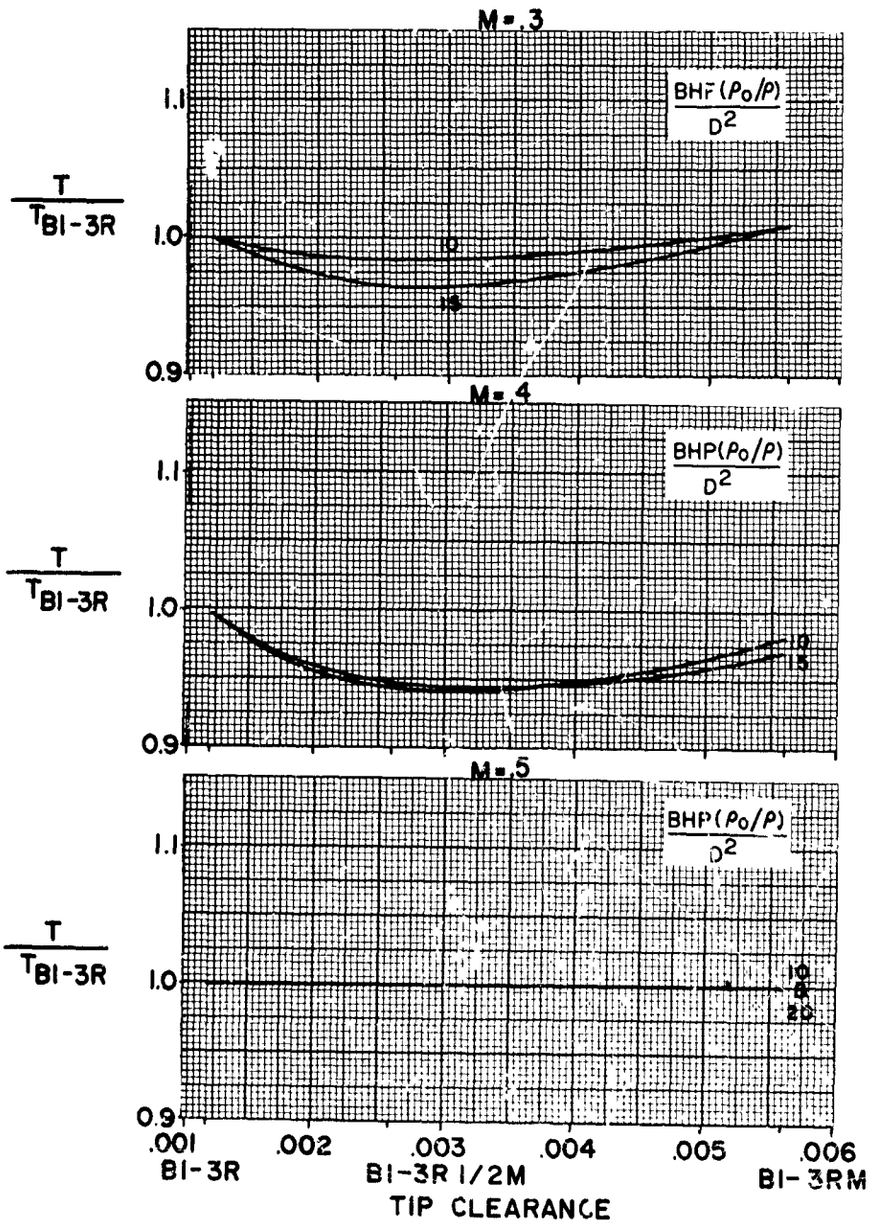

FIGURE 200

HS SHROUDED PROPELLER TEST

PERFORMANCE COMPARISON OF UNSHROUDED PROPELLER, 3WT, WITH BASIC CONFIGURATION BI-3WT

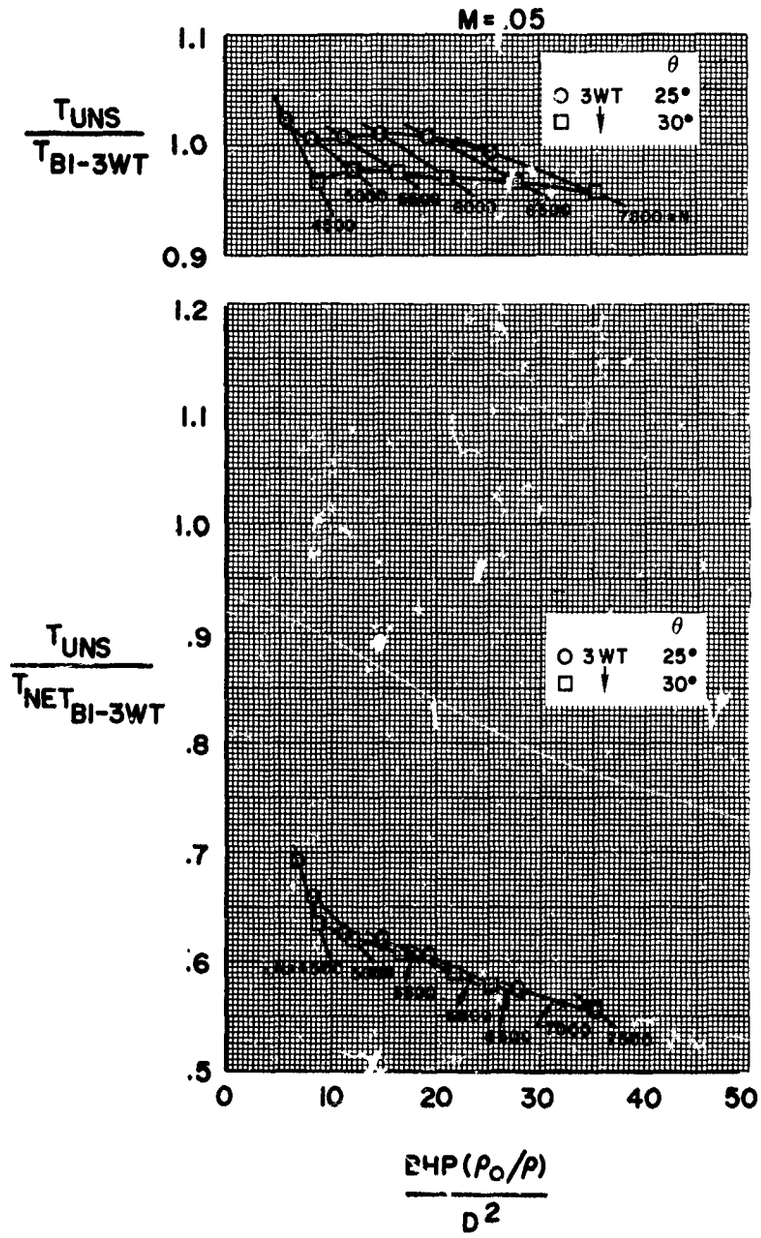

FIGURE 291

HS SHROUDED PROPELLER TEST

PERFORMANCE COMPARISON OF UNSHROUDED PROPELLER, 3WT, WITH BASIC CONFIGURATION BI-3WT

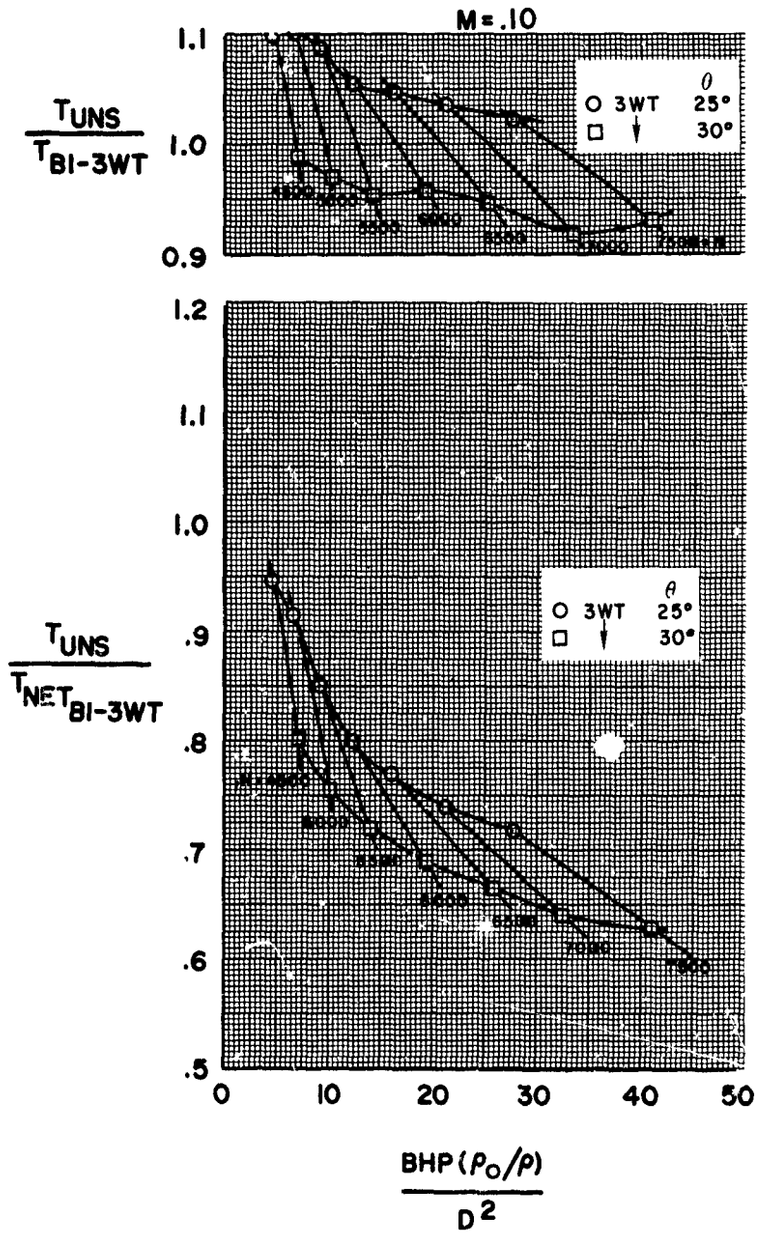

FIGURE 202

HS SHROUDED PROPELLER TEST

PERFORMANCE COMPARISON OF UNSHROUDED PROPELLER, 3WT, WITH BASIC CONFIGURATION BI-3WT

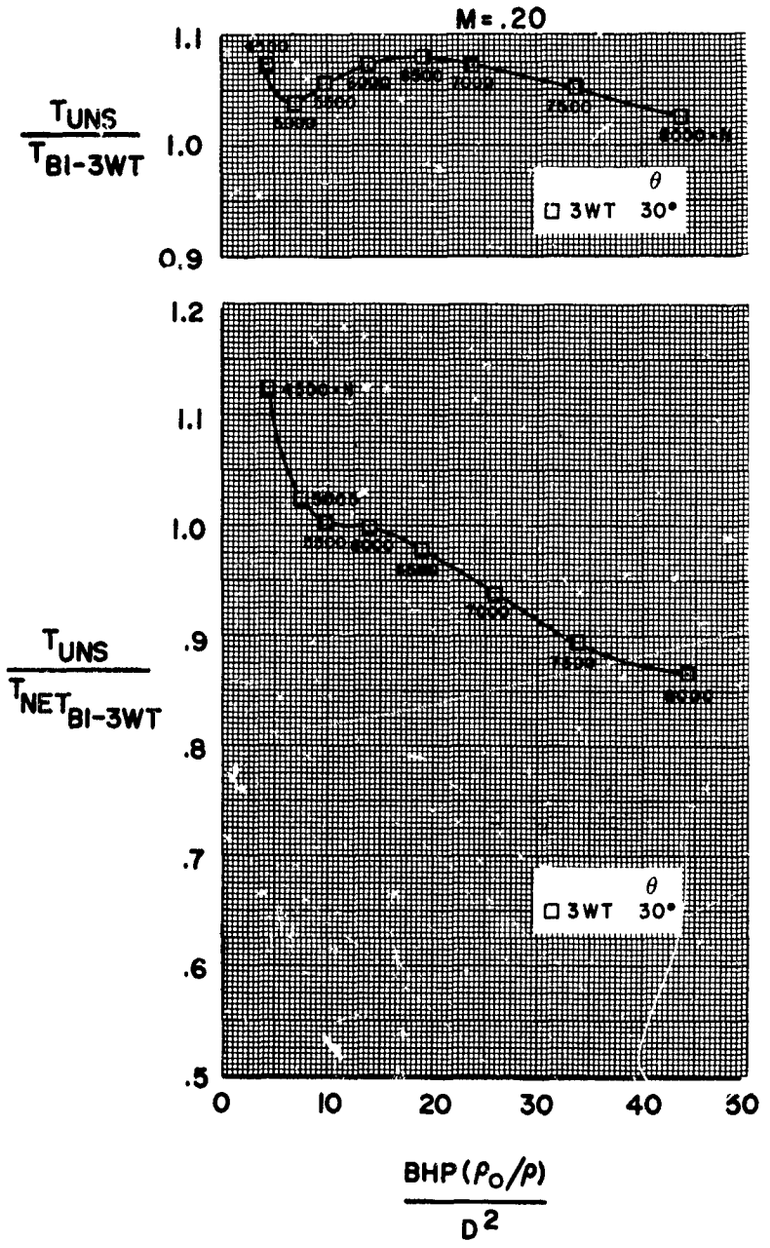

FIGURE 203

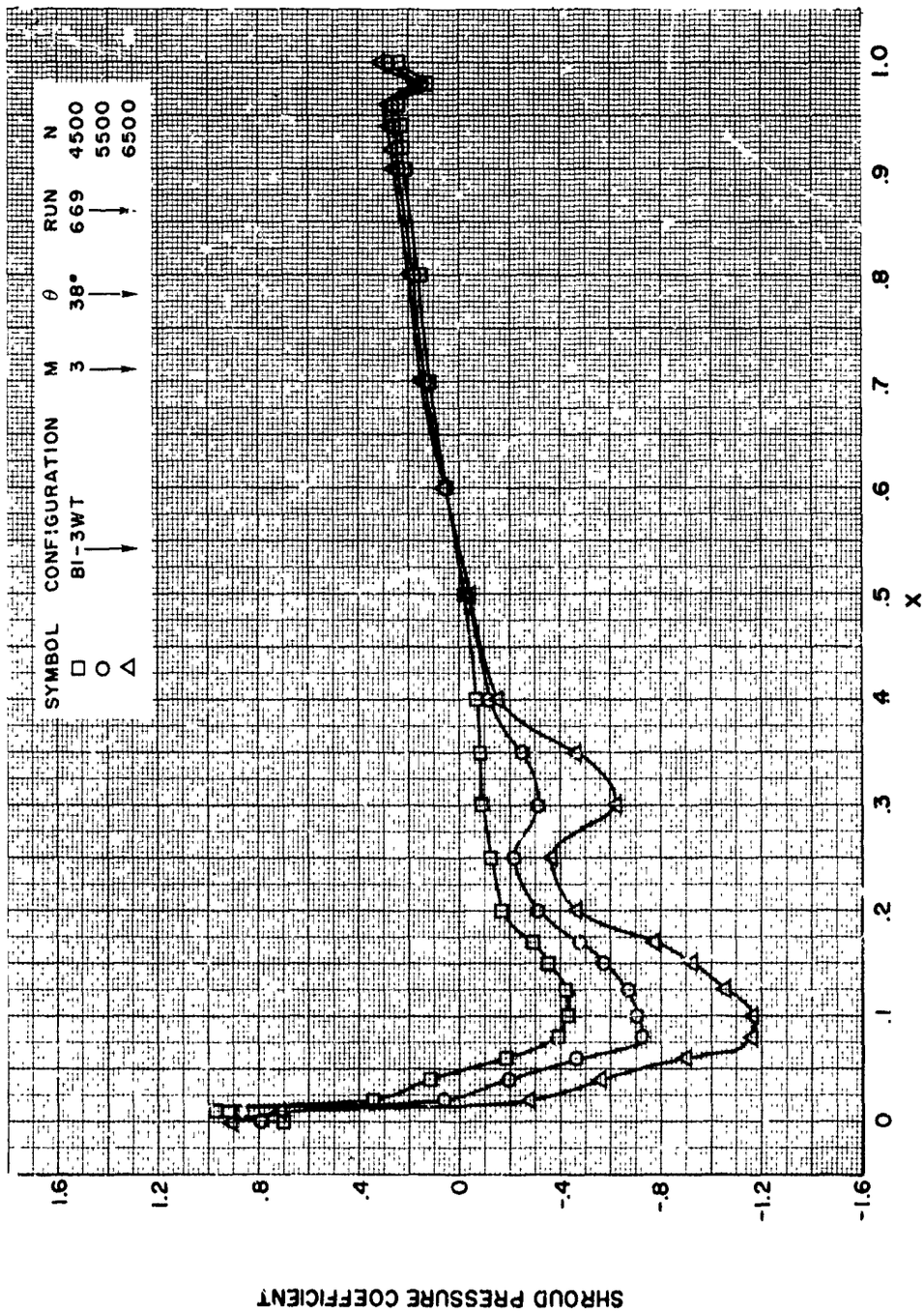

HS SHROUDED PROPELLER TEST
INSIDE SHROUD SURFACE PRESSURE DISTRIBUTION
EFFECT OF RPM

FIGURE 204

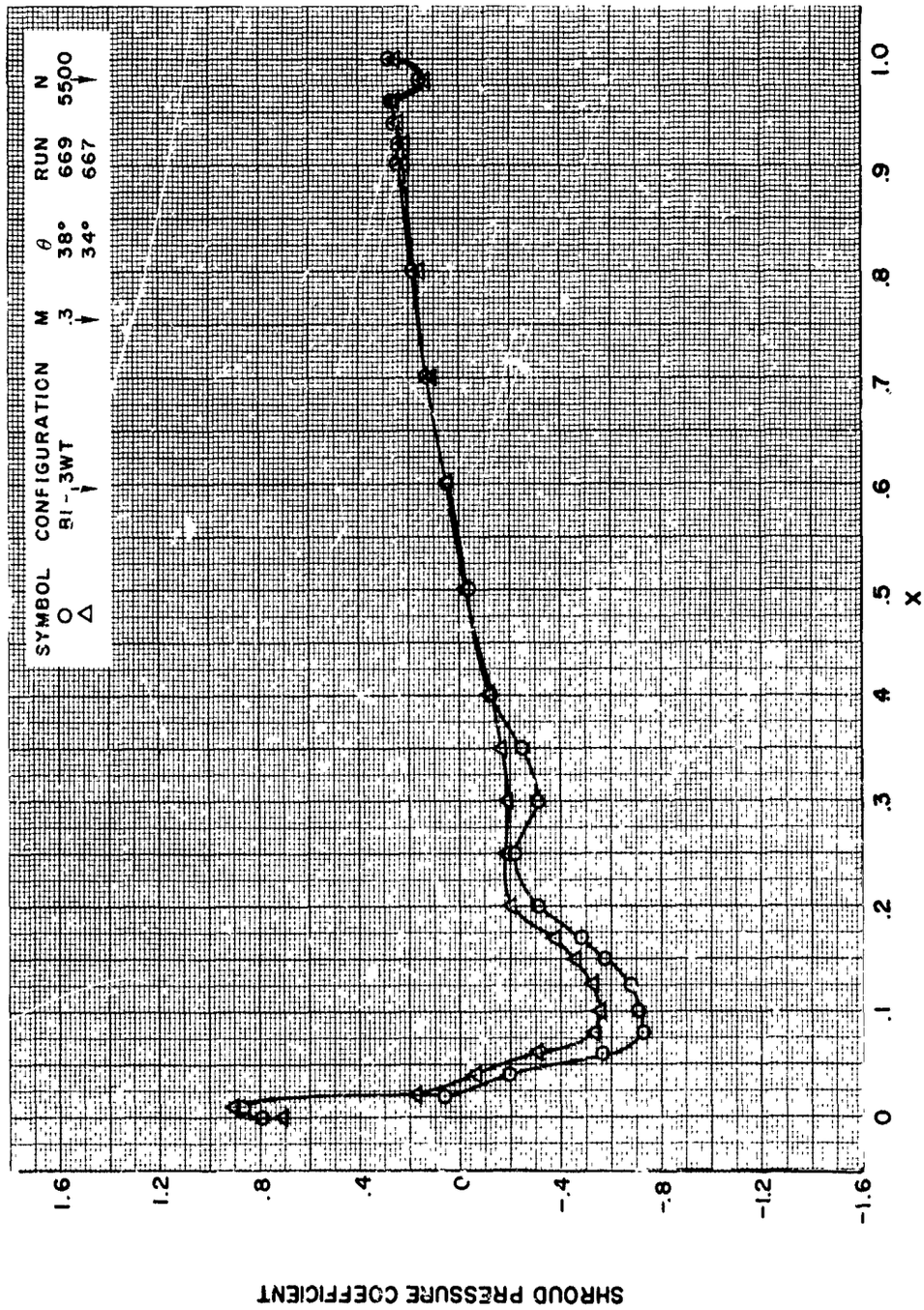

HS SHROUDED PROPELLER TEST
INSIDE SHROUD SURFACE PRESSURE DISTRIBUTION
EFFECT OF BLADE ANGLE

FIGURE 205

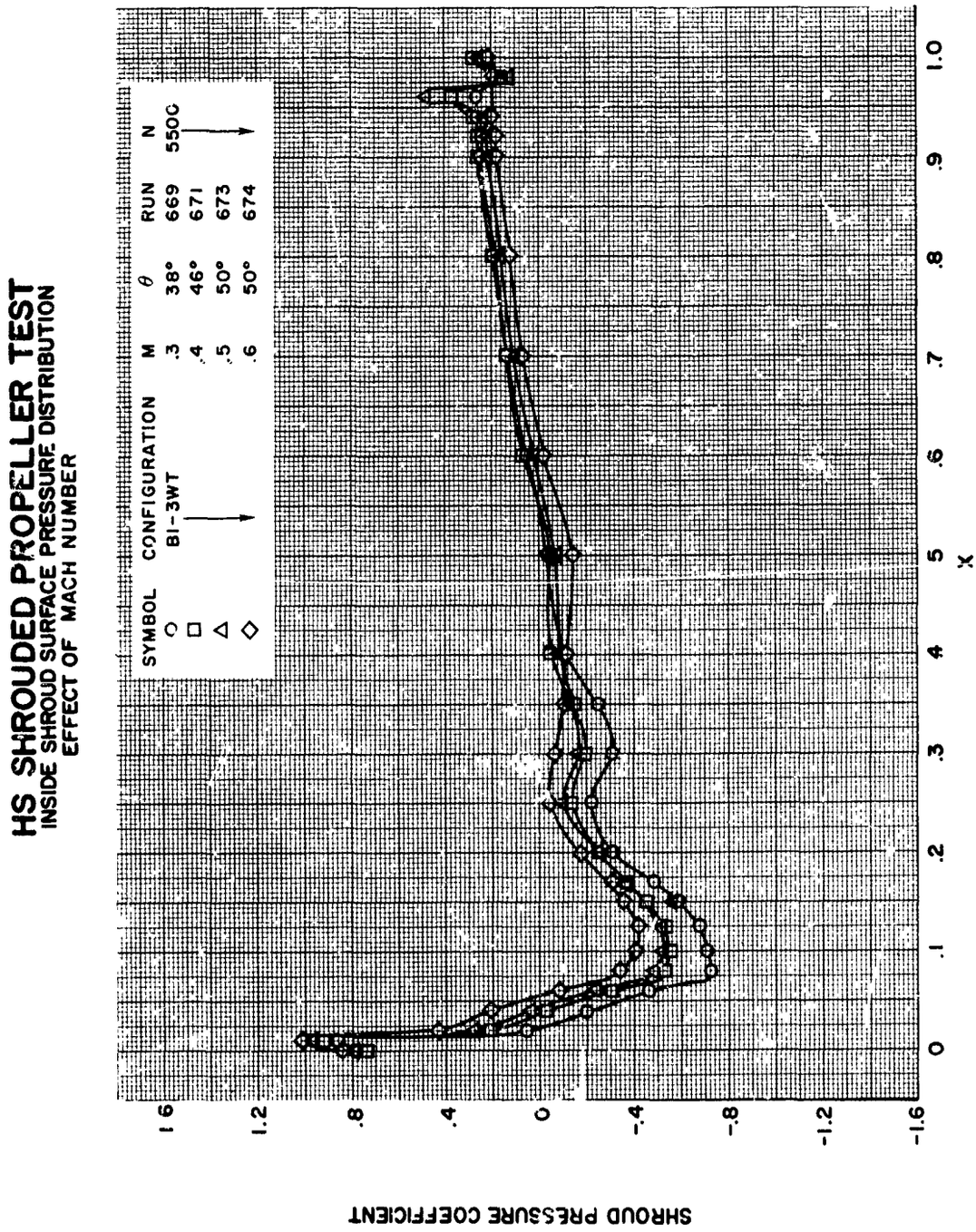
HS SHROUDED PROPELLER TEST
INSIDE SHROUD SURFACE PRESSURE DISTRIBUTION
EFFECT OF MACH NUMBER
SYMBOL CONFIGURATION M θ RUN N
○ BI-3WT .3 38° 669 550G
□ .4 46° 671
△ .5 50° 673
◇ .6 50° 674
SHROUD PRESSURE COEFFICIENT
1.6
1.2
.8
.4
0
-.4
-.8
-1.2
-1.6
0
.1
.2
.3
.4
.5
.6
.7
.8
.9
1.0
X

FIGURE 206

HS SHROUDED PROPELLER TEST
INSIDE SHROUD SURFACE PRESSURE DISTRIBUTION
EFFECT OF AREA RATIO

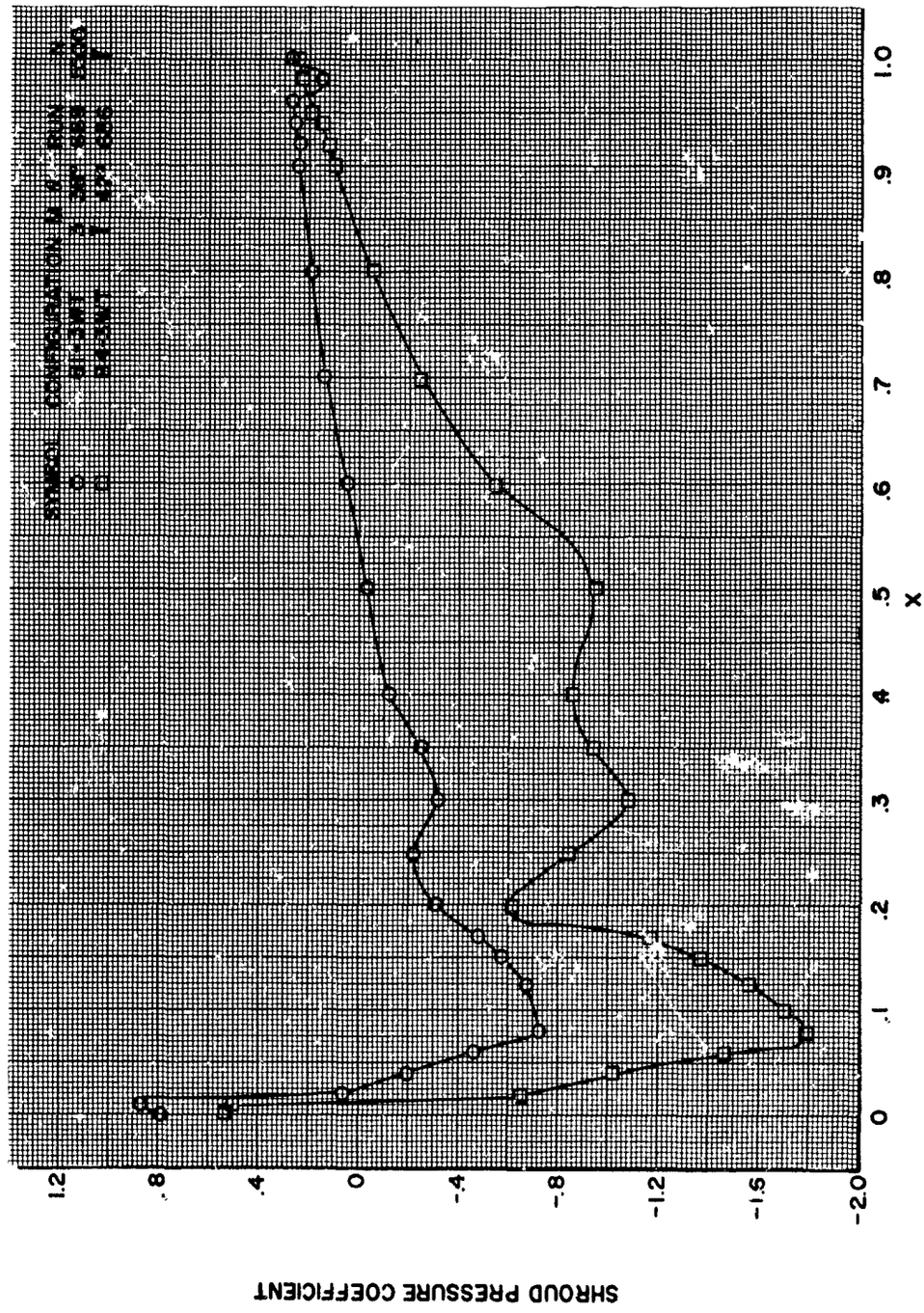

FIGURE 207

HS SHROUDED PROPELLER TEST
INSIDE SHROUD SURFACE PRESSURE DISTRIBUTION
EFFECT OF SHROUD LENGTH

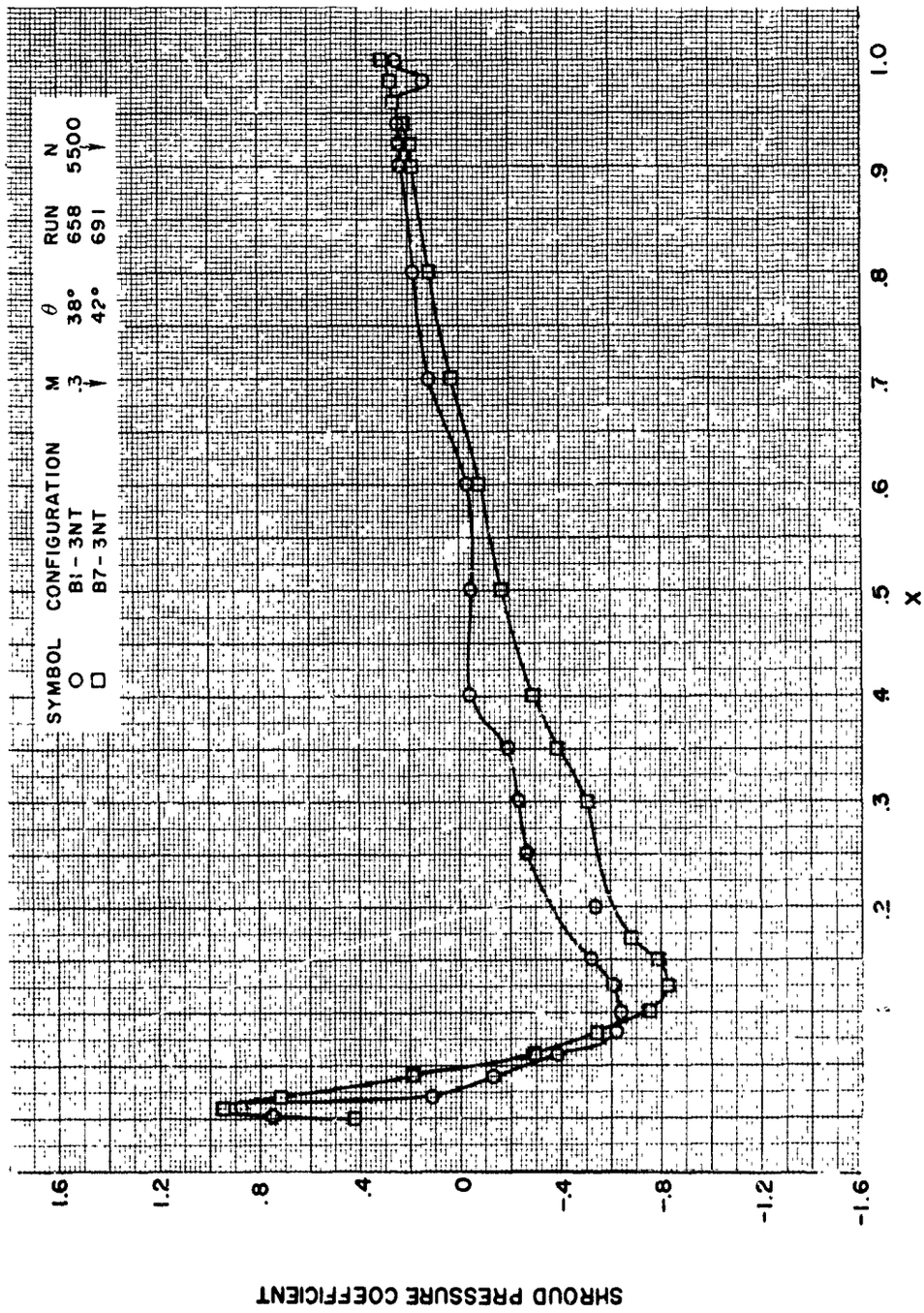

FIGURE 208

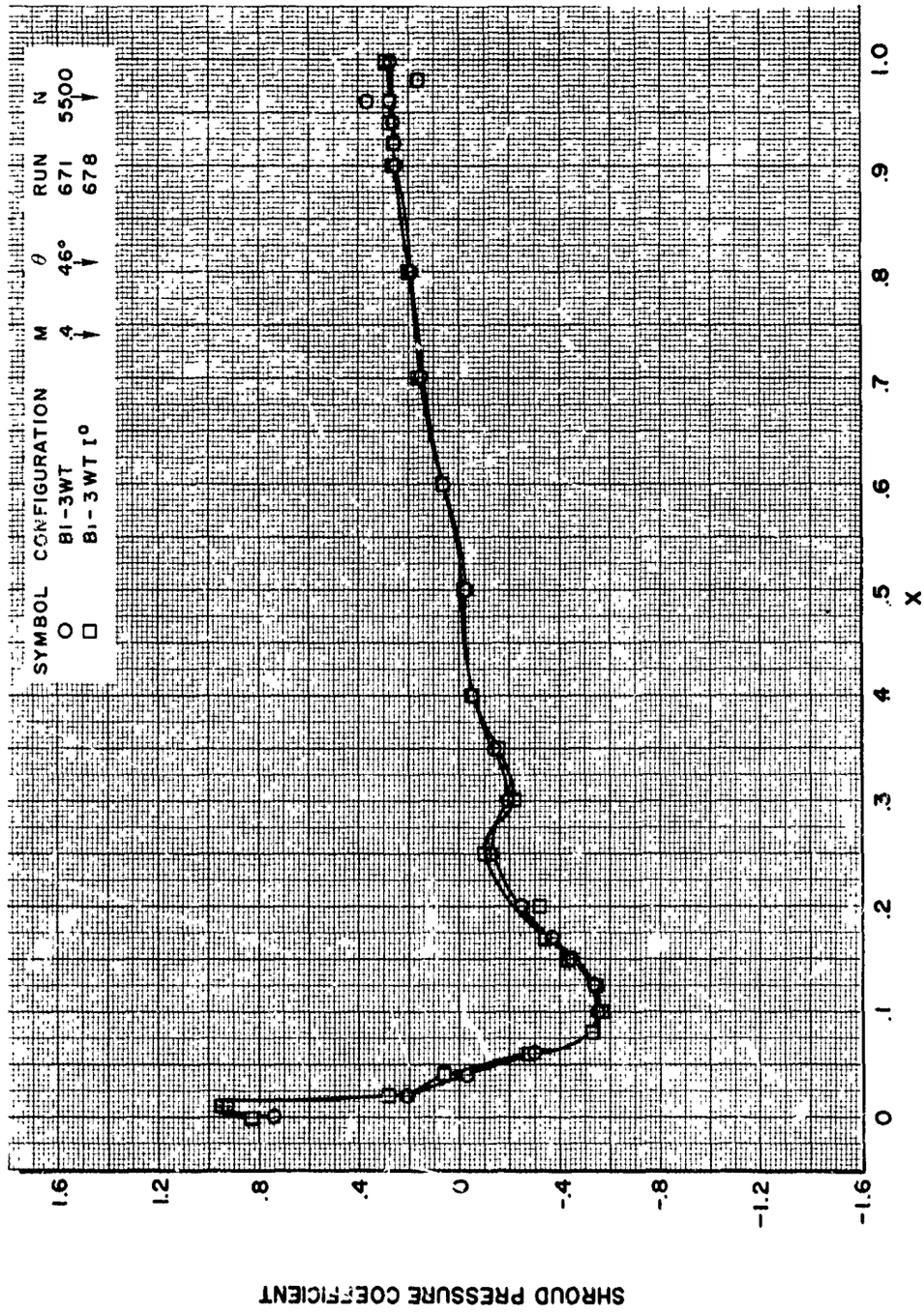

HS SHROUDED PROPELLER TEST
INSIDE SHROUD SURFACE PRESSURE DISTRIBUTION
EFFECT OF INLET VANE

FIGURE 209

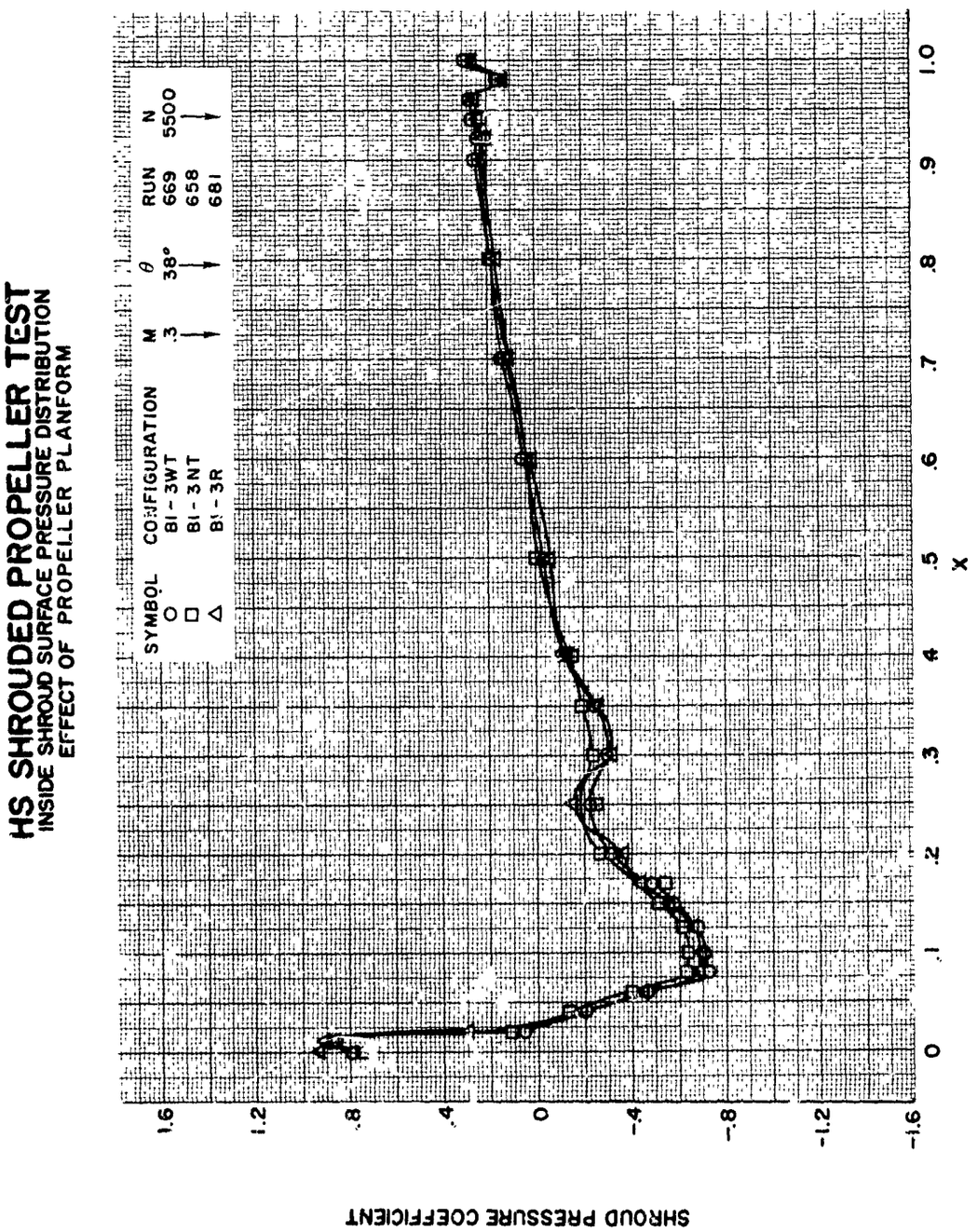
HS SHROUDED PROPELLER TEST
INSIDE SHROUD SURFACE PRESSURE DISTRIBUTION
EFFECT OF PROPELLER PLANFORM
SYMBOL CONFIGURATION M θ RUN N
○ BI-3WT .3 38° 669 5500
□ BI-3NT 658
△ BI-3R 681
SHROUD PRESSURE COEFFICIENT
1.6
1.2
.8
.4
0
-.4
-.8
-1.2
-1.6
0
.1
.2
.3
.4
.5
.6
.7
.8
.9
1.0
X

FIGURE 210

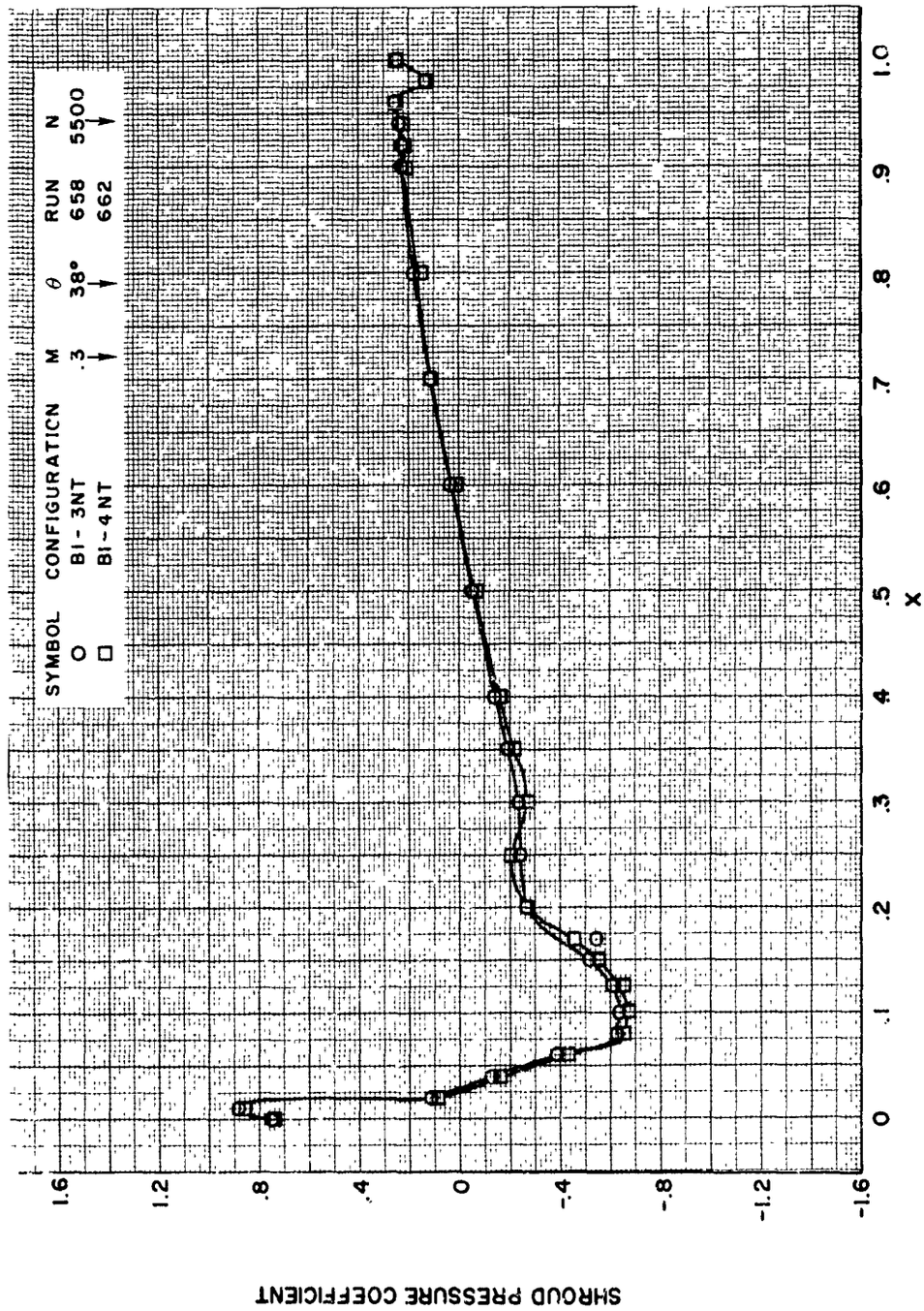

HS SHROUDED PROPELLER TEST
INSIDE SHROUD SURFACE PRESSURE DISTRIBUTION
EFFECT OF NUMBER OF BLADES

FIGURE 211

HS SHROUDED PROPELLER TEST

INSIDE SHROUD SURFACE PRESSURE DISTRIBUTION

EFFECT OF TIP CLEARANCE

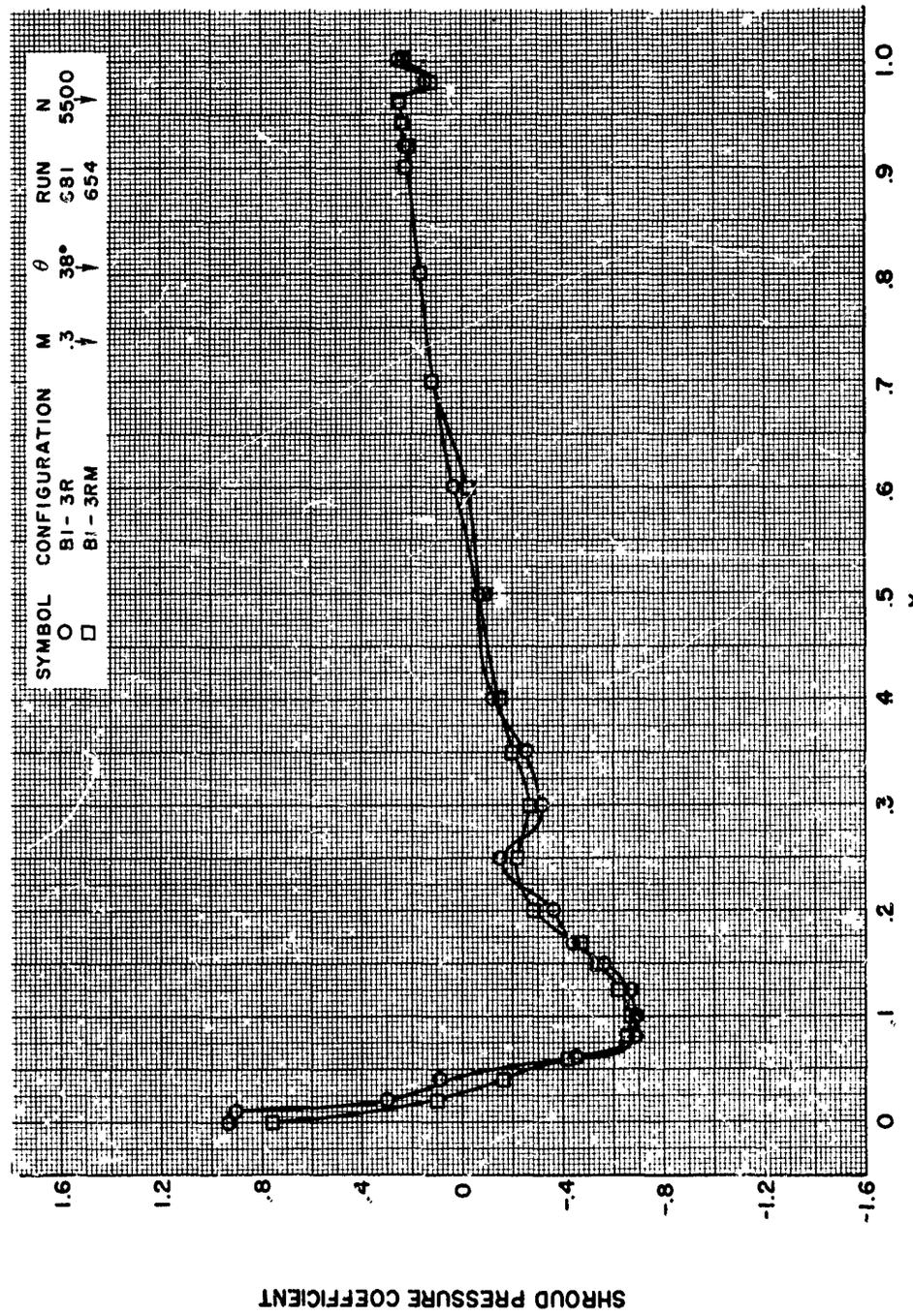

FIGURE 212

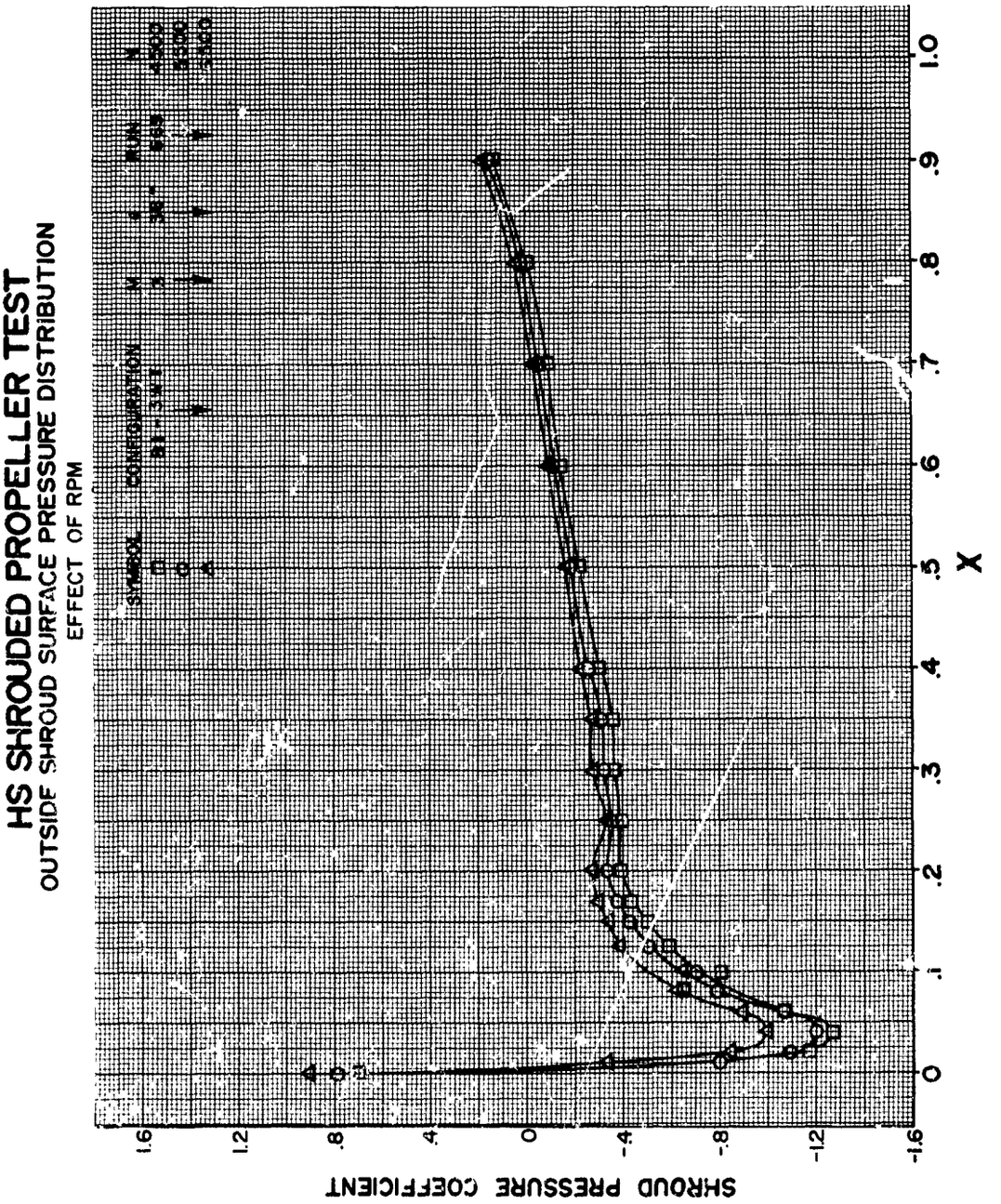
HS SHROUDED PROPELLER TEST
OUTSIDE SHROUD SURFACE PRESSURE DISTRIBUTION
EFFECT OF RPM
SYMBOL
CONFIGURATION
RUN
N
4500
4000
2500
SHROUD PRESSURE COEFFICIENT
1.6
1.2
.8
.4
0
-.4
-.8
-1.2
-1.6
0
.1
.2
.3
.4
.5
.6
.7
.8
.9
1.0
X

FIGURE 213

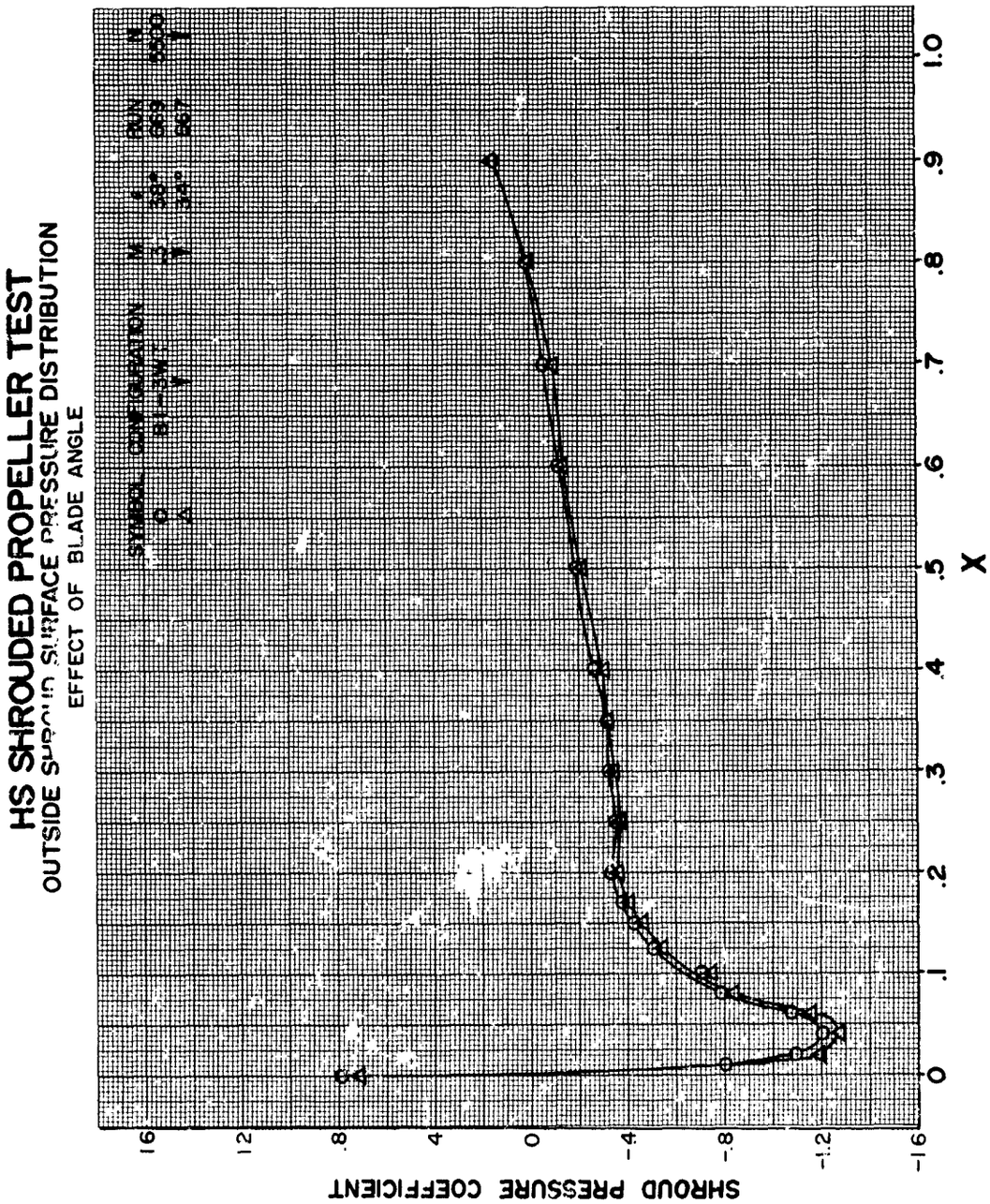
HS SHROUDED PROPELLER TEST
OUTSIDE SURFACE PRESSURE DISTRIBUTION
EFFECT OF BLADE ANGLE
SYMBOL CONFIGURATION M β RUN
○ 8L-5W-1 .39 39° 669
□ 8L-5W-1 .39 34° 667
△ 8L-5W-1 .39 [illegible] [illegible]
SHROUD PRESSURE COEFFICIENT
16
12
.8
4
0
-.4
-.8
-1.2
-1.6
0
.1
.2
.3
.4
.5
.6
.7
.8
.9
1.0
X

FIGURE 214

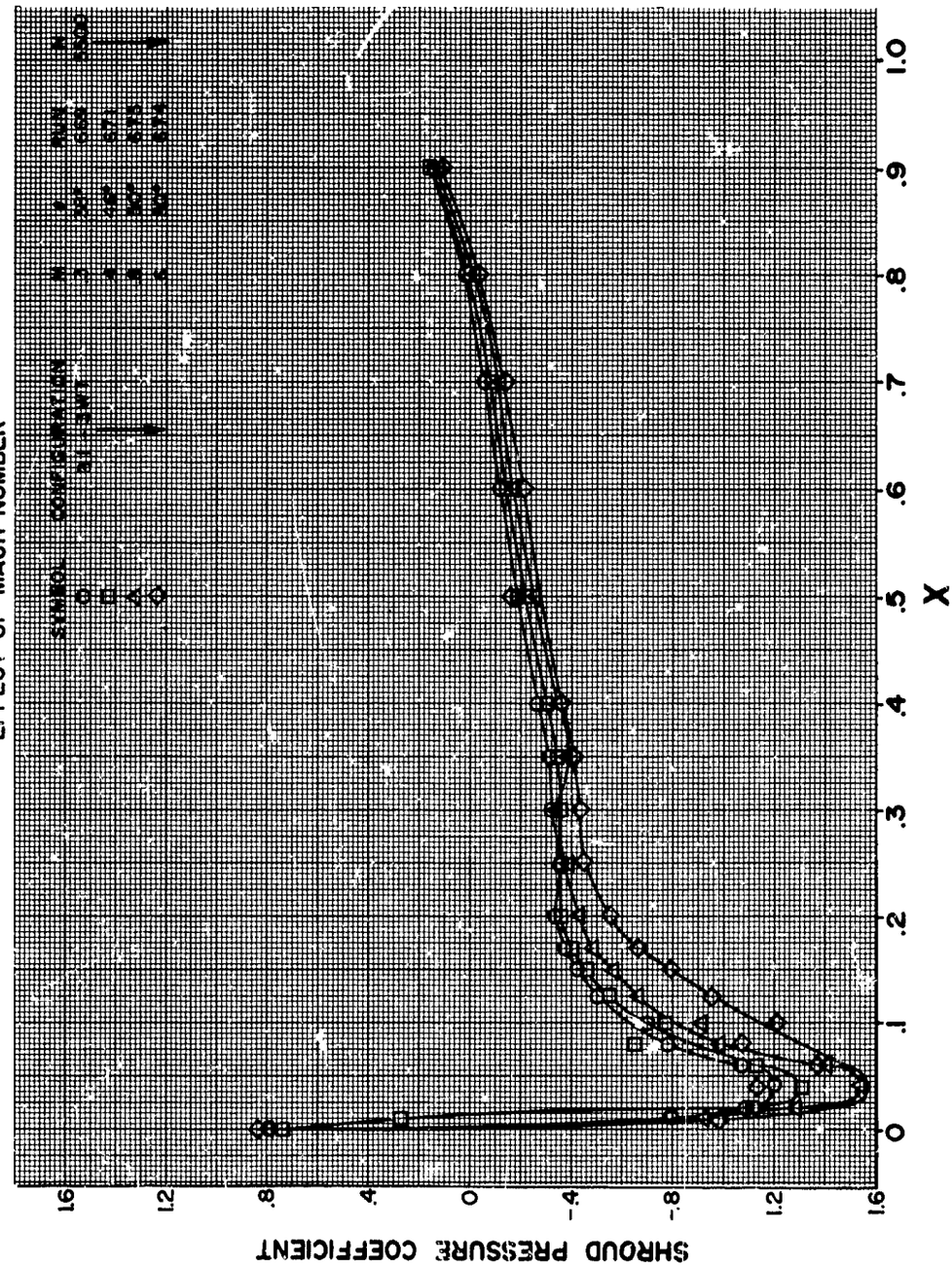
HS SHROUDED PROPELLER TEST
OUTSIDE SHROUD SURFACE PRESSURE DISTRIBUTION
EFFECT OF MACH NUMBER
SYMBOL
CONFIGURATION
SHROUD PRESSURE COEFFICIENT
X
1.6
1.2
.8
.4
0
-.4
-.8
-1.2
-1.6
0
.1
.2
.3
.4
.5
.6
.7
.8
.9
1.0

FIGURE 215

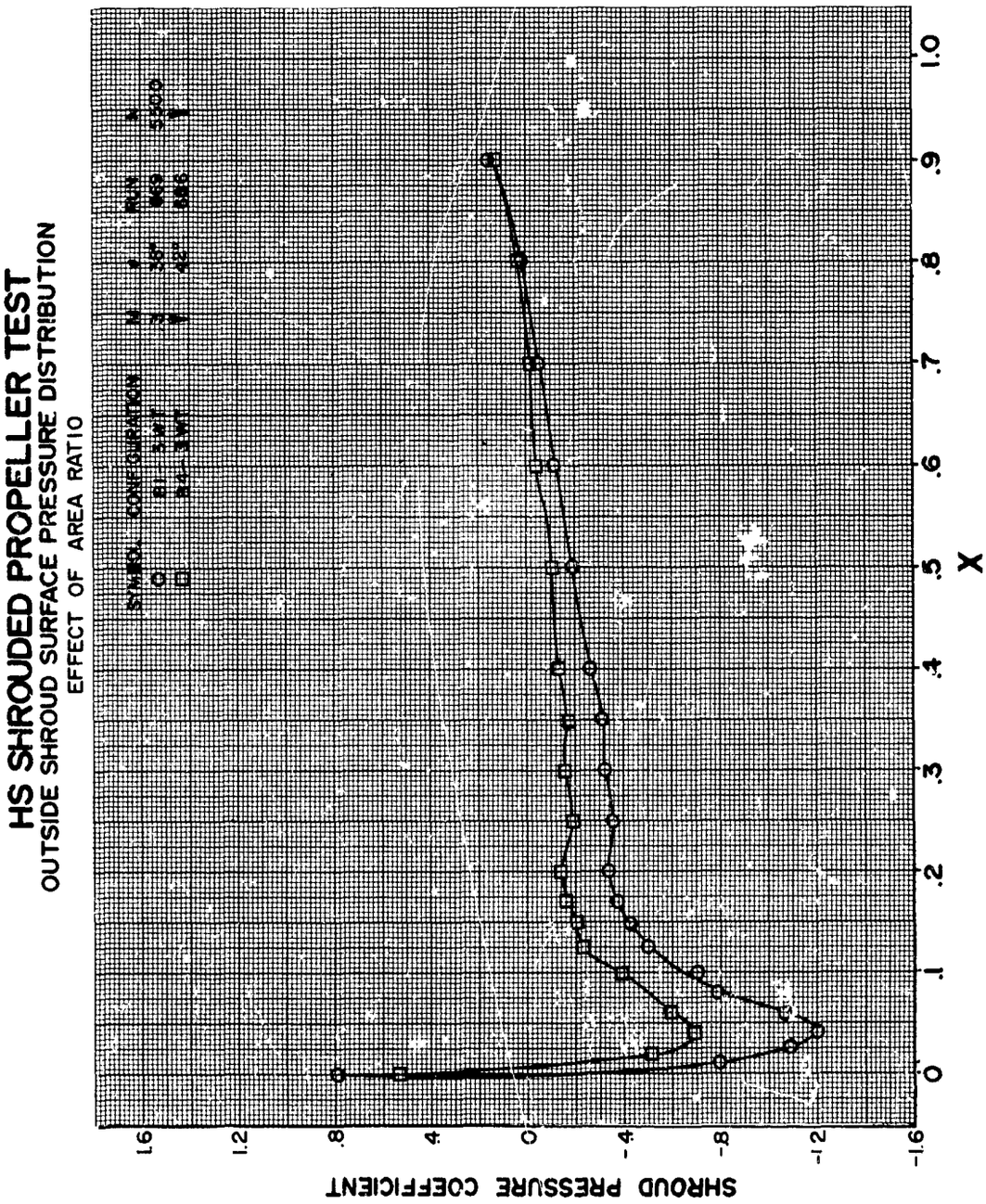
HS SHROUDED PROPELLER TEST
OUTSIDE SHROUD SURFACE PRESSURE DISTRIBUTION
EFFECT OF AREA RATIO
SYMBOL CONFIGURATION
SHROUD PRESSURE COEFFICIENT
X
1.6
1.2
.8
.4
0
-.4
-.8
-1.2
-1.6
0
.1
.2
.3
.4
.5
.6
.7
.8
.9
1.0

FIGURE 216

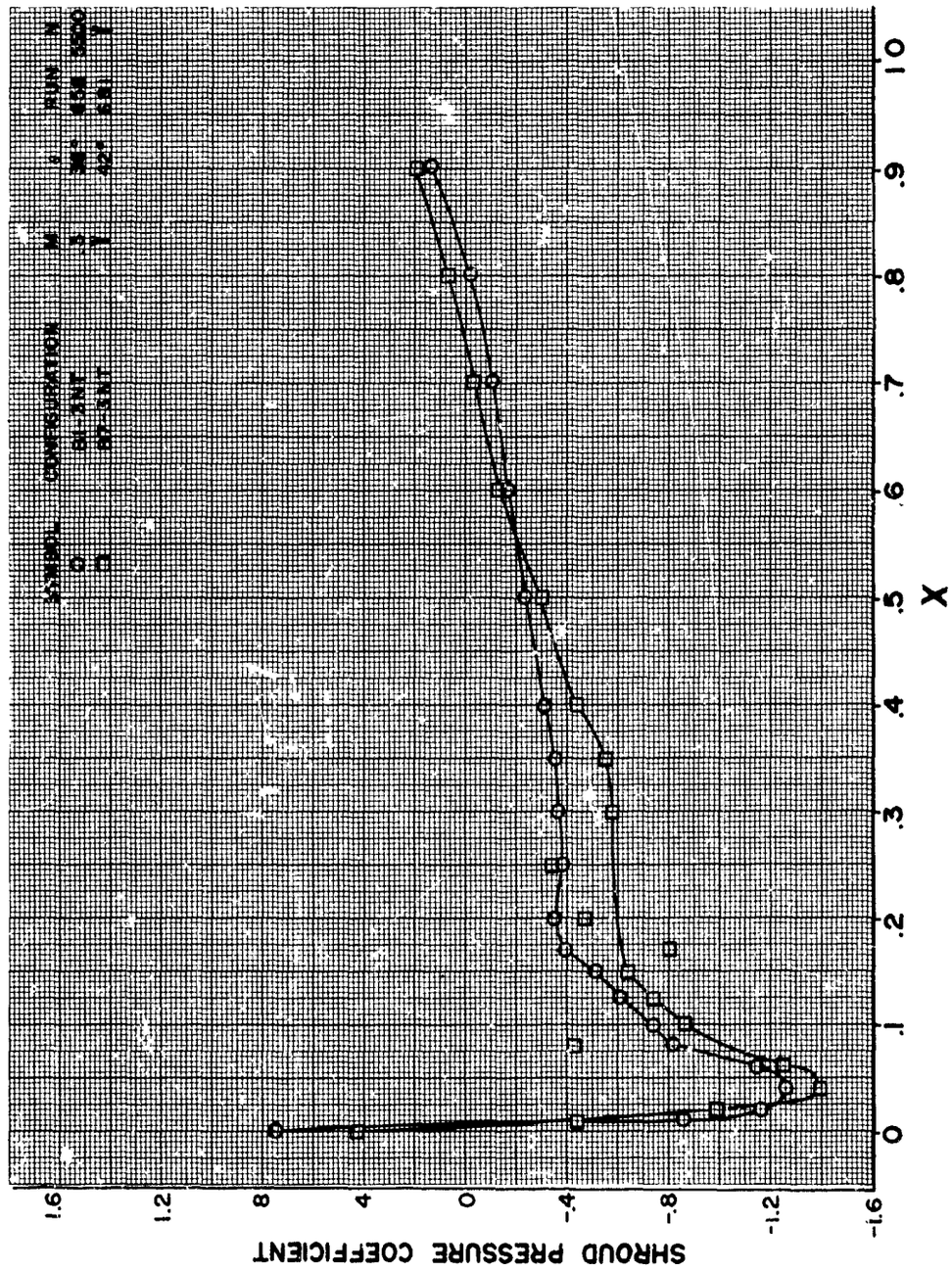

HS SHROUDED PROPELLER TEST

OUTSIDE SHROUD SURFACE PRESSURE DISTRIBUTION

EFFECT OF SHROUD LENGTH

FIGURE 217

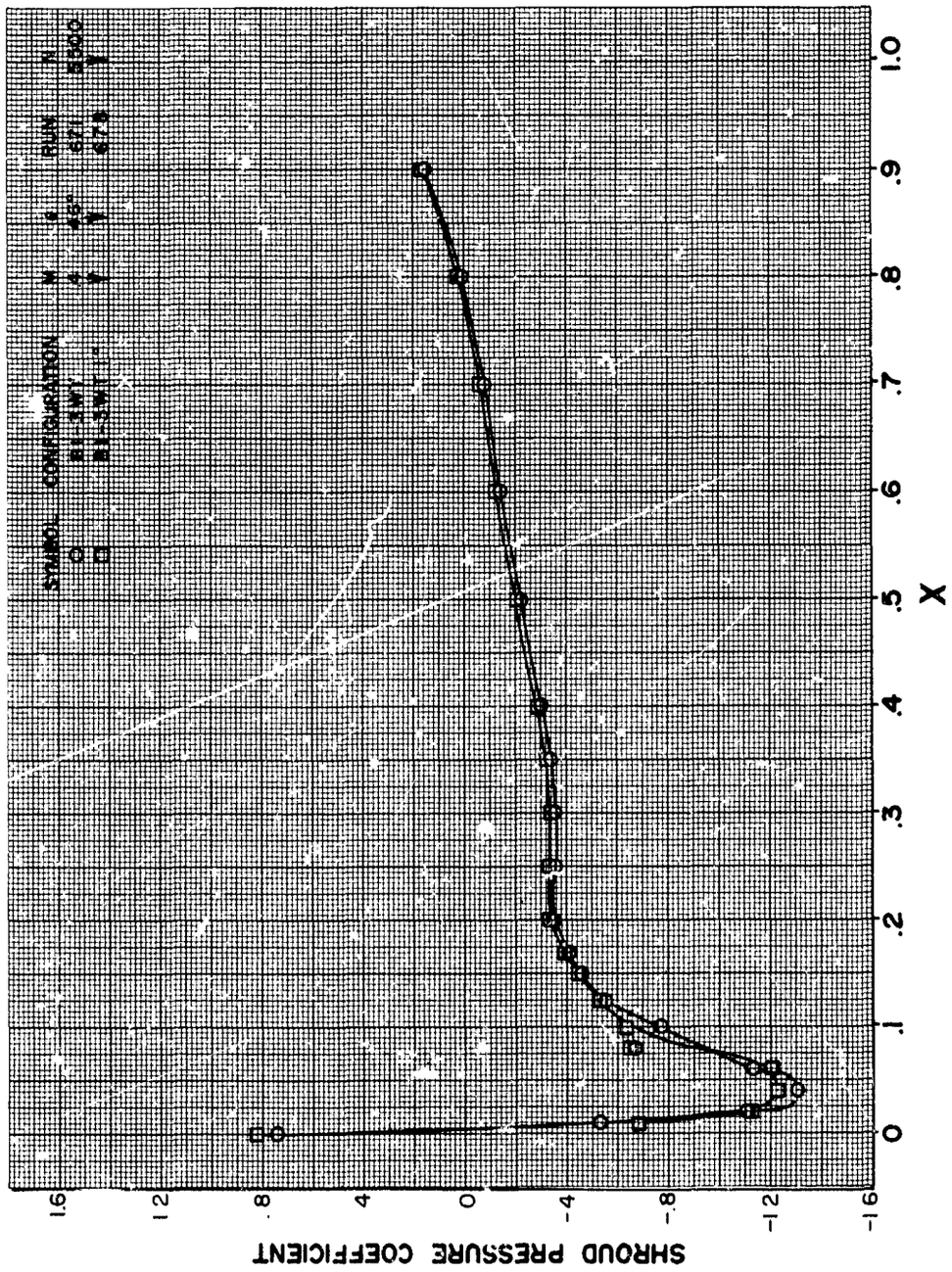

HS SHROUDED PROPELLER TEST
OUTSIDE SHROUD SURFACE PRESSURE DISTRIBUTION
EFFECT OF INLET VANE

FIGURE 218

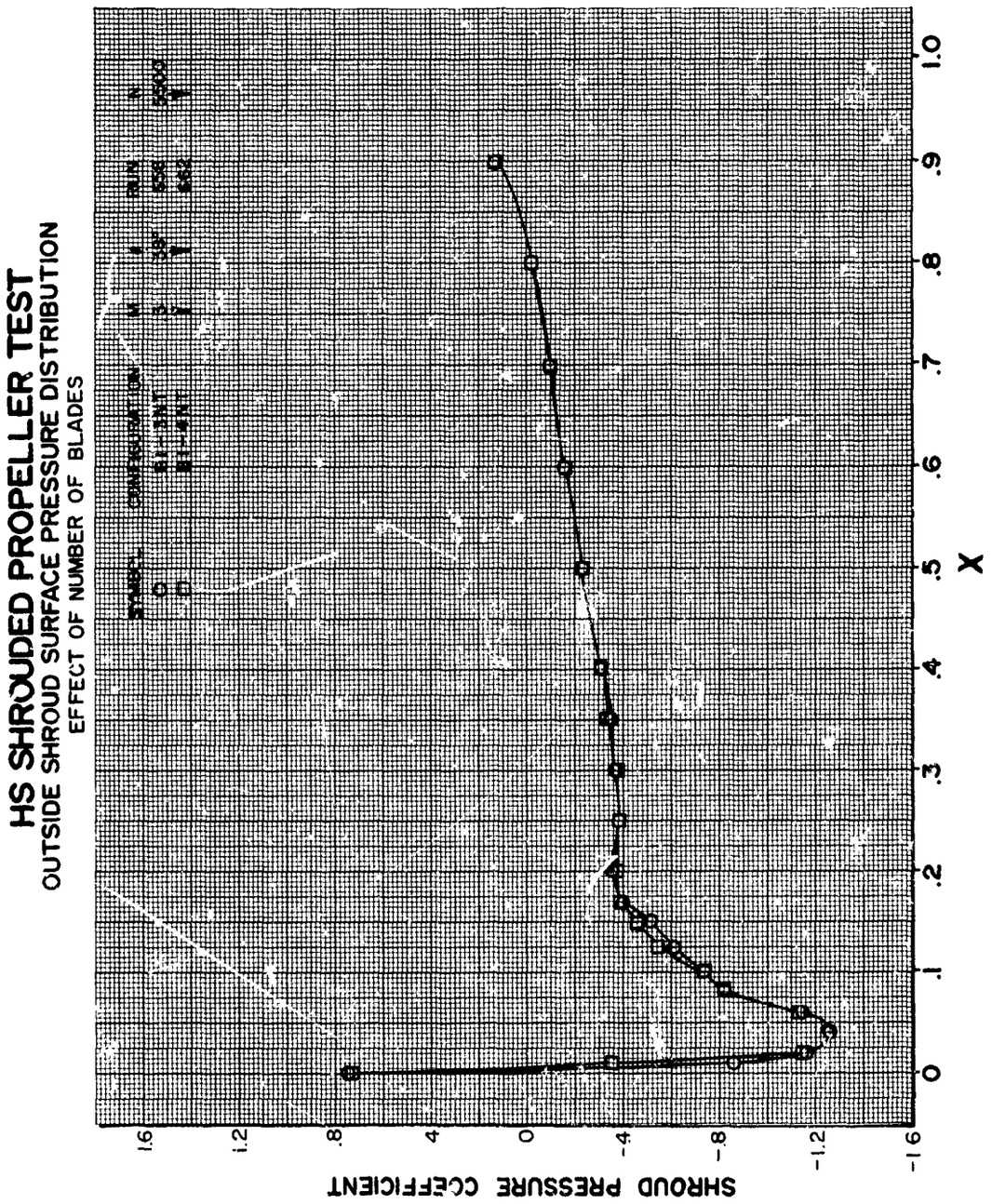
HS SHROUDED PROPELLER TEST
OUTSIDE SHROUD SURFACE PRESSURE DISTRIBUTION
EFFECT OF NUMBER OF BLADES
SYMBOL
CONFIGURATION
RUN
SHROUD PRESSURE COEFFICIENT
X
1.6
1.2
.8
.4
0
-.4
-.8
-1.2
-1.6
0
.1
.2
.3
.4
.5
.6
.7
.8
.9
1.0

FIGURE 219

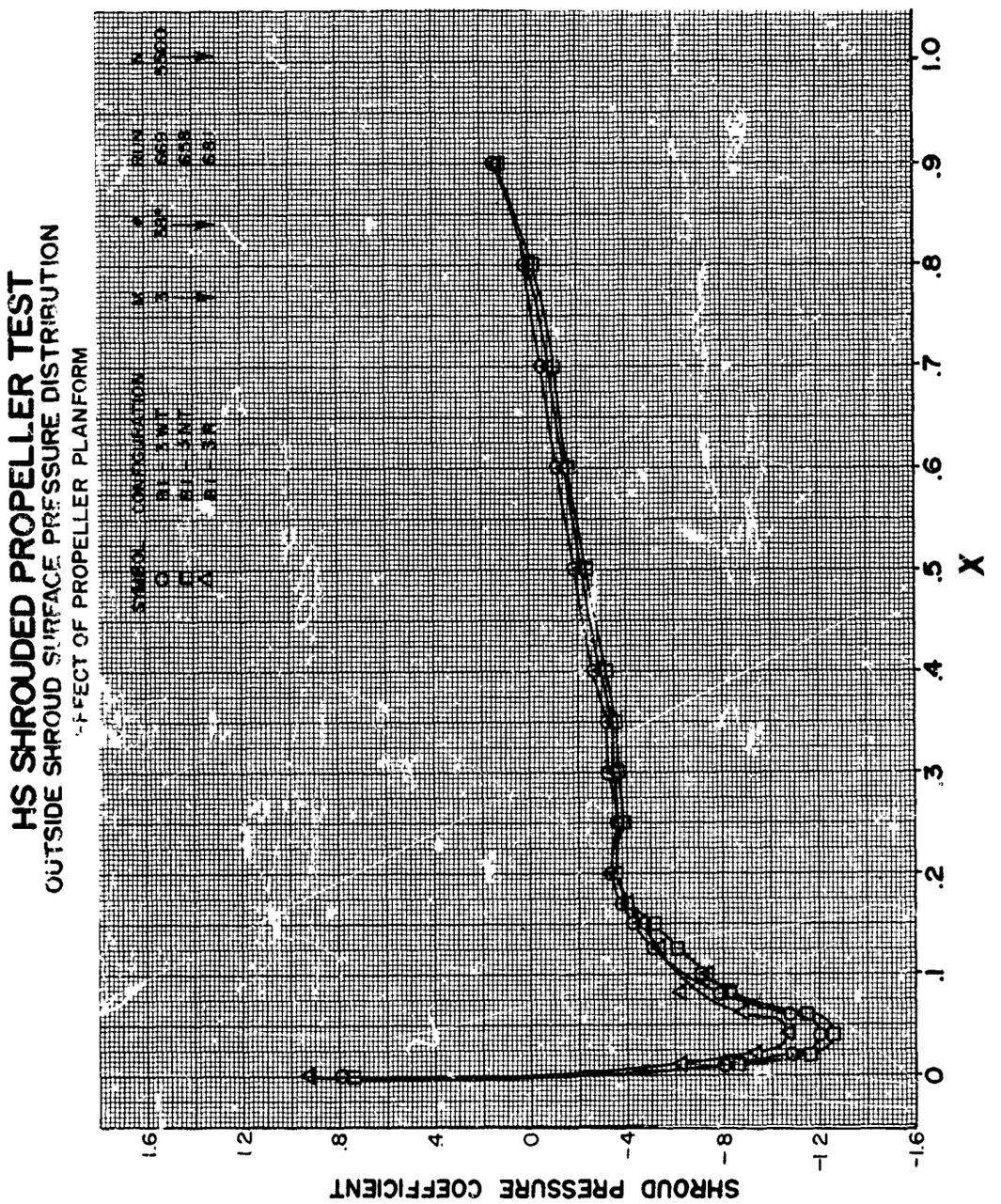
HS SHROUDED PROPELLER TEST
OUTSIDE SHROUD SURFACE PRESSURE DISTRIBUTION
EFFECT OF PROPELLER PLANFORM
SYMBOL CONFIGURATION
RUN
SHROUD PRESSURE COEFFICIENT
X
1.6
1.2
.8
.4
0
-.4
-.8
-1.2
-1.6
0
.1
.2
.3
.4
.5
.6
.7
.8
.9
1.0

FIGURE 220

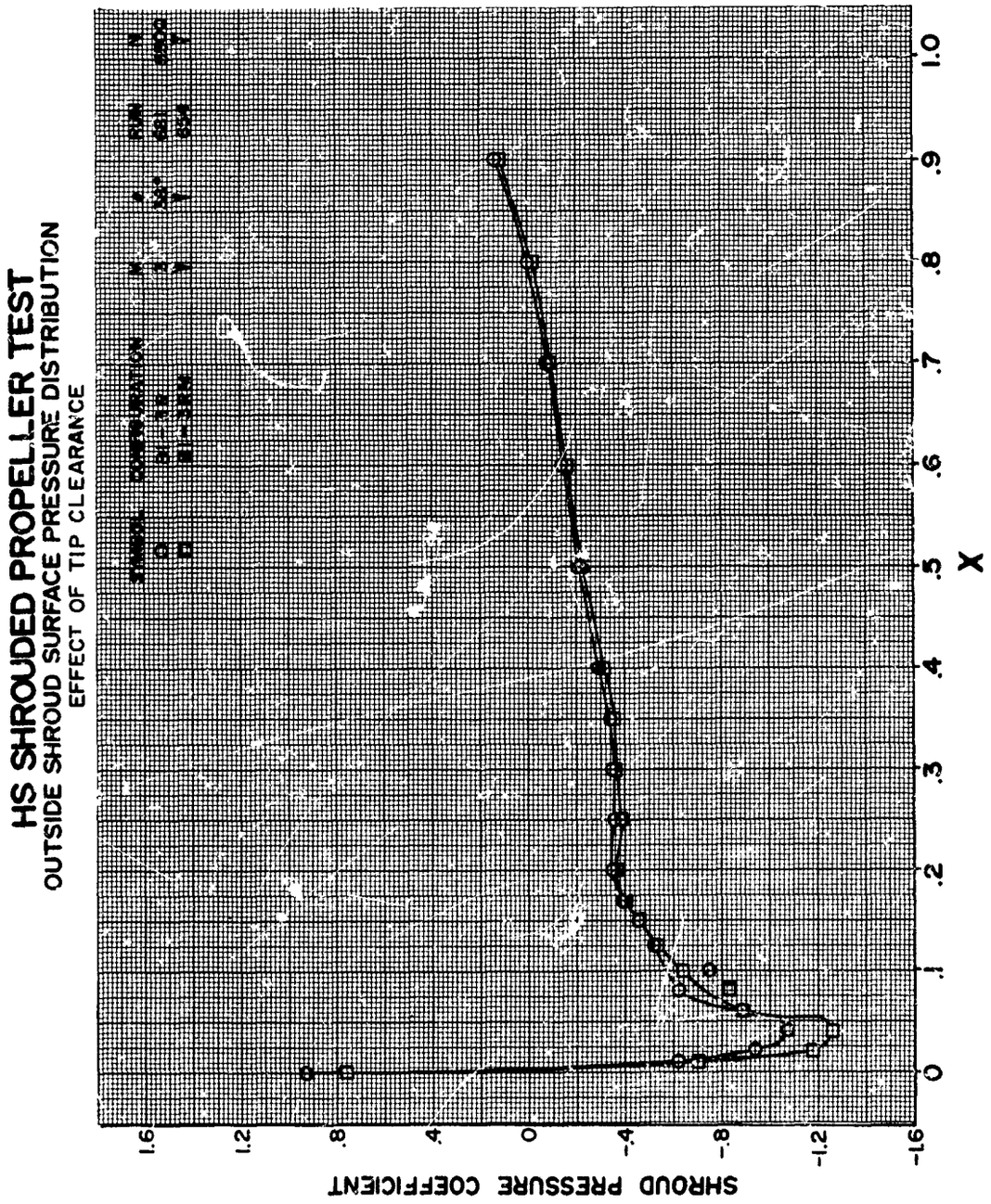
HS SHROUDED PROPELLER TEST
OUTSIDE SHROUD SURFACE PRESSURE DISTRIBUTION
EFFECT OF TIP CLEARANCE
SHROUD PRESSURE COEFFICIENT
X
1.6
1.2
.8
.4
0
-.4
-.8
-1.2
-1.6
0
.1
.2
.3
.4
.5
.6
.7
.8
.9
1.0

FIGURE 221

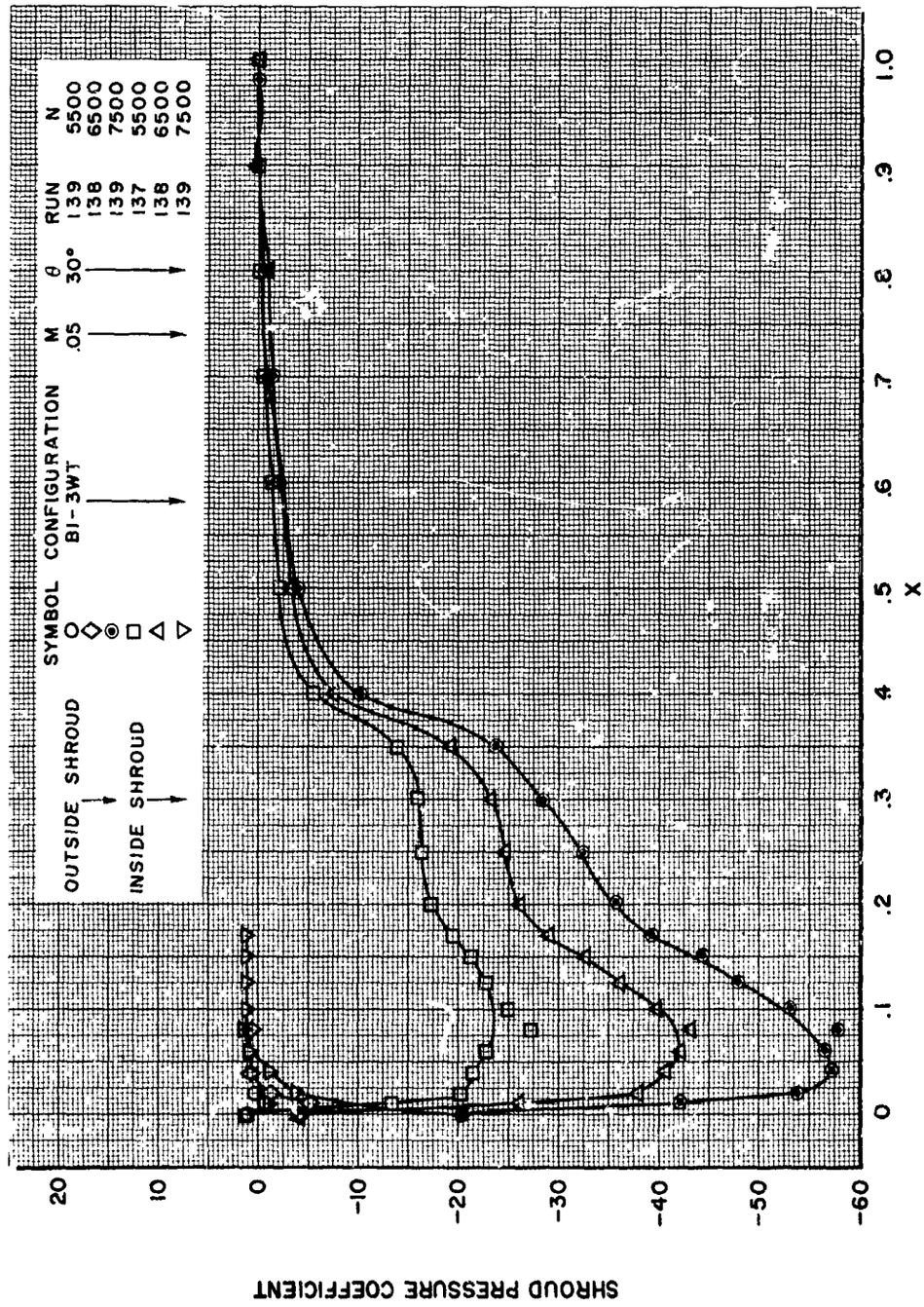
HS SHROUDED PROPELLER TEST
SHROUD SURFACE PRESSURE DISTRIBUTION
EFFECT OF RPM
OUTSIDE SHROUD
INSIDE SHROUD
SYMBOL
CONFIGURATION
BI-3WT
M
.05
θ
30°
RUN
N
139 5500
138 6500
139 7500
137 5500
138 6500
139 7500
SHROUD PRESSURE COEFFICIENT
20
10
0
-10
-20
-30
-40
-50
-60
0
.1
.2
.3
.4
.5
.6
.7
.8
.9
1.0
X

FIGURE 222

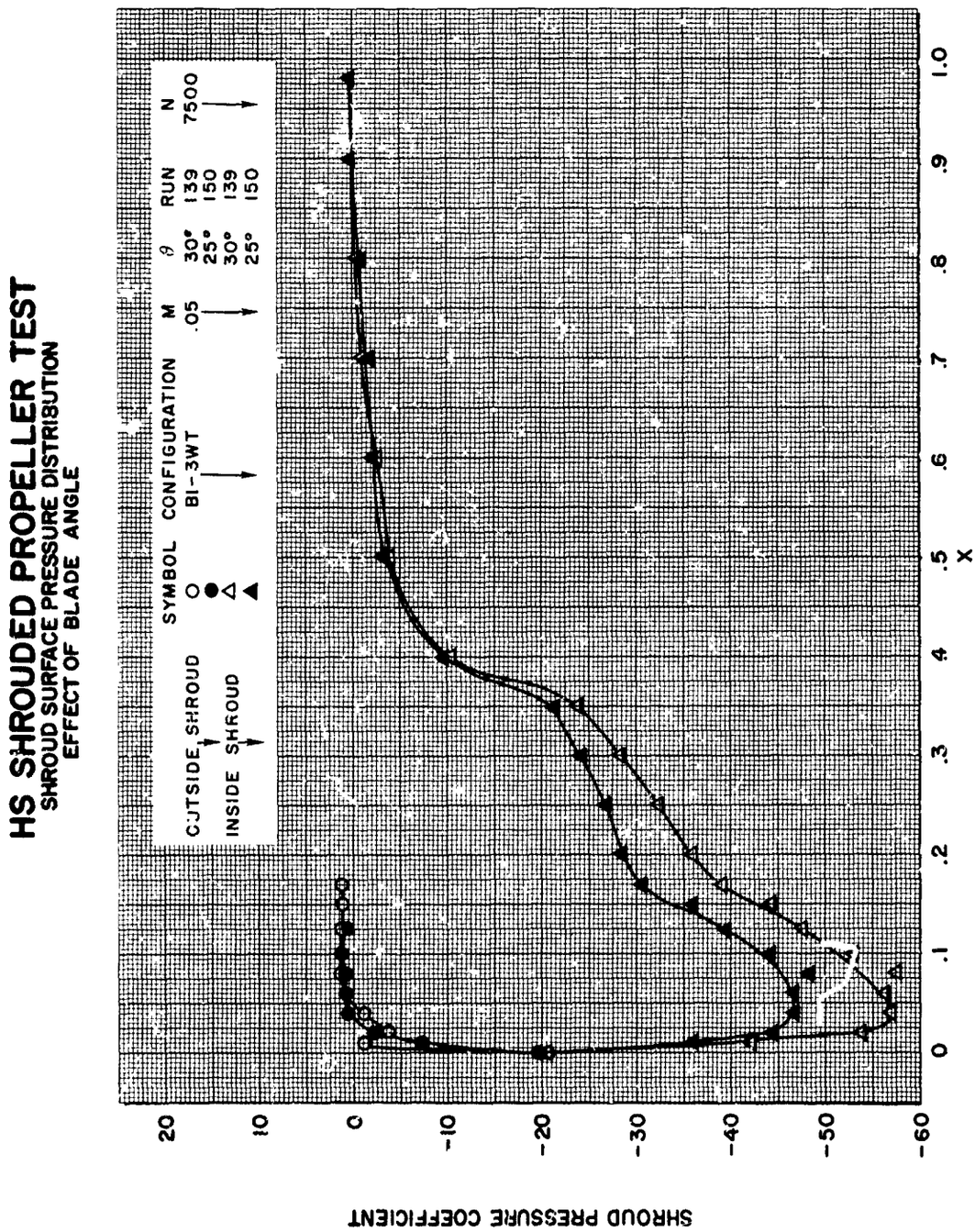
HS SHROUDED PROPELLER TEST
SHROUD SURFACE PRESSURE DISTRIBUTION
EFFECT OF BLADE ANGLE
SYMBOL CONFIGURATION M θ RUN N
OUTSIDE SHROUD ○ BI-3WT .05 30° 139 7500
● 25° 150
INSIDE SHROUD △ 30° 139
▲ 25° 150
SHROUD PRESSURE COEFFICIENT
20
10
0
-10
-20
-30
-40
-50
-60
0
.1
.2
.3
.4
.5
.6
.7
.8
.9
1.0
X

FIGURE 223

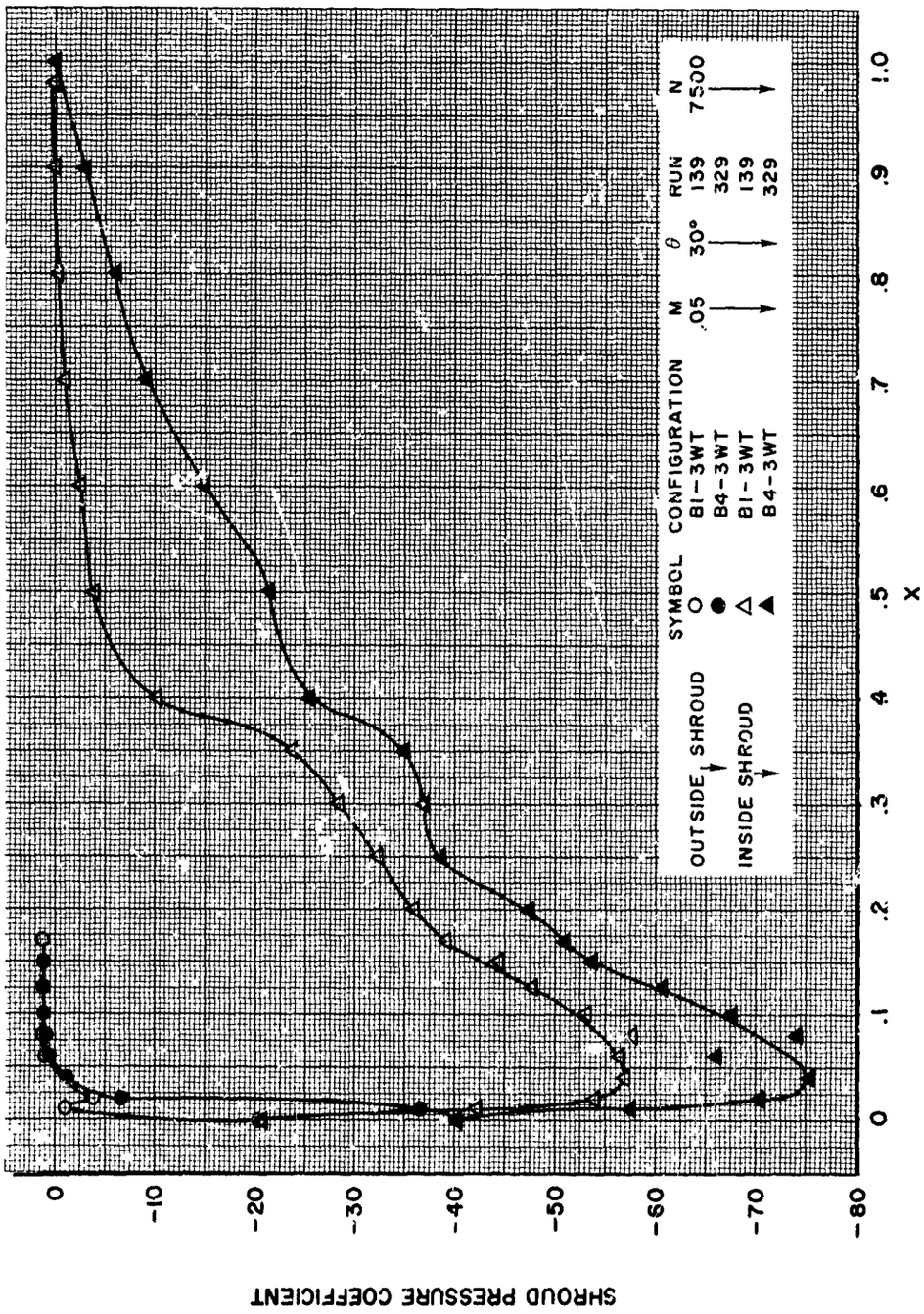

HS SHROUDED PROPELLER TEST
SHROUD SURFACE PRESSURE DISTRIBUTION
EFFECT OF AREA RATIO

FIGURE 224

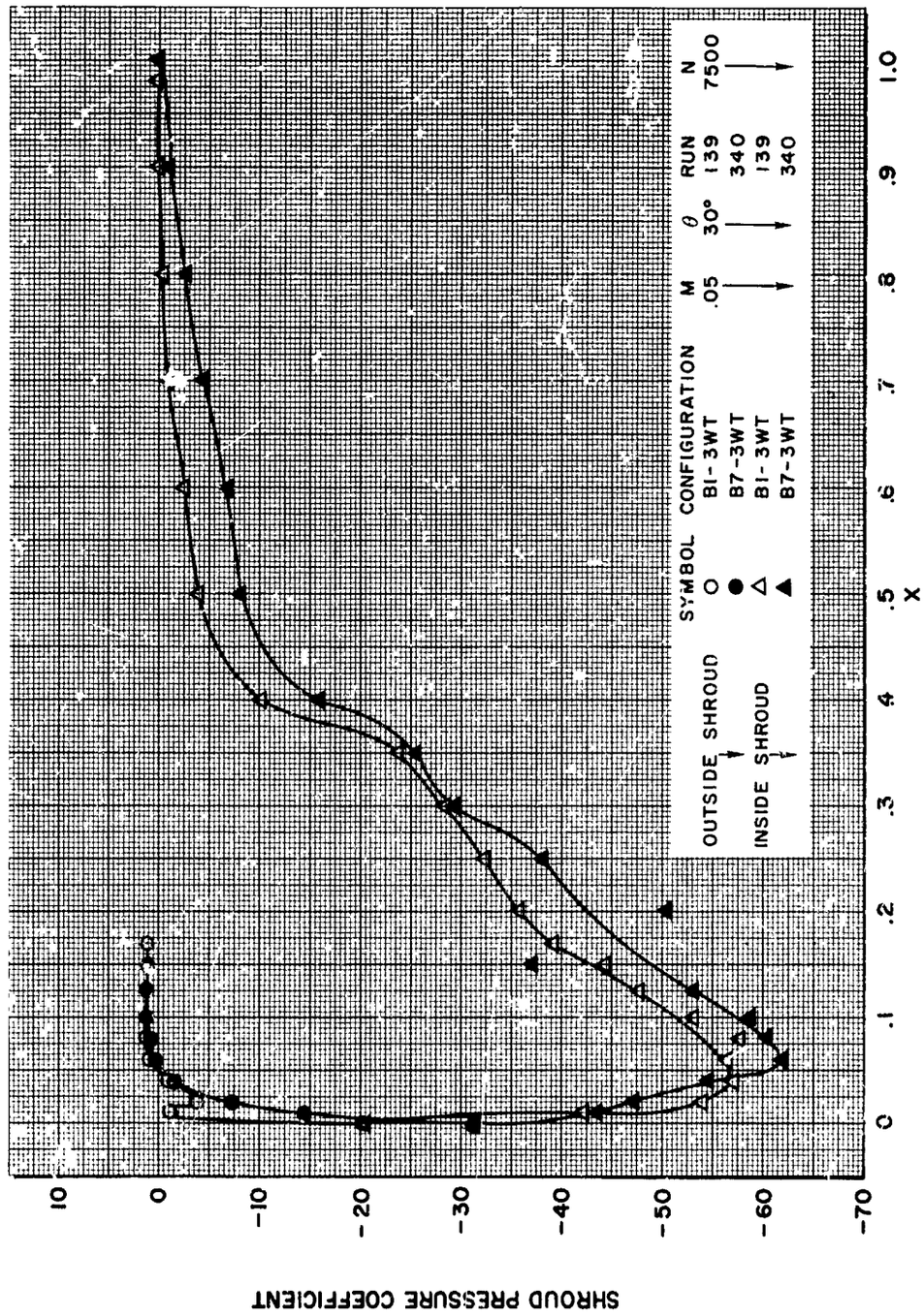

HS SHROUDED PROPELLER TEST
SHROUD SURFACE PRESSURE DISTRIBUTION
EFFECT OF SHROUD LENGTH

FIGURE 225

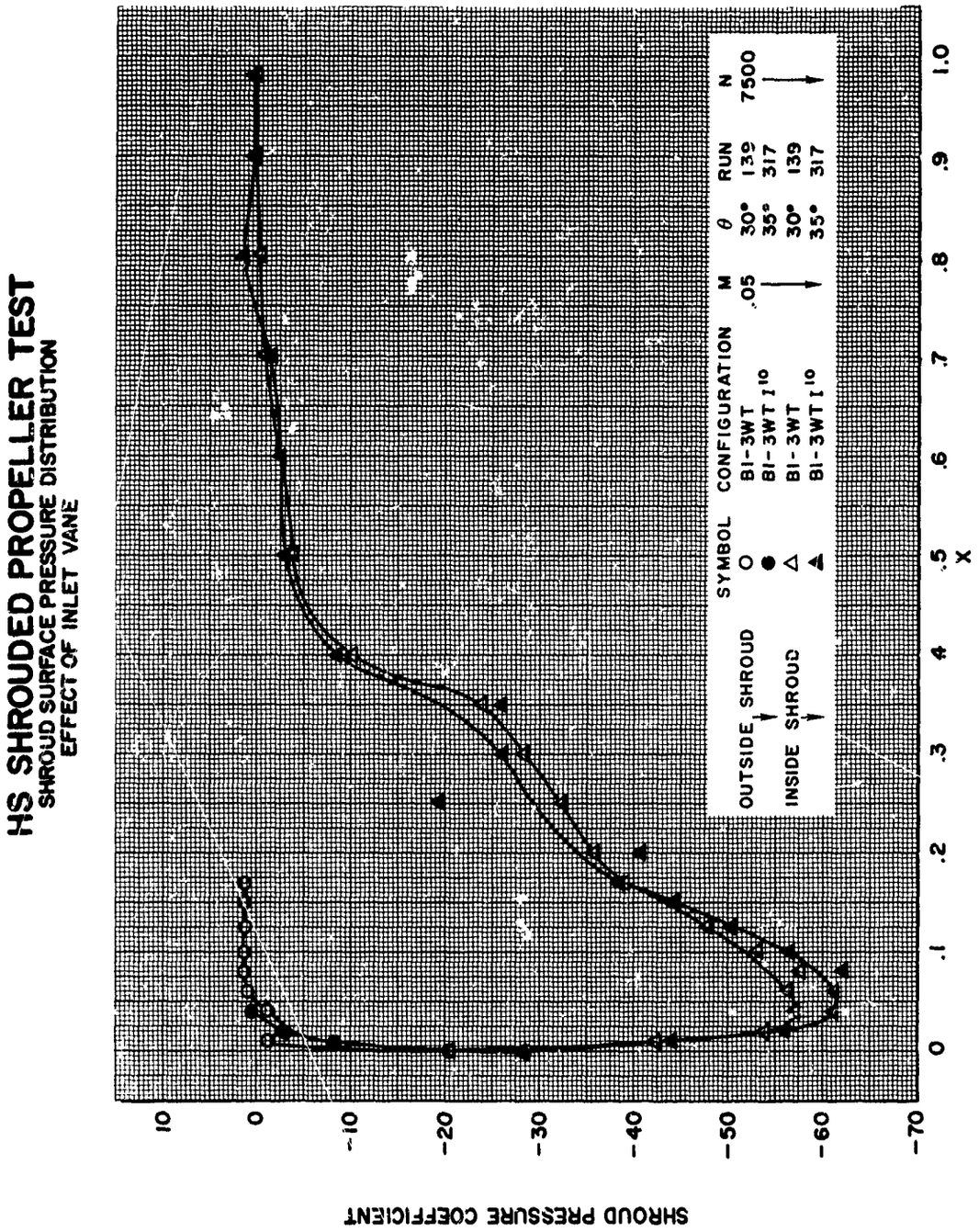
HS SHROUDED PROPELLER TEST
SHROUD SURFACE PRESSURE DISTRIBUTION
EFFECT OF INLET VANE
SYMBOL CONFIGURATION M θ RUN N
OUTSIDE SHROUD
INSIDE SHROUD
BI-3WT .05 30° 139 7500
BI-3WT I10 35° 317
BI-3WT 30° 139
BI-3WT I10 35° 317
SHROUD PRESSURE COEFFICIENT
10
0
-10
-20
-30
-40
-50
-60
-70
0
.1
.2
.3
.4
.5
.6
.7
.8
.9
1.0
X

FIGURE 226

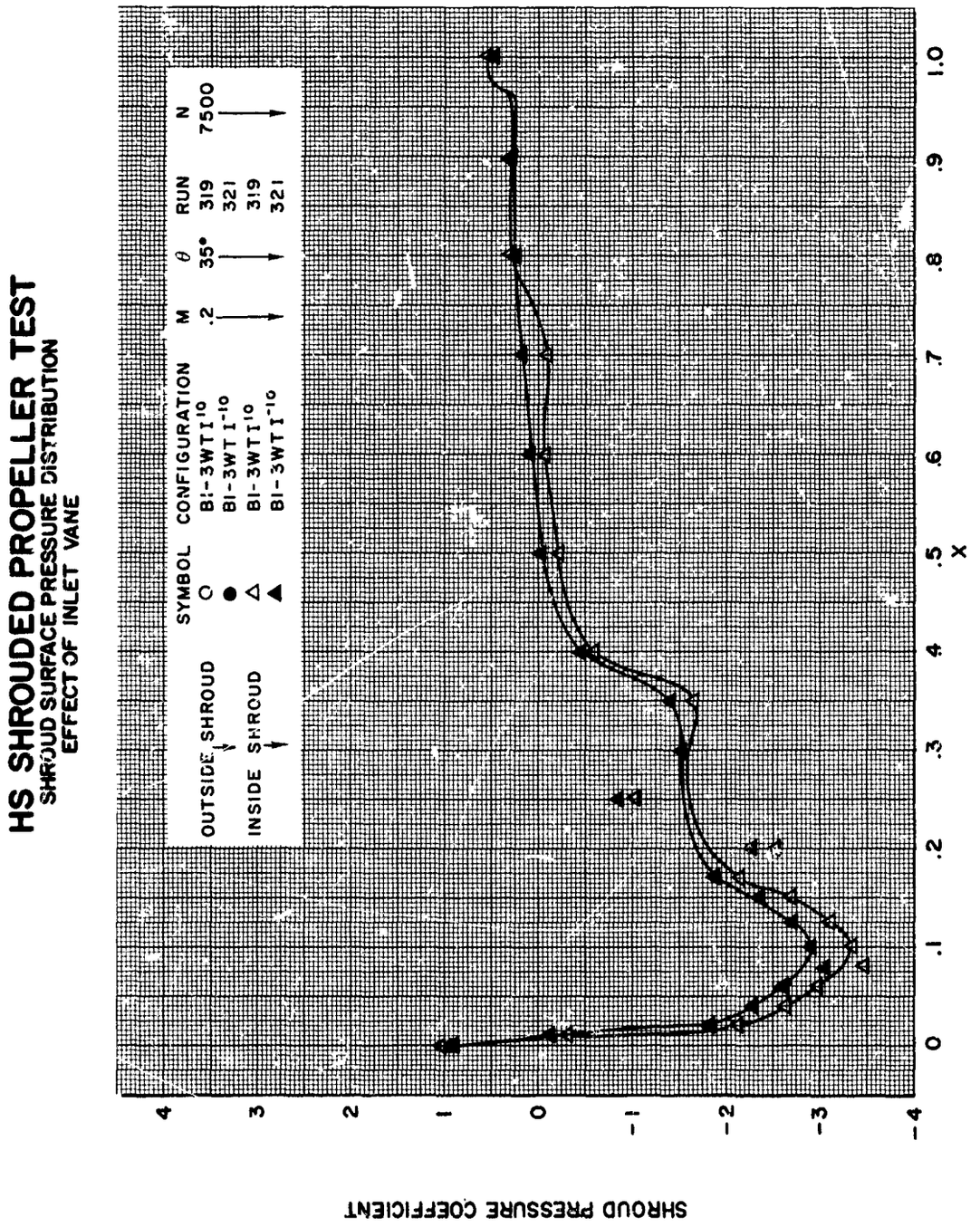
HS SHROUDED PROPELLER TEST
SHROUD SURFACE PRESSURE DISTRIBUTION
EFFECT OF INLET VANE
SYMBOL CONFIGURATION M θ RUN N
OUTSIDE SHROUD ○ BI-3WTI10 .2 35° 319 7500
● BI-3WTI-10 321
INSIDE SHROUD △ BI-3WTI10 319
▲ BI-3WTI-10 321
SHROUD PRESSURE COEFFICIENT
4
3
2
1
0
-1
-2
-3
-4
0
.1
.2
.3
.4
.5
.6
.7
.8
.9
1.0
X

FIGURE 227

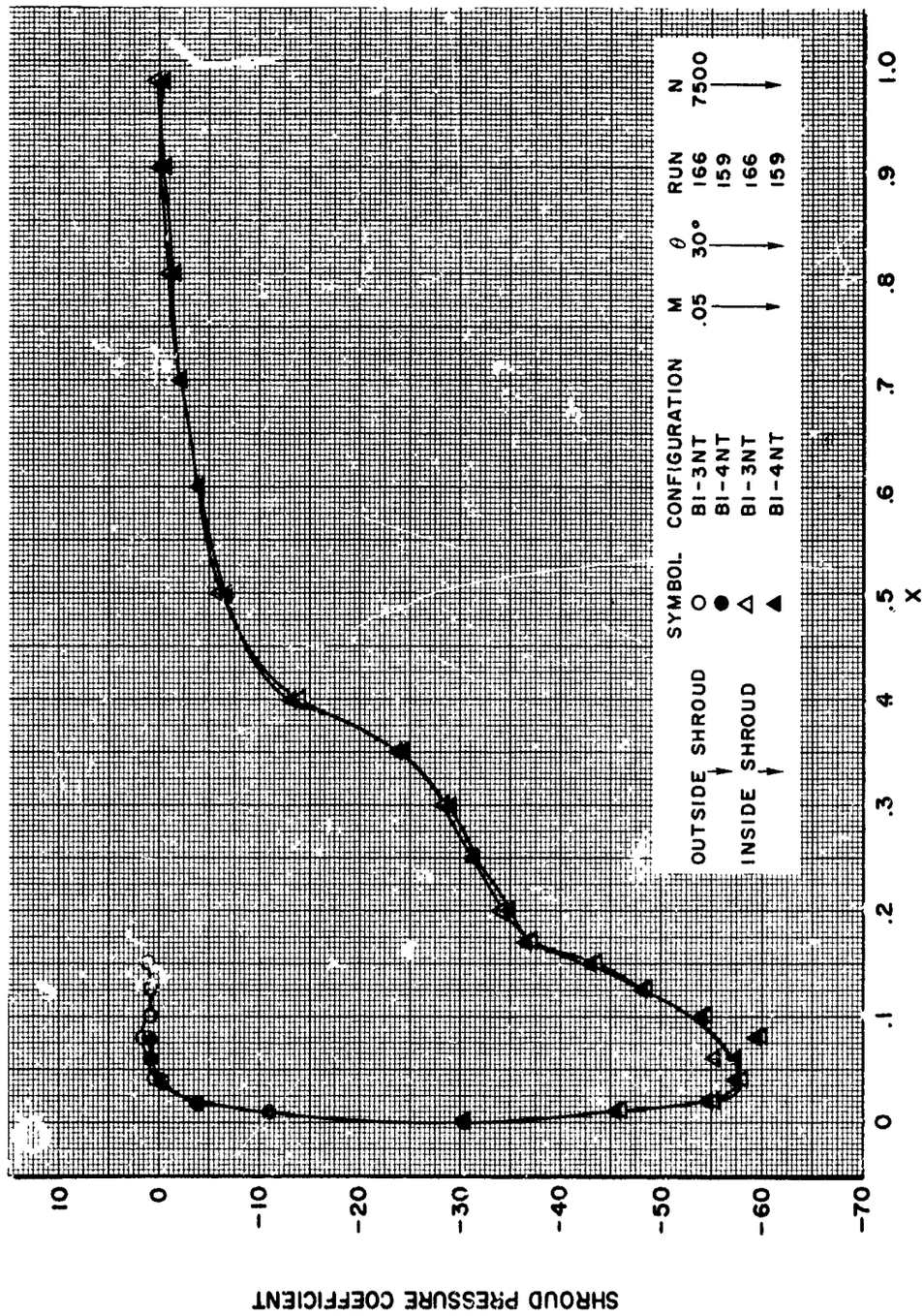
HS SHROUDED PROPELLER TEST
SHROUD SURFACE PRESSURE DISTRIBUTION
EFFECT OF NUMBER OF BLADES
SHROUD PRESSURE COEFFICIENT
10
0
-10
-20
-30
-40
-50
-60
-70
0
.1
.2
.3
.4
.5
.6
.7
.8
.9
1.0
X
OUTSIDE SHROUD
INSIDE SHROUD
SYMBOL
CONFIGURATION
M
θ
RUN
N
BI-3NT
BI-4NT
BI-3NT
BI-4NT
.05
30°
166
159
166
159
7500

FIGURE 228

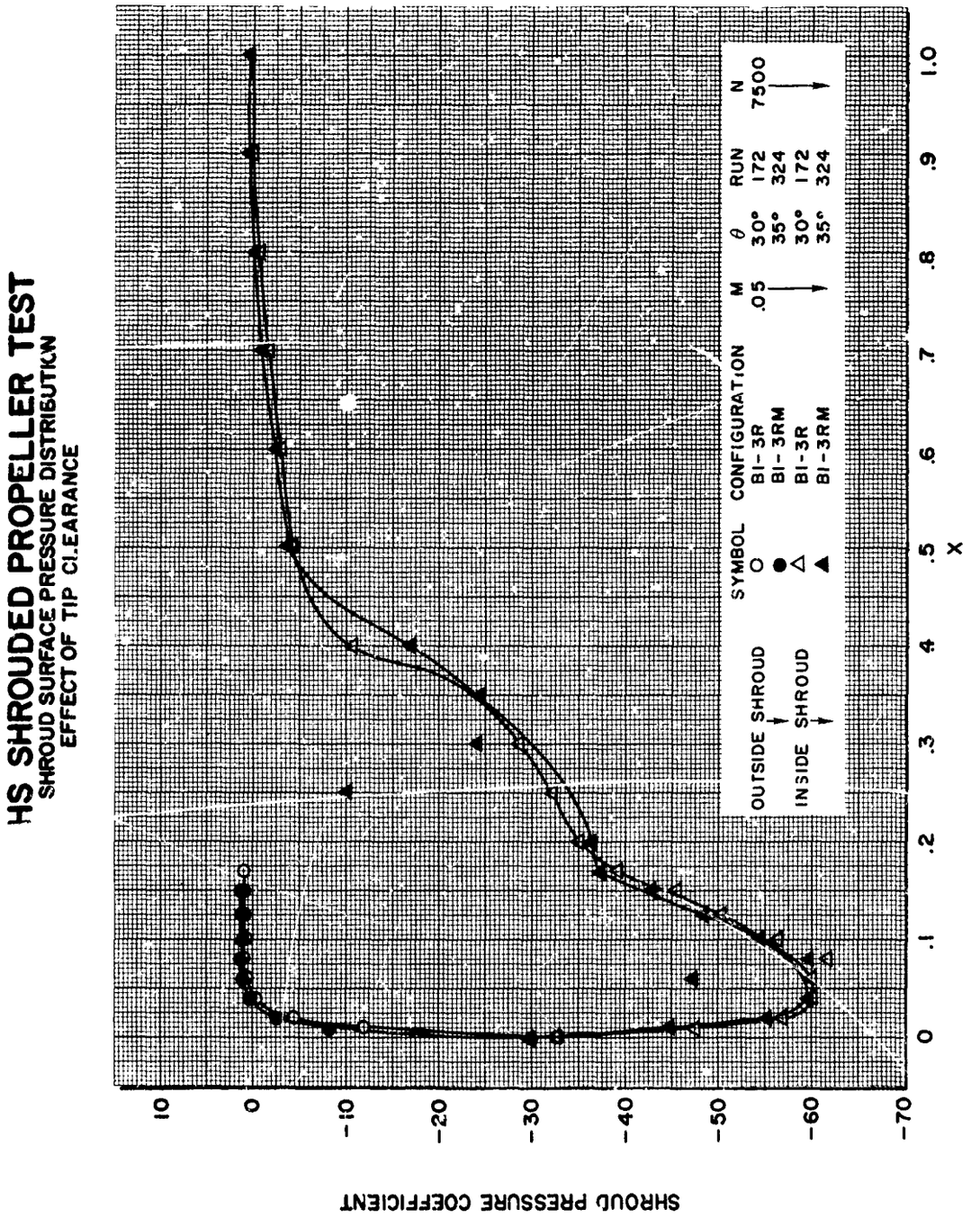
HS SHROUDED PROPELLER TEST
SHROUD SURFACE PRESSURE DISTRIBUTION
EFFECT OF TIP CLEARANCE
SHROUD PRESSURE COEFFICIENT
10
0
-10
-20
-30
-40
-50
-60
-70
0
.1
.2
.3
.4
.5
.6
.7
.8
.9
1.0
X
OUTSIDE SHROUD
INSIDE SHROUD
SYMBOL
CONFIGURATION
M
θ
RUN
N
BI-3R
BI-3RM
BI-3R
BI-3RM
.05
30°
35°
30°
35°
172
324
172
324
7500

FIGURE 229

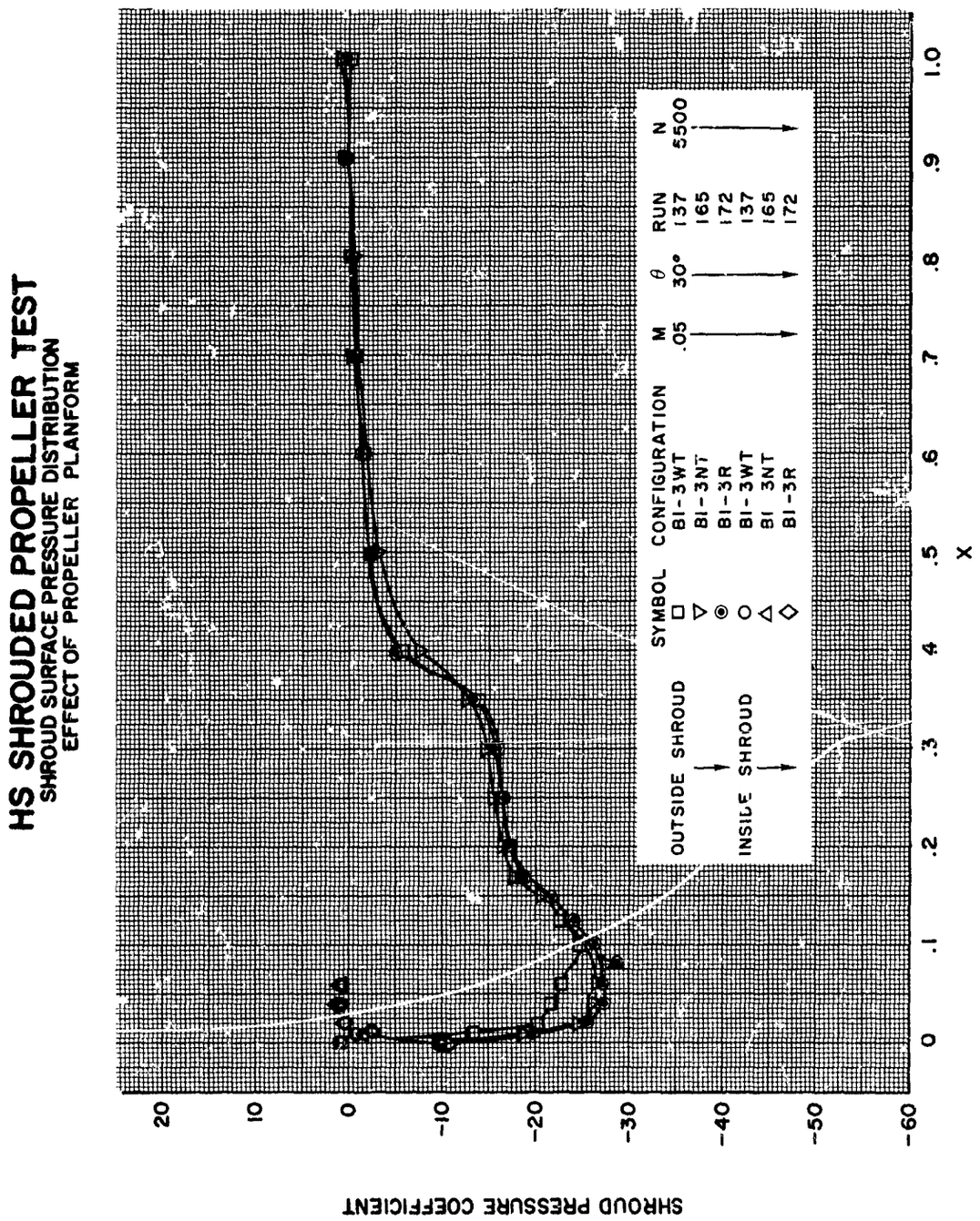
HS SHROUDED PROPELLER TEST
SHROUD SURFACE PRESSURE DISTRIBUTION
EFFECT OF PROPELLER PLANFORM
SHROUD PRESSURE COEFFICIENT
20
10
0
-10
-20
-30
-40
-50
-60
0
.1
.2
.3
.4
.5
.6
.7
.8
.9
1.0
X
OUTSIDE SHROUD
INSIDE SHROUD
SYMBOL
CONFIGURATION
M
θ
RUN
N
BI-3WT
BI-3NT
BI-3R
BI-3WT
BI 3NT
BI-3R
.05
30°
137
165
172
137
165
172
5500

FIGURE 230

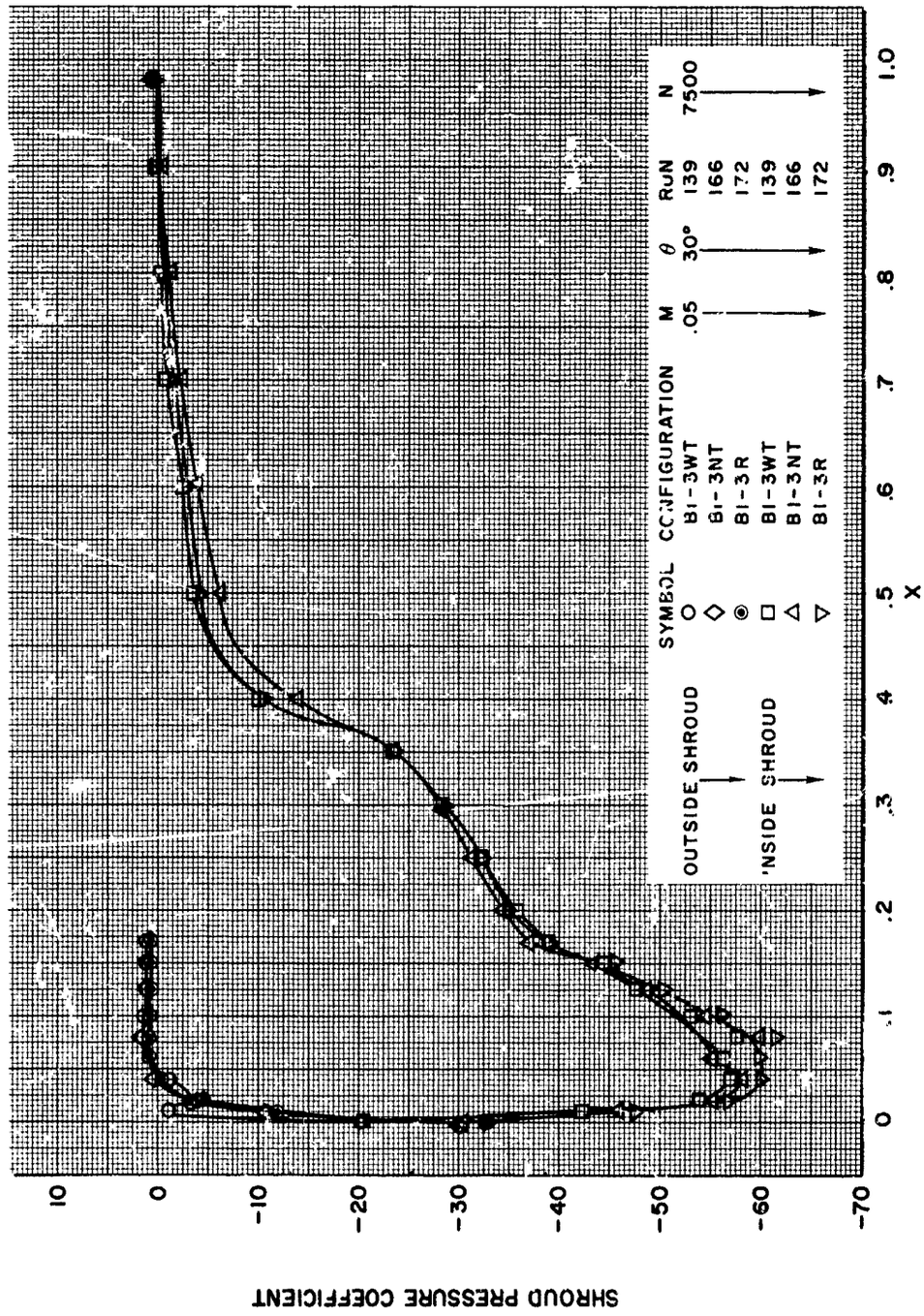
HS SHROUDED PROPELLER TEST
SHROUD SURFACE PRESSURE DISTRIBUTION
EFFECT OF PROPELLER PLANFORM
SHROUD PRESSURE COEFFICIENT
10
0
-10
-20
-30
-40
-50
-60
-70
0
.1
.2
.3
.4
.5
.6
.7
.8
.9
1.0
X
OUTSIDE SHROUD
INSIDE SHROUD
SYMBOL CONFIGURATION M θ RUN N
BI-3WT .05 30° 139 7500
BI-3NT 166
BI-3R 172
BI-3WT 139
BI-3NT 166
BI-3R 172

FIGURE 231

HS SHROUDED PROPELLER TEST

RADIAL DISTRIBUTION OF PROPELLER PLANE AXIAL VELOCITIES

EFFECT OF RPM

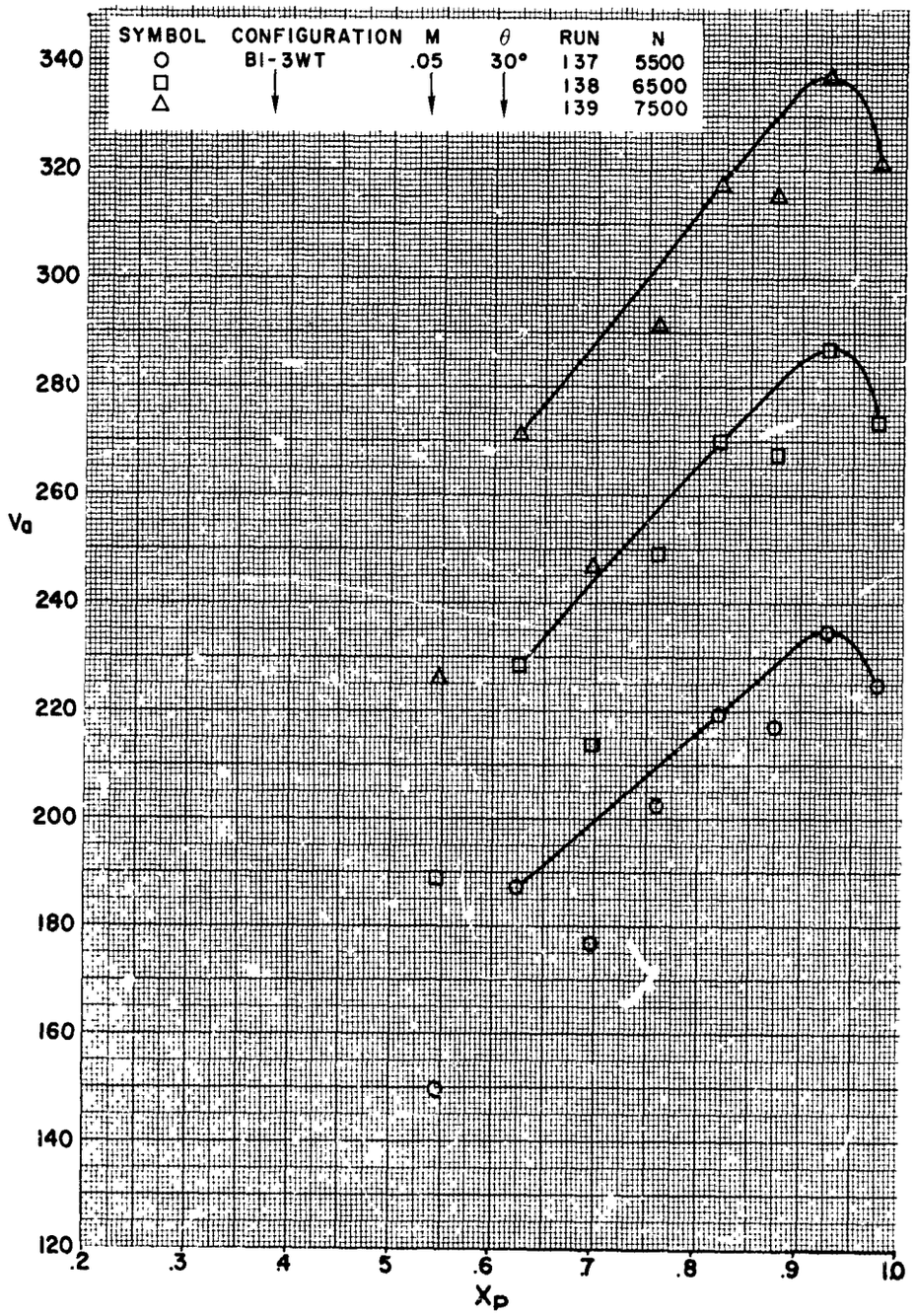

FIGURE 232

HS SHROUDED PROPELLER TEST

RADIAL DISTRIBUTION OF PROPELLER PLANE AXIAL VELOCITIES

EFFECT OF RPM

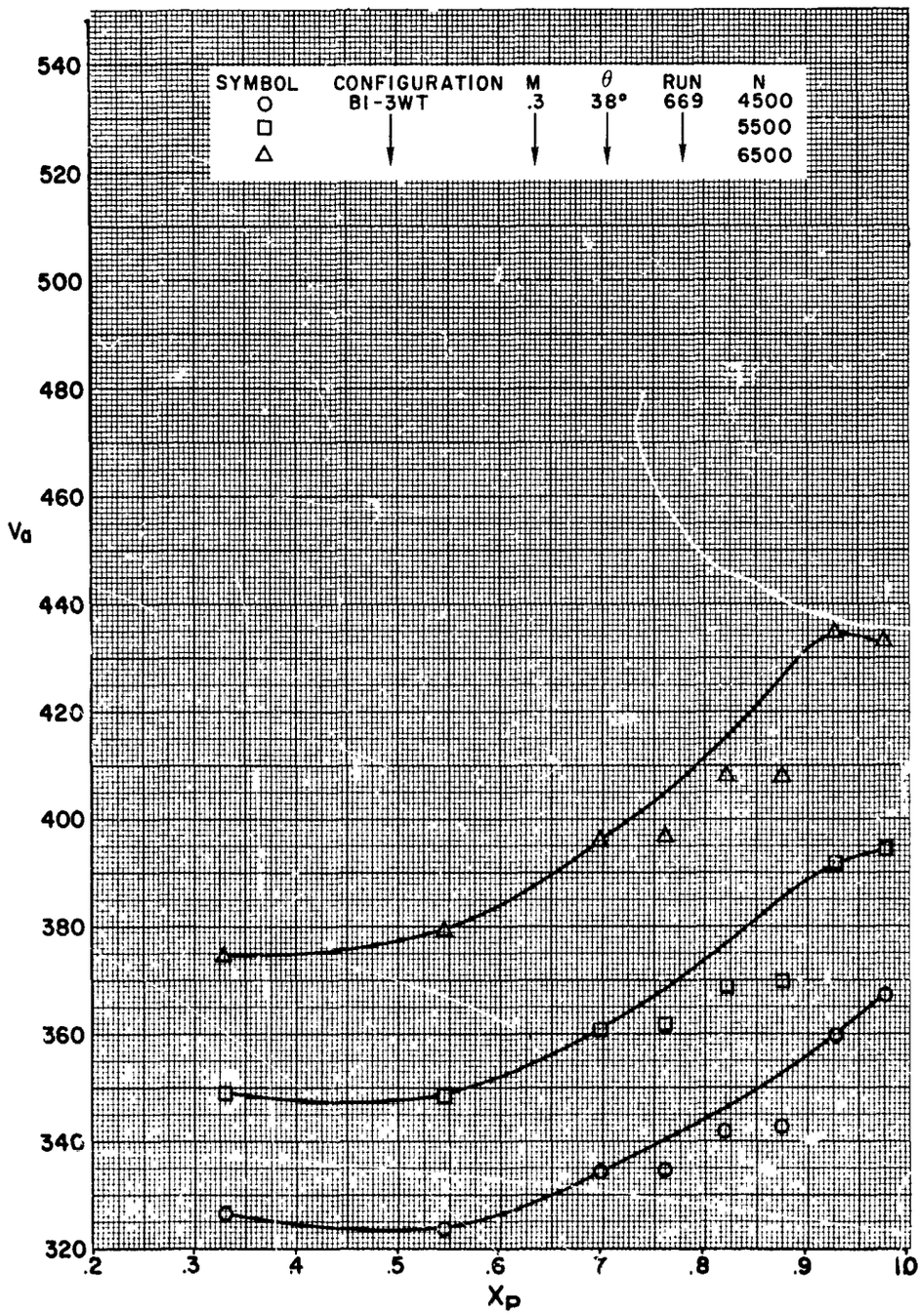

FIGURE 233

HS SHROUDED PROPELLER TEST

RADIAL DISTRIBUTION OF PROPELLER PLANE AXIAL VELOCITIES

EFFECT OF BLADE ANGLE

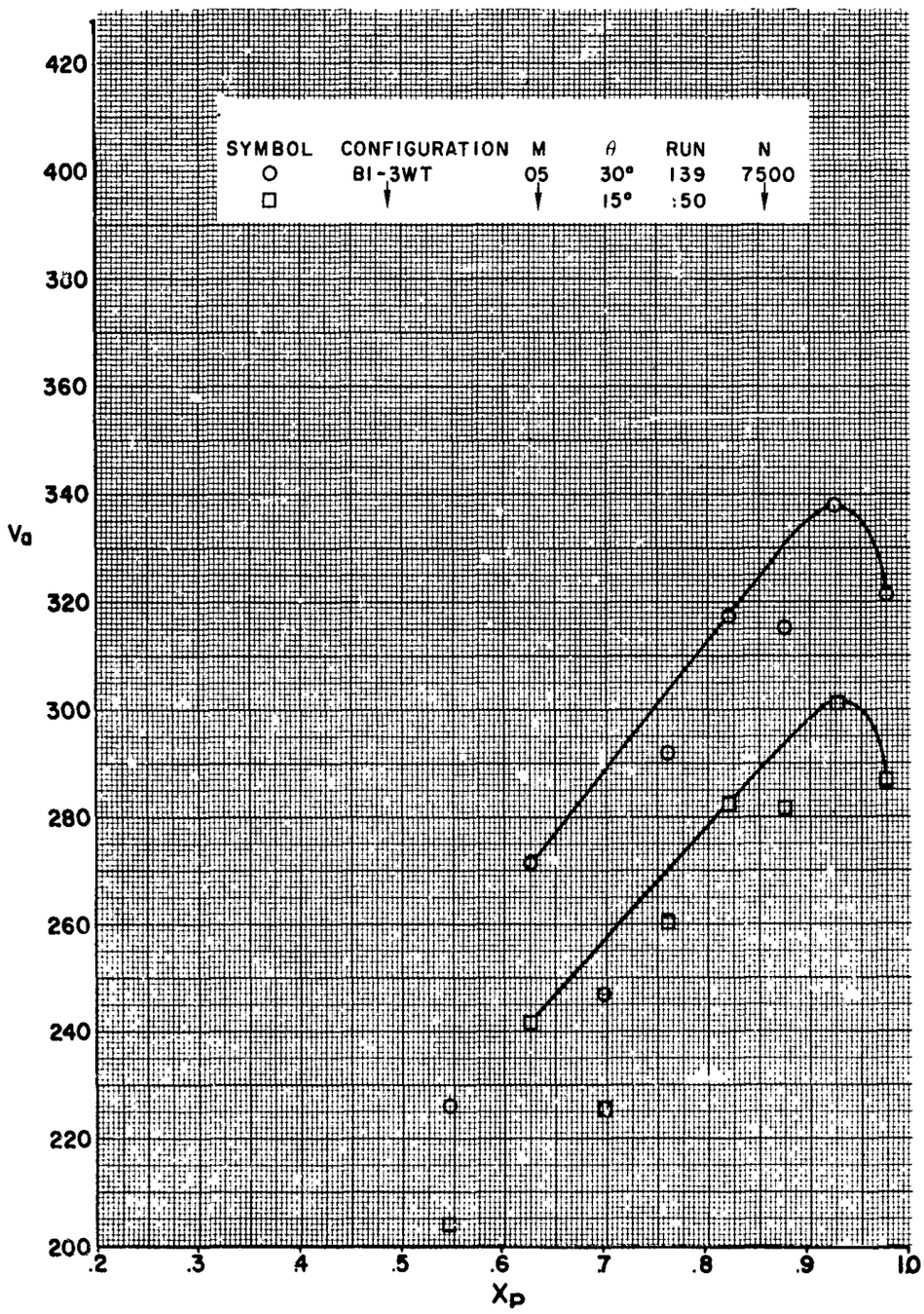

FIGURE 234

HS SHROUDED PROPELLER TEST

RADIAL DISTRIBUTION OF PROPELLER PLANE AXIAL VELOCITIES

EFFECT OF BLADE ANGLE

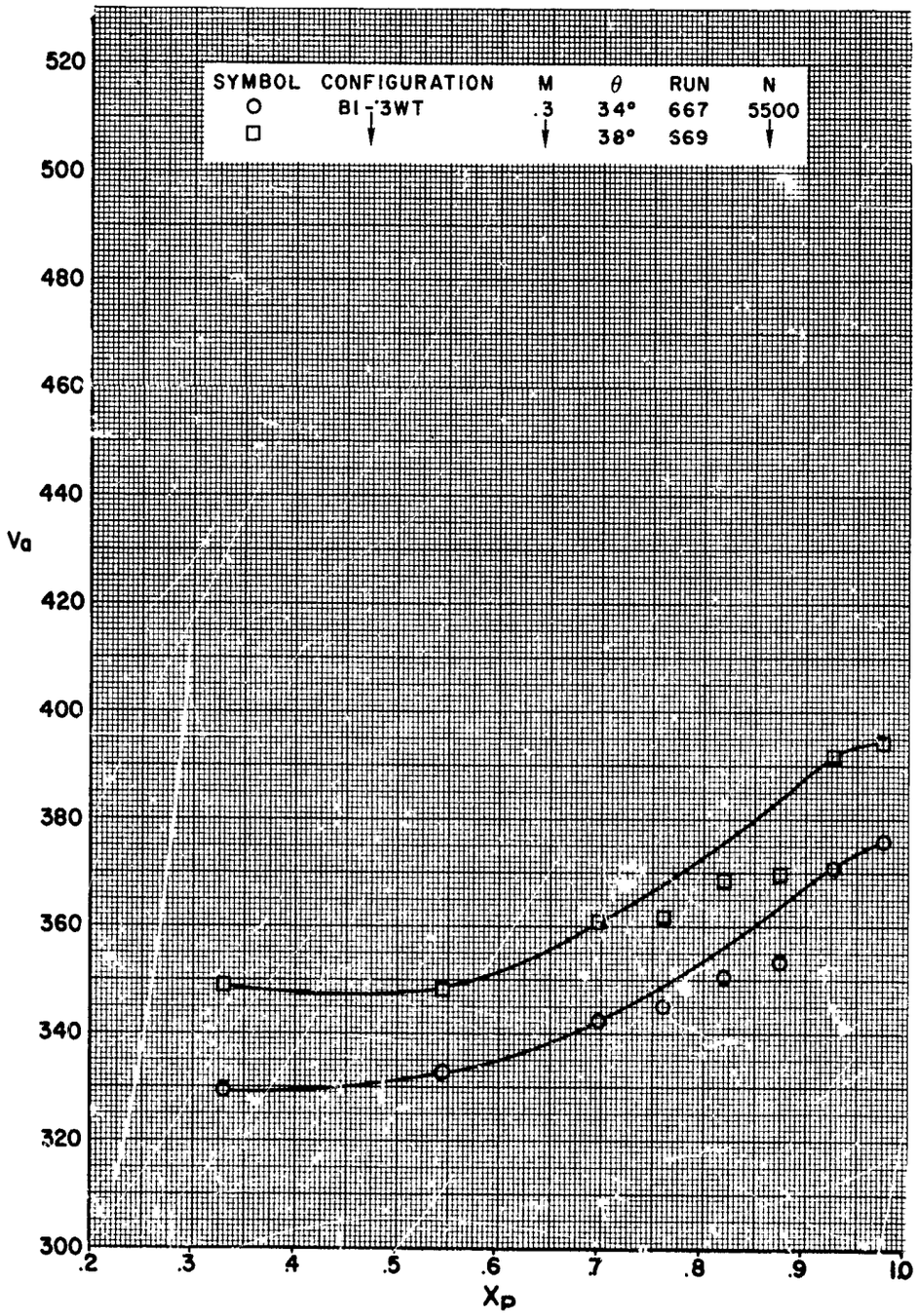

FIGURE 235

HS SHROUDED PROPELLER TEST

RADIAL DISTRIBUTION OF PROPELLER PLANE AXIAL VELOCITIES

EFFECT OF MACH NUMBER

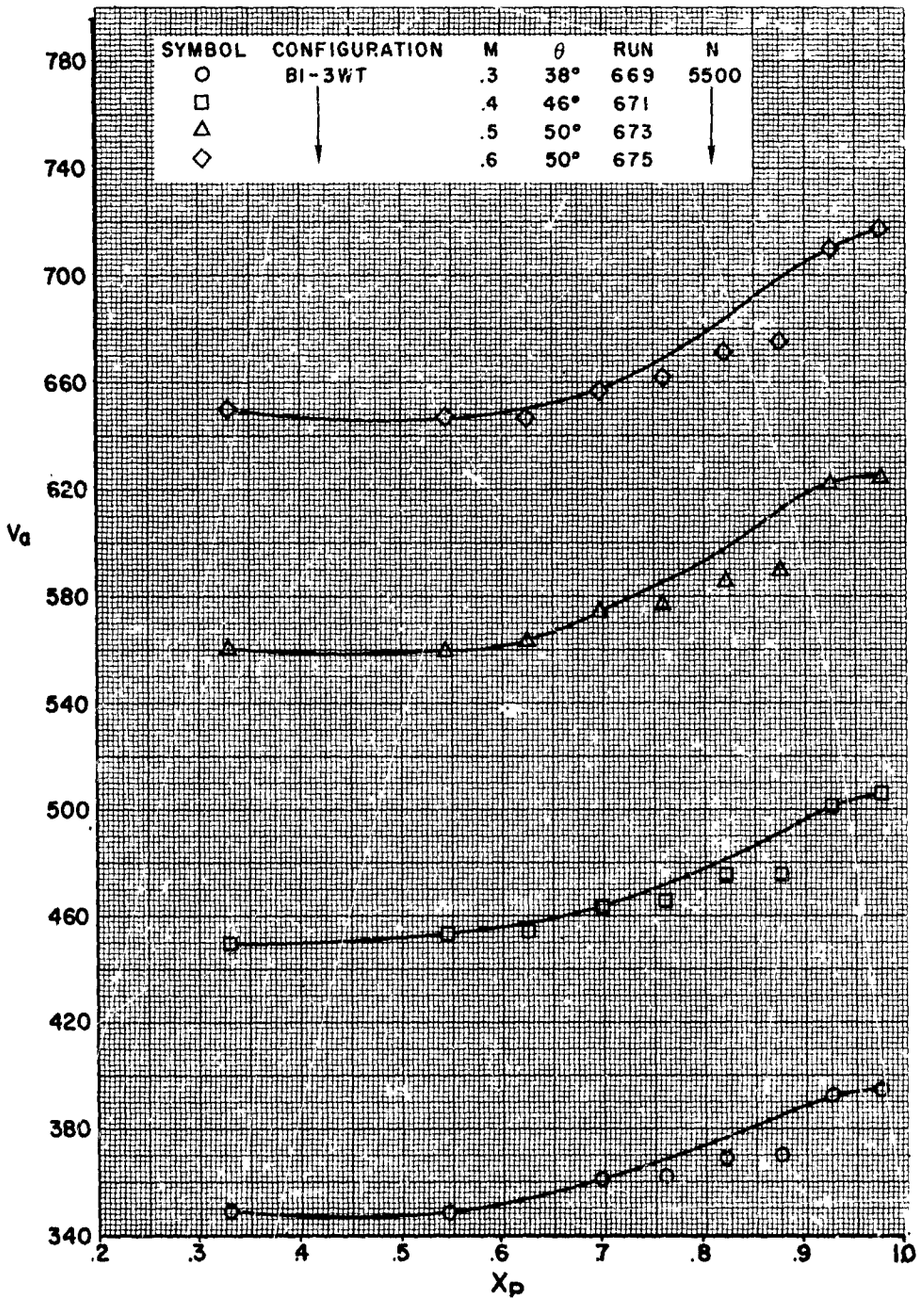

FIGURE 236

HS SHROUDED PROPELLER TEST

RADIAL DISTRIBUTION OF PROPELLER PLANE AXIAL VELOCITIES

EFFECT OF AREA RATIO

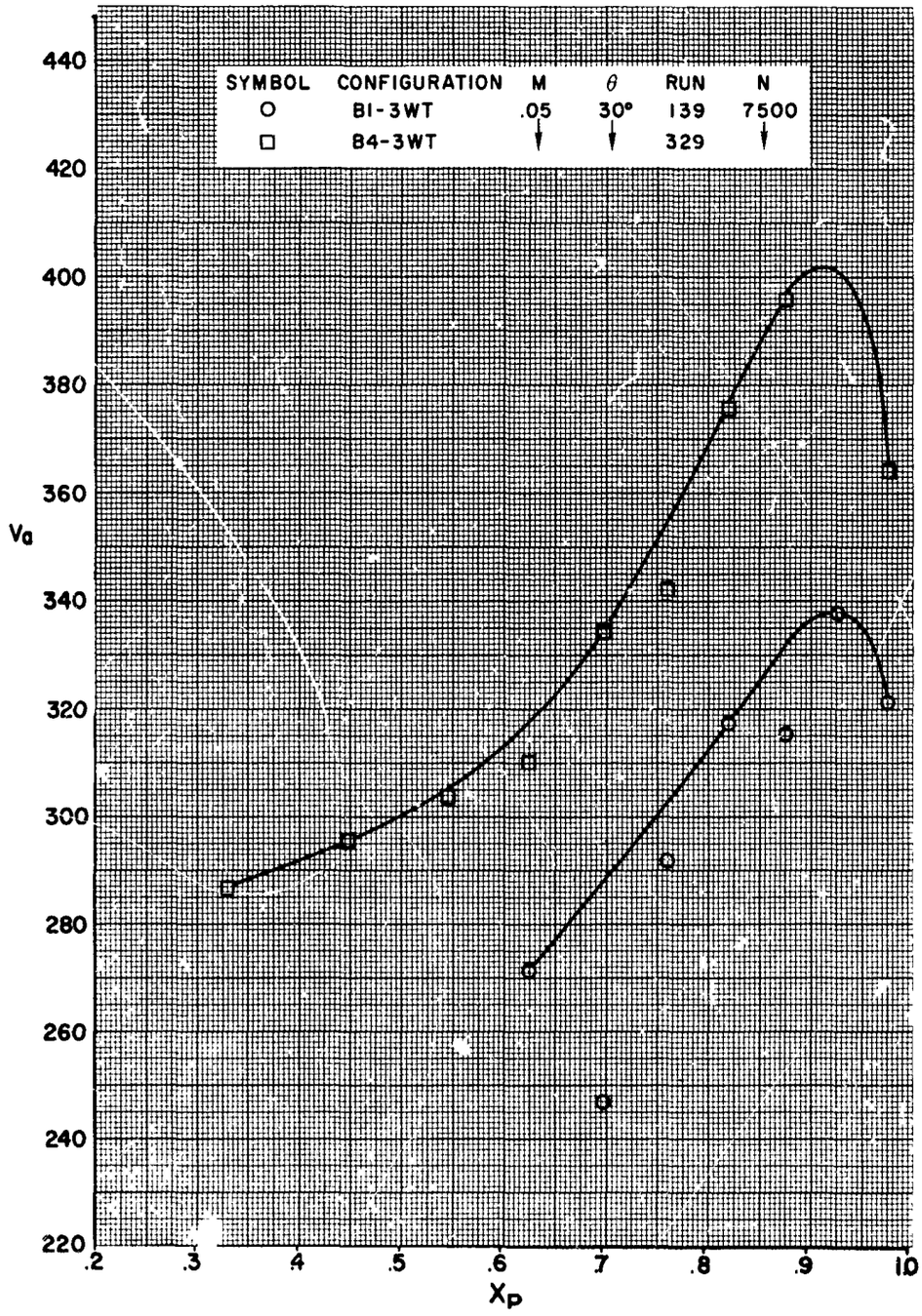

FIGURE 237

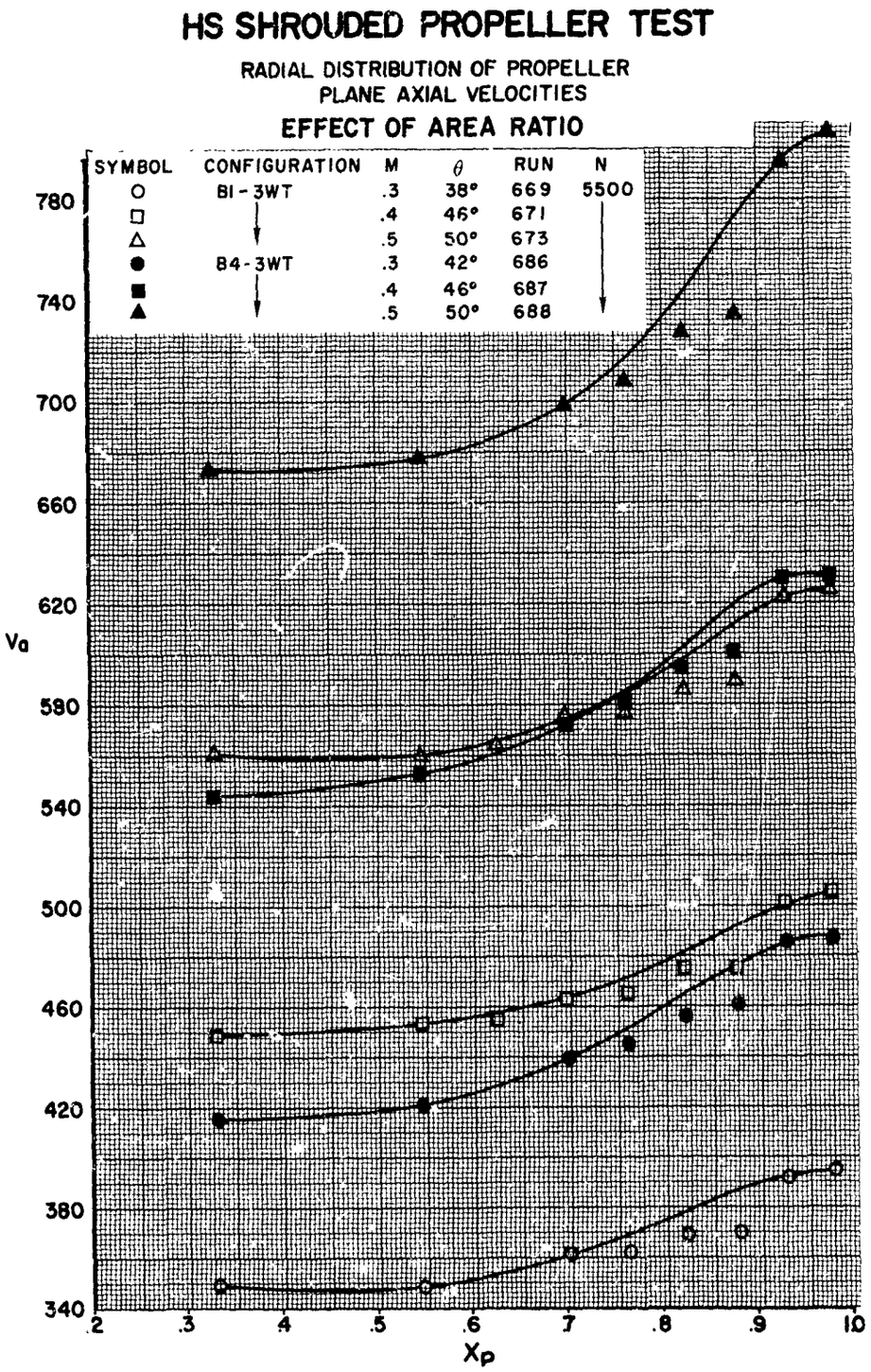
HS SHROUDED PROPELLER TEST
RADIAL DISTRIBUTION OF PROPELLER PLANE AXIAL VELOCITIES
EFFECT OF AREA RATIO
SYMBOL CONFIGURATION M θ RUN N
○ B1-3WT .3 38° 669 5500
□ .4 46° 671
△ .5 50° 673
● B4-3WT .3 42° 686
■ .4 46° 687
▲ .5 50° 688
780
740
700
660
620
580
540
500
460
420
380
340
Va
.2
.3
.4
.5
.6
.7
.8
.9
1.0
Xp

FIGURE 238

HS SHROUDED PROPELLER TEST

RADIAL DISTRIBUTION OF PROPELLER PLANE AXIAL VELOCITIES

EFFECT OF INLET VANE

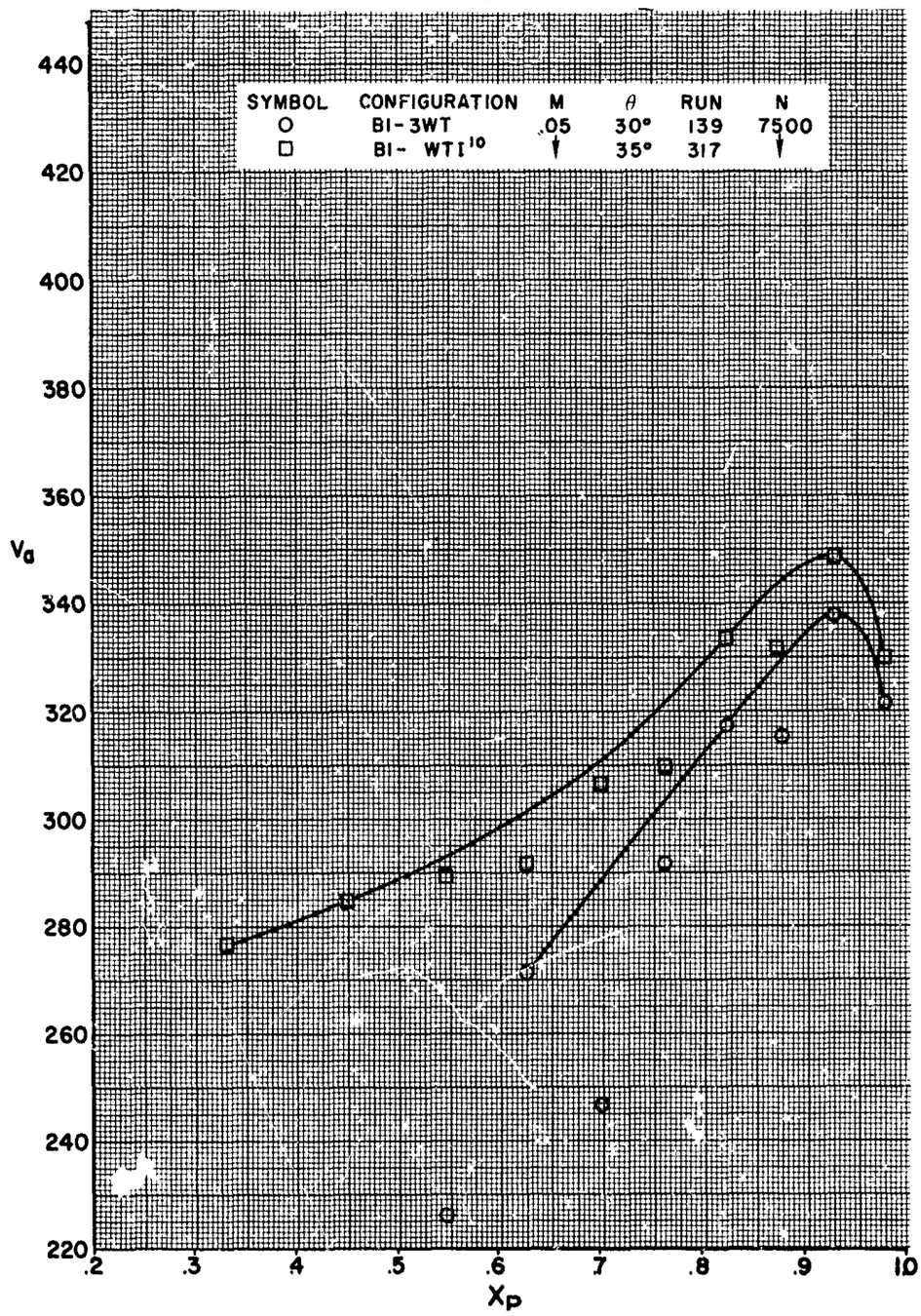

FIGURE 239

HS SHROUDED PROPELLER TEST

RADIAL DISTRIBUTION OF PROPELLER PLANE AXIAL VELOCITIES

EFFECT OF INLET VANE

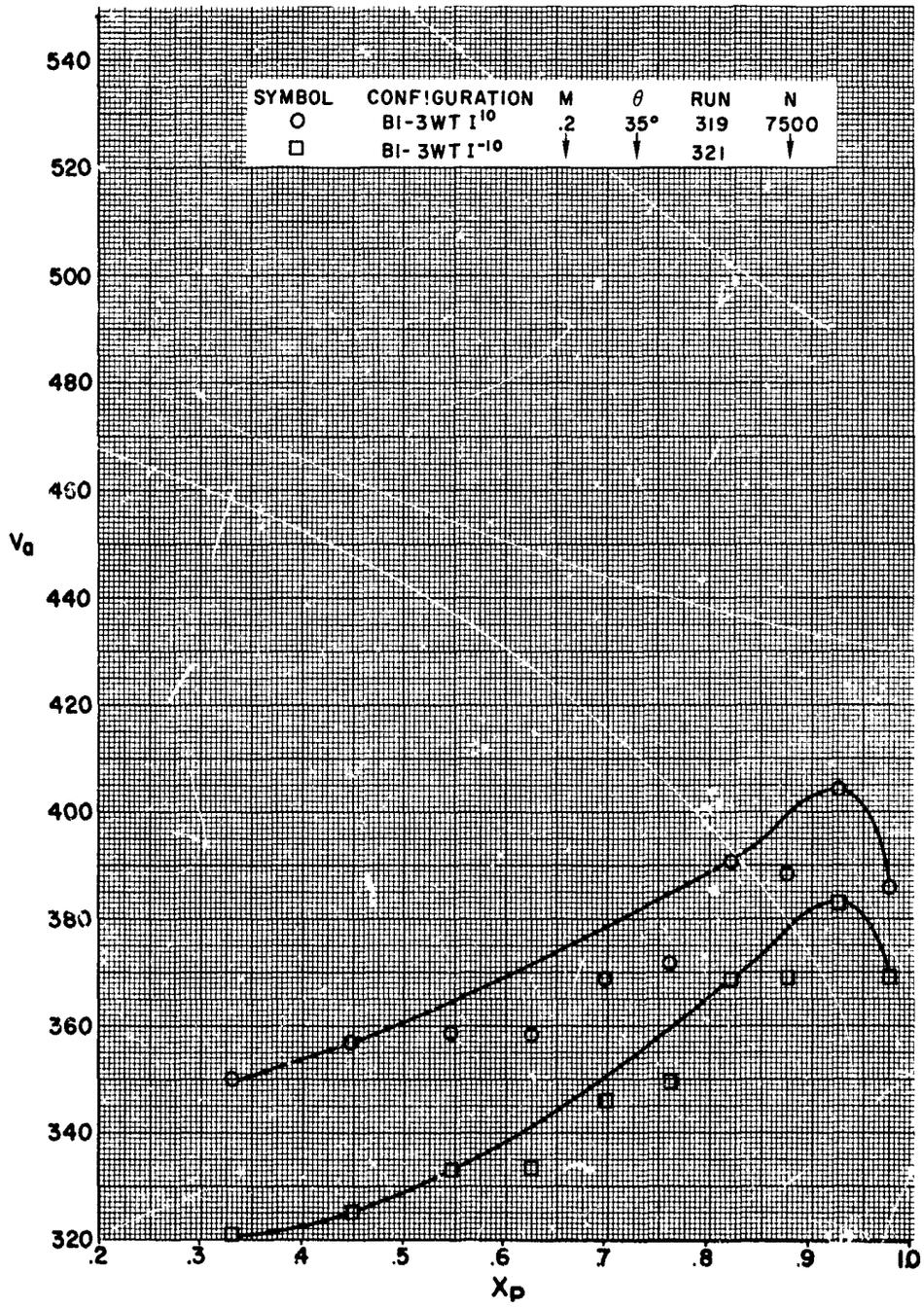

FIGURE 240

HS SHROUDED PROPELLER TEST

RADIAL DISTRIBUTION OF PROPELLER PLANE AXIAL VELOCITIES

EFFECT OF INLET VANE

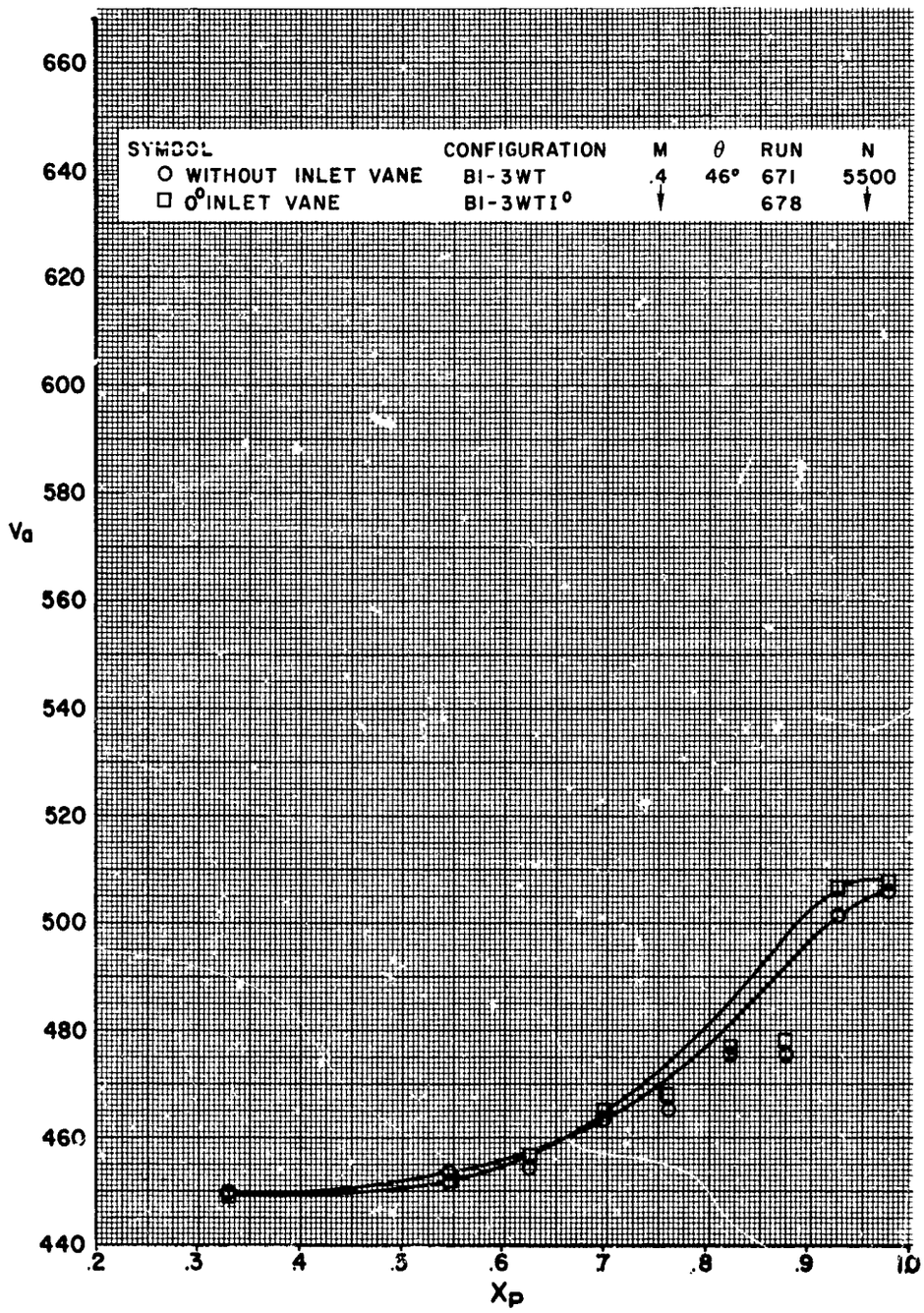

FIGURE 241

HS SHROUDED PROPELLER TEST

RADIAL DISTRIBUTION OF PROPELLER PLANE AXIAL VELOCITIES

EFFECT OF SHROUD LENGTH

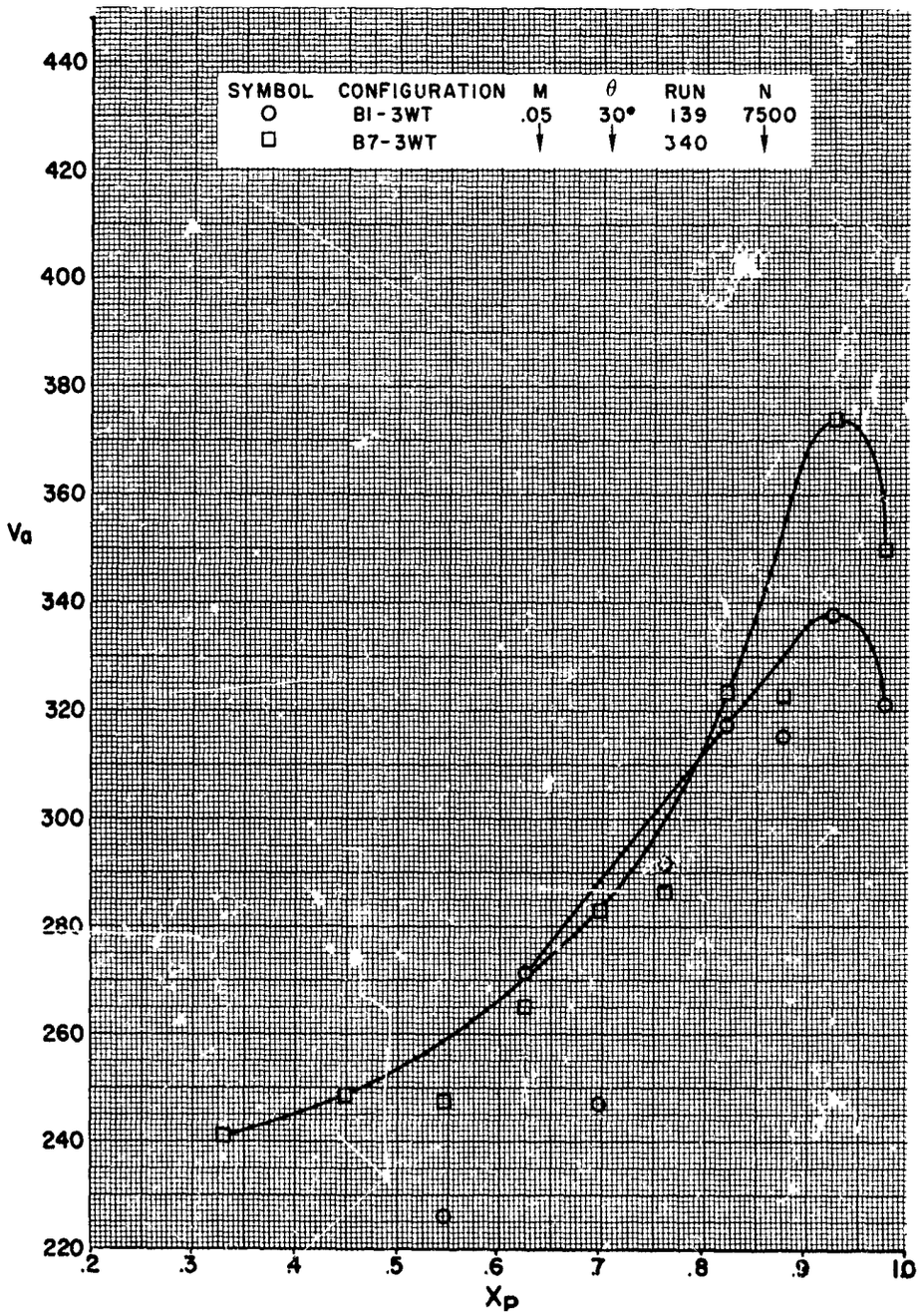

FIGURE 242

HS SHROUDED PROPELLER TEST

RADIAL DISTRIBUTION OF PROPELLER PLANE AXIAL VELOCITIES

EFFECT OF SHROUD LENGTH

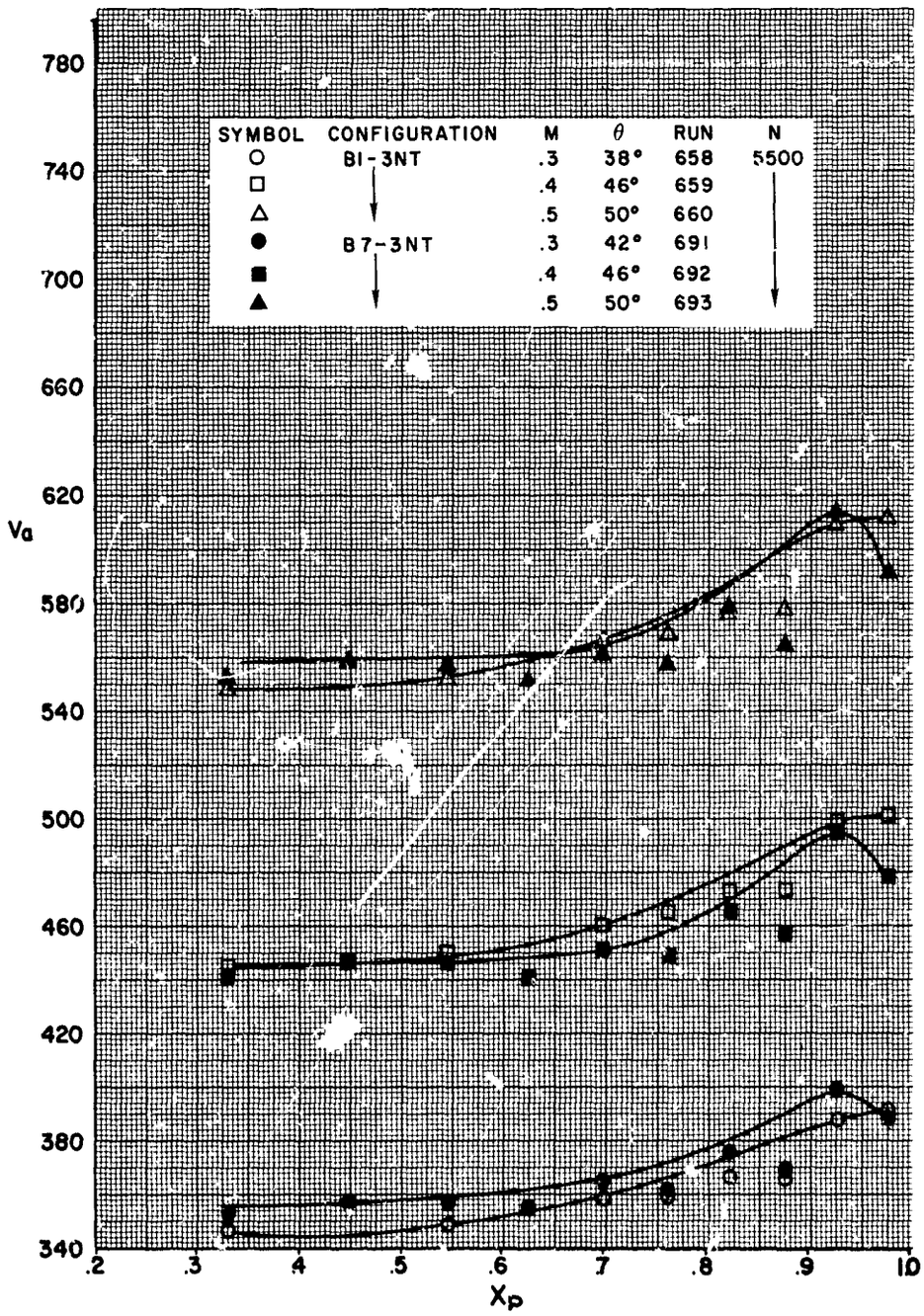

FIGURE 243

HS SHROUDED PROPELLER TEST

RADIAL DISTRIBUTION OF PROPELLER PLANE AXIAL VELOCITIES

EFFECT OF TIP CLEARANCE

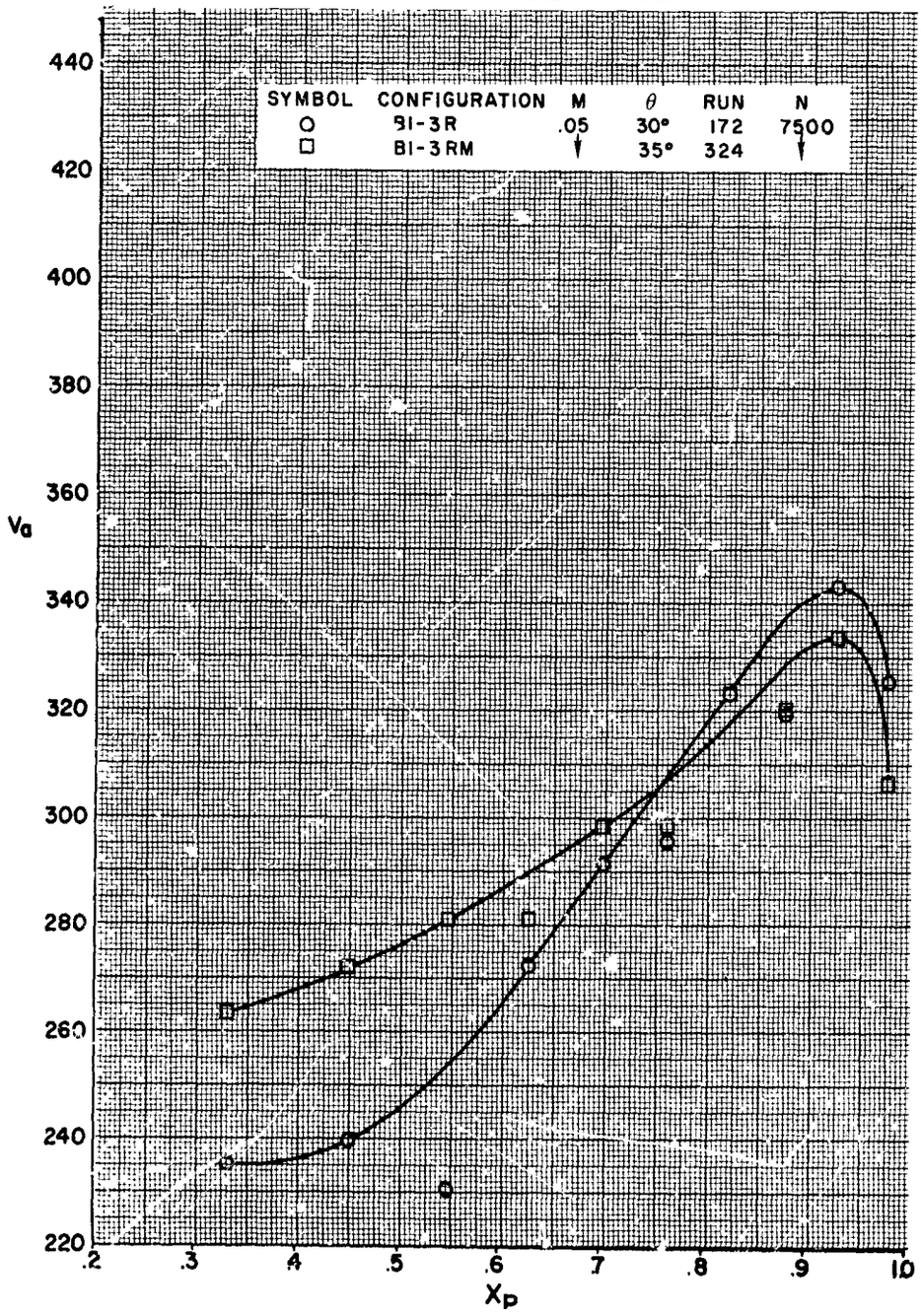

FIGURE 244

HS SHROUDED PROPELLER TEST

RADIAL DISTRIBUTION OF PROPELLER PLANE AXIAL VELOCITIES

EFFECT OF NUMBER OF BLADES

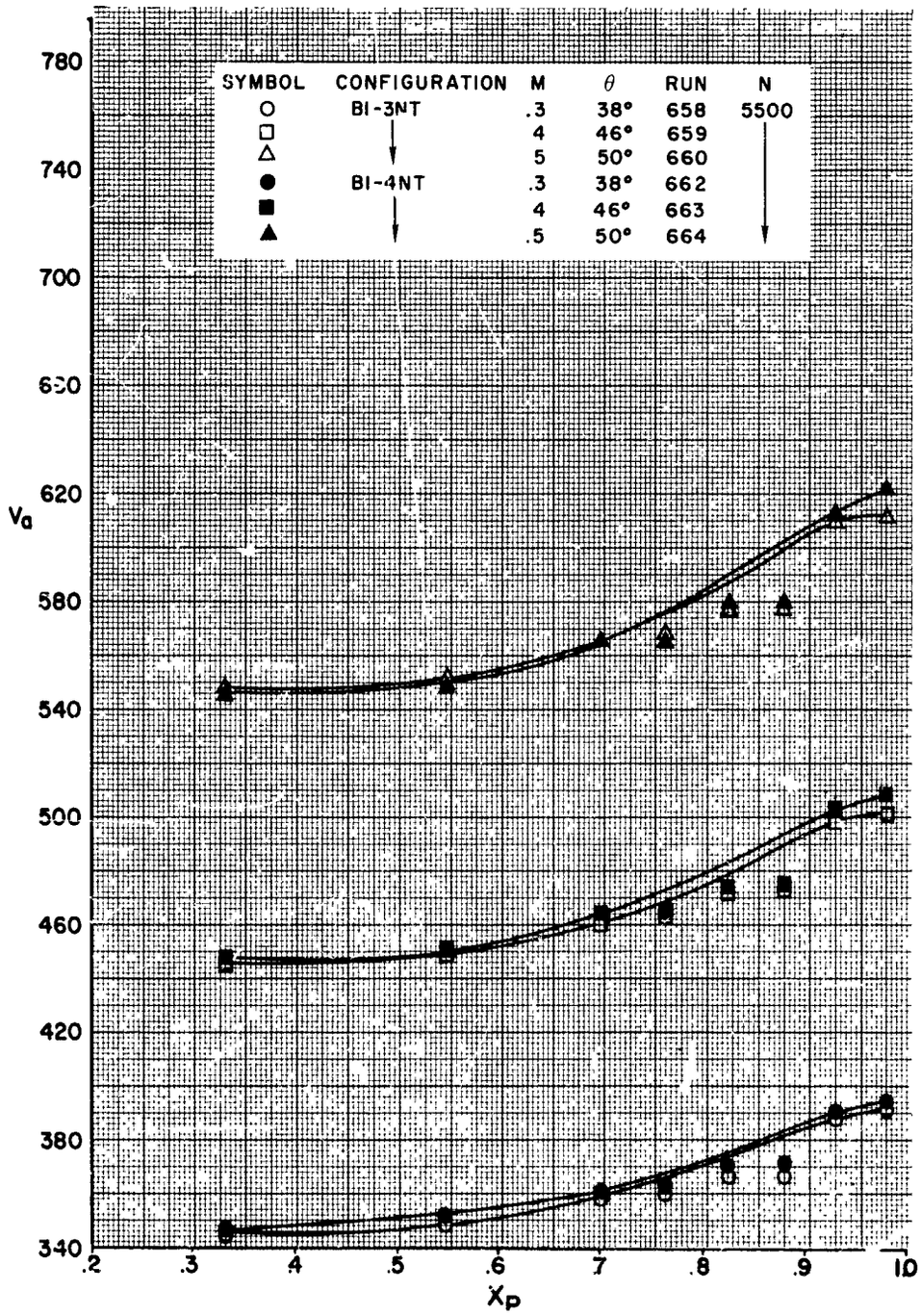

FIGURE 245

HS SHROUDED PROPELLER TEST

RADIAL DISTRIBUTION OF PROPELLER PLANE AXIAL VELOCITIES

EFFECT OF PROPELLER PLANFORM

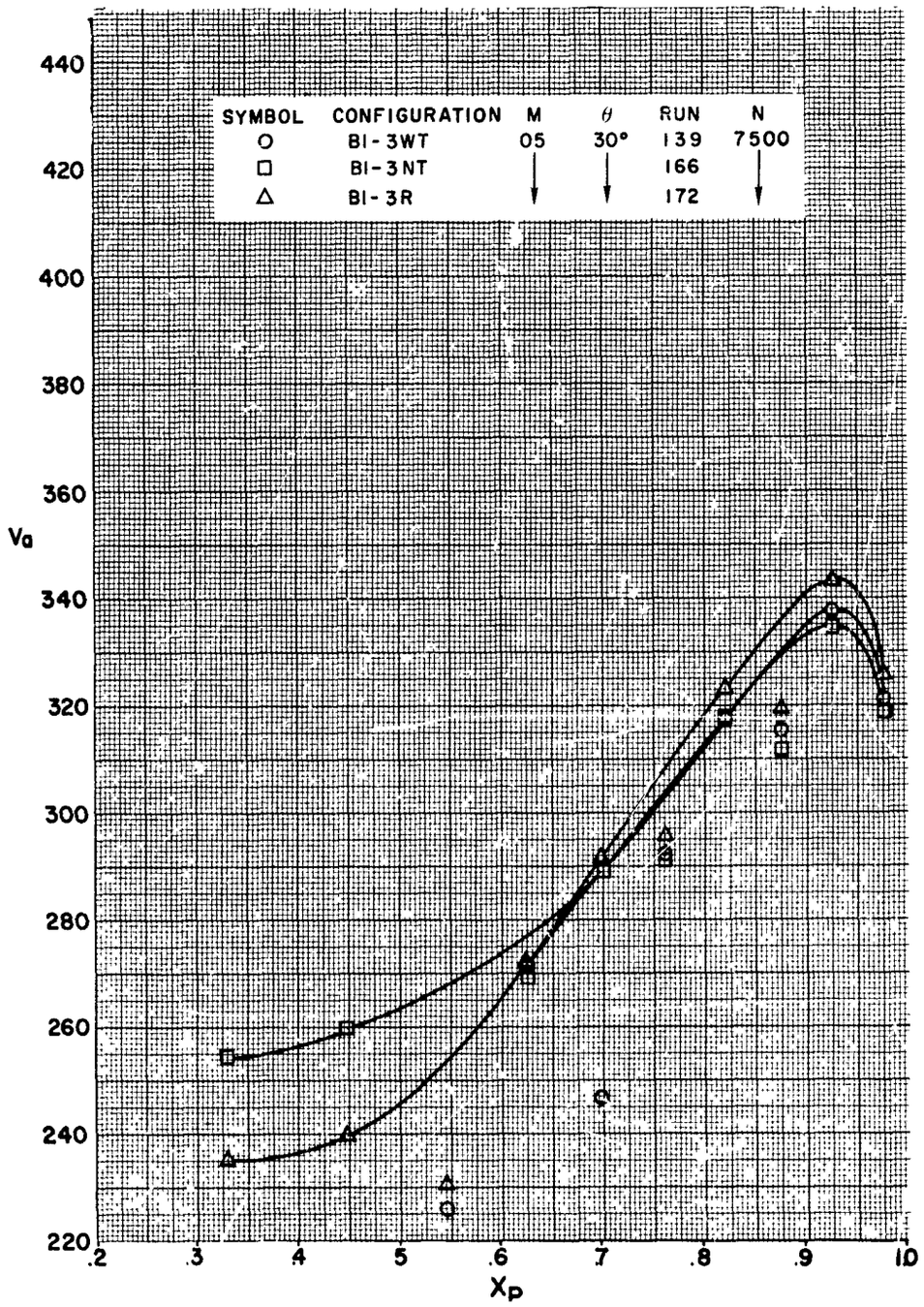

FIGURE 246

HS SHROUDED PROPELLER TEST

RADIAL DISTRIBUTION OF PROPELLER PLANE AXIAL VELOCITIES

EFFECT OF PROPELLER PLANFORM

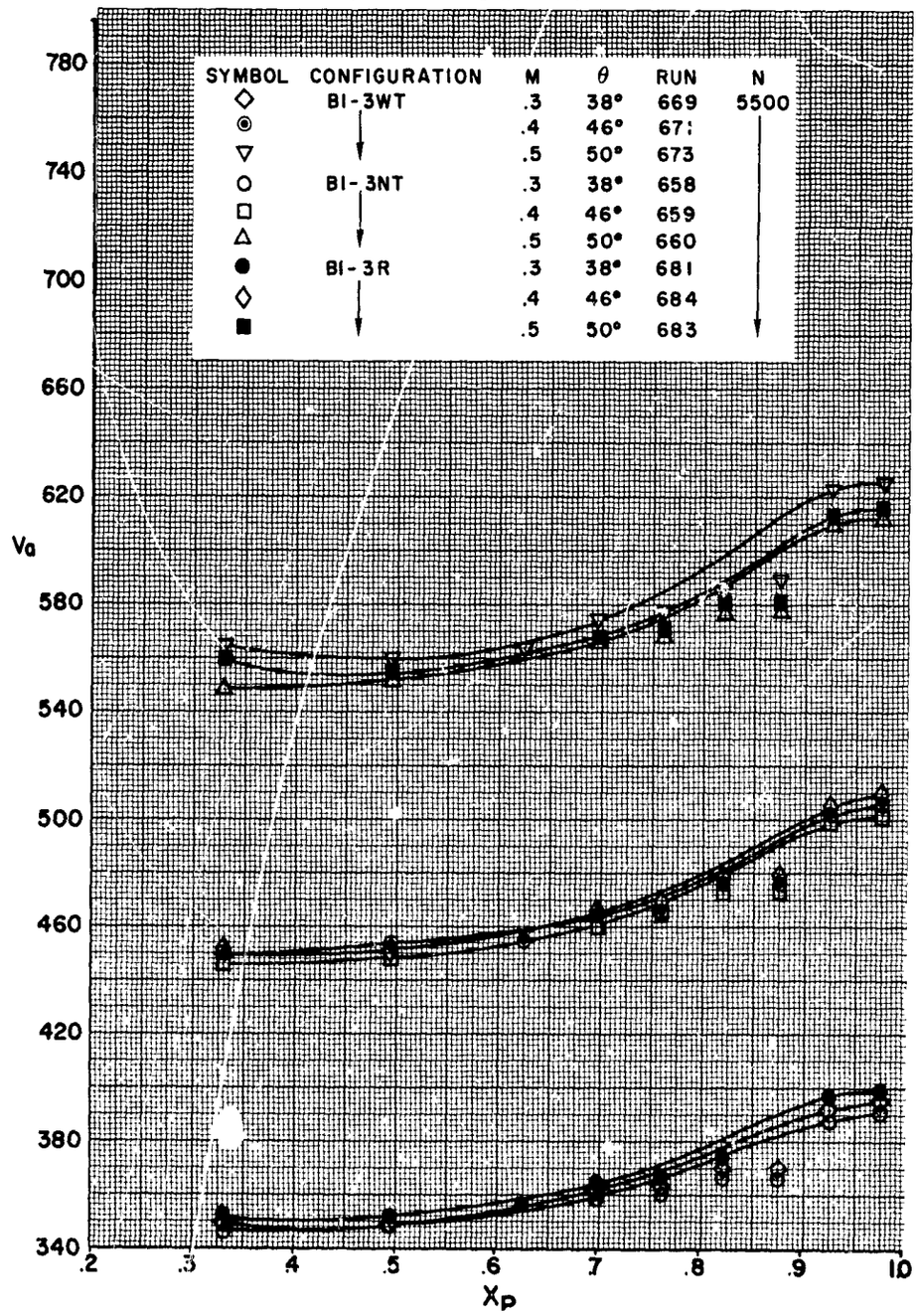

FIGURE 247

HS SHROUDED PROPELLER TEST

RADIAL DISTRIBUTION OF PROPELLER PLANE AXIAL VELOCITIES

EFFECT OF NUMBER OF BLADES

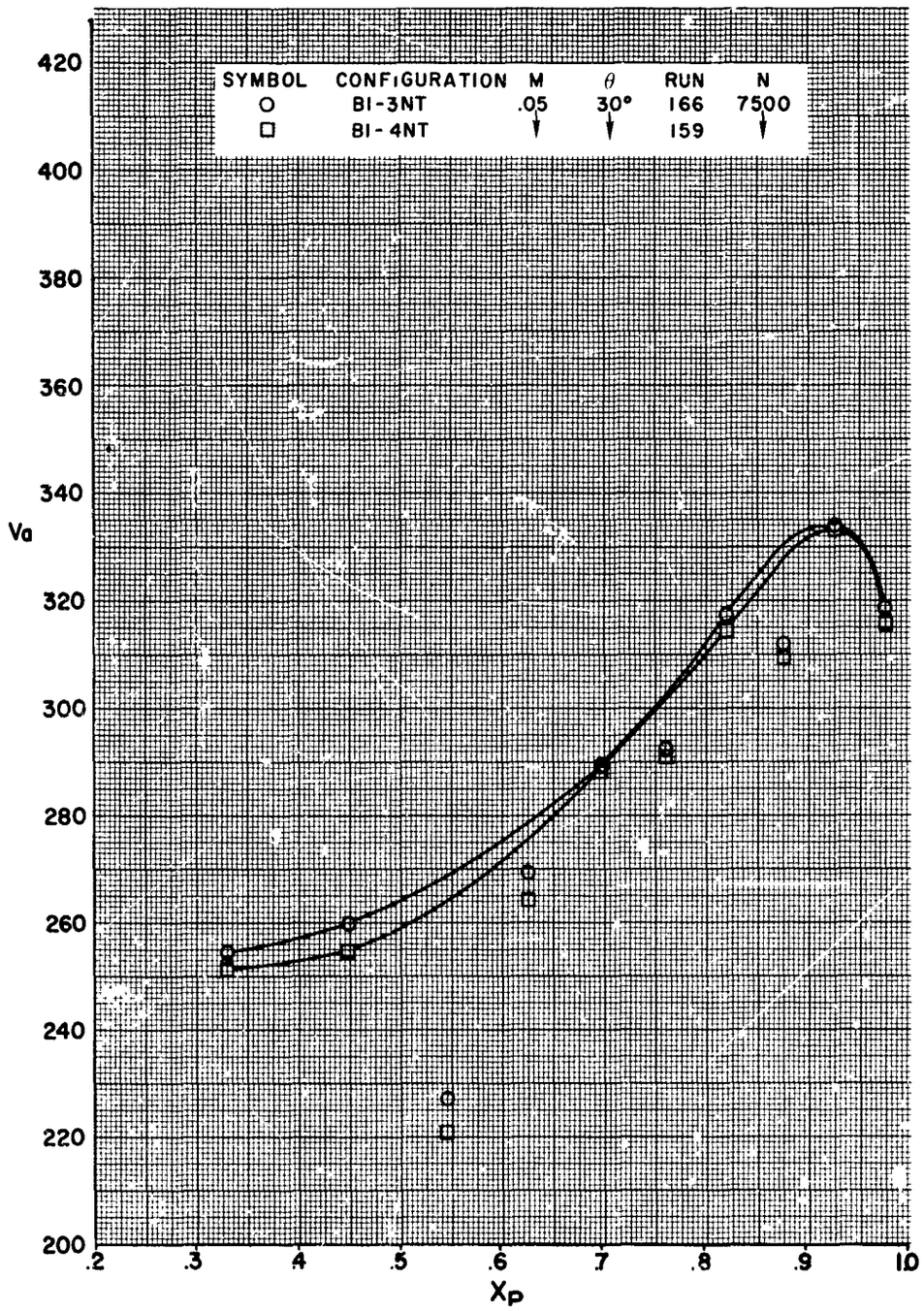

FIGURE 248

HS SHROUDED PROPELLER TEST

RADIAL DISTRIBUTION OF PROPELLER PLANE AXIAL VELOCITIES

EFFECT OF TIP CLEARANCE

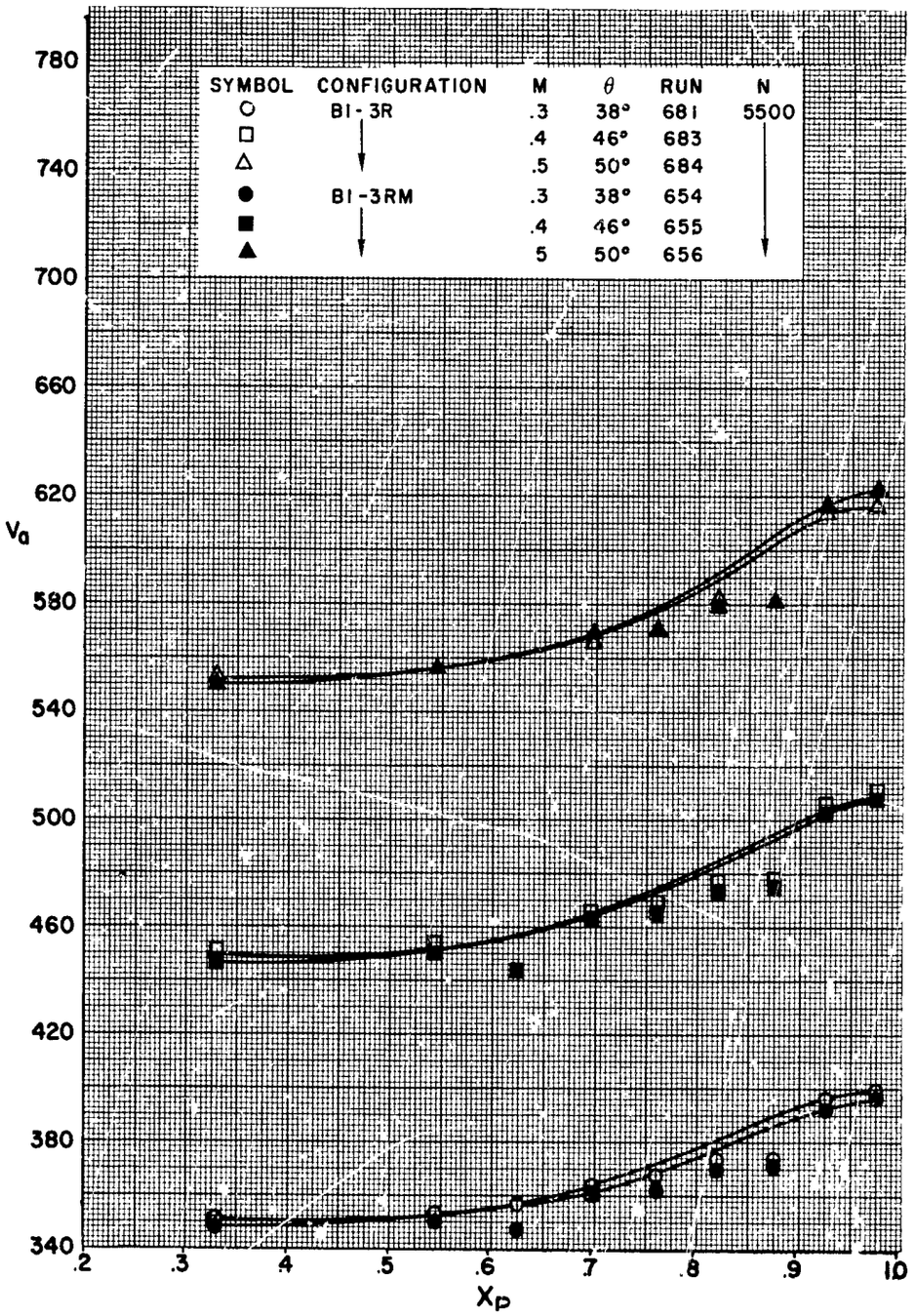

FIGURE 249

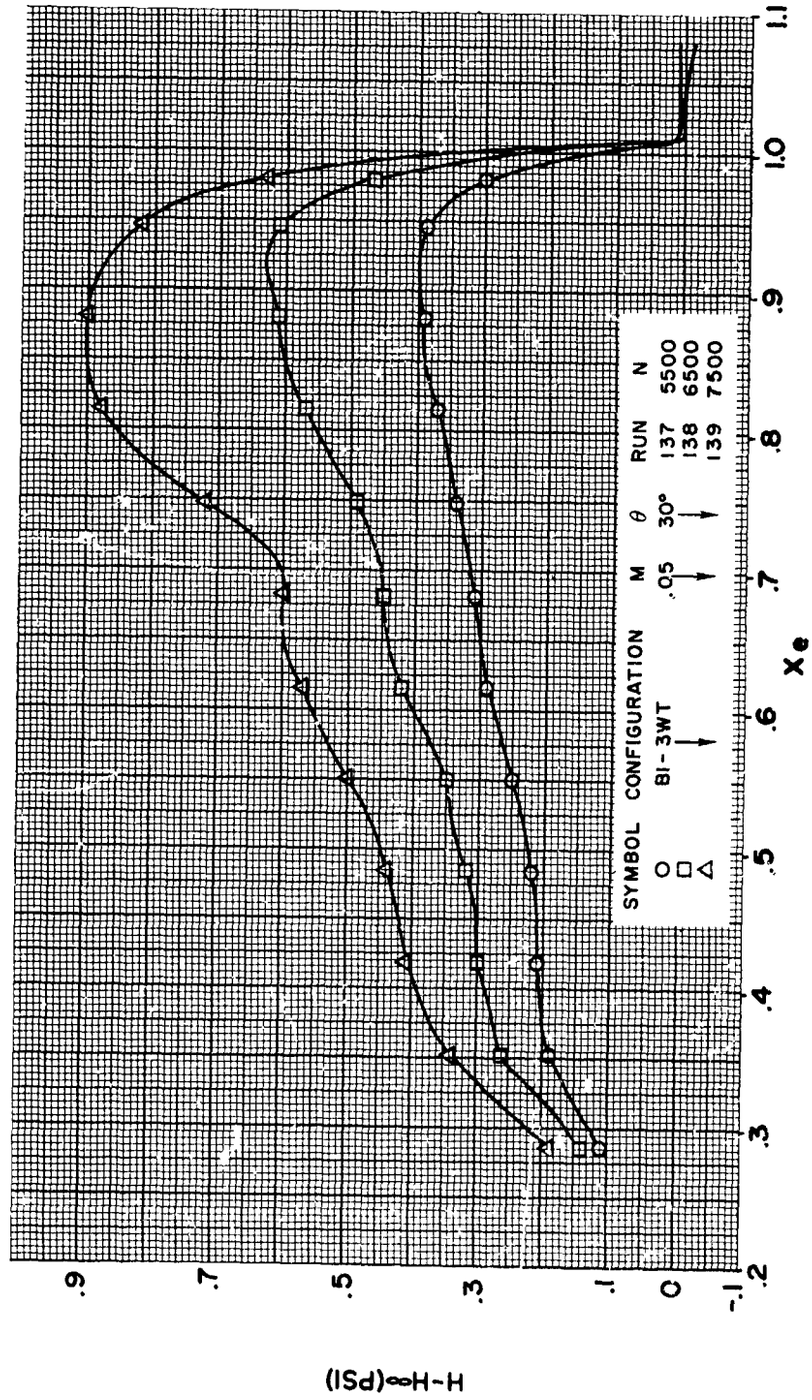

HS SHROUDED PROPELLER TEST
RADIAL TOTAL PRESSURE DISTRIBUTION
AT SHROUD EXIT
EFFECT OF RPM

FIGURE 250

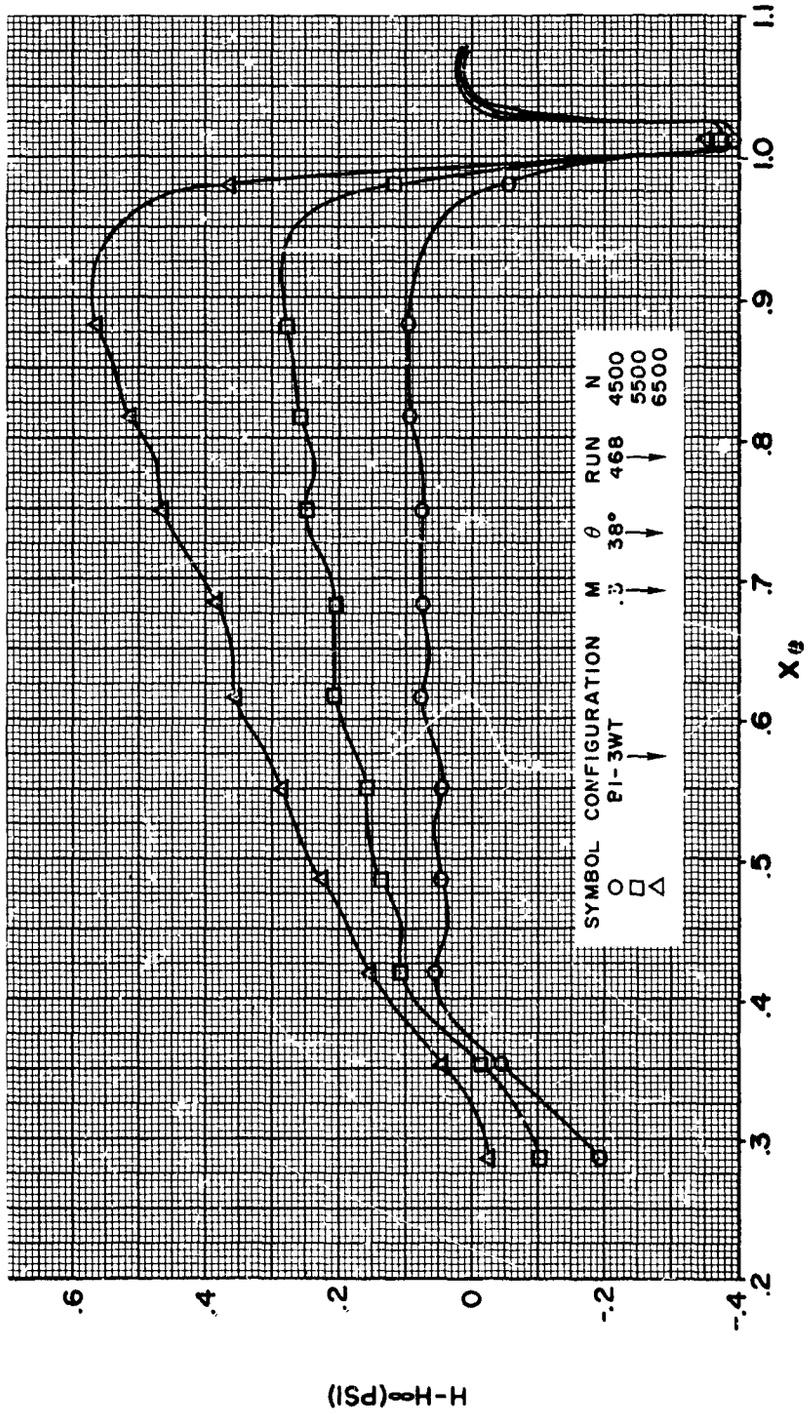

HS SHROUDED PROPELLER TEST
RADIAL TOTAL PRESSURE DISTRIBUTION
AT SHROUD EXIT
EFFECT OF RPM

FIGURE 251

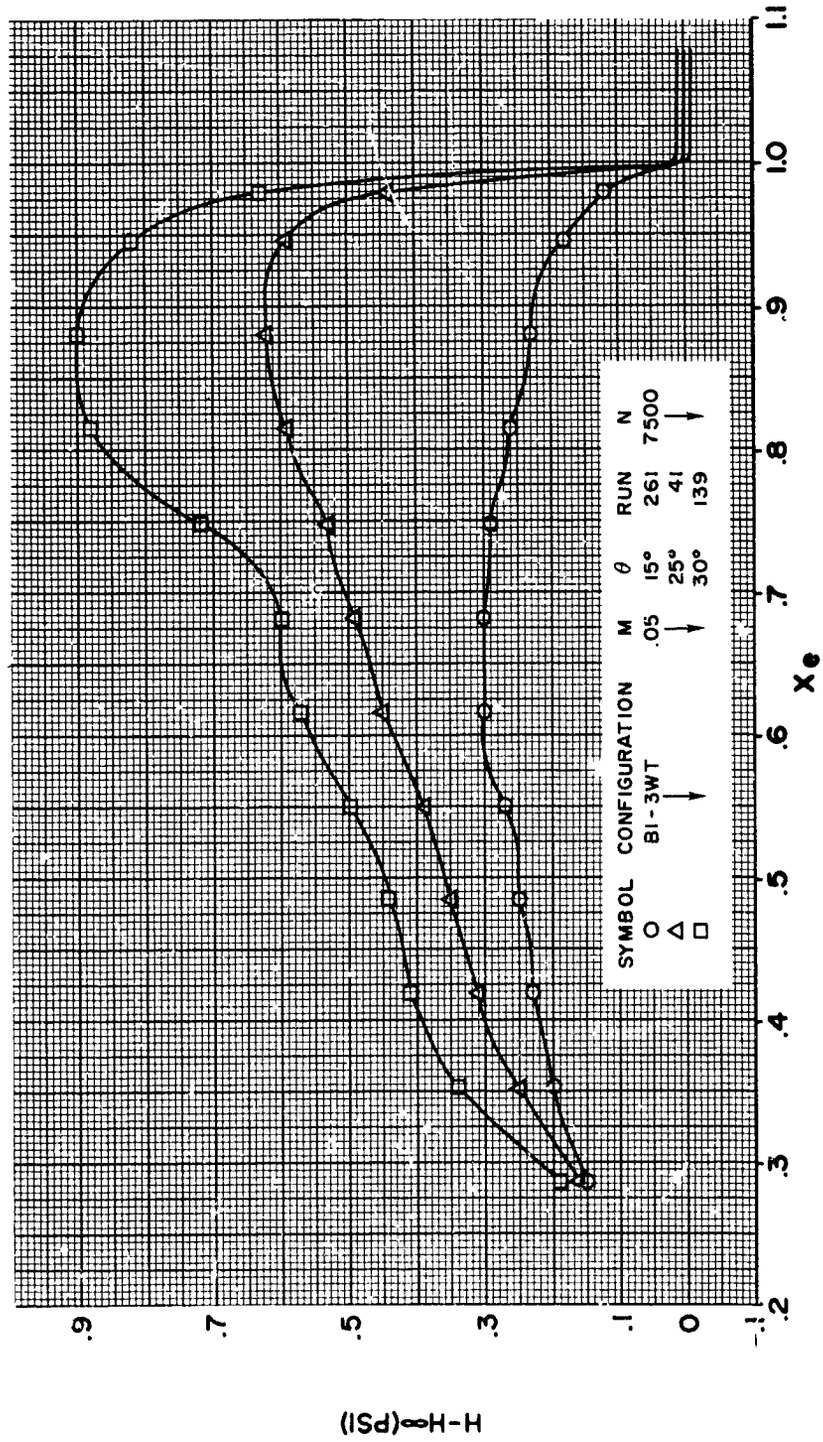

HS SHROUDED PROPELLER TEST
RADIAL TOTAL PRESSURE DISTRIBUTION
AT SHROUD EXIT

EFFECT OF BLADE ANGLE

FIGURE 252

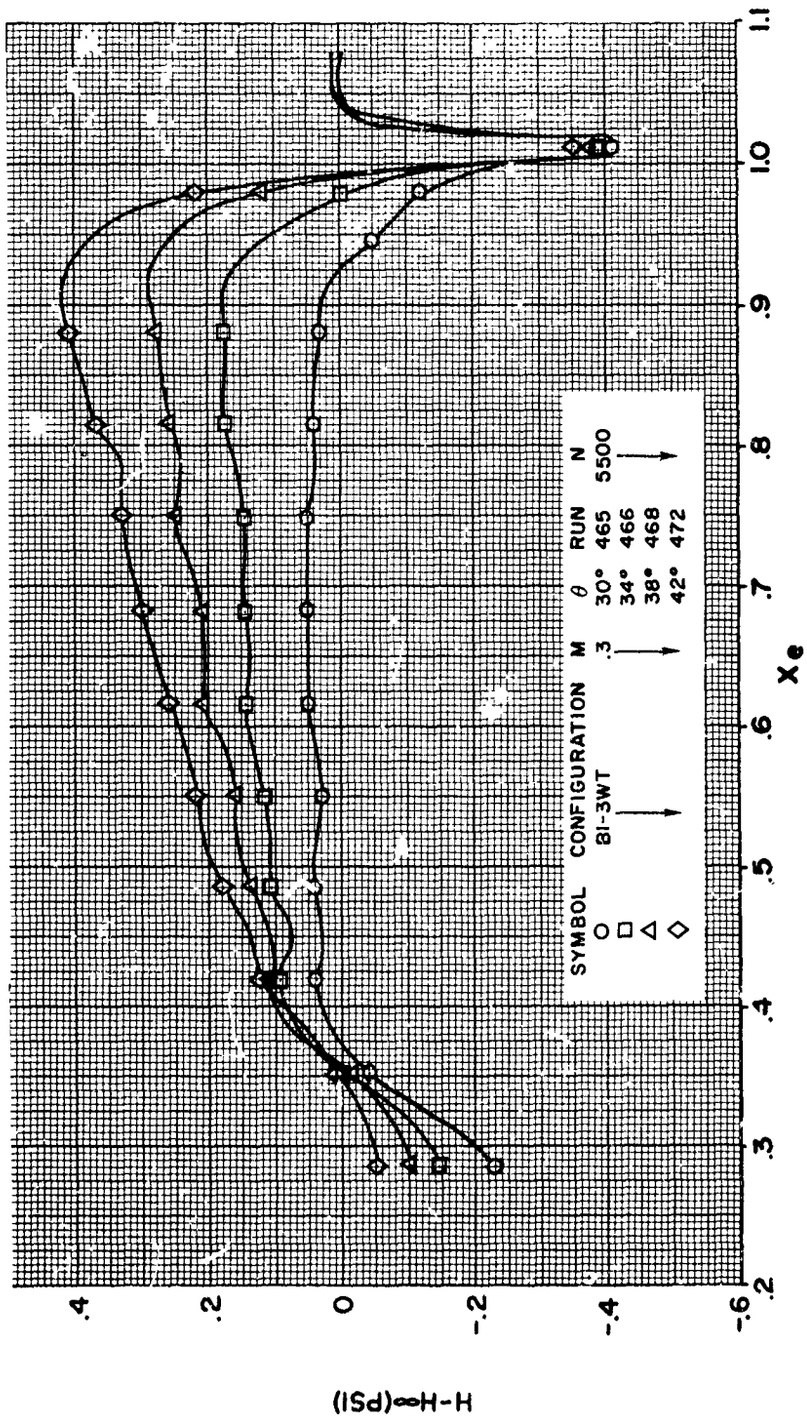

HS SHROUDED PROPELLER TEST
RADIAL TOTAL PRESSURE DISTRIBUTION
AT SHROUD EXIT

EFFECT OF BLADE ANGLE

FIGURE 253

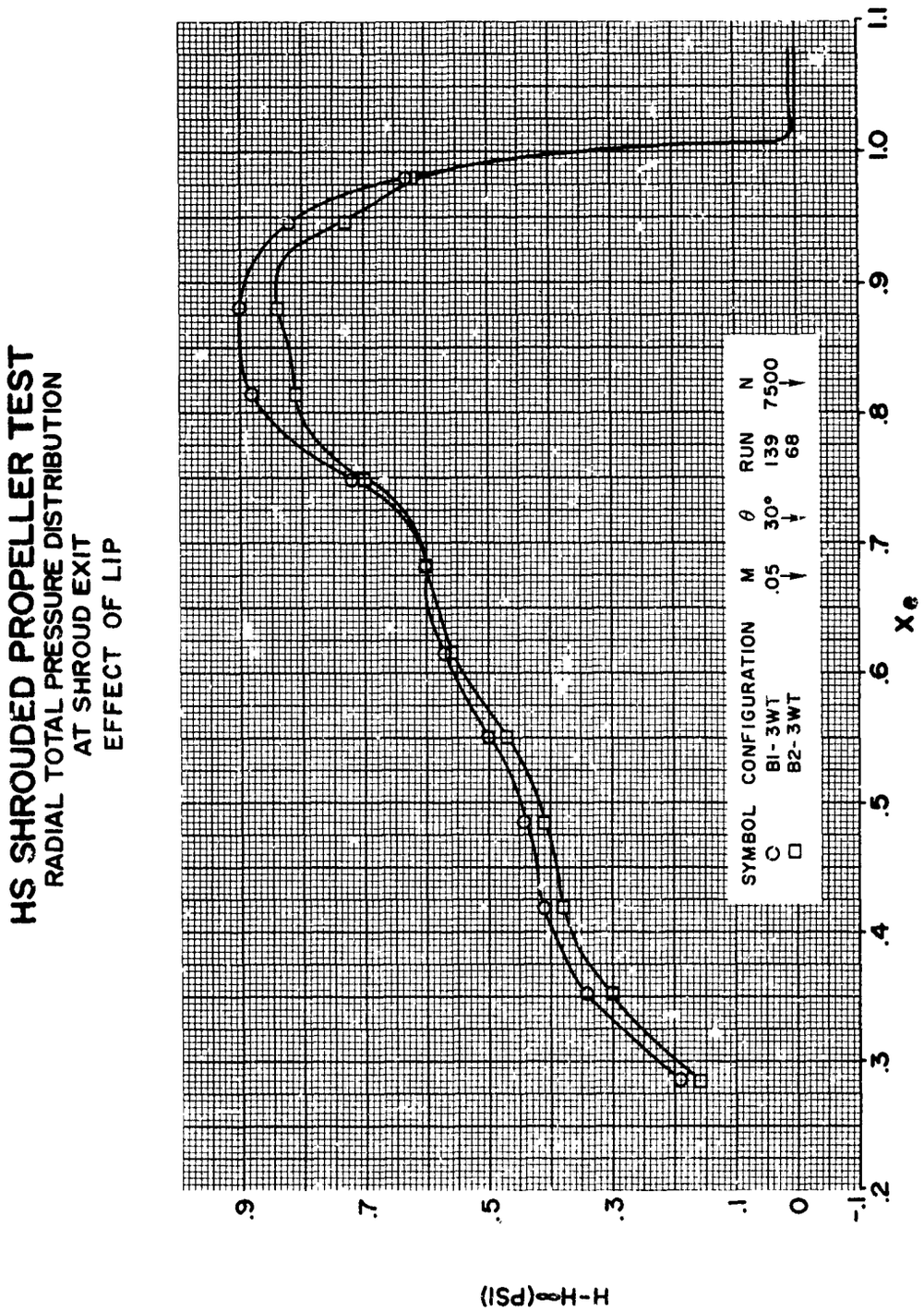
HS SHROUDED PROPELLER TEST
RADIAL TOTAL PRESSURE DISTRIBUTION
AT SHROUD EXIT
EFFECT OF LIP
SYMBOL CONFIGURATION M θ RUN N
○ B1-3WT .05 30° 139 7500
□ B2-3WT 68
H-H∞(PSI)
.9
.7
.5
.3
.1
0
-.1
.2
.3
.4
.5
.6
.7
.8
.9
1.0
1.1
X/R

FIGURE 254

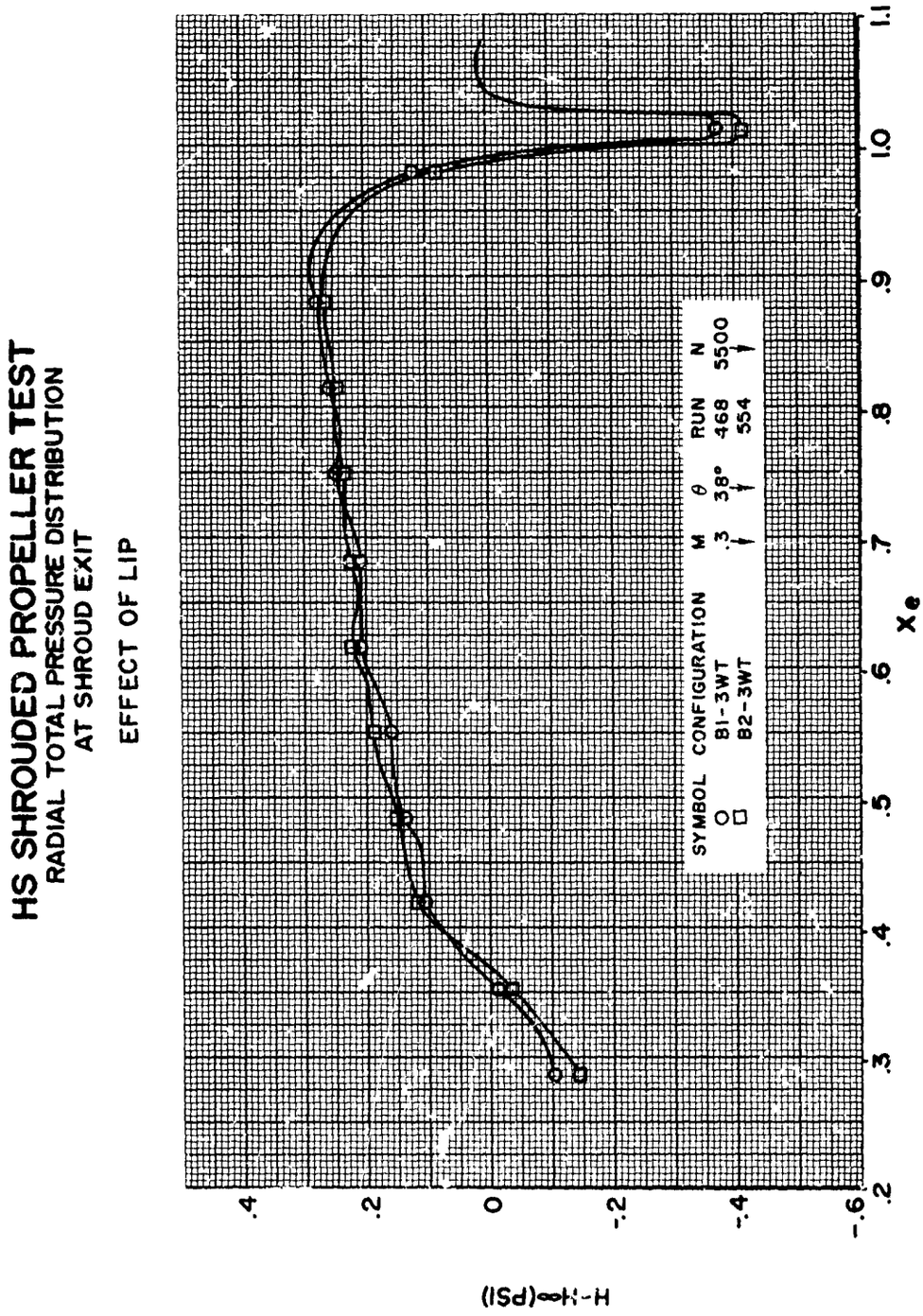
HS SHROUDED PROPELLER TEST
RADIAL TOTAL PRESSURE DISTRIBUTION
AT SHROUD EXIT
EFFECT OF LIP
SYMBOL CONFIGURATION M θ RUN N
○ B1-3WT .3 38° 468 5500
□ B2-3WT ↑ ↑ 554 ↑
.4
.2
0
-.2
-.4
-.6
H-H∞(PSI)
.2
.3
.4
.5
.6
.7
.8
.9
1.0
1.1
Xe

FIGURE 255

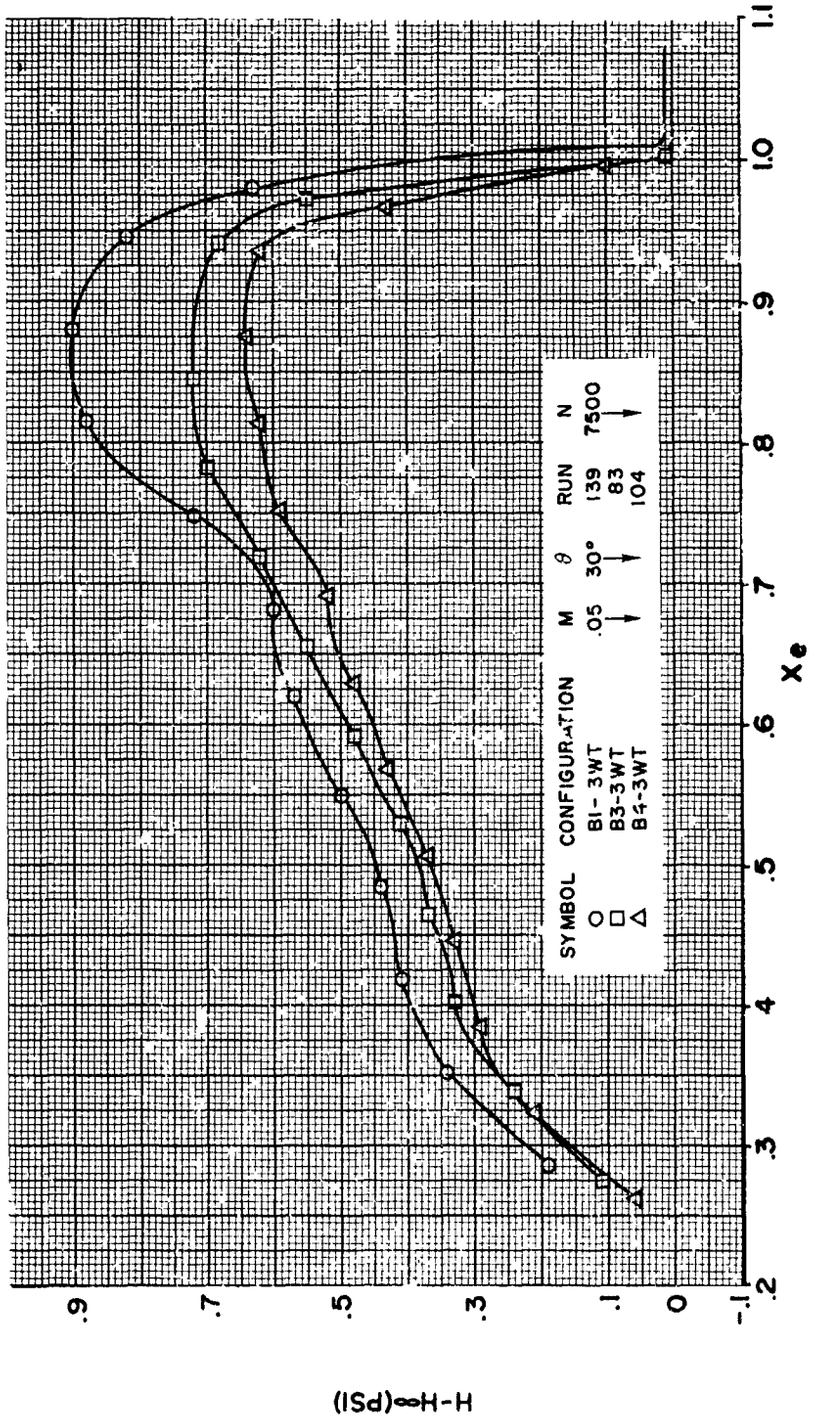

HS SHROUDED PROPELLER TEST
RADIAL TOTAL PRESSURE DISTRIBUTION
AT SHROUD EXIT
EFFECT OF AREA RATIO

FIGURE 256

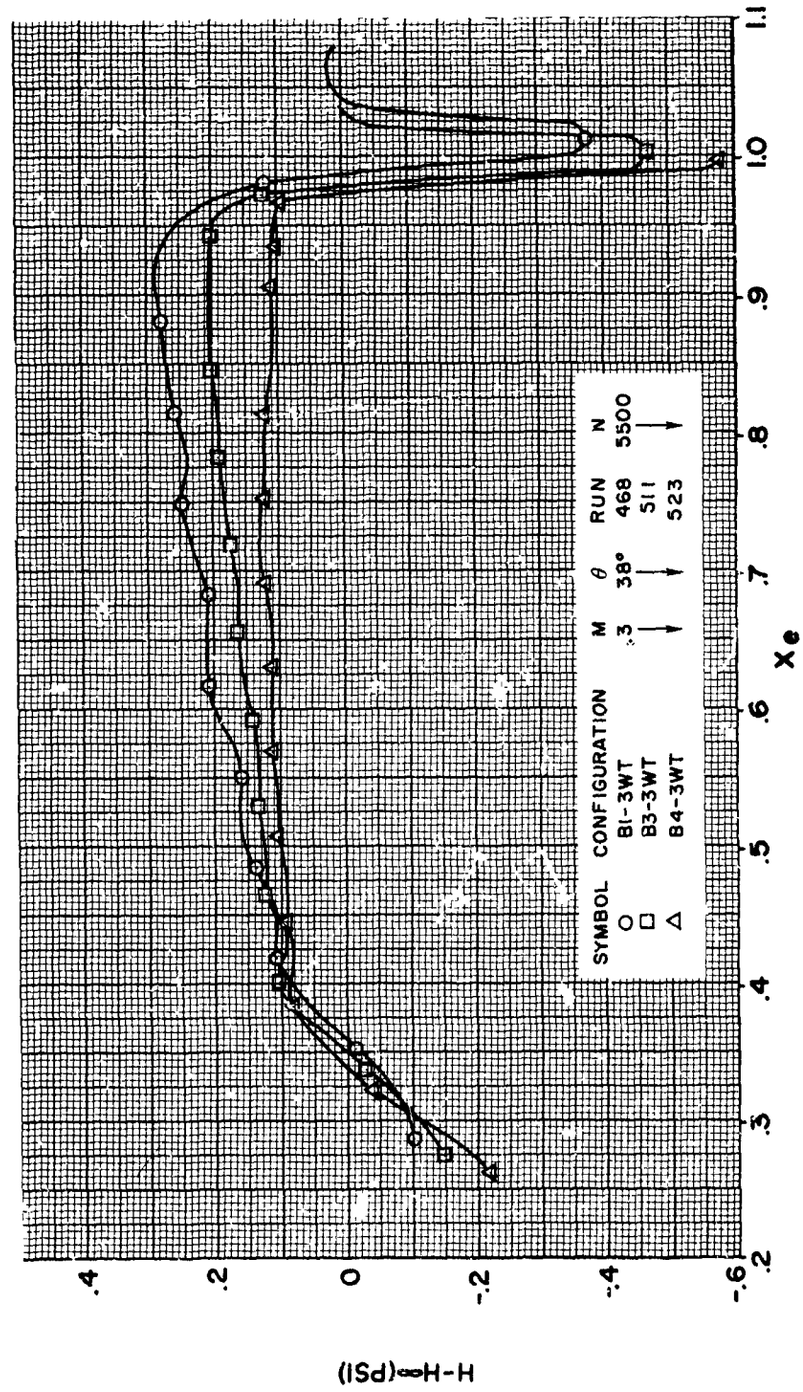

HS SHROUDED PROPELLER TEST
RADIAL TOTAL PRESSURE DISTRIBUTION
AT SHROUD EXIT
EFFECT OF AREA RATIO

FIGURE 257

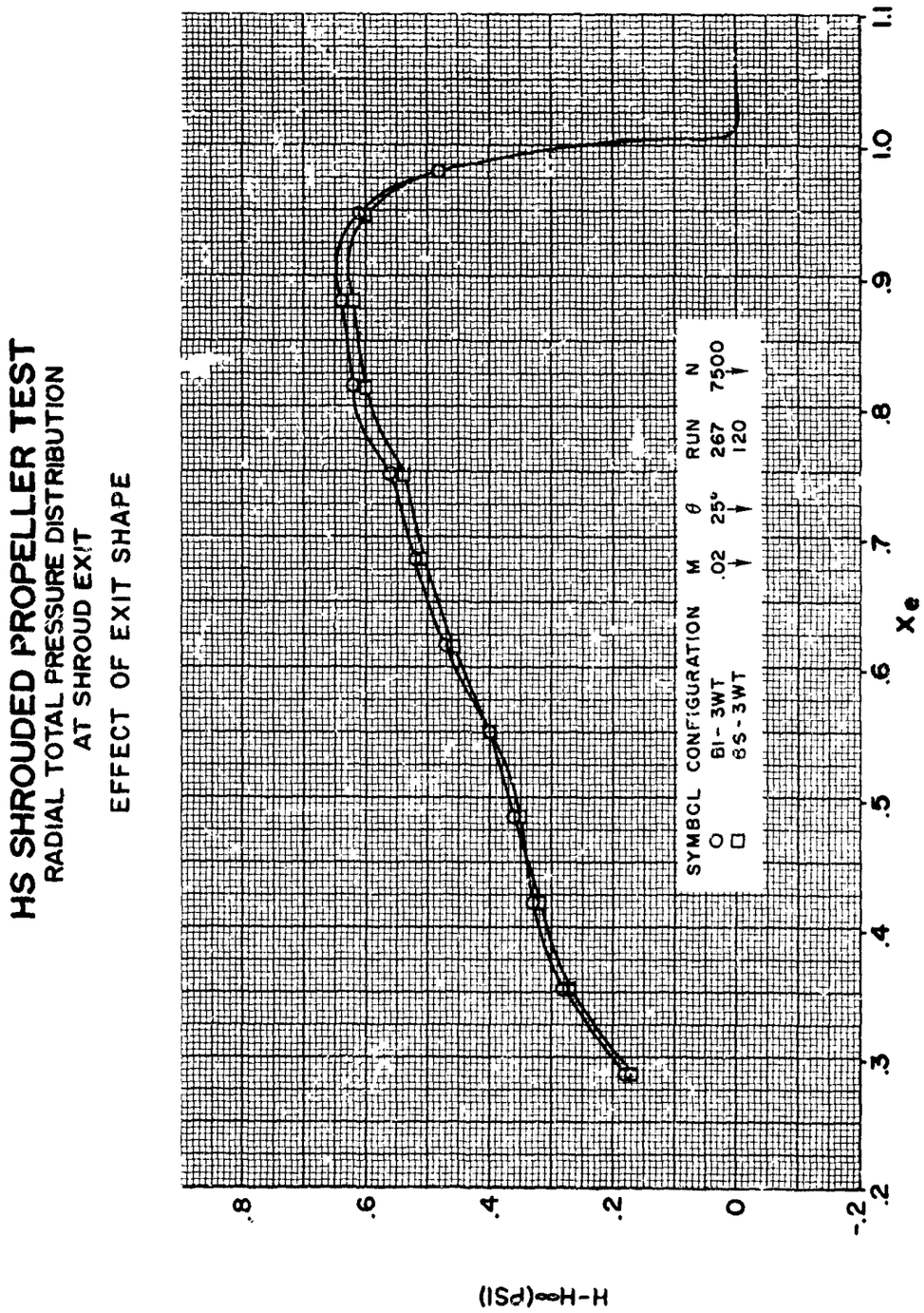
HS SHROUDED PROPELLER TEST
RADIAL TOTAL PRESSURE DISTRIBUTION
AT SHROUD EXIT
EFFECT OF EXIT SHAPE
SYMBOL CONFIGURATION M θ RUN N
○ BI-3WT .02 25° 267 7500
□ BS-3WT 120
H-H∞(PSI)
.8
.6
.4
.2
0
-.2
.2
.3
.4
.5
.6
.7
.8
.9
1.0
1.1
Xe

FIGURE 258

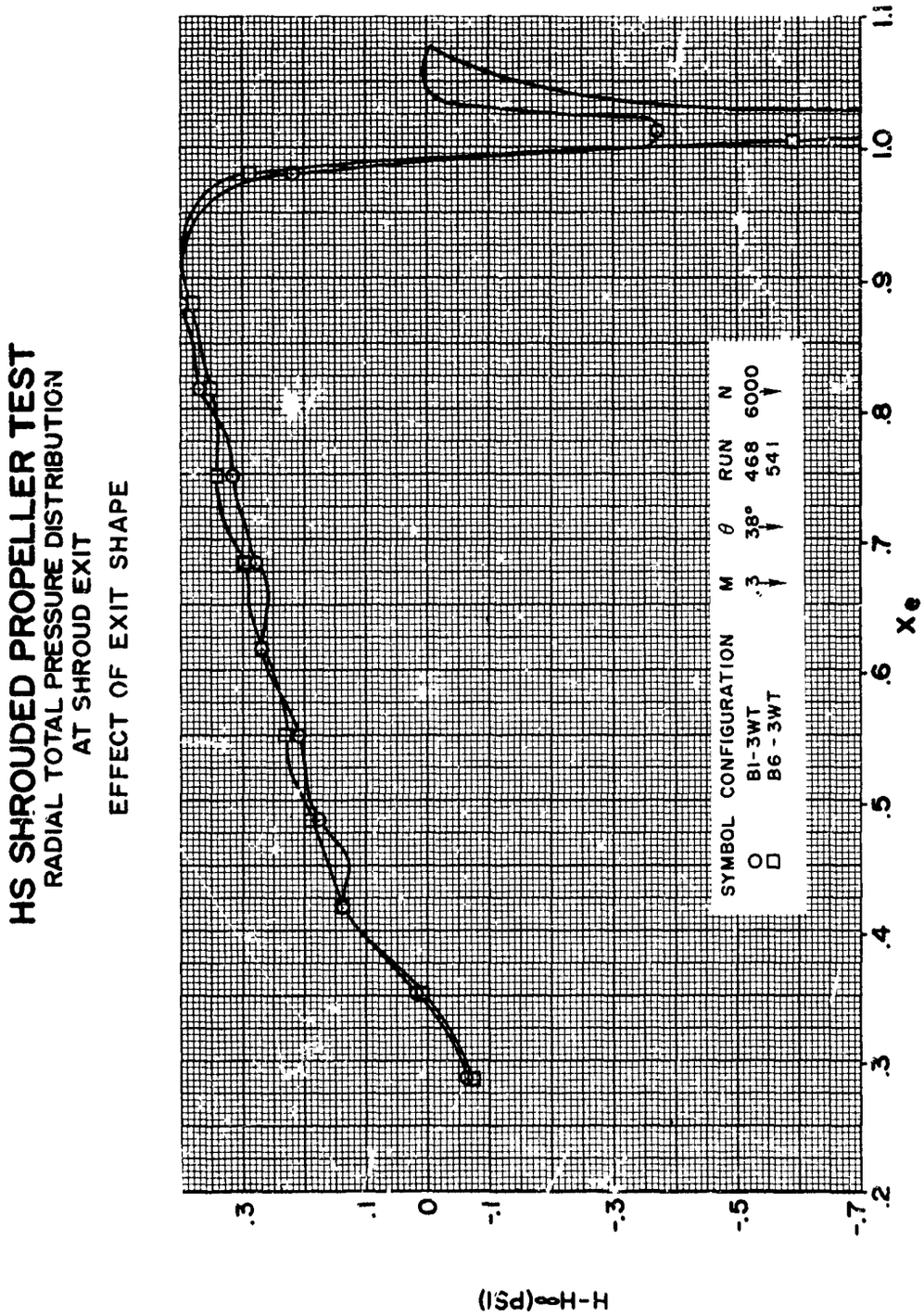
HS SHROUDED PROPELLER TEST
RADIAL TOTAL PRESSURE DISTRIBUTION
AT SHROUD EXIT
EFFECT OF EXIT SHAPE
SYMBOL CONFIGURATION M θ RUN N
O B1-3WT .3 38° 468 6000
□ B6-3WT 541
H-H∞(PSI)
.3
.1
0
-.1
-.3
-.5
-.7
.2
.3
.4
.5
.6
.7
.8
.9
1.0
1.1
Xe

FIGURE 259

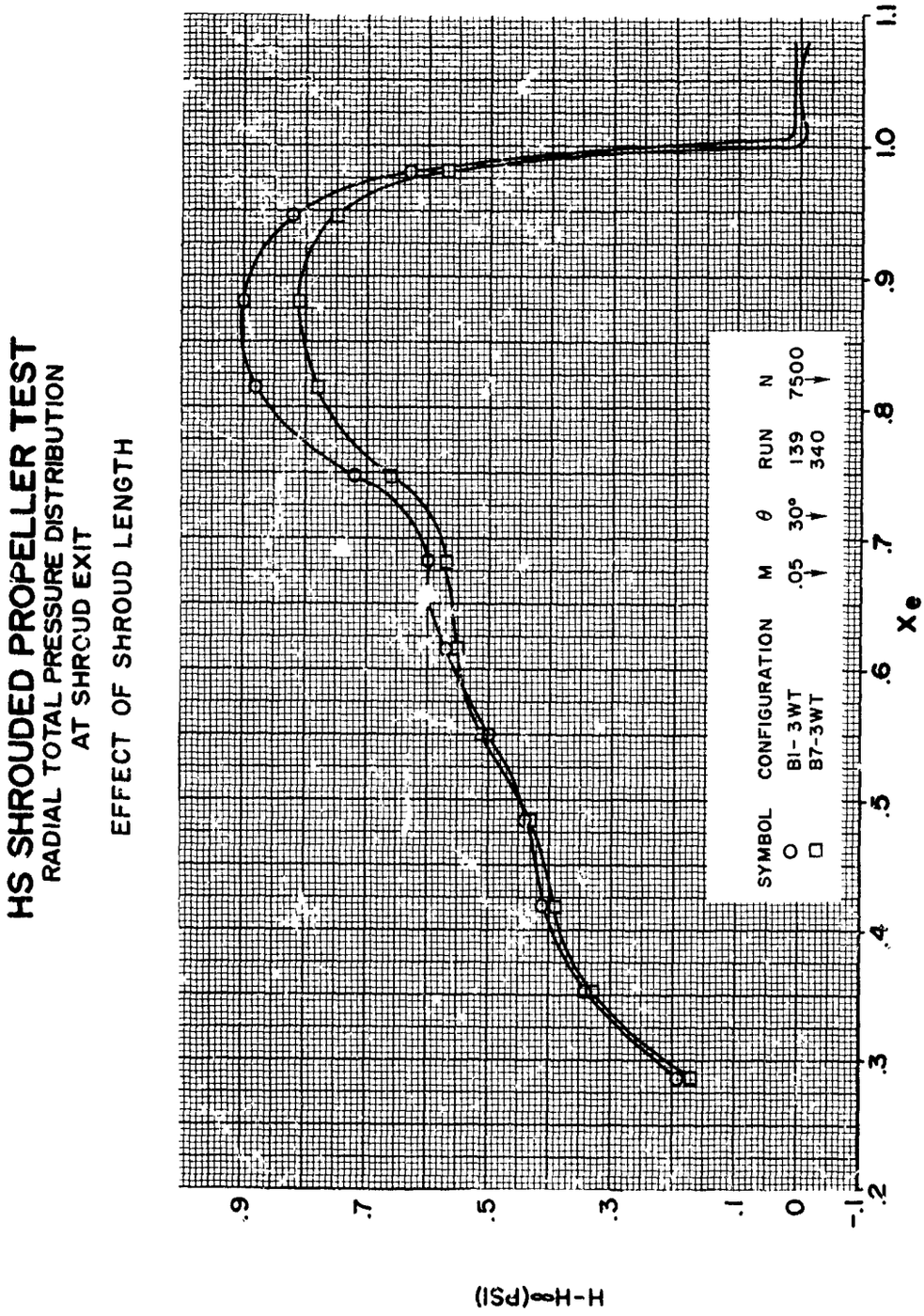
HS SHROUDED PROPELLER TEST
RADIAL TOTAL PRESSURE DISTRIBUTION
AT SHROUD EXIT
EFFECT OF SHROUD LENGTH
SYMBOL CONFIGURATION M θ RUN N
O B1-3WT .05 30° 139 7500
□ B7-3WT 340
H-H∞(PSI)
.9
.7
.5
.3
.1
0
-.1
.2
.3
.4
.5
.6
.7
.8
.9
1.0
1.1
Xe

FIGURE 260

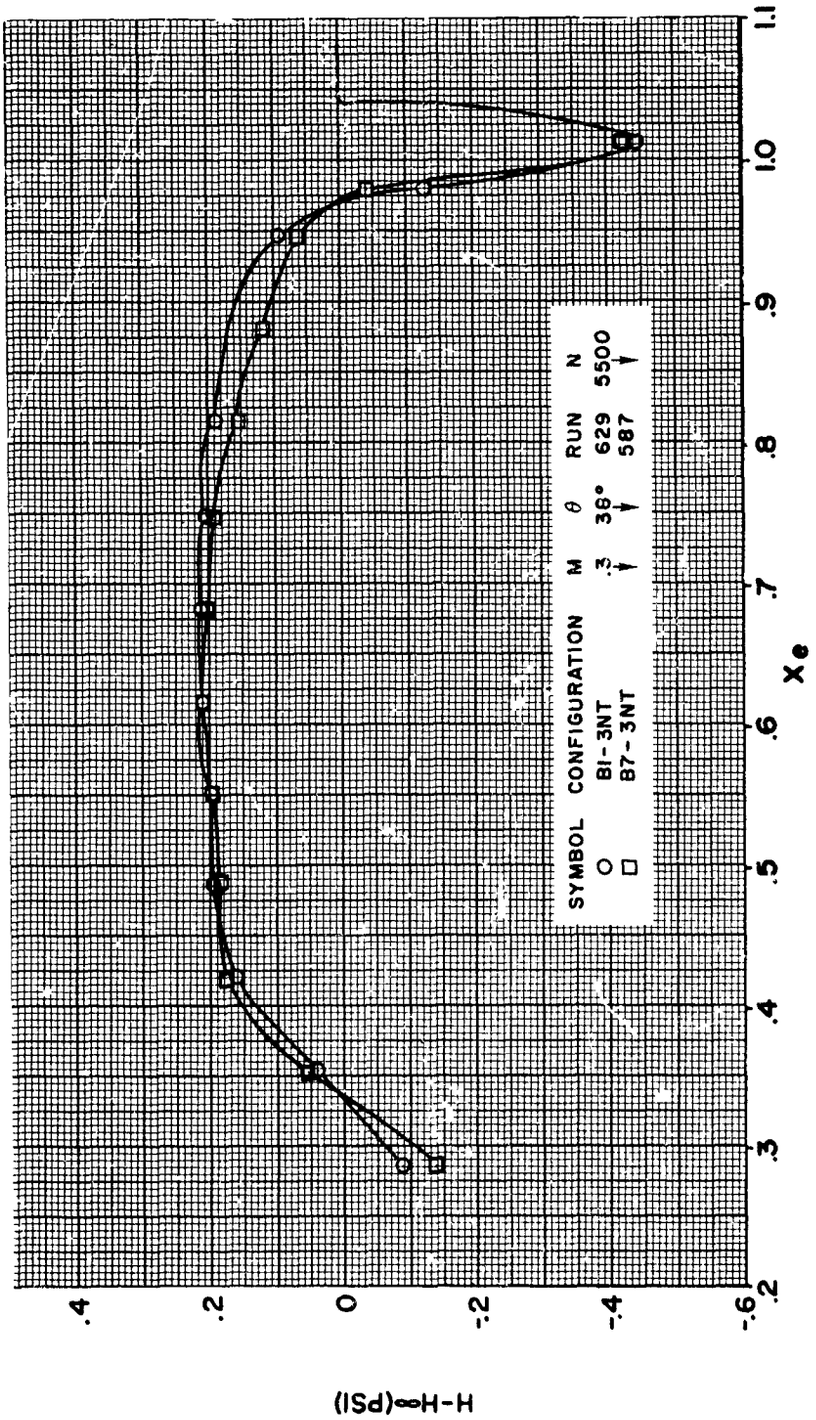

HS SHROUDED PROPELLER TEST
RADIAL TOTAL PRESSURE DISTRIBUTION
AT SHROUD EXIT
EFFECT OF SHROUD LENGTH

FIGURE 261

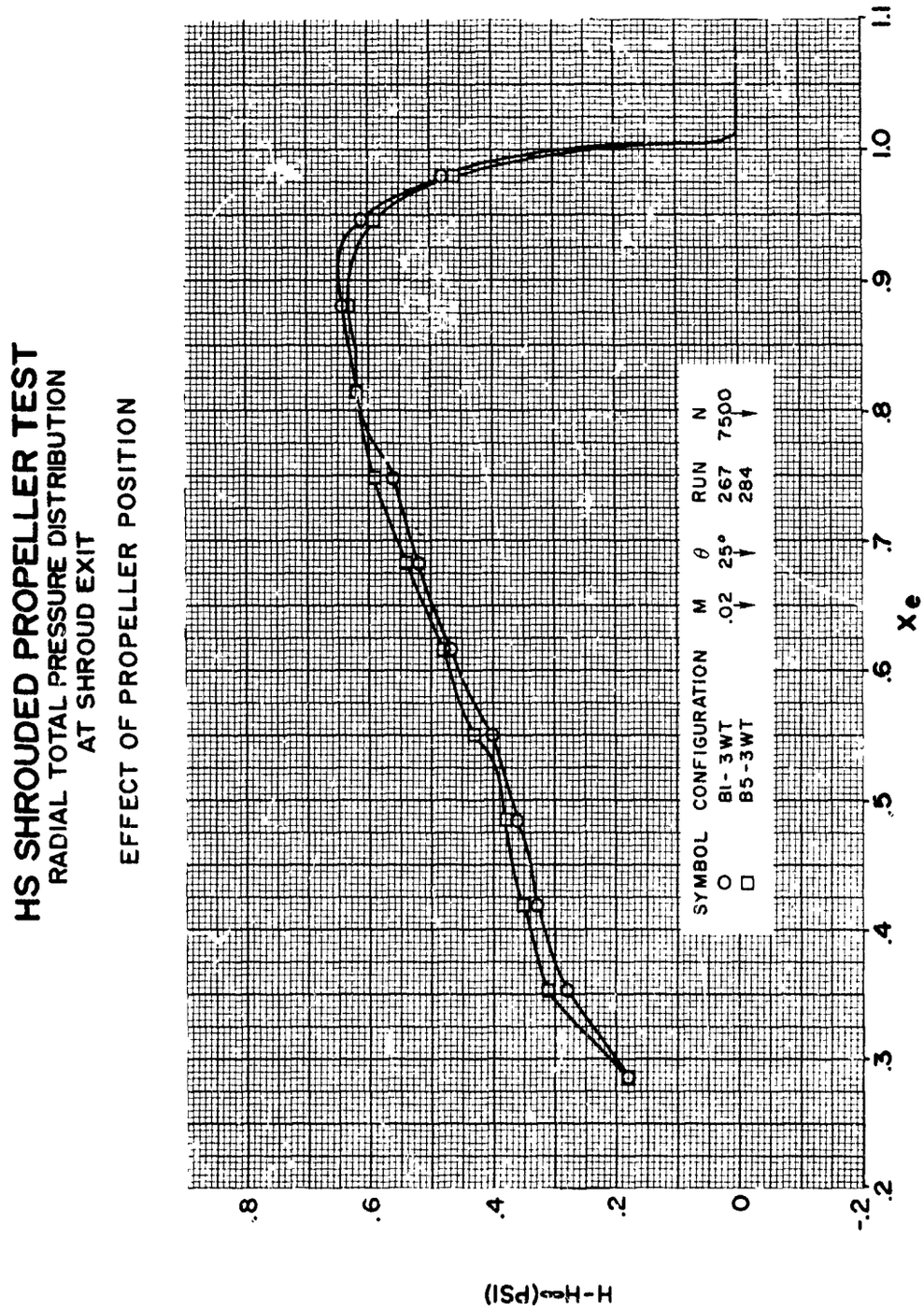
HS SHROUDED PROPELLER TEST
RADIAL TOTAL PRESSURE DISTRIBUTION
AT SHROUD EXIT
EFFECT OF PROPELLER POSITION
SYMBOL CONFIGURATION M θ RUN N
O B1-3WT .02 25° 267 7500
□ B5-3WT 284
H-H∞(PSI)
.8
.6
.4
.2
0
-.2
.2
.3
.4
.5
.6
.7
.8
.9
1.0
1.1
Xe

FIGURE 262

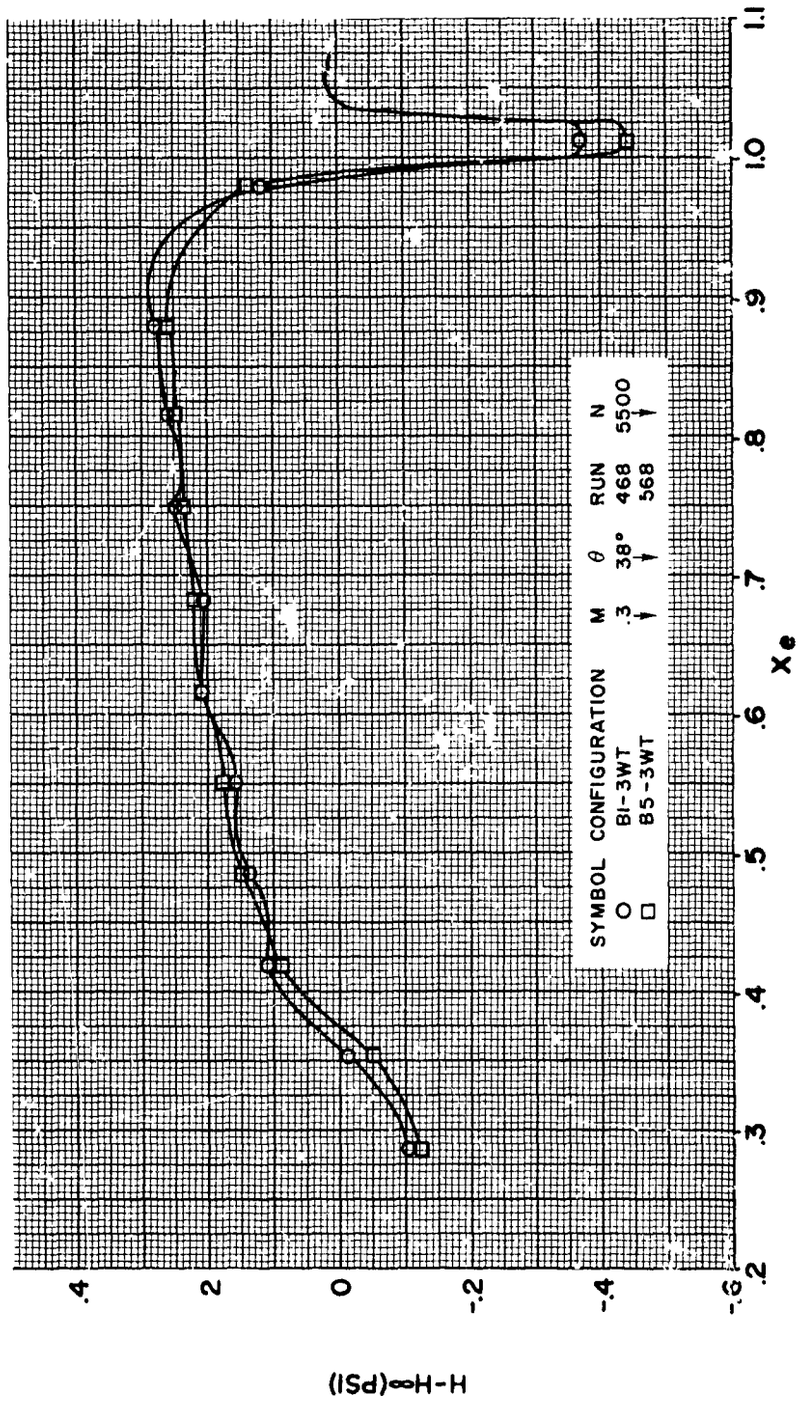

HS SHROUDED PROPELLER TEST
RADIAL TOTAL PRESSURE DISTRIBUTION
AT SHROUD EXIT

EFFECT OF PROPELLER POSITION

FIGURE 263

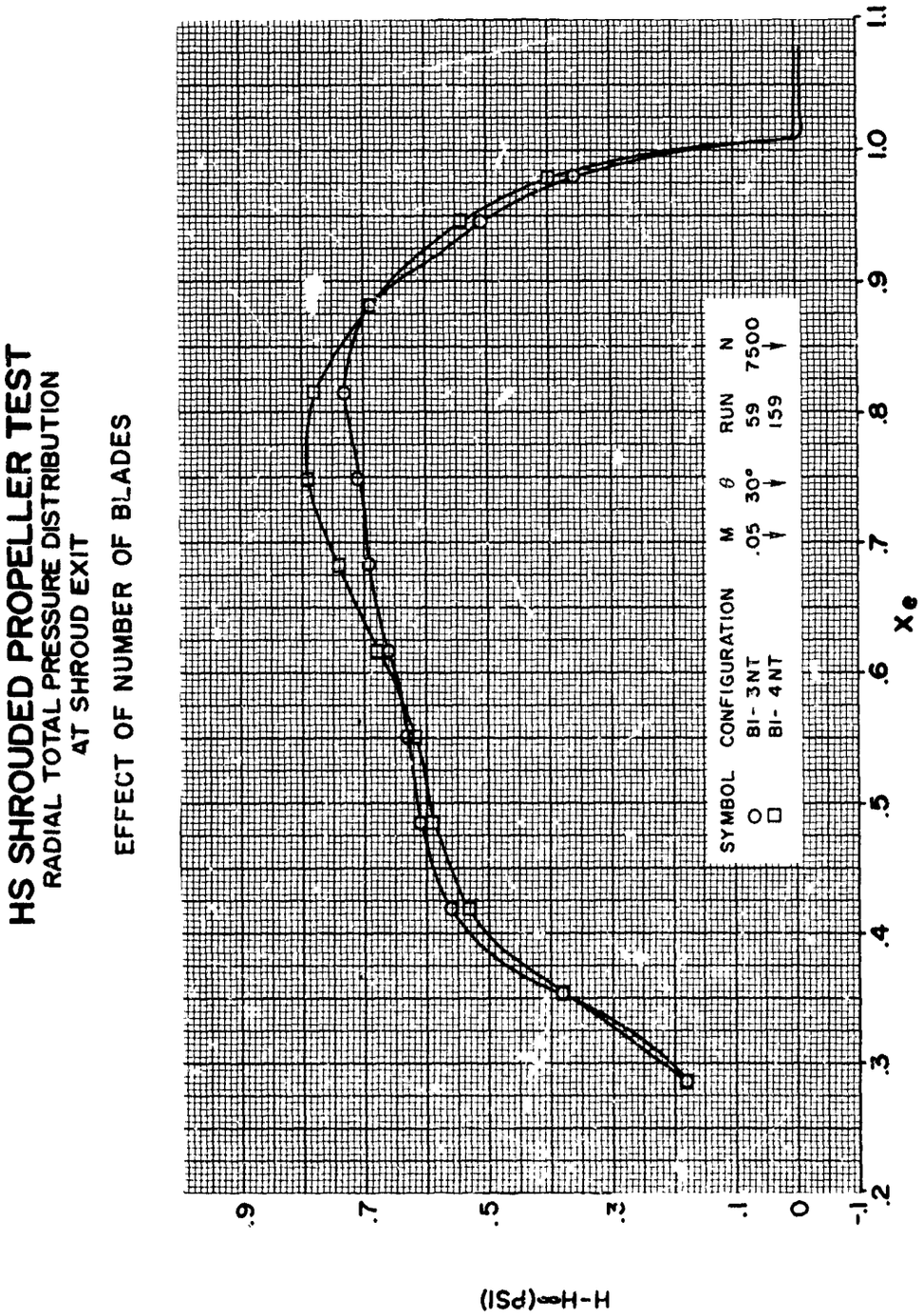
HS SHROUDED PROPELLER TEST
RADIAL TOTAL PRESSURE DISTRIBUTION
AT SHROUD EXIT
EFFECT OF NUMBER OF BLADES
SYMBOL CONFIGURATION M θ RUN N
○ BI-3NT .05 30° 59 7500
□ BI-4NT ↓ ↓ 159 ↓
H-H∞(PSI)
.6
.7
.5
.3
.1
0
-.1
.2
.3
.4
.5
.6
.7
.8
.9
1.0
1.1
Xe

FIGURE 264

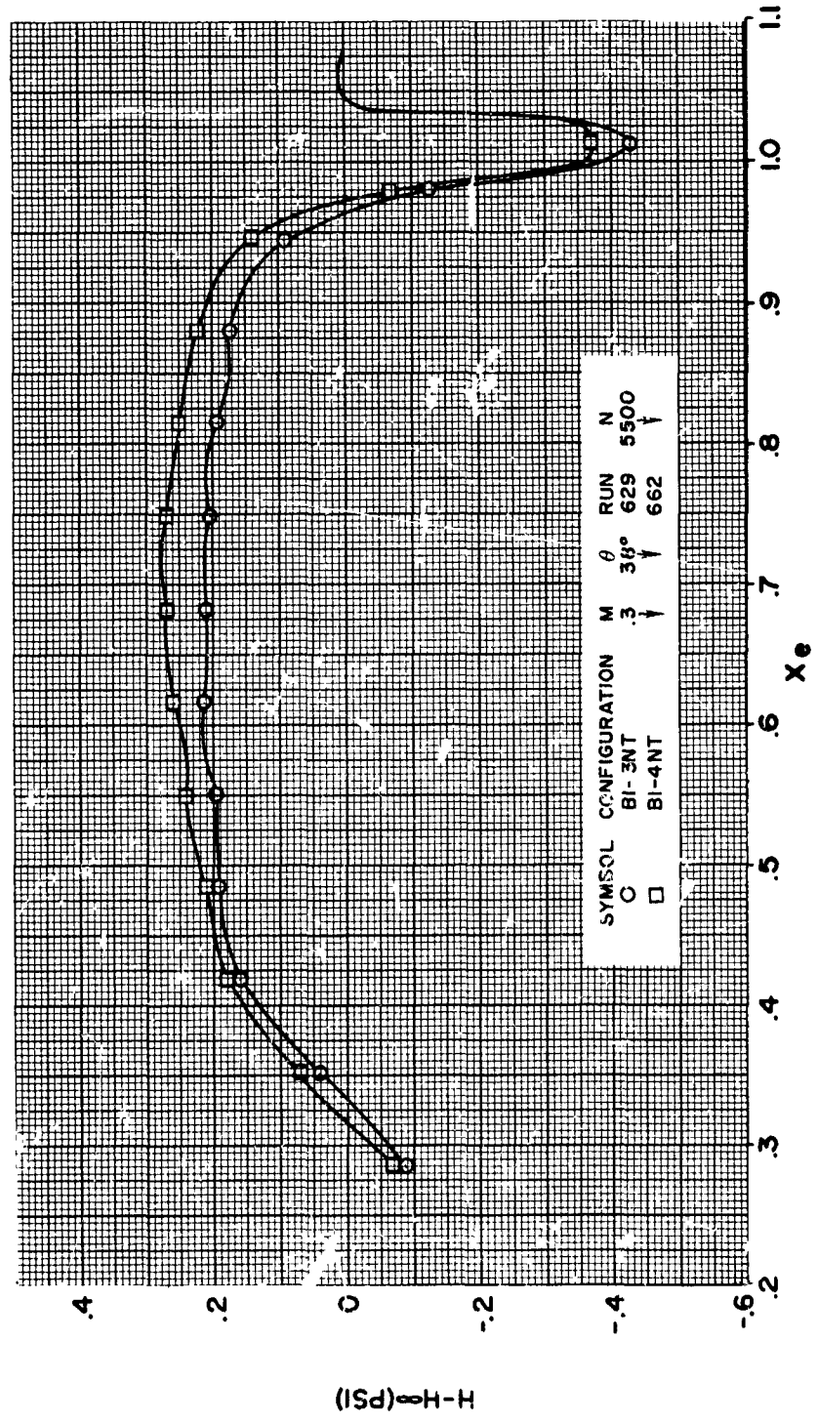

HS SHROUDED PROPELLER TEST
RADIAL TOTAL PRESSURE DISTRIBUTION
AT SHROUD EXIT
EFFECT OF NUMBER OF BLADES

FIGURE 265

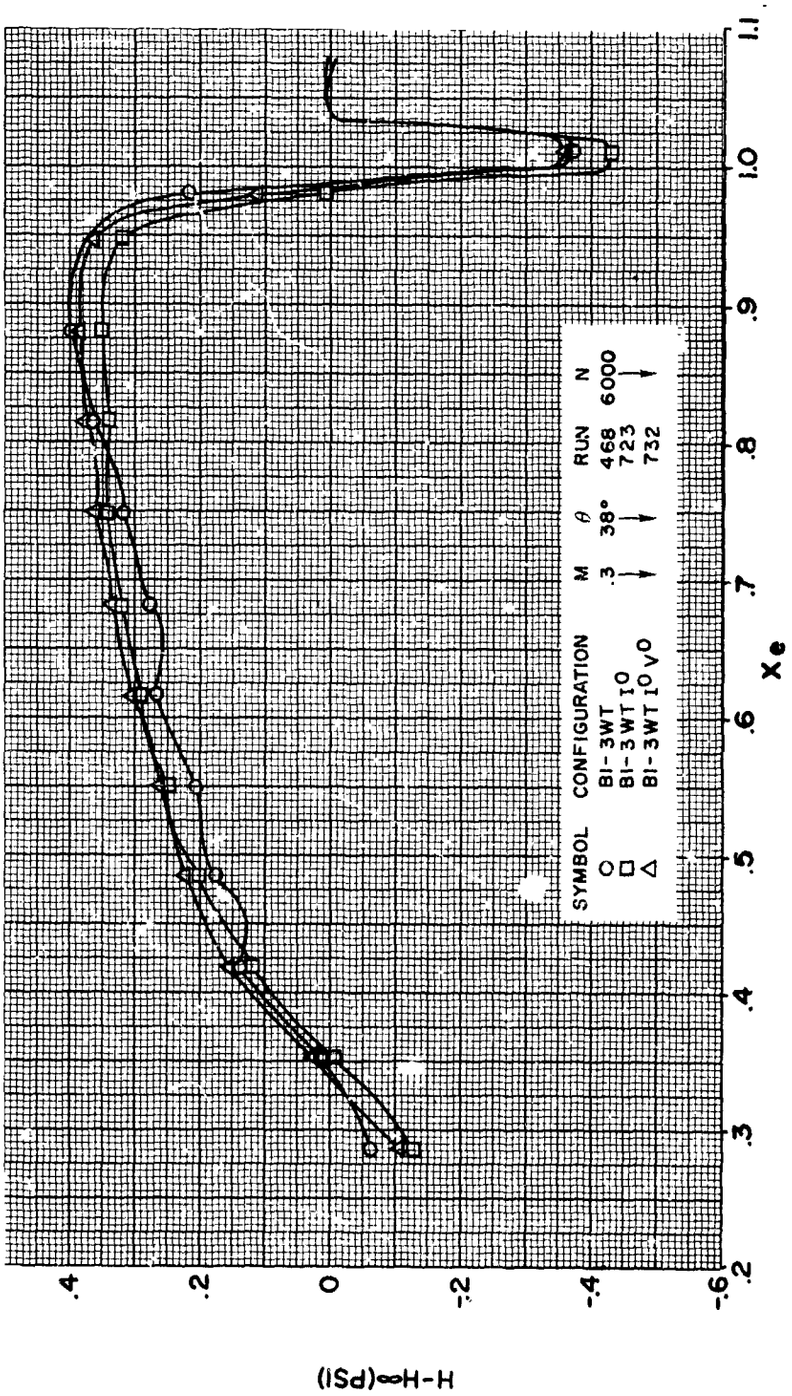

HS SHROUDED PROPELLER TEST
RADIAL TOTAL PRESSURE DISTRIBUTION
AT SHROUD EXIT
EFFECT OF VANE

FIGURE 266

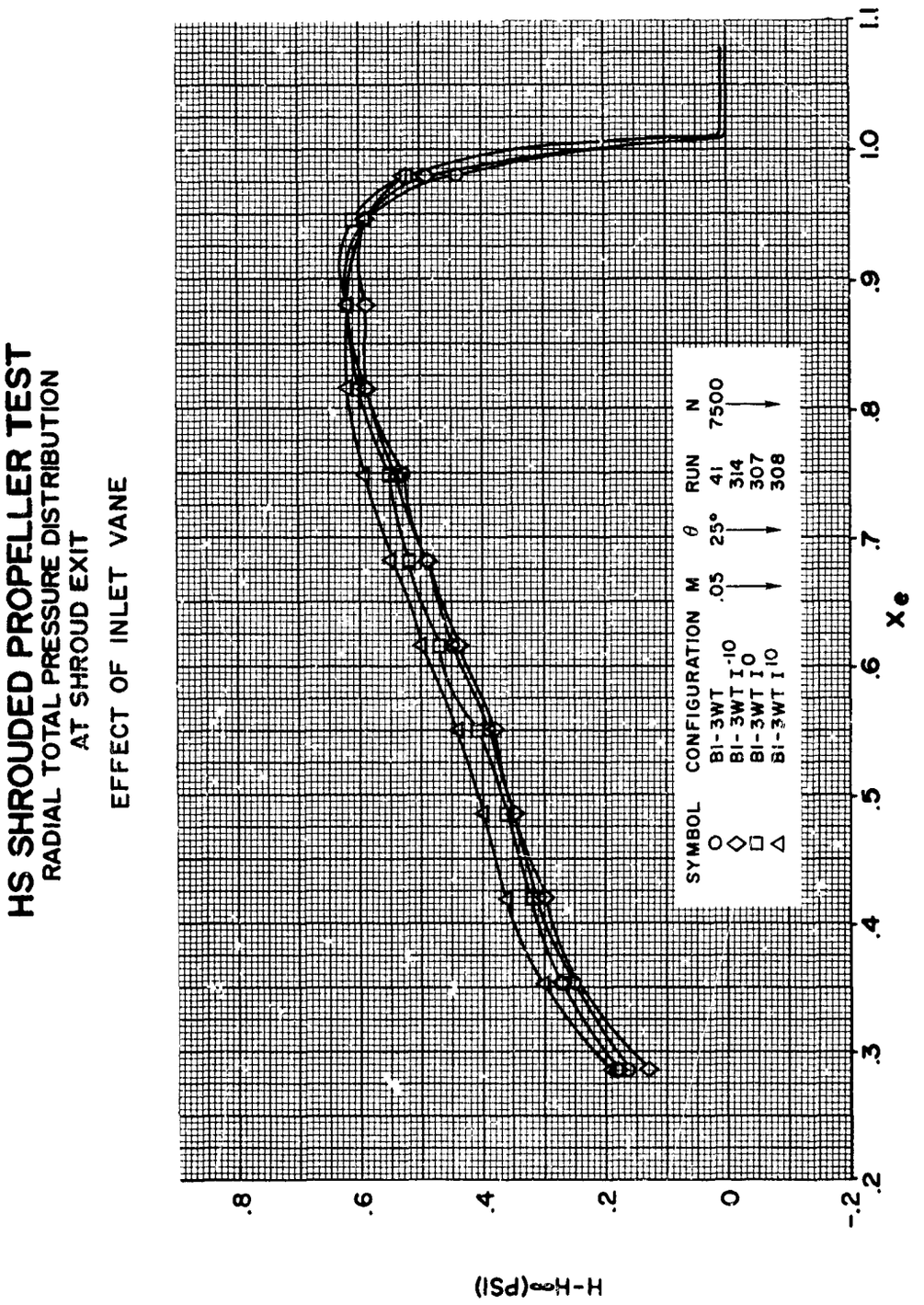
HS SHROUDED PROPELLER TEST
RADIAL TOTAL PRESSURE DISTRIBUTION
AT SHROUD EXIT
EFFECT OF INLET VANE
SYMBOL CONFIGURATION M θ RUN N
○ BI-3WT .05 25° 41 7500
◇ BI-3WT I-10 314
□ BI-3WT I 0 307
△ BI-3WT I 10 308
H-H∞(PSI)
.8
.6
.4
.2
0
-.2
.2
.3
.4
.5
.6
.7
.8
.9
1.0
1.1
Xe

FIGURE 267

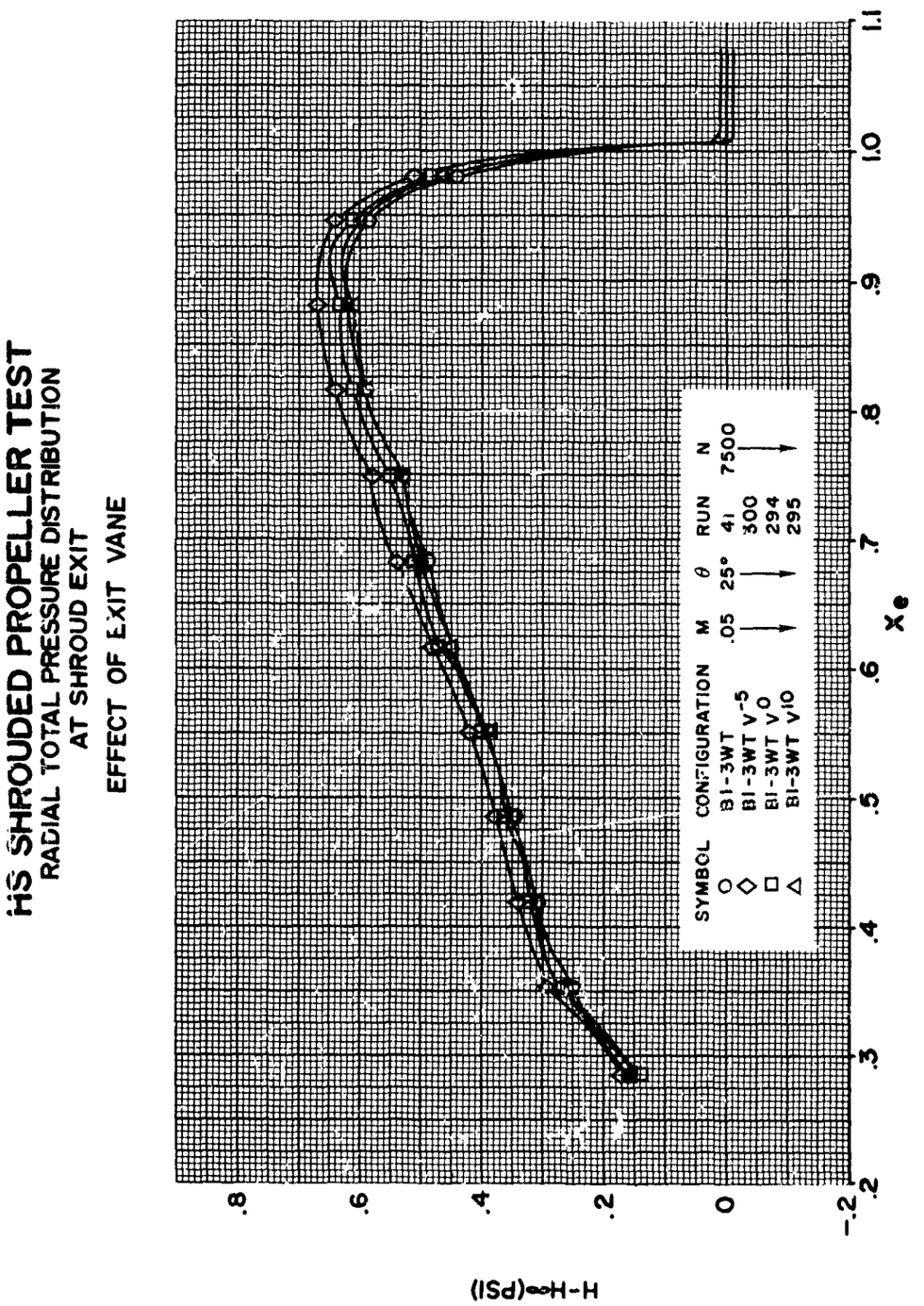
HS SHROUDED PROPELLER TEST
RADIAL TOTAL PRESSURE DISTRIBUTION
AT SHROUD EXIT
EFFECT OF EXIT VANE
SYMBOL CONFIGURATION M θ RUN N
○ BI-3WT .05 25° 41 7500
◇ BI-3WT V-5 300
□ BI-3WT V0 294
△ BI-3WT V10 295
H-H∞(PSI)
Xe
.8
.6
.4
.2
0
-.2
.2
.3
.4
.5
.6
.7
.8
.9
1.0
1.1

FIGURE 268

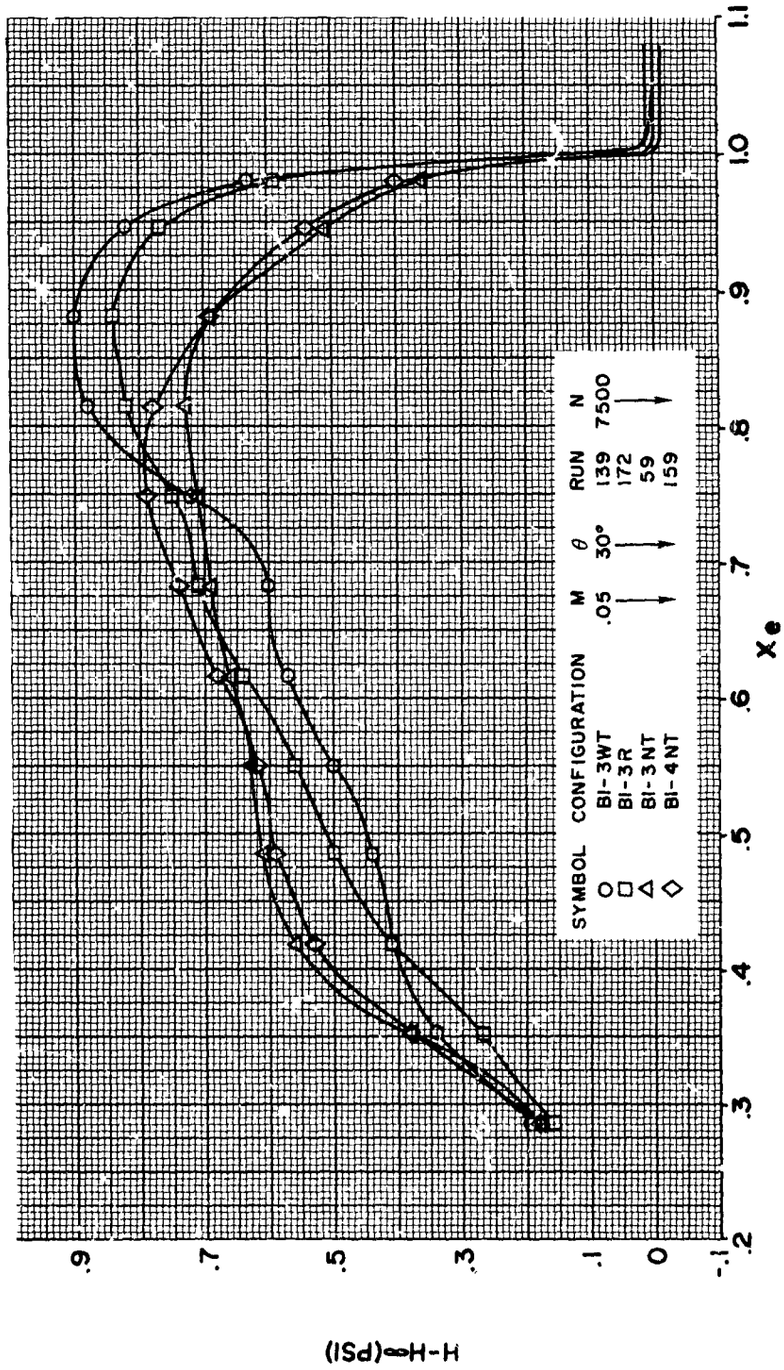

HS SHROUDED PROPELLER TEST
RADIAL TOTAL PRESSURE DISTRIBUTION
AT SHROUD EXIT
EFFECT OF PROPELLER PLANFORM

FIGURE 269

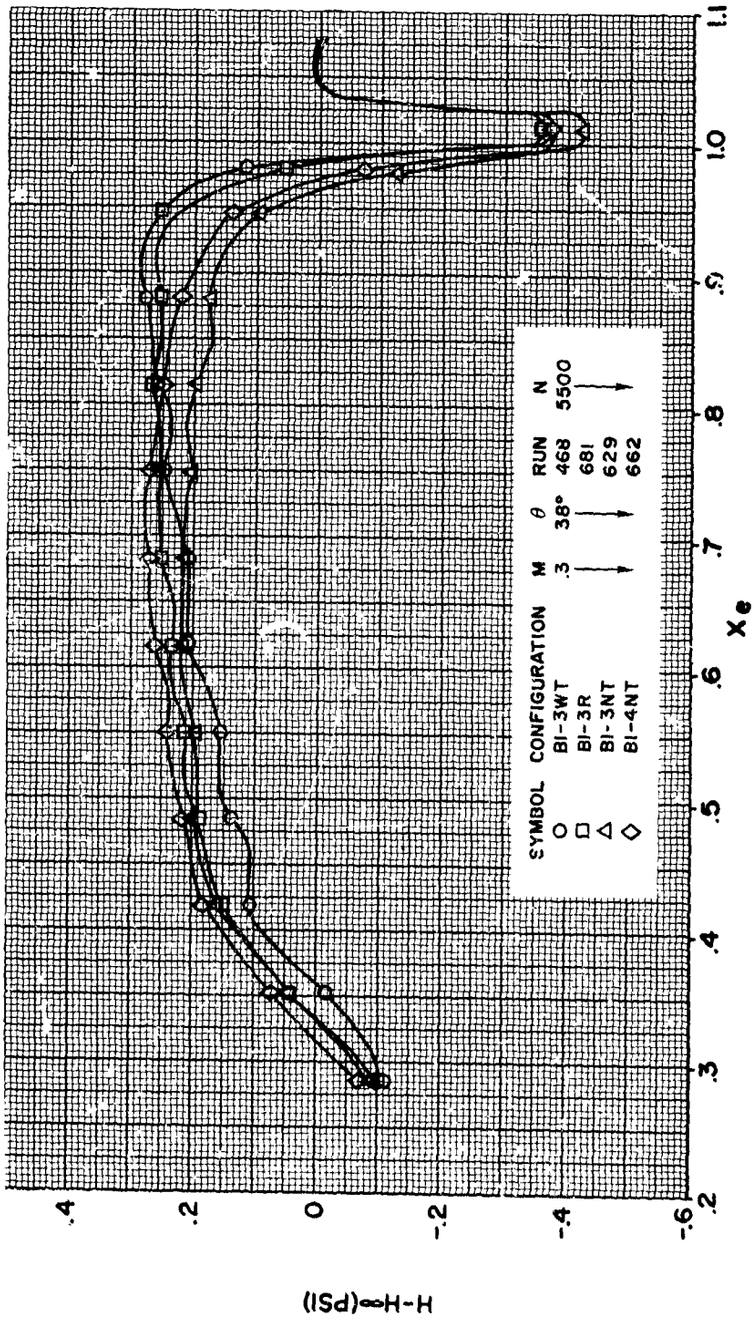

HS SHROUDED PROPELLER TEST
RADIAL TOTAL PRESSURE DISTRIBUTION
AT SHROUD EXIT
EFFECT OF PROPELLER PLANFORM

FIGURE 270

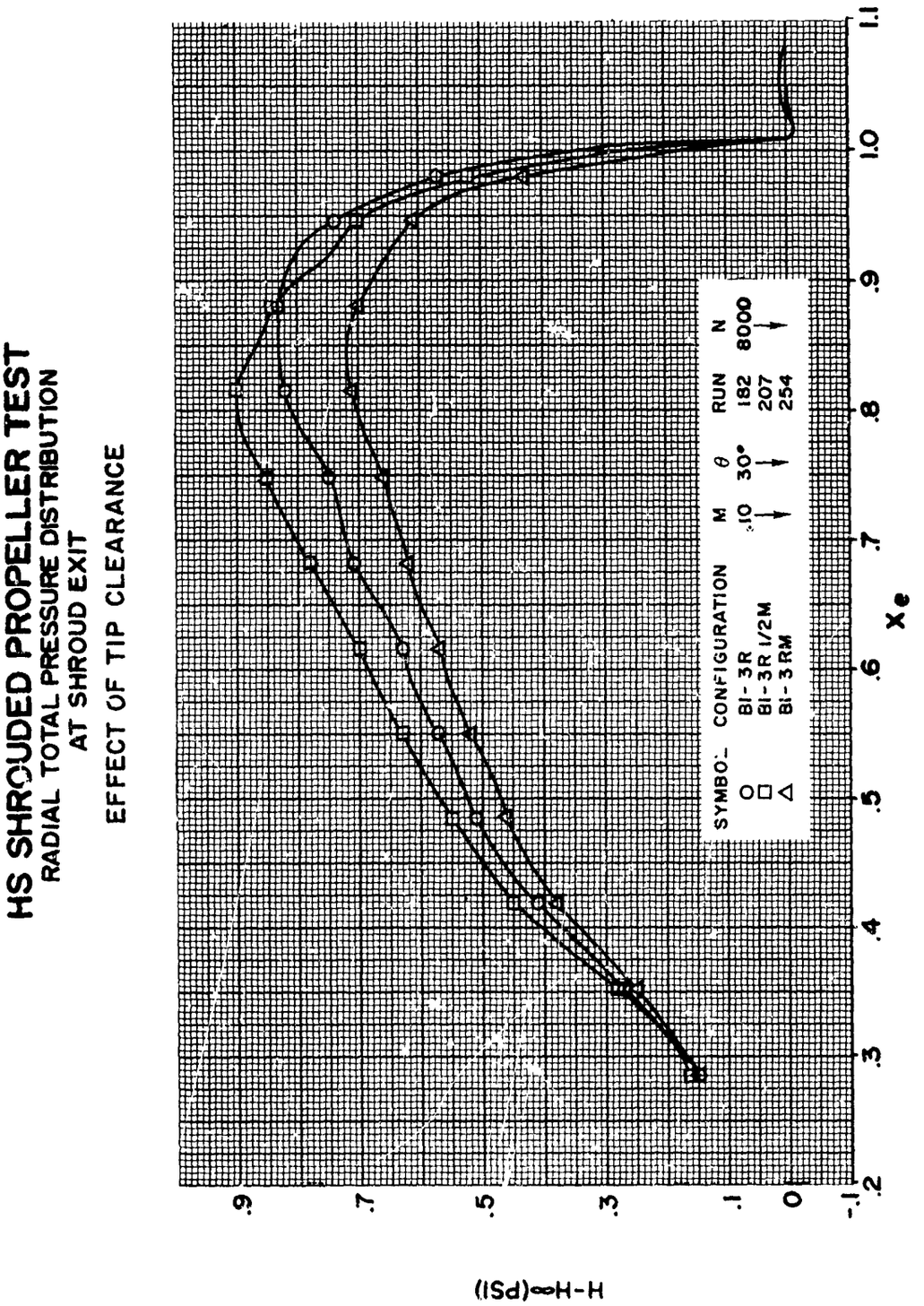
HS SHROUDED PROPELLER TEST
RADIAL TOTAL PRESSURE DISTRIBUTION
AT SHROUD EXIT
EFFECT OF TIP CLEARANCE
SYMBOL CONFIGURATION M θ RUN N
○ BI-3R .10 30° 182 8000
□ BI-3R 1/2M 207
△ BI-3RM 254
H-H∞(PSI)
Xe
.9
.7
.5
.3
.1
0
-.1
.2
.3
.4
.5
.6
.7
.8
.9
1.0
1.1

FIGURE 271

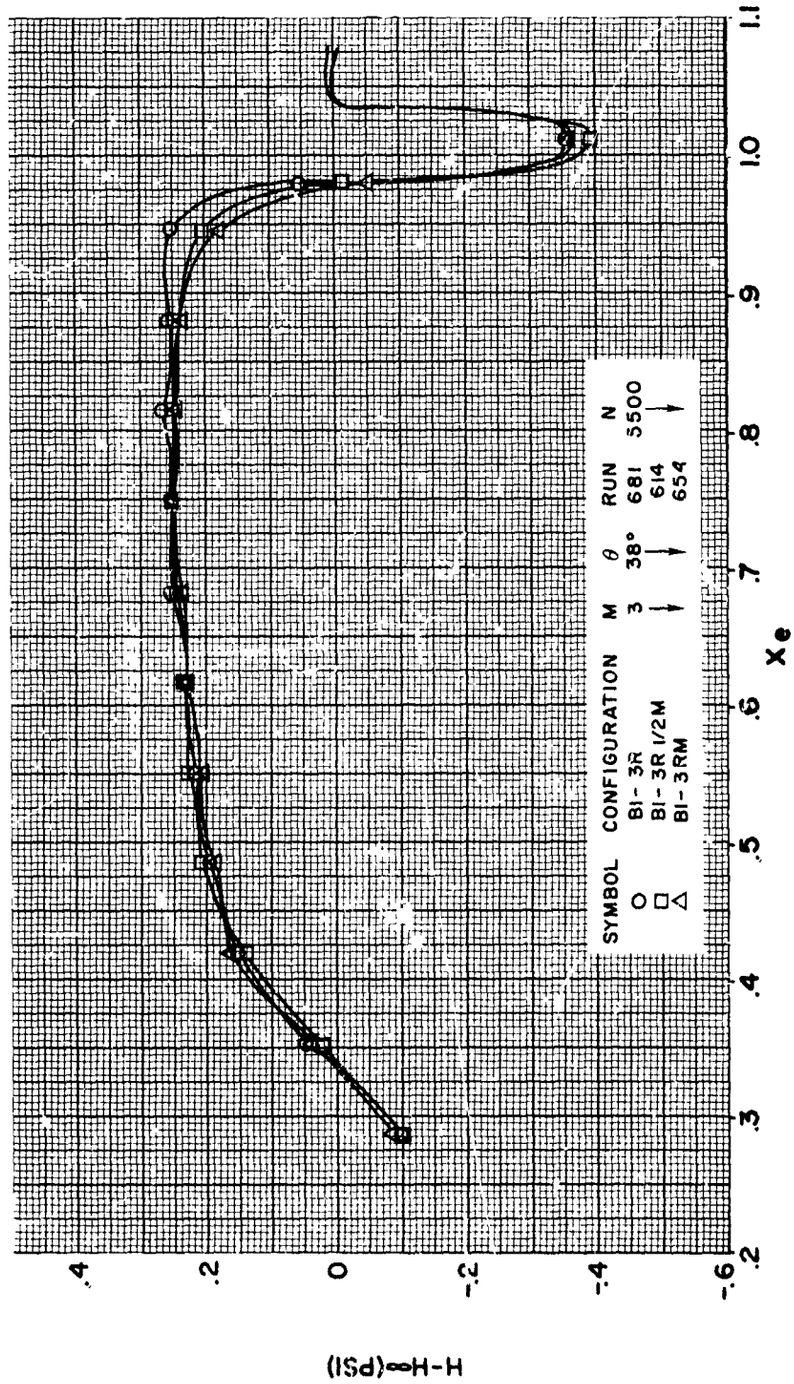

HS SHROUDED PROPELLER TEST
RADIAL TOTAL PRESSURE DISTRIBUTION
AT SHROUD EXIT
EFFECT OF TIP CLEARANCE

FIGURE 272

HS SHROUDED PROPELLER TEST

RADIAL STATIC PRESSURE DISTRIBUTION
AT SHROUD EXIT FROM TRAVERSING
PROBE MEASUREMENTS

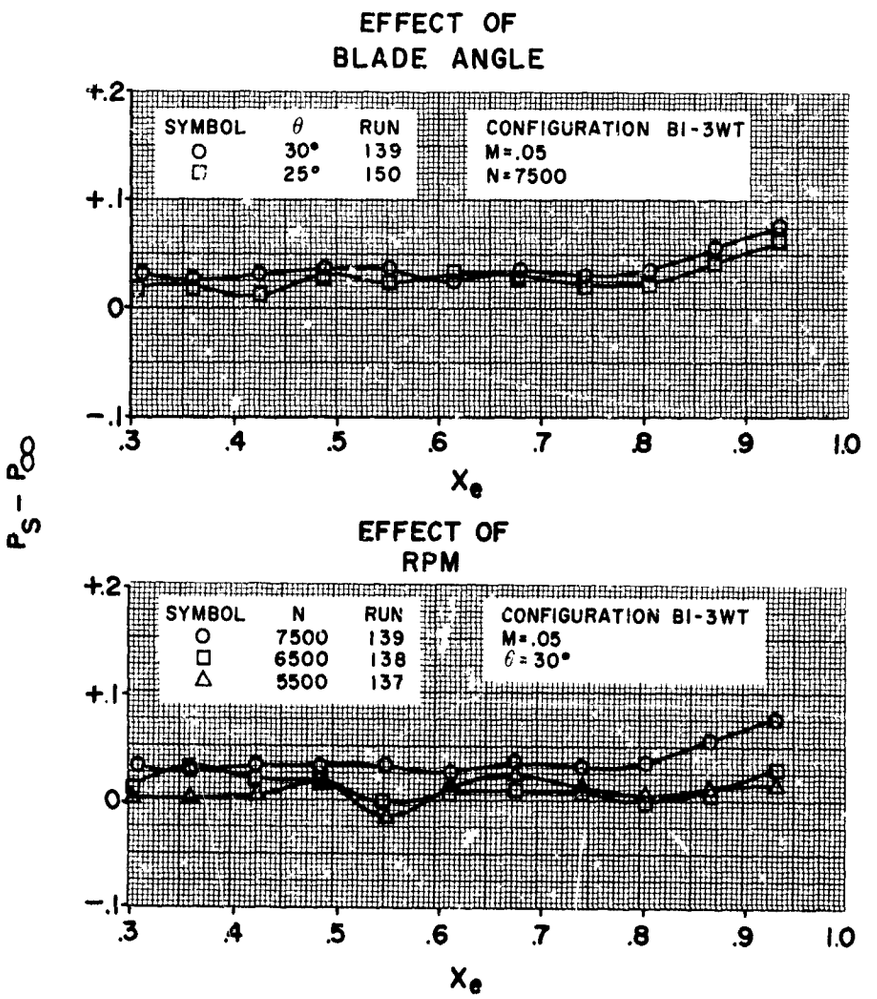

FIGURE 273

HS SHROUDED PROPELLER TEST

RADIAL STATIC PRESSURE DISTRIBUTION
AT SHROUD EXIT FROM TRAVERSING
PROBE MEASUREMENTS

EFFECT OF
BLADE ANGLE

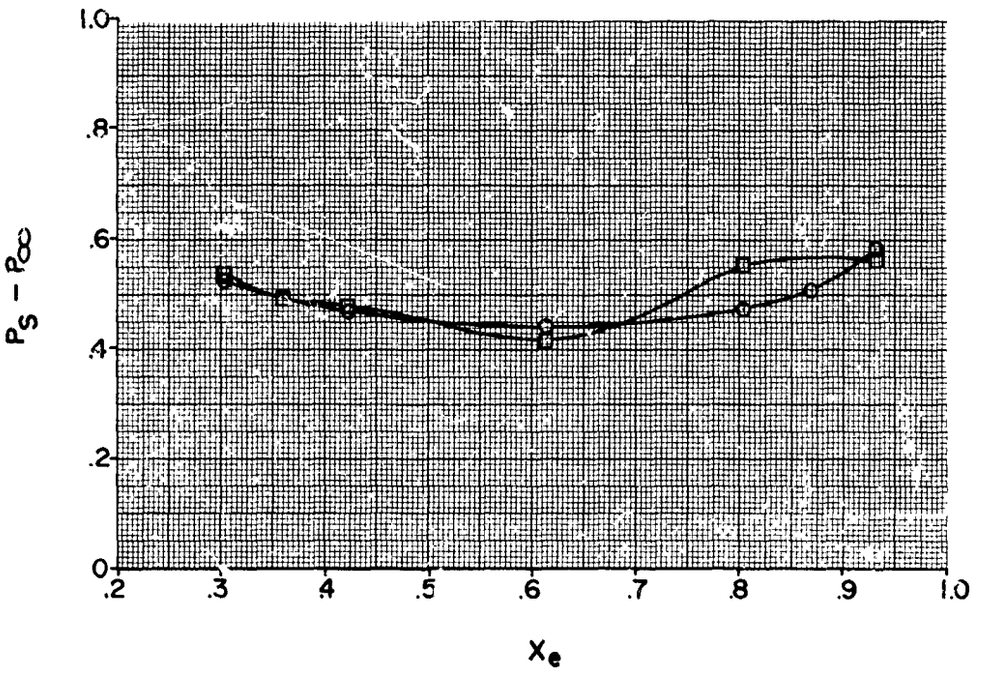

SYMBOL	CONFIGURATION	M	θ	RUN	N
○	BI-3WT	.4	42°	670	5500
□	↓	↓	46°	671	↓

FIGURE 274

HS SHROUDED PROPELLER TEST

RADIAL STATIC PRESSURE DISTRIBUTION
AT SHROUD EXIT FROM TRAVERSING
PROBE MEASUREMENTS

EFFECT OF
MACH NUMBER

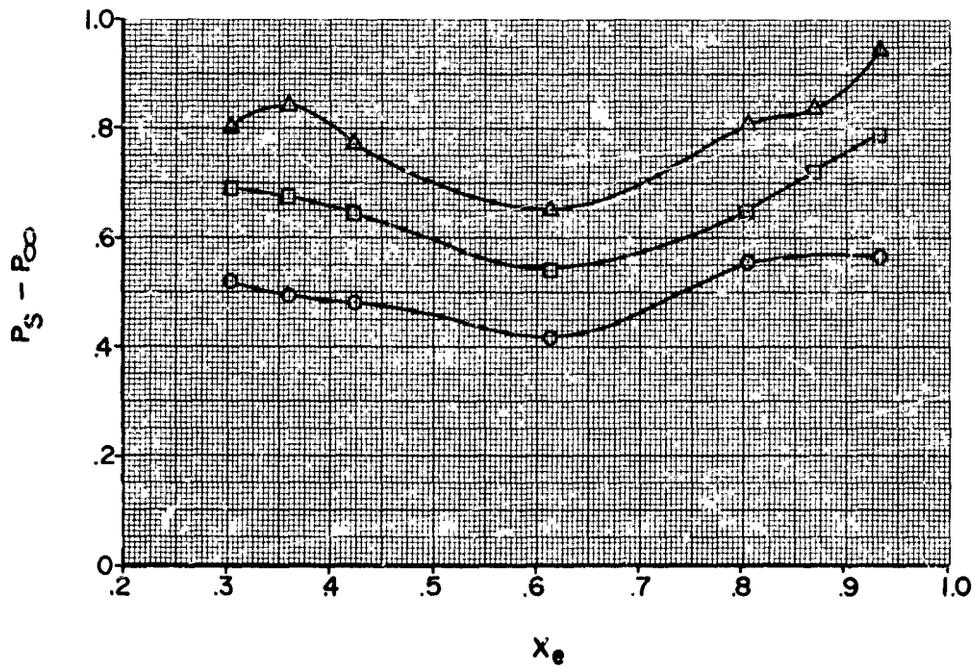

SYMBOL	CONFIGURATION	M	θ	RUN	N
○	BI-3WT	.4	46°	671	5500
□	↓	.5	50°	673	↓
△		.6	50°	674	

FIGURE 275

HS SHROUDED PROPELLER TEST

RADIAL STATIC PRESSURE DISTRIBUTION
AT SHROUD EXIT FROM TRAVERSING
PROBE MEASUREMENTS

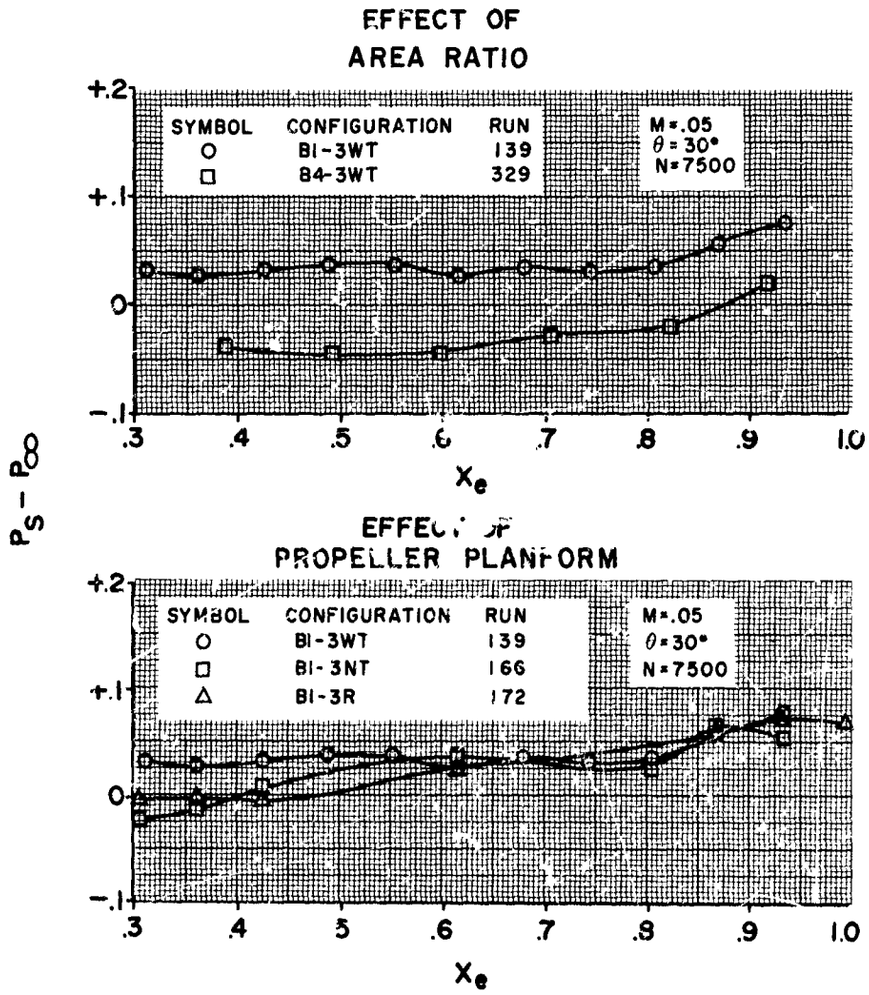

FIGURE 276

HS SHROUDED PROPELLER TEST

RADIAL STATIC PRESSURE DISTRIBUTION
AT SHROUD EXIT FROM TRAVERSING
PROBE MEASUREMENTS

EFFECT OF
AREA RATIO

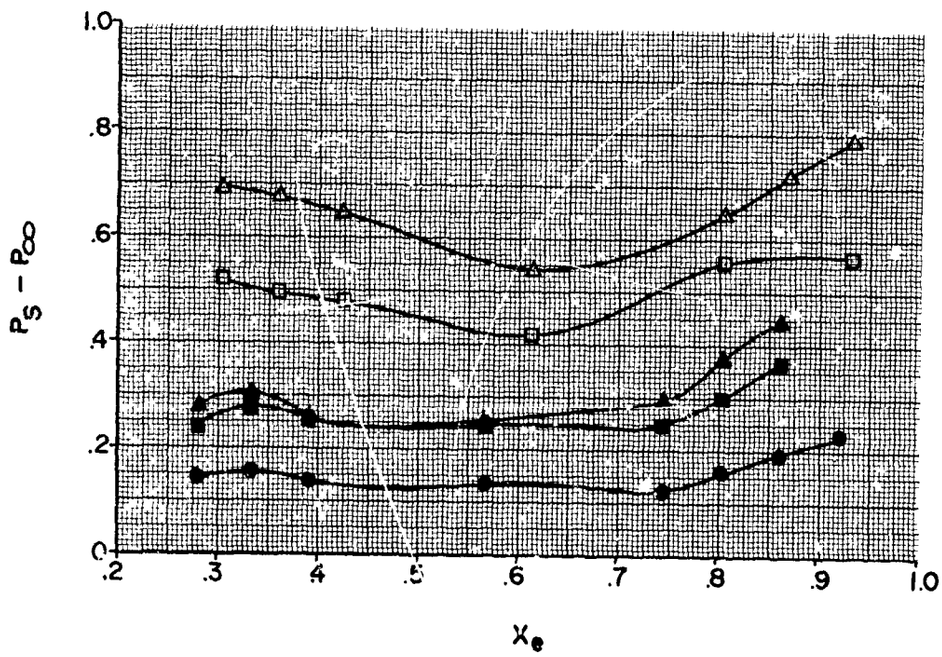

SYMBOL	CONFIGURATION	M	θ	RUN	N
□	B1-3WT	.4	46°	671	5500
△	↓	.5	50°	673	↓
●	B4-3WT	.3	42°	686	
■	↓	.4	50°	687	
▲	↓	.5	58°	688	↓

FIGURE 277

HS SHROUDED PROPELLER TEST

RADIAL STATIC PRESSURE DISTRIBUTION
AT SHROUD EXIT FROM TRAVERSING
PROBE MEASUREMENTS

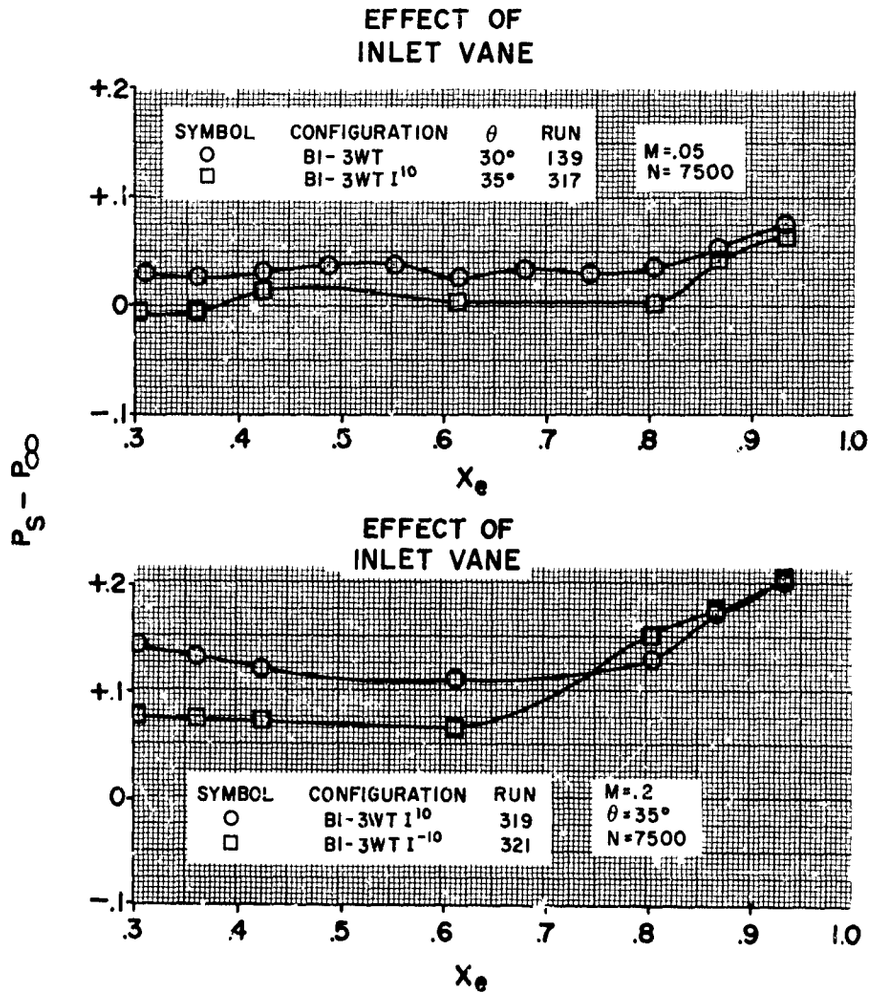

FIGURE 278

HS SHROUDED PROPELLER TEST

RADIAL STATIC PRESSURE DISTRIBUTION
AT SHROUD EXIT FROM TRAVERSING
PROBE MEASUREMENTS

EFFECT OF
INLET VANE

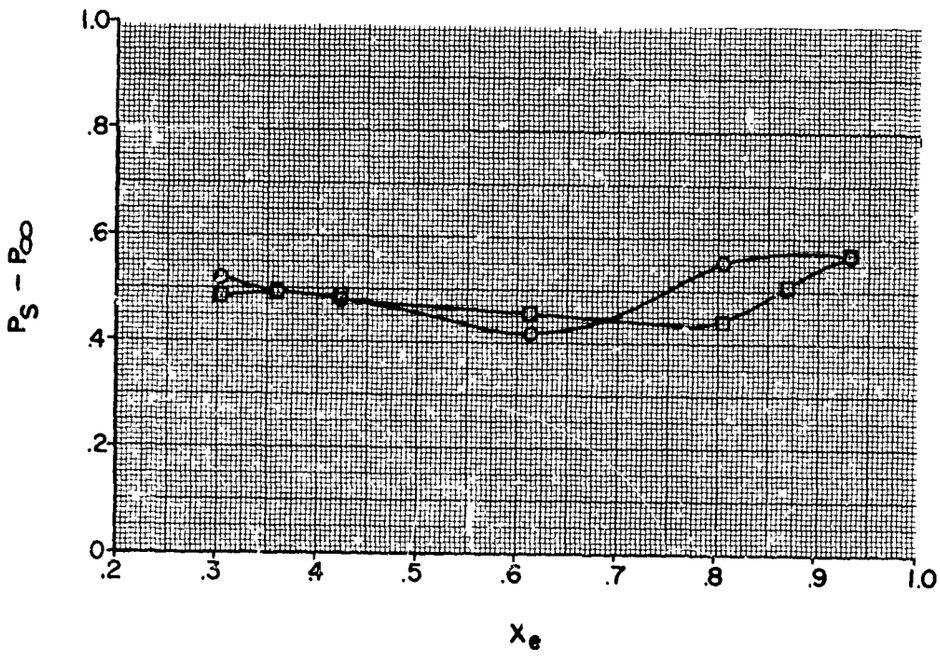

SYMBOL		CONFIGURATION	M	θ	RUN	N
○	WITHOUT INLET VANE	BI-3WT	.4	46°	671	3500
□	0° INLET VANE	BI-3 WTI°	↓	↓	678	↓

FIGURE 279

HS SHROUDED PROPELLER TEST

RADIAL STATIC PRESSURE DISTRIBUTION
AT SHROUD EXIT FROM TRAVERSING
PROBE MEASUREMENTS

EFFECT OF
SHROUD LENGTH

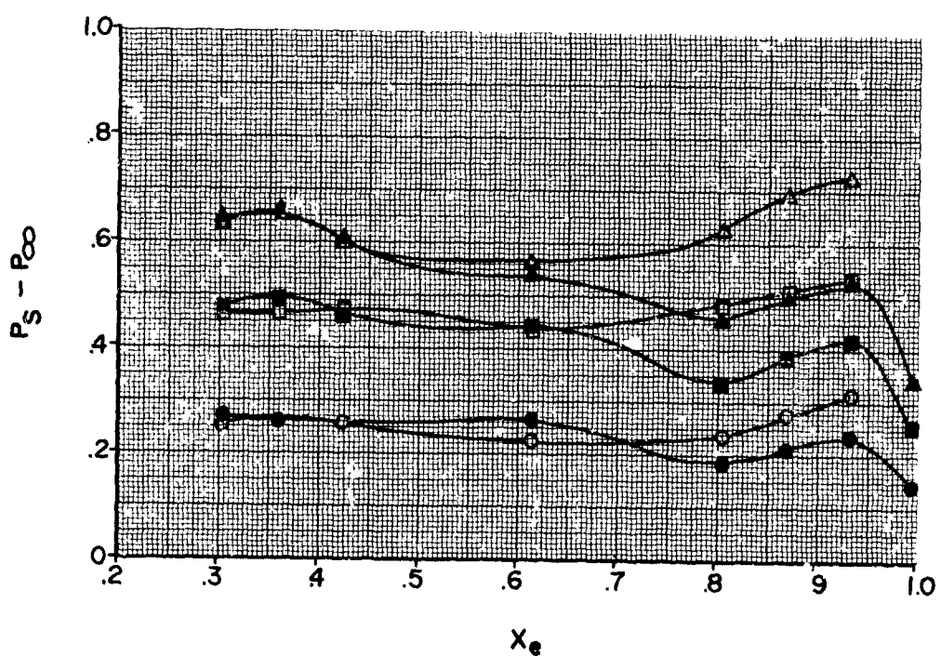

SYMBOL	CONFIGURATION	M	θ	RUN	N
○	B1-3NT	.3	38°	658	5500
□	↓	.4	46°	659	↓
△	↓	.5	50°	660	↓
●	B7-3NT	.3	42°	691	↓
■	↓	4	46°	692	↓
▲	↓	.5	50°	693	↓

FIGURE 280

HS SHROUDED PROPELLER TEST

RADIAL STATIC PRESSURE DISTRIBUTION
AT SHROUD EXIT FROM TRAVERSING
PROBE MEASUREMENTS

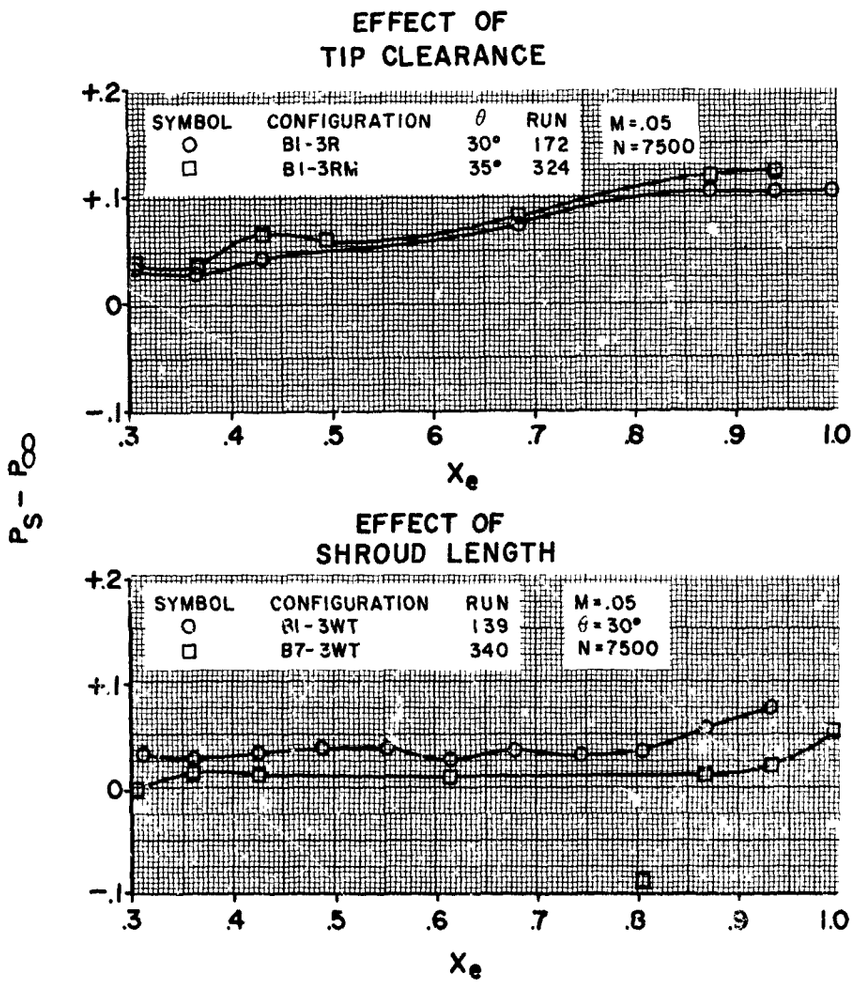

FIGURE 281

HS SHROUDED PROPELLER TEST

RADIAL STATIC PRESSURE DISTRIBUTION
AT SHROUD EXIT FROM TRAVERSING
PROBE MEASUREMENTS

EFFECT OF
PROPELLER PLANFORM

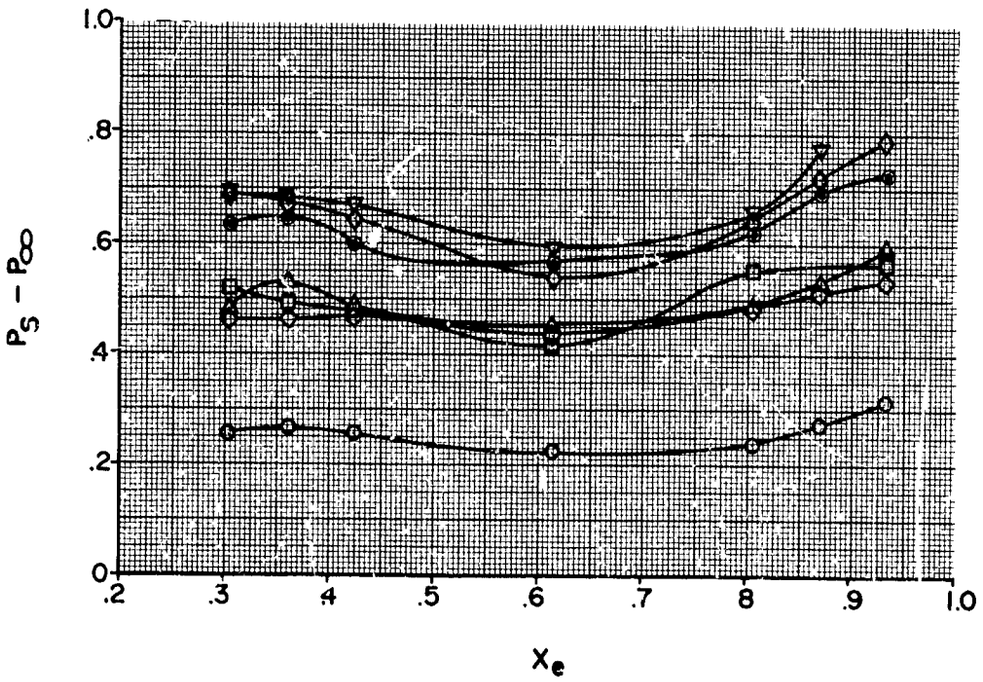

SYMBOL	CONFIGURATION	M	θ	RUN	N
△	BI-3R	.4	46°	684	5500
▽	↓	.5	50°	683	↓
□	BI-3WT	.4	46°	671	↓
◇	↓	.5	50°	673	↓
○	BI-3NT	.3	38°	658	↓
◇	↓	.4	46°	659	↓
◉	↓	.5	50°	660	↓

FIGURE 282

HS SHROUDED PROPELLER TEST

RADIAL STATIC PRESSURE DISTRIBUTION
AT SHROUD EXIT FROM TRAVERSING
PROBE MEASUREMENTS

EFFECT OF
NUMBER OF BLADES

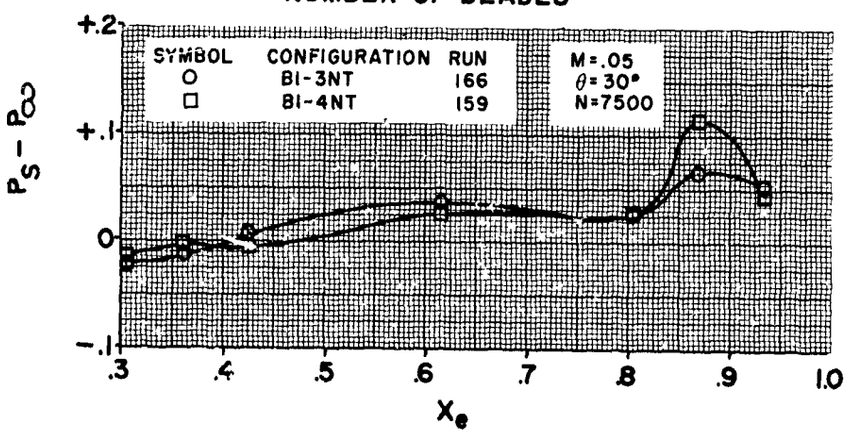

FIGURE 283

HS SHROUDED PROPELLER TEST

RADIAL STATIC PRESSURE DISTRIBUTION
AT SHROUD EXIT FROM TRAVERSING
PROBE MEASUREMENTS

EFFECT OF
NUMBER OF BLADES

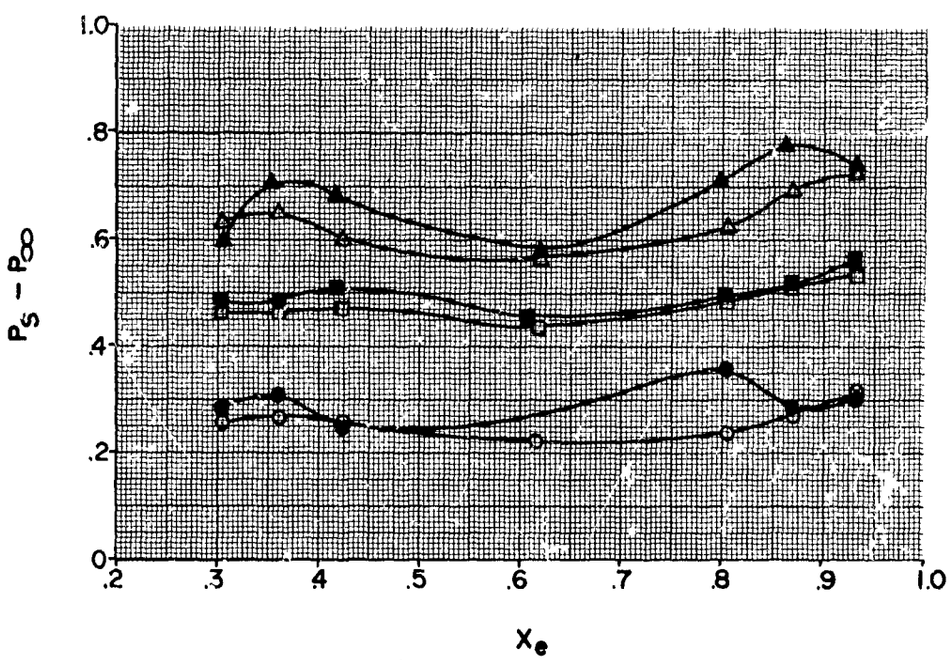

SYMBOL	CONFIGURATION	M	θ	RUN	N
○	BI-3NT	.3	38°	658	5500
□	↓	.4	46°	659	↓
△	↓	.5	50°	660	↓
●	BI-4NT	.3	38°	662	↓
■	↓	.4	46°	663	↓
▲	↓	.5	50°	664	↓

FIGURE 284

HS SHROUDED PROPELLER TEST

RADIAL STATIC PRESSURE DISTRIBUTION
AT SHROUD EXIT FROM TRAVERSING
PROBE MEASUREMENTS

EFFECT OF
TIP CLEARANCE

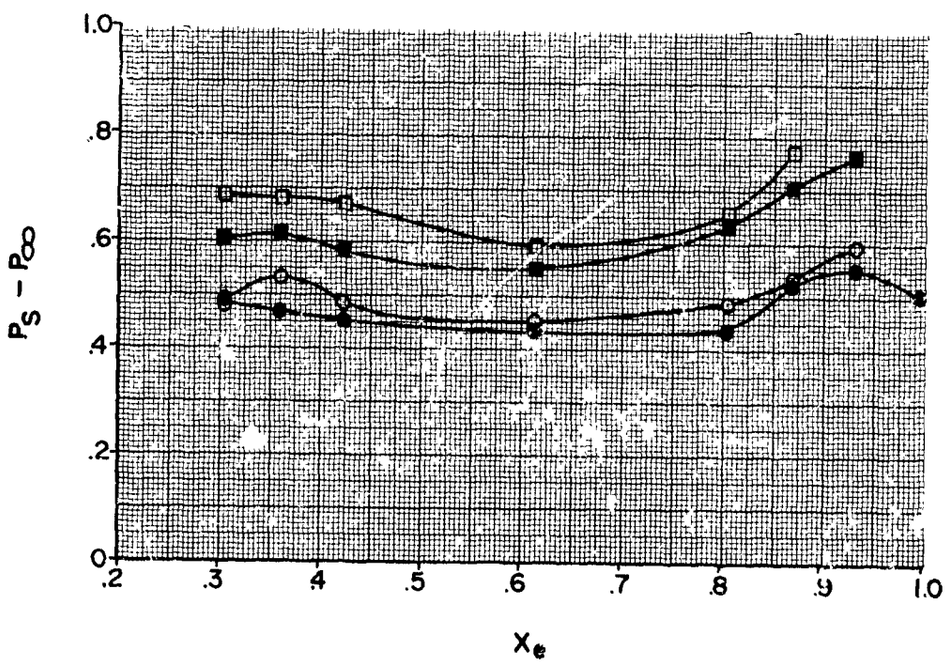

SYMBOL	CONFIGURATION	M	θ	RUN	N
○	BI-3R	.4	46°	684	5500
□	↓	.5	50°	683	↓
●	BI-3RM	.4	46°	655	
■	↓	5	50°	656	↓

FIGURE 285

HS SHROUDED PROPELLER TEST

RADIAL DISTRIBUTION OF AXIAL VELOCITY AT SHROUD EXIT FROM TRAVERSING PROBE MEASUREMENT

EFFECT OF RPM

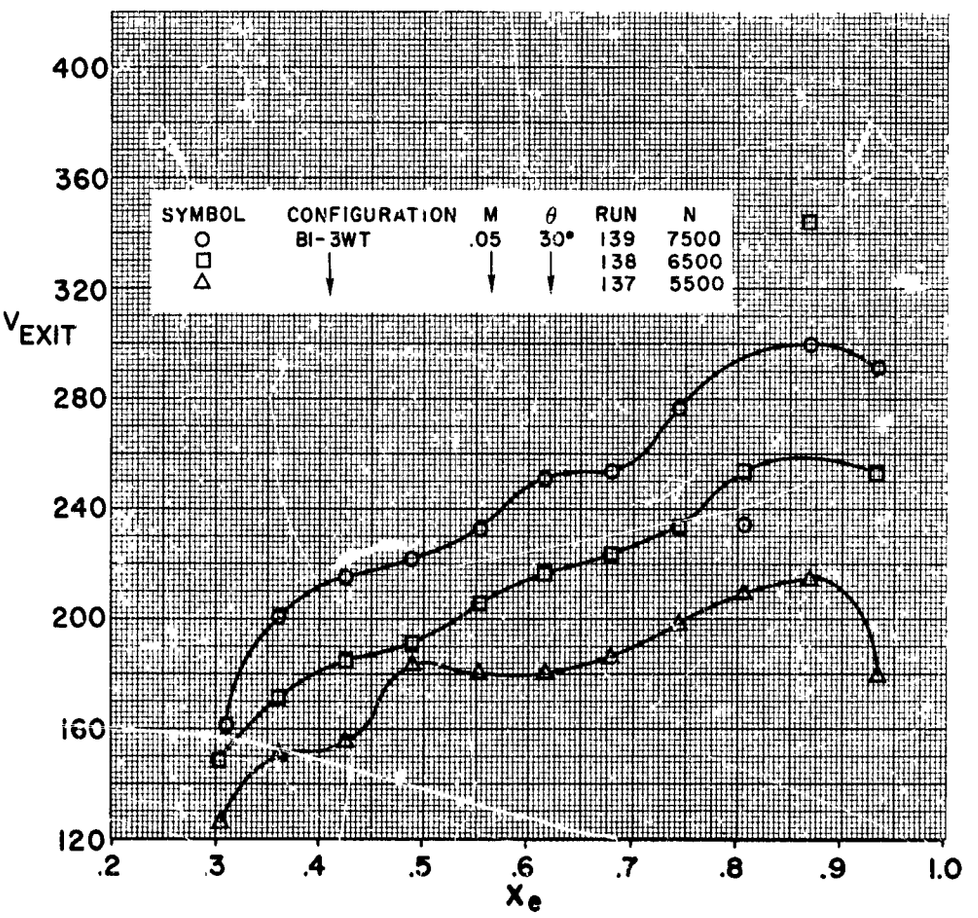

FIGURE 286

HS SHROUDED PROPELLER TEST

RADIAL DISTRIBUTION OF AXIAL VELOCITY AT SHROUD EXIT FROM TRAVERSING PROBE MEASUREMENT

EFFECT OF BLADE ANGLE

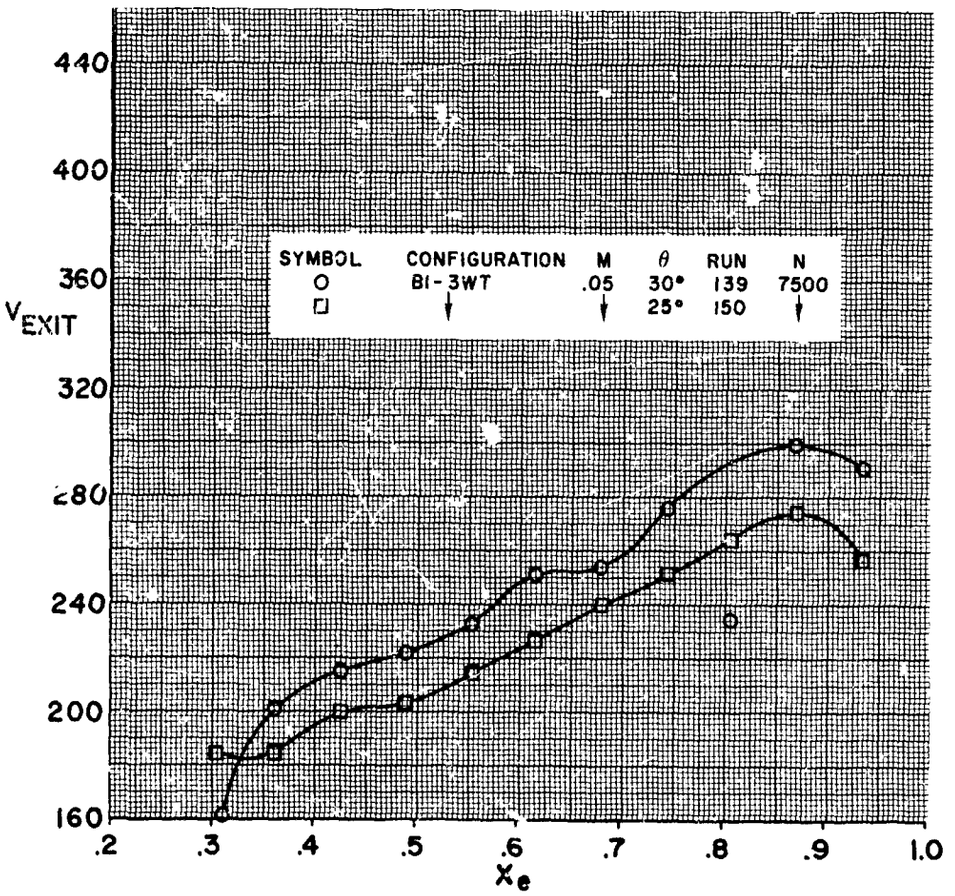

FIGURE 287

HS SHROUDED PROPELLER TEST

RADIAL DISTRIBUTION OF AXIAL VELOCITY AT SHROUD EXIT FROM TRAVERSING PROBE MEASUREMENT

EFFECT OF BLADE ANGLE

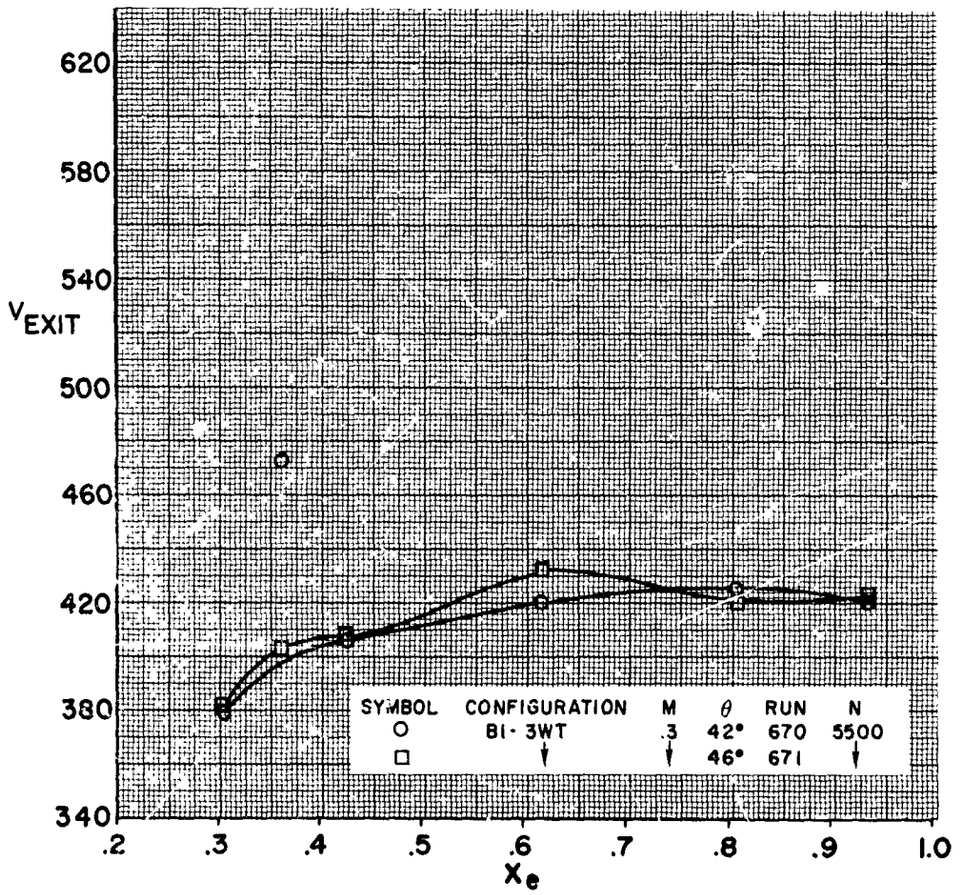

FIGURE 288

HS SHROUDED PROPELLER TEST

RADIAL DISTRIBUTION OF AXIAL VELOCITY AT SHROUD EXIT FROM TRAVERSING PROBE MEASUREMENT

EFFECT OF MACH NUMBER

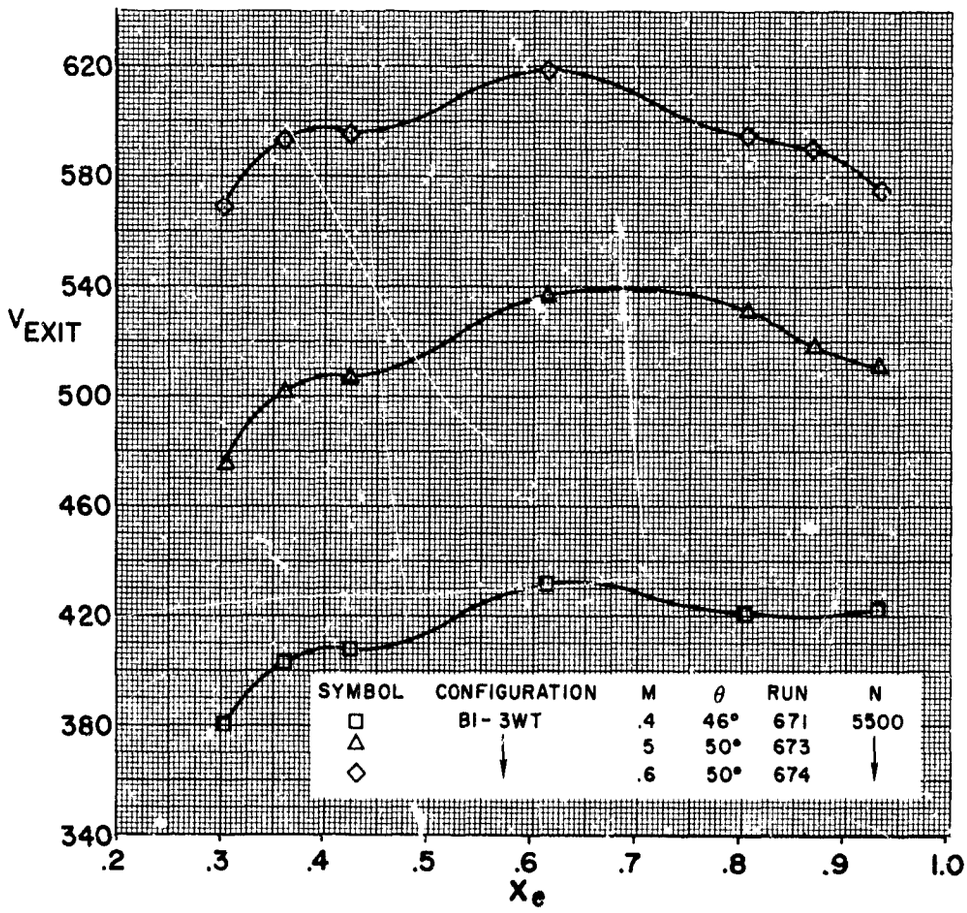

FIGURE 289

HS SHROUDED PROPELLER TEST

RADIAL DISTRIBUTION OF AXIAL VELOCITY AT SHROUD EXIT FROM TRAVERSING PROBE MEASUREMENT

EFFECT OF AREA RATIO

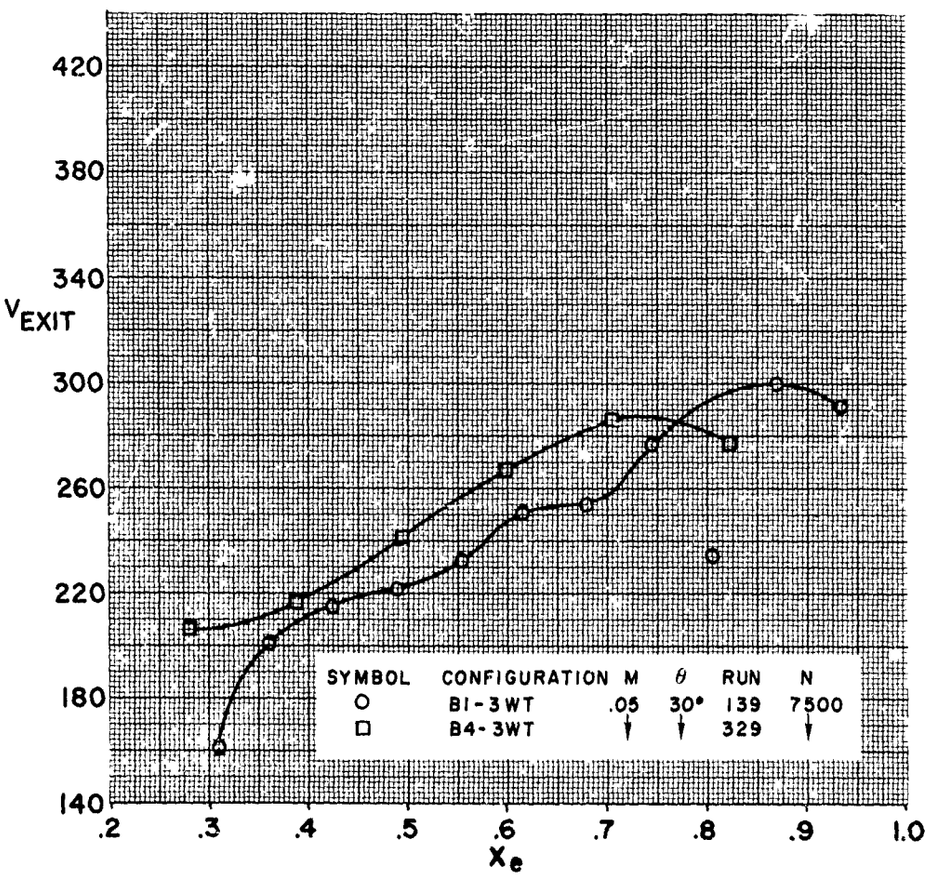

FIGURE 290

HS SHROUDED PROPELLER TEST

RADIAL DISTRIBUTION OF AXIAL VELOCITY AT SHROUD EXIT FROM TRAVERSING PROBE MEASUREMENT

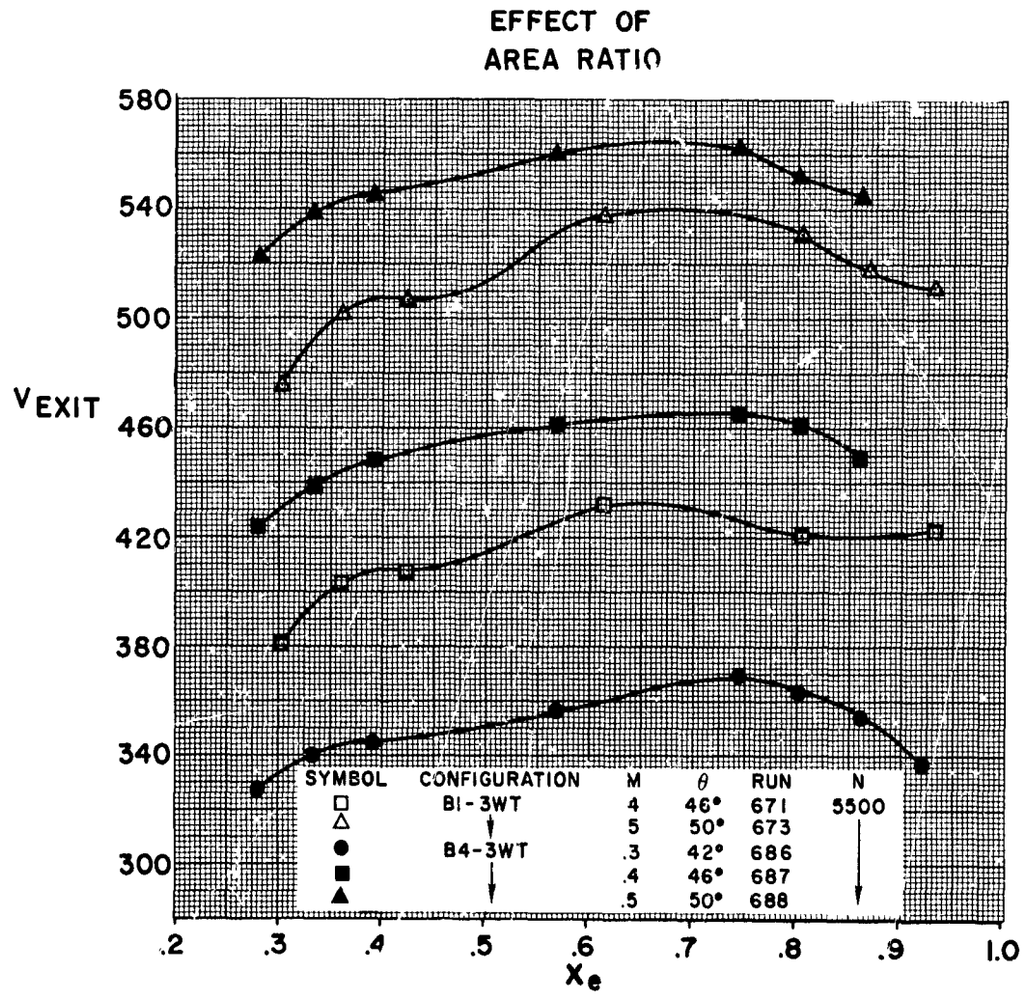

FIGURE 291

HS SHROUDED PROPELLER TEST

RADIAL DISTRIBUTION OF AXIAL VELOCITY AT SHROUD EXIT FROM TRAVERSING PROBE MEASUREMENT

EFFECT OF SHROUD LENGTH

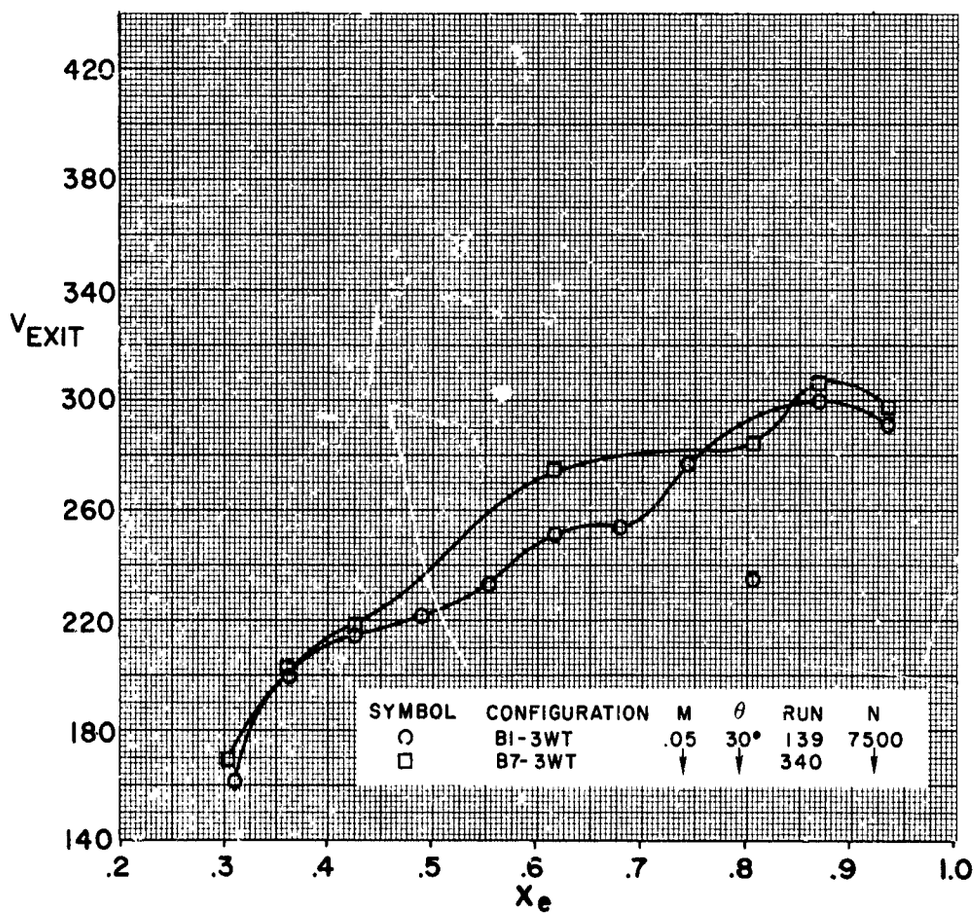

FIGURE 292

HS SHROUDED PROPELLER TEST

RADIAL DISTRIBUTION OF AXIAL VELOCITY AT SHROUD EXIT FROM TRAVERSING PROBE MEASUREMENT

EFFECT OF SHROUD LENGTH

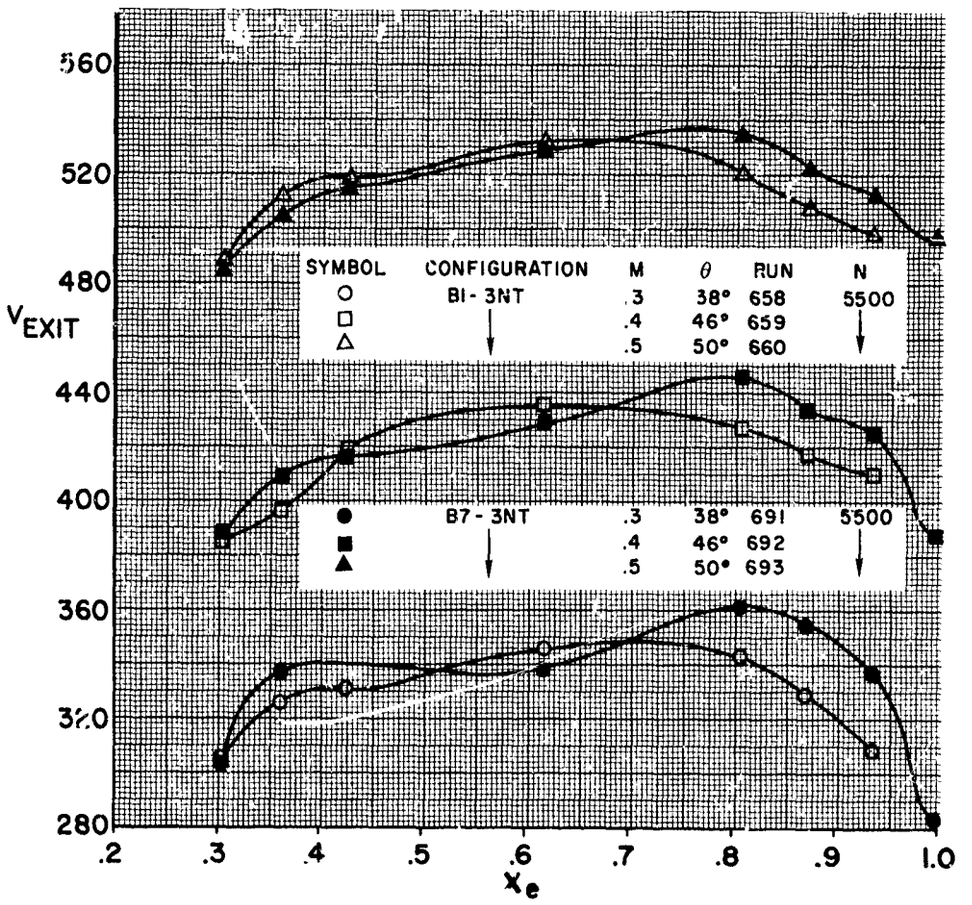

FIGURE 293

HS SHROUDED PROPELLER TEST

RADIAL DISTRIBUTION OF AXIAL VELOCITY AT SHROUD EXIT FROM TRAVERSING PROBE MEASUREMENT

EFFECT OF INLET VANE

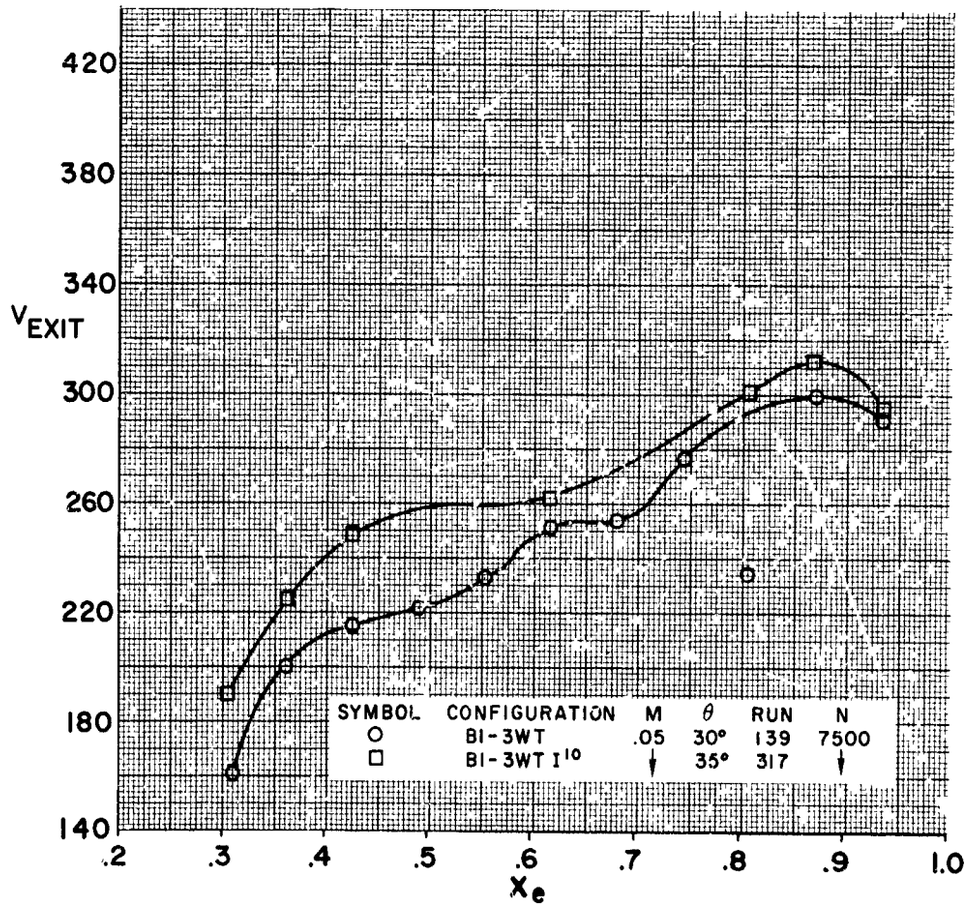

FIGURE 294

HS SHROUDED PROPELLER TEST

RADIAL DISTRIBUTION OF AXIAL VELOCITY AT SHROUD EXIT FROM TRAVERSING PROBE MEASUREMENT

EFFECT OF INLET VANE

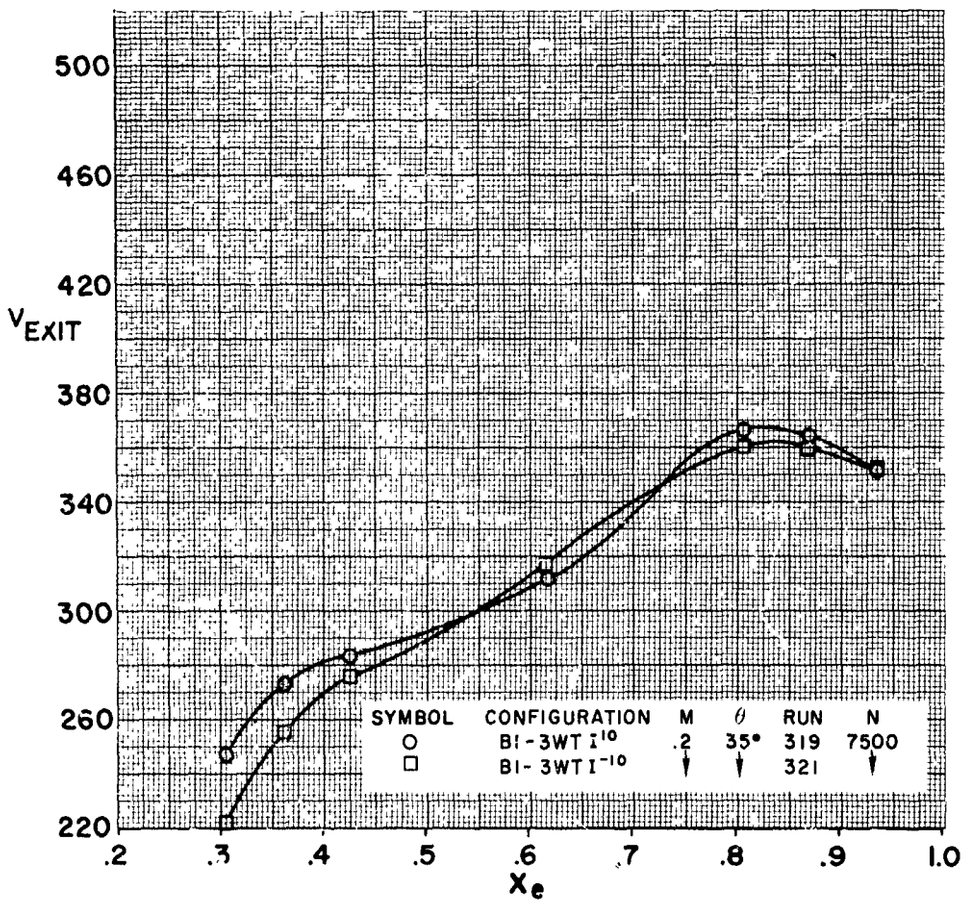

FIGURE 295

HS SHROUDED PROPELLER TEST

RADIAL DISTRIBUTION OF AXIAL VELOCITY AT SHROUD EXIT FROM TRAVERSING PROBE MEASUREMENT

EFFECT OF INLET VANE

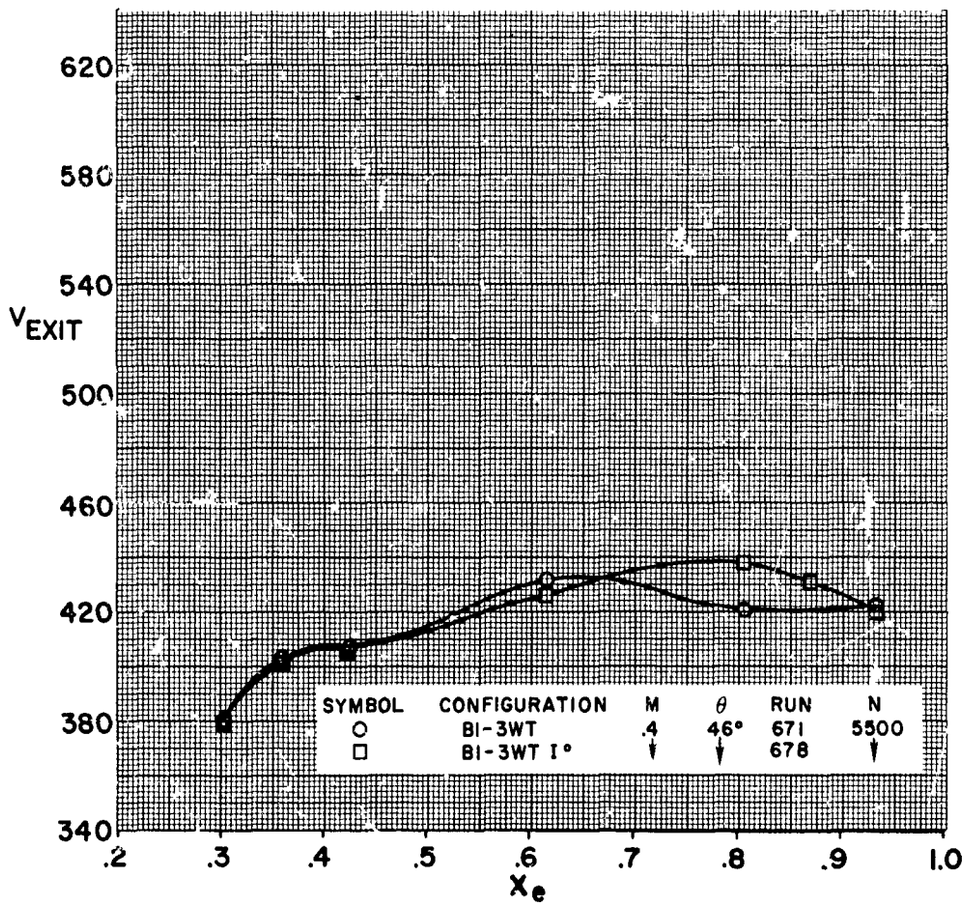

FIGURE 296

HS SHROUDED PROPELLER TEST

RADIAL DISTRIBUTION OF AXIAL VELOCITY AT SHROUD EXIT FROM TRAVERSING PROBE MEASUREMENT

EFFECT OF TIP CLEARANCE

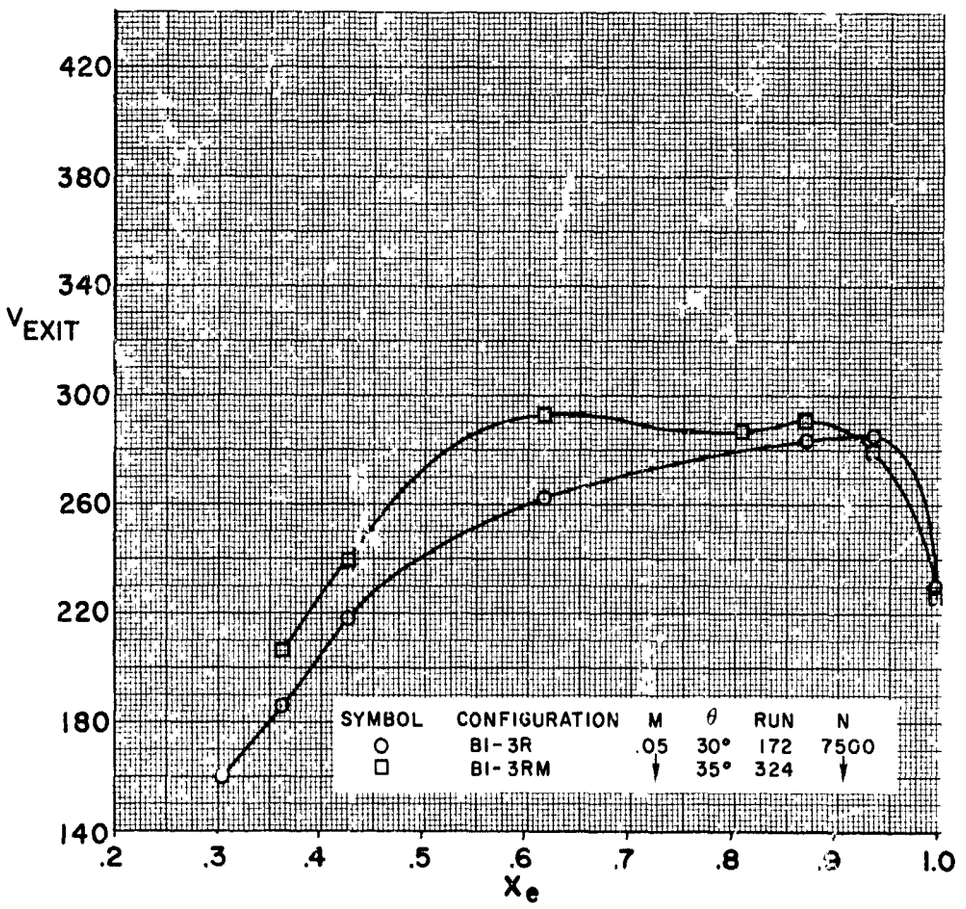

FIGURE 297

HS SHROUDED PROPELLER TEST

RADIAL DISTRIBUTION OF AXIAL VELOCITY AT SHROUD EXIT FROM TRAVERSING PROBE MEASUREMENT

EFFECT OF TIP CLEARANCE

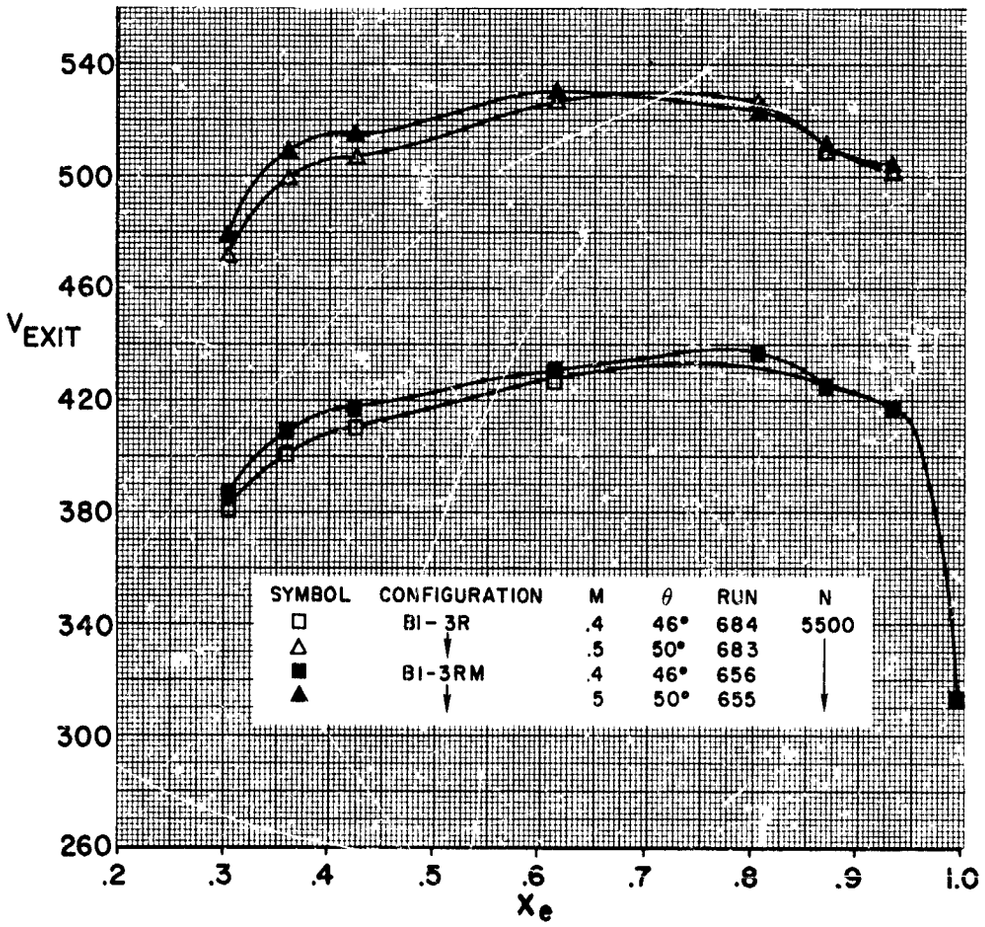

FIGURE 298

HS SHROUDED PROPELLER TEST

RADIAL DISTRIBUTION OF AXIAL VELOCITY AT SHROUD EXIT FROM TRAVERSING PROBE MEASUREMENT

EFFECT OF
NUMBER OF BLADES

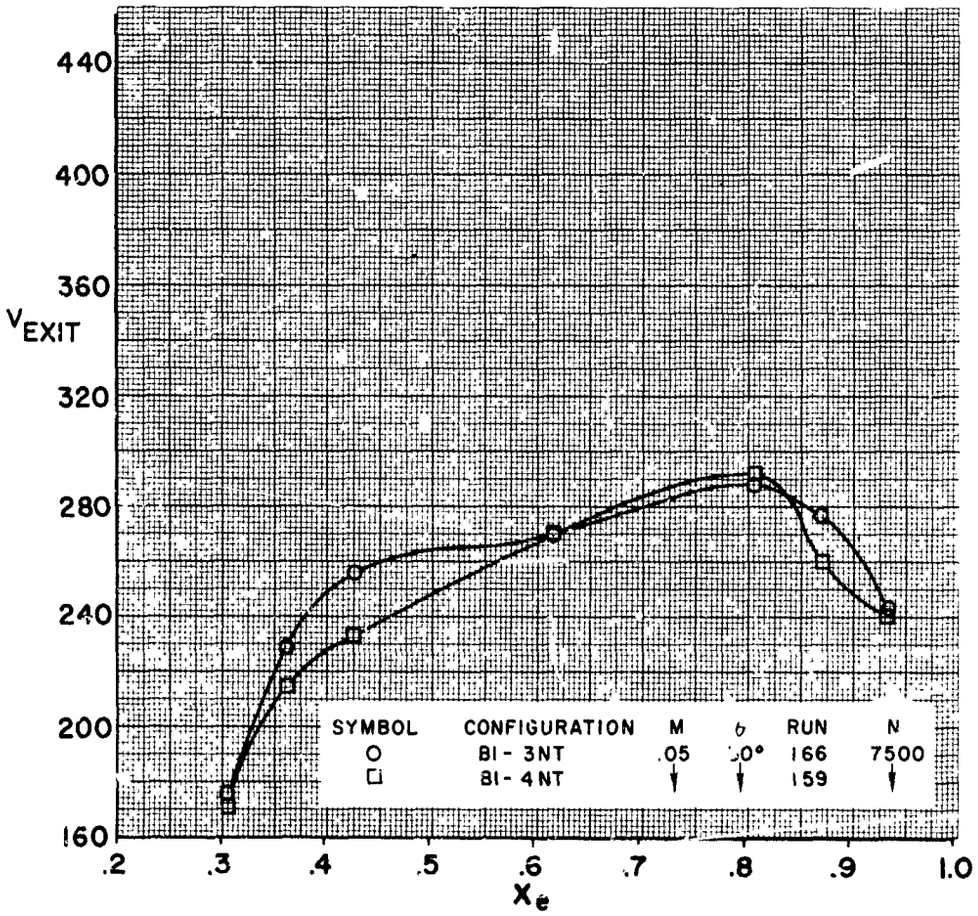

FIGURE 299

HS SHROUDED PROPELLER TEST

RADIAL DISTRIBUTION OF AXIAL VELOCITY AT SHROUD EXIT FROM TRAVERSING PROBE MEASUREMENT

EFFECT OF NUMBER OF BLADES

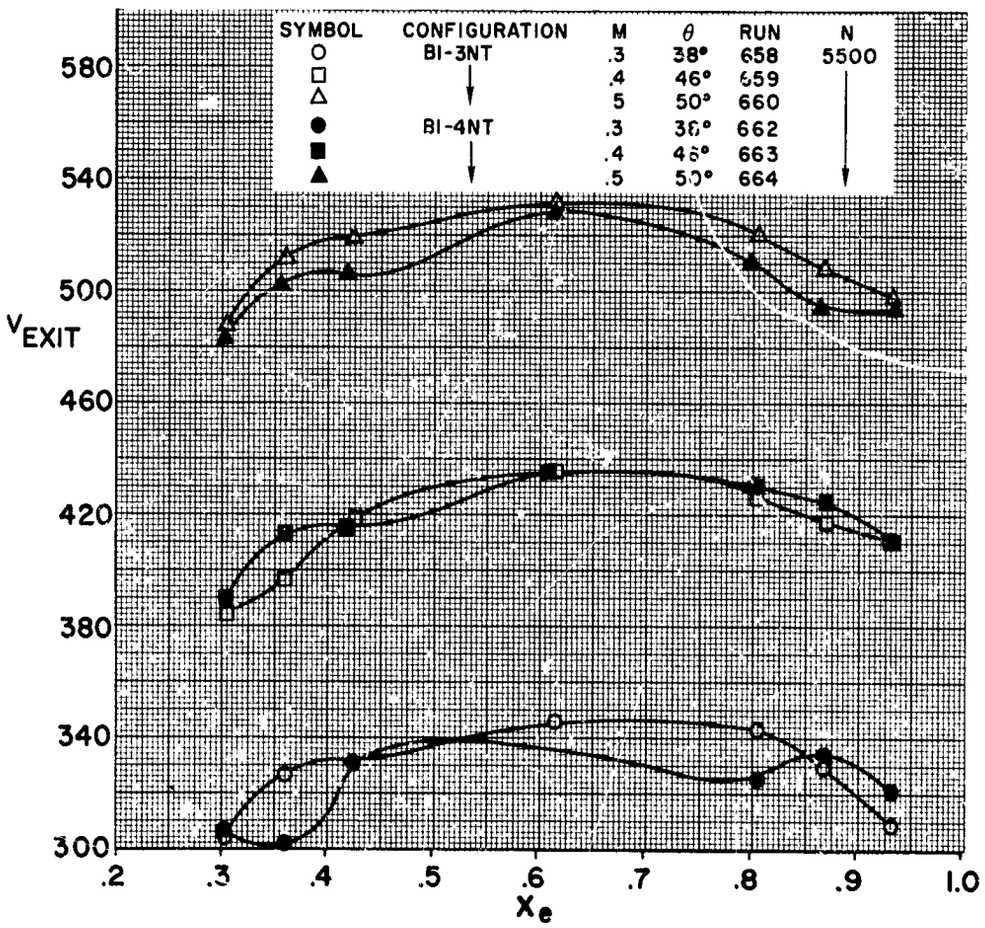

FIGURE 300

HS SHROUDED PROPELLER TEST

RADIAL DISTRIBUTION OF AXIAL VELOCITY AT SHROUD EXIT FROM TRAVERSING PROBE MEASUREMENT

EFFECT OF PROPELLER PLANFORM

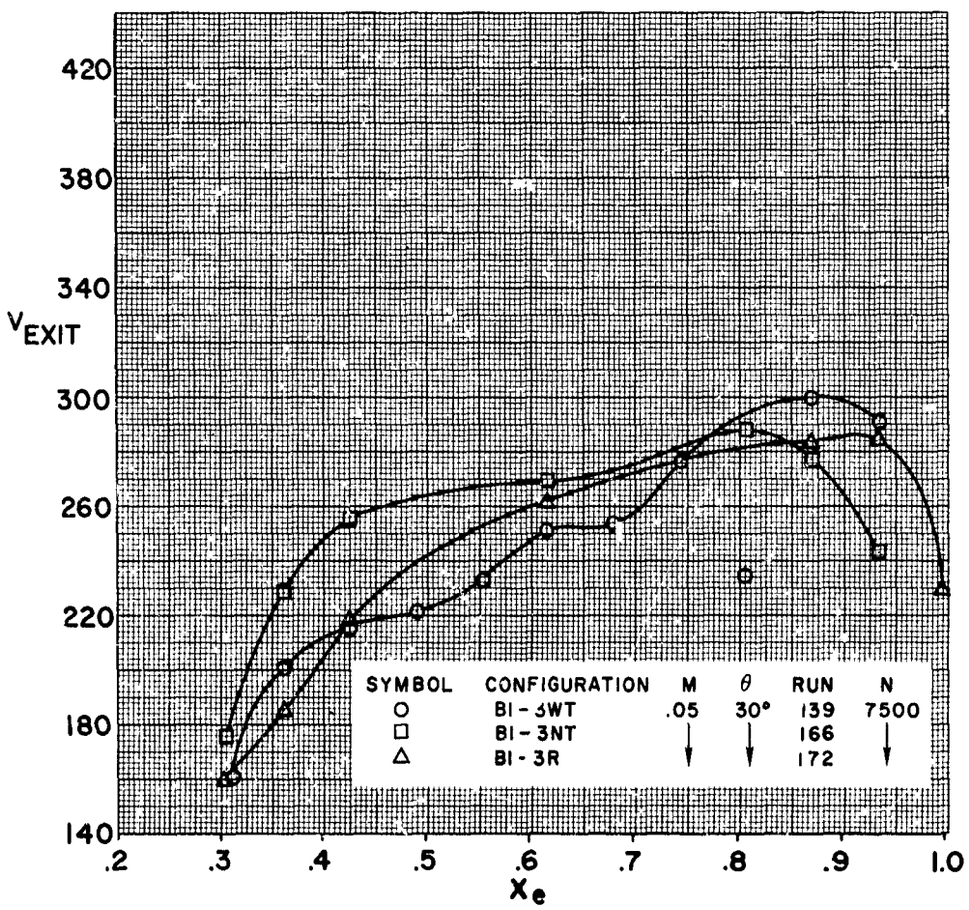

FIGURE 301

HS SHROUDED PROPELLER TEST

RADIAL DISTRIBUTION OF AXIAL VELOCITY AT SHROUD EXIT FROM TRAVERSING PROBE MEASUREMENT

EFFECT OF PROPELLER PLANFORM

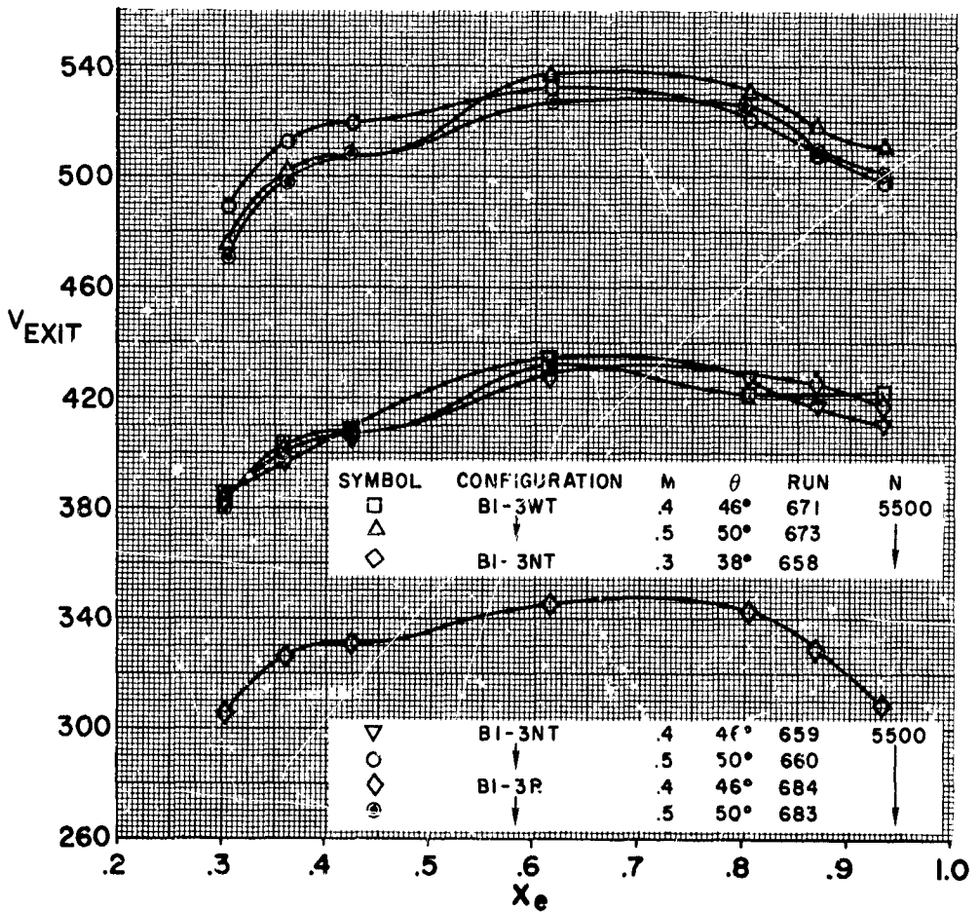

FIGURE 302

XII APPENDICES

12.1 EXTRAPOLATION OF EXPERIMENTAL DATA TO THE STATIC CASE (M = 0)

This experimental program was conducted at tunnel speeds to a minimum 0.02 Mach number. This represented the lowest controllable speed which could be maintained in the tunnel. As a consequence of this, the data had to be extrapolated.

Several methods of obtaining static data were considered and many of these tried. After evaluating the various methods one stood out as being superior. This method employed calculated performance as an extrapolation guideline.

The calculation method used was a modification of the method employed in the Hamilton Standard Preliminary Design Bulletin 6220 referred to as the Blue Book. This is a two-dimensional vortex strip analysis of the propeller forces coupled with a momentum representation of the shroud. The shroud thrusts were corrected in accordance with the Blue Book empirical drag corrections. Figure 12.1-1 is a plot of calculated and experimental values of power coefficients (Cp) vs net thrust coefficient (Ctnet) for a constant tip speed at several Mach numbers. This plot was employed so that any blade angle setting inaccuracies could be eliminated; i.e. the plot is not dependent upon a fixed angle setting. The experimental data in figure 12.1-2 is shown by symbols connected with broken lines for 0.02, 0.05, 0.10, 0.15, and 0.20 Mach number. The calculated data is shown at each of these Mach numbers and at M = 0 with a solid line. Figure 12.1-2 is a crossplot at fixed values of Cp, of the data shown in Figure 12.1-1. Again symbols and broken lines represent the experimental data taken from the faired curves of Figure 12.1-1. The extrapolation from M = 0.02 to M = 0 followed the guideline established by the calculated data.

The need for an extraplation guideline is exhibited in Figure 12.1-2 where the slope of Ctnet vs M is seen to be very steep near M = 0. The same guideline approach was considered for the extrapolation of the propeller thrust coefficients. The agreement between calculated and experimental Ct's was very good, but the shallow slopes of Ct vs M did not necessitate a guideline for extrapolation.

Due to the limitations in the vortex and momentum theory, guidelines for six of the test models (B2-3WT, B5-3WT, B6-3WT, B1-3R1/2M, B1-3RM and B7-3NT) could not be computed. The extrapolation for these six models was based upon slopes of C_{TNET} vs Mach number established for the other models.

Ctnet for each model at each of the reported tip speeds (785, 915 and 985) was extrapolated to M = 0 in this manner. The resulting values are believed to fairly, consistently and accurately represent the model static thrust.

Some of the other methods attempted which did not yield consistent or accurate results are:

(Continued)

1. Extrapolations of experimental figures of merit to M = 0.

2. Duct flows were computed from measured thrusts and plotted against M. The slope of flow vs M was fairly shallow but the resultant thrust computed at M = 0 flow did not produce consistent static data.

3. Semilogarithmic, squared, cubed and inverse plots of the experimental data.

HS SHROUDED PROPELLER TEST

VARIATION OF NET THRUST COEFFICIENT
WITH POWER COEFFICIENT FOR
CALCULATED AND EXPERIMENTAL VALUES

CONFIGURATION BI-3WT
N = 6000

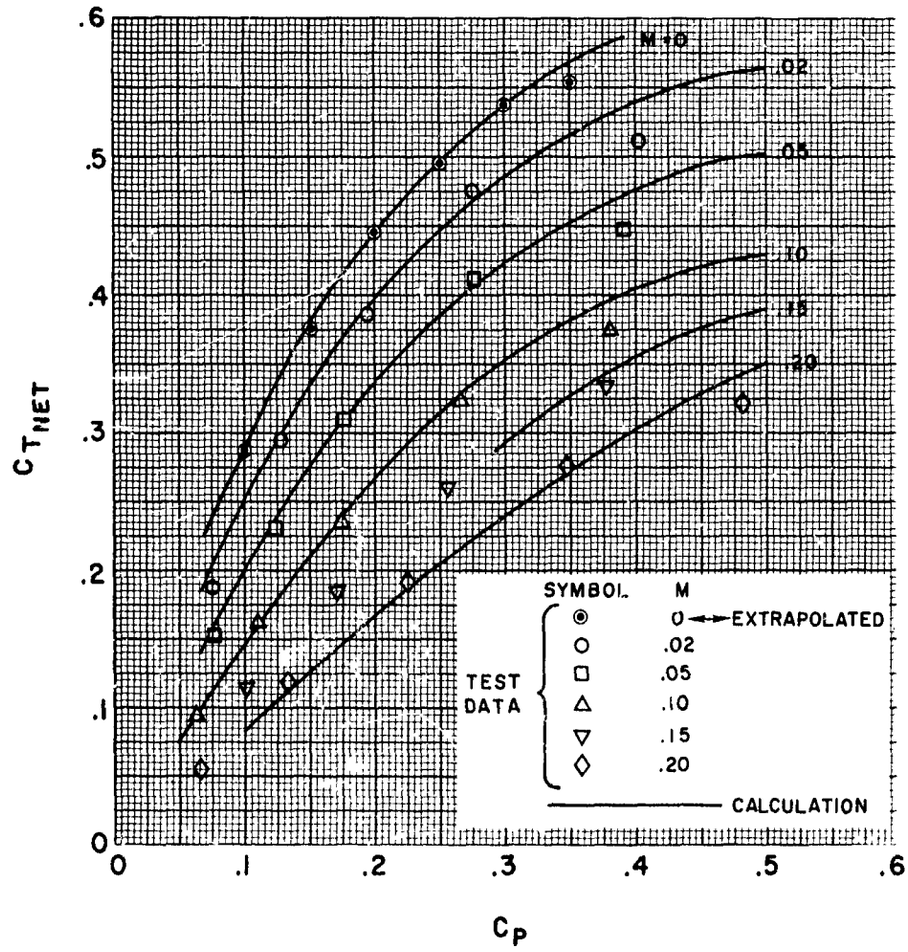

FIGURE 12.1-1

HS SHROUDED PROPELLER TEST

VARIATION OF NET THRUST COEFFICIENT
WITH MACH NUMBER FOR EXPERIMENTAL AND
CALCULATED VALUES

CONFIGURATION BI-3WT
N = 6000

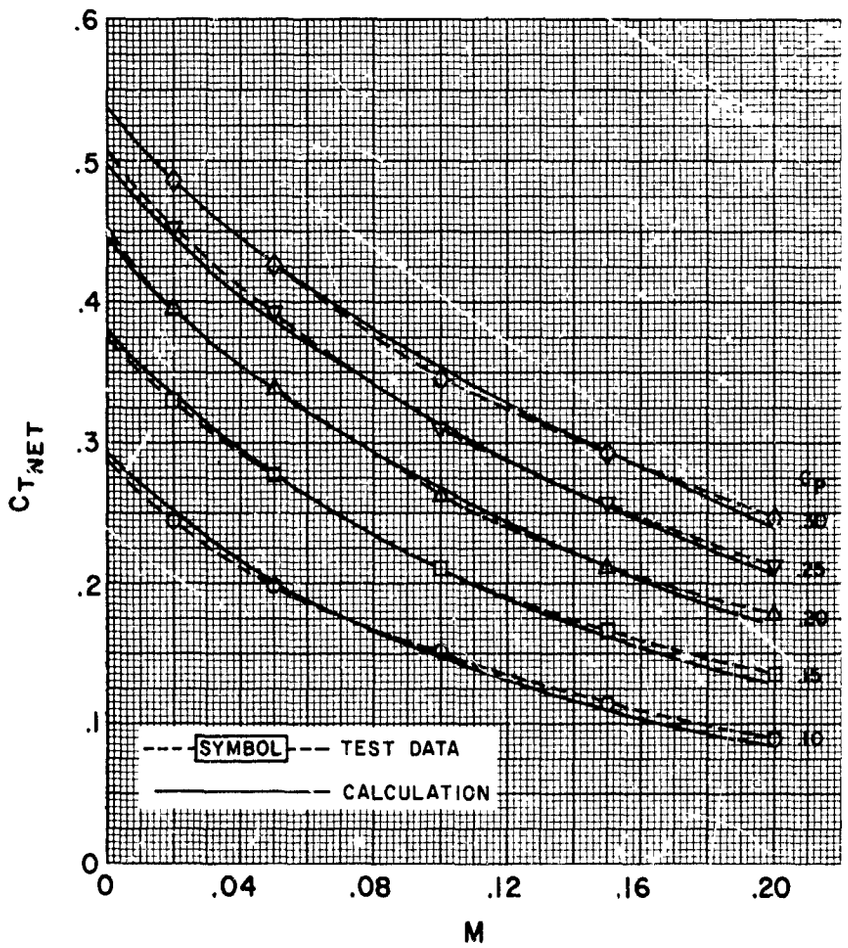

FIGURE 12.1-2

APPENDICES

12.2 CONVERSION OF EXPERIMENTAL DATA FROM COEFFICIENT FORM

The experimental measurements were reduced to propeller coefficient form through the data reduction program. These coefficients are defined in the list of symbols, and the relationships and the constants used to generate the curves of this report are listed below.

Propeller Configuration	Nominal Propeller Diameter Used in Coefficients
3RM	2.472'
3R1/2M	2.487'
All Others	2.494'

Power Loading ($BHP/D^2 X \rho_o/\rho$)

The power loading is based upon the shroud ID(2.5') at the propeller plane, and is equal to $k_1 C_p$. Values of k_1 are shown in Table 12.2-1.

Thrust per Shaft Horsepower (T/BHP and Tnet/BHP)

Thrust per shaft horsepower curves are shown for the basic model (B1-3WT) and are related to the coefficients in this manner:

$$T/BHP = k_2\ Ct/Cp$$

$$Tnet/SHP = k_2\ Ctnet/Cp$$

Values of k_2 are shown in Table B-1.

Thrust Ratios (T/TB1-3WT, Tnet/Tnet B1-3WT, etc.)

$$T/TB1\text{-}3WT = k_3 \frac{Ct}{Ct\ (B1\text{-}3WT)} \text{ (at same RPM and power loading)}$$

$$Tnet/Tnet\ B1\text{-}3WT = k_3 \frac{Ctnet}{Ctnet\ (B1\text{-}3WT)}$$

where CtB1-3WT and Ctnet B1-3WT are read @ Cp = Cp (B1-3WT)

and Ct and Ctnet are read @ Cp = k_4 Cp (B1-3WT)

Values of k_3 and k_4 are shown in Table 12.2-1.

(Continued)

Thrust Ratios (where basic model is not used in denominator)

$$\frac{T}{Tx} = \frac{T}{T\,(B1\text{-}3WT)} \div \frac{Tx}{T\,(B1\text{-}3WT)}$$

$$\text{and } \frac{Tnet}{Tnetx} = \frac{Tnet}{Tnet\,(B1\text{-}3WT)} \div \frac{Tnetx}{Tnet\,(B1\text{-}3WT)}$$

For example, the effect of tip clearance is shown by comparing the thrusts of B1-3R1/2m and B1-3RM with B1-3R i.e., $\frac{T\,(B1\text{-}3R1/2M)}{T\,(B1\text{-}3R)} = \frac{T\,(B1\text{-}3R1/2M)}{T\,(B1\text{-}3WT)} \div \frac{T(B1\text{-}3R)}{T\,(B1\text{-}3WT)}$

TABLE 12.2-1

PROPELLER CONFIGURATION	RPM	K1	K2	K3	K4
3RM	5000	36.95	—	0.9653	1.047
	6000	63.8	—	0.9653	1.047
	7000	101.3	—	0.9653	1.047
	7500	124.6	—	0.9653	1.047
3R1/2M	5000	38.1	—	0.9888	1.013
	6000	65.8	—	0.9888	1.013
	7000	104.4	—	0.9888	1.013
	7500	128.4	—	0.9888	1.013
3R	5000	38.6	2.645	1.0	1.0
	6000	66.7	2.205	1.0	1.0
	7000	105.9	1.890	1.0	1.0
	7500	130.3	1.764	1.0	1.0

APPENDICES

12.3 SHROUD SURFACE PRESSURE INTEGRATIONS - FRICTION DRAG

Several of the shroud surface static pressure distributions have been integrated to obtain a shroud friction drag. Whereas this effort did not yield the quality of results which were hoped for, it did provide a better understanding of the distribution of thrust load on the shroud. The friction drag obtained from these pressure integrations has been compared with analytically determined friction drags from methods described in references 1 and 5. These friction drags have two applications of prime importance, and they are: (1) to explain the apparent shroud ineffectiveness at low power loadings $\left(\frac{BHP}{D^2} \times \rho_o/\rho\right)$ and (2) to provide a friction correction to be applied to the theoretical performance prediction method under development for Phase III of this contract.

Measurements

The shroud surface pressures were measured at two azimuthal locations. At each azimuthal location there were twenty three static taps on the inside surface, nineteen on the external surface and a leading and trailing edge tap. In figure 12.3-2 the pressure distributions at both locations are shown and some differences can be observed. These differences are not fully understood but could be due to several contributing factors. Some of these factors are: surface irregularities, leaks in pressure loads, model pitch or yaw, tolerances on pressure tap locations, and shroud asymmetry. The degree to which these differences affect the friction evaluation cannot be fully established, but both measurements as well as the average measurement have been integrated.

METHOD OF INTEGRATION AND FRICTION DRAG EVALUATION

$$C_{P_L} = \frac{P_L - P_\infty}{q_\infty} \quad \begin{array}{l} + \text{Cp indicates } P_L > P_\infty \\ - \text{Cp indicates } P_L < P_\infty \end{array}$$

With the shroud divided into three sections, as shown in figure 12.3-1, the pressure integration can quite easily be visualized. Section I starts at the leading edge and extends aft to the points of minimum radius on the inside surface and to the maximum radius on the outside surface. Section II is that portion of the center section of the shroud which has a constant inside and outside radius and hence no projected surface area in the thrust direction. Section III is the aft portion of the shroud commencing where the inner and outer radii again change from the minimum and maximum dimensions. Therefore:

(Continued)

$$\Delta Ts = \Delta P_L \times \Delta A$$

where $\Delta A = 2\pi r \Delta r$

$$\Delta P_L = P_{LIII} @ r - P_{LI} @ r$$

proceeding to the limit and integrating yields =

$$T_s = \int_{R_i}^{Ro} 2\pi r \, (P_{III} - P_I)_{@ r} \, dr$$

but $2\pi r dr = \pi d(r^2)$

$$\& \; (P_{LIII} - P_{LI}) @r = q_\infty \left(\frac{P_L - P_\infty}{q_\infty}_{III} - \frac{P_L - P_\infty}{q_\infty}_{I}\right) @ r = q_\infty (C_{P_{LIII}} - C_{P_{LI}}) @r$$

$$Ts = \frac{\pi q_\infty}{144} \int_{Ri^2 = 225}^{Ro^2 = 324} (C_{P_{LIII}} - C_{P_{LI}}) \, d(r^2)$$

and with C_{P_L} plotted against r^2 (inches ^{2}) and integrated Ts is obtained. The various shroud sections (I, II and III) and the shroud axial locations (x) are denoted on figure 12.3-2. The association of ri^2 and ro^2 with static tap location for the various shroud models is shown in Table 10.3-I. A perusal of this tabulation readily shows that the projected area in the thrust direction, measured by r^2. changes very abruptly near the leading edge. This is also shown in figure 12.3-2 and creates some inaccuracy in the pressure integrals.

Several pressure distributions were integrated to define the friction drag and to explain the loss of shroud effectiveness at low values of $BHP/D^2 \times \rho_o/\rho$. Figure 12.3-3 presents a summary of the pressure integrals, the measured force and the friction drag for several M = 0.3 data points. Superimposed upon this curve is the friction drag as deduced by the method of reference 1. (The friction drag from reference 5 was very similar to that from reference 1). The reasonably good correlation shown here between the experimental and analytical approaches was not found to be consistently true for all cases examined. Therefore, for purpose of this report the method of reference 1 will be used to define the shroud friction drag and to establish conclusions on shroud effectiveness. However, for the shroud friction addition to the theoretical method of Phase III of this contract, additional effort will be expended on the experimental pressure distribution as well as on purely analytical methods.

(Continued)

The analytically determined values of shroud friction drag (reference 1) are summarized in Table 12.3-II for the B1 and B4 shrouds (1.1 and 1.3 area ratio). The equation derived from reference 1 from which these drags were determined is:

$$\rho_o/\rho\, F_D = \pi D C^{0.8} \frac{\rho_o}{2} \left(\frac{\mu}{\rho}\right)^{0.2} \quad 1.8\left\{1 + \left(\frac{A_1}{A_2}\right)^{1.8} \quad 1 + \frac{2}{\rho_o \Pi/4\,(1 - X_n^2)} \quad \frac{T\,\rho_o/\rho}{D^2}\right\}.074$$

TABLE 12.3—II

$T/D^2 X\, \rho_o/\rho$ = V (fps)	0	20	40	60	0	20	40	60
	$F_D\ \rho_o/\rho$ FOR B1 SHROUD (POUNDS)				$F_D\ \rho_o/\rho$ FOR B4 SHROUD (POUNDS)			
0	0	1.8	3.3	4.8	0	2.5	4.5	6.5
100	1.7	3.3	4.8	6.2	2.6	4.7	6.8	8.7
200	5.5	6.8	8.2	9.6	6.7	8.7	10.7	12.5
300	11.6	13.0	14.3	15.7	13.4	15.2	17.1	18.9
400	19.4	20.6	22.0	23.3	22.6	24.4	26.2	28.2
500	28.7	29.9	31.2	32.5	34.0	35.6	37.3	39.2
600	40.0	41.2	42.3	43.5	47.1	48.7	50.2	52.2

Table 12.3-II was based upon the B1 and B4 shroud model dimensions and upon air viscosity at 65°F.

The friction drag for the 1.2 area ratio shroud (B3) can be attained from the equation for $F_D\ \rho_o/\rho$ or from a linear interpolation of the drags on Table 12.3-II. For all the remaining models, except B7 (short chord) the drags are the same as for B1. For the short chord shroud the drags are twenty percent less than the tabulated values.

TABLE 12.3-I

A_4/A_2 =	1.1		1.1		1.2		1.3		1.1	
%C	r_i^2	r_o^2	r_i^2	r_o^2	r_i^2	r_o^2	r_i^2	r_o^2	r_i^2	r_o^2
L.E.	289.5	289.5	280.8	280.8	289.5	289.5	289.5	289.5	289.5	289.5
01	266.8	306.5	260.	299.	266.8	306.5	266.8	306.5	170.0	304.5
02	258.	311.8	252.	305.5	258.	311.8	258.0	311.8	262.0	309.5
04	245.	318.	241.8	313.2	245.	318.	245.	318.	251.5	315.2
06	237.5	320.2	235.9	317.8	237.5	320.2	239.5	320.2	243.2	318.5
08	232.5	322.	231.	320.	232.5	322.	232.5	322.	238.	320.5
10	229.	323.	228.2	322.	229.	323.	229.	323.	233.5	321.8
12.5	226.5	323.5	226.6	323.2	226.5	323.5	226.5	323.5	230.	322.7
15	225.2	324.	225.3	323.7	225.2	324.	225.2	324.	227.	323.5
17	225.	324	225.1	324.	225.	324.	225.	324.	226.5	323.8
20	225.	324.	225.	324.	225.	324.	225	324.	225.3	323.9
25	225.	324.	225.	324.	225.	324.	225.	324.	225.	224.
30	225.	323.	225.	323.	225.	323.	225.	323.8	225.	322.5
35	225.	321.	225.	321.	225.	322.2	225.	323.5	225.	319.2
40	225.	318.5	225.	318.5	225.	320.5	225.	322.7	225.	316.
50	225.	311.5	225.	311.5	225.	315.5	225.	321.	225.3	307.
60	228.8	302.	228.8	302.	231.5	308.5	234.7	317.5	228.2	296.6
70	233.	291.	233.	291.	240.8	301.5	248.	311.5	233.	284.5
80	238.	279.	238.	279.	250.	293.	261.5	304.8	237.5	273.5
90	242.5	265.	242.5	265.	259.	282.	275.5	277.8	242.7	261.3
92	244.	X	244.	X	261.	X	278.	X	244.	X
94	245.	X	245.	X	263.	X	281.	X	245.	X
96	245.5	X	245.5	X	265.	X	284.	X	245.8	X
98	246.5	X	246.5	X	267.	X	286.8	X	246.5	X
T.E.	248.2	248.2	248.2	248.2	269.3	269.3	290.	290.	248.2	248.2
SHROUD DESIGNATION	B1		B2		B3		B4		B7	

HS SHROUDED PROPELLER TEST

SHROUD CHORD FORCE INTEGRATION ZONES

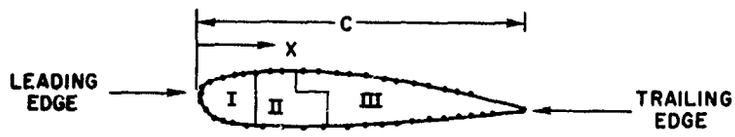

CROSS-SECTIONAL VIEW AT 90° AND 315°

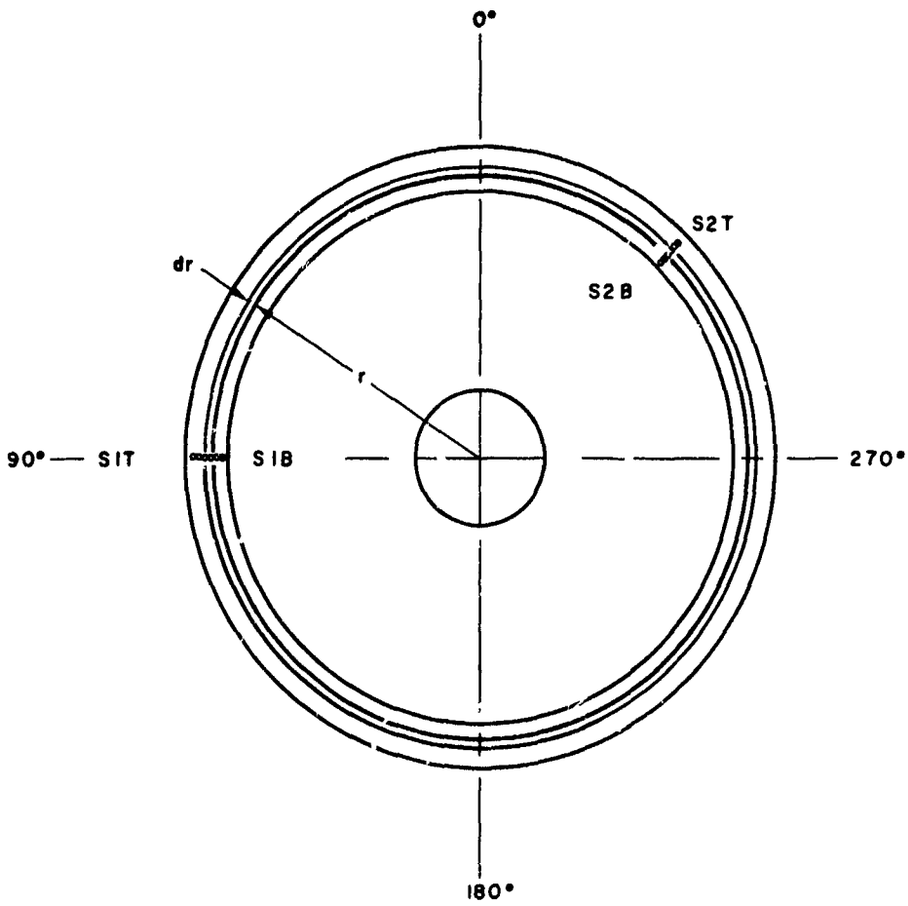

VIEW LOOKING DOWNSTREAM

FIGURE 12.3–1

HS SHROUDED PROPELLER TEST

SHROUD SURFACE PRESSURE

CONFIGURATION BI-3WT
TIP SPEED = 850 FPS
M = .30
θ = 34°
RUN 667

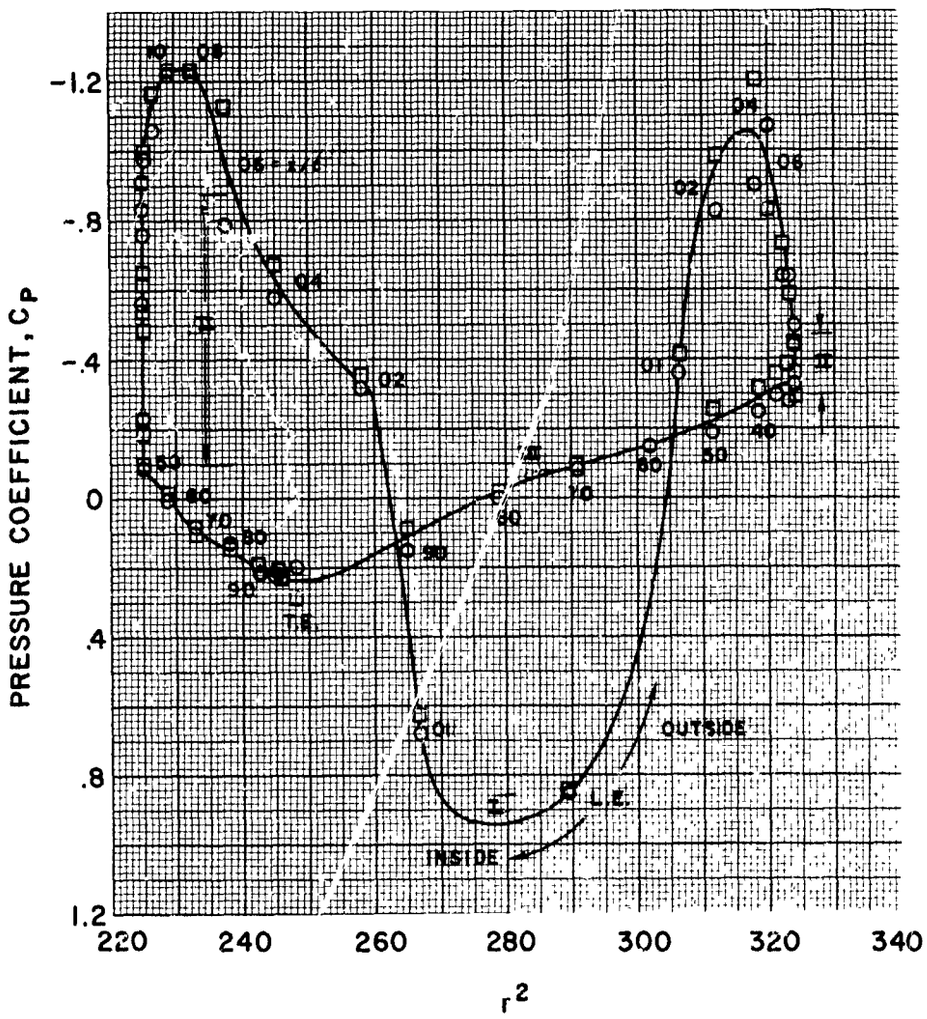

FIGURE 12.3—2

HS SHROUDED PROPELLER TEST

SUMMARY OF SHROUD FRICTION DRAG

CONFIGURATION BI-3WT
M = .3

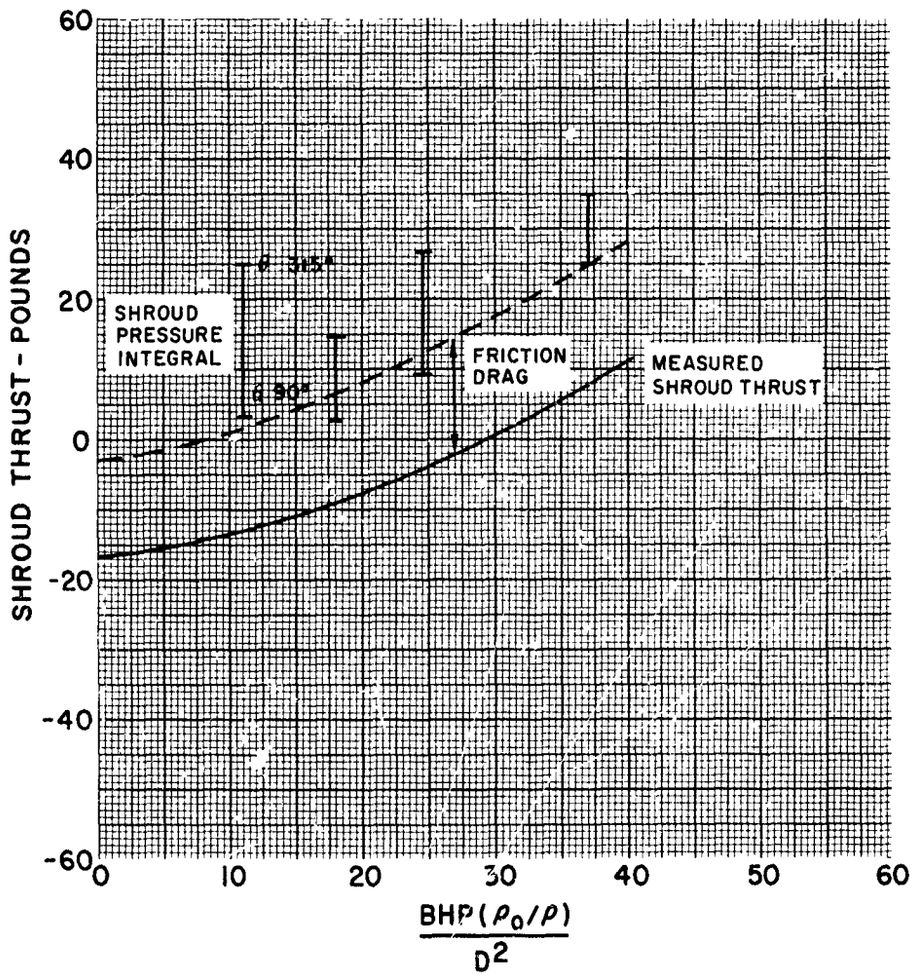

I REPRESENTS RANGE OF INVISCID SHROUD THRUST FROM PRESSURE INTEGRATION AT TWO AZIMUTHAL LOCATIONS

---- REPRESENTS INVISCID SHROUD THRUST OBTAINED FROM MEASURED THRUST PLUS ANALYTICALLY DETERMINED FRICTION DRAG.

FIGURE 12.3—3

APPENDICES

12.4 PROPELLER THRUST AND POWER DISTRIBUTIONS FROM SHROUD EXIT TRAVERSE PROBE MEASUREMENTS

A three dimensional traversing probe was installed at the shroud exit for approximately 95 runs to obtain total and static pressure distributions and flow magnitude and direction. This probe was traversed across the shroud exit plane with measurements taken at six or more radial locations for one azimuthal position. These data are completely tabulated in Volume IV of this report and will be used extensively in establishing and checking out the theoretical method for Phase III of this contract. The traversing probe is described in detail in the Test Methods section of this report and also in Volume II.

Propeller Thrust Distribution

An incompressible flow analysis was employed to compute propeller thrust distributions (dCt/dx). The velocities and pressures used were from traverse probe measurements at the shroud exit plane. With notation as defined in the Figure 3 the derivation of the equations for dCt/dx for the 1.1 area ratio shrouds with C/D = 0.667 is:

Constants:

Xh3 = 0.25	H denotes total pressure
Xhe = 0.251	P denotes static pressure
R3 = 1.25'	V denotes axial velocity
Re = 1.313'	V zeta denotes tangetial or swirl velocity
A2 = A3	Radial velocities are neglected.
	$dT = 16dC_t \; n^2R^4$
	$x = r/R$

From Bernoulli:

$$H_3 = P_3 + 1/2\rho V_3^2 + 1/2\rho V^2 ZETA \qquad \text{(d1)}$$

$$H_2 = P_2 + 1/2\rho V_2^2 \qquad \text{(d2)}$$

For a control volume around an elemental propeller area dA.

$$(P_3 - P_2)\, dA_3 = dT + \rho dA_3 V_2^2 - \rho dA_3 V_3^2 \qquad \text{(d3)}$$

XII (Continued)

which for incompressible flow becomes

$$(P_3 - P_2) = dT/dA_3 = \frac{16dC_T \rho n^2 R_3^4}{dA_3} \qquad (d4)$$

$$\text{and } dA_3 = 2\pi r_3 dr_3 = 2\pi R_3^2 X_3 d X_3 \qquad (d5)$$

Subtracting (d_2) from (d_1) substituting (d_4) and (d_5) and letting V2 = V3 (Va)

$$H_3 - H_2 = \frac{8\rho n^2 R_3^2}{\pi x} dC_T/d_x + 1/2\rho V^2 \text{ ZETA} \qquad (d6)$$

$H_2 = H\infty$ (assumes no inlet total pressure loss) (d7)

which was quite well substantiated by inlet rake measurements)

$$H_3 = He + \Delta H \qquad (d8)$$

The measurements made at the shroud exit are transferred to the propeller plane so that dCt/dx can be defined. ΔH is the loss in total pressure due to the diffuser inefficiency and is estimated from the one dimensional computed loss for a conical diffuser in axial flow.

$$\Delta H = (1 - \eta_D)\ 1/2\,\rho \bar{V}_3^2 \left[1 - \left(\frac{A_3}{A_e}\right)^2\right] \qquad (d9)$$

where η_D = diffuser efficiency = 92% by assumption
$\bar{V}_3$ = average velocity @ 3
$Ae/A_3 = 1.1$

In order to distribute the total pressure loss in a realistic manner the inefficiency, as represented by $(1 - \eta_D)$ was distributed linearly at the outer and inner boundaries (Xe = 0.035 to 1.0 and Xe = 0.25 to 0.35). The loss magnitude was assumed to be twice as large at the outer wall as at the inner wall representing a net loss equal to the loss implied by equation (d9).

The streamline at the exit plane are assumed to be represented at the propeller plane by the following expression:

$$X_3 = \frac{1 - X_{h3}}{1 - X_{he}} (Xc - Xhe) + Xh3 \qquad (10)$$

(Continued)

and $$dX_3 = \left(\frac{1 - X_{h_3}}{1 - X_{h_e}}\right) dXe \qquad \text{(d11)}$$

but for the 1.1 area ratio shrouds, where $X_{h_3} = 0.250$ and $X_{h_e} = 0.251$

$$X_3 = X_e \text{ and } dX_3 = dX_e \qquad \text{(d12)}$$

and from conservation of angular momemtum

$$r3\ V_{ZETA_3} = re\ V_{ZETA_e}$$

or $$V_{ZETA_3} = \frac{X_e R_e}{X_3 R_3}\ V_{ZETA_e} \qquad \text{(d13)}$$

which for the model being considered ($1.1A_e/A_3$, $C/D = 0.667$) reduces to:

$$V_{ZETA_3} = 1.05\ V_{ZETA_e} \qquad \text{(d14)}$$

Combining (d6), (d10), (d11) and (d14)

$$dC_T/d_X = \frac{\pi X_e}{8\rho\, n^2 R_3{}^2}\left[(H_e - H\infty) + \Delta H - 0.55\rho\, V^2{}_{ZETA_e}\right] \qquad \text{(d15)}$$

and (d15) reduces to:

$$dC_T/d_X = \frac{908\ X_e}{\rho\, N^2}\left[(H_e - H\infty) + \Delta H - 0.55\rho\ V^2{}_{ZETA_e}\right] \qquad \text{(d16)}$$

where ρ = free stream density
N = propeller RPM
$H_e - H\infty$ = psf
V_{ZETA_e} = Ve tan ZETA

A numerical example utilizing equation (d16) is shown in Table 12.4-I and several dCt/dx distributions are shown in figures 12.4-1 through 12.4-7. Integrations of these distributions gave thrust coefficients which agreed very well with measured values.

Power Coefficient Distributions

An incompressible flow analysis was employed to compute the propeller power distribution (dCp/dx) from traverse probe measurements. Due to the direct dependence of

XII

(Continued)

dCp/dx upon the measured swirl angle ZETA, and due to the tolerance in the ZETA measurement, correlations between measured and computed powers have been poor. Because of the poor correlation no refinements in the analysis and no measurement corrections were attempted since they could only bring about minor improvements. The formulation of the equation is:

$$550\ dHP = \Omega\, dQ_3 = 32\ \rho n^3 R_3^{\ 5} dC_p \tag{d21}$$

and from conservation of angular momentum

$$dQ_3 = dQ_e, \text{ where } Q = \text{input torque} \tag{d22}$$

$$\&\ dQ_e = (V_{ZETA_e}\, r_c)\ (\rho\, 2\, \pi r_e d\, r_e\, V_e) \tag{d23}$$

with $r = xR$, $\Omega = 2\pi n$ and $n = N/60$

$$\frac{d\,C_p}{dX} = \frac{3280}{N^2}\ X_e^{\ 2}\ V_{ZETA_e}\ V_e \tag{d24}$$

Several power distributions were calculated and are shown in figure 12.4-8 through 12.4-9. For the power distributions a ± 2° tolerance was assumed on the swirl angle (ZETA), and the effect of this tolerance is shown in figures 10.4-7 and 10.4-8. These distributions were integrated and compared with the measured values, but because of the errors in the swirl angle the agreement with test was poor.

TABLE 12.4—I

CONDITION $M = 0.03$, RPM $= 6500$, $\Theta\ 3/4 = 30^{o}$, RUN 137

$\rho = 0.00246$, $\frac{908}{\rho N^2} = 0.000871$

X_E	[1] $H_E - H_\infty$ (PSF)	[2] ΔH(PSF)	[3] $0.55\ \rho V_Z^2$(PSF)	[4] [1] + [2] − [3] (PSF)	[5] $0.00871 - X_E$ [4] $= d\frac{C_T}{d_X}$
0.995	60.50	15.2	4.95	70.75	0.614
0.933	86.40	—	1.88	84.52	0.685
0.868	85.00	—	2.78	82.22	0.621
0.805	80.60	—	2.03	78.57	0.551
0.743	69.15	—	1.56	67.59	0.437
0.678	63.35	—	1.50	61.85	0.367
0.615	59.00	—	1.72	57.28	0.306
0.552	51.80	—	1.69	50.11	0.241
0.488	47.50	—	1.71	45.79	0.194
0.425	44.65	—	2.08	42.57	0.157
0.361	40.30	—	2.69	37.61	0.118
0.304	28.80	1.4	2.98	27.22	0.072

$$C_T = \int_{X = 0.25}^{X = 1.0} \left(\frac{DCT}{DX}\right) d_X = 0.258$$

TEST VALUE OF $C_T = 0.258$

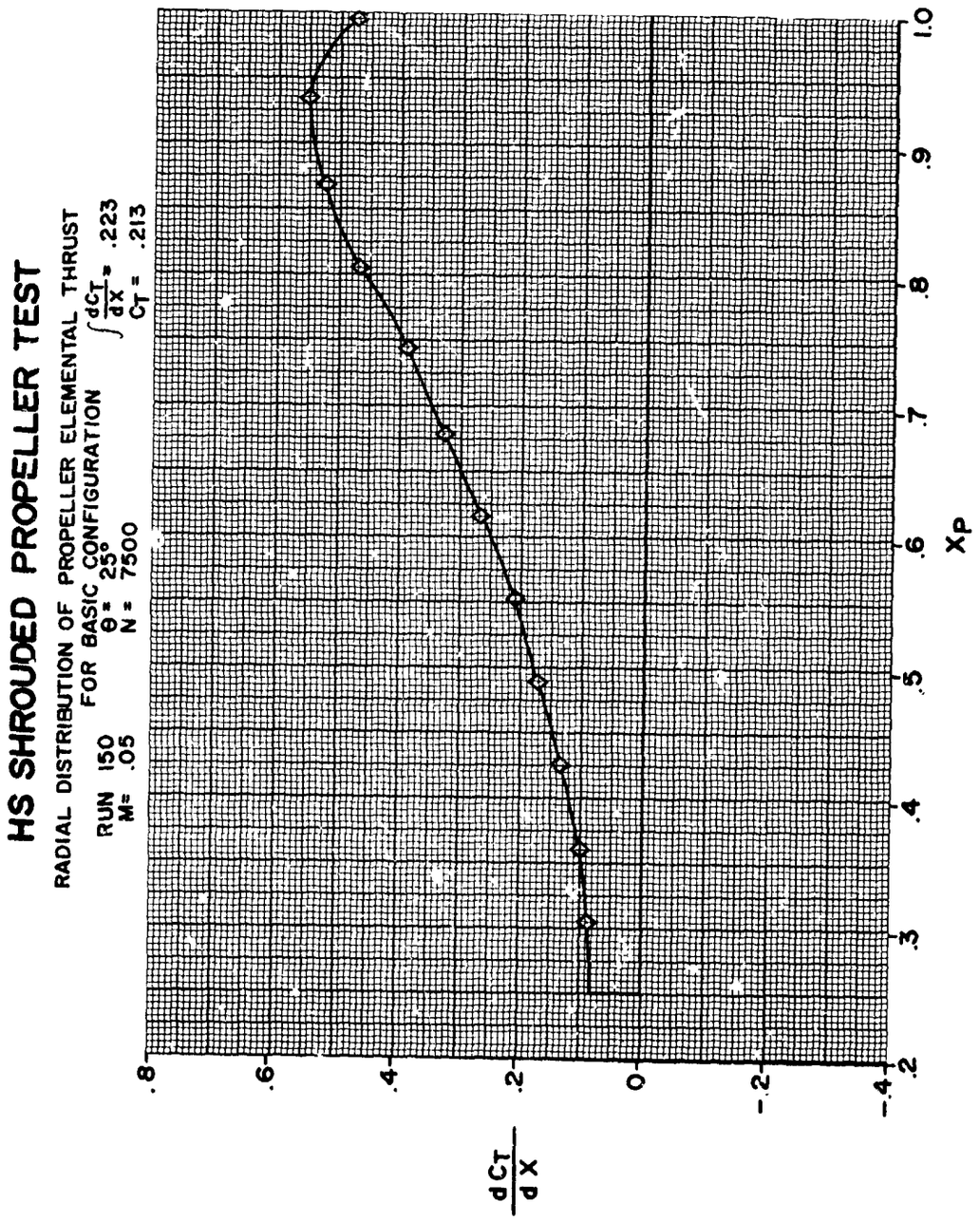
HS SHROUDED PROPELLER TEST
RADIAL DISTRIBUTION OF PROPELLER ELEMENTAL THRUST
FOR BASIC CONFIGURATION
RUN 150
M= .05
θ= 25°
N= 7500
∫ dCT/dX = .223
CT = .213
dCT/dX
.8
.6
.4
.2
0
-.2
-.4
.2
.3
.4
.5
.6
.7
.8
.9
1.0
XP

FIGURE 12.4-1

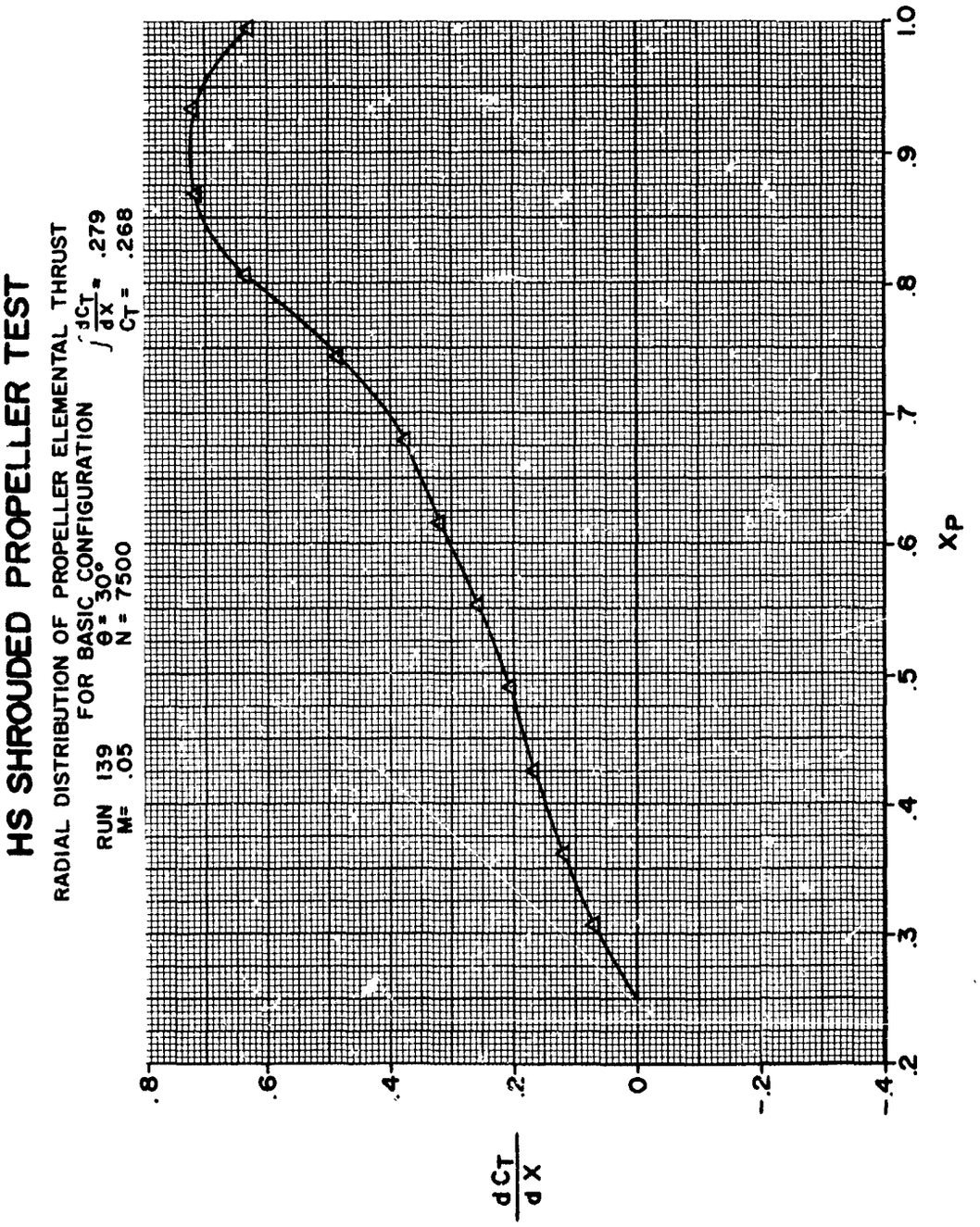
HS SHROUDED PROPELLER TEST
RADIAL DISTRIBUTION OF PROPELLER ELEMENTAL THRUST
FOR BASIC CONFIGURATION
RUN 139
M= .05
θ= 30°
N = 7500
∫ dCT/dX = .279
CT = .268
dCT/dX
.8
.6
.4
.2
0
-.2
-.4
.2
.3
.4
.5
.6
.7
.8
.9
1.0
XP

FIGURE 12.4-2

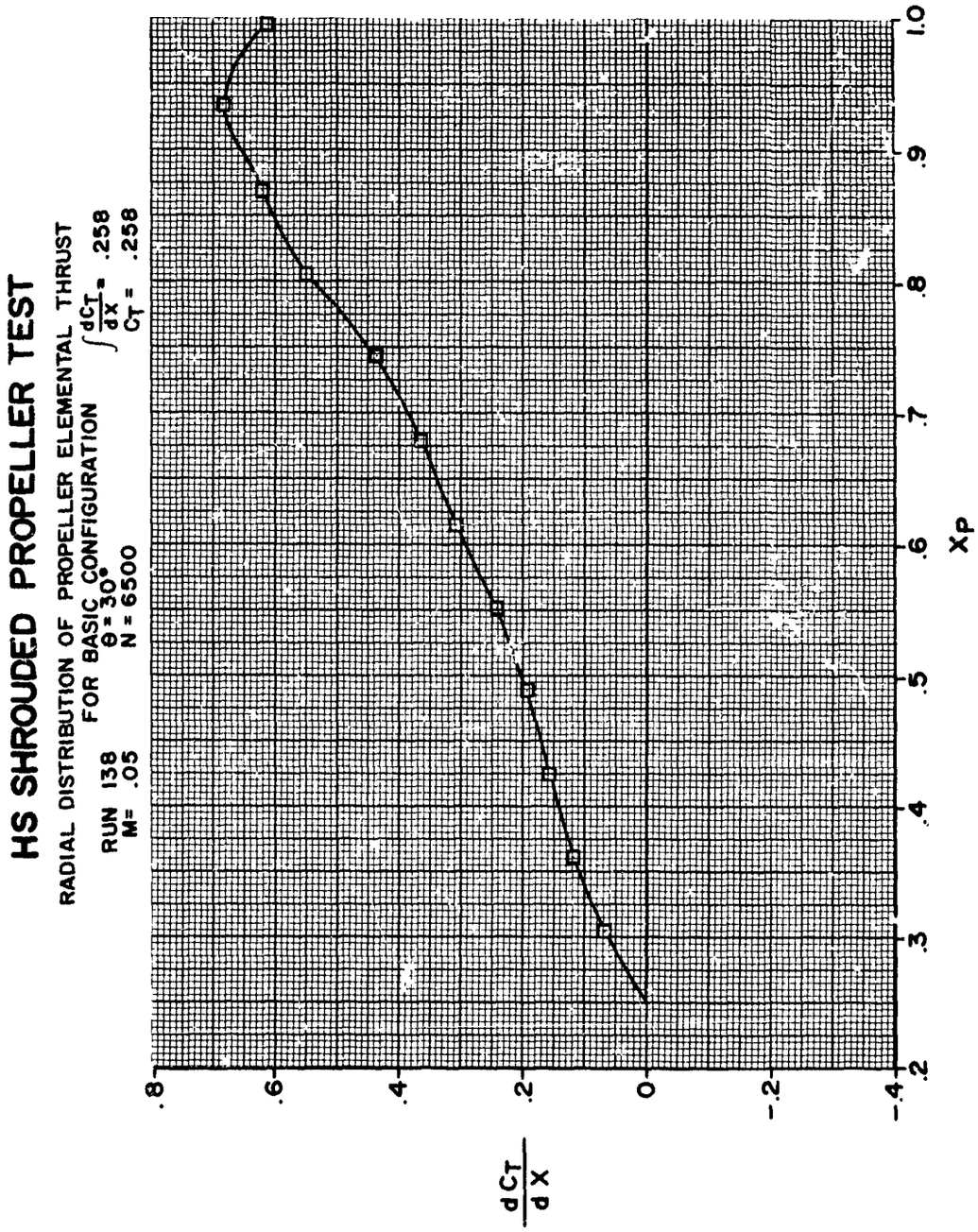
HS SHROUDED PROPELLER TEST
RADIAL DISTRIBUTION OF PROPELLER ELEMENTAL THRUST
FOR BASIC CONFIGURATION
RUN 138
M= .05
θ = 30°
N = 6500
∫ dCT/dX = .258
CT = .258
dCT/dX
.8
.6
.4
.2
0
-.2
-.4
.2
.3
.4
.5
.6
.7
.8
.9
1.0
XP

FIGURE 12.4–3

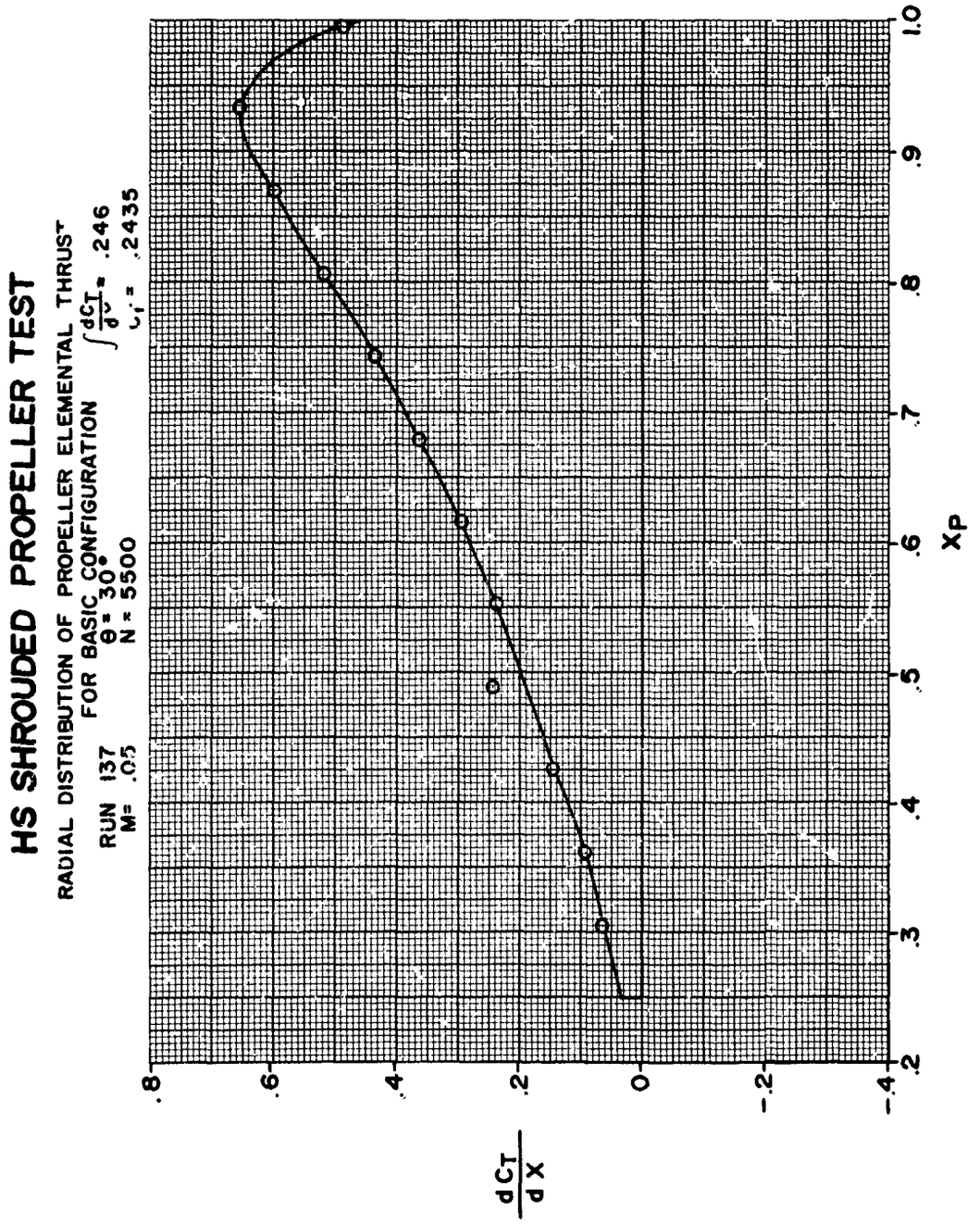
HS SHROUDED PROPELLER TEST
RADIAL DISTRIBUTION OF PROPELLER ELEMENTAL THRUST
FOR BASIC CONFIGURATION
RUN 137
M= .05
θ= 30°
N = 5500
∫ dCT/dν = .246
ci = .2435
dCT/dX
.8
.6
.4
.2
0
-.2
-.4
.2
.3
.4
.5
.6
.7
.8
.9
1.0
XP

FIGURE 12.4-4

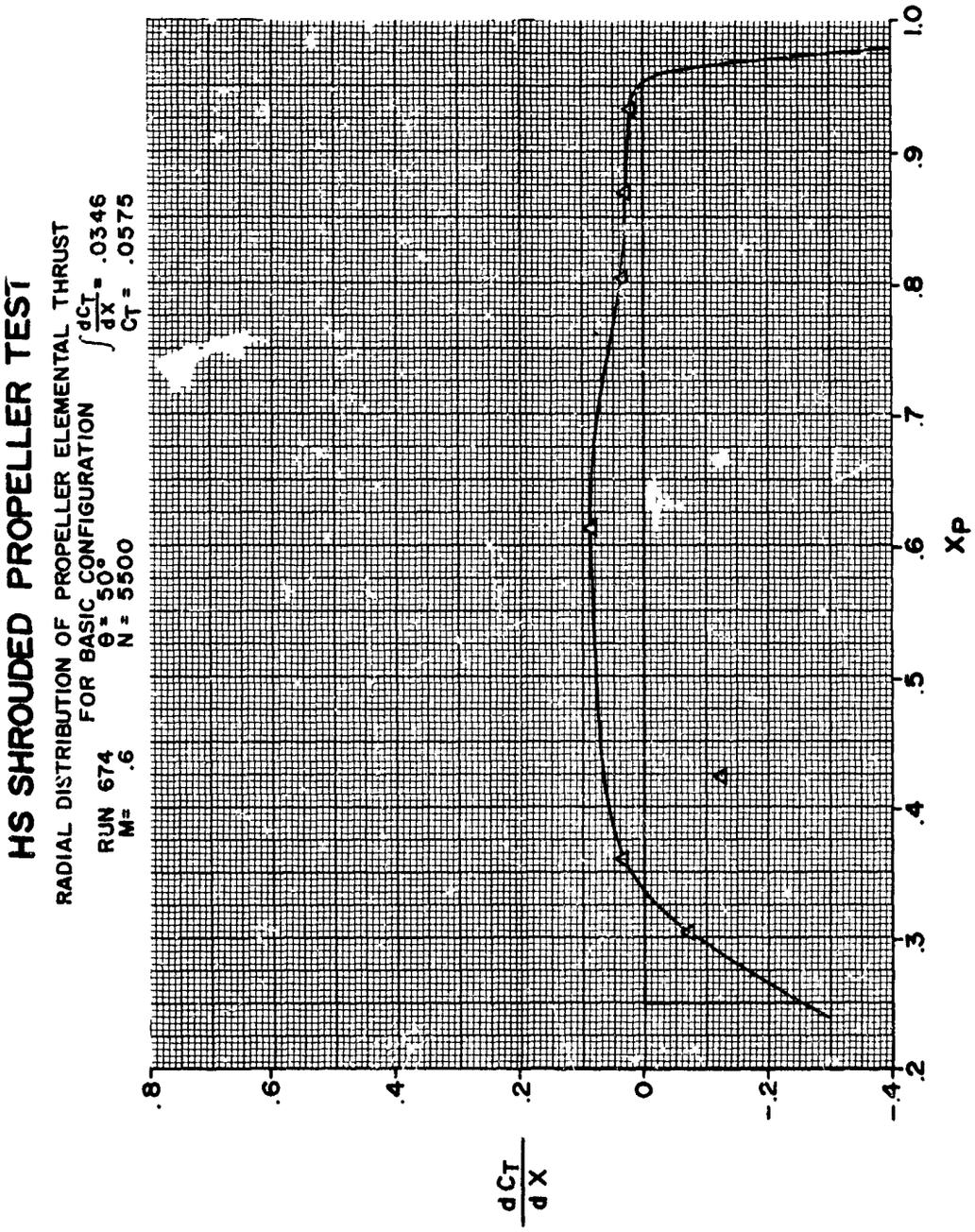
HS SHROUDED PROPELLER TEST
RADIAL DISTRIBUTION OF PROPELLER ELEMENTAL THRUST
FOR BASIC CONFIGURATION
RUN 674
M= .6
θ= 50°
N = 5500
∫ dCT/dX = .0346
CT = .0575
dCT/dX
.8
.6
.4
.2
0
-.2
-.4
.2
.3
.4
.5
.6
.7
.8
.9
1.0
XP

FIGURE 12.4–5

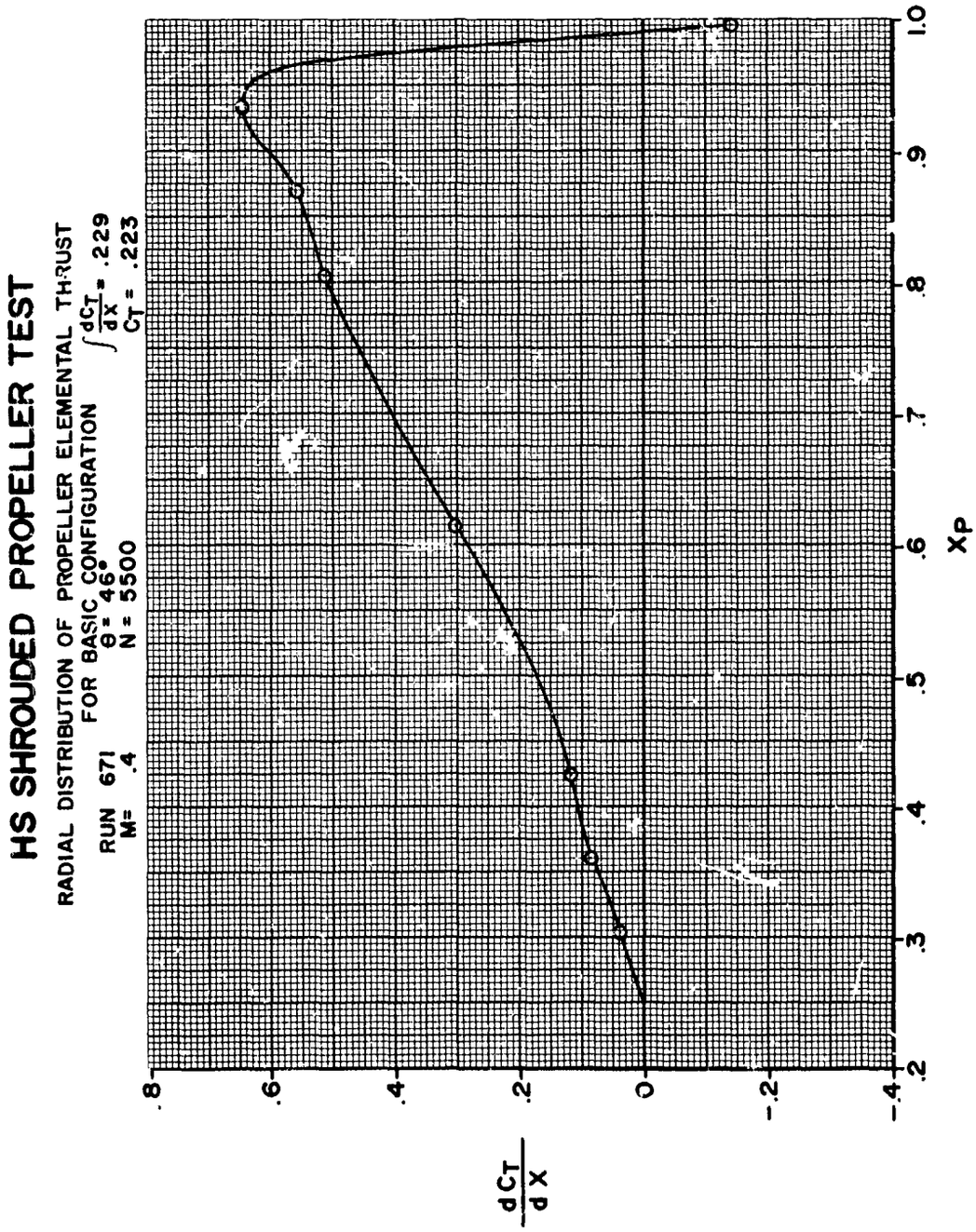
HS SHROUDED PROPELLER TEST
RADIAL DISTRIBUTION OF PROPELLER ELEMENTAL THRUST
FOR BASIC CONFIGURATION
RUN 671
M= .4
θ= 46°
N = 5500
∫ dCT/dX = .229
CT = .223
dCT/dX
.8
.6
.4
.2
0
-.2
-.4
.2
.3
.4
.5
.6
.7
.8
.9
1.0
XP

FIGURE 12.4-6

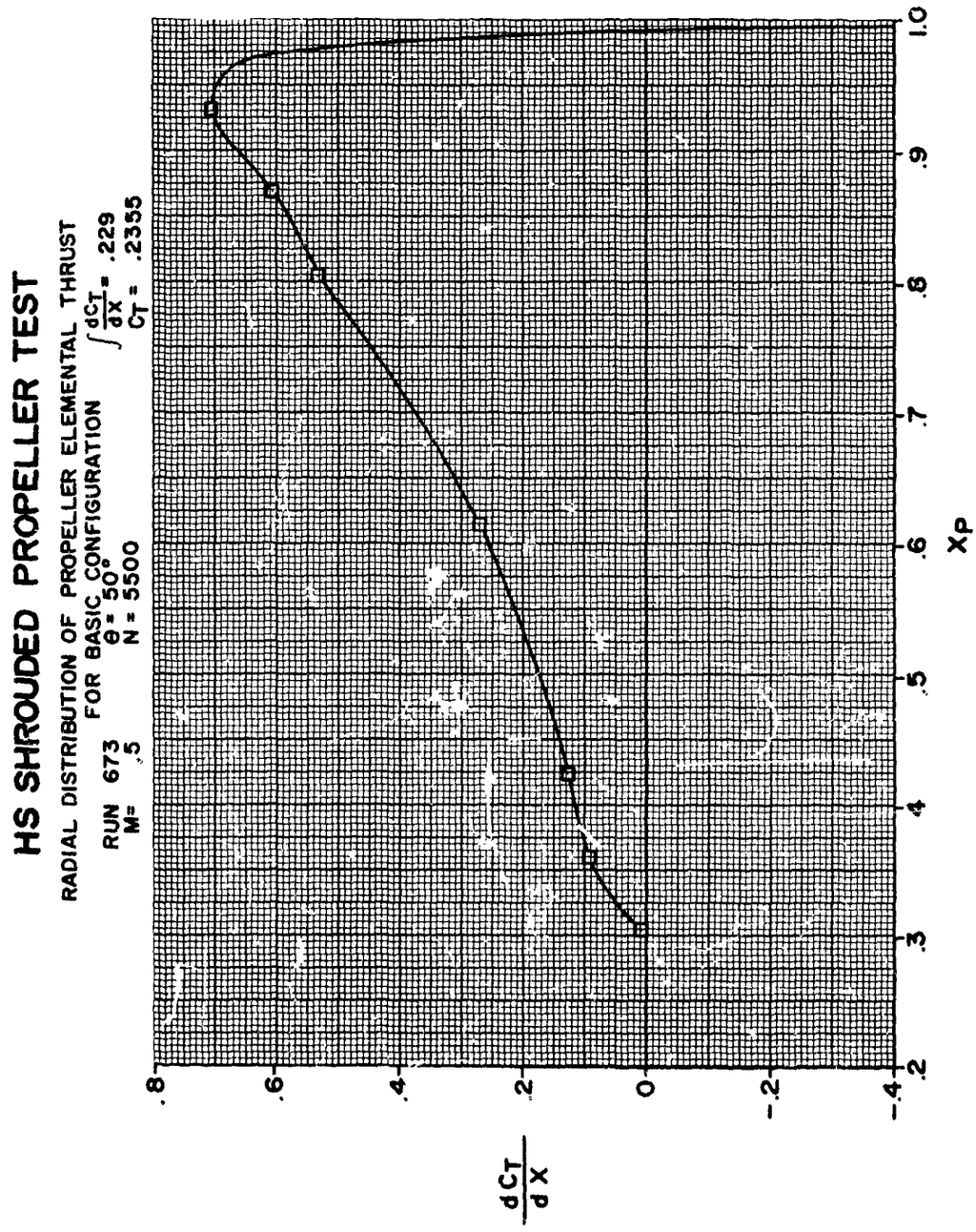
HS SHROUDED PROPELLER TEST
RADIAL DISTRIBUTION OF PROPELLER ELEMENTAL THRUST
FOR BASIC CONFIGURATION
RUN 673
M= .5
θ= 50°
N = 5500
∫ dCT/dX = .229
CT = .2355
dCT/dX
.8
.6
.4
.2
0
-.2
-.4
.2
.3
.4
.5
.6
.7
.8
.9
1.0
XP

FIGURE 12.4-7

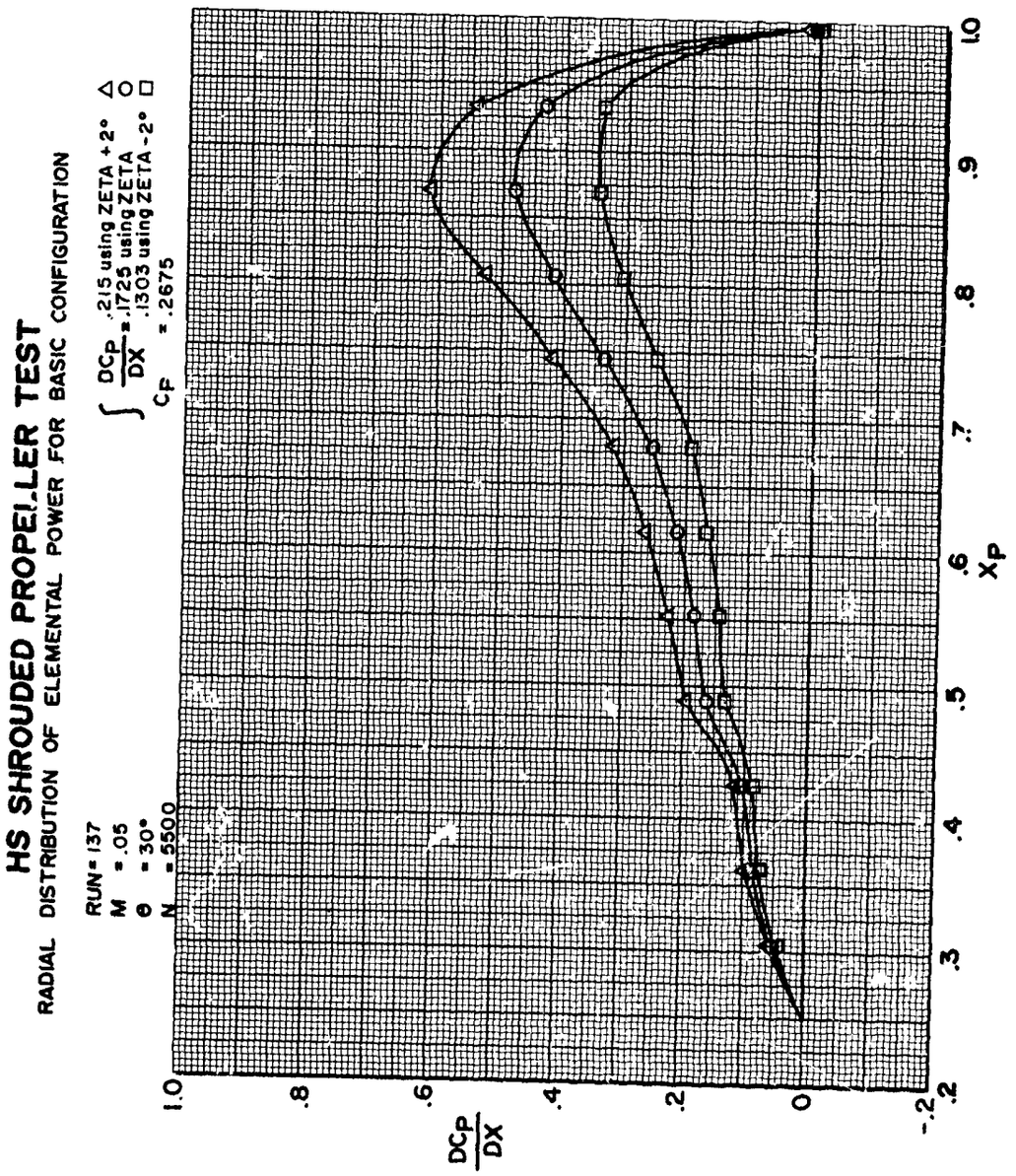
HS SHROUDED PROPELLER TEST
RADIAL DISTRIBUTION OF ELEMENTAL POWER FOR BASIC CONFIGURATION
RUN = 137
M = .05
θ = 30°
N = 5500
∫ DCP/DX dCP = .215 using ZETA + 2° △
.1725 using ZETA ○
.1303 using ZETA - 2° □
= .2675
DCP/DX
XP
1.0
.8
.6
.4
.2
0
-.2
.2
.3
.4
.5
.6
.7
.8
.9
1.0

FIGURE 12.4-8

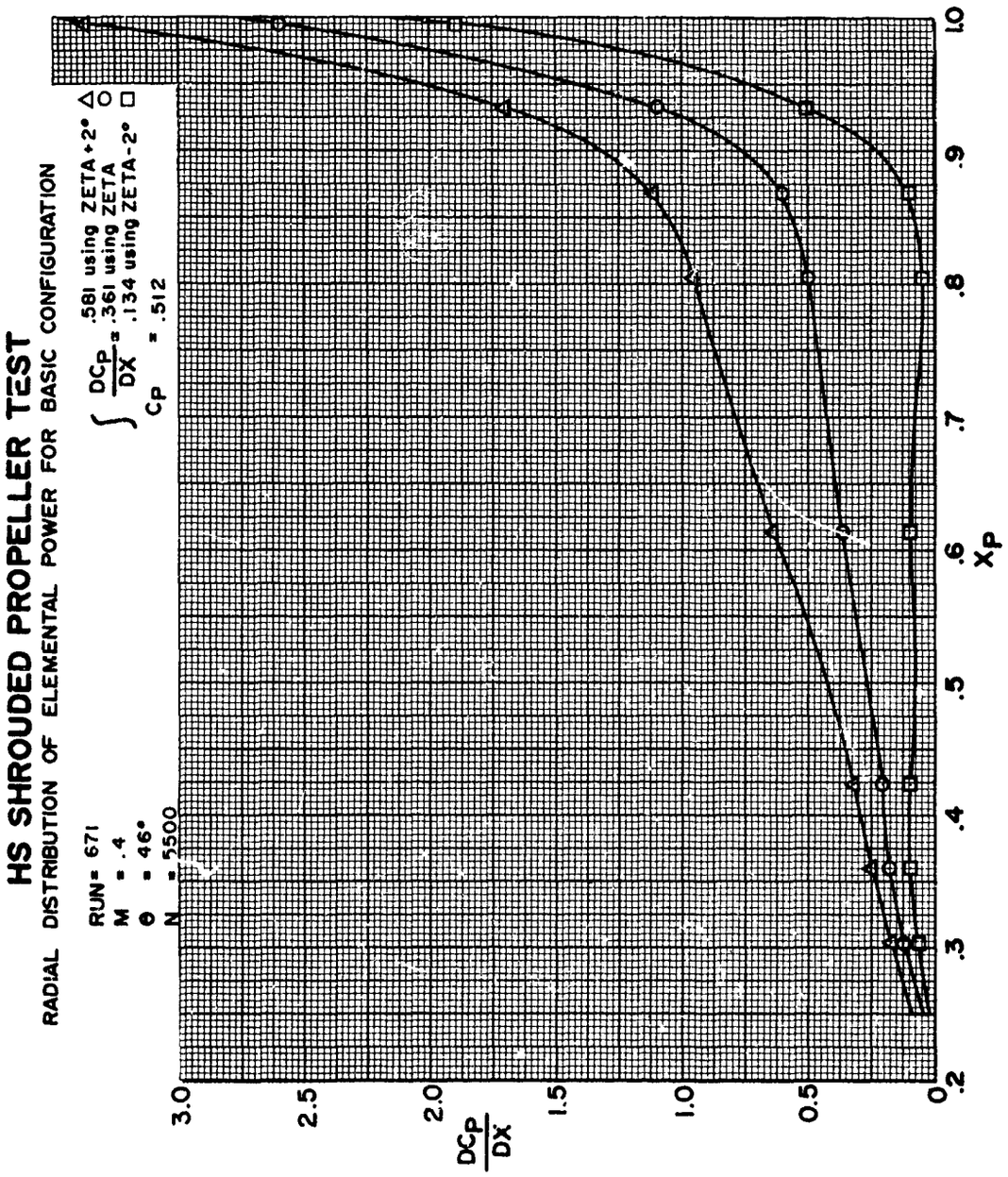
HS SHROUDED PROPELLER TEST
RADIAL DISTRIBUTION OF ELEMENTAL POWER FOR BASIC CONFIGURATION
RUN = 671
M = .4
θ = 46°
N = 5500
∫ DCP/DX = .581 using ZETA+2° △
.361 using ZETA ○
.134 using ZETA-2° □
CP = .512
DCP/DX
XP
3.0
2.5
2.0
1.5
1.0
0.5
0
.2
.3
.4
.5
.6
.7
.8
.9
1.0

FIGURE 12.4–9

XII APPENDICES

12.5 CALCULATION OF SLIPSTREAM CONTRACTION AND NET THRUST FROM PRESSURE DISTRIBUTION

Several pressure runs have been selected to evaluate the net thrust and the slipstream contraction. A semi-viscid evaluation of the net thrust can be obtained from the flow measurements at the shroud exit from the traverse probe. The internal viscous effects of the shroud are included in these flow measurements. The external momemtum deficiency due to the shroud friction drag is not, however, included in these flow measurements. The slipstream contraction is based upon these measurements and the assumption that the static pressure in the ultimate wake is equal to the atmospheric static pressure. For these analysis the pressures and velocities have been averaged and the problem has been reduced to a one-dimensional one.

Analysis

Assumptions:

1. Rotational effects are negligible and equilibrium in the jet is satisfied by a uniform jet static pressure where $P_{jet} = P_\infty$

2. Average exit axial velocity = $V_e = \dfrac{\int_{Xh_e}^{1.0} \rho_e V_e X_e dX_e}{\int_{Xh_e}^{1.0} \rho_e X_e dX_e}$

3. Average exit static pressure = Pe = arithmetic average of static pressure distributions from figures 273 through 285.

4. $A^*_{jet} = A^*_e$ (equivalence of areas where M = 1.0)

5. $H_j = H_e$ (total pressure equivalence)

Making use of compressible relationships and Mach tables as in reference 7, Table 12.5-I shows the pertinent values used and the results which evolved.

where:

pressures are in psf	Temperature is in degrees Rankine
thrusts are in pounds	M is nominal free stream Mach No.
velocities are in fps	density is in slugs/ft^3

XII

(Continued)

In Table 12.5-I:

1. A_j/Ae is the computed slipstream area contraction and is equal to $A_j/A^*/Ae/A^*$

2. $Tnet_i = \rho_e A_e V_e (V_j - V_\infty)$

   where $Ae_{(B1-3WT)} = 5.06\ ft^2$ (Area ratio = 1.1)

   and $Ae_{(B4-3WT)} = 5.975\ ft^2$ (Area ratio = 1.3)

3. F_D is the shroud friction drag based upon Table 12.3-II.

4. $Tnet_c = Tnet_i - F_D$

Table 12.5-I shows that the slipstream leaving the shroud generally contracts to its ultimate or jet size where the static pressure is again atmospheric. Of the two models the contraction is about 5% greater for the 1.1 area ratio shroud (B1-3WT), indicating that the jet area for this model is only about 80% as large as for the 1.3 area ratio shroud. The corrected net thrusts ($Tnet_c$) are nearly always greater than the measured net thrusts indicating that there is an incompatability either in the pressures and velocities or in the formulation. The disagreement between these values is worse for the 1.3 area ratio shrouds.

The lack of agreement between the computed and the measured net thrusts could be due to several factors which will be further evaluated in the theoretical formulation in Phase III of this contract. This investigation will look into:

1. A 2-D analysis where distributions of pressures and velocities will be used in lieu of average values.

2. Using the inlet rake velocities and exit rake total pressures in generating the required information to determine $Tnet_c$ and Aj/Ae.

3. Incorporating measured radial and tangetial velocities in determining the distribution of Pj.

4. Using the shroud surface pressure at the trailing edge as the static pressure at the shroud exit.

TABLE 12.5–I

RUN NO. / MODEL	P_∞ / V_∞	ρ_e / $\bar{T}_{TE}$	$\bar{V}_e$ / $\bar{M}_e$	$\bar{H}_e-\bar{H}_j$ / $\bar{M}_j$	$\bar{A}_j$ / $\bar{A}_e$	$\bar{V}_j$ / $\bar{V}_j-V_\infty$	T_{NET} / A_j/A_e	F_D / T_{NET_C}	M / $T_{NET\ MEAS.}$
139	2110	.00251	257	2198	2.45	266.5	680	6.	0.05
B1–3WT	58.5	497	0.2365	0.245	2.53	208	0.968	674.	690.
329	2135	00242	256	2215	2.60	253.	711.	7.	0.05
B4–3WT	60.0	508	0.232	0.230	2.58	193	1.007	704.	680.
671	1907.	00221	419.	2182	1.47	494.	158.	25.	0.40
B1–3WT	460.2	540.	0.373	0.442	1.68	33.8	0.875	133.	118.
673	1788.	0.00209	522.	2185.	1.26	605.	166.	34.	0.5
B1–3WT	574.8	548.	0.465	0.543	1.41	30.2	0.894	132.	121.
686	2004.	0.00226	349.	2170.	1.83	379.	155.	19.	0.3
B4–3WT	346.2	534.	0.311	0.338	1.92	32.8	0.953	136.	111.
687	1902.	0.00220	449.	2172.	1.47	492.	187.	29.	0.4
B4–3WT	460.4	537.	0.401	0.441	1.59	31.6	0.925	158.	126.
688	1784.	0.00206	550.	2167.	1.27	599.	164.	40.	0.5
B4–3WT	574.9	543.	0.496	0.538	1.35	24.[illegible]	0.940	124.	47.

APPENDICES

12.6 APPLICATIONS TO X-22

The data obtained in this test program were used to determine the potential performance benefits available to the Bell X-22A through shroud and propeller shape changes. To do this the performance of each model was determined at three X-22A operating conditions. From these data, the relative effect on X-22A performance was obtained for a given shape parameter change by interpolating the performance of the X-22A from the test data and making a ratio of that performance to the performance of the variable. No consideration was given as to whether the shape parameter change was structurally feasible within the present framework of the X-22A. These results are shown in Table 12.6-I on the following page.

TABLE 12.6–I

SHAPE PARAMETER *	PRESENT X–22A	CHANGE TO	CONDITIONS HOVER 761 HP,2590 RPM	225 KTS 600 BHP,1840 RPM	305 KTS 1328 BHP,2220 RPM
AREA RATIO (INCREASE)	1.17	B4–3WT	3.5 % **	–25 %	–40%
AREA RATIO (DECREASE)	1.17	B1–3WT	–3.5	7	15
TIP CLEARANCE	0.0043	B1–3R	4.0	3.0	1.0
LIP SHAPE	0.117	B1–3WT	0.5	–3.0	– 3.0
SHROUD LENGTH	0.575	B1–3WT	0	4.0	11.0
PROPELLER PLANFORM	NT	R	2.0	2.0	0
PROPELLER POSITION	0.29	B5–3WT	0	2.0	2.0

* AS DEFINED IN PRESENT REPORT.

** INDICATES PERCENTAGE INCREASE IN NET PERFORMANCE OVER THE PRESENT X–22A CONFIGURATION, – INDICATES A PERCENTAGE LOSS IN NET PERFORMANCE.

(Continued)

This table summarizes the findings for the three conditions shown. The largest changes in performance are noted for area ratio. The test data indicate that had the X-22A incorporated an area ratio of 1.3, a gain of 3.5% in net thrust could be realized at static conditions but this would have resulted in a 40% loss in cruise. Similarly, the effect of the other shape changes can be seen in Table 12.6-I. The effect of the shroud external shape (B6-3WT) and the number of propeller blades (B1-4NT) are not shown since there were no performance benefits with these two variables.

It should be pointed out that even larger gains may be possible than indicated in this table if it is possible to combine shape parameters not investigated in this test. For example, the B4-3WT model with the 3R or minimum tip clearance blade may produce an even greater gain in hover performance than is indicated in this table. Similarly, other combinations are possible.